Chapter 11

Control of Active Power and Reactive Power

So far this book has concentrated on the characteristics and modelling of individual elements of the power systems. This chapter will examine control of active power and reactive power by considering the system as an entity. In addition, the characteristics and modelling of equipment used for control will be described.

The flows of active power and reactive power in a transmission network are fairly independent of each other and are influenced by different control actions (see Section 6.3). Hence, they may be studied separately for a large class of problems. Active power control is closely related to frequency control, and reactive power control is closely related to voltage control. As constancy of frequency and voltage are important factors in determining the quality of power supply, the control of active power and reactive power is vital to the satisfactory performance of power systems.

11.1 ACTIVE POWER AND FREQUENCY CONTROL

For satisfactory operation of a power system, the frequency should remain nearly constant. Relatively close control of frequency ensures constancy of speed of induction and synchronous motors. Constancy of speed of motor drives is particularly important for satisfactory performance of generating units as they are highly dependent on the performance of all the auxiliary drives associated with the fuel, the feed-water and the combustion air supply systems. In a network, considerable drop in frequency could result in high magnetizing currents in induction motors and transformers. The extensive use of electric clocks and the use of frequency for other timing purposes require accurate maintenance of synchronous time which is

proportional to integral of frequency. As a consequence, it is necessary to regulate not only the frequency itself but also its integral.

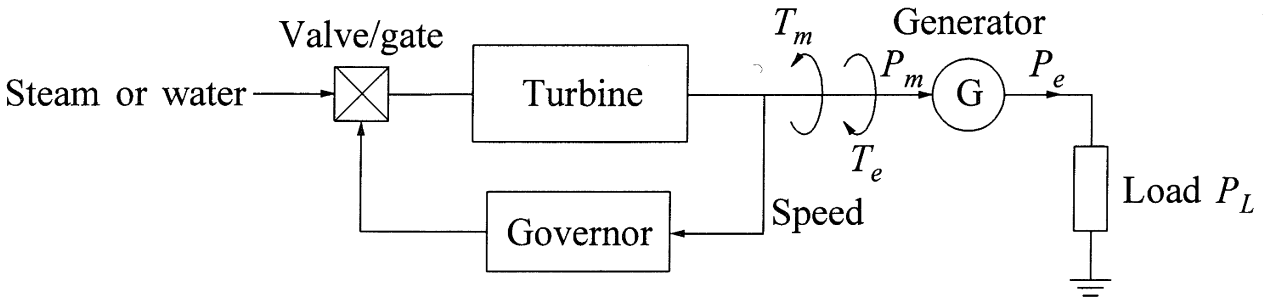
The frequency of a system is dependent on active power balance. As frequency is a common factor throughout the system, a change in active power demand at one point is reflected throughout the system by a change in frequency. Because there are many generators supplying power into the system, some means must be provided to allocate change in demand to the generators. A speed governor on each generating unit provides the primary speed control function, while supplementary control originating at a central control centre allocates generation.

In an interconnected system with two or more independently controlled areas, in addition to control of frequency, the generation within each area has to be controlled so as to maintain scheduled power interchange. The control of generation and frequency is commonly referred to as *load-frequency control* (LFC).

We will first review the requirements for primary speed governing and then discuss supplementary control.

11.1.1 Fundamentals of Speed Governing

The basic concepts of speed governing are best illustrated by considering an isolated generating unit supplying a local load as shown in Figure 11.1.

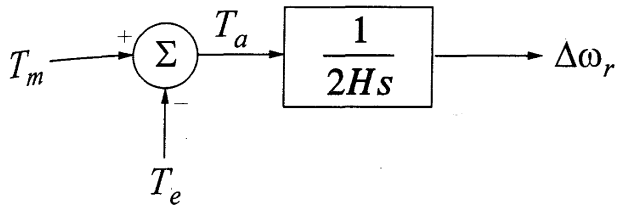


T_m = mechanical torque T_e = electrical torque
P_m = mechanical power P_e = electrical power P_L = load power

Figure 11.1 Generator supplying isolated load

Generator response to load change

When there is a load change, it is reflected instantaneously as a change in the electrical torque output T_e of the generator. This causes a mismatch between the mechanical torque T_m and the electrical torque T_e which in turn results in speed variations as determined by the equation of motion. As shown in Chapter 3 (Section 3.9), the following transfer function represents the relationship between rotor speed as a function of the electrical and mechanical torques.



s = Laplace operator
T_m = Mechanical torque (pu)
T_e = Electrical torque (pu)
T_a = Accelerating torque (pu)
H = Inertia constant (MW-Sec/MVA)
$\Delta\omega_r$ = Rotor speed deviation (pu)

Figure 11.2 Transfer function relating speed and torques

For load-frequency studies, it is preferable to express the above relationship in terms of mechanical and electrical power rather than torque. The relationship between power P and torque T is given by

$$P = \omega_r T \tag{11.1}$$

By considering a small deviation (denoted by prefix Δ) from initial values (denoted by subscript 0), we may write

$$\begin{aligned} P &= P_0 + \Delta P \\ T &= T_0 + \Delta T \\ \omega_r &= \omega_0 + \Delta\omega_r \end{aligned} \tag{11.2}$$

From Equation 11.1,

$$P_0 + \Delta P = (\omega_0 + \Delta\omega_r)(T_0 + \Delta T)$$

The relationship between the perturbed values, with higher-order terms neglected, is given by

$$\Delta P = \omega_0 \Delta T + T_0 \Delta\omega_r \tag{11.3}$$

Therefore,

$$\Delta P_m - \Delta P_e = \omega_0(\Delta T_m - \Delta T_e) + (T_{m0} - T_{e0})\Delta\omega_r \tag{11.4}$$

Since, in the steady state, electrical and mechanical torques are equal, $T_{m0} = T_{e0}$. With speed expressed in pu, $\omega_0 = 1$. Hence,

$$\Delta P_m - \Delta P_e = \Delta T_m - \Delta T_e \tag{11.5}$$

Figure 11.2 can now be expressed in terms of ΔP_m and ΔP_e as follows:

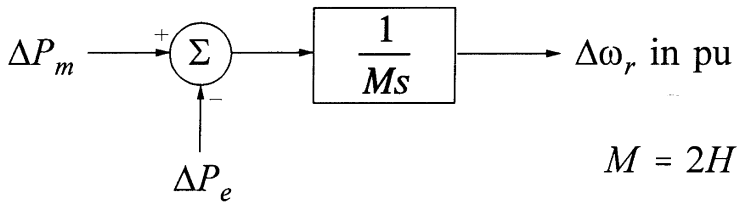


Figure 11.3 Transfer function relating speed and power

Within the range of speed variations with which we are concerned, the turbine mechanical power is essentially a function of valve or gate position and independent of frequency.

Load response to frequency deviation

In general, power system loads are a composite of a variety of electrical devices. For resistive loads, such as lighting and heating loads, the electrical power is independent of frequency. In the case of motor loads, such as fans and pumps, the electrical power changes with frequency due to changes in motor speed. The overall frequency-dependent characteristic of a composite load may be expressed as

$$\Delta P_e = \Delta P_L + D\Delta\omega_r \tag{11.6}$$

where

ΔP_L = non-frequency-sensitive load change
$D\Delta\omega_r$ = frequency-sensitive load change
D = load-damping constant

The damping constant is expressed as a percent change in load for one percent change in frequency. Typical values of D are 1 to 2 percent. A value of D=2 means that a 1% change in frequency would cause a 2% change in load.

The system block diagram including the effect of the load damping is shown in Figure 11.4.

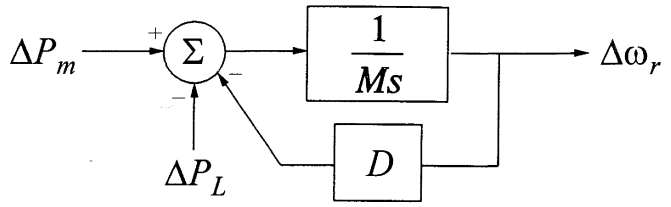


Figure 11.4

This may be reduced to the form shown in Figure 11.5.

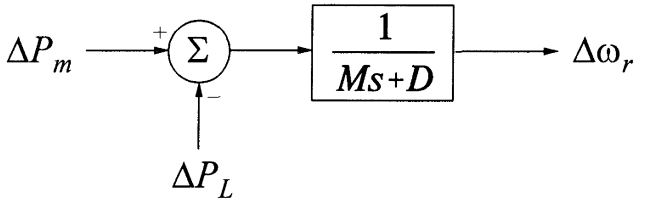


Figure 11.5

In the absence of a speed governor, the system response to a load change is determined by the inertia constant and the damping constant. The steady-state speed deviation is such that the change in load is exactly compensated by the variation in load due to frequency sensitivity. This is illustrated in the following example.

Example 11.1

A small system consists of 4 identical 500 MVA generating units feeding a total load of 1,020 MW. The inertia constant H of each unit is 5.0 on 500 MVA base. The load varies by 1.5% for a 1% change in frequency. When there is a sudden drop in load by 20 MW,

(a) Determine the system block diagram with constants H and D expressed on 2,000 MVA base.

(b) Find the frequency deviation, assuming that there is no speed-governing action.

Solution

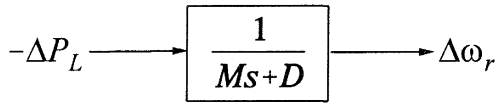
(a) For 4 units on 2,000 MVA base, H = 5.0×(500/2000)×4 = 5.0. Hence,

$$M = 2H = 10.0 \text{ s}$$

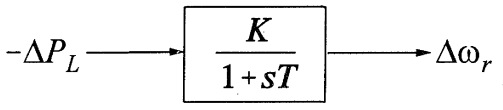
Expressing D for the remaining load (1020-20=1000 MW) on 2,000 MVA base,

$$D = 1.5\times1000/\ 2000 = 0.75\%$$

(b) With $\Delta P_m = 0$ (no speed governing), the system block diagram with parameters expressed in pu on 2,000 MVA is



This may be expressed in the standard form in terms of a gain and a time constant:



where

$$K = \frac{1}{D} = \frac{1}{0.75} = 1.33$$

$$T = \frac{M}{D} = \frac{10}{0.75} = 13.33 \quad \text{s}$$

The load change is

$$\Delta P_L = -20 \quad \text{MW}$$

$$= \frac{-20}{2000} = -0.01 \quad \text{pu}$$

For a step reduction in load by 0.01 pu, Laplace transform of the change in load is

$$\Delta P_L(s) = \frac{-0.01}{s}$$

Hence, from the block diagram

$$\Delta\omega_r(s) = -\left(\frac{-0.01}{s}\right)\left(\frac{K}{1+sT}\right)$$

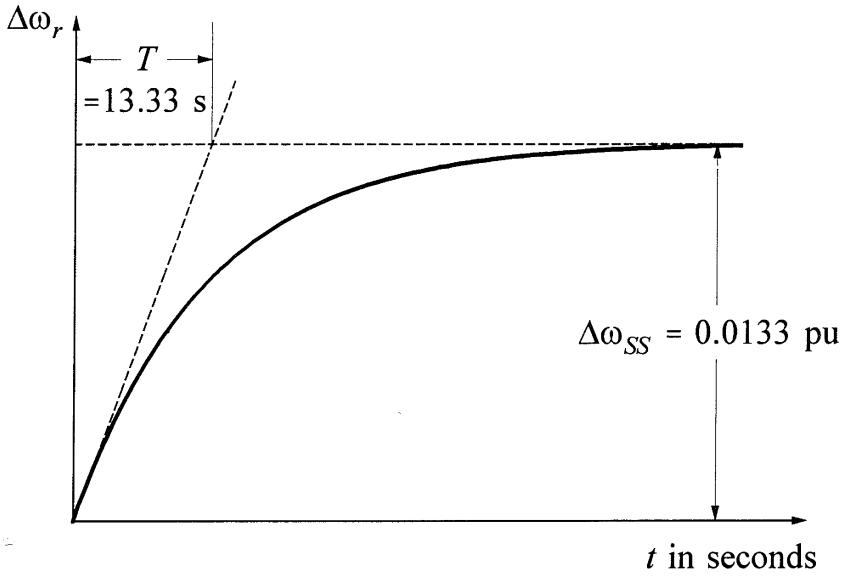
Taking the inverse transform,

$$\Delta\omega_r(t) = -0.01K e^{-\frac{t}{T}} + 0.01K$$

$$= -0.01\times 1.33\, e^{-\frac{t}{13.33}} + 0.01\times 1.33$$

$$= -0.0133\, e^{-0.075t} + 0.0133$$

The pu speed deviation as function of time is shown in the following figure.



The time constant T is 13.33 s and the steady-state speed deviation is

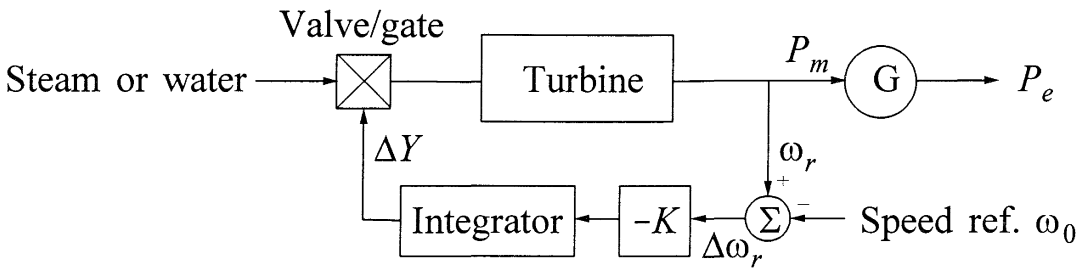
$$\Delta\omega_{ss} = -\frac{\Delta P_L}{D} = 0.0133 \text{ pu}$$

$$= 0.0133\times 60 = 0.8 \text{ Hz}$$

■

Isochronous governor [1,2]

The adjective isochronous means constant speed. An isochronous governor adjusts the turbine valve/gate to bring the frequency back to the nominal or scheduled value. Figure 11.6 shows the schematic of such a speed-governing system. The measured rotor speed ω_r is compared with reference speed ω_0. The error signal (equal to speed deviation) is amplified and integrated to produce a control signal ΔY which actuates the main steam supply valves in the case of a steam turbine, or gates in the case of a hydraulic turbine. Because of the reset action of this integral controller, ΔY will reach a new steady state only when the speed error $\Delta\omega_r$ is zero.



ω_r = rotor speed
P_m = mechanical power
Y = valve/gate position

Figure 11.6 Schematic of an isochronous governor

Figure 11.7 shows the time response of a generating unit, with an isochronous governor, when subjected to an increase in load. The increase in P_e causes the frequency to decay at a rate determined by the inertia of rotor. As the speed drops, the turbine mechanical power begins to increase. This in turn causes a reduction in the rate of decrease of speed, and then an increase in speed when the turbine power is in excess of the load power. The speed will ultimately return to its reference value and the steady-state turbine power increases by an amount equal to the additional load.

An isochronous governor works satisfactorily when a generator is supplying an isolated load or when only one generator in a multigenerator system is required to respond to changes in load. For power load sharing between generators connected to the system, speed regulation or droop characteristic must be provided as discussed next.

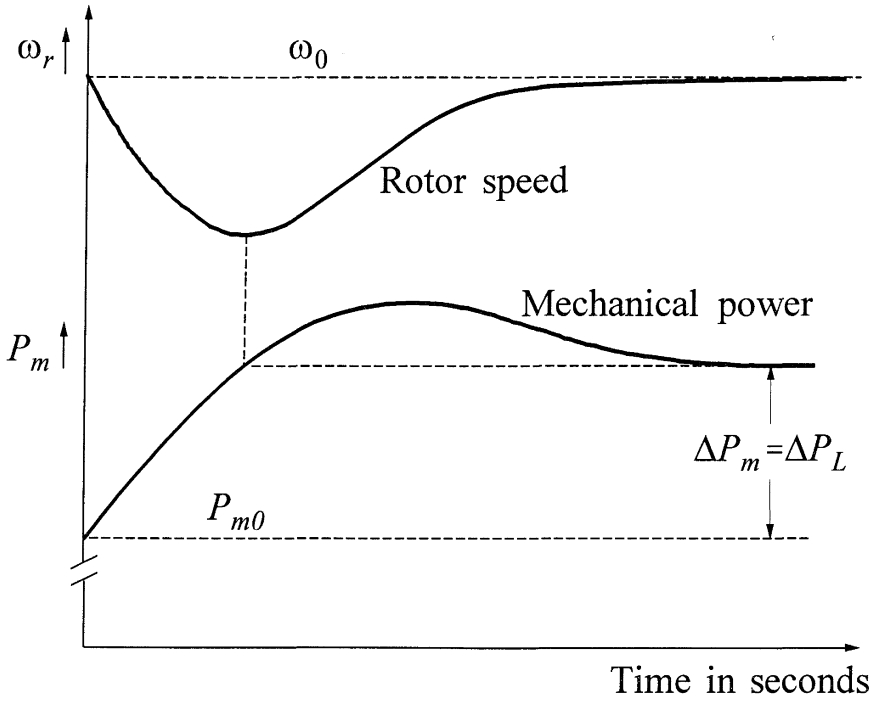


Figure 11.7 Response of generating unit with isochronous governor

Governors with speed-droop characteristic [1,2]

The isochronous governors cannot be used when there are two or more units connected to the same system since each generator would have to have precisely the same speed setting. Otherwise, they would fight each other, each trying to control system frequency to its own setting. For stable load division between two or more units operating in parallel, the governors are provided with a characteristic so that the speed drops as the load is increased.

The speed-droop or regulation characteristic may be obtained by adding a steady-state feedback loop around the integrator as shown in Figure 11.8.

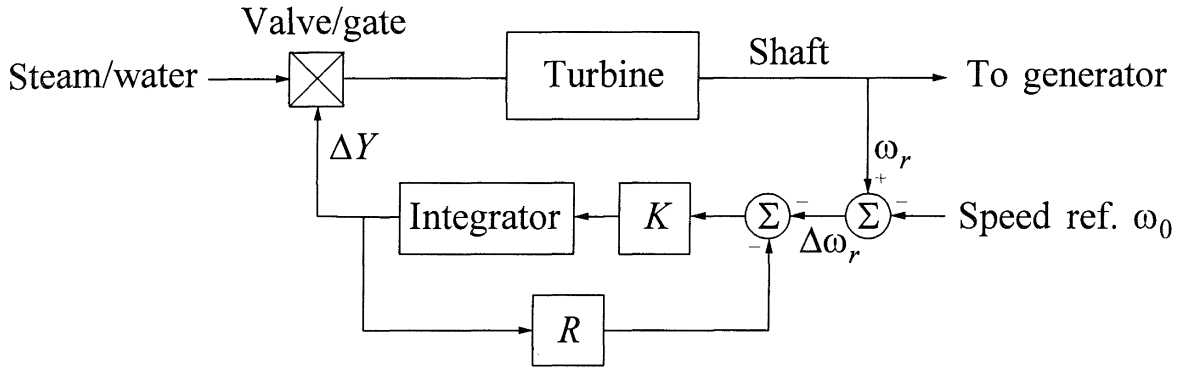
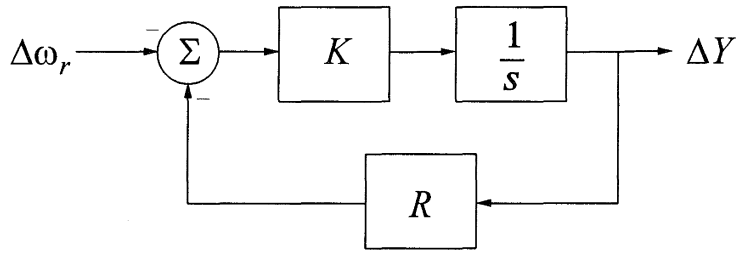
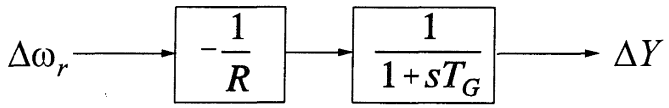


Figure 11.8 Governor with steady-state feedback

The transfer function of the governor of Figure 11.8 reduces to the form shown in Figure 11.9. This type of governor is characterized as a *proportional controller* with a gain of $1/R$.



(a) Block diagram with steady-state feedback



$$T_G = \frac{1}{KR}$$

(b) Reduced block diagram

Figure 11.9 Block diagram of a speed governor with droop

Percent speed regulation or droop:

The value of R determines the steady-state speed versus load characteristic of the generating unit as shown in Figure 11.10. The ratio of speed deviation ($\Delta\omega_r$) or frequency deviation (Δf) to change in valve/gate position (ΔY) or power output (ΔP) is equal to R. The parameter R is referred to as speed regulation or droop. It can be expressed in percent as

$$\text{Percent } R = \frac{\text{percent speed or frequency change}}{\text{percent power output change}} \times 100$$

$$= \left(\frac{\omega_{NL} - \omega_{FL}}{\omega_0}\right) \times 100$$

where

ω_{NL} = steady-state speed at no load
ω_{FL} = steady-state speed at full load
ω_0 = nominal or rated speed

For example, a 5% droop or regulation means that a 5% frequency deviation causes 100% change in valve position or power output.

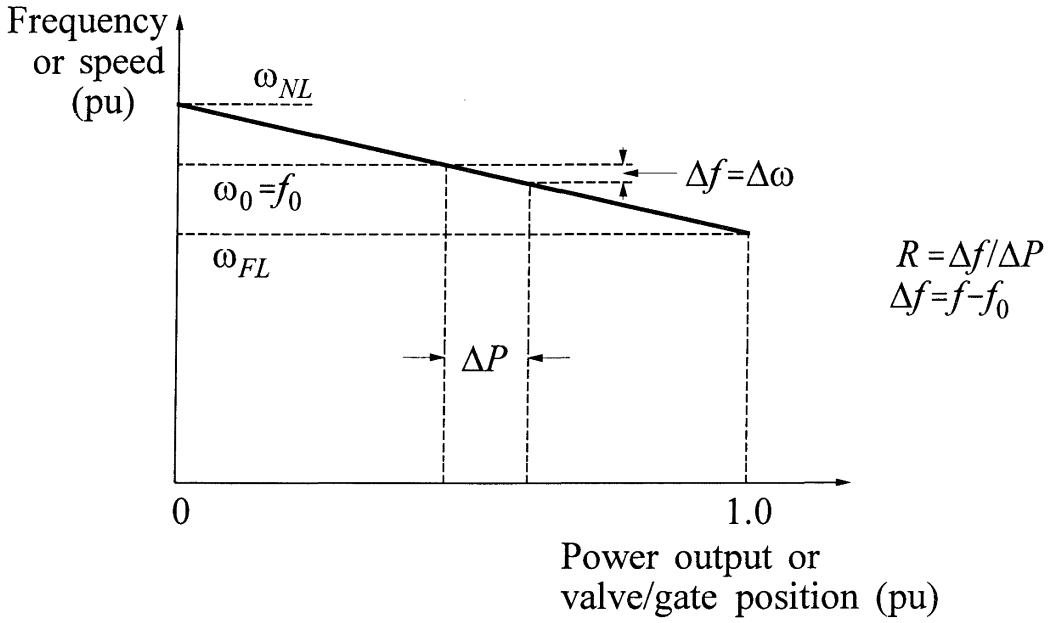


Figure 11.10 Ideal steady-state characteristics of a governor with speed droop

Load sharing by parallel units:

If two or more generators with drooping governor characteristics are connected to a power system, there will be a unique frequency at which they will share a load change. Consider two units with droop characteristics as shown in Figure 11.11. They are initially at nominal frequency f_0, with outputs P_1 and P_2. When a load increase ΔP_L causes the units to slow down, the governors increase output until they reach a new common operating frequency f'. The amount of load picked up by each unit depends on the droop characteristic:

$$\Delta P_1 = P_1' - P_1 = \frac{\Delta f}{R_1}$$

$$\Delta P_2 = P_2' - P_2 = \frac{\Delta f}{R_2}$$

Hence,

$$\frac{\Delta P_1}{\Delta P_2} = \frac{R_2}{R_1}$$

If the percentages of regulation of the units are nearly equal, the change in the outputs of each unit will be nearly in proportion to its rating.

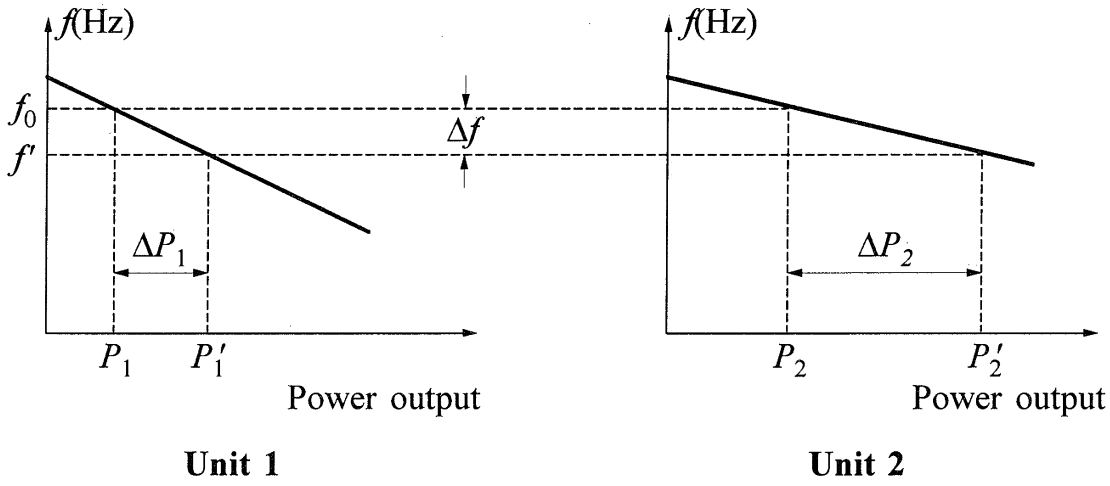


Figure 11.11 Load sharing by parallel units with drooping governor characteristics

Time response

Figure 11.12 shows the time response of a generating unit, with a speed-droop governor, when subjected to an increase in load. Because of the droop characteristic, the increase in power output is accompanied by a steady-state speed or frequency deviation ($\Delta\omega_{SS}$).

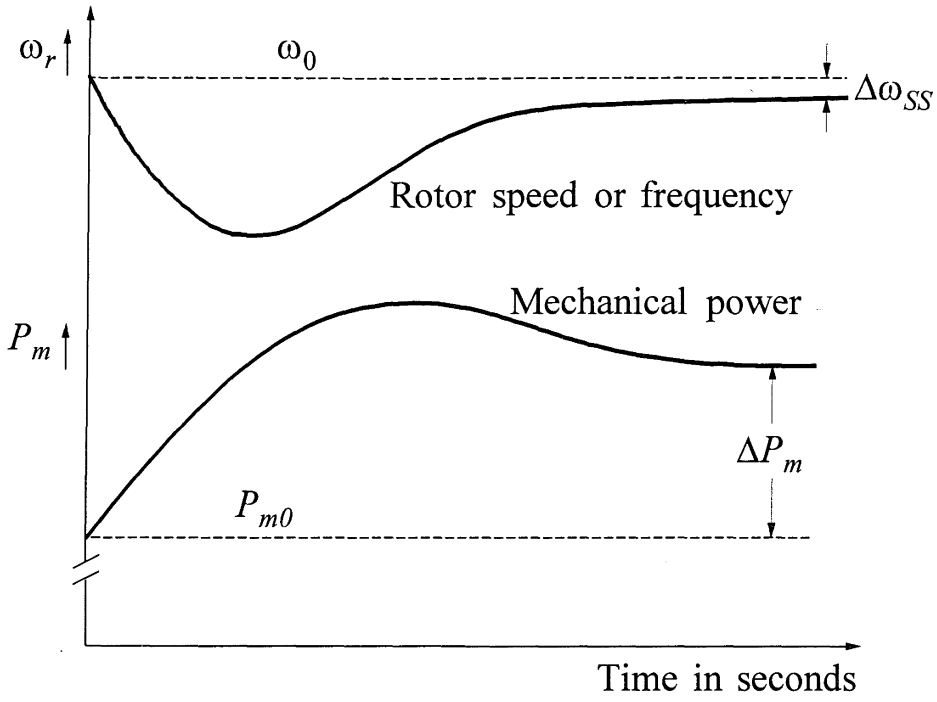


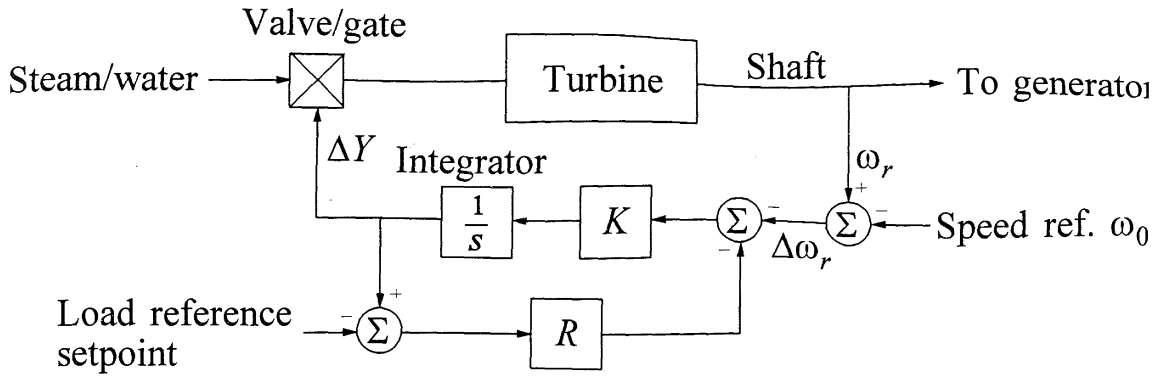
Figure 11.12 Response of a generating unit with a governor having speed-droop characteristic

11.1.2 Control of Generating Unit Power Output

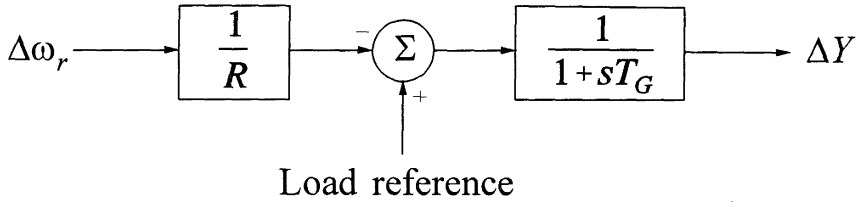
The relationship between speed and load can be adjusted by changing an input shown as "load reference setpoint" in Figure 11.13.

In practice, the adjustment of load reference setpoint is accomplished by operating the "speed-changer motor." The effect of this adjustment is depicted in Figure 11.14, which shows a family of parallel characteristics for different speed-changer motor settings. The characteristics shown are for a governor associated with a 60 Hz system. Three characteristics are shown representing three load reference settings. At 60 Hz, characteristic A results in zero output, characteristic B results in 50% output, and characteristic C results in 100% output. Thus, the power output of the generating unit at a given speed may be adjusted to any desired value by adjusting the load reference setting through actuation of the speed-changer motor. For each setting, the speed-load characteristic has a 5% droop; that is, a speed change of 5% (3 Hz) causes a 100% change in power output.

When two or more generators are operating in parallel, the speed-droop characteristic (corresponding to a load reference setting) of each generating unit merely establishes the proportion of the load picked up by the unit when a sudden change in system load occurs. The output of each unit at any given system frequency can be varied only by changing its load reference, which in effect moves the speed-droop characteristic up and down.



(a) Schematic diagram of governor and turbine



(b) Reduced block diagram of governor

Figure 11.13 Governor with load reference control for adjusting speed-load relationship

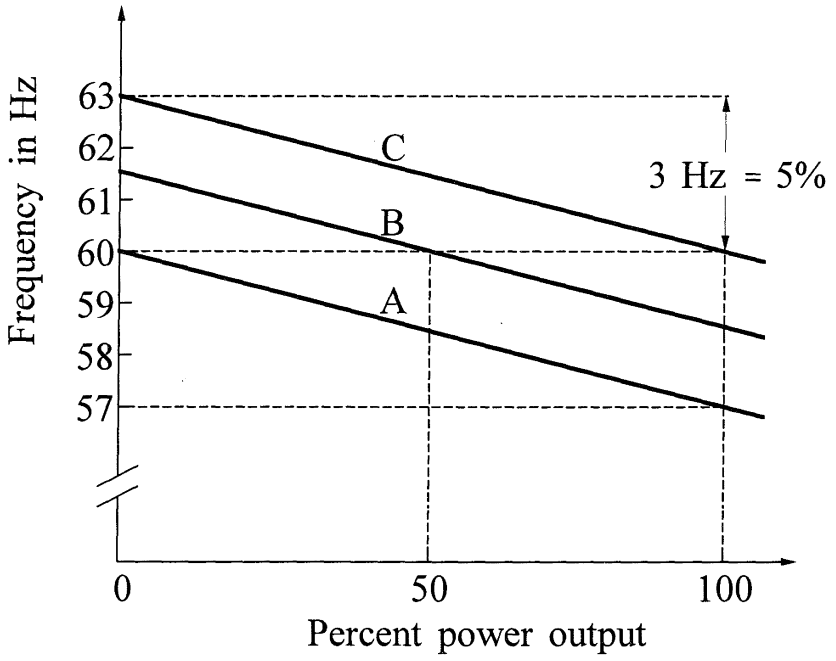


Figure 11.14 Effect of speed-changer setting on governor characteristic

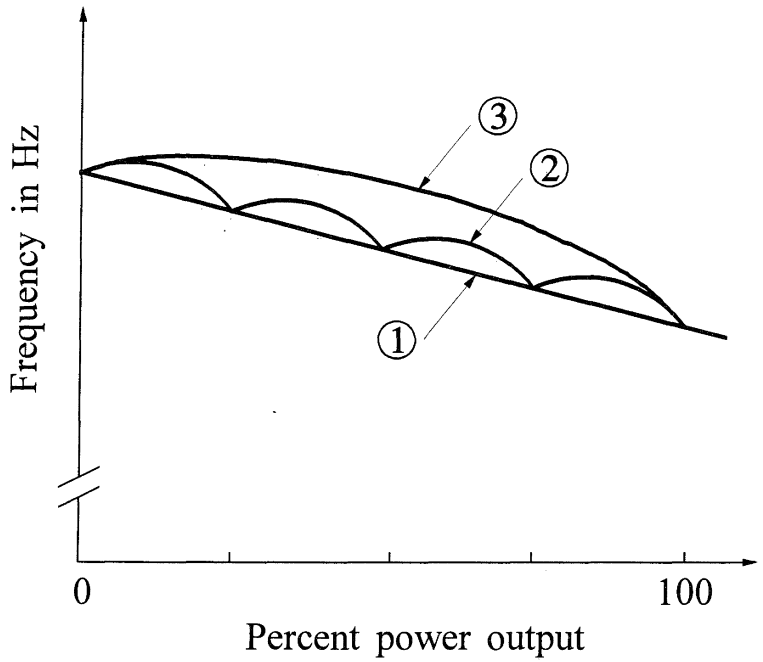
When a generating unit is feeding an isolated load, the adjustment of the speed changer changes the unit speed. However, when the unit is synchronized to a power system, the speed-changer adjustment changes the unit power output; it has only a minor effect on system frequency, depending on the size of the unit relative to that of the total system generation.

Actual speed-droop characteristic [1]

The governor speed-droop characteristic we have considered so far (Figures 11.10 and 11.14) represents the ideal relationship. In actual practice the characteristic departs from the straight-line relationship as depicted in Figure 11.15.

As discussed in Chapter 9, steam turbines have a number of control valves, each having nonlinear flow area versus position characteristic. Hence, they have the speed-droop characteristics of the general nature of curve 2 in Figure 11.15. Each section of curve 2 represents the effect of one control valve. Hydraulic turbines, which have a single gate, tend to have the characteristic similar to curve 3.

The actual speed-droop characteristic may thus exhibit *incremental regulation* ranging from 2% to 12%, depending on the unit output. Modern electrohydraulic governing systems minimize these variations in incremental regulation by using linearizing circuits or first-stage pressure feedback.



Curve 1: Ideal linear characteristic
Curve 2: Actual characteristic for steam units
Curve 3: Actual characteristic for hydraulic units

Figure 11.15 Actual and ideal governor speed-droop characteristics

11.1.3 Composite Regulating Characteristic of Power Systems

In the analysis of load-frequency controls (LFCs), we are interested in the collective performance of all generators in the system. The intermachine oscillations and transmission system performance are therefore not considered. We tacitly assume the coherent response of all generators to changes in system load and represent them by an equivalent generator. The equivalent generator has an inertia constant M_{eq} equal to the sum of the inertia constants of all the generating units and is driven by the combined mechanical outputs of the individual turbines as illustrated in Figure 11.16. Similarly, the effects of the system loads are lumped into a single damping constant D. The speed of the equivalent generator represents the system frequency, and in per unit the two are equal. We will therefore use rotor speed and frequency interchangeably in our discussion of load-frequency control.

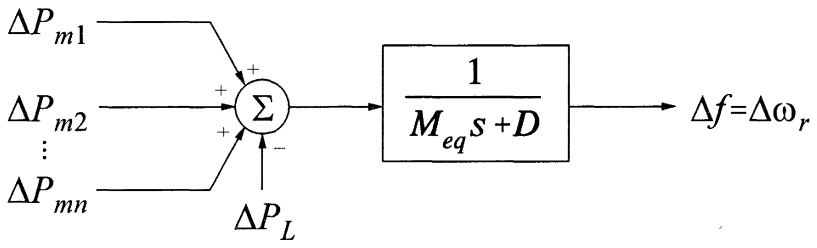


Figure 11.16 System equivalent for LFC analysis

The composite power/frequency characteristic of a power system thus depends on the combined effect of the droops of all generator speed governors. It also depends on the frequency characteristics of all the loads in the system. For a system with n generators and a composite load-damping constant of D, the steady-state frequency deviation following a load change ΔP_L is given by

$$\begin{aligned}\Delta f_{SS} &= \frac{-\Delta P_L}{(1/R_1+1/R_2+\cdots+1/R_n)+D} \\ &= \frac{-\Delta P_L}{1/R_{eq}+D}\end{aligned} \tag{11.7}$$

where

$$R_{eq} = \frac{1}{1/R_1+1/R_2+\cdots+1/R_n} \tag{11.8}$$

Thus, the composite frequency response characteristic of the system is

$$\beta = \frac{-\Delta P_L}{\Delta f_{SS}} = \frac{1}{R_{eq}} + D \tag{11.9}$$

The composite frequency response characteristic β is normally expressed in MW/Hz. It is also sometimes referred to as the *stiffness* of the system. The composite regulating characteristic of the system is equal to 1/β.

The effects of governor speed droop and the frequency sensitivity of load on the net frequency change are illustrated in Figure 11.17, which considers the composite effects of all the generating units and load in the system. An increase of system load by ΔP_L (at nominal frequency) results in a total generation increase of ΔP_G due to governor action and a total system load reduction of ΔP_D due to its frequency-sensitive characteristic.

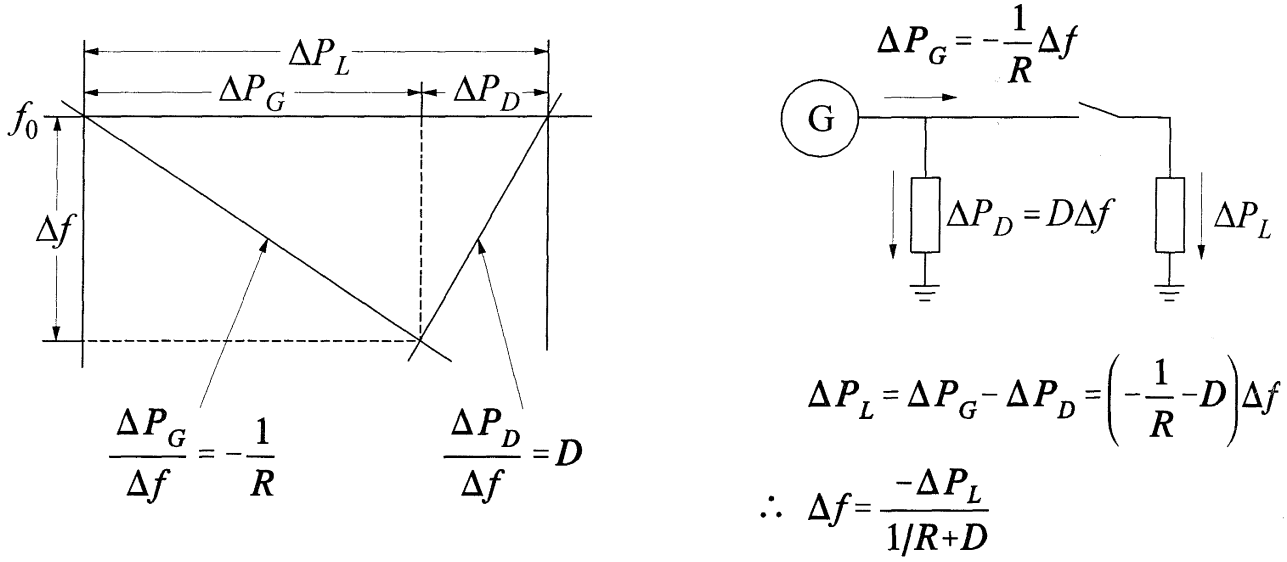


Figure 11.17 Composite governor and load characteristic

Example 11.2

A power system has a total load of 1,260 MW at 60 Hz. The load varies 1.5% for every 1% change in frequency (D=1.5). Find the steady-state frequency deviation when a 60 MW load is suddenly tripped, if

(a) There is no speed control.

(b) The system has 240 MW of spinning reserve evenly spread among 500 MW of generation capacity with 5% regulation based on this capacity. All other generators are operating with valves wide open. Assume that the effect of governor dead bands is such that only 80% of the governors respond to the reduction in system load.

Neglect the effects of transmission losses.

Solution

Total remaining load is 1260−60 = 1200 MW. The damping constant of remaining load is

$$D = \left(\frac{1.5}{100}\times 1200\right)\times\left(\frac{100}{60\times 1}\right) = 30 \quad \text{MW/Hz}$$

(a) With no speed control, the resulting increase in steady-state frequency is

$$\Delta f = \frac{-\Delta P_L}{D} = \frac{-(-60)\ \text{MW}}{30\ \text{MW/Hz}}$$

$$= 2.0 \quad \text{Hz}$$

(b) Since there is a reduction in system load and an increase in frequency, all generating units (not just those on spinning reserve) respond. However, due to the effects of dead band, only 80% of the total generation contributes to speed regulation.

The total spinning generation capacity is equal to

$$\text{Load} + \text{reserve} = 1260 + 240 = 1500 \text{ MW}$$

Generation contributing to regulation is

$$0.8\times 1500 = 1200 \text{ MW}$$

A regulation of 5% means that a 5% change in frequency causes a 100% change in power generation. Therefore,

$$\frac{1}{R} = \frac{1200}{(5/100)\times 60} = 400 \quad \text{MW/Hz}$$

The composite system frequency response characteristic is

$$\beta = \frac{1}{R} + D = 400 + 30$$

$$= 430 \quad \text{MW/Hz}$$

Steady-state increase in frequency is

$$\Delta f = \frac{-\Delta P_L}{\beta} = \frac{-(-60)\ \text{MW}}{430\ \text{MW/Hz}}$$

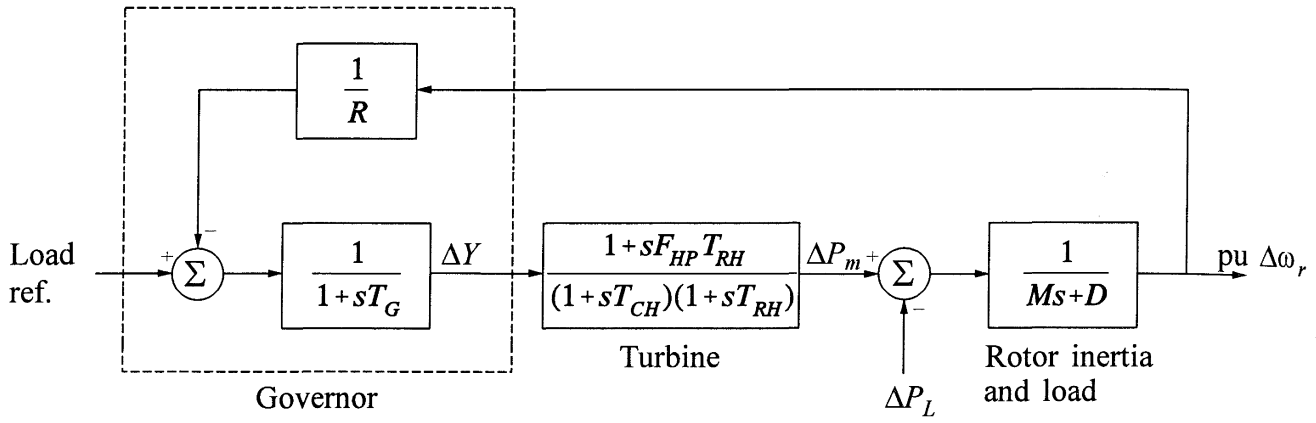
$$= 0.1395 \quad \text{Hz}$$

■

11.1.4 Response Rates of Turbine-Governing Systems

So far, we have analyzed steady-state performance of speed-governing systems. We will now examine the relative response rates of steam and hydraulic turbines and their governing systems.

As discussed in Chapter 9, steam turbines may be of either reheat type or non-reheat type. Figure 11.18 shows the block diagram of a generating unit with a reheat turbine. The block diagram includes representation of the speed governor, turbine, rotating mass and load, appropriate for load-frequency analysis. The turbine representation is based on the simplified transfer function developed in Chapter 9 (Section 9.2.1), and assumes constant boiler pressure.

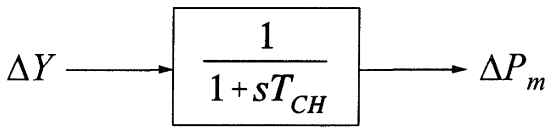


Typical values:

R = 0.05	T_G = 0.2 s	F_{HP} = 0.3	T_{RH} = 7.0 s
T_{CH} = 0.3 s	F_{LP} = 0.7	M = 10.0 s	D = 1.0

Figure 11.18 Block diagram of a generating unit with a reheat steam turbine

The block diagram of Figure 11.18 is also applicable to a unit with non-reheat turbine. However, in this case T_{RH}=0, and the turbine transfer function simplifies to that shown in Figure 11.19.



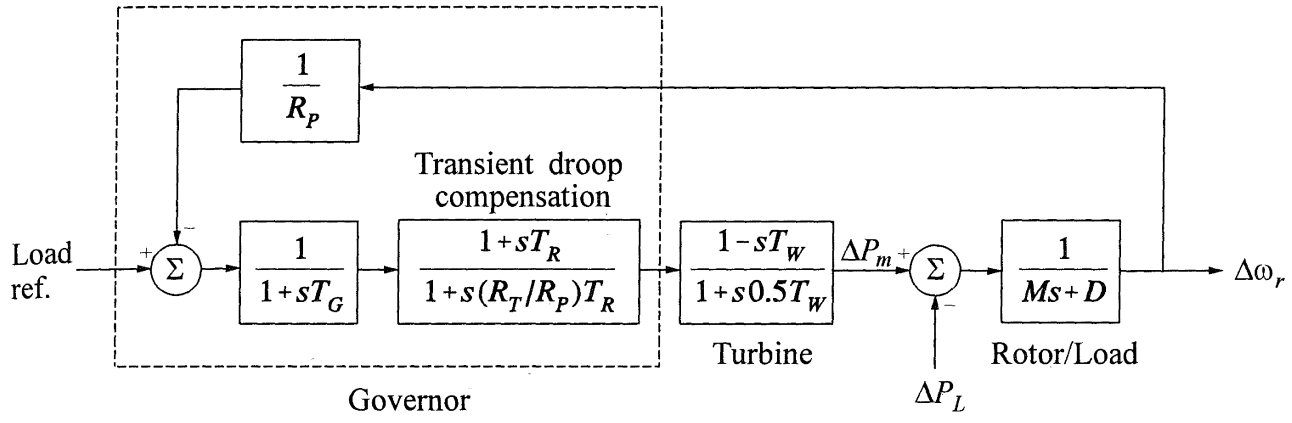
Typical value:

T_{CH} = 0.3 s

Figure 11.19 Non-reheat turbine transfer function

In Chapter 9 (Section 9.1.3), we showed that the governors of hydraulic units require *transient droop compensation* for stable speed control performance. Because a change in the position of the gate at the foot of the penstock produces an initial short-term turbine power change which is opposite to that sought, hydro turbine governors are designed to have relatively large transient droop, with long resetting times. This ensures stable frequency regulation under isolated operating conditions (islanding). Consequently, the response of a hydraulic unit to speed change or to changes in speed-changer setting is relatively slow.

The block diagram of a generating unit with a hydraulic turbine is shown in Figure 11.20. The governor includes transient droop. The transfer functions for the turbine and the speed governor used in the block diagram were developed in Chapter 9. For fast-frequency deviations, the governor exhibits a high regulation (or low gain); for slow changes and in the steady state it has a lower regulation (or high gain).



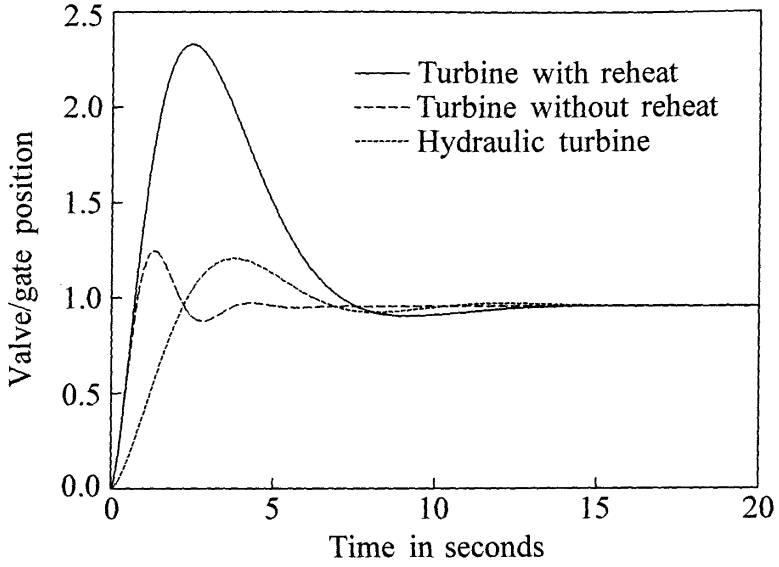
Typical values:

$R_P = 0.05$	$T_G = 0.2$ s	$M = 6.0$ s	$D = 1.0$
$T_W = 1.0$ s	$R_T = 0.38$	$T_R = 5.0$ s	

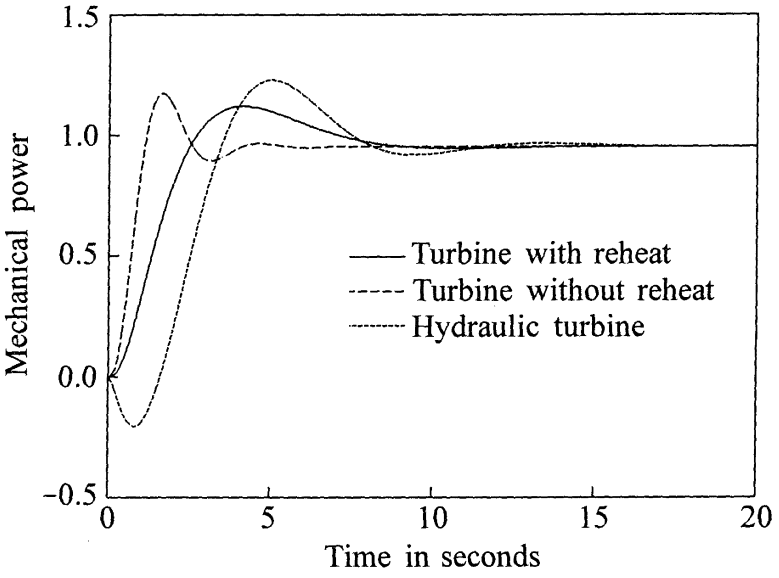
Figure 11.20 Block diagram of hydraulic unit

The nature of the responses of generating units with reheat and non-reheat steam turbines, and hydraulic turbines when subjected to a step change in load (ΔP_L), is illustrated in Figure 11.21. These responses have been computed by using the linearized models and typical parameters shown in Figures 11.18 and 11.19. Constant boiler pressure has been assumed for the steam turbines. Depending on the type of boiler and its controls, and on the size of the load change, the response of the steam turbines may be significantly slower than that shown. On the other hand, a low-head hydraulic unit may have a significantly faster response than the one considered here.

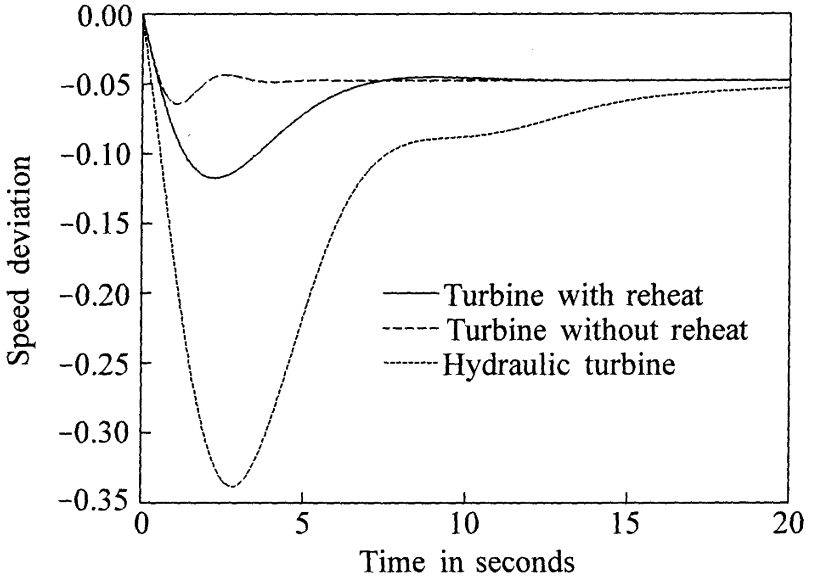
The results presented here demonstrate that, although the steady-state speed deviation is the same for all three units considered, there are significant differences in their transient responses. Unit response characteristics, in fact, vary widely



(a) Turbine valve/gate position



(b) Mechanical power



(c) Speed deviation

Figure 11.21 Responses of steam and hydraulic generating units to a small step increase in load demand; values shown are in per unit of the step change.

depending on many factors. These include, in addition to the type of plant, plant controls and mode of operation (e.g., boiler-follow, turbine-follow), and operating point (e.g., nearness to valve point, load limit).

11.1.5 Fundamentals of Automatic Generation Control [3-6]

With primary speed control action, a change in system load will result in a steady-state frequency deviation, depending on the governor droop characteristic and frequency sensitivity of the load. All generating units on speed governing will contribute to the overall change in generation, irrespective of the location of the load change. Restoration of system frequency to nominal value requires supplementary control action which adjusts the load reference setpoint (through the speed-changer motor). Therefore, the basic means of controlling prime-mover power to match variations in system load in a desired manner is through control of the load reference setpoints of selected generating units. As system load is continually changing, it is necessary to change the output of generators automatically.

The primary objectives of *automatic generation control* (AGC) are to regulate frequency to the specified nominal value and to maintain the interchange power between control areas at the scheduled values by adjusting the output of selected generators. This function is commonly referred to as *load-frequency control* (LFC). A secondary objective is to distribute the required change in generation among units to minimize operating costs.

AGC in isolated power systems

In an isolated power system, maintenance of interchange power is not an issue. Therefore, the function of AGC is to restore frequency to the specified nominal value. This is accomplished by adding a reset or integral control which acts on the load reference settings of the governors of units on AGC, as shown in Figure 11.22. The integral control action ensures zero frequency error in the steady state.

The supplementary generation control action is much slower than the primary speed control action. As such it takes effect after the primary speed control (which acts on all units on regulation) has stabilized the system frequency. Thus, AGC adjusts load reference settings of selected units, and hence their output power, to override the effects of the composite frequency regulation characteristics of the power system. In so doing, it restores the generation of all other units not on AGC to scheduled values.

AGC in interconnected power systems

To form the basis for supplementary control of interconnected power systems, let us first look at the performance with primary speed control only.

Consider the interconnected system shown in Figure 11.23(a). It consists of two areas connected by a tie line of reactance X_{tie}. For load-frequency studies, each area may be represented by an equivalent generating unit exhibiting its overall

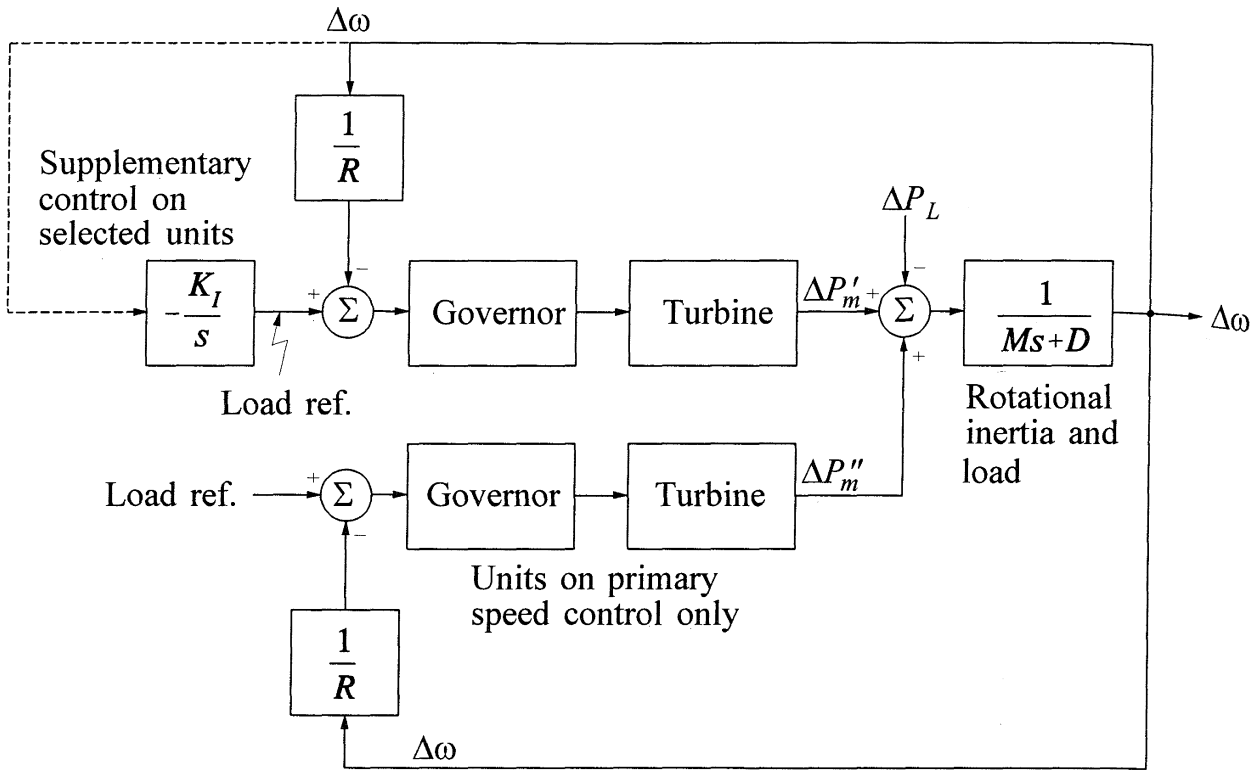


Figure 11.22 Addition of integral control on generating units selected for AGC

performance. Such composite models are acceptable since we are not concerned about intermachine oscillations within each area.

Figure 11.23(b) shows the electrical equivalent of the system, with each area represented by a voltage source behind an equivalent reactance as viewed from the tie bus. The power flow on the tie line from area 1 to area 2 is

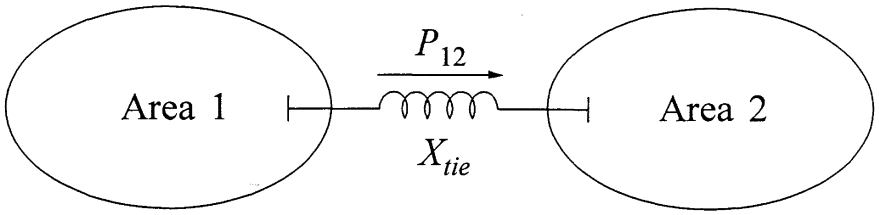
$$P_{12} = \frac{E_1 E_2}{X_T} \sin(\delta_1 - \delta_2)$$

Linearizing about an initial operating point represented by $\delta_1 = \delta_{10}$ and $\delta_2 = \delta_{20}$, we have

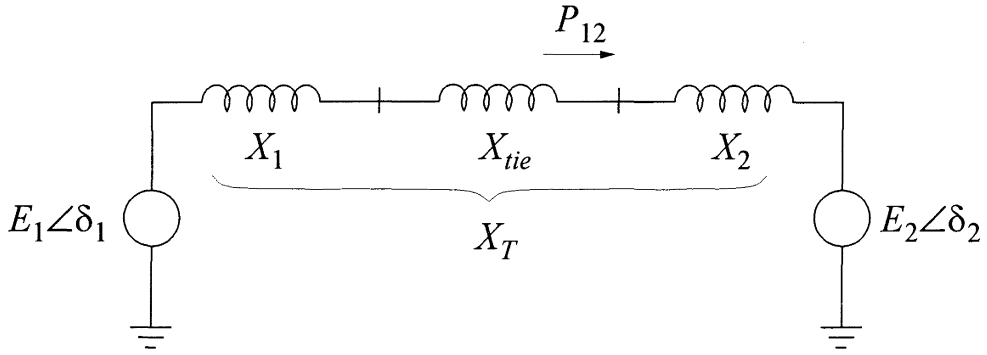
$$\Delta P_{12} = T \Delta \delta_{12}$$

where $\Delta\delta_{12} = \Delta\delta_1 - \Delta\delta_2$, and T is the synchronizing torque coefficient given by

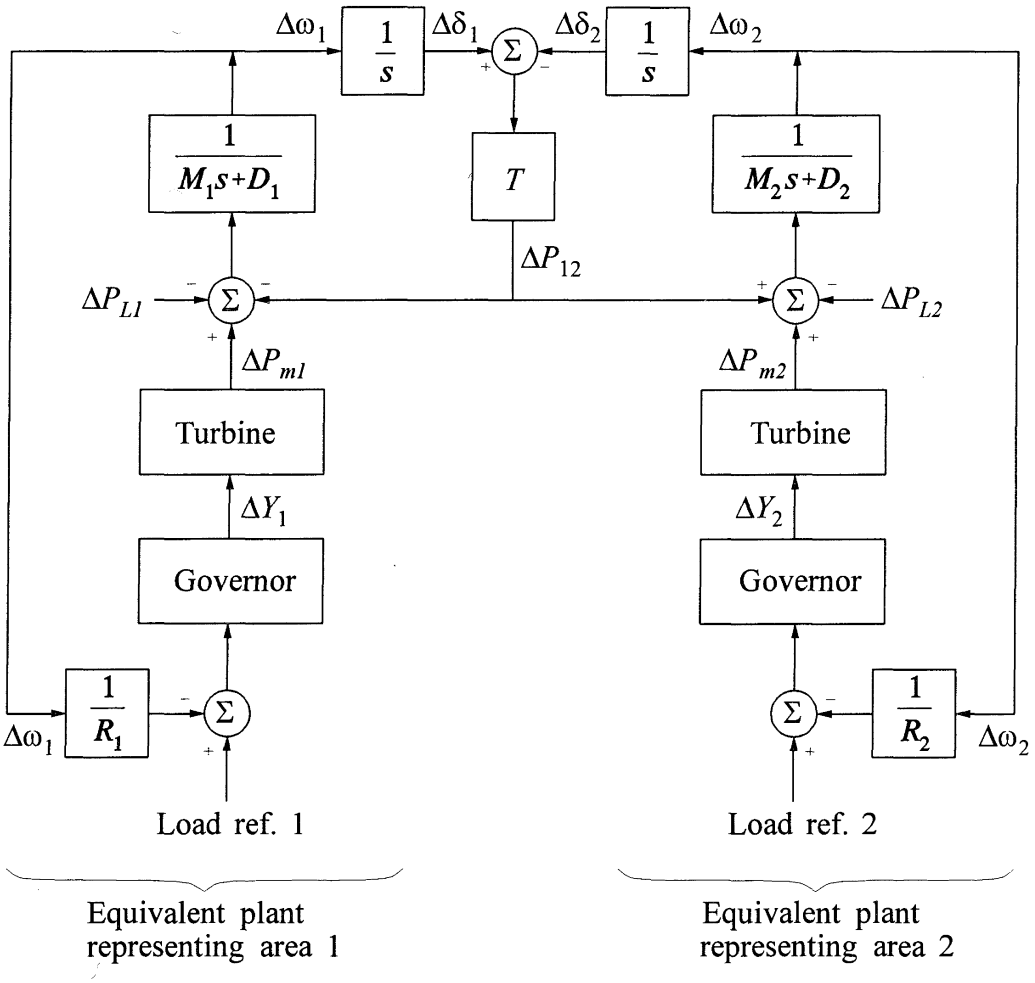
$$T = \frac{E_1 E_2}{X_T} \cos(\delta_{10} - \delta_{20}) \tag{11.10}$$



(a) Two-area system



(b) Electrical equivalent



(c) Block diagram

Figure 11.23 Two-area system with only primary speed control

The block diagram representation of the system is shown in Figure 11.23(c) with each area represented by an equivalent inertia M, load-damping constant D, turbine, and governing system with an effective speed droop R. The tie line is represented by the synchronizing torque coefficient T. A positive ΔP_{12} represents an increase in power transfer from area 1 to area 2. This in effect is equivalent to increasing the load of area 1 and decreasing the load of area 2; therefore, feedback of ΔP_{12} has a negative sign for area 1 and a positive sign for area 2.

The steady-state frequency deviation $(f-f_0)$ is the same for the two areas. For a total load change of ΔP_L,

$$\Delta f = \Delta\omega_1 = \Delta\omega_2 = \frac{-\Delta P_L}{(1/R_1+1/R_2)+(D_1+D_2)} \tag{11.11}$$

Consider the steady-state values following an increase in area 1 load by ΔP_{L1}. For area 1, we have

$$\Delta P_{m1} - \Delta P_{12} - \Delta P_{L1} = \Delta f D_1 \tag{11.12}$$

and for area 2,

$$\Delta P_{m2} + \Delta P_{12} = \Delta f D_2 \tag{11.13}$$

The change in mechanical power depends on regulation. Hence,

$$\Delta P_{m1} = -\frac{\Delta f}{R_1} \tag{11.14}$$

$$\Delta P_{m2} = -\frac{\Delta f}{R_2} \tag{11.15}$$

Substitution of Equation 11.14 in Equation 11.12 and Equation 11.15 in Equation 11.13 yields

$$\Delta f\left(\frac{1}{R_1}+D_1\right) = -\Delta P_{12} - \Delta P_{L1} \tag{11.16}$$

and

$$\Delta f\left(\frac{1}{R_2}+D_2\right) = \Delta P_{12} \tag{11.17}$$

Solving Equations 11.16 and 11.17, we get

$$\Delta f = \frac{-\Delta P_{L1}}{(1/R_1+D_1)+(1/R_2+D_2)} = \frac{-\Delta P_{L1}}{\beta_1+\beta_2} \tag{11.18}$$

and

$$\Delta P_{12} = \frac{-\Delta P_{L1}(1/R_2+D_2)}{(1/R_1+D_1)+(1/R_2+D_2)} = \frac{-\Delta P_{L1}\beta_2}{\beta_1+\beta_2} \tag{11.19}$$

where β_1 and β_2 are the composite frequency response characteristics of areas 1 and 2, respectively. The above relationships are depicted in Figure 11.24.

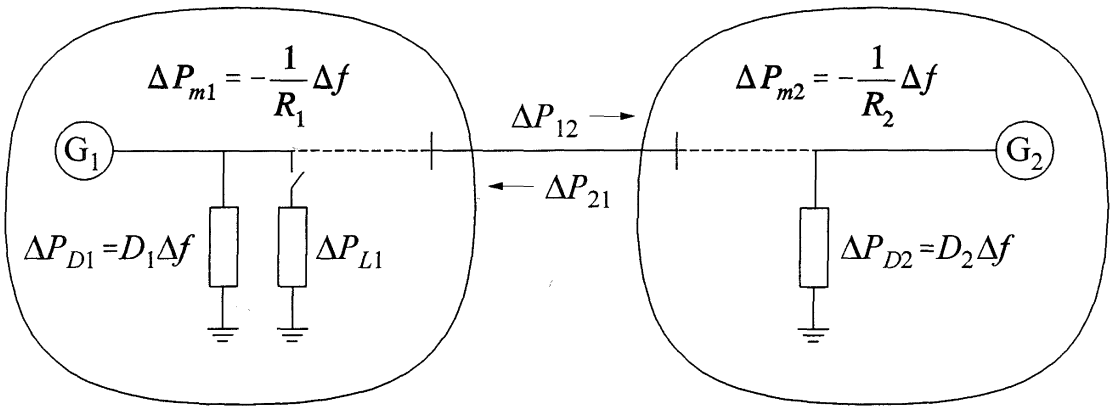


Figure 11.24 Effect of change in area 1 load

An increase in area 1 load by ΔP_{L1} results in a frequency reduction in both areas and a tie line flow of ΔP_{12}. A negative ΔP_{12} is indicative of flow from area 2 to area 1. The tie line flow deviation reflects the contribution of the regulation characteristics $(1/R+D)$ of one area to another.

Similarly, for a change in area 2 load by ΔP_{L2}, we have

$$\Delta f = \frac{-\Delta P_{L2}}{\beta_1+\beta_2} \tag{11.20}$$

and

$$\Delta P_{12} = -\Delta P_{21} = \frac{\Delta P_{L2}\beta_1}{\beta_1+\beta_2} \tag{11.21}$$

The above relationships form the basis for the load-frequency control of interconnected systems.

Frequency bias tie line control

The basic objective of supplementary control is to restore balance between each area load and generation. This is met when the control action maintains

- Frequency at the scheduled value
- Net interchange power with neighbouring areas at scheduled values

The supplementary control in a given area should ideally correct only for changes in that area. In other words, if there is a change in area 1 load, there should be supplementary control action only in area 1 and not in area 2.

Examination of Equations 11.18 to 11.21 indicates that a control signal made up of tie line flow deviation added to frequency deviation weighted by a *bias factor* would accomplish the desired objectives. This control signal is known as *area control error* (ACE).

From Equations 11.16 and 11.17, it is apparent that a suitable bias factor for an area is its frequency-response characteristic β. Thus, the area control error for area 2 is

$$\text{ACE}_2 = \Delta P_{21} + B_2 \Delta f \tag{11.22}$$

where

$$B_2 = \beta_2 = \frac{1}{R_2} + D_2 \tag{11.23}$$

Similarly, for area 1

$$\text{ACE}_1 = \Delta P_{12} + B_1 \Delta f \tag{11.24}$$

where

$$B_1 = \beta_1 = \frac{1}{R_1} + D_1 \tag{11.25}$$

The ACE represents the required change in area generation, and its unit is

MW.[1] The unit normally used for expressing the frequency bias factor B is MW/0.1 Hz.

The block diagram shown in Figure 11.25 illustrates how supplementary control is implemented. It is applied to selected units in each area and acts on the load reference setpoints.

The area frequency-response characteristic $(1/R+D)$ required for establishing the bias factors can be estimated by examination of chart records following a significant disturbance such as a sudden loss of a large unit.

Basis for selection of bias factor [3-8]

Actually, from steady-state performance considerations, the choice of bias factor is not important. Any combination of area control errors containing components of tie line power deviation and frequency deviation will result in steady-state restoration of the tie flow and frequency since the integral control action ensures that ACE is reduced to zero. In order to illustrate this, consider the following area control error signals applicable to a two-area system:

$$\text{ACE}_1 = A_1\Delta P_{12}+B_1\Delta f = 0 \tag{11.26}$$

$$\text{ACE}_2 = A_2\Delta P_{21}+B_2\Delta f = 0 \tag{11.27}$$

The above equations result in $\Delta P_{12}=0$ and $\Delta f=0$ for all non-zero values of A_1, A_2, B_1 and B_2.

However, the composition of area control error signals is more important from *dynamic performance* considerations. This can be illustrated by considering the transient response of the AGC system to a sudden increase in area 1 load. The sudden increase in load will result in a decrease in system frequency, followed by governor response (primary speed control of units in both areas) which limits the maximum frequency excursion and subsequently (typically on the order of 10 seconds) brings the frequency deviation back to a value Δf_R determined by the regulation characteristics of both systems:

$$\Delta f_R = \frac{-\Delta P_{L1}}{\beta_1+\beta_2} \tag{11.28}$$

---

[1] In the literature, several alternative equations have been used to express ACE. A commonly used alternative form is

$$\text{ACE} = \Delta P_{tie} - B\Delta f$$

where $B=-\beta$, a negative number.

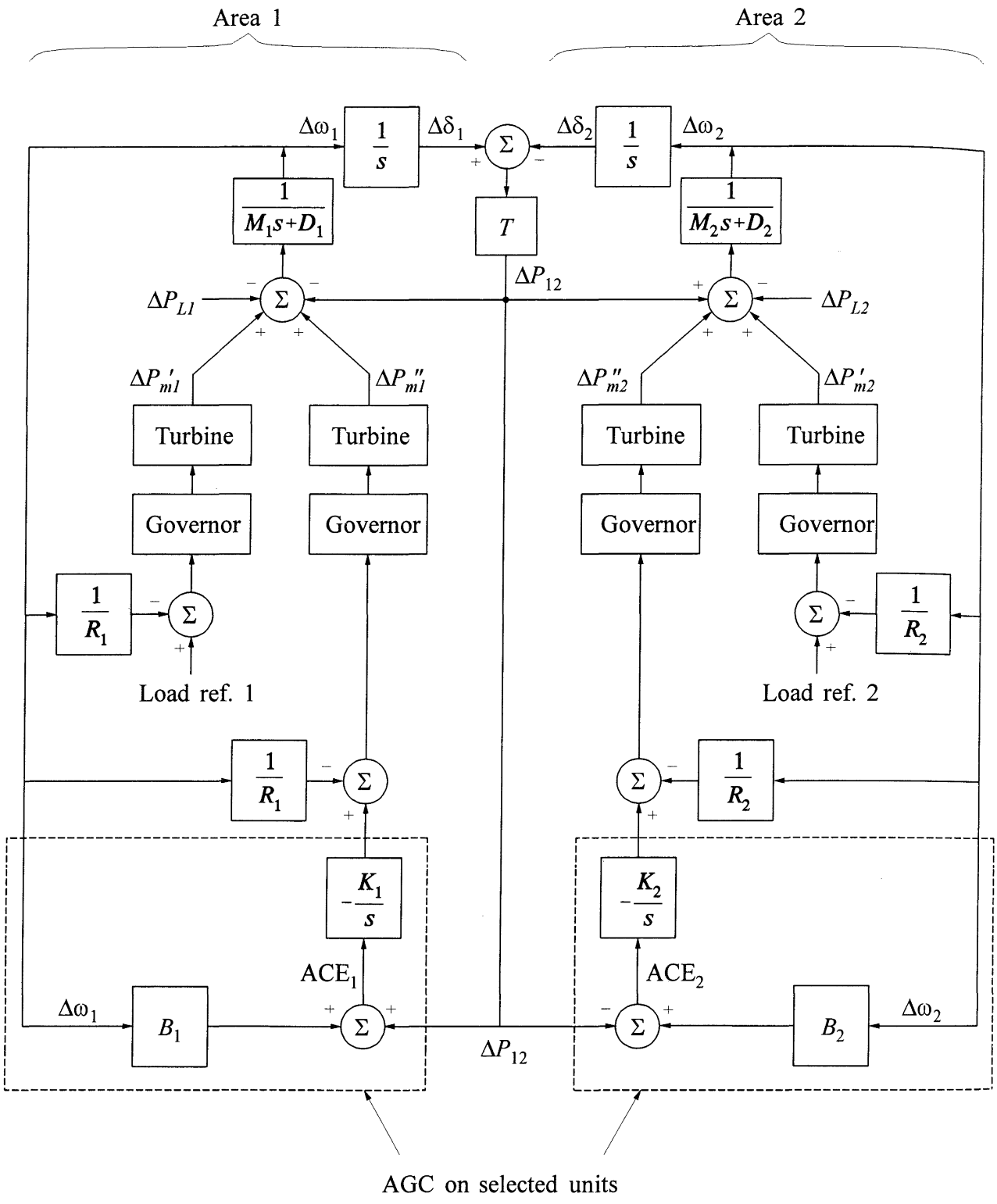


Figure 11.25 Block diagram of two-area system with supplementary control

At this point, there is a deviation of tie line power flow from the scheduled value. The

supplementary control, which is much slower than the primary speed control, will now commence responding. Let us examine the performance of the supplementary control for different settings of the area frequency bias factors at the instant when the frequency deviation is Δf_R.

(a) With B_1 equal to β_1, and B_2 equal to β_2, we have

$$\begin{aligned} \text{ACE}_1 &= \Delta P_{12} + B_1 \Delta f_R \\ &= \frac{-\Delta P_{L1}}{\beta_1 + \beta_2}(\beta_2 + \beta_1) \\ &= -\Delta P_{L1} \end{aligned}$$

and

$$\begin{aligned} \text{ACE}_2 &= -\Delta P_{12} + B_2 \Delta f_R \\ &= \frac{-\Delta P_{L1}}{\beta_1 + \beta_2}(-\beta_2 + \beta_2) \\ &= 0 \end{aligned}$$

Only the supplementary control in area 1 will respond to ΔP_{L1} and change generation so as to bring ACE_1 to zero. The load change in area 1 is thus unobservable to the supplementary control in area 2.

(b) If, on the other hand, B_1 and B_2 were set to double their respective area frequency-response characteristics,

$$\begin{aligned} \text{ACE}_1 &= \Delta P_{12} + B_1 \Delta f_R \\ &= \frac{-\Delta P_{L1}}{\beta_1 + \beta_2}(\beta_2 + 2\beta_1) \\ &= -\Delta P_{L1}\left(1 - \frac{1}{\beta_2}\right) \end{aligned}$$

Similarly,

$$\begin{aligned} \text{ACE}_2 &= -\Delta P_{12} + 2\beta_2 \Delta f_R \\ &= \frac{-\Delta P_{L1}}{\beta_2} \end{aligned}$$

Thus, both area 1 and area 2 supplementary controls would respond and

correct the frequency deviation twice as fast. However, the generation picked up by area 2 will subsequently reflect itself as a component of ACE_2, and will be backed off again in the steady state.

(c) If we set the bias factors significantly lower than the respective area βs, a situation opposite to the above would exist. In this case, the supplementary control in area 2 would tend to back off the generation picked up by its generators as a result of primary speed control or governor action. This would result in a degradation of system frequency control.

In addition to the above considerations, a very high value of bias factor is not desirable from the control stability viewpoint. At values significantly higher than the area β, the control action may become unstable.

The appropriateness of setting the frequency bias factor B nearly equal to the area β from dynamic considerations has been examined by a number of investigators [3-8]. A recommendation made in reference 7 to use significantly lower bias settings (B equal to nearly 0.5β) has not gained acceptance. A subsequent optimization study reported in reference 8 showed that $B=\beta$ is indeed a logical choice.

Systems with more than two areas

The description of the frequency bias tie line control described above applies equally well to systems with more than two areas. The interchange schedule applicable to each area is the algebraic sum of power flows on all the tie lines from that area to the other areas.

When an area is interconnected with more than one additional area, scheduled interchange transfers between them do not necessarily flow directly through the tie lines connecting the respective areas. Actual flows could split over parallel paths through other areas, depending on the relative impedances of the parallel paths. This is illustrated in Figure 11.26 which considers a three-area system.

Performance of AGC under normal and abnormal conditions

Under *normal conditions*, with each area able to carry out its control obligations, steady-state corrective action of AGC is confined to the area where the deficit or excess of generation occurs. Interarea power transfers are maintained at scheduled levels and system frequency is held constant.

Under *abnormal conditions*, one or more areas may be unable to correct for the generation-load mismatch due to insufficient generation reserve on AGC. In such an event, other areas assist by permitting the interarea power transfers to deviate from scheduled values and by allowing system frequency to depart from its pre-disturbance value. Each area participates in frequency regulation in proportion to its available regulating capacity relative to that of the overall system.

The following example illustrates the above aspects of AGC performance.

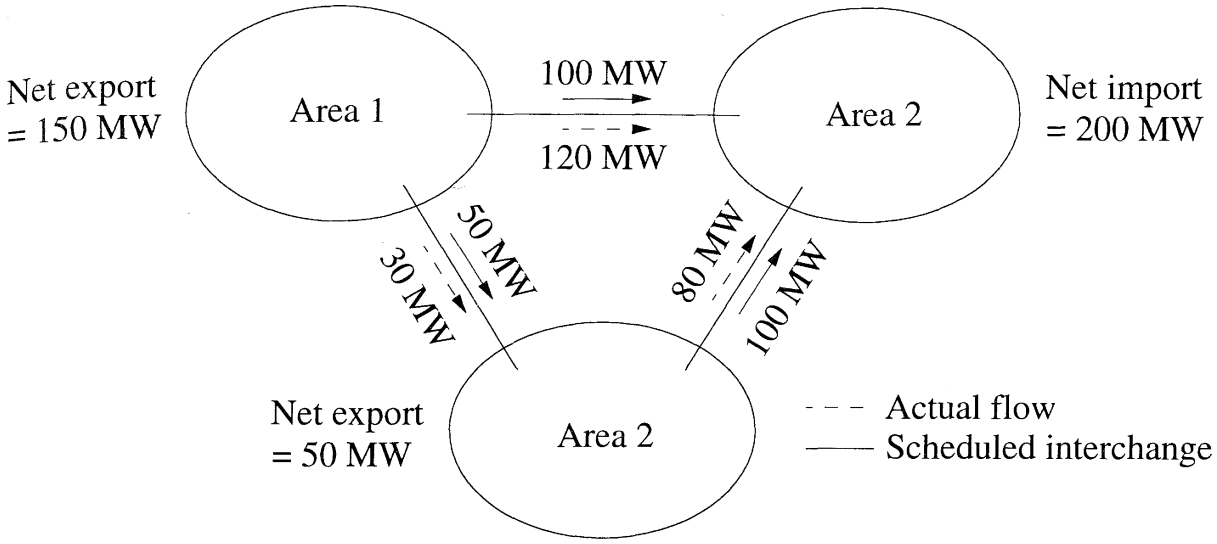
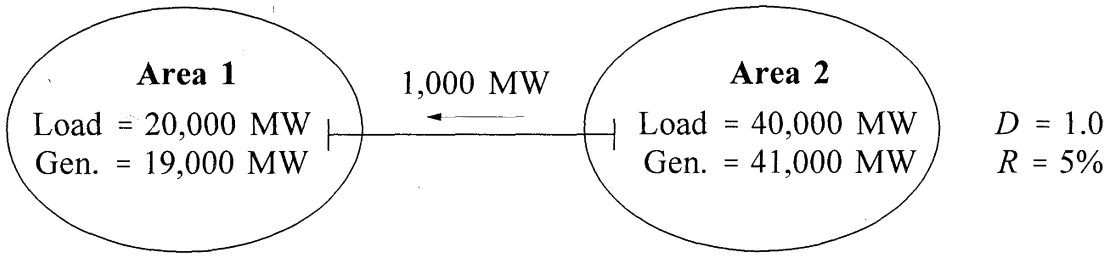


Figure 11.26 Three areas connected by tie lines

Example 11.3

Consider two interconnected areas as follows:



The connected load at 60 Hz is 20,000 MW in area 1 and 40,000 MW in area 2. The load in each area varies 1% for every 1% change in frequency. Area 1 is importing 1,000 MW from area 2. The speed regulation, R, is 5% for all units.

Area 1 is operating with a spinning reserve of 1,000 MW spread uniformly over a generation of 4,000 MW capacity, and area 2 is operating with a spinning reserve of 1,000 MW spread uniformly over a generation of 10,000 MW.

Determine the steady-state frequency, generation and load of each area, and tie line power for the following cases.

(a) Loss of 1,000 MW load in area 1, assuming that there are no supplementary controls.

(b) Each of the following contingencies, when the generation carrying spinning reserve in each area is on supplementary control with frequency bias factor settings of 250 MW/0.1 Hz for area 1 and 500 MW/0.1 Hz for area 2.

(i) Loss of 1,000 MW load in area 1

(ii) Loss of 500 MW generation, carrying part of the spinning reserve, in area 1

(iii) Loss of 2,000 MW generation, not carrying spinning reserve, in area 1

(iv) Tripping of the tie line, assuming that there is no change to the interchange schedule of the supplementary control

(v) Tripping of the tie line, assuming that the interchange schedule is switched to zero when the ties are lost

Solution

(a) *With no supplementary control.*

Assuming that none of the governors are blocked, all generating units in the two areas respond to the loss of load.

A 5% regulation on 20,000 MW generating capacity (including spinning reserve of 1,000 MW) in area 1 corresponds to

$$\frac{1}{R_1} = \frac{1}{0.05} \times \frac{20{,}000}{60} = 6{,}666.67 \quad \text{MW/Hz}$$

Similarly, a 5% regulation on 42,000 MW generating capacity in area 2 corresponds to

$$\frac{1}{R_2} = \frac{1}{0.05} \times \frac{42{,}000}{60} = 14{,}000.00 \quad \text{MW/Hz}$$

Total regulation due to 62,000 MW generating capacity in the two areas is

$$\frac{1}{R} = \frac{1}{R_1} + \frac{1}{R_2} = 20{,}666.67 \quad \text{MW/Hz}$$

Load damping due to 19,000 MW load (remaining after loss of 1,000 MW load) in area 1 is

$$D_1 = 1 \times \frac{19{,}000}{100} \times \frac{100}{60} = 316.67 \quad \text{MW/Hz}$$

Load damping due to 40,000 MW load in area 2 is

$$D_2 = 1 \times \frac{40{,}000}{100} \times \frac{100}{60} = 666.67 \quad \text{MW/Hz}$$

Total effective load damping of the two areas is

$$D = D_1 + D_2 = 983.33 \quad \text{MW/Hz}$$

Change in system frequency due to loss of 1,000 MW load in area 1 is

$$\Delta f = \frac{-\Delta P_L}{1/R + D} = \frac{-(-1000)}{20{,}666.67 + 983.33} = 0.04619 \quad \text{Hz}$$

Load changes in the two areas due to increase in frequency are

$$\Delta P_{D1} = D_1 \Delta f = 316.67 \times 0.04619 = 14.63 \quad \text{MW}$$
$$\Delta P_{D2} = D_2 \Delta f = 666.67 \times 0.04619 = 30.79 \quad \text{MW}$$

Generation changes in the two areas due to speed regulation are

$$\Delta P_{G1} = -\frac{1}{R_1}\Delta f = 6{,}666.67 \times 0.04619 = -307.93 \quad \text{MW}$$

$$\Delta P_{G2} = -\frac{1}{R_2}\Delta f = 14{,}000.00 \times 0.04619 = -646.65 \quad \text{MW}$$

The new load, generation and tie line power flows are as follows.

Area 1		Area 2	
Load	= 20,000.00 − 1,000.00 + 14.63 = 19,014.63 MW	Load	= 40,000.00 + 30.79 = 40,030.79 MW
Generation	= 19,000.00 − 307.93 = 18,692.07 MW	Generation	= 41,000.00 − 646.65 = 40,353.35 MW

Tie line power flow from area 2 to area 1 is 322.56 MW. Steady-state frequency is 60.04619 Hz.

(b) *With supplementary control.*

(i) Loss of 1,000 MW load in area 1:

Area 1 has a generating capacity of 4,000 MW on supplementary control, and this will reduce generation so as to bring ACE_1 to zero. Similarly, area 2 generation on supplementary control will keep ACE_2 at zero:

$$ACE_1 = B_1 \Delta f + \Delta P_{12} = 0$$
$$ACE_2 = B_2 \Delta f - \Delta P_{12} = 0$$

Hence,

$$\Delta f = 0 \qquad \Delta P_{12} = 0$$

Area 1 generation and load are reduced by 1,000 MW. There is no steady-state change in area 2 generation and load, or the tie flow.

(ii) Loss of 500 MW generation carrying part of spinning reserve in area 1:

Prior to loss of generation, area 1 had a spinning reserve of 1,000 MW spread uniformly over a generation of 4,000 MW capacity (3,000 MW generation plus 1,000 MW reserve). Spinning reserve lost with generation loss is

$$\frac{500}{3{,}000} \times 1{,}000 = 166.67 \quad \text{MW}$$

Spinning reserve remaining is 1,000.00 − 166.67 = 833.33 MW. This is sufficient to make up for 500 MW generation loss. Hence, the generation and load in the two areas are restored to their pre-disturbance values. There are no changes in tie line flow or system frequency. However, area 1 spinning reserve is reduced from 1,000 MW to 833.33 MW.

(iii) Loss of 2,000 MW generation in area 1, not carrying spinning reserve:

Half of the generation loss will be made up by the 1,000 MW spinning reserve on supplementary control in area 1. When this limit is reached, area 1 is no longer able to control ACE. Supplementary control in area 2, however, is able to control its ACE. Hence,

$$\text{ACE}_2 = B_2 \Delta f - \Delta P_{12} = 0$$

or

$$\Delta P_{12} = B_2 \Delta f = 5{,}000 \Delta f$$

There is thus a net reduction in system frequency. This causes a reduction in loads due to frequency sensitivity.

Area 1 load damping is

$$D_1 = 1 \times \frac{20{,}000}{100} \times \frac{100}{60} = 333.33 \quad \text{MW/Hz}$$

The balance of generation loss in area 1 is made up by a reduction in load and tie flow from area 2. Hence,

$$-1{,}000 = D_1\Delta f + \Delta P_{12}$$
$$= 333.33\Delta f + 5{,}000\Delta f$$

Solving for Δf, we have

$$\Delta f = \frac{-1{,}000}{5{,}000+333.33} = -0.1875 \quad \text{Hz}$$

Change in area 1 load is

$$\Delta P_{D1} = D_1\Delta f = 333.33\times(-0.1875)$$
$$= -62.5 \quad \text{MW}$$

The tie flow change is

$$\Delta P_{12} = 5{,}000\times(-0.1875) = -937.5 \quad \text{MW}$$

Change in area 2 load is

$$\Delta P_{D2} = D_2\Delta f = 666.67\times(-0.1875)$$
$$= -125.00 \quad \text{MW}$$

The area load and generation are as follows.

Area 1		Area 2	
Load	= 20,000.0 − 62.5 = 19,937.5 MW	Load	= 40,000.0 − 125.0 = 39,875.0 MW
Generation	= 19,000.0 − 1,000.0 = 18,000.0 MW	Generation	= 41,000.0 − 125.0 + 937.5 = 41,812.5 MW

The steady-state tie line power flow from area 2 to area 1 is 1,937.50 MW, and the system frequency is 60.0 − 0.1875 = 59.8125 Hz.

(iv) Tripping of the tie line, assuming no change in interchange schedule:

The supplementary control of area 1 attempts to maintain interchange schedule at 1,000 MW. Hence,

$$\text{ACE}_1 = \Delta P_{12} + B_1\Delta f_1 = 1{,}000 + 2{,}500\Delta f = 0$$

Solving, we find

$$\Delta f_1 = -\frac{1000}{2500} = -0.4 \quad \text{Hz}$$

Change in area 1 load is

$$\Delta P_{D1} = D_1 \Delta f_1 = 333.33 \times (-0.4) = -133.33 \quad \text{MW}$$

Similarly for area 2, we have

$$\Delta f_2 = \frac{1{,}000}{5{,}000} = 0.2 \quad \text{Hz}$$

and

$$\Delta P_{D2} = 666.67 \times 0.2 = 133.33 \quad \text{MW}$$

The area load, generation, and frequencies are as follows:

Area 1		Area 2	
Load	= 20,000.00 − 133.33 = 19,866.67 MW	Load	= 40,000.00 + 133.33 = 40,133.33 MW
Generation	= 19,866.67 MW	Generation	= 40,133.33 MW
f_1	= 59.6 Hz	f_2	= 60.2 Hz

(v) Tripping of the tie line, with interchange schedule switched to zero:

With interchange schedule switched to zero, area 1 supplementary control will pick up 1,000 MW generation to make up for loss of import power. Similarly, area 2 supplementary control reduces generation by 1,000 MW to compensate for loss of export. The generation in each area is equal to the respective loads and the area frequencies are equal to 60 Hz. ■

Economic allocation of generation

As noted earlier, an important secondary function of automatic generation control is to allocate generation so that each power source is loaded most economically. This function is referred to as *economic dispatch control* (EDC). The theory of economic dispatch is based on the principle of equal incremental costs.

For control of tie line power and frequency, it is necessary to send signals to generating plants to control generation. It is possible to use these signals to control generation to satisfy economic dispatch criteria. Thus, the requirements for EDC can be handled as part of the AGC function.

Since system load is continually changing, economic dispatch calculations have to be made at frequent intervals. The allocation of individual generation output is accomplished by using *base points* and *participation factors* (PFs). The base point represents the most economic output for each generating unit, and the participation

factor is the rate of change of the unit output with respect to a change in total generation. The new desired output for each generator is calculated as follows [2]:

$$P_{desired} = P_{base\ point} + \mathrm{PF}(\Delta P_{total}) \tag{11.29}$$

where

ΔP_{total} = total new generation − sum of $P_{base\ point}$ for all generation

Sum of participation factors of all units is equal to unity.

11.1.6 Implementation of AGC

In modern AGC schemes, the control actions are usually determined for each control area at a central location called the dispatch centre. Information pertaining to tie line flows, system frequency, and unit MW loadings is telemetered to the central location where the control actions are determined by a digital computer. The control signals are transmitted via the same telemetering channels to the generating units on AGC as shown in Figure 11.27. The normal practice is to transmit raise or lower pulses of varying lengths to the units. The control equipment at the plants then changes the reference setpoints of the units up or down in proportion to the pulse length.

Figure 11.27 illustrates the implementation of AGC for one control area (normally the service area of an individual utility). Each control area of an interconnected system is controlled in a similar manner, but independently of the other control areas. That is, the control of generation in the interconnected system is "area-wise decentralized."

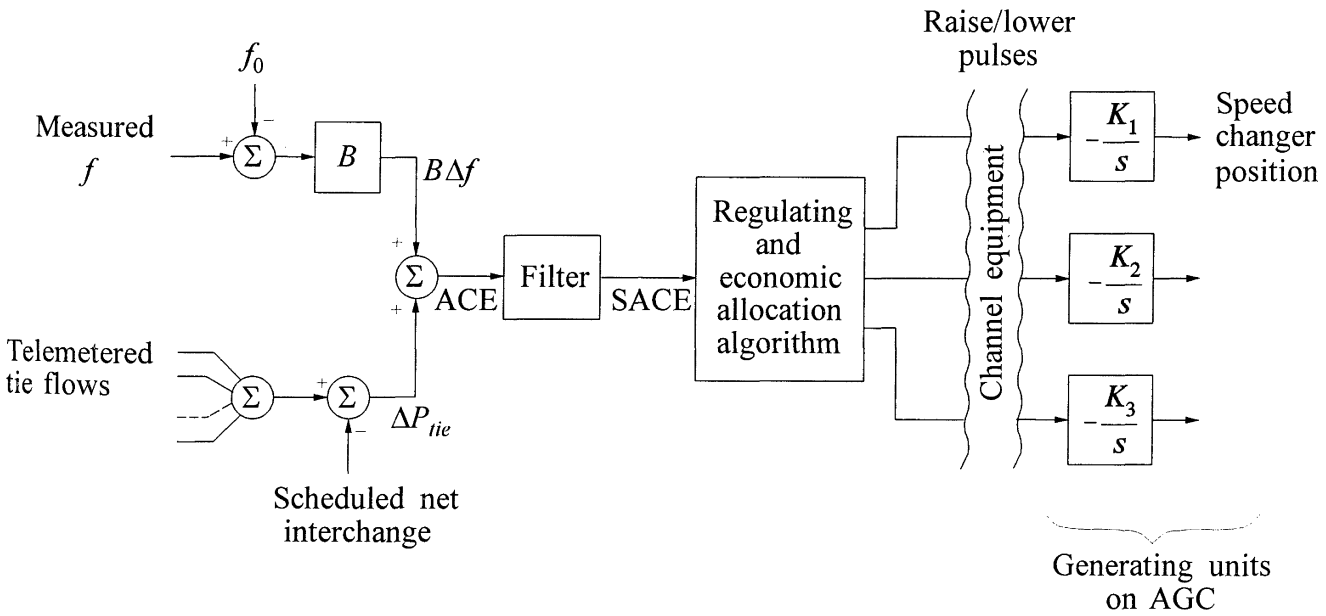


Figure 11.27 AGC control logic for each area

Early AGC systems, developed in the 1950s, were based on analog control equipment. These were gradually superseded by digital systems beginning in the late 1960s. Now, all-digital systems are the universal choice for AGC applications.

Filtering of ACE

Much of the change in ACE is usually due to fast random variations in load to which generating units need not respond. In fact, control action in response to these random components does not reduce ACE but merely causes unnecessary wear and tear on governor motors and turbine valves. Therefore, AGC programs normally use filtering schemes to filter out random variations, and *smoothed ACE* (SACE) is used to control generation.

The conventional approach is to use a low-order filter which reduces noise at the expense of speed of response.

Reference 9 suggests a method of distinguishing random variations and sustained load-change requirements by evaluating whether or not the error is in the direction of correct inadvertent interchange.

Rate limits

In establishing AGC signals, it should be recognized that there is a limit to the rate at which generating unit outputs can be changed. This is particularly true of thermal units where mechanical and thermal stresses are the limiting factors. The maximum loading rate for thermal units is on the order of 2% MCR (*maximum continuous rating*) per minute. For hydro units, the rate is on the order of 100% MCR per minute.

Control performance criteria

The guidelines followed by North American utilities for load-frequency control are developed by the Operating Committee of the North American Electric Reliability Council (NERC). The following criteria specify the minimum control performance standards set by NERC [10].

Under *normal conditions* the following criteria apply:

1. A1 criterion – The ACE must return to zero within 10 minutes of previously reaching zero. Violations of this criterion count for each subsequent 10-minute period that the ACE fails to return to zero.

2. A2 criterion – The average ACE for each of the six 10-minute periods during the hour (i.e., for the 10-minute periods ending at 10, 20, 30, 40, 50, and 60 minutes past the hour) must be within specific limits, referred to as L_d, that are determined from the control area's rate of change of demand characteristics:

$$L_d = 5 + 0.025\,\Delta L \quad \text{MW}$$

where ΔL is the greatest hourly change in the net system load of a control area on the day of its maximum summer or winter peak load.

Under *disturbance conditions* (sudden loss of generation or increase of load) the following criteria apply:

1. B1 criterion – The ACE must return to zero within 10 minutes following the start of the disturbance.

2. B2 criterion – The ACE must start to return to zero within 1 minute following the start of the disturbance.

A disturbance is said to have occurred when a sampled value of ACE exceeds $3L_d$.

Time deviation correction

It is the practice of U.S. and Canadian interconnected systems to assign to one area the maintenance of a system time standard. For example, the standard for the eastern systems is maintained by the American Electric Power (AEP) company at Canton, Ohio. Through designated communication channels, information on the status of the system time deviation is relayed to all control areas, and certain periods are designated as time-correction periods. During such periods, all areas are expected to simultaneously offset their frequency schedules by an amount related to accumulated system time deviation.

Frequency of AGC execution

The stability of an AGC system and its ability to react to changing inputs are influenced by phase lags in the input system quantities and in the transmission of its control signals.

With digitally based systems, experience has shown that the execution of AGC once every 2 to 4 seconds results in good performance. This means the ACE is computed and the raise/lower control signals are transmitted to the generating plant once every 2 to 4 seconds.

Figure 11.28 shows the overall function diagram of a typical AGC system.

Frequency bias setting

The general practice in North America is to establish frequency bias in each control area once a year based on the area's natural regulation characteristic $(1/R+D)$ corresponding to the forecasted peak load of the coming year. The average frequency bias setting employed is about 2% per 0.1 Hz based on the estimated peak load and spinning reserve. The bias factor remains fixed through the year for all load levels.

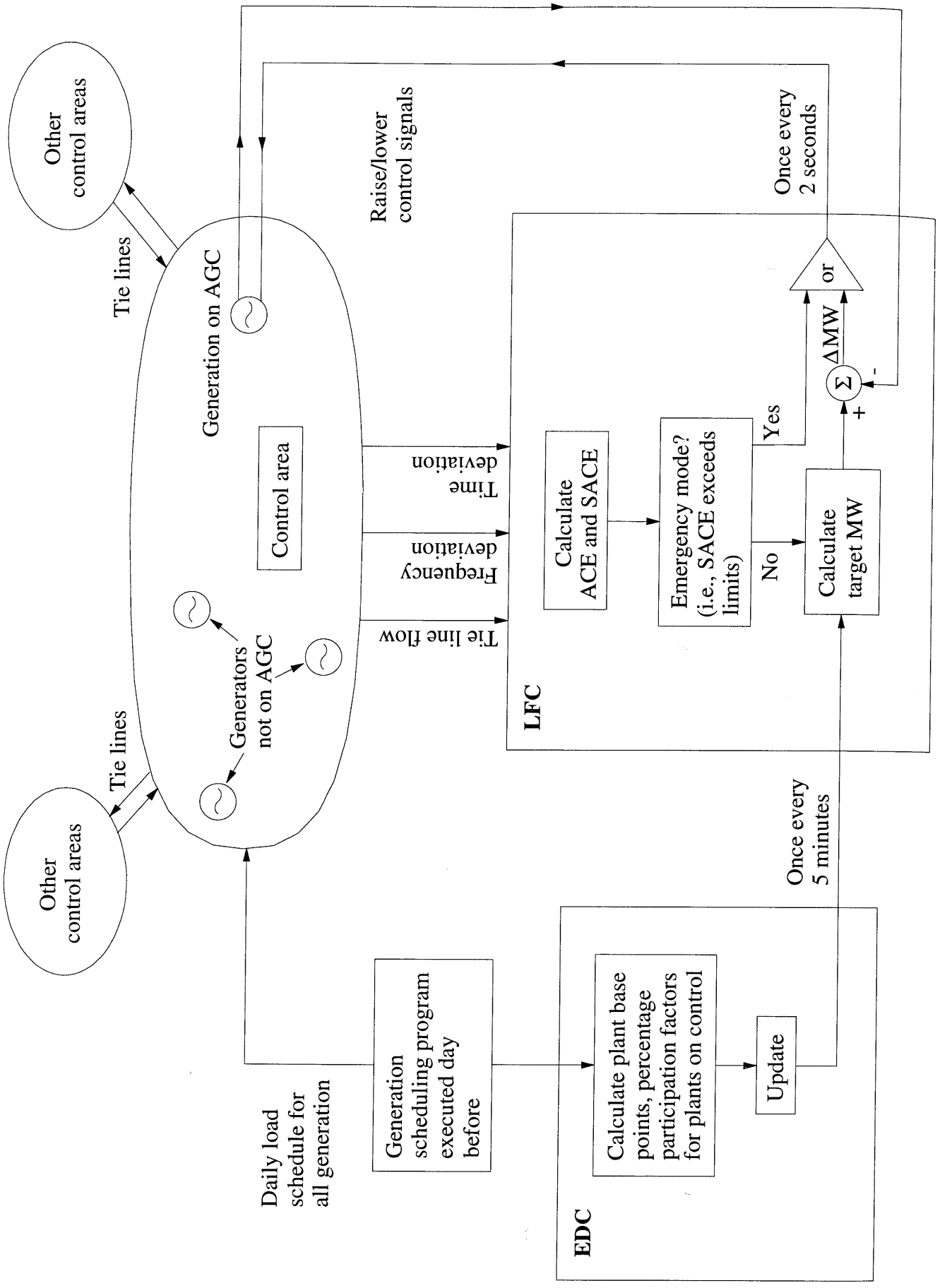


Figure 11.28 *Functional diagram of a typical AGC system*

A result of the above practice appears to be that, at times of low loads, the bias factor is much higher than the actual frequency regulation characteristic of the area. This is suspected of sometimes causing unstable control action resulting in limit cycle oscillations, large inadvertent interchange power accumulation and time deviation [3].

Reference 11 describes a scheme using a variable, nonlinear frequency bias, which results in improved control performance.

AGC tuning and performance [18,19]

The overriding consideration in the design and tuning of the AGC system is the impact on the power plants that are controlled. The characteristics of power plants vary widely and a number of physical constraints exist with regard to their manoeuvrability. A simple system that results in smooth control and a fairly well-damped system is preferable to a rapid control that attempts to bring ACE to zero rapidly. The plant characteristics in relation to variations in ACE are such that it is impossible to perfectly match generation and load continuously. The realization of the control function is limited by the amount of stored energy in the generating units and the rapidity with which generation can be changed. Therefore, the control attempts to match the average of generation and load over a time.

The control strategy should include the following objectives:

- To minimize fuel cost
- To avoid sustained operation of the generating units in the undesirable ranges (e.g., valve points for steam units)
- To minimize equipment wear and tear by avoiding unnecessary manoeuvring of generating units

Practical AGC systems achieve the above objectives by keeping the control strategies simple, robust, and reliable.

The stability of the control system and its ability to respond to the ACE signals are influenced by the phase lags associated with the measurement and transmission of control signals.

The ideal way to determine the AGC system parameters is by means of simulations. An important parameter that has an influence on the stability of AGC system is the overall loop gain; its value should be finalized based on field tests.

Emergency mode operation

For major system upsets causing splitting of the interconnected system into separate islands or opening of tie lines, AGC is suspended. This may be based on detection of very large changes in frequency or ACE. In some cases, AGC may be suspended for intentional tripping of load/generation so that AGC may not defeat the purpose of such tripping.

Effect of speed-governor dead band

The dead band associated with a speed governor is defined as "the total magnitude of the change in steady-state speed within which there is no resulting measurable change in the position of the governor-controlled valves or gates" [12]. Dead band is expressed in percent of the rated speed.

The effect of the dead band on the governor speed-droop characteristic is depicted in Figure 11.29. The speed-droop characteristic appears as a band rather than a line.

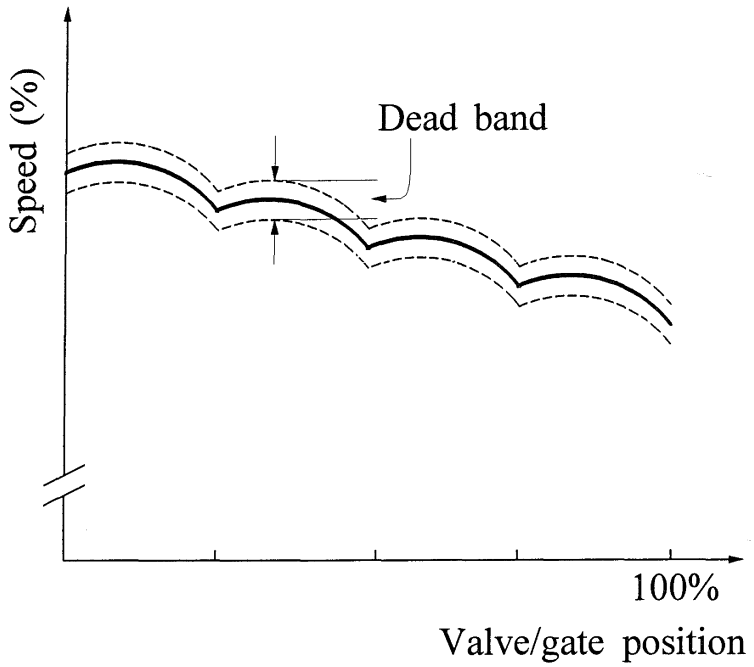


Figure 11.29

Dead band is caused by coulomb friction and backlash effects in various governor linkages, and by valve overlap in the hydraulic relays [1].

The current IEEE standards specify a maximum dead band of 0.06% (0.036 Hz) for governors of large steam turbines [12]. For governors of hydraulic turbines, the standards specify a maximum speed dead band of 0.02% and a maximum blade control dead band of 1.0% [13]. Dead bands of modern electrohydraulic governors are in fact much smaller. In some cases, special measures have been taken to practically eliminate the dead band [14]. However, there are many older units in operation with significant governor dead band.

The effect of the dead band on the speed governor response depends on the magnitude of the frequency deviation. If the deviation is small, it may remain entirely within the dead band; consequently, the speed control will be inactive. In any given situation, however, the entire dead band width will not have to be overcome. The position of each governor would be randomly distributed within its dead band; hence, for small changes in input signal the response of the individual generating units will

tend to be random [15]. Speed governor dead bands result in random frequency fluctuations. In large power systems, these random fluctuations have a magnitude on the order of 0.01 Hz.

Results of investigations of the effects of governor dead bands on the performance of AGC systems are reported in references 5, 16 and 17. One effect of the dead band is to reduce the area frequency response characteristic β (i.e., to increase the effective frequency regulation). This requires a reduction in the frequency bias setting to ensure satisfactory AGC performance [16]. Reference 3 provides an in-depth analysis of AGC system dynamic performance and hypothesizes that governor dead bands may cause AGC system limit cycling with periods ranging from 30 seconds to 90 seconds.

Further reading on AGC

The state-of-the-art AGC systems have evolved from the early analog systems to the present digital systems. The result is a simple, yet robust, decentralized system that controls a complex, highly nonlinear, and continuously changing power system. There is a large amount of literature on the subject, some of which has attempted to use modern control theory in an effort to achieve optimal performance. However, these techniques have not been applied to practical AGC systems.

Reference 20 provides a good review of the properties of the conventional AGC systems and of some of the systems proposed in the literature that are based on modern control theory. It identifies potential areas in which the conventional approach may be improved by using concepts based on modern control theory.

Reference 21 presents a general approach to the analysis and synthesis of AGC systems based on multivariable control theory. It proposes two criteria for the design of the load-frequency controllers: (a) non-interaction between controls of frequency and tie line powers; (b) autonomy of controls of each area in taking care of its load variations during steady-state as well as transient conditions.

References 20 and 21 provide additional insight into the requirements and performance of AGC systems. They are both recommended for further reading.

11.1.7 Underfrequency Load Shedding

Severe system disturbances can result in cascading outages and isolation of areas, causing formation of electrical islands. If such an islanded area is undergenerated, it will experience a frequency decline. Unless sufficient generation with ability to rapidly increase output is available, the decline in frequency will be largely determined by frequency sensitive characteristics of loads. In many situations, the frequency decline may reach levels that could lead to tripping of steam turbine generating units by underfrequency protective relays, thus aggravating the situation further. To prevent extended operation of separated areas at lower than normal frequency, load-shedding schemes are employed to reduce the connected load to a level that can be safely supplied by available generation.

Hazards of underfrequency operation

There are two main problems associated with the operation of a power system at low frequency, both related to thermal generating units.

The first problem is concerned with the vibratory stress on the long low-pressure turbine blades. As discussed in Chapter 9 (Section 9.2.3), operation of steam turbines below 58.5 Hz is severely restricted. Since the effects of vibratory stress are cumulative with time, restoration of normal frequency operation as soon as possible is essential.

The second problem is concerned with the performance of plant auxiliaries driven by induction motors. At frequencies below 57 Hz, the plant capability may be severely reduced because of the reduced output of boiler feed pumps or fans supplying combustion air [22]. In the case of nuclear power plants, the reactors may overheat due to reduced flow of coolant as the frequency declines. Low-flow protections or underfrequency relays are normally used to guard against this condition. If the frequency decline is excessive, the generating units may be tripped off the power system.

In addition to avoiding the above consequences, it is necessary to restore normal frequency as soon as possible so that the affected area may be reconnected to the main power system.

Limitations of prime mover systems

The prime movers have several limitations which affect their ability to control frequency decay:

1. The generation can be increased only to the limits of available spinning reserve within each affected area.

2. The load that can be picked up by a thermal unit is limited due to thermal stress in the turbine. Initially, about 10% of turbine rated output can be picked up quickly without causing damage by too rapid heating. This is followed by a slow increase of about 2% per minute.

3. The ability of a boiler to pick up a significant amount of load is limited. An increase in steam flow when the turbine valves open results in a pressure drop. An increase in fuel input to the boiler is required to restore pressure. This takes several minutes and is of little use in limiting frequency drop.

4. The speed governors have a time delay of 3 to 5 seconds.

As a consequence of the above, generation reserve available for control of frequency is limited to a fraction of the remaining generation.

Factors influencing frequency decay

Assuming that the separated area has negligible spinning reserve with speed governing, the extent to which the frequency of the separated area will decrease and the rate of decay depend mainly on three factors: the magnitude of the overload ΔL (i.e., generation deficiency), load-damping constant D applicable to the area load, and the inertia constant M representing the total rotational inertia of the generators in the area.

Based on the results of Example 11.1, we may write the following expression for the frequency decay:

$$\Delta f = -\Delta L(1-e^{-\frac{t}{T}})K \tag{11.30}$$

where $K=1/D$ and $T=M/D$.

For example, with $D=1.0$ and $M=10$ s, the frequency reduction as a function of time t is

$$\Delta f = -\Delta L(1-e^{-\frac{t}{10}}) \text{ pu}$$

$$= -\Delta L(1-e^{-\frac{t}{10}})60 \text{ Hz}$$

Figure 11.30 shows the frequency decay for four values of ΔL.

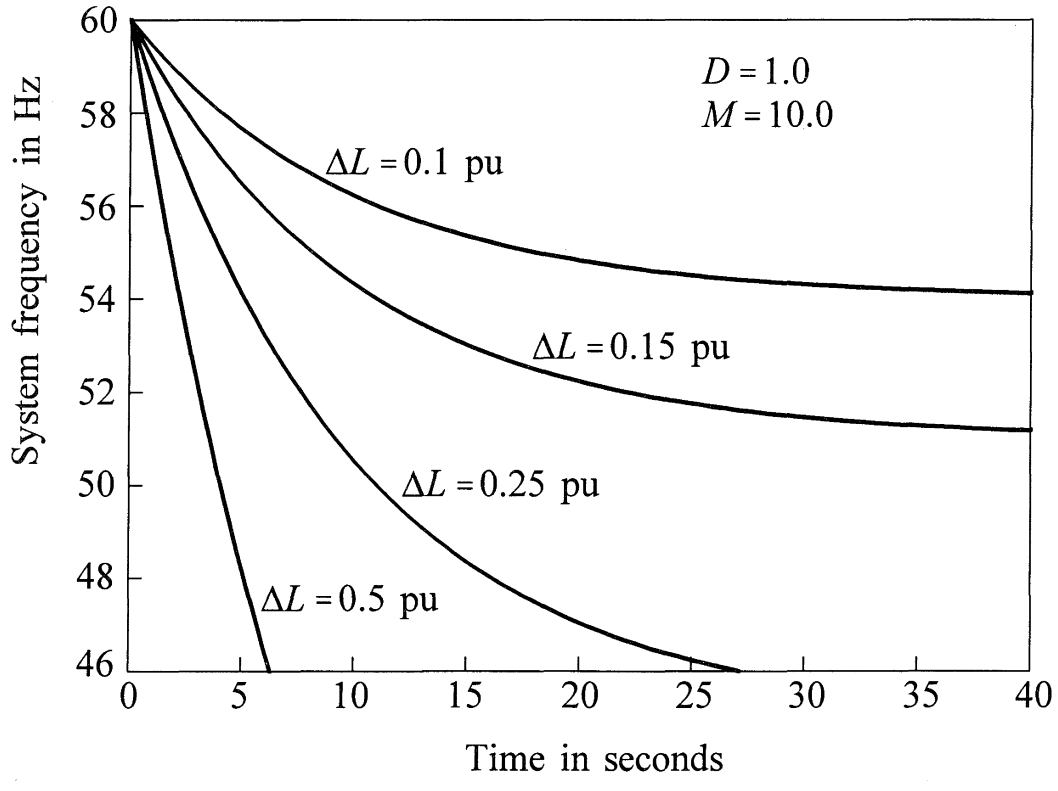


Figure 11.30 Frequency decay due to generation deficiency

Basis for selection of load-shedding schemes

Results such as those presented in Figure 11.30 are helpful as a first step in establishing the basis for load-shedding schemes. Considerations in the selection of the scheme include the maximum generation deficiency for which protection is required, the minimum permissible frequency, likely areas of system separation, and the range of inertia constant M and load-damping constant D.

Reference 23 describes a procedure for developing a load-shedding scheme. A typical scheme shedding load in three steps is as follows:

- 10% load is shed when frequency drops to 59.2 Hz
- 15% additional load is shed when frequency drops to 58.8 Hz
- 20% additional load is shed when frequency reaches 58.0 Hz

Typical operating time with solid-state relays is in the range of 0.1 to 0.2 second.

A scheme based on frequency drop alone is generally acceptable for generation deficiencies up to 25%. For greater generation deficiencies, a scheme which takes into account both frequency drop and rate of change of frequency provides increased selectivity by preventing unnecessary tripping of load [24]. Ontario Hydro uses such a relay to trip appropriate amounts of load in an area. The relay is referred to as a *frequency trend relay* (FTR), and its tripping logic is shown in Figure 11.31. The relay sheds up to 50% of area load. The system within Ontario is divided into 22 areas, and the load shedding is applied to several stations in each area to maintain the integrity of the area under disturbance conditions.

The procedure described above provides a simple means of determining the settings for underfrequency load shedding. After selection of possible areas of separation and specific load blocks for shedding, *detailed dynamic simulation should be carried out to ensure satisfactory system performance, with due regard to power plant and network protections/controls and to system voltages* (see Chapter 16, Section 16.5.2).

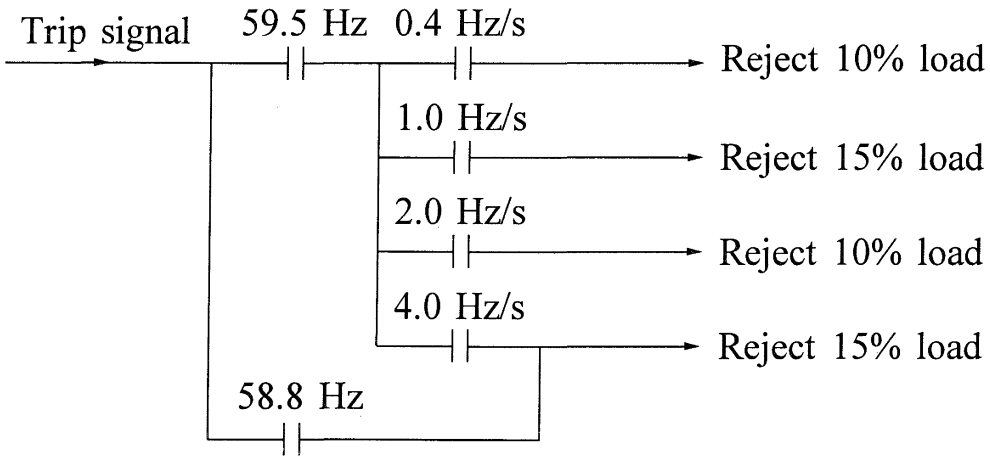


Figure 11.31 Tripping logic for frequency trend relay

11.2 REACTIVE POWER AND VOLTAGE CONTROL

For efficient and reliable operation of power systems, the control of voltage and reactive power should satisfy the following objectives:

(a) Voltages at the terminals of all equipment in the system are within acceptable limits. Both utility equipment and customer equipment are designed to operate at a certain voltage rating. Prolonged operation of the equipment at voltages outside the allowable range could adversely affect their performance and possibly cause them damage.

(b) System stability is enhanced to maximize utilization of the transmission system. As we will see later in this section, and in Chapters 12 to 14, voltage and reactive power control have a significant impact on system stability.

(c) The reactive power flow is minimized so as to reduce RI^2 and XI^2 losses to a practical minimum (see Chapter 6, Section 6.3). This ensures that the transmission system operates efficiently, i.e., mainly for active power transfer.

The problem of maintaining voltages within the required limits is complicated by the fact that the power system supplies power to a vast number of loads and is fed from many generating units. As loads vary, the reactive power requirements of the transmission system vary. This is abundantly clear from the performance characteristics of transmission lines discussed in Chapter 6. Since reactive power cannot be transmitted over long distances, voltage control has to be effected by using special devices dispersed throughout the system. This is in contrast to the control of frequency which depends on the overall system active power balance. The proper selection and coordination of equipment for controlling reactive power and voltage are among the major challenges of power system engineering.

We will first briefly review the characteristics of power system components from the viewpoint of reactive power and then we will discuss methods of voltage control.

11.2.1 Production and Absorption of Reactive Power

Synchronous generators can generate or absorb reactive power depending on the excitation. When overexcited they supply reactive power, and when underexcited they absorb reactive power. The capability to continuously supply or absorb reactive power is, however, limited by the field current, armature current, and end-region heating limits, as discussed in Chapter 5 (Section 5.6). Synchronous generators are normally equipped with automatic voltage regulators which continually adjust the excitation so as to control the armature voltage.

Overhead lines, depending on the load current, either absorb or supply reactive power. At loads below the natural (surge impedance) load, the lines produce net

reactive power; at loads above the natural load, the lines absorb reactive power. The reactive power characteristics of transmission lines are discussed in detail in Chapter 6.

Underground cables, owing to their high capacitance, have high natural loads. They are always loaded below their natural loads, and hence generate reactive power under all operating conditions.

Transformers always absorb reactive power regardless of their loading; at no load, the shunt magnetizing reactance effects predominate; and at full load, the series leakage inductance effects predominate.

Loads normally absorb reactive power. A typical load bus supplied by a power system is composed of a large number of devices. The composition changes depending on the day, season, and weather conditions. The composite characteristics are normally such that a load bus absorbs reactive power. Both active power and reactive power of the composite loads vary as a function of voltage magnitudes. Loads at low-lagging power factors cause excessive voltage drops in the transmission network and are uneconomical to supply. Industrial consumers are normally charged for reactive as well as active power; this gives them an incentive to improve the load power factor by using shunt capacitors.

Compensating devices are usually added to supply or absorb reactive power and thereby control the reactive power balance in a desired manner. In what follows, we will discuss the characteristics of these devices and the principles of application.

11.2.2 Methods of Voltage Control

The control of voltage levels is accomplished by controlling the production, absorption, and flow of reactive power at all levels in the system. The generating units provide the basic means of voltage control; the automatic voltage regulators control field excitation to maintain a scheduled voltage level at the terminals of the generators. Additional means are usually required to control voltage throughout the system. The devices used for this purpose may be classified as follows:

(a) Sources or sinks of reactive power, such as shunt capacitors, shunt reactors, synchronous condensers, and static var compensators (SVCs).

(b) Line reactance compensators, such as series capacitors.

(c) Regulating transformers, such as tap-changing transformers and boosters.

Shunt capacitors and reactors, and series capacitors provide *passive* compensation. They are either permanently connected to the transmission and distribution system, or switched. They contribute to voltage control by modifying the network characteristics.

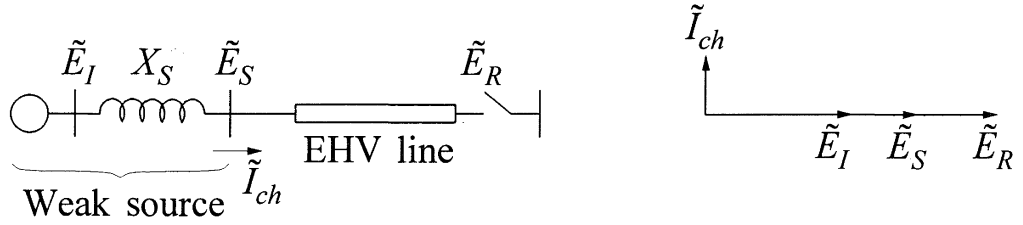
Synchronous condensers and SVCs provide *active* compensation; the reactive power absorbed/supplied by them is automatically adjusted so as to maintain voltages of the buses to which they are connected. Together with the generating units, they establish voltages at specific points in the system. Voltages at other locations in the system are determined by active and reactive power flows through various circuit elements, including the passive compensating devices.

The following is a description of the basic characteristics and forms of application of devices commonly used for voltage and reactive power control.

11.2.3 Shunt Reactors

Shunt reactors are used to compensate for the effects of line capacitance, particularly to limit voltage rise on open circuit or light load.

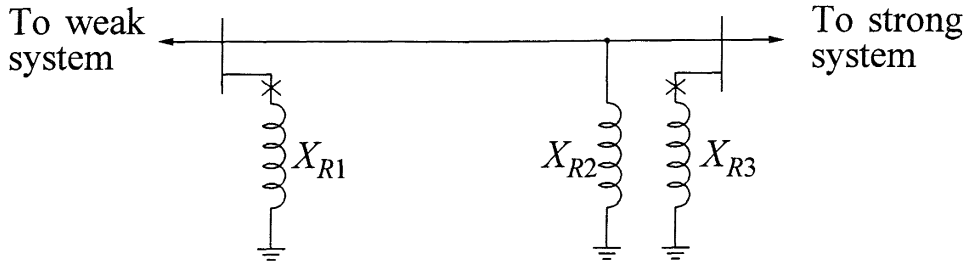
They are usually required for EHV overhead lines longer than 200 km. A shorter overhead line may also require shunt reactors if the line is supplied from a weak system (low short-circuit capacity) as shown in Figure 11.32. When the far end of the line is opened, the capacitive line-charging current flowing through the large source inductive reactance (X_S) will cause a rise in voltage E_S at the sending end of the line. The "Ferranti" effect (see Chapter 6, Section 6.1) will cause a further rise in receiving-end voltage E_R.



(a) System diagram (b) Phasor diagram

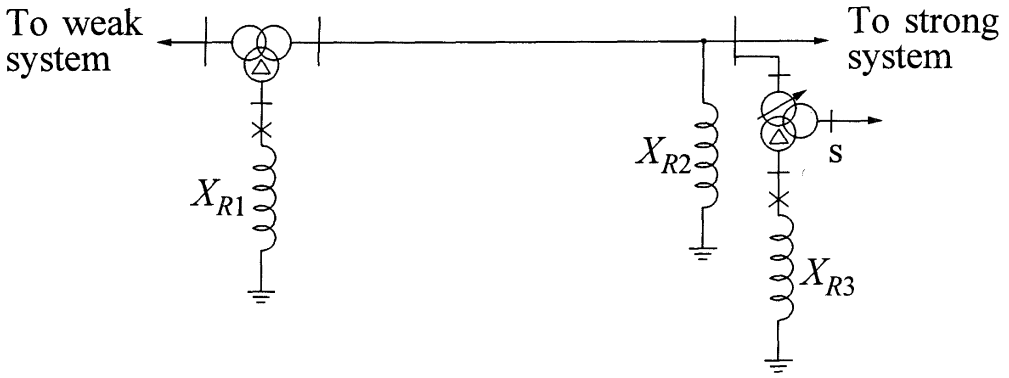
Figure 11.32 EHV line connected to a weak system

A shunt reactor of sufficient size must be permanently connected to the line to limit fundamental-frequency temporary overvoltages to about 1.5 pu for a duration of less than 1 second. Such line-connected reactors also serve to limit energization overvoltages (switching transients). Additional shunt reactors required to maintain normal voltage under light-load conditions may be connected to the EHV bus as shown in Figure 11.33, or to the tertiary windings of adjacent transformers as shown in Figure 11.34. During heavy loading conditions some of the reactors may have to be disconnected. This is achieved by switching reactors using circuit-breakers.



X_{R2} – permanently line-connected reactor
X_{R1}, X_{R3} – switchable bus-connected reactor

Figure 11.33 Line and bus-connected EHV reactors



X_{R2} – permanently line-connected reactor
X_{R1}, X_{R3} – switchable reactors connected to tertiary windings of transformers

Figure 11.34 Line and transformer-connected reactors

For shorter lines supplied from strong systems, there may not be a need for reactors connected to the line permanently. In such cases, all the reactors used may be switchable, connected either to the tertiary windings of transformers or to the EHV bus. In some applications, tapped reactors with on-voltage tap-change control facilities have been used, as shown in Figure 11.35, to allow variation of the reactance value.

Shunt reactors are similar in construction to transformers, but have a single winding (per phase) on an iron core with air-gaps and immersed in oil. They may be of either single-phase or three-phase construction.

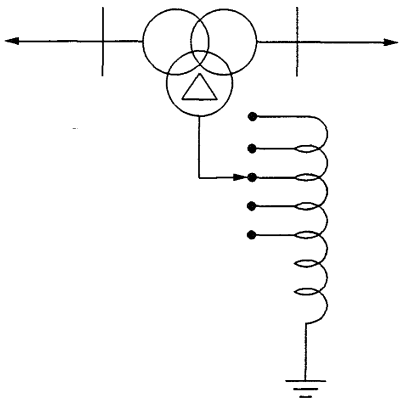


Figure 11.35 Tapped shunt reactor

11.2.4 Shunt Capacitors

Shunt capacitors supply reactive power and boost local voltages. They are used throughout the system and are applied in a wide range of sizes.

Shunt capacitors were first used in the mid-1910s for power factor correction. The early capacitors employed oil as the dielectric. Because of their large size and weight, and high cost, their use at the time was limited. In the 1930s, the introduction of cheaper dielectric materials and other improvements in capacitor construction brought about significant reductions in price and size. The use of shunt capacitors has increased phenomenally since the late 1930s. Today, they are a very economical means of supplying reactive power. The principal advantages of shunt capacitors are their low cost and their flexibility of installation and operation. They are readily applied at various points in the system, thereby contributing to efficiency of power transmission and distribution. The principal disadvantage of shunt capacitors is that their reactive power output is proportional to the square of the voltage. Consequently, the reactive power output is reduced at low voltages when it is likely to be needed most.

Application to distribution systems [25,26]

Shunt capacitors are used extensively in distribution systems for power-factor correction and feeder voltage control. Distribution capacitors are usually switched by automatic means responding to simple time clocks, or to voltage or current-sensing relays.

The objective of *power-factor correction* is to provide reactive power close to the point where it is being consumed, rather than supply it from remote sources. Most loads absorb reactive power; that is, they have lagging power factors. Table 11.1 gives typical power factors and voltage-dependent characteristics of some common types of loads.

Table 11.1 Typical characteristics of individual loads

Type of load	Power factor (lag)	Voltage dependence	
		P	Q
Large industrial motor	0.89	$V^{0.05}$	$V^{0.5}$
Small industrial motor	0.83	$V^{0.1}$	$V^{0.6}$
Refrigerator	0.84	$V^{0.8}$	$V^{2.5}$
Heat pump (cool/heat)	0.81/0.84	$V^{0.2}$	$V^{2.5}$
Dishwasher	0.99	$V^{1.8}$	$V^{3.5}$
Clothes washer	0.65	$V^{0.08}$	$V^{1.6}$
Clothes dryer	0.99	$V^{2.0}$	$V^{3.3}$
Colour TV	0.77	$V^{2.0}$	$V^{5.0}$
Fluorescent lighting	0.90	$V^{1.0}$	$V^{3.0}$
Incandescent lighting	1.00	$V^{1.55}$	-
Range, water or space heat	1.00	$V^{2.0}$	-

Power-factor correction is provided by means of fixed (permanently connected) and switched shunt capacitors at various voltage levels throughout the distribution systems. Low voltage banks are used for large customers and medium voltage banks are used at intermediate switching stations. For large industrial plants, as shown in Figure 11.36, power factor correction is applied at different levels: (i) individual motors, (ii) groups of motors, and (iii) the overall plant.

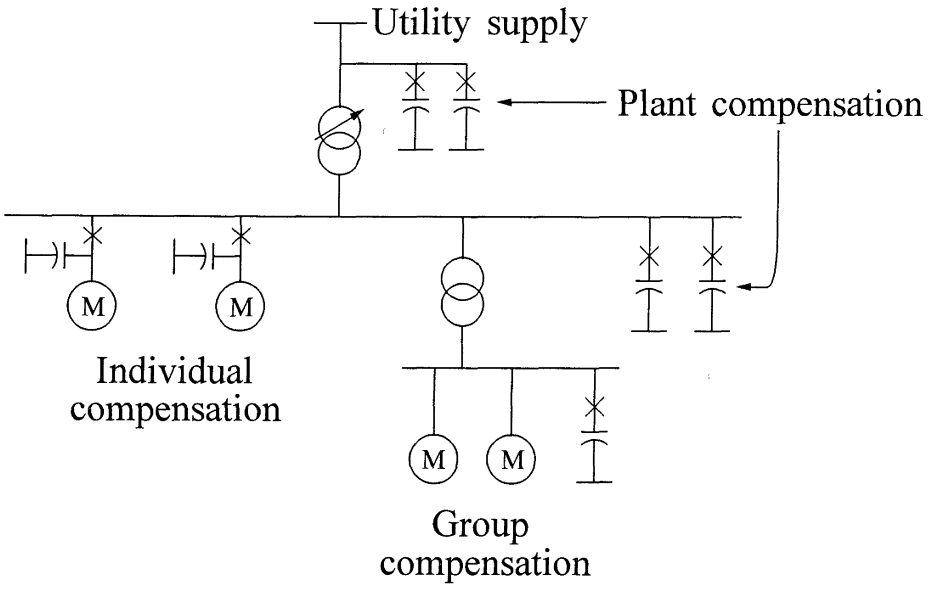


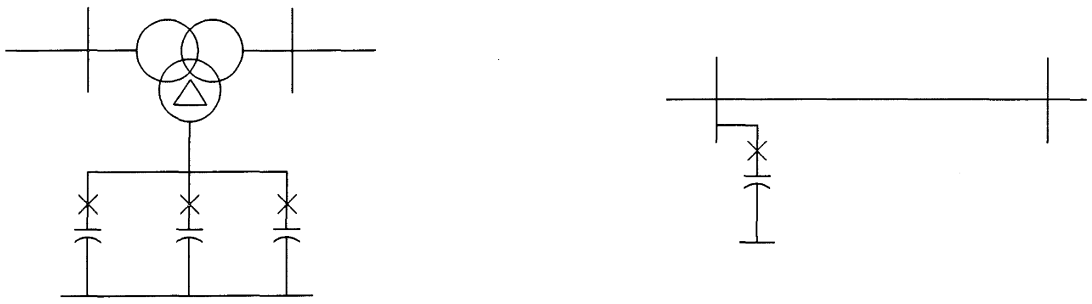
Figure 11.36 Power factor correction in industrial plants [26]

Switched shunt capacitors are also used extensively for *feeder voltage control.* They are installed at appropriate locations along the length of the feeder to ensure that voltages at all points remain within the allowable maximum and minimum limits as the loads vary. As discussed in Section 11.2.10, the application of shunt capacitors is coordinated with that of feeder voltage regulators or booster transformers.

Application to transmission system

Shunt capacitors are used to compensate for the XI^2 losses in transmission systems and to ensure satisfactory voltage levels during heavy loading conditions. Capacitor banks of appropriate sizes are connected either directly to the high voltage bus or to the tertiary winding of the main transformer, as shown in Figure 11.37. They are breaker-switched either automatically by a voltage relay or manually. Switching of capacitor banks provides a convenient means of controlling transmission system voltages. They are normally distributed throughout the transmission system so as to minimize losses and voltage drops. Detailed power-flow studies are performed to determine the size and location of capacitor banks to meet the system design criteria which specify maximum allowable voltage drop following specified contingencies. Procedures for power-flow analysis are discussed in Section 11.3.

The principles of application of shunt capacitors and other forms of transmission system compensation are presented in Section 11.2.8.



(a) Tertiary connected capacitor banks

(b) HV capacitor bank

Figure 11.37 Capacitor bank connections

11.2.5 Series Capacitors

Series capacitors are connected in series with the line conductors to compensate for the inductive reactance of the line. This reduces the transfer reactance between the buses to which the line is connected, increases maximum power that can be transmitted, and reduces the effective reactive power (XI^2) loss. Although series

capacitors are not usually installed for voltage control as such, they do contribute to improved voltage control and reactive power balance. The reactive power produced by a series capacitor increases with increasing power transfer; a series capacitor is self-regulating in this regard.

Application to distribution feeders

Series capacitors have been applied to improve voltage regulation of distribution and industrial feeders since the 1930s. Welders and arc furnaces are typical of loads with poor power factor and intermittent demand. A series capacitor not only reduces voltage drop in the steady state, but it responds almost instantaneously to changes in load current. The series capacitor, by reducing the impedance between the bulk power source and the fluctuating load, is effective in solving light-flicker problems.

There are a number of problems associated with the application of series capacitors to industrial feeders that need careful attention [27-29]:

- Self-excitation of large induction and synchronous motors during starting. The motor may lock in at a fraction of synchronous (subsynchronous) speed due to resonance conditions.

  The most common remedy is to connect, during starting, a suitable resistance in parallel with the series capacitor.

- Hunting of synchronous motors (in some cases induction motors) at light load, due to the high R/X ratio of the feeder.

- Ferroresonance between transformers and series capacitors resulting in harmonic overvoltages. This may occur when energizing an unloaded transformer or when suddenly removing a load.

Because of the above problems and the difficulty in protecting the capacitors from system fault currents, series capacitors are not very widely used in today's distribution systems. They are, however, used in subtransmission systems to modify load division between parallel lines and to improve voltage regulation.

Application to EHV transmission system

Because series capacitors permit economical loading of long transmission lines, their application to EHV transmission has grown. They have been primarily used to improve system stability and to obtain the desired load division among parallel lines.

Complete compensation of the line is never considered. At 100% compensation, the effective line reactance would be zero, and the line current and power flow would be extremely sensitive to changes in the relative angles of terminal voltages. In addition, the circuit would be series resonant at the fundamental frequency. High compensation levels also increase the complexity of protective

relaying and the probability of subsynchronous resonance. A practical upper limit to the degree of series compensation is about 80%.

It is not practical to distribute the capacitance in small units along the line. Therefore, lumped capacitors are installed at a few locations along the line. The use of lumped series capacitors results in an uneven voltage profile.

Series capacitors operate at line potential; hence, they must be insulated from ground. A widely accepted practice is to mount the capacitors on platforms insulated from ground. Alternatively, ground-base capacitor banks consisting of capacitor cans placed inside oil-insulated tanks may be used.

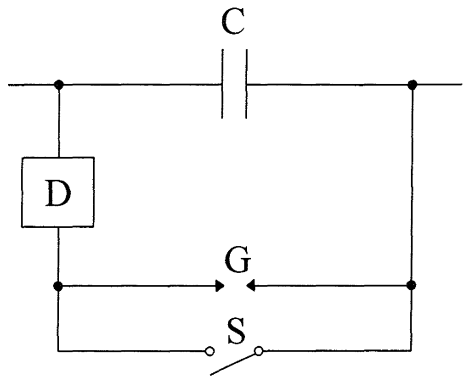
The following are some of the key considerations in the application of series-capacitor banks:

(a) *Voltage rise due to reactive current.* Voltage rise on one side of the capacitor may be excessive when the line reactive-current flow is high, as might occur during power swings or heavy power transfers. This may impose unacceptable stress on equipment on the side of the bank experiencing high voltage. The system design must limit the voltage to acceptable levels, or the equipment must be rated to withstand the highest voltage that might occur.

(b) *Bypassing and reinsertion.* The series capacitors are normally subjected to a voltage which is on the order of the regulation of the line, i.e., only a few percent of the rated line voltage. If, however, the line is short-circuited by a fault beyond the capacitor, a voltage on the order of the line voltage will appear across the capacitor. It would not be economical to design the capacitor for this voltage, since both size and cost of the capacitor increase with the square of the voltage. Therefore, provision is made for bypassing the capacitor during faults and reinsertion after fault clearing. Speed of reinsertion may be an important factor in maintaining transient stability.

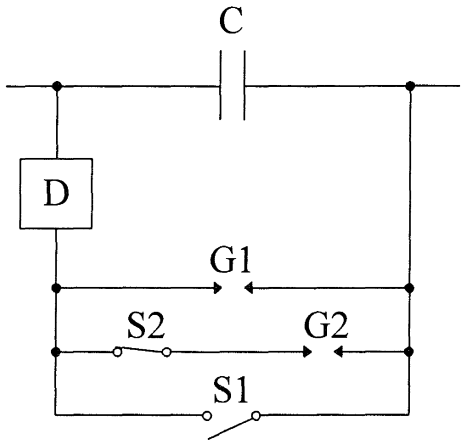
Traditionally, bypassing was provided by a spark gap across the bank or each module of the bank. However, the present trend is to use nonlinear resistors of zinc oxide which have the advantage that reinsertion is essentially instantaneous. Figure 11.38 shows alternative bypass schemes [30]. The scheme shown in Figure 11.38(a) consists of a single spark gap (G) which bypasses the capacitor bank when the capacitor voltage exceeds a set value, usually about three to four times the capacitor rated voltage. The damping circuit (D) limits the discharge current and absorbs the capacitor energy. Upon detection of gap current, the bypass breaker (S) is closed, diverting the current from the gap. When the current returns to normal, the breaker is opened, thereby reinserting the capacitor into the line. This scheme is designed to provide a reinsertion time of 200 to 400 ms.

A dual-gap scheme with reinsertion time on the order of 80 ms is shown in Figure 11.38(b). It has an extra spark gap (G2) which is set low so that it will spark over first. Breaker S2 is normally closed. In the event of a fault, gap



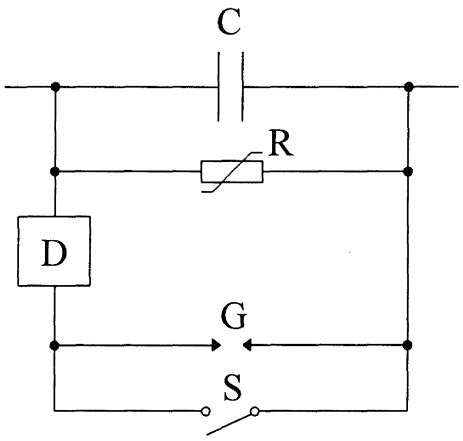
C Capacitor bank
D Damping circuit
G Spark gap
S Bypass breaker

(a) Single-gap protective scheme



C Capacitor bank
D Damping circuit
G1 Spark gap, high-set
G2 Spark gap, low-set
S1 Bypass breaker
S2 Reinsertion breaker

(b) Dual-gap protective scheme



C Capacitor bank
R Nonlinear resistor (ZnO)
D Damping circuit
G Spark gap
S Bypass breaker

(c) Zinc-oxide protective scheme

Figure 11.38 Series capacitor bypass protective schemes [30]

G2 bypasses the capacitor bank. Breaker S2 opens immediately after the line fault has been cleared and reinserts the capacitor bank into the line. As a result, reinsertion is not delayed due to the de-ionization time. The other gap G1, which is high-set, and the bypass breaker S1 serve as backup protection.

In the scheme shown in Figure 11.38(c), a nonlinear resistor of zinc oxide (ZnO) limits the voltage across the capacitor bank during a fault and reinserts the bank immediately on termination of the fault current. The energy is absorbed by the ZnO resistor without the need to fire the spark gap (G). The spark gap is provided as a backup overvoltage protection for the resistor. The capacitor bank and the ZnO resistor remain in circuit during the fault, with the resistor bypassing most of the current; reinsertion takes place automatically without delay when the fault is cleared.

(c) *Location.* A series-capacitor bank can theoretically be located anywhere along the line. Factors influencing choice of location include cost, accessibility, fault level, protective relaying considerations, voltage profile and effectiveness in improving power transfer capability.

The following are the usual locations considered:

- Midpoint of the line
- Line terminals
- 1/3 or 1/4 points of the line

In practice all of the above arrangements have been used.

The midpoint location has the advantage that the relaying requirements are less complicated if compensation is less than 50%. In addition, short-circuit current is lower. However, it is not very convenient in terms of access for maintenance, monitoring, security, etc.

Splitting of the compensation into two parts, with one at each end of the line, provides more accessability and availability of station service and other auxiliaries. The disadvantages are higher fault current, complicated relaying, and higher rating of the compensation.

The effectiveness of the compensation scheme depends on the location of the series capacitors and the associated shunt reactors. References 31 and 32 present results of comprehensive studies evaluating the effectiveness of different capacitor locations.

The choice of configuration of the compensation scheme for any particular application requires a detailed study with regard to the overall economy and system reliability. The study should take into account voltage profiles, compensation effectiveness, effect on transmission losses, overvoltages, and proximity to an attended station. References 33 and 34 provide details of engineering considerations related to series-capacitor applications on two power systems.

Adding a capacitor in series with the inductance of a transmission line forms a series-resonant circuit. The natural frequency of the resonant circuit so formed, for the usual range of compensation (20 to 70% of line reactance), is below the power frequency. The transmission network thus has a natural frequency in the subsynchronous range. Consequently, transient current components of subharmonic frequency are excited during any disturbance and are superimposed on the power-frequency currents. The subharmonic currents are usually damped rapidly within a few cycles, due to the resistances of the line and of any connected equipment such as loads. Therefore, the subharmonic natural mode introduced by the use of a series capacitor is rarely troublesome. One notable exception is the possible interaction with a natural frequency of the shaft mechanical system of nearby steam turbine generating units. It may lead to a buildup of torsional oscillations, either spontaneously or after a disturbance. This phenomenon is known as *subsynchronous resonance* (SSR). A detailed discussion of the SSR problem and measures available to counter it are presented in Chapter 15.

11.2.6 Synchronous Condensers

A synchronous condenser is a synchronous machine running without a prime mover or a mechanical load. By controlling the field excitation, it can be made to either generate or absorb reactive power. With a voltage regulator, it can automatically adjust the reactive power output to maintain constant terminal voltage. It draws a small amount of active power from the power system to supply losses.

Synchronous condensers have been used since the 1930s for voltage and reactive power control at both transmission and subtransmission levels. They are often connected to the tertiary windings of transformers. They fall into the category of *active shunt compensators*. Because of their high purchase and operating costs, they have been largely superseded by static var compensators (discussed next). Recent applications of synchronous condensers have been mostly at HVDC converter stations connected to weak systems [35]. There are many old synchronous condensers still in operation, and they serve as an excellent form of voltage and reactive power control devices.

Synchronous compensators have several advantages over static compensators. Synchronous compensators contribute to system short-circuit capacity. Their reactive power production is not affected by the system voltage. During power swings (electromechanical oscillations) there is an exchange of kinetic energy between a synchronous condenser and the power system. During such power swings, a synchronous condenser can supply a large amount of reactive power, perhaps twice its continuous rating. It has about 10 to 20% overload capability for up to 30 minutes. Unlike other forms of shunt compensation, it has an internal voltage source and is better able to cope with low system voltage conditions.

Some combustion turbine peaking units can be operated as synchronous condensers if required. Such units are often equipped with clutches which can be used to disconnect the turbine from the generator when active power is not required from them.

11.2.7 Static Var Systems [36-38]

Terminology [36]

Static var compensators (SVCs) are shunt-connected static generators and/or absorbers whose outputs are varied so as to control specific parameters of the electric power system. The term "static" is used to indicate that SVCs, unlike synchronous compensators, have no moving or rotating main components. Thus an SVC consists of static var generator (SVG) or absorber devices and a suitable control device.

A static var system (SVS) is an aggregation of SVCs and mechanically switched capacitors (MSCs) or reactors (MSRs) whose outputs are coordinated.

Types of SVC

The following are the basic types of reactive power control elements which make up all or part of any static var system:

- Saturated reactor (SR)
- Thyristor-controlled reactor (TCR)
- Thyristor-switched capacitor (TSC)
- Thyristor-switched reactor (TSR)
- Thyristor-controlled transformer (TCT)
- Self- or line-commutated converter (SCC/LCC)

A number of different SVS configurations made up of a combination of one or more of the basic types of SVC and fixed capacitor (FC) banks (i.e., capacitors not switched via local automatic control) have been used in practice for transmission system compensation.

We will first discuss the general principle of SVS operation in an HVAC system using a somewhat idealized compensator and then examine the characteristics of specific configurations.

Static var systems are capable of controlling individual phase voltages of the buses to which they are connected. They can therefore be used for control of negative-sequence as well as positive-sequence voltage deviations. However, we are interested here in the balanced fundamental frequency performance of power systems and therefore our analysis will consider only this aspect of SVS performance.

Fundamental frequency performance of an SVS [36,38]

Characteristic of an ideal SVS:

From the viewpoint of power system operation, an SVS is equivalent to a shunt capacitor and a shunt inductor, both of which can be adjusted to control voltage and reactive power at its terminals (or a nearby bus) in a prescribed manner (see Figure 11.39).

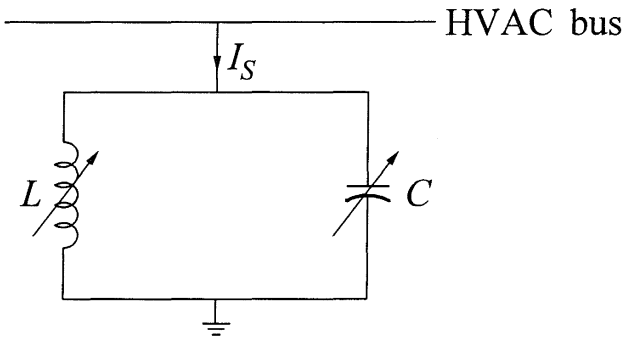


Figure 11.39 Idealized static var system

Ideally, an SVS should hold constant voltage (assuming that this is the desired objective), possess unlimited var generation/absorption capability with no active and reactive power losses and provide instantaneous response. The performance of the SVS can be visualized on a graph of controlled ac bus voltage (V) plotted against the SVS reactive current (I_S). The V/I characteristic of an ideal SVS is shown in Figure 11.40. It represents the steady-state and quasi steady-state characteristics of the SVS.

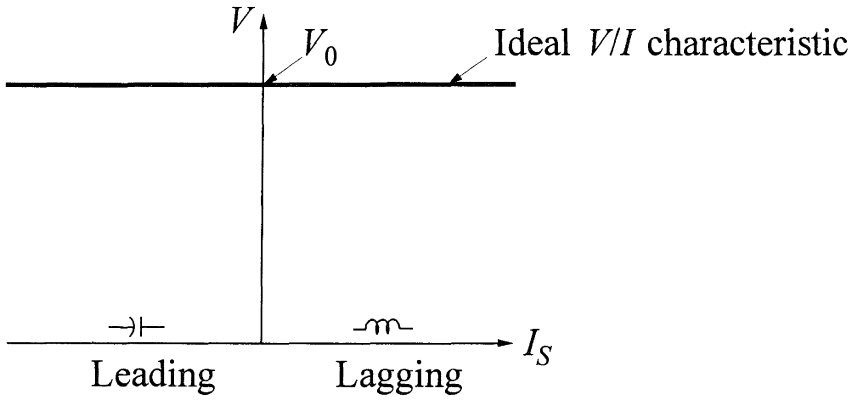
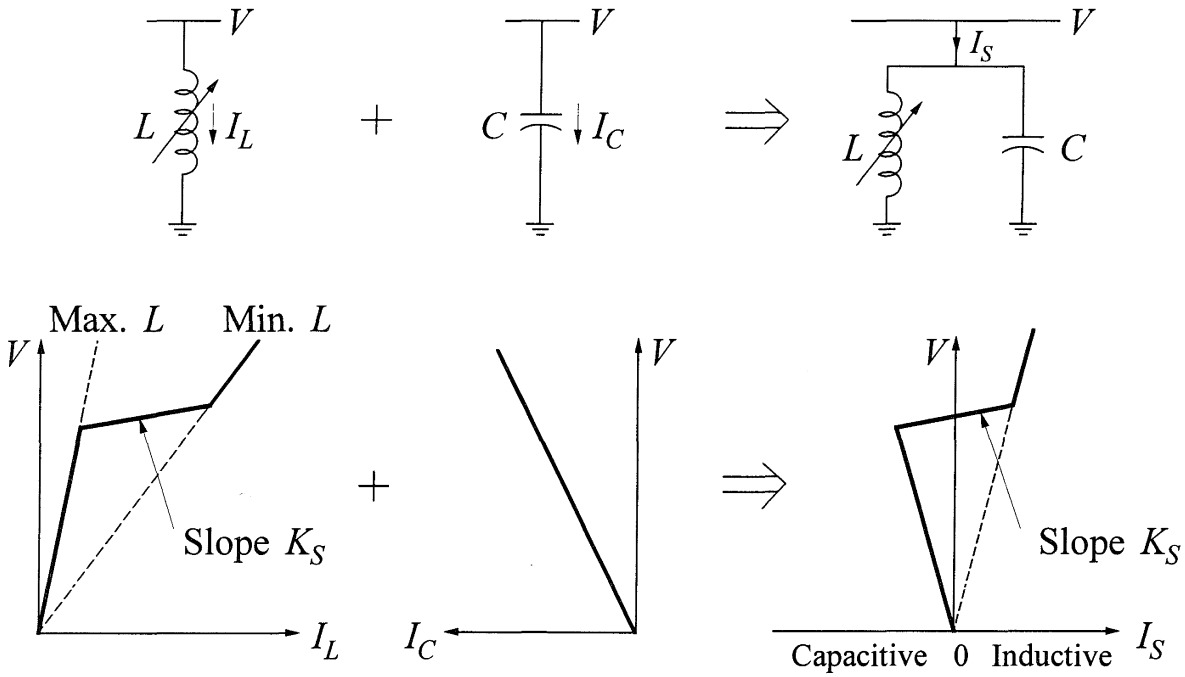


Figure 11.40 V/I characteristic of ideal compensator

Characteristic of a realistic SVS:

We consider an SVS composed of a controllable reactor and a fixed capacitor. The resulting characteristics are sufficiently general and are applicable to a wide range of practical SVS configurations.

Figure 11.41 illustrates the derivation of the characteristic of an SVS consisting of a controllable reactor and a fixed capacitor. The composite characteristic is derived by adding the individual characteristics of the components. The characteristic shown in Figure 11.41(a) is representative of the characteristics of practical controllable reactors.

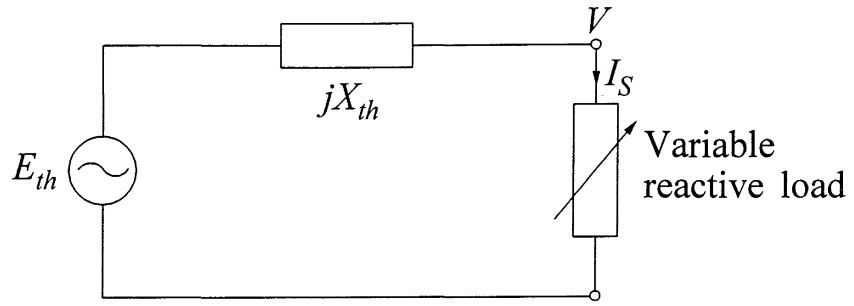


(a) Controllable reactor (b) Fixed capacitor (c) SVS

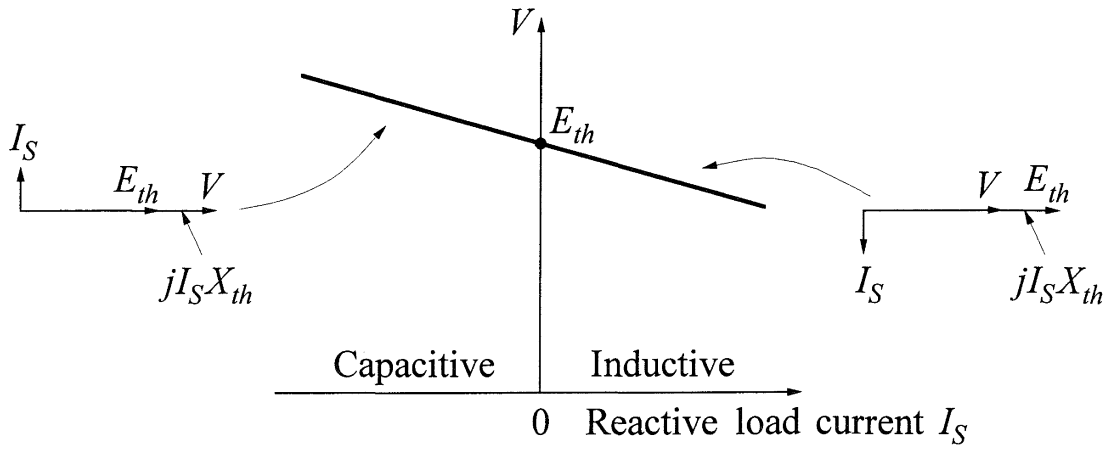
Figure 11.41 Composite characteristics of an SVS

Power system characteristic:

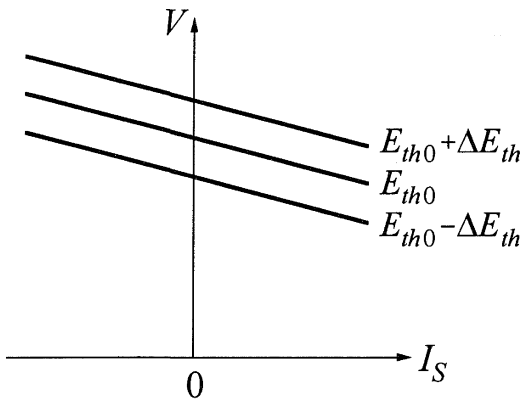
In order to examine how the SVS performs when applied to a power system, the characteristics of the SVS and the power system need to be examined together. The system *V/I* characteristic may be determined by considering the Thevenin equivalent circuit as viewed from the bus whose voltage is to be regulated by the SVS. This is illustrated in Figure 11.42. The Thevenin impedance in Figure 11.42(a) is predominantly an inductive reactance. The corresponding voltage versus reactive current characteristic is shown in Figure 11.42(b). The voltage V increases linearly with capacitive load current and decreases linearly with inductive load current.



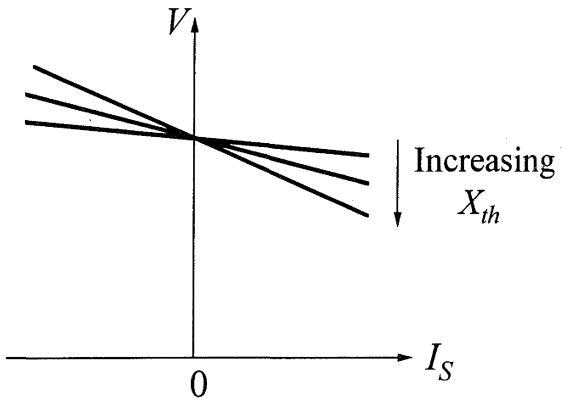
(a) Thevenin equivalent circuit of HVAC network



(b) Voltage-reactive current characteristic



(c) Effect of varying source voltage E_{th}



(d) Effect of varying system reactance X_{th}

Figure 11.42 Power system voltage versus reactive current characteristic [38]

For each network condition, an equivalent circuit such as that shown in Figure 11.42(a) can be defined. Figures 11.42(c) and (d) show how the network *V/I* characteristic is affected by changes in source voltage E_{th} and the system equivalent reactance X_{th}, respectively.

Composite SVS - power system characteristic:

The system characteristic may be expressed as

$$V = E_{th} - X_{th} I_S \tag{11.31}$$

The SVS characteristic, within the control range defined by the slope reactance X_{SL}, is given by

$$V = V_0 + X_{SL} I_S \tag{11.32}$$

For voltages outside the control range, the ratio V/I_S is equal to the slopes of the two extreme segments of Figure 11.41(c). These are determined by the ratings of the inductor and capacitor.

The solution of SVS and power system characteristic equations is graphically illustrated in Figure 11.43. Three system characteristics are considered in the figure, corresponding to three values of the source voltage. The middle characteristic

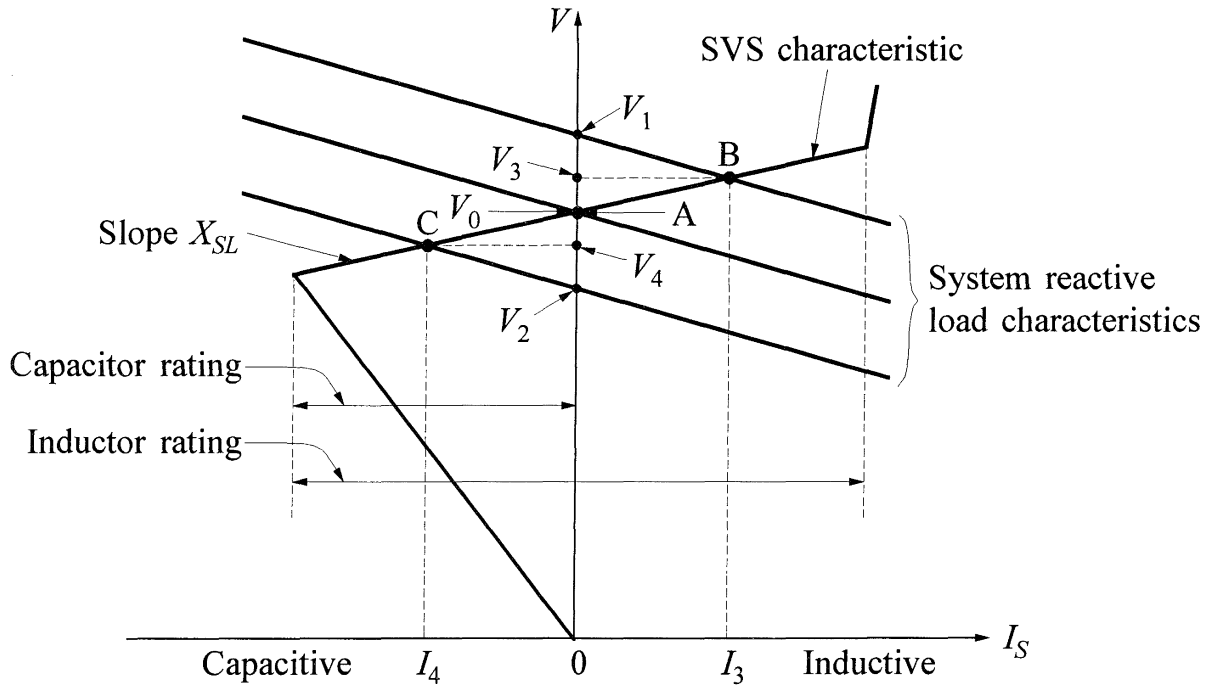


Figure 11.43 Graphical solution of SVS operating point for given system conditions

represents nominal system conditions, and is assumed to intersect the SVS characteristic at point A where $V=V_0$ and $I_S=0$.

If the system voltage increases by ΔE_{th} (for example, due to a decrease in system load level), V will increase to V_1, without an SVS. With the SVS, however, the operating point moves to B; by absorbing inductive current I_3, the SVS holds the voltage at V_3. Similarly, if the source voltage decreases (due to increase in system load level), the SVS holds the voltage at V_4, instead of at V_2 without the SVS. If the slope K_S of the SVS characteristic were zero, the voltage would have been held at V_0 for both cases considered above.

Effect of using switched capacitors:

In the example considered in Figure 11.43, the SVS control range would be exceeded for larger variations in system conditions. The use of switched capacitor banks can extend the continuous control range of the SVS. This is illustrated in Figure 11.44, which considers three capacitor banks, two of which are switchable. Either thyristors or mechanical switches may be used for switching the capacitors in and out automatically by local voltage-sensing controls. In the figure the unswitched capacitor includes a reactor for filtering harmonics.

We see that an SVS is not a source of voltage as is a synchronous condenser. Instead, it alters the system voltage at the point of connection by varying the reactive current drawn or supplied to the system. In effect, the SVS acts as a variable reactive load which is adjusted so as to keep the ac voltage nearly constant.

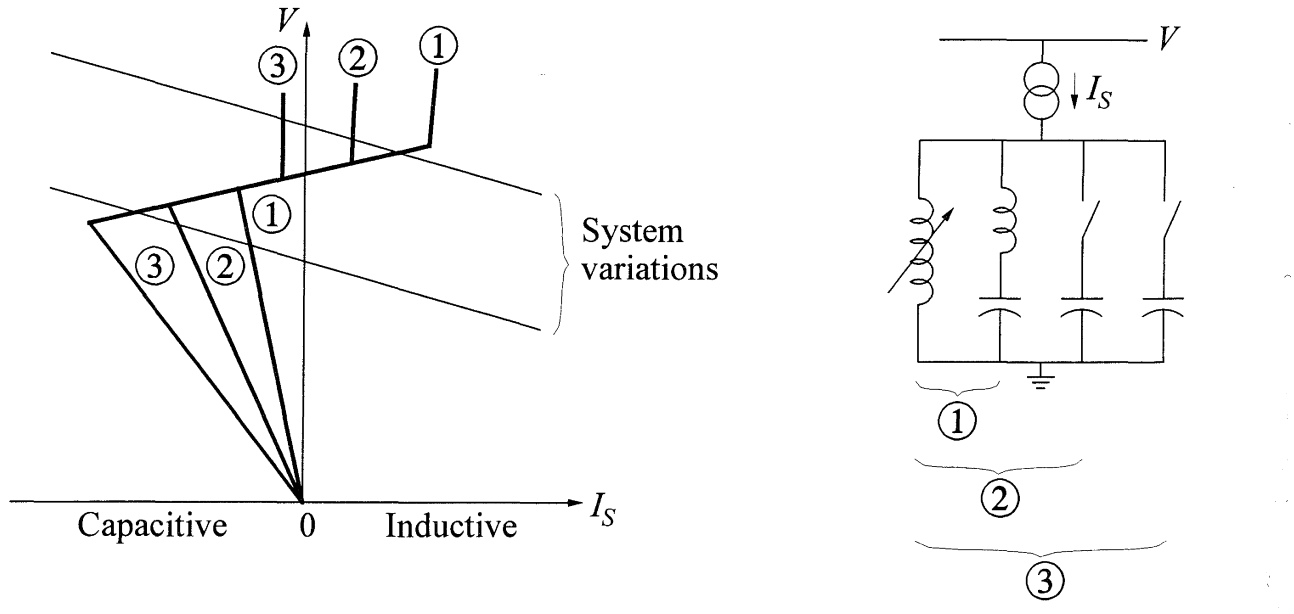


Figure 11.44 Use of switched capacitors to extend continuous control range

In general, the elements of an SVS operate on the principle of adjustable susceptance. The controlled susceptance is either a reactor or a capacitor. We will discuss next the operation of the more commonly used elements: TCR, TSC, and MSC. For a description of other forms of static compensators readers may consult references 36 and 37.

Thyristor-controlled reactor (TCR) [36,37]

Principle of operation:

The basic elements of a TCR are a reactor in series with a bidirectional thyristor switch as shown in Figure 11.45(a).

The thyristors conduct on alternate half-cycles of the supply frequency depending on the firing angle α, which is measured from a zero crossing of voltage. Full conduction is obtained with a firing angle of 90°. The current is essentially reactive and sinusoidal. Partial conduction is obtained with firing angles between 90° and 180°, as shown in Figure 11.45(b). Firing angles between 0 and 90° are not allowed as they produce asymmetrical currents with a dc component.

Let σ be the conduction angle, related to α by

$$\sigma = 2(\pi - \alpha) \tag{11.33}$$

The instantaneous current i is given by

$$i = \begin{cases} \dfrac{\sqrt{2}V}{X_L}(\cos\alpha - \cos\omega t) & \text{for } \alpha < \omega t < \alpha + \sigma \\ 0 & \text{for } \alpha + \sigma < \omega t < \alpha + \pi \end{cases} \tag{11.34}$$

Fourier analysis of the current waveform gives the fundamental component:

$$I_1 = \frac{V}{X_L}\frac{\sigma - \sin\sigma}{\pi} \tag{11.35}$$

where I_1 and V are RMS values, and X_L is the reactance of the reactor at fundamental frequency.

The effect of increasing α (i.e., decreasing σ) is to reduce the fundamental component I_1. This is equivalent to increasing the effective inductance of the reactor.

In effect, so far as the fundamental frequency current component is concerned, the TCR is a controllable susceptance. The effective susceptance as a function of the firing angle α is

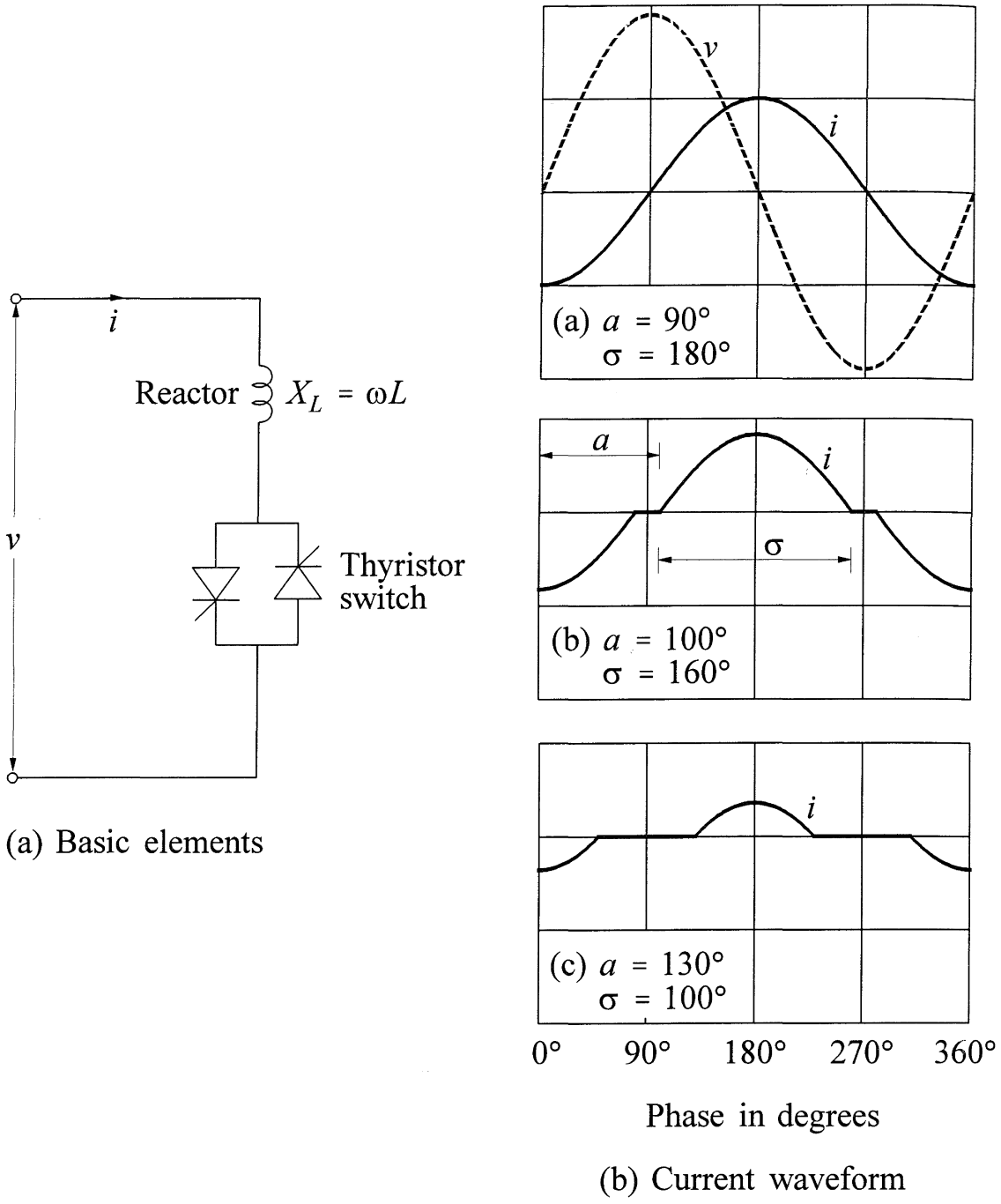


Figure 11.45 Thyristor-controlled reactor

$$B(\alpha) = \frac{I_1}{V} = \frac{\sigma - \sin\sigma}{\pi X_L} = \frac{2(\pi - \alpha) + \sin 2\alpha}{\pi X_L} \tag{11.36}$$

The maximum value of the effective susceptance is at full conduction (α=90°, σ=180°), and is equal to $1/X_L$; the minimum value is zero, obtained with α=180° or σ=0°.

This susceptance control principle is known as *phase control*. The susceptance is switched into the system for a controllable fraction of every half cycle. The variation in susceptance as well as the TCR current is smooth or continuous.

The TCR requires a control system which determines the firing instants (i.e., firing angle α) measured from the last zero crossing of the voltage (synchronization of firing angles). In some designs the control system responds to a signal that directly represents the desired susceptance. In others, the control responds to error signals such as voltage deviation, auxiliary stabilizing signals, etc. The result is a steady-state *V/I* characteristic shown in Figure 11.46, which can be described by

$$V = V_{ref} + X_{SL} I_1 \tag{11.37}$$

where X_{SL} is the slope reactance determined by the control system gain.

As illustrated in Figure 11.44, the TCR voltage control characteristic can be extended into the capacitive region by adding in parallel a fixed capacitor bank or switched capacitor banks.

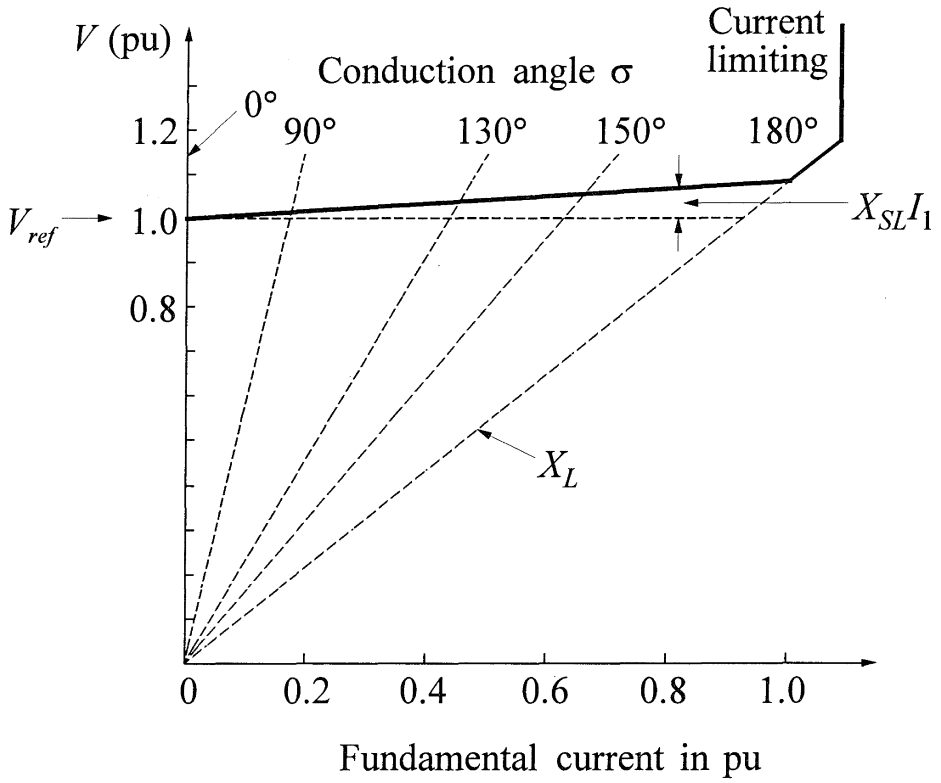
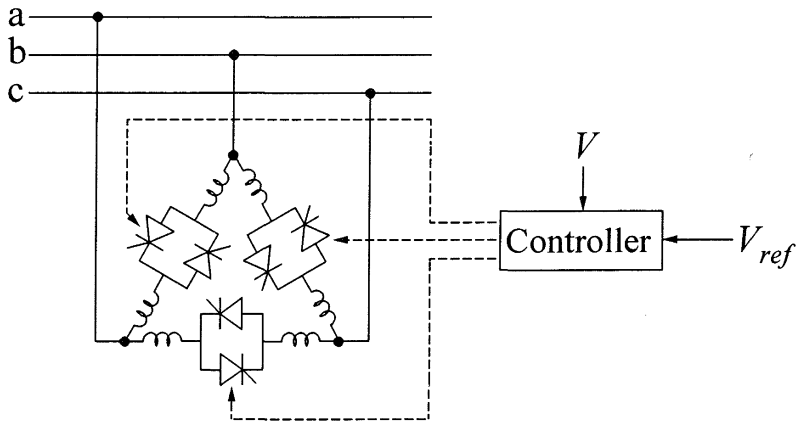


Figure 11.46 Fundamental voltage-current characteristic of TCR

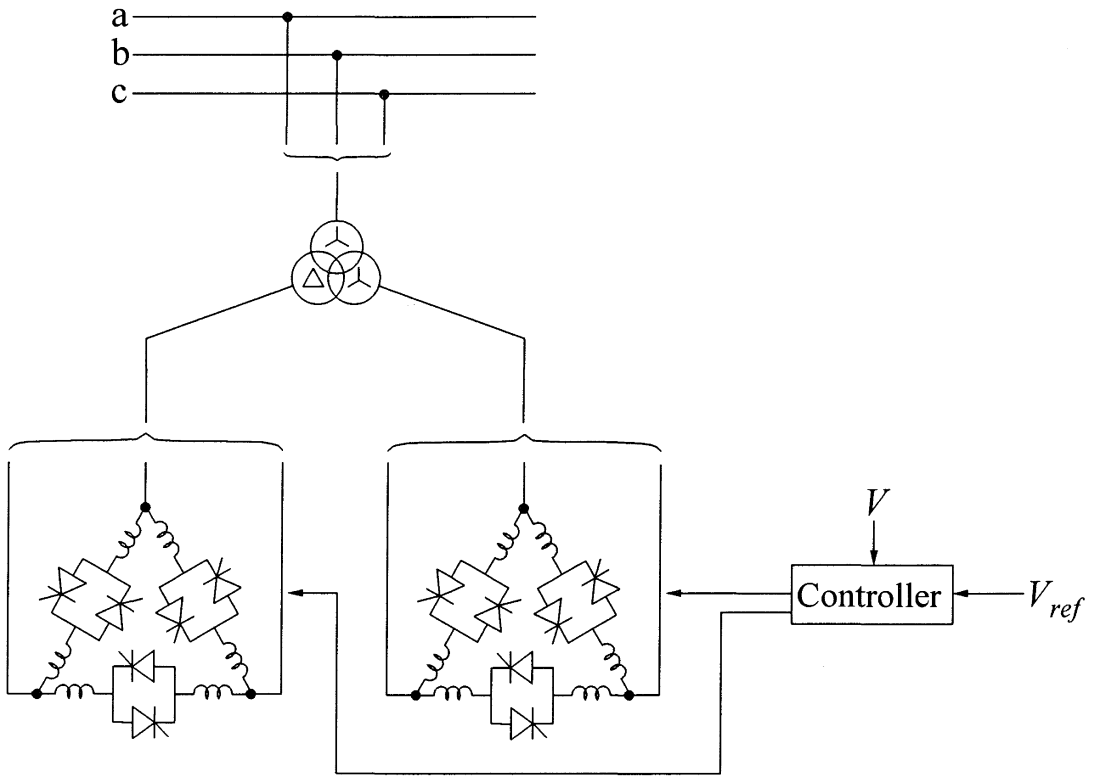
Harmonics:

As α is increased from 90° to 180°, the current waveform becomes less and less sinusoidal; in other words, the TCR generates harmonics. For the single-phase

device considered so far, if the firing of the thyristors is symmetrical (equal for both thyristors), only odd harmonics are generated. For a three-phase system, the preferred arrangement is to have the three single-phase TCR elements connected in delta (6-pulse TCR) as shown in Figure 11.47(a). For balanced conditions, all triple (3, 9, ...) harmonics circulate within the closed delta and are therefore absent from the line currents. Filters are often used to remove harmonic currents.



(a) 6-pulse TCR



(b) 12-pulse TCR

Figure 11.47 Three-phase TCR arrangements

Elimination of 5^{th} and 7^{th} harmonics can be achieved by using two 6-pulse TCRs of equal rating, fed from two secondary windings of the step-down transformers, one connected in Y and the other in Δ as shown in Figure 11.47(b). Since the voltages applied to the TCRs have a phase difference of 30°, 5^{th} and 7^{th} harmonics are eliminated from the primary-side line current. This is known as a 12-pulse arrangement because there are 12 thyristor firings every cycle of the three-phase line voltage. With the 12-pulse scheme, the lowest-order characteristic harmonics are the 11^{th} and 13^{th}. These can be filtered with a simple capacitor bank.

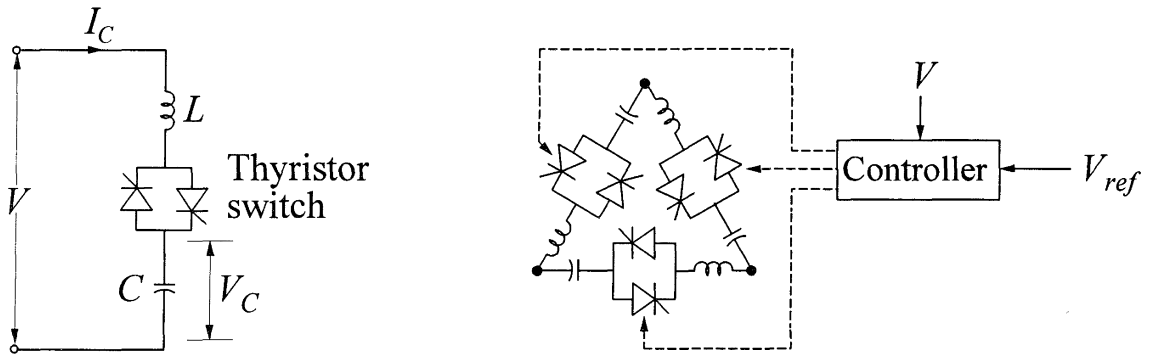
Dynamic response:

The TCR responds in about 5 to 10 ms, but delays are introduced by measurement and control circuits. To ensure control loop stability the response rate may have to be limited. For these reasons response times are typically around 1 to 5 cycles of supply frequency.

Thyristor-switched capacitor (TSC) [26,36,37]

Principle of operation:

A thyristor-switched capacitor scheme consists of a capacitor bank split up into appropriately sized units, each of which is switched on and off by using thyristor switches. Each single-phase unit consists of a capacitor (C) in series with a bidirectional thyristor switch and a small inductor (L) as shown in Figure 11.48(a). The purpose of the inductor is to limit switching transients, to damp inrush currents, and to prevent resonance with the network. In three-phase applications, the basic units are connected in Δ as shown in Figure 11.48(b).



(a) Single-phase unit (b) Three-phase unit

Figure 11.48 Thyristor-switched capacitor (TSC)

The switching of capacitors excites transients which may be large or small depending on the resonant frequency of the capacitors with the external system. The thyristor firing controls are designed to minimize the switching transients. This is achieved by choosing the switching instant when the voltage across the thyristor switch is at a minimum, ideally zero. Figure 11.49 illustrates the operating principle. The switching-on instant (t_1) is chosen so that the bus voltage V is at its maximum and of the same polarity as the capacitor voltage; this ensures a transient-free switching. The switching-off instant (t_2) corresponds to a current zero. The capacitor will then remain charged to a peak voltage, either positive or negative, ready for the next switch-on operation.

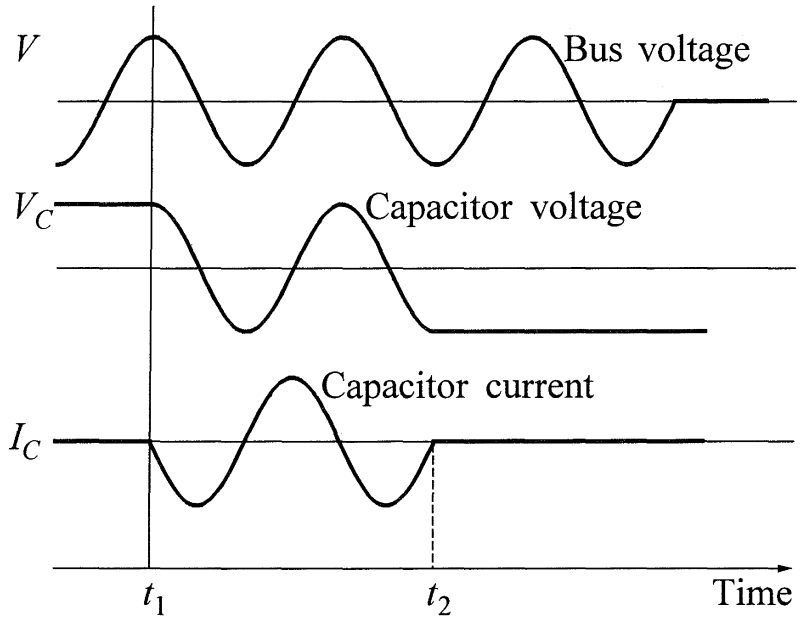


Figure 11.49 Switch operation of a TSC

The susceptance control principle used by a TSC is known as the *integral cycle control*; the susceptance is switched in for an integral number of exact half cycles. The susceptance is divided into several parallel units, and the susceptance is varied by controlling the number of units in conduction. A change can be made every half cycle. This form of control does not generate harmonics.

Figure 11.50 shows the basic scheme of a TSC consisting of parallel Δ connected TSC elements and a controller. When the bus voltage deviates from the reference value (V_{ref}) beyond the dead band in either direction, the control switches in (or out) one or more capacitor banks until the voltage returns inside the dead band, provided that not all the banks have been switched in (or out).

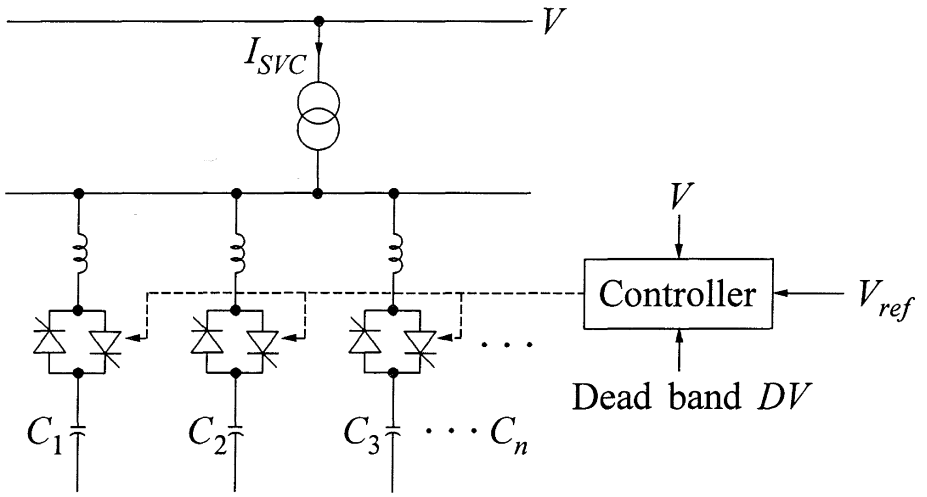


Figure 11.50 TSC scheme

Dynamic response:

The *V/I* characteristic of a TSC compensator is shown in Figure 11.51. We see that the voltage control provided is discontinuous or stepwise. It is determined by the rating and number of parallel connected units. In high voltage applications, the number of shunt capacitor banks is limited because of the high cost of thyristors. The power system *V/I* characteristics, as system conditions change, intersect the TSC *V/I* characteristics at discrete points. The bus voltage V is controlled within the range $V_{ref} \pm DV/2$, where DV is the dead band. When the system is operating so that its

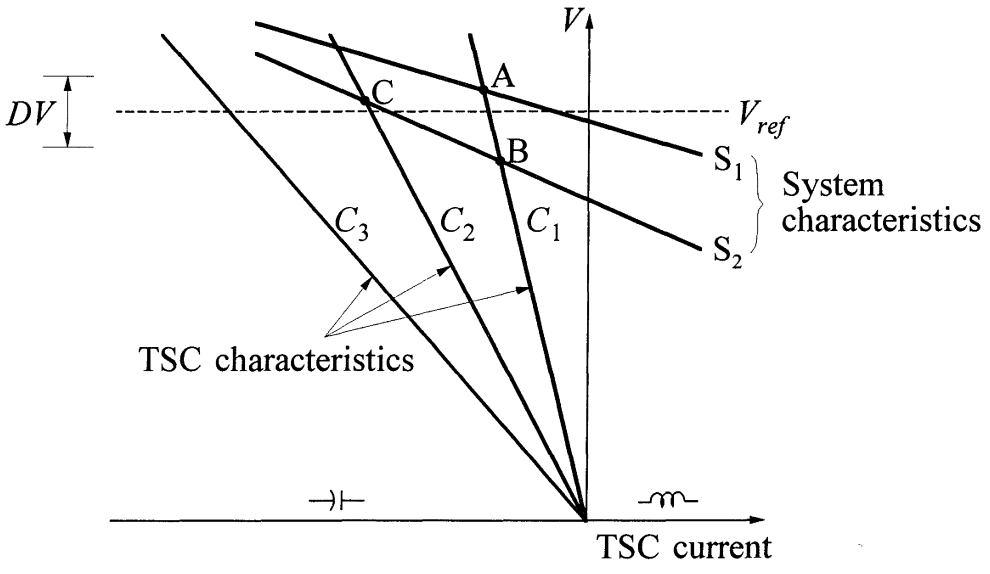


Figure 11.51 *V/I* characteristics of a TSC and power system

characteristic is represented by line S_1, then capacitor C_1 will be switched in and operating point A prevails. If the system characteristic suddenly changes to S_2, the bus voltage drops initially to a value represented by operating point B. The TSC control switches in bank C_2 to change the operating point to C, bringing the voltage within the desired range. Thus the compensator current can change in discrete steps. The time taken for executing a command from the controller ranges from one-half cycle to one cycle.

Mechanically switched capacitor (MSC)

Typically, an MSC scheme consists of one or more capacitor units connected to the power system by a circuit-breaker. A small reactor might be connected in series with the capacitor to damp energizing transients and reduce harmonics. Prestrike and restrike-free circuit-breakers have to be used to avoid system overvoltages due to capacitor-switching transients.

The *V/I* characteristic is linear and similar to that of a TSC. The response time is equal to the switching time of the circuit-breaker arrangement which is on the order of 100 ms following the initiation of switching operation instruction. Frequent switching is not possible unless discharge devices are provided.

Practical static var systems

A static var compensation scheme with any desired control range can be formed by using combinations of the elements described above. Several SVS configurations have been successfully applied to meet differing system requirements. The required speed of response, size range, flexibility, losses, and cost are among the important considerations in selecting a configuration for any particular application.

Figure 11.52 shows a typical SVS scheme consisting of a TCR, a three-unit TSC, and harmonic filters (for filtering TCR-generated harmonics). At power frequency, the filters are capacitive and produce reactive power of about 10 to 30% of TCR MVAr rating. In order to ensure a smooth control characteristic, the TCR current rating should be slightly larger than that of one TSC unit; otherwise dead bands arise (see reference 37, Chapter 4).

The steady-state *V/I* characteristic of the SVS is shown in Figure 11.53(a), and the corresponding *V/Q* characteristic is shown in Figure 11.53(b). The linear control range lies within the limits determined by the maximum susceptance (B_{LMX}) of the reactor, the total capacitive susceptance (B_C) as determined by the capacitor banks in service and the filter capacitance. If the voltage drops below a certain level (typically 0.3 pu) for an extended period, control power and thyristor gating energy can be lost, requiring a shutdown of the SVS. The SVS can restart as soon as the voltage recovers. However, the voltage may drop to low values for short periods, such as during transient faults, without causing the SVS to trip.

Within the linear control range, the SVS is equivalent to a voltage source V_{ref} in series with a reactance of X_{SL}. As is evident from Figure 11.43, the slope reactance

X_{SL} has a significant effect on the performance of the SVS. A large value of X_{SL} makes the SVS less responsive, i.e., changes in system conditions cause large voltage variations at the SVS high voltage bus. The value of X_{SL} is determined by the steady-state gain of the controller (voltage regulator). It may also be effected by a current feedback (with PI controller). Its choice should be based on detailed power-flow and stability studies. Typically, the slope is set within the range of 1 to 5%, depending on the ac system strength.

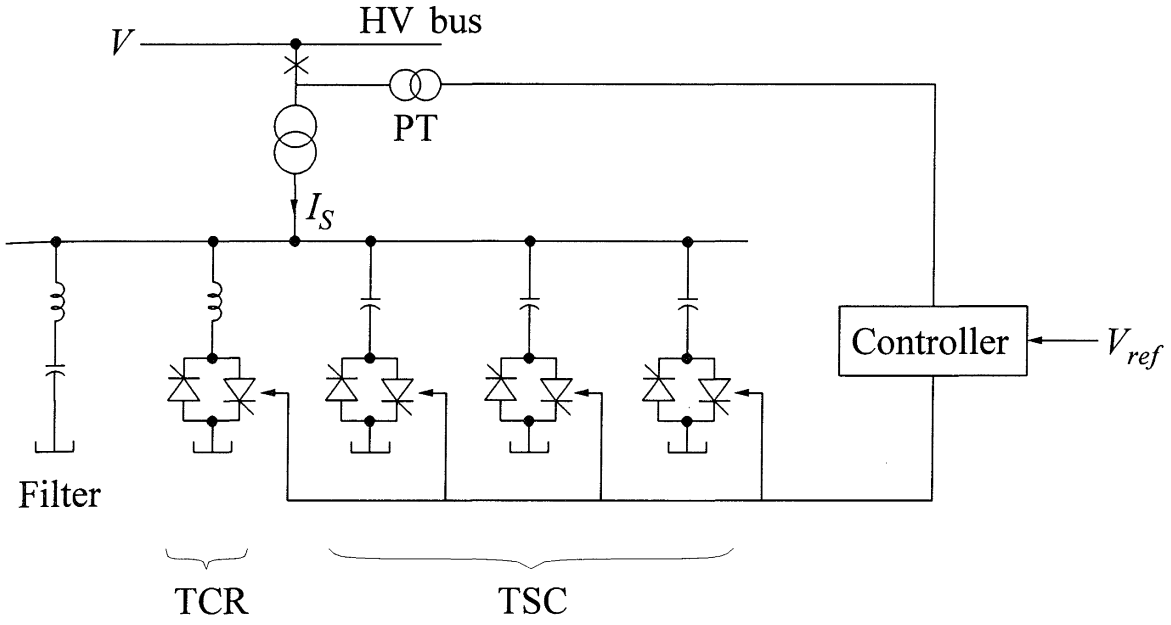
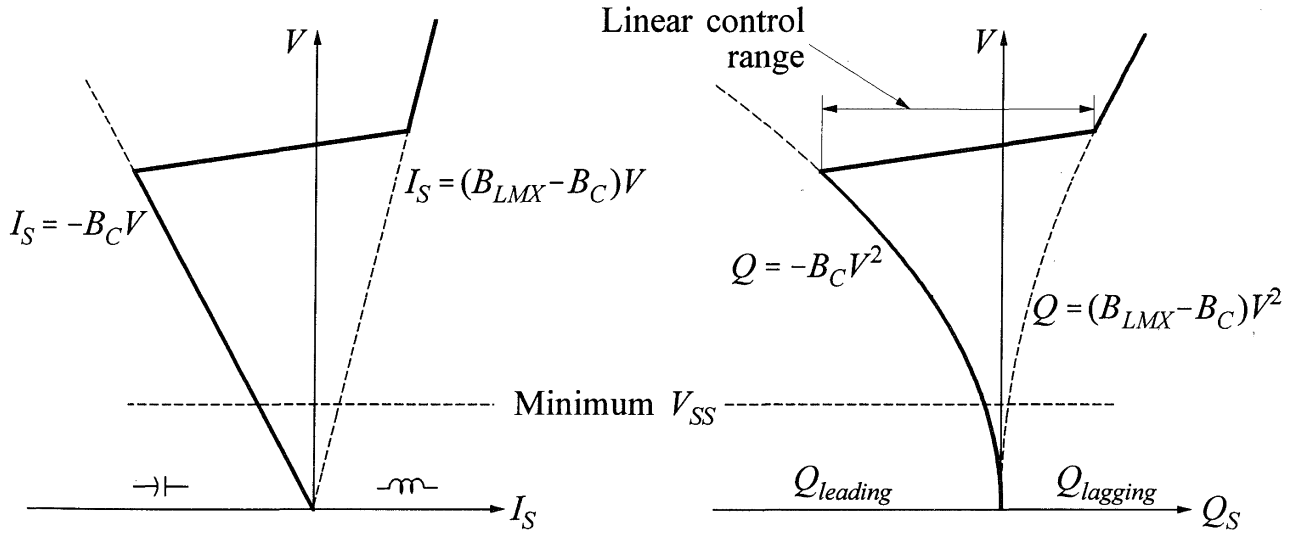


Figure 11.52 A typical static var system



(a) Voltage-current characteristic

(b) Voltage-reactive power characteristic

Figure 11.53 SVS steady-state characteristics

Application of static var compensators

Since their first application in the late 1970s, the use of SVCs in transmission systems has been increasing steadily. By virtue of their ability to provide continuous and rapid control of reactive power and voltage, SVCs can enhance several aspects of transmission system performance. Applications to date include the following:

- Control of temporary (power frequency) overvoltages
- Prevention of voltage collapse
- Enhancement of transient stability
- Enhancement of damping of system oscillations

References 39 to 42 provide details of SVC applications on a number of power systems.

At the subtransmission and distribution system levels, SVCs are used for balancing the three phases of systems supplying unbalanced loads. They are also used to minimize fluctuations in supply voltage caused by repetitive-impact loads such as dragline loads of mining plants, rolling mills, and arc furnaces.

Arc furnaces are a special case of impact loads. They cause voltage fluctuations with frequencies randomly varying between 2 and 10 Hz. These result in flicker of filament lamps in the adjacent load areas. Some electronic equipment and television receivers may also be adversely affected. The term "voltage flicker" is used to describe such rapid fluctuations in voltage. To minimize the adverse effects on the adjacent load areas, the voltage fluctuations must be kept below the acceptable minimum level (typically 0.3%). SVCs provide an effective and economical means of eliminating the voltage flicker problems and have been widely used for such applications since the early 1970s.

11.2.8 Principles of Transmission System Compensation

In the previous sections we have described various devices used for reactive compensation of transmission systems. A well-planned and coordinated application of these devices is essential for the economical design and operation of a reliable system. As reactive compensation affects the steady-state as well as the dynamic performance of the system, detailed power-flow and stability studies are required for establishing appropriate compensation schemes. We will describe the power-flow studies in Section 11.3. Stability studies will be covered in Chapters 12 to 17 in which we consider different aspects of system stability.

In addition to detailed simulations, an understanding of the principles of reactive compensation in transmission systems is invaluable for proper selection and application of the compensating devices. This subject is covered very well by T.J.E.

Miller in reference 37. Here we will briefly review these principles by considering how different forms of compensation affect the performance of a transmission line.

We will first consider the ideal cases of uniformly distributed compensation as they lead to simple relationships which help us to understand the fundamental nature of each type of compensation. We will then consider specific configurations of lumped or concentrated compensation to see how they compare with the ideal cases.

Uniformly distributed fixed series and shunt compensation

In Chapter 6 (Section 6.1) we saw that the line performance is determined by the characteristic impedance Z_C and the electrical length (also referred to as line angle) θ. The objective of compensation is to modify these parameters so as to result in the desired voltage and power transfer characteristics.

Without compensation, assuming a lossless line, the expressions for the two line parameters are

$$Z_C = \sqrt{\frac{L}{C}} = \sqrt{\frac{x_L}{b_C}} = \sqrt{\frac{X_L}{B_C}} \tag{11.38}$$

$$\theta = \beta l \tag{11.39}$$

with the phase constant β given by

$$\beta = \omega\sqrt{LC} = \sqrt{x_L b_C} = \frac{\sqrt{X_L B_C}}{l} \tag{11.40}$$

where

L = series inductance per unit length
C = shunt capacitance per unit length
x_L = series inductive reactance per unit length
b_C = shunt capacitive susceptance per unit length
X_L = total series inductive reactance
B_C = total shunt susceptance
l = line length

Let us designate the corresponding quantities *with compensation* by using a superscript prime ($'$).

With a uniformly distributed *shunt compensation* having a susceptance of b_{sh} per unit length, the effective shunt susceptance is given by

$$b'_C = b_C - b_{sh} = b_C(1 - k_{sh}) \tag{11.41}$$

where k_{sh} is the *degree of shunt compensation* defined as follows:

$$k_{sh} = \frac{b_{sh}}{b_C} \tag{11.42}$$

It is positive for inductive shunt compensation and is negative for capacitive shunt compensation.

The effective values of the characteristic impedance and phase constant with shunt compensation are related to the uncompensated values as follows:

$$Z_C' = \sqrt{\frac{x_L}{b_C'}} = \frac{Z_C}{\sqrt{1-k_{sh}}} \tag{11.43}$$

and

$$\beta' = \beta\sqrt{1-k_{sh}} \tag{11.44}$$

Shunt capacitive compensation in effect decreases Z_C and increases β, whereas shunt inductive compensation increases Z_C and decreases β.

With a uniformly distributed *series capacitive compensation* of C_{se} per unit length, the effective series reactance is

$$\begin{aligned} x_L' &= x_L - \frac{1}{\omega C_{se}} = x_L - x_{Cse} \\ &= x_L(1-k_{se}) \end{aligned} \tag{11.45}$$

where k_{se} is the *degree of series capacitive compensation* defined as follows:

$$k_{se} = \frac{x_{Cse}}{x_L} \tag{11.46}$$

It is positive for capacitive series compensation.

The effective values of characteristic impedance and phase constant with series compensation are given by

$$Z_C' = \sqrt{\frac{x_L'}{b_C}} = Z_C\sqrt{1-k_{se}} \tag{11.47}$$

and

$$\beta' = \beta\sqrt{1-k_{se}} \tag{11.48}$$

Series (capacitive) compensation decreases both Z_C and β.

With *both shunt and series compensation*, the combined effects are as follows:

$$Z_C' = Z_C\sqrt{\frac{1-k_{se}}{1-k_{sh}}} \tag{11.49}$$

$$\beta' = \beta\sqrt{(1-k_{sh})(1-k_{se})} \tag{11.50}$$

The effective line angle (θ') and natural load (P_0') are given by

$$\theta' = \theta\sqrt{(1-k_{sh})(1-k_{se})} \tag{11.51}$$

$$P_0' = P_0\sqrt{\frac{1-k_{sh}}{1-k_{se}}} \tag{11.52}$$

Effect of compensation on line voltage:

Under light load conditions, a flat voltage profile is achieved by inductive shunt compensation. For example, with k_{sh}=1 (100% inductive compensation), θ' and P_0' are reduced to zero and Z_C' is increased to infinity; this results in a flat voltage at zero load.

Under heavy load conditions, a flat voltage can be achieved by adding shunt capacitive compensation. For example, in order to transmit $1.4P_0$ with a flat voltage profile, a shunt capacitive compensation of k_{sh}=−0.96 is required.

Series capacitive compensation may, in theory, be used instead of shunt compensation to give a flat voltage profile, under heavy loading. For example, a flat voltage profile can be achieved at a load of $1.4P_0$ with a distributed series compensation of k_{se}=0.49. In practice, lumped series capacitors are not suitable for obtaining a smooth voltage profile along the line. Obviously, step changes in voltage occur at points where the series capacitors are applied. They do, however, improve voltage regulation at any given point, i.e., voltage changes with load are reduced.

Effect of compensation on maximum power:

In Chapter 6 we developed the expression (Equation 6.51) for power transferred by a line. With compensation, this expression becomes

$$P_R = \frac{E_S E_R}{Z_C' \sin\theta'} \sin\delta \tag{11.53}$$

The maximum power (corresponding to δ=90°) can be increased by decreasing either Z_C', or θ', or both.

The characteristic impedance Z_C' can be decreased with capacitive shunt compensation, but it is accompanied by an increase in the electrical length θ'. On the other hand, inductive shunt compensation decreases θ', but increases Z_C'. Only series capacitor compensation contributes to the decrease of both Z_C' and θ'.

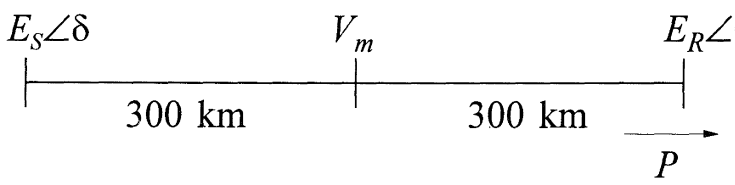
We should, however, recognize that compensation is not required in all cases to satisfy both objectives: (i) increasing P_0', the power level at which the voltage profile is flat, and (ii) decreasing electrical length in order to improve stability. Short lines may require voltage support, i.e., an increase in P_0', even though the inherent electrical length is small. This may be achieved by shunt capacitors, provided that θ' does not become excessive as a result. On the other hand, as we saw in Chapter 6 (see Figure 6.13), lines longer than about 500 km cannot be loaded even up to P_0 because of excessive θ; in such cases, reduction of θ' is the first priority.

Illustrative example

For purposes of illustration, we will consider a lossless 500 kV line having the following parameters:

β = 0.0013 rad/km $\qquad$ Z_C = 250 Ω (P_0 = 1,000 MW)
x_L = 0.325 Ω/km $\qquad$ b_C = 5.2 μS/km

The line is 600 km long and transfers power between two sources as shown in Figure 11.54. The magnitudes of the source voltages are held at 1.0 pu. Our objective is to examine the line performance without and with compensation. We will consider shunt capacitor and series capacitor compensations chosen so as to maintain 1.0 pu midpoint voltage when the power transferred (P) is equal to $1.4P_0$.



$E_S = E_R$ = 1.0 pu
$\theta = \beta l$ = 0.0013×600
= 0.78 rad = 44.7°

Figure 11.54

(a) With *no compensation*, the power-angle relationship is

$$P = \frac{E_S E_R}{Z_C \sin\theta} \sin\delta$$

With E_S and E_R at rated values,

$$\frac{P}{P_0} = \frac{1}{\sin\theta}\sin\delta = \frac{1}{\sin 44.7^\circ}\sin\delta = 1.42\sin\delta$$

Also, considering one half of the symmetrical line, P may be expressed in terms of V_m as

$$P = \frac{E_S V_m}{Z_C \sin(\theta/2)} \sin(\delta/2)$$

$$= P_0 \frac{V_m \sin(\delta/2)}{\sin(44.7^\circ/2)}$$

Hence, the per unit value of midpoint voltage as a function of P is given by

$$V_m = \frac{P}{P_0}\frac{0.38}{\sin(\delta/2)}$$

(b) With *uniformly distributed fixed shunt compensation*, to maintain V_m at 1.0 pu when $P=1.4P_0$, we have

$$1.4P_0 = P_0' = P_0\sqrt{1-k_{sh}}$$

Therefore, $k_{sh}=-0.96$. This will, in fact, result in 1.0 pu voltage throughout the line length at $P=1.4P_0$. The corresponding values of Z_C' and θ' are

$$Z_C' = \frac{Z_C}{\sqrt{1-k_{sh}}} = \frac{250}{\sqrt{1+0.96}} = 178.57 \quad \Omega$$

$$\theta' = \theta\sqrt{1-k_{sh}} = 10.92 \quad \text{rad} = 62.57^\circ$$

The power transferred is given by

$$P = \frac{E_S E_R}{Z_C' \sin\theta'} \sin\delta$$

Hence,

$$\frac{P}{P_0} = \frac{Z_C}{Z_C'}\frac{\sin\delta}{\sin\theta'} = 1.58\sin\delta$$

The midpoint voltage is now given by

$$V_m = \frac{P}{P_0}\frac{Z_C'}{Z_C}\frac{\sin(\theta'/2)}{\sin(\delta/2)} = \frac{P}{P_0}\frac{0.371}{\sin(\delta/2)}$$

(c) With *uniformly distributed fixed series compensation*, to maintain V_m at 1.0 pu when $P=1.4P_0$, we have

$$1.4P_0 = P_0' = P_0/\sqrt{1-k_{se}}$$

Therefore, $k_{se}=0.49$. The line parameters change to

$$Z_C' = Z_C\sqrt{1-k_{se}} = 250\sqrt{1-0.49} = 178.57 \quad \Omega$$

$$\theta' = \theta\sqrt{1-k_{se}} = 0.557 \quad \text{rad} = 31.92°$$

The power transfer and midpoint voltage equations now become

$$\frac{P}{P_0} = \frac{Z_C}{Z_C'}\frac{\sin\delta}{\sin\theta'} = 2.65\sin\delta$$

and

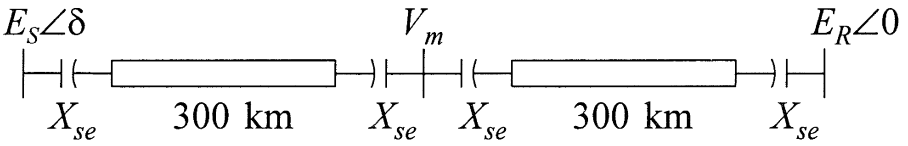
$$V_m = \frac{P}{P_0}\frac{Z_C'}{Z_C}\frac{\sin(\theta'/2)}{\sin(\delta/2)} = \frac{P}{P_0}\frac{0.1964}{\sin(\delta/2)}$$

Next, we consider the performance of lumped shunt capacitor and series capacitor compensations. With lumped compensation, the expression for P-δ and V_m-P relationships cannot be obtained by a simple modification of the corresponding equations for an uncompensated line. We will, therefore, use a power-flow program to analyze the performance of the compensated line.

(d) With *lumped midpoint shunt compensation*, a capacitor bank of 412 MVAr is required to maintain V_m at 1.0 pu when the power transferred is $1.4P_0$.

A distributed shunt compensation of -0.96 represents a total MVAr of about 749. This is nearly twice the MVAr rating of the lumped shunt compensation. The two sources at the ends of the line supply about half of the reactive power compensation required when lumped compensation is used.

(e) With *lumped series compensation*, split into four units (two at the ends and two in the middle of the line), as shown in Figure 11.55, the degree of compensation k_{se} required is 0.505 to maintain V_m at 1.0 pu when the power transferred is $1.4P_0$.



$$X_{se} = 24.625 \ \Omega \qquad k_{se} = \frac{4\times 24.625}{600\times 0.325} = 0.505$$

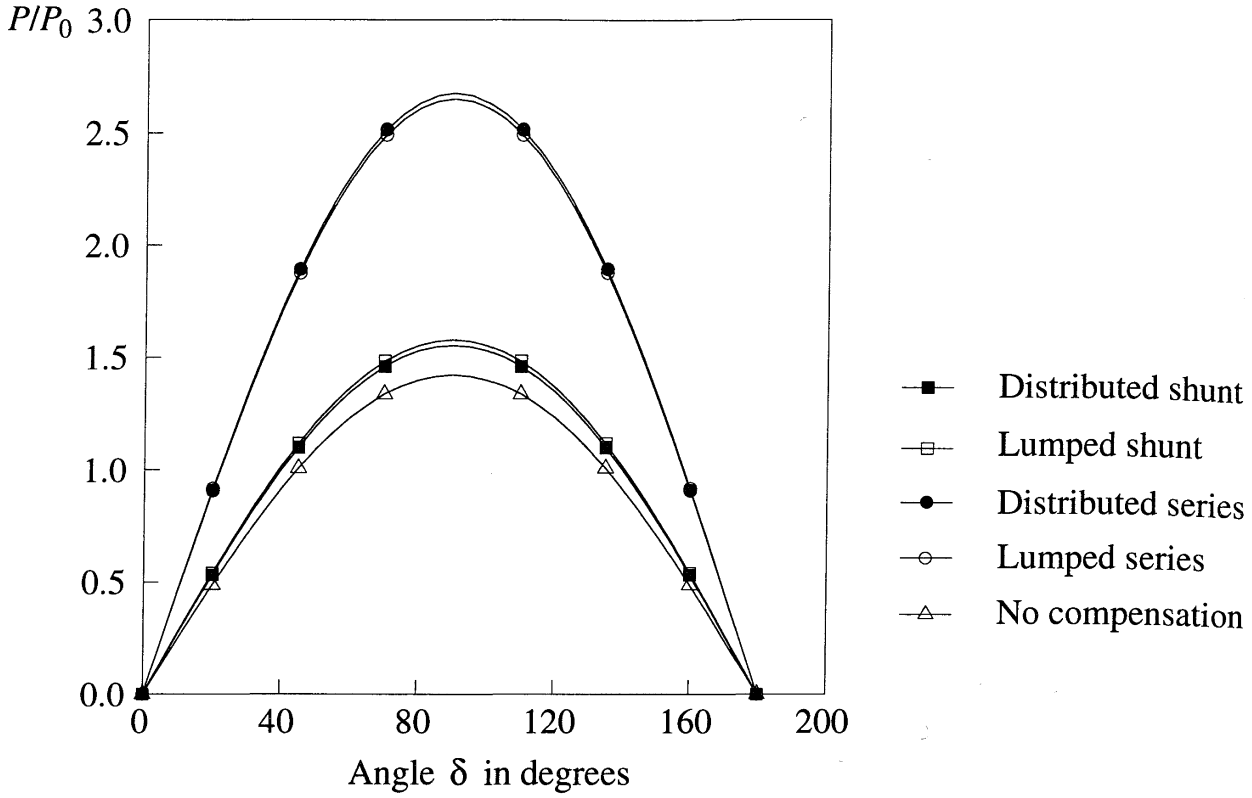
Figure 11.55 Lumped series compensation

Figure 11.56(a) shows plots of power transferred as a function of transmission angle δ for all the five cases we have considered: (a) no compensation, (b) distributed shunt compensation, (c) distributed series compensation, (d) lumped shunt compensation, and (e) lumped series compensation. Plots of midpoint voltage as a function of power transferred for the five cases are shown in Figure 11.56(b). We have considered here a 500 kV line. With line losses neglected and power expressed in per unit of natural power (P_0), the only parameter that has an impact on line performance is β. As noted in Chapter 6, β is practically the same for lines of all voltage levels. Hence, the results presented are generally applicable to a 600 km line of any voltage level.

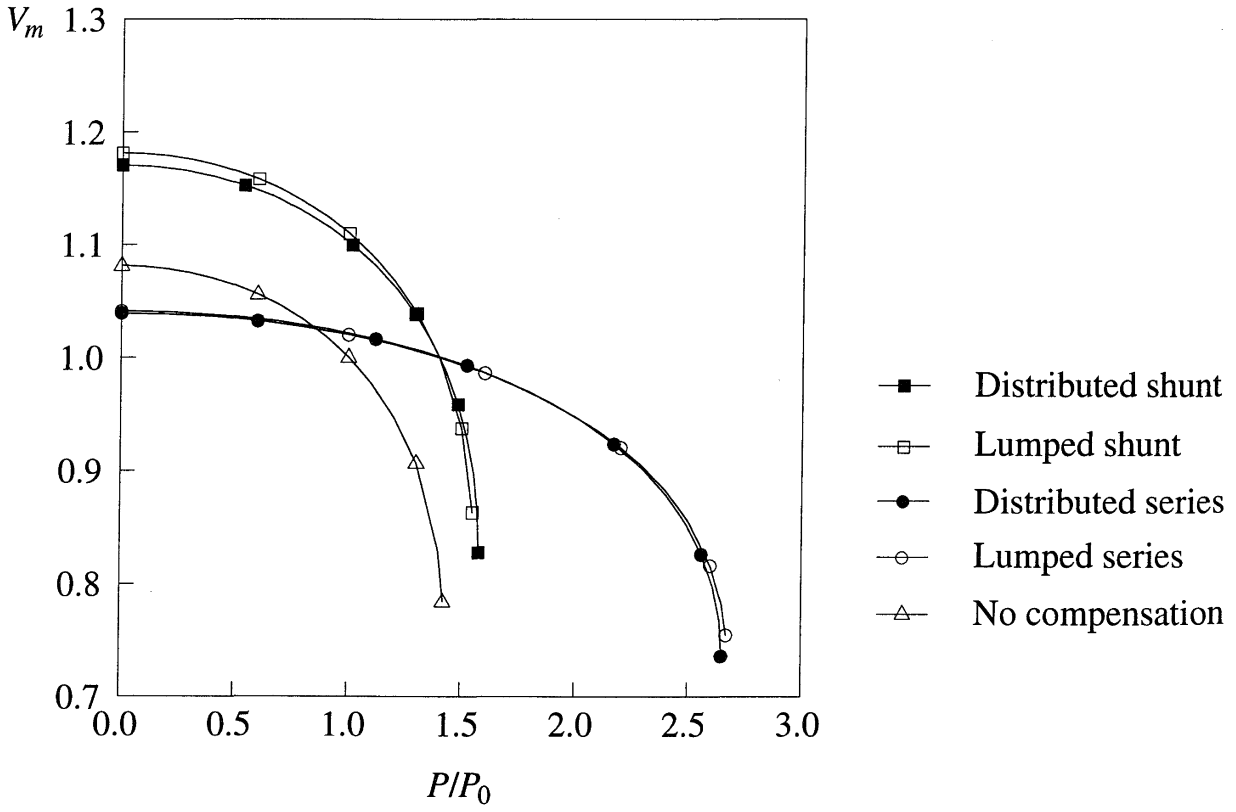
The P-δ and V_m-P characteristics with each type of lumped compensation, for the system considered, are practically identical to the characteristics computed with the corresponding uniformly distributed compensation.

From the results presented in Figure 11.56, we can make some general observations:

1. The shunt capacitor compensation (chosen to keep midpoint voltage at 1.0 pu when $P=1.4P_0$) increases the maximum power capability to 1.58 pu of natural power. This represents an increase of 0.16 pu over the limit of 1.42 pu for the uncompensated case.



(a) Power transfer as a function of transmission angle δ



(b) Midpoint voltage as a function of power transfer

Figure 11.56 Performance of 600 km line with and without compensation

While the shunt compensation has helped maintain the midpoint voltage at the rated values when P is equal to 1.4 pu, the voltage magnitude is very sensitive to variations in power transfer level. For example, when the shunt compensated line is operating near the effective natural load ($1.4P_0$), a small change in power changes the voltage magnitude significantly.

We also see that, when operating at a power transfer level corresponding to V_m of 1.0 pu, the shunt compensated line is much closer to the stability limit than the uncompensated line. Thus, shunt compensation has increased the effective natural load at the expense of stability margin and voltage regulation.

2. The series capacitor compensation (chosen so as to keep midpoint voltage at 1.0 pu when $P=1.4P_0$) increases the maximum transfer capability to 2.65 pu. In addition to nearly doubling the stability limit, the voltage regulation is significantly improved; for example, at $P=1.4P_0$, a large variation in P causes a very small change in V_m.

Uniformly distributed regulated shunt compensation

Consider a shunt compensation in which k_{sh} is continuously *regulated* so that the effective natural load (P_0') is equal to the power transmitted (P) at all times. From Equation 11.53,

$$P = \frac{P_0'}{\sin\theta'}\sin\delta$$

Therefore, when a line is operating at natural load, the transmission angle is equal to the line angle (see Chapter 6, Section 6.1.9). As a result, with continuously regulated shunt compensation, $\theta'=\delta$ at all times. Hence,

$$\frac{P}{\delta} = \frac{P_0'}{\theta'} = \frac{P_0\sqrt{1-k_{sh}}}{\theta\sqrt{1-k_{sh}}} = \frac{P_0}{\theta} = \text{constant} \qquad (11.54)$$

We thus have a *linear* relationship between P and δ, instead of the sinusoidal relationship with fixed or no compensation. This means that the small-signal (steady-state) stability limit with the regulated compensation is infinite. With V_0 denoting the rated line voltage, the slope of the P-δ characteristic is given by

$$\frac{P_0}{\theta} = \frac{V_0^2}{Z_C\theta} = \frac{V_0^2}{X_L} \qquad (11.55)$$

This is equal to the peak of the sinusoidal P-δ characteristic with 100% shunt inductive compensation (k_{sh}=1).

Let us consider the 600 km, 500 kV line for illustration. From Equation 11.54, with δ and θ expressed in radians,

$$\frac{P/P_0}{\delta} = \frac{1}{\theta} = \frac{1}{0.78} = 1.282 \quad \text{pu/rad}$$

This is illustrated in Figure 11.57, which shows P-δ characteristics with uniformly distributed regulated compensation and with fixed distributed shunt compensation of k_{sh}=1.0.

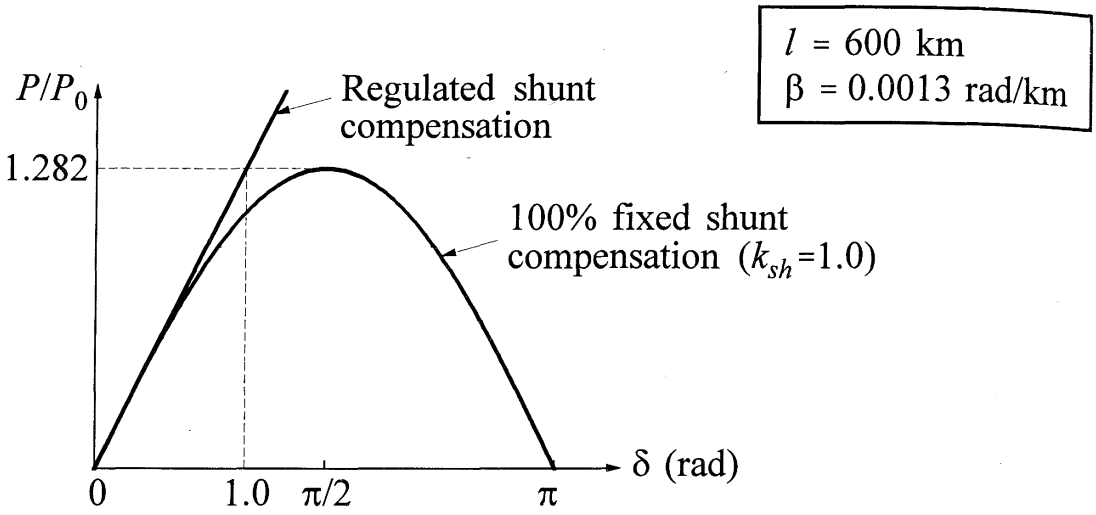


Figure 11.57 Power-angle characteristics of a 600-km line with regulated and shunt inductive compensation

The regulated shunt compensation effectively changes k_{sh} continuously so that $P_0' = P$. For each value of k_{sh}, there is a sinusoidal P-δ characteristic. As the transmitted power P changes, the regulator effectively adjusts k_{sh} so that the operating point shifts from one curve to another in such a way that it lies on a straight line with a positive slope. For satisfactory operation at high power transfer levels, the regulator must be rapid and continuous to prevent movement along the sinusoidal characteristic corresponding to the current value of k_{sh} before moving to the new characteristic.

In practice, this form of compensation can be nearly achieved by placing active compensators, such as synchronous condensers or static var systems, at discrete intervals along the line. The compensators would hold constant voltage equal to V_0 at many points along the line for all load levels; this nearly satisfies the requirement for the effective natural load (P_0') to be equal to the current value of power (P) being transmitted.

The regulators must, however, have sufficient capacity to satisfy the reactive power requirements for maintaining constant voltage at all possible load levels. For the ideal case, the total reactive power supplied or absorbed by the constant voltage regulators is given by

$$\begin{aligned} Q_V &= (V^2\omega C - I^2\omega L)\,l \\ &= P_0\theta\left[1-(P/P_0)^2\right] \end{aligned} \tag{11.56}$$

For P greater than P_0, the reactive power required is capacitive. The reactive power increases as the square of the power transmitted.

Satisfactory performance of such a scheme depends on the ability of all regulators to maintain constant voltage along the line. If one regulator fails or if it reaches a reactive power limit, the stability of the entire system may be affected.

Hydro Quebec's James Bay transmission system [39] uses this form of compensation. It is of historical interest to note that the concept of long distance ac power transmission using distributed regulated shunt compensation was proposed by F.G. Baum as far back as 1921 [43]. He envisioned a 220 kV line having its voltage maintained by synchronous condensers at intervals of about 100 mi. He showed that with equal voltage (within 3%) at all compensator stations, there was virtually no limit to transmission distance.

Regulated compensation at discrete intervals

We will now examine how regulated compensation applied at discrete intervals approximates the performance of uniformly distributed compensation. We will first consider a midpoint compensator as shown in Figure 11.58, and then we extend the analysis to an arbitrary number of compensators.

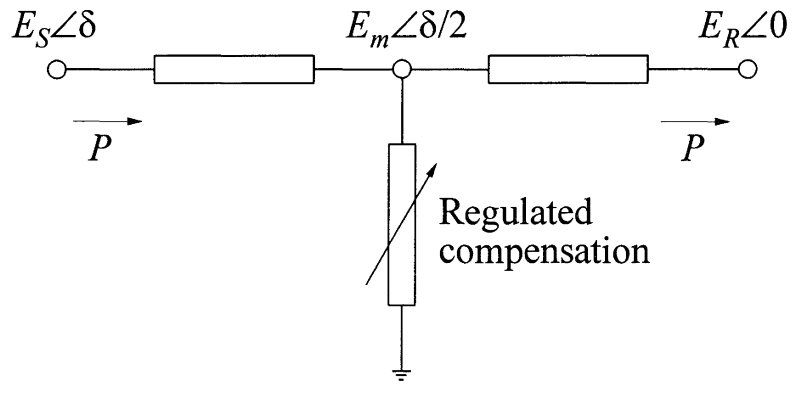


Figure 11.58 Line with midpoint regulated compensation

Midpoint regulated compensation:

The compensating susceptance is continuously varied such that E_m is constant. For simplicity, we will assume that $E_S=E_R=E_m=E$. The line may be considered to be made up of two *independent sections*, each section having a line angle of $\theta/2$, where θ is line angle of the entire line. By applying Equation 11.53 to each section, the expression for power transmitted is

$$P = \frac{E^2}{Z_C \sin(\theta/2)} \sin(\delta/2) \tag{11.57}$$

If E is equal to rated voltage, the expression for P may be expressed in terms of the natural power P_0 of the uncompensated line as follows:

$$P = \frac{P_0}{\sin(\theta/2)} \sin(\delta/2) \tag{11.58}$$

For an uncompensated line, the power transmitted is given by

$$P = \frac{P_0}{\sin\theta} \sin\delta \tag{11.59}$$

The ratio of maximum power that can be transmitted with and without midpoint regulated compensation is

$$\frac{P'_{max}}{P_{max}} = \frac{\sin\theta}{\sin(\theta/2)} \tag{11.60}$$

Table 11.2 lists the values of the above ratio for different line lengths (assuming $\beta=0.0013$ rad/km).

Figure 11.59 shows plots of power versus angle characteristics with and without midpoint regulated compensation for a line length of 600 km ($\theta=44.7°$).

If the regulated compensation has unlimited reactive power capability, it will hold the midpoint voltage through any load level as seen above. On the other hand, if it has a finite size, it can regulate only up to its maximum capacitive output. Its performance beyond this limit depends on the type of device.

Table 11.2

Line Length l (km)	Line Angle θ (degrees)	P'_{max}/P_{max}
200	14.9	1.98
400	29.8	1.93
600	44.7	1.85
800	59.6	1.73
1000	74.5	1.59
1200	89.4	1.42

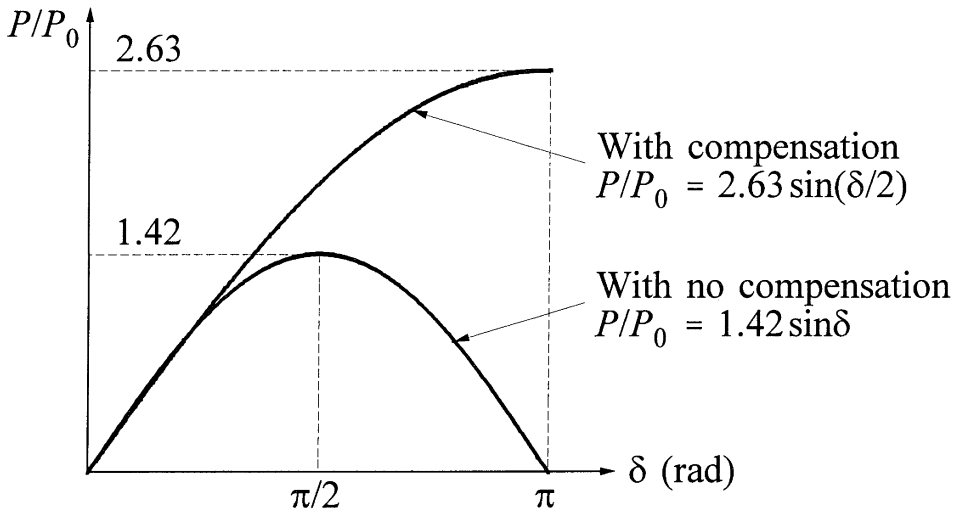


Figure 11.59 Power-angle relationship with and without midpoint regulated compensation

As an example, let us consider an SVS applied to the midpoint of the 600 km line considered above. The SVS performs as a regulated compensation until the reactive power output limit is reached. If the SVS has unlimited capacity, the P-δ characteristic is shown as curve 1 in Figure 11.60. If the SVS has a maximum capacitive rating of 750 MVAr at rated voltage, when the capacitive limit is reached the SVS behaves as a simple capacitor. Thus point A in Figure 11.60 represents the transition from a variable susceptance voltage control operation to a constant-B_{sh} operation represented by curve 2.

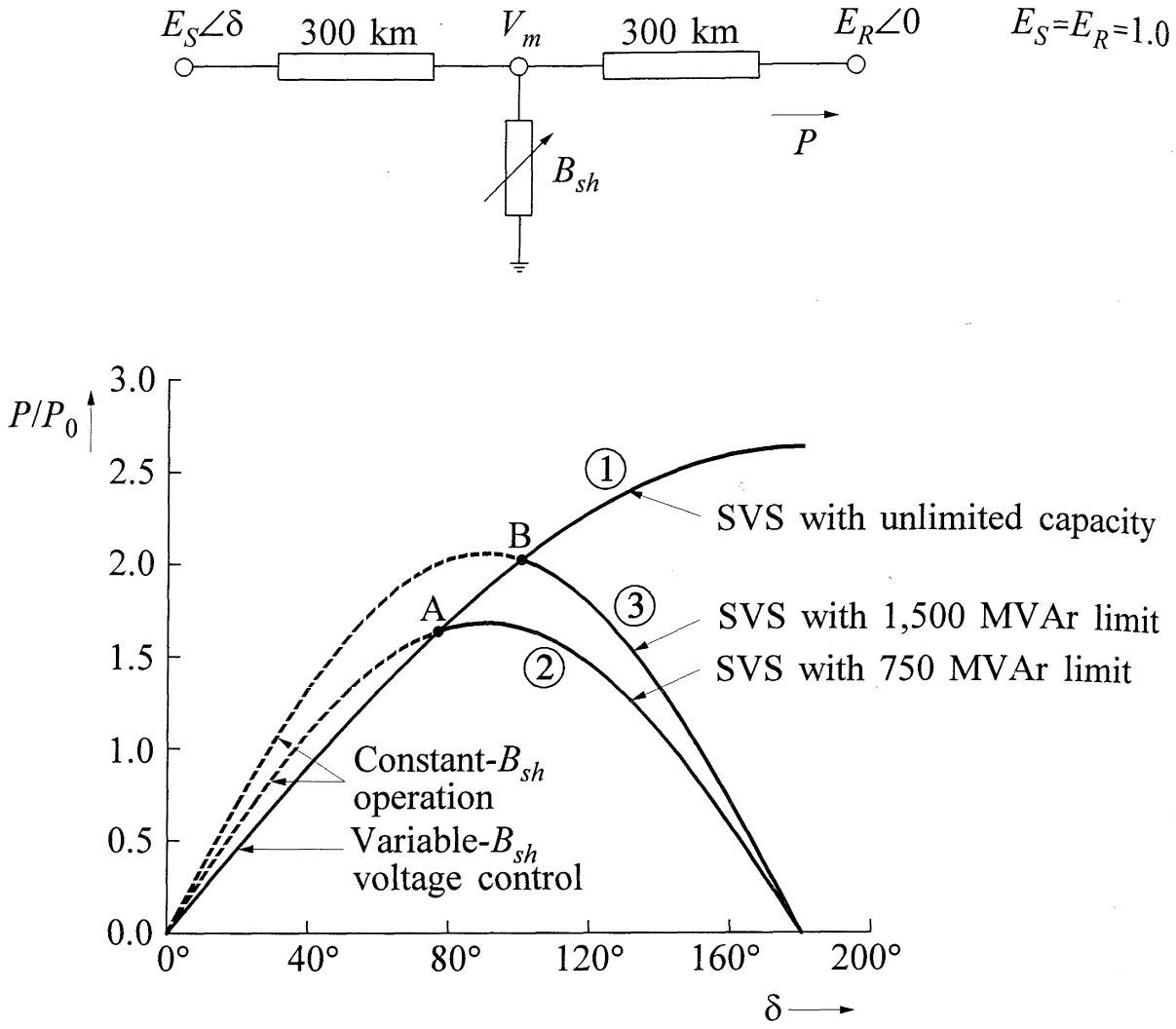


Figure 11.60 Performance of a 600 km line with an SVS regulating midpoint voltage

If the SVS capacitive limit is 1,500 MVAr, the corresponding constant-B_{sh} characteristic is represented by curve 3. In this case, the transition point (B) is on the unstable part (beyond $\delta=90°$) of the power-angle curve. The operation would be unstable immediately following the transition from the variable susceptance mode to the fixed capacitor mode.

With an SVS of unlimited capacity, the maximum power that can be transmitted is $2.63P_0$. However, this is achieved by the SVS supplying very large amounts of reactive power at high values of P. Figure 11.61 shows a plot of the reactive power (Q) supplied (or absorbed) by the SVS to maintain 1.0 pu midpoint voltage as the transmitted power P is varied. The SVS absorbs Q when P is less than P_0, and supplies Q when P is greater than P_0. The Q supplied is not excessive for P less than about $1.4P_0$. Beyond a certain limit, it may not be economical to provide an SVS with the required reactive power capability; it may be cheaper to achieve the desired transmission capability by an alternative means.

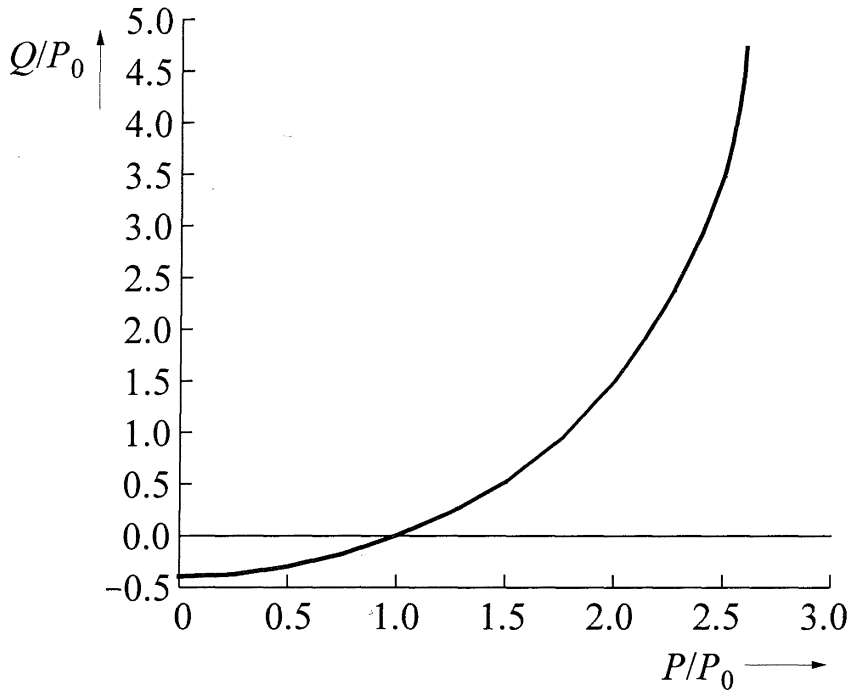


Figure 11.61 Reactive power supplied by SVS as a function of transmitted power

In our analysis, we have neglected the effect of the SVS droop characteristic; that is, we have assumed the slope reactance X_{SL} to be zero. The effect of a finite X_{SL} is to reduce the maximum power and the reactive power requirements.

Arbitrary number of regulated compensators:

We will next consider the general case where $n-1$ regulated compensators are applied to the line at regular intervals so that the line is divided into n independent sections. The power transmitted is now given by

$$P = \frac{P_0}{\sin(\theta/n)}\sin(\delta/n) \tag{11.61}$$

The ratio of maximum power that can be transmitted with and without the compensation is

$$\frac{P'_{max}}{P_{max}} = \frac{\sin\theta}{\sin(\theta/n)} \tag{11.62}$$

Table 11.3 lists the above ratio for different values of n for a line length of 600 km (assuming β=0.0013 rad/km).

Table 11.3

n	θ/n (degrees)	P'_{max}/P_{max}
1	44.70	1.00
2	22.35	1.85
3	14.90	2.74
4	11.17	3.63
6	7.45	5.42
8	5.59	7.22
10	4.47	9.03

Figure 11.62 shows plots of P-δ characteristics for different values of n.

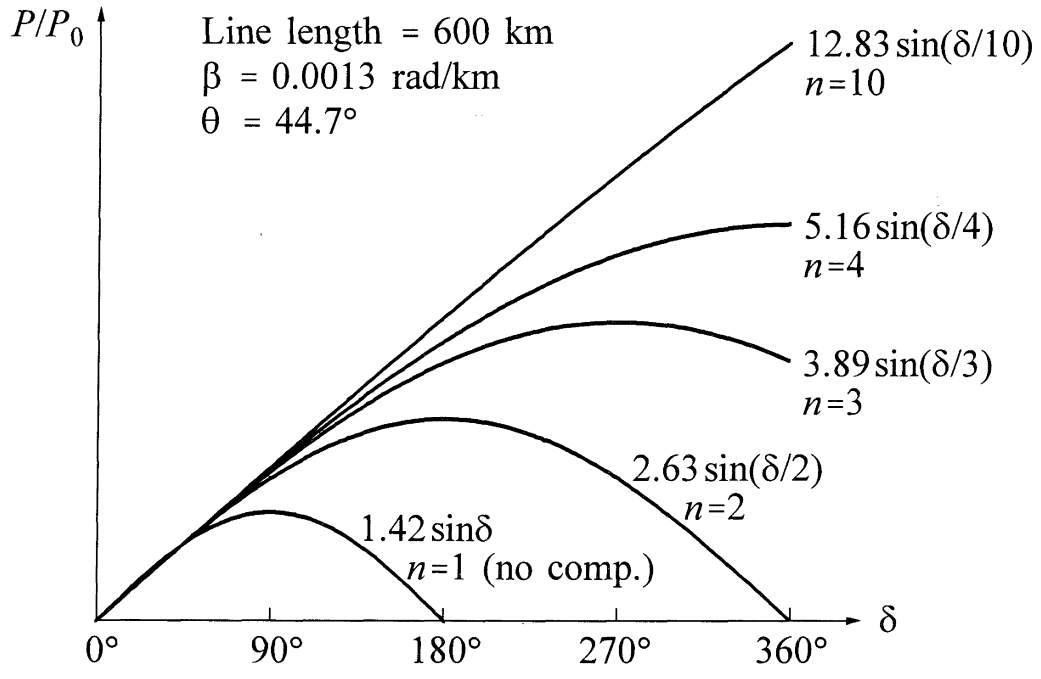


Figure 11.62 Power-angle relationships with regulated compensation at discrete intervals dividing line into n independent sections

Comparative summary of alternative forms of compensation [44-46]

1. Switched shunt capacitor compensation generally provides the most economical reactive power source for voltage control. It is ideally suited for compensating transmission lines if reduction of the effective characteristic impedance (Z'_C), rather than reduction of the effective line angle (θ') is the primary consideration.

   However, heavy use of shunt capacitor compensation could lead to reduction of small-signal (steady-state) stability margin and poor voltage regulation.

2. Series capacitor compensation is self-regulating, i.e., its reactive power output increases with line loading. It is ideally suited for applications where reduction of the effective line angle (θ') is the primary consideration. It increases the effective natural load as well as the small-signal stability limit and it improves voltage regulation. It is normally used to improve system stability and to obtain the desired load division among parallel lines.

   Series capacitor compensation could cause subsynchronous resonance problems requiring special solution measures. In addition, protection of lines with series capacitors requires special attention.

3. A combination of series and shunt capacitors may provide the ideal form of compensation in some cases. This allows independent control of the effective characteristic impedance and the load angle δ. An example of such an application is a long line requiring compensation which, in addition to increasing the effective SIL, causes the phase angle across the line to take a desired value so as not to adversely affect loading patterns on parallel lines.

4. A static var system is ideally suited for applications requiring direct and rapid control of voltage. It has a distinct advantage over series capacitors where compensation is required to prevent voltage sag at a bus involving multiple lines. Since shunt compensation is connected to the bus and not to particular lines, the total cost of the regulated shunt compensation may be substantially less than that for series compensation of each of the lines.

   When an SVS is used to permit a high power transfer over a long distance, the possibility of instability when the SVS is pushed to its limit must be recognized. When operating at its capacitive limit, the SVS becomes a simple capacitor; it offers no voltage control and its reactive power drops with the square of the voltage. Systems heavily dependent on shunt compensation may experience nearly instantaneous collapse when loadings exceed the levels for which the SVS is sized. The ratings of the SVS should be based on very thorough studies which define its total MVAr and the switched and dynamically controlled portions. An SVS has limited overload capability and has higher losses than series capacitor compensation.

11.2.9 Modelling of Reactive Compensating Devices

In power-flow and stability studies, the passive compensating devices (shunt capacitors, shunt reactors, and series capacitors) are modelled as admittance elements of fixed values. They are included in the network admittance matrix (see Chapter 6, Section 6.4.1) along with the other transmission network passive elements.

Synchronous condensers are modelled as synchronous generators but with no steady-state active power output. Except for the fact that there is no prime mover, the representation of a synchronous condenser and the associated excitation system is similar to that for a synchronous generator.

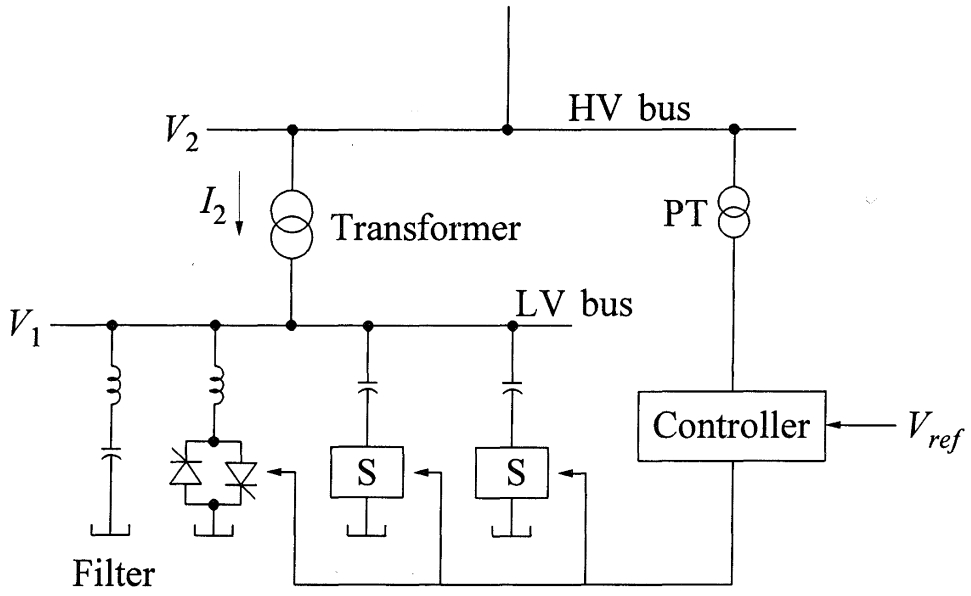
However, special models are required for representing static var compensators.

Modelling of static var systems [36,38,47]

Figure 11.63 shows the schematic diagram of a typical SVS. It consists of a TCR and switched (thyristor or mechanical) capacitors, and has the steady-state characteristic shown in Figure 11.64. The characteristics and modelling of SVSs with different configurations comprising other types of SVCs are conceptually the same.

Representation of SVS in power-flow studies:

From Figure 11.64 we see that the SVS has three possible modes of operation. The corresponding equivalent circuits of the SVS as seen from the HV bus are shown in Figure 11.65.



S = thyristor or mechanically controlled switch

Figure 11.63 Schematic of a typical SVS

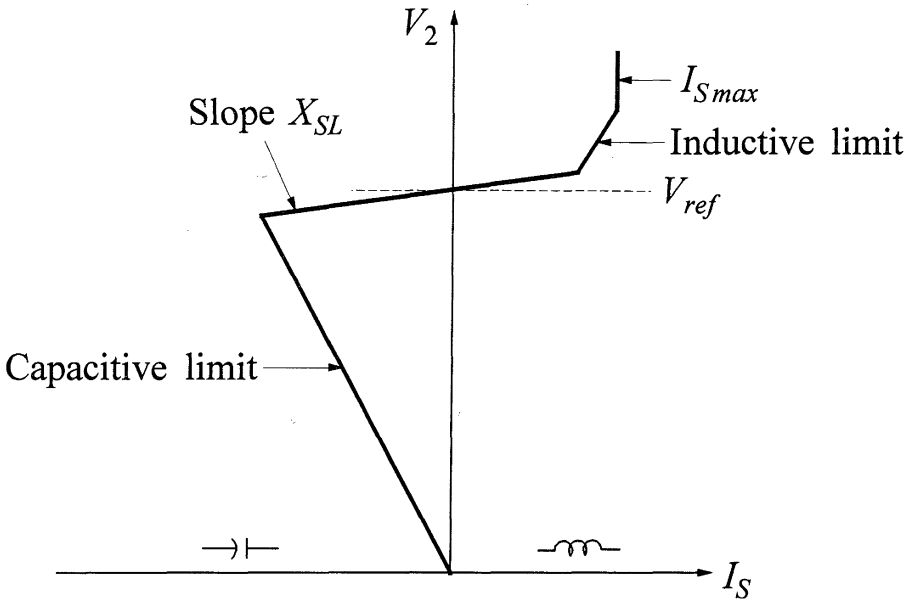
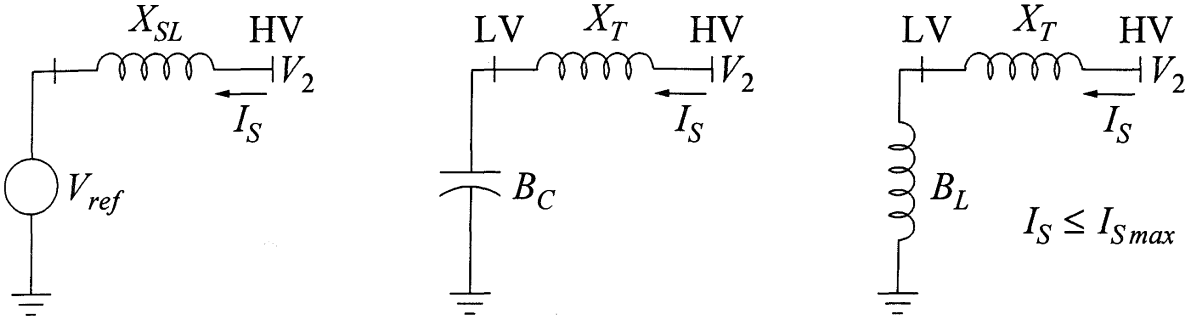


Figure 11.64 Steady-state *V-I* characteristic



(a) Linear control range

(b) Capacitive limit

(c) Inductive limit

Figure 11.65 Steady-state equivalent circuits of an SVS

The normal mode of operation is in the linear control range. In this mode, the SVS as seen from the HV bus is equivalent to a voltage source V_{ref} in series with the slope reactance X_{SL}. When the SVS operation reaches the capacitive limit, it becomes a fixed capacitive susceptance (B_C) connected to the LV bus. The reactance between the LV bus and the HV bus is the transformer leakage reactance X_T. Similarly, when the SVS operation hits the inductive limit, it becomes a fixed susceptance (B_L) whose net value is inductive. The maximum value of the SVS current is limited to I_{Smax}.

For power-flow analysis, the network configuration shown in Figure 11.66 may be used to represent the SVS. The transformer reactance X_T is split into X_{SL} and X_T-X_{SL}, thereby creating a phantom bus (M). This allows proper representation of the SVS while operating in the linear control mode, including the effect of the slope reactance. In this mode, the SVS is represented as a PV bus (with P=0) remotely controlling the bus M voltage equal to V_{ref}.

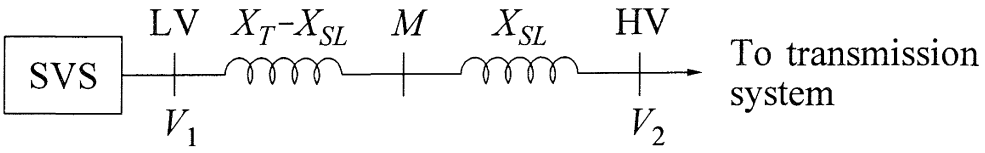


Figure 11.66 SVS representation in power-flow studies

When either of the reactive limits is reached, the SVS becomes a simple susceptance of fixed value connected to the LV bus; bus M voltage is no longer controlled. The SVS current is limited to $I_{S\,max}$.

The above representation accounts for the SVS performance appropriately in all three modes. In addition, it retains the identity of the LV bus to which the SVS is connected.

Representation in stability studies:

Static var systems are usually configured to meet individual system requirements. The control techniques used vary depending on the equipment suppliers and on the vintage of equipment. Therefore, standard stability models capable of representing in detail the wide range of SVSs in use have not been developed. Instead, basic models appropriate for general purpose studies have been recommended by CIGRE [36]. A new set of basic models covering recent developments has been prepared by the IEEE [47]. Such basic models are adequate for general purpose studies in which the special features specific to individual installations do not affect stability analysis. These models may also be used for preliminary studies involving new installations. For detailed studies, however, accurate models reflecting actual controls may be necessary.

Here, we will describe the general approach to modelling of an SVS of the type shown in Figure 11.63. A functional block diagram representation of the SVS is shown in Figure 11.67. The stability model may be developed by identifying the mathematical model for each functional block.

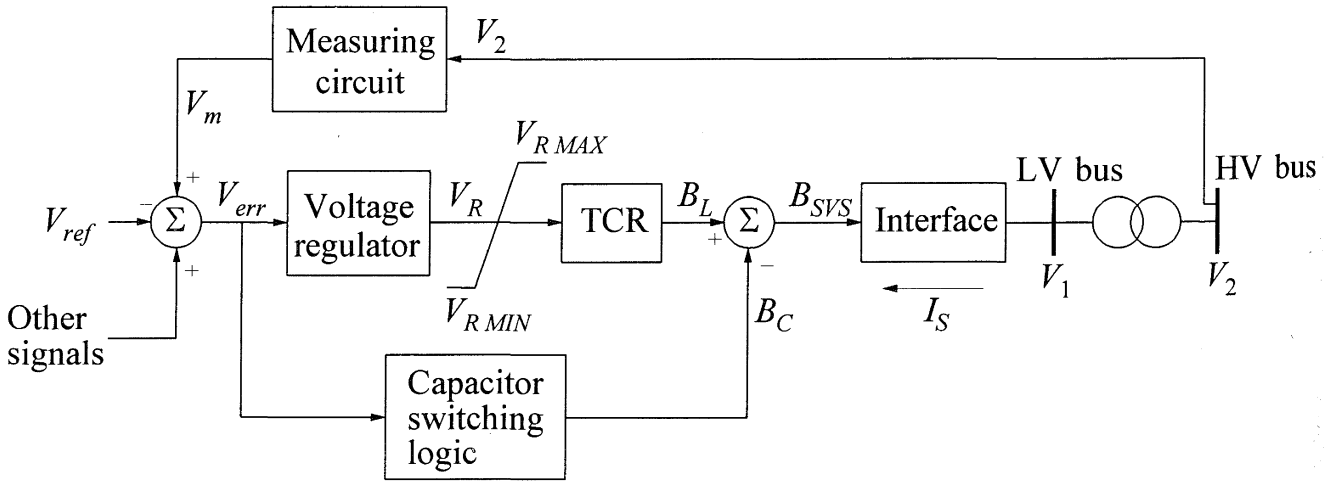


Figure 11.67 SVS functional block diagram

The *thyristor-controlled reactor* (TCR) block represents the variation of reactor susceptance as a function of the firing angle, thyristor firing circuits (Equation 11.36), and linearizing circuit used for compensating the nonlinear relationship between the susceptance B_L and the conduction angle σ. Figure 11.68 shows a model of the TCR block with parameters expressed in per unit with the MVA rating (Q_{TCR}) and kV rating of the TCR as base values. The conduction angle σ is in per unit on a base of 180°.

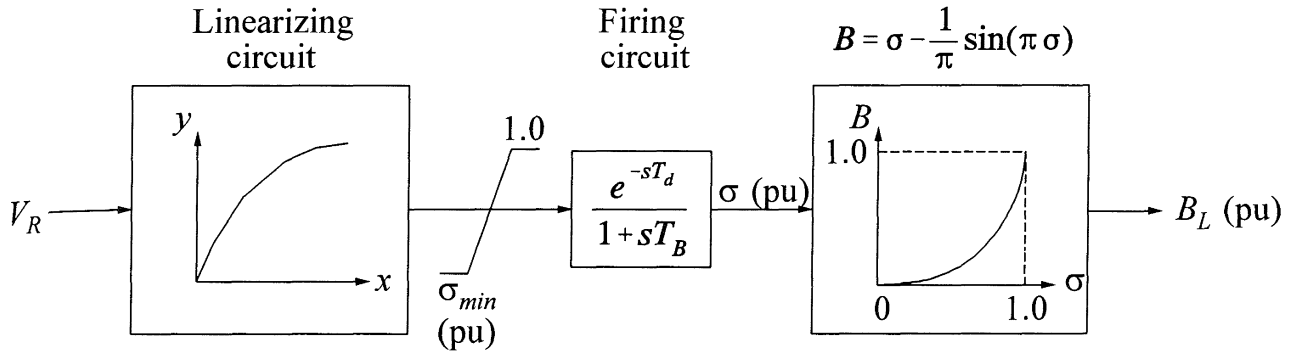


Figure 11.68 Model of TCR block

The limits shown in the firing circuit block represent the limits on the conduction angle, which in turn determine the limiting values of B_L. In per unit, the maximum value of B_L is 1.0. Typically, the minimum value of B_L for a TCR is 0.02 pu; it may be assumed to be zero. The parameter T_d is the gating transport delay; it has a value of about 1 ms and is normally neglected, making $e^{-sT_d} \approx 1.0$. The time constant T_B associated with the thyristor firing sequence control has a value of about 5 ms; it may also be neglected for most studies.

If the nonlinear relationship between σ and B_L is assumed to be perfectly compensated and T_d and T_B are neglected, the TCR block may be represented by a unit gain with limits as shown in Figure 11.69.

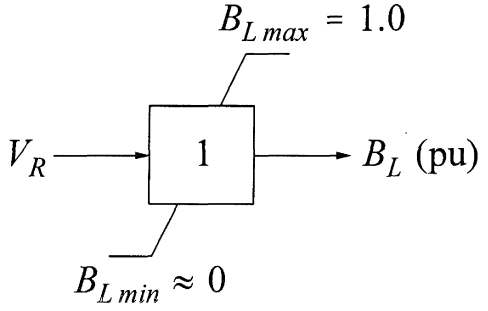


Figure 11.69 Simplified model of TCR block

The structure of the *voltage regulator* block in Figure 11.67 is very much dependent on the particular application as it provides a means of optimizing the SVS dynamic performance. Figure 11.70 shows models of two commonly used forms of regulators.

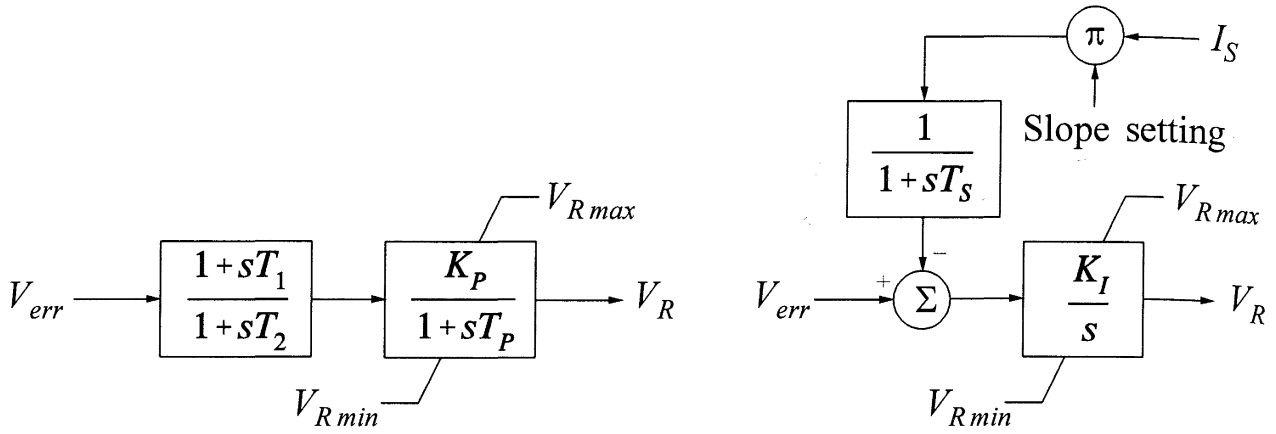


Figure 11.70 Voltage regulator models

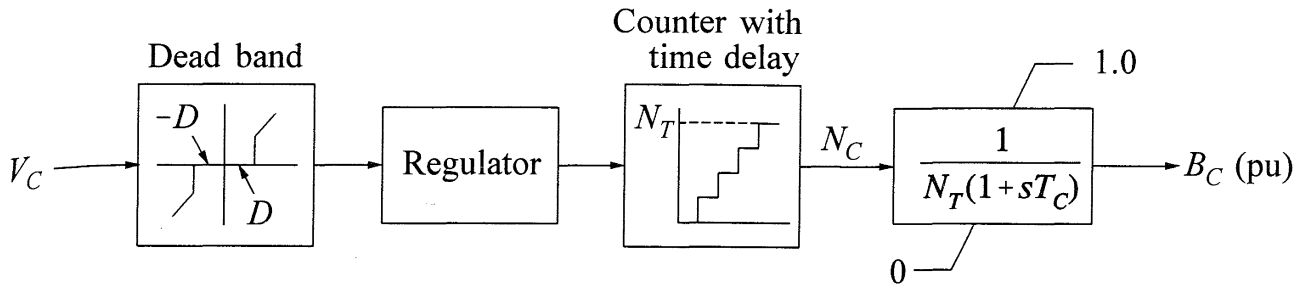
With the proportional type regulator shown in Figure 11.70(a), the gain K_P is the reciprocal of the droop characteristic, i.e., the slope reactance X_{SL}. The time constant T_P is usually in the range of 50 ms to 100 ms. Figure 11.70(b) shows an integral type regulator. The droop characteristic is obtained through feedback of SVS current. The limiters associated with both forms of regulators are of the non-windup type.

The *measuring circuit* block in Figure 11.67 includes instrument transformers, A/D converters, and rectifiers. It contains a transport delay and time constants which are very small. Consequently, the measuring circuit may be represented by a simple time constant on the order of 5 ms or as a unit gain.

The *capacitor-switching logic* may be represented by a switching sequence depending on the means used for switching, i.e., mechanical or thyristor switches. The intelligence used for switching depends on the requirements of the particular application.

Figure 11.71 shows a model suitable for representing a thyristor switched capacitor (TSC) with parameters expressed in per unit with the MVA rating (Q_{TSC}) and kV rating of the TSC as base values. In the model, T_C is the time constant associated with the thyristor sequence control.

In the model shown, N_T is the total number of individually switched capacitor bank units (assumed to be of equal size), N_C is the number of units switched in at any given time, and T_C is a time constant associated with the thyristor firing sequence control. The control signal V_C attempts to maintain V_2 within a narrow band, with the control action coordinated with that of the TCR.



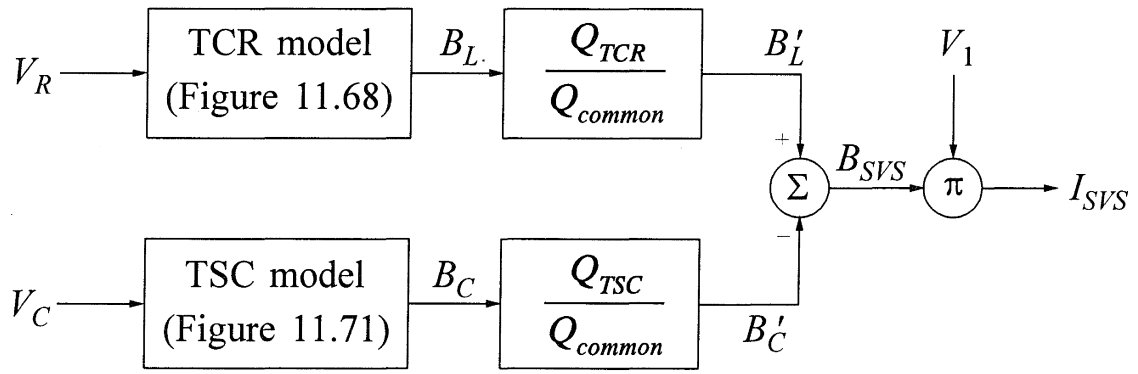
MVA base = Q_{TSC} = TSC MVAr rating

Figure 11.71 TSC model

Figure 11.72 shows the per unit representation of a combined TCR and TSC system. TCR and TSC are each modelled by using a per unit system with their respective MVAr ratings as base MVA. The susceptances B_L and B_C are converted to the common per unit system (usually with 100 MVA base) used to model the entire power system. In Figure 11.72, the net susceptance B_{SVS} and the total SVS current are expressed in the common per unit system. The net susceptance B_{SVS} is inductive if positive, and is capacitive if negative. The current into the SVS represented by I_{SVS} is positive when inductive (load convention). This is consistent with the convention commonly used for representing the *V-I* characteristic of the SVS (Figure 11.64).

For most system studies, it is not necessary to represent a TSC explicitly as shown in Figure 11.72. The TSC response may be assumed to be instantaneous, and the SVS is represented by a TCR and an FC with the MVAr ratings appropriately selected.

With a fixed capacitor there is no switching logic; the susceptance B_C has a fixed value. Figure 11.73 shows a simplified model of an SVC consisting of a TCR and a fixed capacitor. The TCR is assumed to have a proportional type regulator. The parameters are in per unit with TCR ratings as base values.



Q_{TCR} = MVAr rating of TCR
Q_{TSC} = MVAr rating of TSC
Q_{common} = common MVA base
V_1 = LV bus voltage

Figure 11.72 Combined TCR and TSC representation

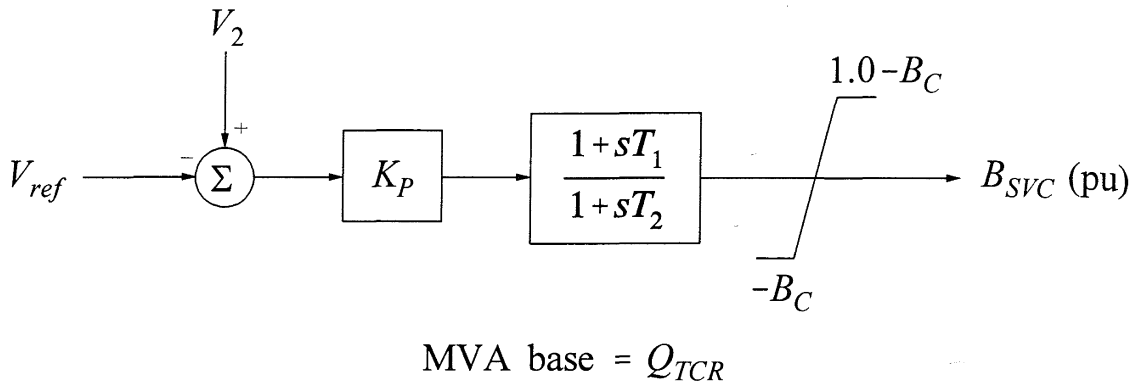


Figure 11.73 Simplified model of an SVC comprising a TCR and an FC

In addition to the feedback of HV bus voltage to control the SVS, additional signals may be used to enhance system stability.

11.2.10 Application of Tap-Changing Transformers to Transmission Systems

Transformers with tap-changing facilities constitute an important means of controlling voltage throughout the system at all voltage levels. In Chapter 6, we discussed the principle of operation and modelling of tap-changing transformers. Here we will consider how they are used to control voltage and reactive power at the transmission system level.

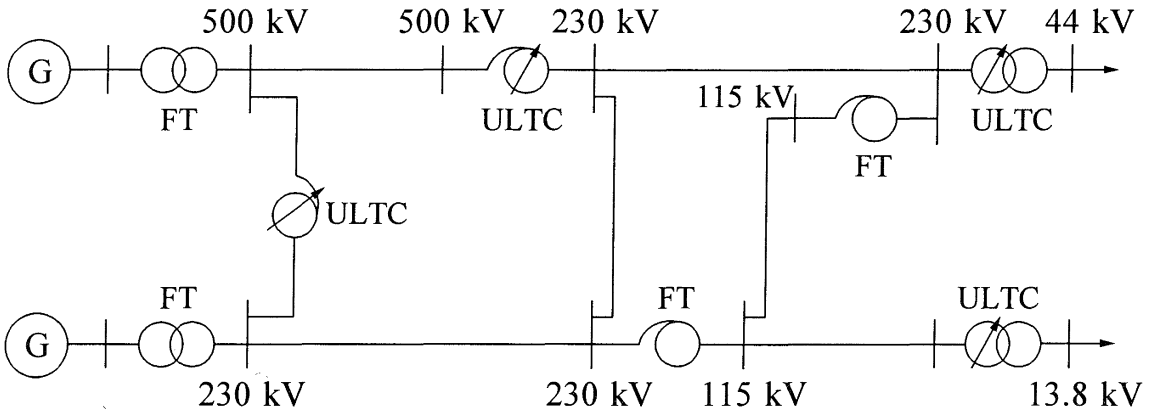
Autotransformers used to change voltage from one subsystem to another (for example, 500 kV to 230 kV) are often furnished with under-load tap-changing (ULTC) facilities. These may be controlled either automatically or manually. Usually there are many such transformers throughout the network interconnecting transmission systems of different levels. The taps on these transformers provide a convenient means of controlling reactive power flow between subsystems. This in turn can be used to control the voltage profiles, and minimize active and reactive power losses.

The control of a single transformer will cause changes in voltages at its terminals. In addition, it influences the reactive power flow through the transformer. The resulting effect on the voltages at other buses will depend on the network configuration and load/generation distribution. Coordinated control of the tap changers of all the transformers interconnecting the subsystems is required if the general level of voltage is to be changed.

During high system load conditions, the network voltages are kept at the highest practical level to minimize reactive power requirements and increase the effectiveness of shunt capacitors and line charging. The highest allowable operating voltage of the transmission network is governed by the requirement that insulation levels of equipment not be exceeded, taking into consideration possible switching operations and outage conditions. During light load conditions, it is usually required to lower the network voltages to reduce line charging and avoid underexcited operation of generators.

Transformers with off-load tap-changing facilities can also help maintain satisfactory voltage profiles. While transformers with ULTC can be used to take care of daily, hourly, and minute-by-minute variations in system conditions, settings of off-load tap-changing transformers have to be carefully chosen depending on long-term variations due to system expansion, load growth, or seasonal changes. Optimal power-flow analysis provides a convenient method of determining appropriate tap settings with either type of tap-changing facility [49-51].

Utility practices with regard to application of ULTC transformers to transmission systems vary widely. For example, Ontario Hydro's practice is to provide ULTC facilities on most 500/230 kV autotransformers and on all "area supply" transformers stepping down from 230 kV or 115 kV to 44 kV, 27.6 kV, or 13.8 kV. All 230/115 kV autotransformers and generator step-up transformers are provided with off-load tap-changing facilities. Figure 11.74 illustrates the general arrangement.



FT = Fixed tap or off-load tap changing
ULTC = Under-load tap changing

Figure 11.74 Single-line diagram of transmission network illustrating transformer tap change facilities

As an additional example, the practice in the United Kingdom is to provide ULTC on all generator step-up transformers and on autotransformers connecting a 400 kV or 275 kV "supergrid network" to a 132 kV or 66 kV "secondary network." Autotransformers connecting the 400 kV and 275 kV networks have fixed ratios.

Many utilities, on the other hand, do not provide for under-load tap changing of transmission network autotransformers.

11.2.11 Distribution System Voltage Regulation [25,48]

Automatic voltage regulation of distribution systems is provided by using one or more of the following methods:

- Bus regulation at the substation
- Individual feeder regulation in the substation
- Supplementary regulation along the feeders

Substation bus regulation

A distribution substation transformer is usually equipped with ULTC equipment that automatically controls the secondary voltage. Alternatively, the substation may have a separate voltage regulator that regulates the secondary side bus voltage.

Bus regulation generally employs three-phase units, although single-phase regulators could be used in applications where phase voltages have a significant unbalance.

Feeder regulation

Feeder voltage regulators control the voltage of each feeder. Either single-phase units or three-phase units may be used, the former being more common. Single-phase regulators are necessary when the individual phases serve diverse forms of loads. Three-phase regulators can provide the same high quality performance as the single-phase regulators, when the phases are similarly loaded and when the supply voltage is balanced.

If there are several feeders supplied by a substation, feeders with similar characteristics may be grouped, and a common regulator may be used to control the voltages of each group of feeders.

In applications where the feeders are very long, additional regulators and shunt capacitors located at selected points on the feeders provide supplementary regulation.

Feeder regulators are also sometimes referred to as booster transformers. A conventional transformer with ULTC performs two functions: voltage transformation and voltage control. Feeder voltage regulators perform only the latter function; that is, they buck or boost the voltage without changing the basic voltage level.

Types of feeder regulators

There are two basic types of feeder voltage regulators: the induction type and the step type. The following is a brief description of their operating principles.

Induction voltage regulator:

Figure 11.75 shows a schematic of an induction voltage regulator. It consists of two sets of windings: (a) primary winding wound on the rotor and connected across the line, and (b) regulating winding wound on the stator and connected in series with the line.

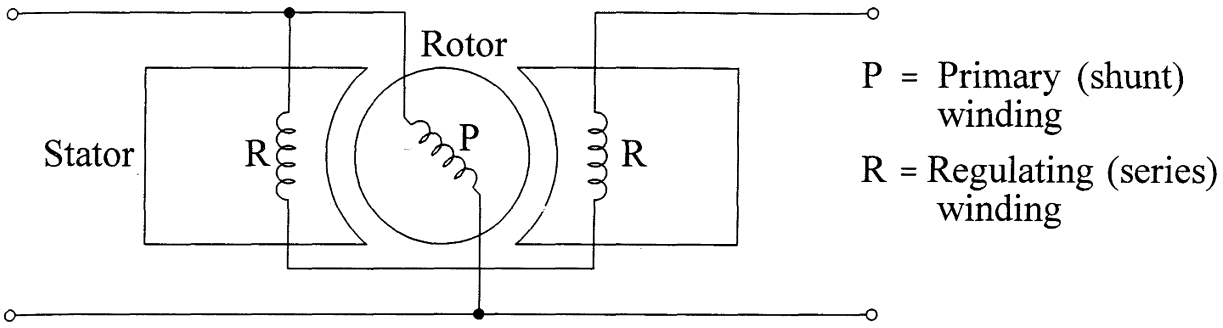


Figure 11.75 Schematic of an induction regulator

The voltage induced in the regulating series winding is added to the primary winding to give the output voltage. The magnitude and polarity of the induced voltage depend on the relative orientation of the regulating winding with respect to the primary winding. By changing the rotor position, the output voltage can be varied between the maximum and minimum limits. The position of the rotor is controlled by an electric motor which responds to a control signal.

The induction regulator provides accurate and continuous control, and performs reliably. Many of the older regulators in service are of this type. It is, however, costly and has been largely superseded by the step type regulator.

Step voltage regulator (SVR):

The step voltage regulator is basically an autotransformer with taps or steps in the series winding, as shown in Figure 11.76. However, it is purely a voltage control device; that is, it is not used for voltage transformation.

The voltage induced in the series winding is either added to or subtracted from the primary voltage depending on the polarity of the series winding. A reversing switch (RS) is provided to change this polarity. The series-winding output voltage magnitude is varied by changing the tap position, which can be done under load.

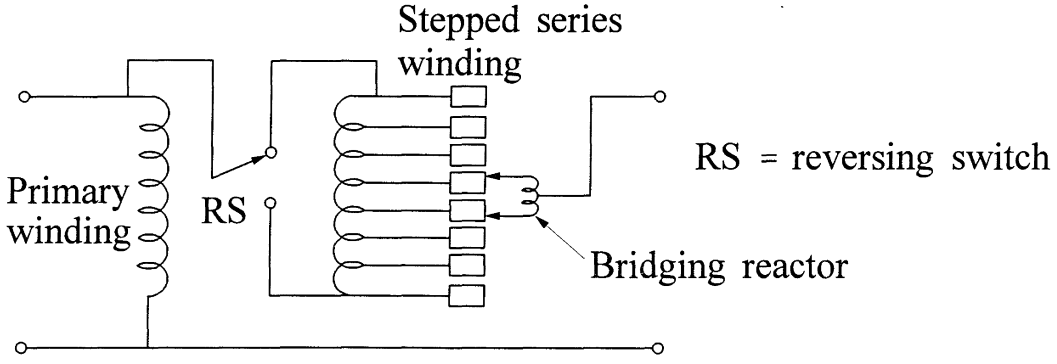


Figure 11.76 Schematic of a step voltage regulator

Typically, the SVR has provision for correcting the voltage by ±10% in 32 steps, each step representing a 5/8% change in voltage. This is achieved by tapping the series winding into eight equal parts, with each part providing one-eighth of the 10% change in voltage. The output terminal is connected to the centre tap of the bridging reactor associated with the tap-changing mechanism. This in effect further divides each step into two equal parts, giving a total of 16 steps of 5/8% each. The reversing switch allows the regulator to raise as well as lower the output voltage, covering a range of plus or minus 10% voltage regulation in a total of 32 steps.

Figure 11.77 shows the major elements of the SVR control mechanism. The SVR is set to hold a constant voltage (within a narrow range) at its secondary terminals or at some selected point out on the feeder as determined by the settings (R and X) of the *line drop compensator*. The voltage sensor compares the input voltage to a preset voltage level. If the input voltage deviates from the setpoint beyond a tolerance or spread for a certain time, the tap-changing motor operates the tap-changing mechanism in a direction so as to bring the voltage back to within a narrow range. This range is called the "bandwidth," and is typically ±2% around the setpoint. The time delay, which is adjustable, prevents the regulator from responding to temporary or self-correcting voltage variations. The time delay setting for the first tap movement can range from 30 to 60 seconds; a 30 seconds setting is typical [48].

The time taken by the tap-changing mechanism for each additional tap movement is in the 2 to 8 seconds range, with 6 seconds being a typical value. Thus, a change from the neutral tap position to full boost or buck takes about 2 minutes.

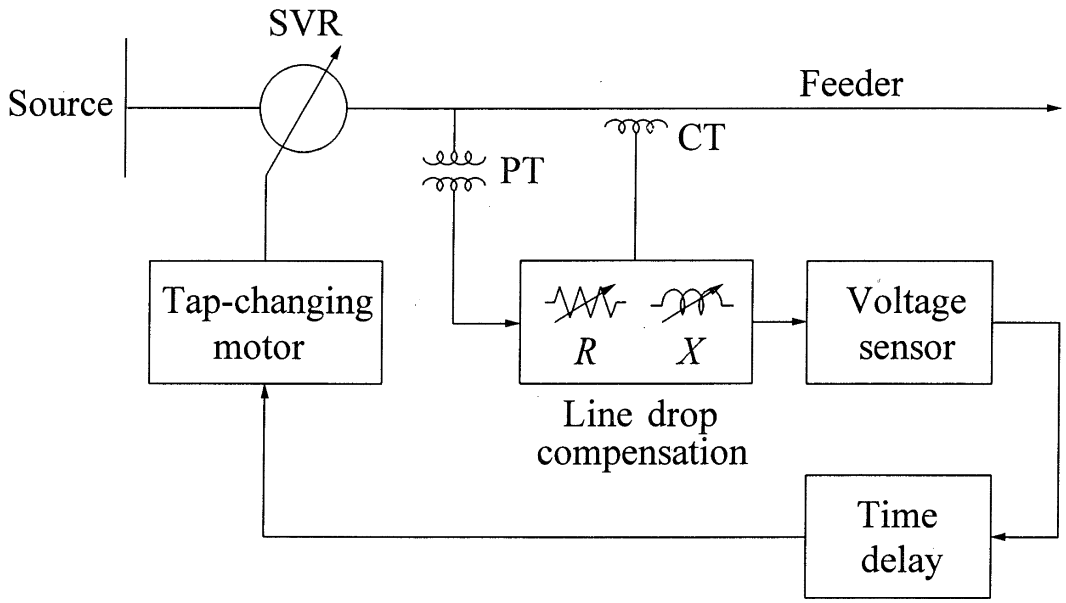


Figure 11.77 SVR control mechanism

Application of voltage regulators and capacitors

Figure 11.78 illustrates the application of regulators and shunt capacitors for control of voltage profile along a feeder. Curve 1 shows the voltage profile with a fairly evenly distributed load along the line, without any regulator or capacitor. The voltage for most parts of the feeder is seen to be below the permissible minimum value. The addition of a voltage regulator (R_1) moves the voltage profile up, as shown by curve 2. A capacitor bank (C), located at approximately two-thirds of the feeder length from the substation, moves the voltage profile to curve 3. The addition of a supplementary regulator (R_2) at approximately one-third of the feeder length from the substation will bring the voltage profile along the entire length of the feeder (from the first consumer to the last) to within the maximum and minimum permissible limits.

For very long feeders, it may be necessary to use two regulators in cascade. One regulator is placed at approximately the middle of the feeder and the other regulator at about one-fifth the distance from the station end. In such cases, it is necessary to ensure proper sequence of operation of the two regulators by setting the time delay of the regulator farther from the station longer than that for the closer regulator. Typical settings are 30 seconds for the regulator closer to the station and 40 seconds for the other regulator.

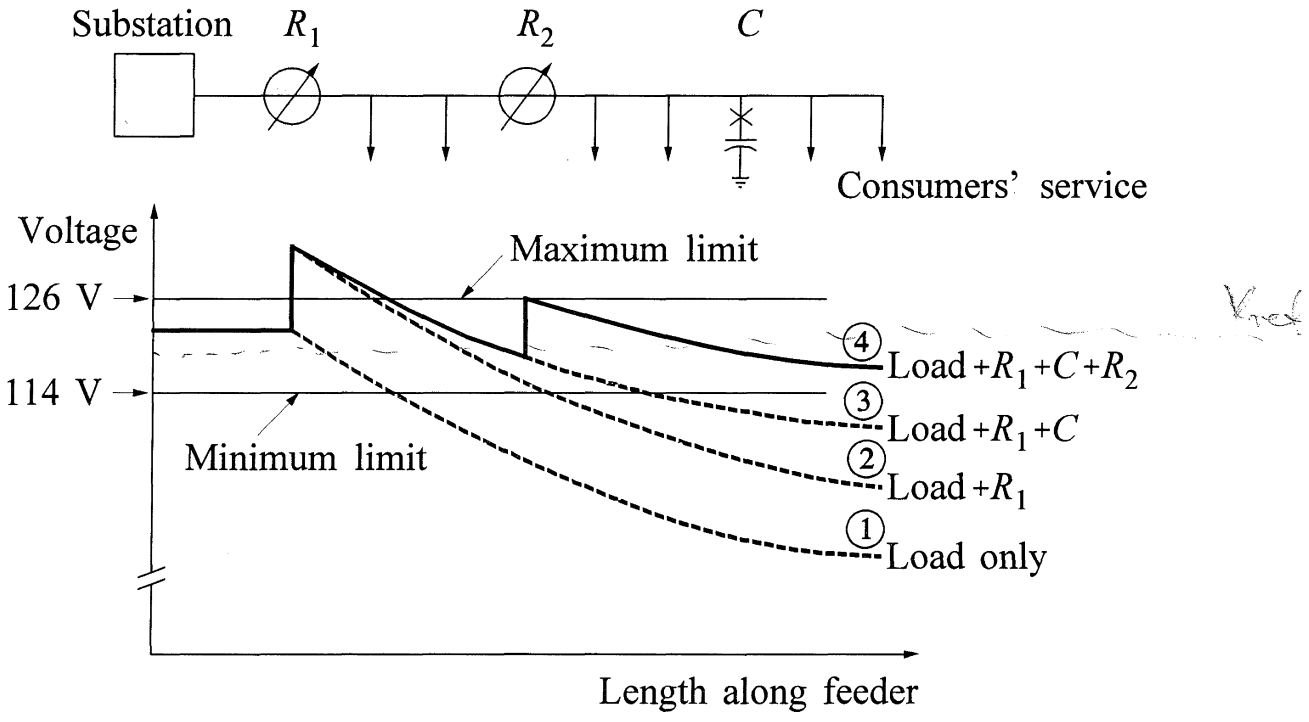


Figure 11.78 Voltage profile of a feeder with a station regulator (R_1), supplementary regulator (R_2) and a shunt capacitor bank (C)

11.2.12 Modelling of Transformer ULTC Control Systems

Modelling of transformers with tap-changing facilities is described in Chapter 6 (Section 6.2). Here we will focus on models for the control systems used for automatically changing transformer taps under load.

The functional block diagram of the control system is shown in Figure 11.79. It consists of the following basic elements [52]:

(a) Tap-changing mechanism driven by a motor unit

(b) Voltage regulator consisting of a measuring element and a time-delay element

(c) Line drop compensator

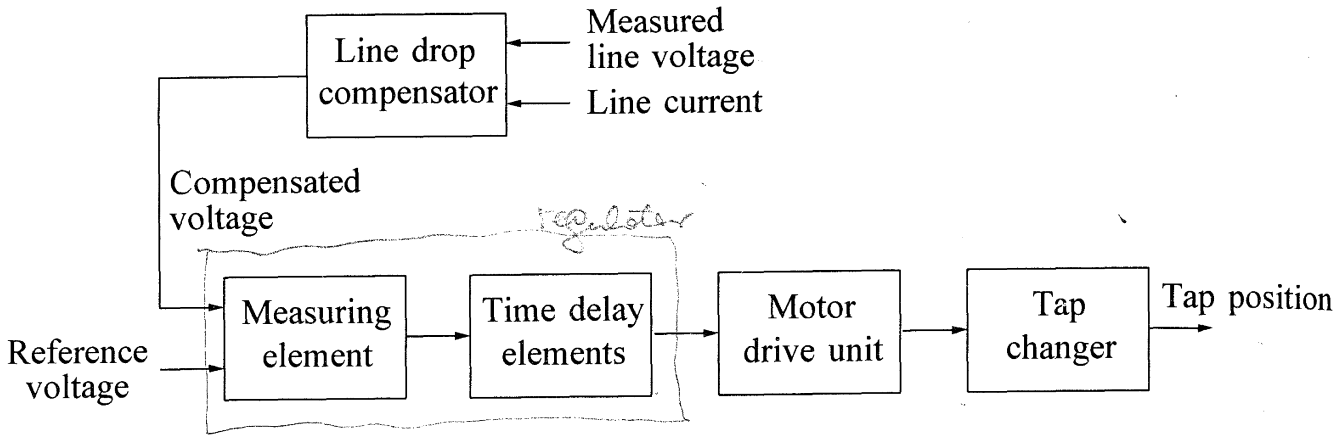


Figure 11.79 Functional block diagram of control system for automatic changing of transformer taps

Figure 11.80 shows the block diagram of the ULTC control system suitable for system studies.

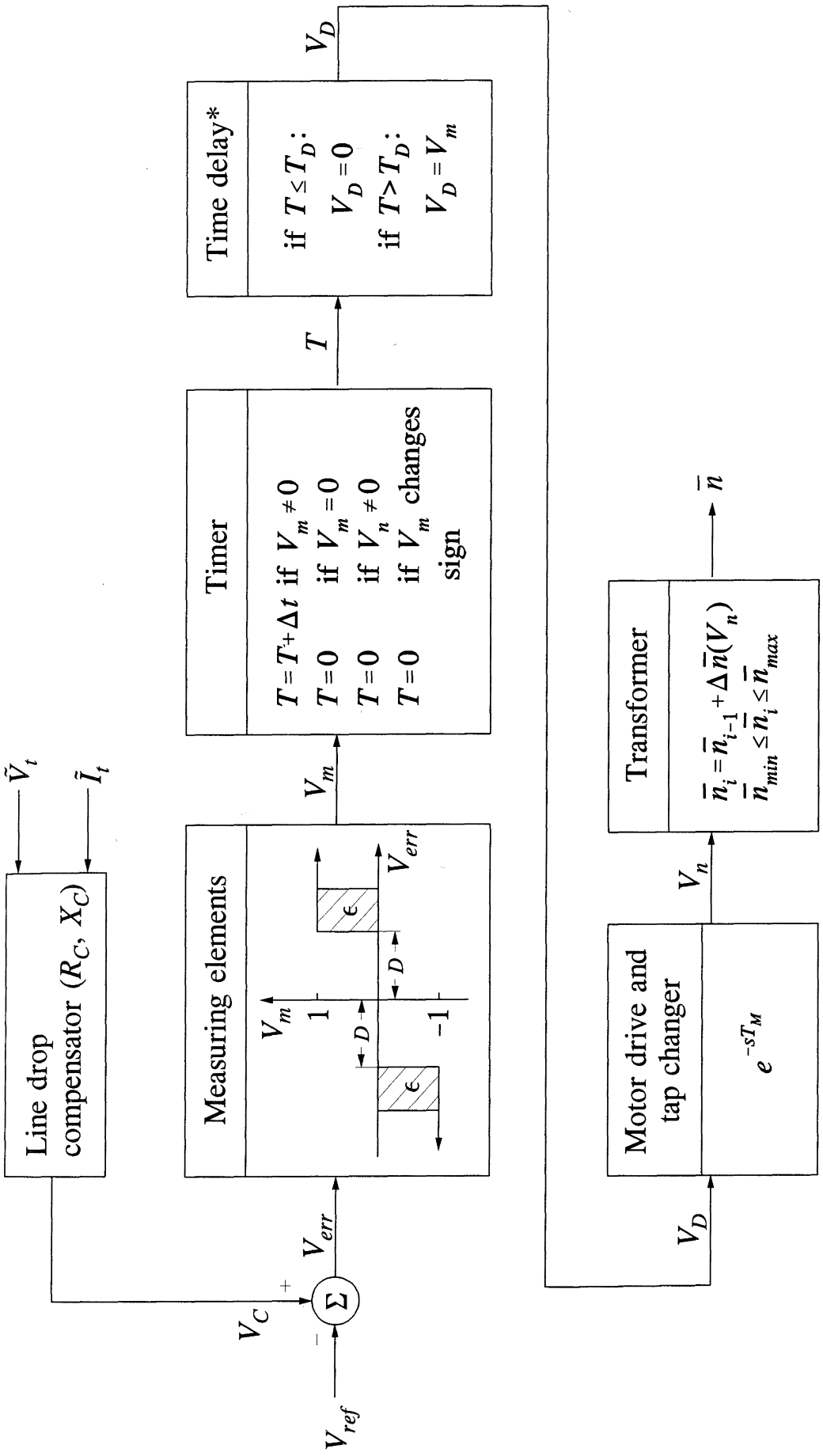
The function of the *line drop compensator*, as discussed in the previous section, is to regulate voltage at a remote point along the line or feeder. The voltage at the remote point is simulated by computing the voltage across the compensator impedance (R_C+jX_C). The magnitude of the compensated voltage is given by

$$V_C = |\tilde{V}_t+(R_C+jX_C)\tilde{I}_t|$$

where $\tilde{V}_t$ is the measured phasor voltage at the transformer secondary side.

The *measuring element* of the voltage regulator consists of an adjustable dead band relay with hysteresis. The input to the regulator is the voltage error.

$$V_{err} = V_{ref}-V_C$$



* $T_D = T_{D0}$ for first tap change
$= T_{D1}$ for subsequent tap change

Figure 11.80 ULTC control system model

The output of the measuring element is V_m, which takes a value of 0, 1, or -1, depending on the input V_{err}. With a regulator dead band of D and a hysteresis band of ε, the output is

$$V_m = \begin{cases} 0 & \text{for } -D \le V_{err} \le +D \\ 0 & \text{for } D < V_{err} \le D+\epsilon; \quad V_{err} \text{ increasing} \\ 0 & \text{for } -D-\epsilon \le V_{err} < -D; \quad V_{err} \text{ decreasing} \\ +1 & \text{for } V_{err} > D+\epsilon \\ +1 & \text{for } D < V_{err} \le D+\epsilon; \quad V_{err} \text{ decreasing} \\ -1 & \text{for } V_{err} < -D-\epsilon \\ -1 & \text{for } -D-\epsilon \le V_{err} < -D; \quad V_{err} \text{ increasing} \end{cases}$$

The *time delay element* is used to prevent unnecessary tap changes in response to transient voltage variations and to introduce the desired time delay before a tap movement. The *timer unit* determines the time duration of the error voltage (V_{err}) exceeding the dead band. The timer is advanced if V_{err} is outside the dead band. It is reset if V_{err} is within the dead band, if there is a tap movement ($v_n \neq 0$), or if V_{err} oscillates above and below the dead band. The output V_D of the time delay unit is normally zero. If the accumulated time T of the timer exceeds T_D, then V_D is set to V_m (i.e., 1 or -1), thereby sending a signal to the tap-changer motor to move the tap up or down.

The time delay T_D is equal to T_{D0} for the first tap movement. Some regulators have an inverse time-delay characteristic, in which case the time delay is inversely proportional to the voltage error:

$$T_D = \frac{T_{D0}}{V_{err}/D}$$

For the second and subsequent tap movements the time delay T_D is equal to T_{D1}. This allows introduction of intentional time delay between consecutive tap movements, if so desired.

The *motor-drive unit and the tap-changer mechanism* may be represented by a simple time delay T_M inherent to the equipment. The output signal V_n represents an incremental change in tap position, and is equal to 0, 1, or -1.

A change in tap position is reflected in the *transformer* model (see Chapter 6, Section 6.2.1) as an incremental change in per unit turns ratio. The per unit turns ratio after the i^{th} operation is

$$\bar{n}_i = \bar{n}_{i-1} + \Delta\bar{n}(V_n)$$

where $\Delta\bar{n}$ represents the per unit turns ratio step corresponding to a change in tap position by one step.

The above assumes that the controlled bus is on the secondary side (see Figure 6.17 of Chapter 6). If the controlled bus is on the primary side, we have

$$\bar{n}_i = \bar{n}_{i-1} - \Delta\bar{n}(V_n)$$

The tap ratio is subject to the maximum and minimum limits ($\bar{n}_{max}$ and $\bar{n}_{min}$).

The following sample data apply to the ULTC control system of the 42 MVA, 110/28.4 kV two-winding transformer considered in Chapter 6, Section 6.2.1:

$\Delta\bar{n} = 0.0059524$	$\bar{n}_{max} = 1.04762$	$\bar{n}_{min} = 0.85714$
$T_M = 0.5$ s	$T_{D0} = 30.0$ s	$T_{D1} = 0$
$D = 0.00835$ (0.835%)	$\varepsilon = 0$	$R_C = X_C = 0$

11.3 POWER-FLOW ANALYSIS PROCEDURES

The main analytical tools used in the planning of reactive power resources are the power-flow and stability programs. The methods of analysis of various aspects of stability are discussed in Chapters 12 to 16.

For reactive power dispatching, in addition to conventional power flows, optimal power-flow programs are being increasingly used. *Optimal power-flow* (OPF) theory was first formulated by Carpentier in 1962 [53]. Since then much research work has been carried out on OPF analysis techniques [49-51,54]. A discussion of the OPF methods and their application is beyond the scope of this book.

In this section, we will limit our discussion to conventional power-flow analysis. Analytical techniques for the solution of the power-flow problem are covered in Chapter 6. We focus on practical considerations and modelling assumptions in power-flow studies of bulk transmission systems. In such studies, the distribution system is not usually represented and loads are represented at substation levels.

The purpose of power-flow analysis is to investigate equipment loadings, power losses, bus voltages and reactive power requirements for the possible range of system operating conditions and contingencies specified by the design criteria. For any given study, the network configuration, load level, and generation schedule are specified. Assumptions regarding equipment modelling depend on the type of power flow: prefault or postfault.

11.3.1 Prefault Power Flows

Prefault power flows generally consider normal system conditions. The basic assumption is that all control actions have taken place and the system is operating in a true steady-state condition. Consequently the system is represented as follows:

- Loads are represented as constant P and Q; this assumes that ULTCs have been successful in holding bus voltages.

- Generator terminal voltages are held at specified values, subject to reactive power outputs being within limits based on capability curves (see Chapter 5, Section 5.4).

- All control actions are accounted for. This includes

  – Transformer tap/phase shift controls
  – Area interchange controls

11.3.2 Postfault Power Flows

Several types of postfault power flows (PFPFs) are generally considered in system studies to ensure satisfactory system performance. These look at *snapshots* of system conditions at various time frames following a disturbance.

Modelling assumptions related to the following should be consistent with the time period considered, purpose of study, and the degree of conservatism required:

- Transmission system transformer ULTCs

- Load characteristics, including effects of distribution system transformer ULTCs and voltage regulators

- Phase shifters

- Tie line power control (AGC)

- Reactive power compensation

- Generator reactive power limits

- Operator actions

For situations that do not involve loss of generation or load, net interchange between AGC control areas does not change significantly; the only changes are due to the voltage sensitive loads and changes in line losses. Therefore, the effect of the tie line power control in such cases is to change the generation on AGC slightly to make up for the changes in the system load and line losses. On the other hand, primary speed controls, frequency dependence of loads, and AGC could be important for contingencies resulting in significant mismatches between generation and load.

Analysis of contingencies not involving loss of generation/load

(a) For PFPFs representing the time period before automatic control actions of ULTCs and AGC (i.e., several seconds following the disturbance), the following modelling assumptions are made:

- Generator AVRs hold terminal voltages. Normally, there is no automatic control action limiting Q; however, depending on the nature of the study, it may be conservative to assume Q to be within generator capability limits.
- Loads vary as a function of bus voltage (since distribution system ULTCs/regulators have not operated).
- Capacitors/reactors are switched by voltage relays (if applicable).
- Tie line power flows are not controlled.

(b) For PFPFs representing the time period after automatic control actions, and before operator actions, the following modelling assumptions are made:

- Generator AVRs hold terminal voltages, subject to the generator reactive power output capability limits.
- ULTCs on automatic control operate; load P and Q are restored to their scheduled values.
- Tie line flows are controlled by AGC.

(c) For PFPFs representing the time period after operator actions, depending on the scope of the study, some or all of the following control actions are assumed to have taken place:

- ULTCs on manual control adjusted.
- Phase shifter angle adjusted.
- Generator Q adjusted to hold HT bus voltage (if applicable), subject to limits on Q.
- Operating reserve generation and exports adjusted to reduce equipment loadings to continuous rating.

Analysis of contingencies resulting in generation-load mismatch

The events that follow loss of generation or load may be categorized as follows:

- Stage 1, representing conditions immediately after the disturbance. During this stage, generator outputs change in approximately inverse proportion to the reactance between the generators and the point where generation or load is lost.

- Stage 2, representing conditions 0.5 s to 2.0 s following the disturbance. The generators accelerate or decelerate due to imbalance between mechanical power input and electrical power output.

  In a small system, all generators accelerate together; the loss of generation/load is shared among the generators in proportion to their inertia.

  In a large system, propagation of the effects of the disturbance to remote parts takes time; there will be time-phase difference between the rotor oscillations of units in different parts of the system.

- Stage 3, representing conditions from 2.0 s to 20.0 s following the disturbance. The speed governors respond and change the turbine outputs. At the end of this stage, the generators throughout the system share the power change in proportion to their capacity, available reserve, and the droop setting. System loads change, depending on their frequency and voltage sensitivity.

- Stage 4, representing conditions tens of seconds to several minutes following the disturbance. The AGC system attempts to correct for deviations in tie line flows and frequency. Depending on the amount of generation reserve on AGC, the tie line flows and frequency are restored. This is followed by manual action by operators.

Special features can be added to power-flow programs representing stages 3 and 4 described above. The corresponding power-flow analyses are referred to as *governor response power flow* and *AGC response power flow*, respectively. Some programs also provide facilities for the *inertial power flow*, which is intended to represent stage 2 identified above. However, such an analysis is meaningful only for small isolated systems in which all generators swing together during the concerned period, sharing generation-load mismatch in proportion to their inertia. For large interconnected systems, this stage can be analyzed only through dynamic simulations such as those used for transient stability analysis.

REFERENCES

[1] L.K. Kirchmayer, *Economic Control of Interconnected Systems*, John Wiley & Sons, 1959.

[2] A.J. Wood and B.F. Wollenberg, *Power Generation, Operation, and Control*, John Wiley & Sons, 1984.

[3] D.N. Ewart, "Automatic Generation Control - Performance under Normal Conditions," *Systems Engineering for Power: Status and Prospects*, CONF. 750867, U.S. Energy Research and Development Administration, Henniker, N.H., August 17-22, 1975.

[4] C. Concordia and L.K. Kirchmayer, "Tie line Power and Frequency Control of Electric Power Systems," Part I: *AIEE Trans.*, Vol. 72, Part III, p. 562, 1953; Part II: *AIEE Trans.*, Vol. 73, Part III-A, p. 133, 1954.

[5] N. Cohn, "Some Aspects of Tie line Bias Control on Interconnected Power Systems," *AIEE Trans.*, Vol. 75, Part III, pp. 1415-1436, February 1957.

[6] O.I. Elgerd, *Electric Energy Systems Theory: An Introduction*, McGraw-Hill, 1971.

[7] O.I. Elgerd and C.E. Fosha, "Optimum Megawatt-Frequency Control of Multi-Area Electric Energy Systems," *IEEE Trans.*, Vol. PAS-89, pp. 556-563, April 1970.

[8] J.L. Willems, "Sensitivity Analysis of the Optimum Performance of Conventional Load-Frequency Control," *IEEE Trans.*, Vol. PAS-93, pp. 1287-1291, September/October 1974.

[9] C.W. Ross, "Error Adaptive Control Computer for Interconnected Power Systems," *IEEE Trans.*, Vol. PAS-85, pp. 742-749, July 1966.

[10] NERC Operating Guide I: *Systems Control*, February 27, 1991.

[11] T. Kennedy, S.M. Hoyt, and C.F. Abell, "Variable, Non-Linear Tie line Frequency Bias for Interconnected Systems Control," *IEEE Trans.*, Vol. PWRS-3, No. 3, pp. 1244-1253, August 1988.

[12] IEEE Standard 122-1991, *Recommended Practice for Functional and Performance Characteristics of Control Systems for Steam Turbine-Generator Units*, February 1992.

[13] IEEE Standard 125-1988, *Recommended Practice for Preparation of Equipment Specifications for Speed-Governing of Hydraulic Turbines Intended to Drive Electric Generators*, October 1988.

[14] L.E. Eilts and F.R. Schlief, "Governing Features and Performance of the First 600 MW Hydrogenerating Units at Grand Coulee," *IEEE Trans.*, Vol. PAS-96, pp. 457-466, March/April 1977.

[15] C. Concordia, "Effect of Prime-Mover Speed Control Characteristics on Electric Power System Performance," *IEEE Trans.*, Vol. PAS-88, pp. 752-756, May 1969.

[16] C. Concordia, L.K. Kirchmayer, and E.A. Szymanski, "Effect of Speed-Governor Dead Band on Tie line Power and Frequency Control Performance," *AIEE Trans.*, Vol. 76, Part III, pp. 429-434, August 1957.

[17] C.W. Taylor, K.Y. Lee, and D.P. Dave, "Automatic Generation Control Analysis with Governor Deadband Effects," *IEEE Trans.*, Vol. PAS-98, pp. 2030-2036, November/December 1979.

[18] F.P. de Mello and J.M. Undrill, "Automatic Generation Control," IEEE Tutorial Course 77 TUDO 010-9-PWR.

[19] IEEE AGC Task Force Report, "Understanding Automatic Generation Control," *IEEE Trans.*, Vol. PWRS-7, No. 3, pp. 1106-1122, August 1992.

[20] J. Carpentier, "To Be or Not to Be Modern - That Is the Question for Automatic Generation Control (Point of View of a Utility Engineer)," *Electric Power & Energy Systems*, Vol. 7, No. 2, pp. 83-90, April 1985.

[21] G. Quazza, "Non-interacting Controls of Interconnected Electric Power Systems," *IEEE Trans.*, Vol. PAS-85, pp. 727-741, July 1966.

[22] H.A. Bauman, G.R. Hahn, and C.N. Metcalf, "The Effect of Frequency Reduction on Plant Capacity and on System Operation," *AIEE Trans.*, Vol. PAS-73, pp. 1632-1637, February 1955.

[23] H.E. Lokay and V. Burtnyk, "Application of Underfrequency Relays for Automatic Load Shedding," *IEEE Trans.*, Vol. PAS-87, pp. 776-783, March 1968.

[24] D.H. Berry, R.D. Brown, J.J. Redmond, and W. Watson, "Underfrequency Protection of the Ontario Hydro System," CIGRE Paper 32-14, August/September 1970.

[25] T. Gönen, *Electric Power Distribution System Engneering*, McGraw Hill, 1986.

[26] T. Petersson, "Reactive Power Compensation," ASEA Publication NK 02-3005 E, May 1983.

[27] J.W. Butler and C. Concordia, "Analysis of Series Capacitor Application Problems," *AIEE Trans.*, Vol. 56, p. 975, 1937.

[28] E.C. Starr and R.D. Evans, "Series Capacitors for Transmission Circuits," *AIEE Trans.*, Vol. 61, pp. 963, 1942.

[29] C.F. Wagner, "Self-Excitation of Induction Motors with Series Capacitors," *AIEE Trans.*, Vol. 62, p. 58, 1943.

[30] *An Introduction to ABB Series Capacitors*, ABB Information Publication, September 9, 1991.

[31] B.S. Ashok Kumar, K. Parthasarathy, F.S. Prabhakara, and H.P. Kincha, "Effectiveness of Series Capacitors in Long Distance Transmission Lines," *IEEE Trans.*, Vol. PAS-89, pp. 941-950, May/June 1970.

[32] F. Iliceto and E. Cinieri, "Comparative Analysis of Series and Shunt Compensation Schemes for AC Transmission Systems," *IEEE Trans.*, Vol. PAS-96, pp. 1819-1830, November/December 1977.

[33] J.A. Maneatis, E.J. Hubacher, W.N. Rothenbuhler, and F. Sabath, "500 kV Series Capacitor Installations in California," *IEEE Trans.*, Vol. PAS-90, pp. 1138-1149, May/June 1971.

[34] G. Jancke, N. Fahlen, and O. Nerf, "Series Capacitors in Power Systems," *IEEE Trans.*, Vol. PAS-94, pp. 915-925, May/June 1975.

[35] C.V. Thio and J.B. Davies, "New Synchronous Compensators for the Nelson River HVDC System - Planning Requirements and Specifications," *IEEE Trans. on Power Delivery*, Vol. 6, No. 2, pp. 922-928, April 1991.

[36] CIGRE Report, "Static VAR Compensators," Prepared by WG 38-01, Task Force No. 2, Paris, 1986.

[37] T.J.E. Miller (editor), *Reactive Power Control in Electric Systems*, John Wiley & Sons, 1982.

[38] U.S. Department of Energy Report, "Static Reactive Power Compensators for

High Voltage Power Systems," Prepared by General Electric Company, DOE/NBM-1010, March 1982.

[39] R. Elsliger, Y. Hotte, and J.C. Roy, "Optimization of Hydro-Quebec's 735 kV Shunt-Compensated System Using Static Compensators on a Large Scale," IEEE Conference paper A 78107-5, Presented at the IEEE PES Winter Meeting, New York, January 29 - February 3, 1978.

[40] R. Gutman, J.J. Keane, M.Ea. Rahman, and Q. Veraas, "Application and Operation of a Static Var System on a Power System - American Electric Experience, Part I: System Studies, Part II: Equipment Design and Installation," *IEEE Trans.*, Vol. PAS-104, pp. 1868-1881, July 1985.

[41] IEEE Publication, "Static Var Compensators: Planning, Operating, and Maintenance Experiences," IEEE/PES 90TH 320-2 PWR.

[42] D. Dickmander, B. Thorvaldsson, G. Stromberg, D. Osborn, A. Poitras, and D. Fisher, "Control System Design and Performance Verification for the Chester Maine Static Var Compensator," *IEEE Trans.*, Vol. PWRD-7, No. 3, pp. 1492-1503, July 1992.

[43] F.G. Baum, "Voltage Regulation and Insulation for Large-Power Long-Distance Transmission Systems," *AIEE Trans.*, Vol. 40, pp. 1017-1032, June 1921.

[44] H.K. Clark, "Voltage Control and Reactive Supply Problems," IEEE course text on Reactive Power: Basics, Problems, and Solutions, Publication 87EH0262-6-PWR.

[45] H.K. Clark, "Considerations in the Evaluation of Series and Shunt Compensation Alternatives," Paper presented at the T & D Expo., Chicago, May 14-16, 1985.

[46] E.W. Kimbark, "A New Look at Shunt Compensation," *IEEE Trans.*, Vol. PAS-102, pp. 212-218, January 1983.

[47] IEEE Special Stability Controls Working Group Report, "Static Var Compensator Models for Power Flow and Dynamic Performance Simulation," Paper 93WM173-5-PWRS, Presented at the IEEE PES Winter Meeting, Columbus, Ohio, February 1993.

[48] General Electric Company, *Voltage Regulation*, Omnitext, 1979.

[49] J.F. Aldrich, R.A. Fernandes, L.W. Wicks, H.H. Happ, and K.A. Wiragu,

"Benefits of Voltage Scheduling in Power Systems," *IEEE Trans.*, Vol. PAS-99, No. 5, pp. 1701-1712, September/October 1980.

[50] M.A. El-Kady, B.D. Bell, V.F. Carvalho, R.C. Burchett, H.H. Happ, and D.R. Vierath, "Assessment of Real-Time Optional Voltage Control," *IEEE Trans.*, Vol. PWRS-1, No. 2, pp. 98-105, May 1986.

[51] N. Flatabø, J.A. Foosnaes, and T.O. Berntsen, "Transformer Tap Setting in Optimal Load Flow," *IEEE Trans.*, Vol. PAS-104, No. 6, pp. 1356-1362, June 1985.

[52] M.S. Ćalović, "Modelling and Analysis of Under-Load Tap-Changing Transformer Control Systems," *IEEE Trans.*, Vol. PAS-103, No. 7, pp. 1909-1915, July 1984.

[53] J. Carpentier, "Contribution à l'Etude du Dispatching Economique," *Bulletin de la Société Française des Electriciens*, Vol., 3, No. 8, August 1962.

[54] H.W. Dommel and W.F. Tinney, "Optimal Power Flow Solutions," *IEEE Trans.*, Vol. PAS-87, pp. 1866-1876, October 1968.

PART III

SYSTEM STABILITY:

physical aspects, analysis, and improvement

Chapter 12

Small-Signal Stability

Chapter 2 provided a general introduction to the power system stability problem, including a discussion of the basic concepts, classification, and definitions of related terms. We will now consider in detail the various categories of system stability, beginning with this chapter on small-signal stability. Knowledge of the characteristics and modelling of individual system components as presented in Chapters 3 to 11 should be helpful in this regard.

Small-signal stability, as defined in Chapter 2, is the ability of the power system to maintain synchronism when subjected to small disturbances. In this context, a disturbance is considered to be small if the equations that describe the resulting response of the system may be linearized for the purpose of analysis. Instability that may result can be of two forms: (i) steady increase in generator rotor angle due to lack of synchronizing torque, or (ii) rotor oscillations of increasing amplitude due to lack of sufficient damping torque. In today's practical power systems, the small-signal stability problem is usually one of insufficient damping of system oscillations. Small-signal analysis using linear techniques provides valuable information about the inherent dynamic characteristics of the power system and assists in its design.

This chapter reviews fundamental aspects of stability of dynamic systems, presents analytical techniques useful in the study of small-signal stability, illustrates the characteristics of small-signal stability problems, and identifies factors influencing them.

12.1 FUNDAMENTAL CONCEPTS OF STABILITY OF DYNAMIC SYSTEMS

12.1.1 State-Space Representation

The behaviour of a dynamic system, such as a power system, may be described by a set of n first order nonlinear ordinary differential equations of the following form:

$$\dot{x}_i = f_i(x_1, x_2, \ldots, x_n;\ u_1, u_2, \ldots, u_r;\ t) \qquad i = 1, 2, \ldots, n \tag{12.1}$$

where n is the order of the system and r is the number of inputs. This can be written in the following form by using vector-matrix notation:

$$\dot{\mathbf{x}} = \mathbf{f}(\mathbf{x}, \mathbf{u}, t) \tag{12.2}$$

where

$$\mathbf{x} = \begin{bmatrix} x_1 \\ x_2 \\ \vdots \\ x_n \end{bmatrix} \qquad \mathbf{u} = \begin{bmatrix} u_1 \\ u_2 \\ \vdots \\ u_r \end{bmatrix} \qquad \mathbf{f} = \begin{bmatrix} f_1 \\ f_2 \\ \vdots \\ f_n \end{bmatrix}$$

The column vector $\mathbf{x}$ is referred to as the *state vector*, and its entries x_i as *state variables*. The column vector $\mathbf{u}$ is the vector of inputs to the system. These are the external signals that influence the performance of the system. Time is denoted by t, and the derivative of a state variable x with respect to time is denoted by $\dot{x}$. If the derivatives of the state variables are not explicit functions of time, the system is said to be *autonomous*. In this case, Equation 12.2 simplifies to

$$\dot{\mathbf{x}} = \mathbf{f}(\mathbf{x}, \mathbf{u}) \tag{12.3}$$

We are often interested in output variables which can be observed on the system. These may be expressed in terms of the state variables and the input variables in the following form:

$$\mathbf{y} = \mathbf{g}(\mathbf{x}, \mathbf{u}) \tag{12.4}$$

where

$$\mathbf{y} = \begin{bmatrix} y_1 \\ y_2 \\ \vdots \\ y_m \end{bmatrix} \qquad \mathbf{g} = \begin{bmatrix} g_1 \\ g_2 \\ \vdots \\ g_m \end{bmatrix}$$

The column vector **y** is the vector of outputs, and **g** is a vector of nonlinear functions relating state and input variables to output variables.

The concept of state

The concept of state is fundamental to the state-space approach. The state of a system represents the minimum amount of information about the system at any instant in time t_0 that is necessary so that its future behaviour can be determined without reference to the input before t_0.

Any set of n linearly independent system variables may be used to describe the state of the system. These are referred to as the *state variables*; they form a minimal set of dynamic variables that, along with the inputs to the system, provide a complete description of the system behaviour. Any other system variables may be determined from a knowledge of the state.

The state variables may be physical quantities in a system such as angle, speed, voltage, or they may be abstract mathematical variables associated with the differential equations describing the dynamics of the system. The choice of the state variables is not unique. This does not mean that the state of the system at any time is not unique; only that the means of representing the state information is not unique. Any set of state variables we may choose will provide the same information about the system. If we overspecify the system by defining too many state variables, not all of them will be independent.

The system state may be represented in an n-dimensional Euclidean space called the *state space*. When we select a different set of state variables to describe the system, we are in effect choosing a different coordinate system.

Whenever the system is not in equilibrium or whenever the input is non-zero, the system state will change with time. The set of points traced by the system state in the state space as the system moves is called the *state trajectory.*

Equilibrium (or singular) points

The equilibrium points are those points where all the derivatives $\dot{x}_1, \dot{x}_2, \ldots, \dot{x}_n$ are simultaneously zero; they define the points on the trajectory with zero velocity. The system is accordingly at rest since all the variables are constant and unvarying with time.

The equilibrium or singular point must therefore satisfy the equation

$$\mathbf{f}(\mathbf{x}_0) = 0 \tag{12.5}$$

where $\mathbf{x}_0$ is the state vector **x** at the equilibrium point.

If the functions $f_i (i=1,2,\ldots,n)$ in Equation 12.3 are linear, then the system is linear. A linear system has only one equilibrium state (if the system matrix is non-singular). For a nonlinear system there may be more than one equilibrium point.

The singular points are truly characteristic of the behaviour of the dynamic system, and therefore we can draw conclusions about stability from their nature.

12.1.2 Stability of a Dynamic System

The stability of a linear system is entirely independent of the input, and the state of a stable system with zero input will always return to the origin of the state space, independent of the finite initial state.

In contrast, the stability of a nonlinear system depends on the type and magnitude of input, and the initial state. These factors have to be taken into account in defining the stability of a nonlinear system.

In control system theory, it is common practice to classify the stability of a nonlinear system into the following categories, depending on the region of state space in which the state vector ranges:

- Local stability or stability in the small
- Finite stability
- Global stability or stability in the large

Local stability

The system is said to be *locally stable* about an equilibrium point if, when subjected to small perturbation, it remains within a small region surrounding the equilibrium point.

If, as t increases, the system returns to the original state, it is said to be *asymptotically stable* in the small.

It should be noted that the general definition of local stability does not require that the state return to the original state and, therefore, includes small limit cycles. In practice, we are normally interested in asymptotic stability.

Local stability (i.e., stability under small disturbance) conditions can be studied by linearizing the nonlinear system equations about the equilibrium point in question. This is illustrated in the next section.

Finite stability

If the state of a system remains within a finite region R, it is said to be stable within R. If, further, the state of the system returns to the original equilibrium point from any point within R, it is asymptotically stable within the finite region R.

Global stability

The system is said to be *globally stable* if R includes the entire finite space.

12.1.3 Linearization

We now describe the procedure for linearizing Equation 12.3. Let $\mathbf{x}_0$ be the initial state vector and $\mathbf{u}_0$ the input vector corresponding to the equilibrium point about which the small-signal performance is to be investigated. Since $\mathbf{x}_0$ and $\mathbf{u}_0$ satisfy Equation 12.3, we have

$$\dot{\mathbf{x}}_0 = \mathbf{f}(\mathbf{x}_0, \mathbf{u}_0) = 0 \tag{12.6}$$

Let us perturb the system from the above state, by letting

$$\mathbf{x} = \mathbf{x}_0 + \Delta\mathbf{x} \qquad \mathbf{u} = \mathbf{u}_0 + \Delta\mathbf{u}$$

where the prefix Δ denotes a small deviation.

The new state must satisfy Equation 12.3. Hence,

$$\begin{aligned} \dot{\mathbf{x}} &= \dot{\mathbf{x}}_0 + \Delta\dot{\mathbf{x}} \\ &= \mathbf{f}[(\mathbf{x}_0 + \Delta\mathbf{x}), (\mathbf{u}_0 + \Delta\mathbf{u})] \end{aligned} \tag{12.7}$$

As the perturbations are assumed to be small, the nonlinear functions $\mathbf{f}(\mathbf{x}, \mathbf{u})$ can be expressed in terms of Taylor's series expansion. With terms involving second and higher order powers of Δx and Δu neglected, we may write

$$\begin{aligned} \dot{x}_i = \dot{x}_{i0} + \Delta\dot{x}_i &= f_i[(\mathbf{x}_0 + \Delta\mathbf{x}), (\mathbf{u}_0 + \Delta\mathbf{u})] \\ &= f_i(\mathbf{x}_0, \mathbf{u}_0) + \frac{\partial f_i}{\partial x_1}\Delta x_1 + \cdots + \frac{\partial f_i}{\partial x_n}\Delta x_n \\ &\quad + \frac{\partial f_i}{\partial u_1}\Delta u_1 + \cdots + \frac{\partial f_i}{\partial u_r}\Delta u_r \end{aligned}$$

Since $\dot{x}_{i0} = f_i(\mathbf{x}_0, \mathbf{u}_0)$, we obtain

$$\Delta\dot{x}_i = \frac{\partial f_i}{\partial x_1}\Delta x_1 + \cdots + \frac{\partial f_i}{\partial x_n}\Delta x_n + \frac{\partial f_i}{\partial u_1}\Delta u_1 + \cdots + \frac{\partial f_i}{\partial u_r}\Delta u_r$$

with $i = 1, 2, \ldots, n$. In a like manner, from Equation 12.4, we have

$$\Delta y_j = \frac{\partial g_j}{\partial x_1}\Delta x_1 + \cdots + \frac{\partial g_j}{\partial x_n}\Delta x_n + \frac{\partial g_j}{\partial u_1}\Delta u_1 + \cdots + \frac{\partial g_j}{\partial u_r}\Delta u_r$$

with $j=1,2,...,m$. Therefore, the linearized forms of Equations 12.3 and 12.4 are

$$\Delta\dot{\mathbf{x}} = \mathbf{A}\,\Delta\mathbf{x} + \mathbf{B}\,\Delta\mathbf{u} \tag{12.8}$$

$$\Delta\mathbf{y} = \mathbf{C}\,\Delta\mathbf{x} + \mathbf{D}\,\Delta\mathbf{u} \tag{12.9}$$

where

$$\mathbf{A} = \begin{bmatrix} \frac{\partial f_1}{\partial x_1} & \cdots & \frac{\partial f_1}{\partial x_n} \\ \cdots & \cdots & \cdots \\ \frac{\partial f_n}{\partial x_1} & \cdots & \frac{\partial f_n}{\partial x_n} \end{bmatrix} \qquad \mathbf{B} = \begin{bmatrix} \frac{\partial f_1}{\partial u_1} & \cdots & \frac{\partial f_1}{\partial u_r} \\ \cdots & \cdots & \cdots \\ \frac{\partial f_n}{\partial u_1} & \cdots & \frac{\partial f_n}{\partial u_r} \end{bmatrix}$$

$$\mathbf{C} = \begin{bmatrix} \frac{\partial g_1}{\partial x_1} & \cdots & \frac{\partial g_1}{\partial x_n} \\ \cdots & \cdots & \cdots \\ \frac{\partial g_m}{\partial x_1} & \cdots & \frac{\partial g_m}{\partial x_n} \end{bmatrix} \qquad \mathbf{D} = \begin{bmatrix} \frac{\partial g_1}{\partial u_1} & \cdots & \frac{\partial g_1}{\partial u_r} \\ \cdots & \cdots & \cdots \\ \frac{\partial g_m}{\partial u_1} & \cdots & \frac{\partial g_m}{\partial u_r} \end{bmatrix} \tag{12.10}$$

The above partial derivatives are evaluated at the equilibrium point about which the small perturbation is being analyzed.

In Equations 12.8 and 12.9,

- $\Delta\mathbf{x}$ is the state vector of dimension n
- $\Delta\mathbf{y}$ is the output vector of dimension m
- $\Delta\mathbf{u}$ is the input vector of dimension r
- $\mathbf{A}$ is the state or plant matrix of size $n\times n$
- $\mathbf{B}$ is the control or input matrix of size $n\times r$
- $\mathbf{C}$ is the output matrix of size $m\times n$
- $\mathbf{D}$ is the (feedforward) matrix which defines the proportion of input which appears directly in the output, size $m\times r$

By taking the Laplace transform of the above equations, we obtain the state equations in the frequency domain:

$$s\Delta\mathbf{x}(s) - \Delta\mathbf{x}(0) = \mathbf{A}\,\Delta\mathbf{x}(s) + \mathbf{B}\,\Delta\mathbf{u}(s) \tag{12.11}$$

$$\Delta\mathbf{y}(s) = \mathbf{C}\,\Delta\mathbf{x}(s) + \mathbf{D}\,\Delta\mathbf{u}(s) \tag{12.12}$$

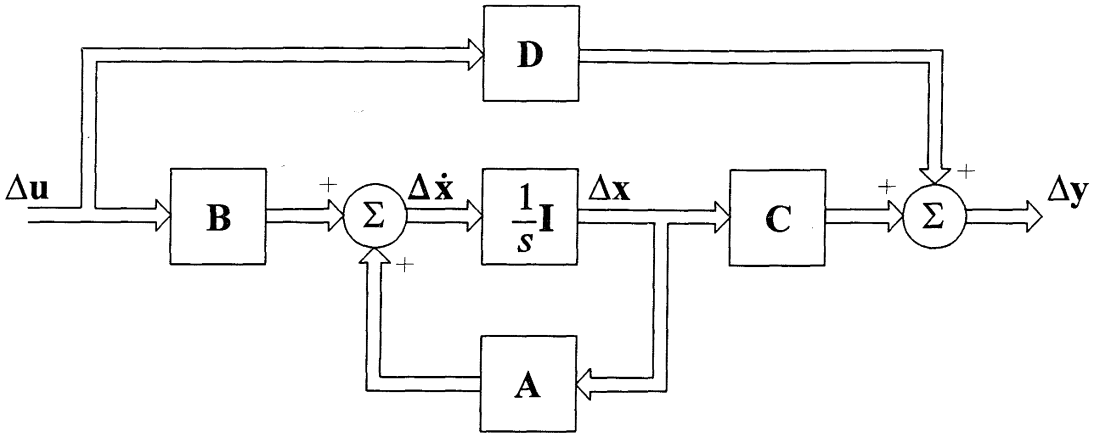


Figure 12.1 Block diagram of the state-space representation

Figure 12.1 shows the block diagram of the state-space representation. Since we are representing the transfer function of the system, the initial conditions $\Delta\mathbf{x}(0)$ are assumed to be zero.

A formal solution of the state equations can be obtained by solving for $\Delta\mathbf{x}(s)$ and evaluating $\Delta\mathbf{y}(s)$, as follows:

Rearranging Equation 12.11, we have

$$(s\mathbf{I}-\mathbf{A})\Delta\mathbf{x}(s) = \Delta\mathbf{x}(0)+\mathbf{B}\,\Delta\mathbf{u}(s)$$

Hence,

$$\begin{aligned}\Delta\mathbf{x}(s) &= (s\mathbf{I}-\mathbf{A})^{-1}[\Delta\mathbf{x}(0)+\mathbf{B}\,\Delta\mathbf{u}(s)] \\ &= \frac{\text{adj}(s\mathbf{I}-\mathbf{A})}{\det(s\mathbf{I}-\mathbf{A})}[\Delta\mathbf{x}(0)+\mathbf{B}\,\Delta\mathbf{u}(s)]\end{aligned} \tag{12.13}$$

and correspondingly,

$$\Delta\mathbf{y}(s) = \mathbf{C}\frac{\text{adj}(s\mathbf{I}-\mathbf{A})}{\det(s\mathbf{I}-\mathbf{A})}[\Delta\mathbf{x}(0)+\mathbf{B}\,\Delta\mathbf{u}(s)]+\mathbf{D}\,\Delta\mathbf{u}(s) \tag{12.14}$$

The Laplace transforms of $\Delta\mathbf{x}$ and $\Delta\mathbf{y}$ are seen to have two components, one dependent on the initial conditions and the other on the inputs. These are the Laplace transforms of the *free* and *zero-state components* of the state and output vectors.

The poles of $\Delta\mathbf{x}(s)$ and $\Delta\mathbf{y}(s)$ are the roots of the equation

$$\det(s\mathbf{I}-\mathbf{A}) = 0 \tag{12.15}$$

The values of s which satisfy the above are known as *eigenvalues* of matrix **A**, and Equation 12.15 is referred to as the *characteristic equation* of matrix **A**.

12.1.4 Analysis of Stability

Lyapunov's first method [1]

The *stability in the small* of a nonlinear system is given by the roots of the characteristic equation of the system of first approximations, i.e., by the eigenvalues of **A**:

(i) When the eigenvalues have negative real parts, the original system is asymptotically stable.
(ii) When at least one of the eigenvalues has a positive real part, the original system is unstable.
(iii) When the eigenvalues have real parts equal to zero, it is not possible on the basis of the first approximation to say anything in the general.

The *stability in the large* may be studied by explicit solution of the nonlinear differential equations using digital or analog computers.

A method that does not require explicit solution of system differential equations is the direct method of Lyapunov.

Lyapunov's second method, or the direct method

The second method attempts to determine stability directly by using suitable functions which are defined in the state space. The sign of the Lyapunov function and the sign of its time derivative with respect to the system state equations are considered.

The equilibrium of Equation 12.3 is *stable* if there exists a positive definite function $V(x_1, x_2, \ldots, x_n)$ such that its total derivative $\dot{V}$ with respect to Equation 12.3 is not positive.[1]

The equilibrium of Equation 12.3 is *asymptotically stable* if there is a positive definite function $V(x_1, x_2, \ldots, x_n)$ such that its total derivative with respect to Equation 12.3 is negative definite.

The system is *stable* in that region in which $\dot{V}$ is negative semidefinite, and *asymptotically stable* if $\dot{V}$ is negative definite.[2]

The stability in the large of power systems is the subject of the next chapter. This chapter is concerned with the stability in the small of power systems, and this is given by the eigenvalues of **A**. As illustrated in the following section, the natural

---

[1] A function is called *definite* in a domain D of state space if it has the same sign for all **x** within D and vanishes for **x**=0. For example, $V(x_1, x_2, x_3) = x_1^2 + x_2^2 + x_3^2$ is positive definite.

[2] A function is called *semidefinite* in a domain D of the state space if it has the same sign or is zero for all **x** within D. For example, $V(x_1, x_2, x_3) = (x_1 - x_2)^2 + x_3^2$ is positive semi-definite since it is zero for $x_1 = x_2$, $x_3 = 0$.

modes of system response are related to the eigenvalues. Analysis of the eigenproperties of **A** provides valuable information regarding the stability characteristics of the system.

It is worth recalling that the matrix **A** is the Jacobian matrix whose elements a_{ij} are given by the partial derivatives $\partial f_i/\partial x_j$ evaluated at the equilibrium point about which the small disturbance is being analyzed. This matrix is commonly referred to as the *state matrix* or the *plant matrix*. The term "plant" originates from the area of process control and is entrenched in control engineering vocabulary. It represents that part of the system which is to be controlled.

12.2 EIGENPROPERTIES OF THE STATE MATRIX

12.2.1 Eigenvalues

The eigenvalues of a matrix are given by the values of the scalar parameter λ for which there exist non-trivial solutions (i.e., other than $\boldsymbol{\phi}=0$) to the equation

$$\mathbf{A}\boldsymbol{\phi} = \lambda\boldsymbol{\phi} \tag{12.16}$$

where

A is an $n\times n$ matrix (real for a physical system such as a power system)
$\boldsymbol{\phi}$ is an $n\times 1$ vector

To find the eigenvalues, Equation 12.16 may be written in the form

$$(\mathbf{A}-\lambda\mathbf{I})\boldsymbol{\phi} = 0 \tag{12.17}$$

For a non-trivial solution

$$\det(\mathbf{A}-\lambda\mathbf{I}) = 0 \tag{12.18}$$

Expansion of the determinant gives the *characteristic equation*. The n solutions of $\lambda=\lambda_1,\lambda_2,...,\lambda_n$ are *eigenvalues* of **A**.

The eigenvalues may be real or complex. If **A** is real, complex eigenvalues always occur in conjugate pairs.

Similar matrices have identical eigenvalues. It can also be readily shown that a matrix and its transpose have the same eigenvalues.

12.2.2 Eigenvectors

For any eigenvalue λ_i, the n-column vector $\boldsymbol{\phi}_i$ which satisfies Equation 12.16 is called the *right eigenvector* of **A** associated with the eigenvalue λ_i. Therefore, we have

$$\mathbf{A}\boldsymbol{\phi}_i = \lambda_i \boldsymbol{\phi}_i \qquad i = 1, 2, \ldots, n \tag{12.19}$$

The eigenvector $\boldsymbol{\phi}_i$ has the form

$$\boldsymbol{\phi}_i = \begin{bmatrix} \phi_{1i} \\ \phi_{2i} \\ \vdots \\ \phi_{ni} \end{bmatrix}$$

Since Equation 12.17 is homogeneous, $k\boldsymbol{\phi}_i$ (where k is a scalar) is also a solution. Thus, the eigenvectors are determined only to within a scalar multiplier.

Similarly, the n-row vector $\boldsymbol{\psi}_i$ which satisfies

$$\boldsymbol{\psi}_i \mathbf{A} = \lambda_i \boldsymbol{\psi}_i \qquad i = 1, 2, \ldots, n \tag{12.20}$$

is called the *left eigenvector* associated with the eigenvalue λ_i.

The left and right eigenvectors corresponding to different eigenvalues are orthogonal. In other words, if λ_i is not equal to λ_j,

$$\boldsymbol{\psi}_j \boldsymbol{\phi}_i = 0 \tag{12.21}$$

However, in the case of eigenvectors corresponding to the same eigenvalue,

$$\boldsymbol{\psi}_i \boldsymbol{\phi}_i = C_i \tag{12.22}$$

where C_i is a non-zero constant.

Since, as noted above, the eigenvectors are determined only to within a scalar multiplier, it is common practice to *normalize* these vectors so that

$$\boldsymbol{\psi}_i \boldsymbol{\phi}_i = 1 \tag{12.23}$$

12.2.3 Modal Matrices

In order to express the eigenproperties of $\mathbf{A}$ succinctly, it is convenient to introduce the following matrices:

$$\boldsymbol{\Phi} = [\, \boldsymbol{\phi}_1 \quad \boldsymbol{\phi}_2 \quad \cdots \quad \boldsymbol{\phi}_n \,] \tag{12.24}$$

$$\boldsymbol{\Psi} = [\, \boldsymbol{\psi}_1^T \quad \boldsymbol{\psi}_2^T \quad \cdots \quad \boldsymbol{\psi}_n^T \,]^T \tag{12.25}$$

$$\boldsymbol{\Lambda} = \text{diagonal matrix, with the eigenvalues } \lambda_1, \lambda_2, \ldots, \lambda_n \text{ as diagonal elements} \tag{12.26}$$

Each of the above matrices is $n \times n$. In terms of these matrices, Equations 12.19 and 12.23 may be expanded as follows.

$$\mathbf{A\Phi} = \mathbf{\Phi\Lambda} \tag{12.27}$$

$$\mathbf{\Psi\Phi} = \mathbf{I} \qquad \mathbf{\Psi} = \mathbf{\Phi}^{-1} \tag{12.28}$$

It follows from Equation 12.27

$$\mathbf{\Phi}^{-1}\mathbf{A\Phi} = \mathbf{\Lambda} \tag{12.29}$$

12.2.4 Free Motion of a Dynamic System

Referring to the state equation 12.9, we see that the free motion (with zero input) is given by

$$\Delta\dot{\mathbf{x}} = \mathbf{A}\,\Delta\mathbf{x} \tag{12.30}$$

A set of equations of the above form, *derived from physical considerations,* is often not the best means of analytical studies of motion. The problem is that the rate of change of each state variable is a linear combination of all the state variables. As the result of cross-coupling between the states, it is difficult to isolate those parameters that influence the motion in a significant way.

In order to eliminate the cross-coupling between the state variables, consider a new state vector $\mathbf{z}$ related to the original state vector $\Delta\mathbf{x}$ by the transformation

$$\Delta\mathbf{x} = \mathbf{\Phi z} \tag{12.31}$$

where $\mathbf{\Phi}$ is the modal matrix of $\mathbf{A}$ defined by Equation 12.24. Substituting the above expression for $\Delta\mathbf{x}$ in the state equation (12.30), we have

$$\mathbf{\Phi}\dot{\mathbf{z}} = \mathbf{A\Phi z} \tag{12.32}$$

The new state equation can be written as

$$\dot{\mathbf{z}} = \mathbf{\Phi}^{-1}\mathbf{A\Phi z} \tag{12.33}$$

In view of Equation 12.29, the above equation becomes

$$\dot{\mathbf{z}} = \mathbf{\Lambda z} \tag{12.34}$$

The important difference between Equations 12.34 and 12.30 is that $\mathbf{\Lambda}$ is a diagonal matrix whereas $\mathbf{A}$, in general, is non-diagonal.

Equation 12.34 represents n uncoupled first order (scalar) equations:

$$\dot{z}_i = \lambda_i z_i \qquad i = 1, 2, \ldots, n \tag{12.35}$$

The effect of the transformation (12.31) is, therefore, to *uncouple* the state equations.

Equation 12.35 is a simple first-order differential equation whose solution with respect to time t is given by

$$z_i(t) = z_i(0) e^{\lambda_i t} \tag{12.36}$$

where $z_i(0)$ is the initial value of z_i.

Returning to Equation 12.31, the response in terms of the original state vector is given by

$$\begin{aligned} \Delta\mathbf{x}(t) &= \mathbf{\Phi z}(t) \\ &= \begin{bmatrix} \boldsymbol{\phi}_1 & \boldsymbol{\phi}_2 & \cdots & \boldsymbol{\phi}_n \end{bmatrix} \begin{bmatrix} z_1(t) \\ z_2(t) \\ \vdots \\ z_n(t) \end{bmatrix} \end{aligned} \tag{12.37}$$

which, in view of Equation 12.36, implies that

$$\Delta\mathbf{x}(t) = \sum_{i=1}^{n} \boldsymbol{\phi}_i z_i(0) e^{\lambda_i t} \tag{12.38}$$

From Equation 12.37, we have

$$\begin{aligned} \mathbf{z}(t) &= \mathbf{\Phi}^{-1} \Delta\mathbf{x}(t) \\ &= \mathbf{\Psi} \Delta\mathbf{x}(t) \end{aligned} \tag{12.39}$$

This implies that

$$z_i(t) = \boldsymbol{\psi}_i \Delta\mathbf{x}(t) \tag{12.40}$$

With $t=0$, it follows that

$$z_i(0) = \boldsymbol{\psi}_i \Delta\mathbf{x}(0) \tag{12.41}$$

By using c_i to denote the scalar product $\boldsymbol{\psi}_i \Delta\mathbf{x}(0)$, Equation 12.38 may be written as

$$\Delta\mathbf{x}(t) = \sum_{i=1}^{n} \boldsymbol{\phi}_i c_i e^{\lambda_i t} \tag{12.42}$$

In other words, the time response of the ith state variable is given by

$$\Delta x_i(t) = \phi_{i1}c_1e^{\lambda_1 t} + \phi_{i2}c_2e^{\lambda_2 t} + \cdots + \phi_{in}c_ne^{\lambda_n t} \tag{12.43}$$

The above equation gives the expression for the free motion time response of the system in terms of the eigenvalues, and left and right eigenvectors.

Thus, the free (or initial condition) response is given by a *linear combination of n dynamic modes* corresponding to the n eigenvalues of the state matrix.

The scalar product $c_i = \boldsymbol{\psi}_i \Delta\mathbf{x}(0)$ represents the *magnitude of the excitation* of the ith mode resulting from the initial conditions.

If the initial conditions lie along the jth eigenvector, the scalar products $\boldsymbol{\psi}_i \Delta\mathbf{x}(0)$ for all $i \neq j$ are identically zero. Therefore, only the jth mode is excited.

If the vector representing the initial condition is not an eigenvector, it can be represented by a linear combination of the n eigenvectors. The response of the system will be the sum of the n responses. If a component along an eigenvector of the initial conditions is zero, the corresponding mode will not be excited (see Example 12.1 for an illustration).

Eigenvalue and stability

The time dependent characteristic of a mode corresponding to an eigenvalue λ_i is given by $e^{\lambda_i t}$. Therefore, the stability of the system is determined by the eigenvalues as follows:

(a) A *real eigenvalue* corresponds to a non-oscillatory mode. A negative real eigenvalue represents a decaying mode. The larger its magnitude, the faster the decay. A positive real eigenvalue represents aperiodic instability.

The values of c's and the eigenvectors associated with real eigenvalues are also real.

(b) *Complex eigenvalues* occur in conjugate pairs, and each pair corresponds to an oscillatory mode.

The associated c's and eigenvectors will have appropriate complex values so as to make the entries of $x(t)$ real at every instant of time. For example,

$$(a+jb)e^{(\sigma-j\omega)t} + (a-jb)e^{(\sigma+j\omega)t}$$

has the form

$$e^{\sigma t}\sin(\omega t+\theta)$$

which represents a damped sinusoid for negative σ.

The real component of the eigenvalues gives the damping, and the imaginary component gives the frequency of oscillation. A negative real part represents a damped oscillation whereas a positive real part represents oscillation of increasing amplitude. Thus, for a complex pair of eigenvalues:

$$\lambda = \sigma \pm j\omega \tag{12.44}$$

The frequency of oscillation in Hz is given by

$$f = \frac{\omega}{2\pi} \tag{12.45}$$

This represents the actual or damped frequency. The damping ratio is given by

$$\zeta = \frac{-\sigma}{\sqrt{\sigma^2+\omega^2}} \tag{12.46}$$

The damping ratio ζ determines the rate of decay of the amplitude of the oscillation. The time constant of amplitude decay is $1/|\sigma|$. In other words, the amplitude decays to $1/e$ or 37% of the initial amplitude in $1/|\sigma|$ seconds or in $1/(2\pi\zeta)$ cycles of oscillation.

Figure 12.2 shows the six different eigenvalue combinations and the corresponding trajectory behaviour around the singular points applicable to a two-dimensional case.

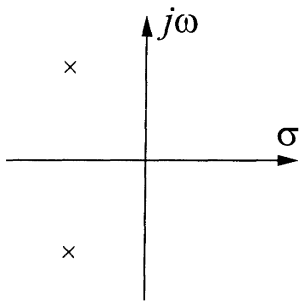
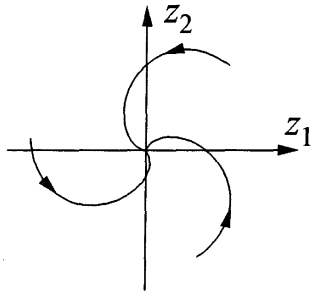
Eigenvalues ($\lambda=\sigma\pm j\omega$)	*Trajectory*	*Type of singularity*
(1) 		Stable focus

Figure 12.2 Singular points corresponding to six possible combinations of eigenvalue pairs
(*Continued on the next page*)

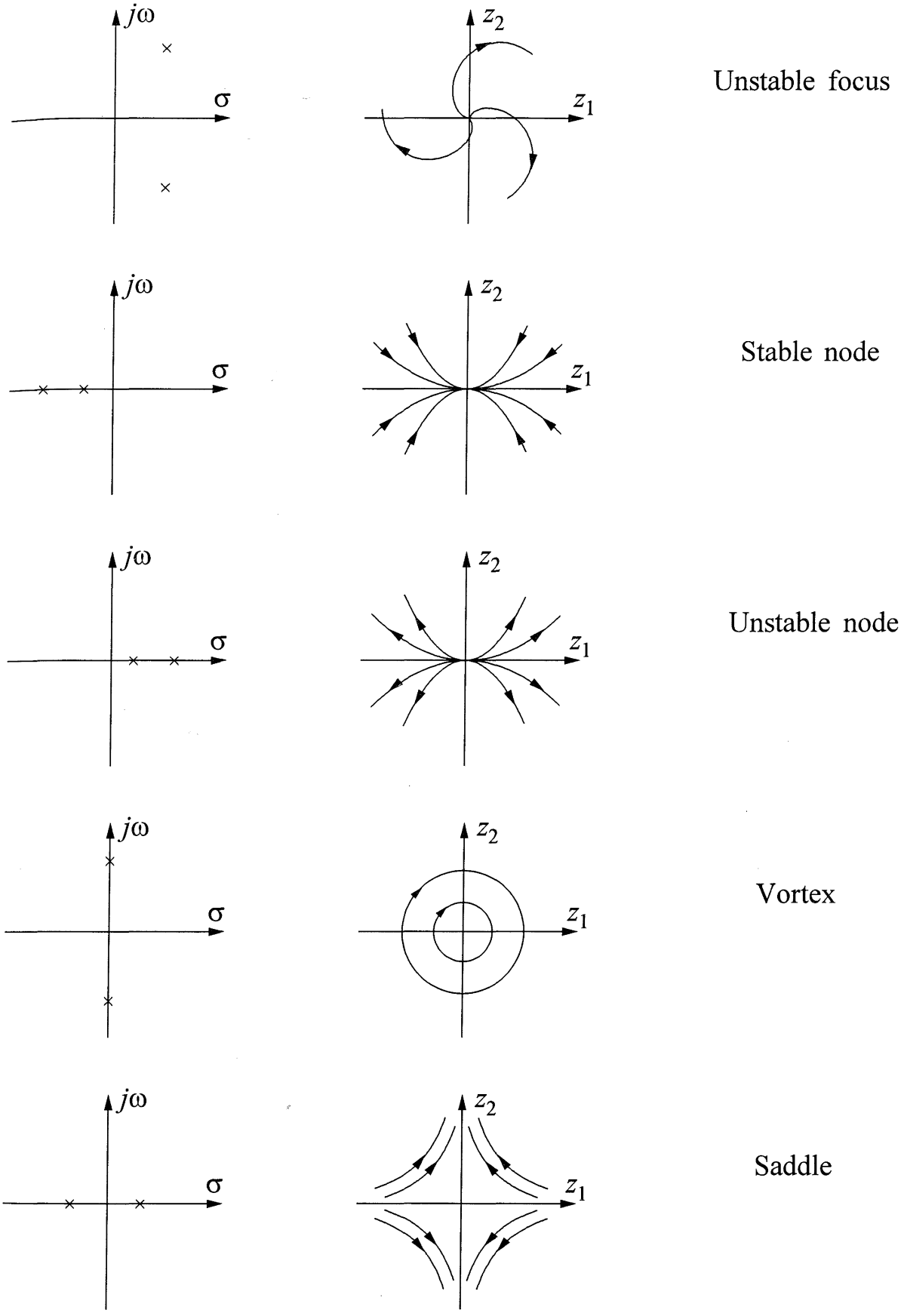


Figure 12.2 (*Continued*) Singular points corresponding to six possible combinations of eigenvalue pairs

Cases (1), (3) and (5) ensure local stability, with (1) and (3) being asymptotically stable.

12.2.5 Mode Shape, Sensitivity, and Participation Factor

(a) Mode shape and eigenvectors

In the previous section, we discussed the system response in terms of the state vectors $\Delta\mathbf{x}$ and $\mathbf{z}$, which are related to each other as follows:

$$\begin{aligned}\Delta\mathbf{x}(t) &= \mathbf{\Phi}\mathbf{z}(t) \\ &= [\ \boldsymbol{\phi}_1 \quad \boldsymbol{\phi}_2 \quad \cdots \quad \boldsymbol{\phi}_n\ ]\mathbf{z}(t)\end{aligned} \tag{12.47A}$$

and

$$\begin{aligned}\mathbf{z}(t) &= \mathbf{\Psi}\Delta\mathbf{x}(t) \\ &= [\ \boldsymbol{\psi}_1^T \quad \boldsymbol{\psi}_2^T \quad \cdots \quad \boldsymbol{\psi}_n^T\ ]^T\Delta\mathbf{x}(t)\end{aligned} \tag{12.47B}$$

The variables $\Delta x_1, \Delta x_2, ..., \Delta x_n$ are the original state variables chosen to represent the dynamic performance of the system. The variables $z_1, z_2, ..., z_n$ are the transformed state variables such that each variable is associated with only one mode. In other words, the transformed variables $\mathbf{z}$ are directly related to the modes.

From Equation 12.47A we see that the *right eigenvector* gives the *mode shape*, i.e., the relative activity of the state variables when a particular mode is excited. For example, the degree of activity of the state variable x_k in the ith mode is given by the element ϕ_{ki} of the right eigenvector $\boldsymbol{\phi}_i$.

The magnitudes of the elements of $\boldsymbol{\phi}_i$ give the extents of the activities of the n state variables in the ith mode, and the angles of the elements give phase displacements of the state variables with regard to the mode.

As seen from Equation 12.47B, the left eigenvector $\boldsymbol{\psi}_i$ identifies which combination of the original state variables displays only the ith mode. Thus the kth element of the right eigenvector $\boldsymbol{\phi}_i$ measures the activity of the variable x_k in the ith mode, and the kth element of the left eigenvector $\boldsymbol{\psi}_i$ weighs the contribution of this activity to the ith mode.

(b) Eigenvalue sensitivity

Let us now examine the sensitivity of eigenvalues to the elements of the state matrix. Consider Equation 12.19 which defines the eigenvalues and eigenvectors:

$$\mathbf{A}\boldsymbol{\phi}_i = \lambda_i\boldsymbol{\phi}_i$$

Differentiating with respect to a_{kj} (the element of **A** in kth row and jth column) yields

$$\frac{\partial \mathbf{A}}{\partial a_{kj}}\boldsymbol{\phi}_i + \mathbf{A}\frac{\partial \boldsymbol{\phi}_i}{\partial a_{kj}} = \frac{\partial \lambda_i}{\partial a_{kj}}\boldsymbol{\phi}_i + \lambda_i\frac{\partial \boldsymbol{\phi}_i}{\partial a_{kj}}$$

Premultiplying by $\boldsymbol{\psi}_i$, and noting that $\boldsymbol{\psi}_i\boldsymbol{\phi}_i = 1$ and $\boldsymbol{\psi}_i(\mathbf{A} - \lambda_i\mathbf{I}) = 0$, we see that the above equation simplifies to

$$\boldsymbol{\psi}_i\frac{\partial \mathbf{A}}{\partial a_{kj}}\boldsymbol{\phi}_i = \frac{\partial \lambda_i}{\partial a_{kj}}$$

All elements of $\partial\mathbf{A}/\partial a_{kj}$ are zero, except for the element in the kth row and jth column which is equal to 1. Hence,

$$\frac{\partial \lambda_i}{\partial a_{kj}} = \psi_{ik}\phi_{ji} \tag{12.48}$$

Thus the sensitivity of the eigenvalue λ_i to the element a_{kj} of the state matrix is equal to the product of the left eigenvector element ψ_{ik} and the right eigenvector element ϕ_{ji}.

(c) Participation factor

One problem in using right and left eigenvectors individually for identifying the relationship between the states and the modes is that the elements of the eigenvectors are dependent on units and scaling associated with the state variables. As a solution to this problem, a matrix called the *participation matrix* (**P**), which combines the right and left eigenvectors as follows is proposed in reference 2 as a measure of the association between the state variables and the modes.

$$\mathbf{P} = [\,\mathbf{p}_1 \quad \mathbf{p}_2 \quad \cdots \quad \mathbf{p}_n\,] \tag{12.49A}$$

with

$$\mathbf{p}_i = \begin{bmatrix} p_{1i} \\ p_{2i} \\ \vdots \\ p_{ni} \end{bmatrix} = \begin{bmatrix} \phi_{1i}\psi_{i1} \\ \phi_{2i}\psi_{i2} \\ \vdots \\ \phi_{ni}\psi_{in} \end{bmatrix} \tag{12.49B}$$

where

ϕ_{ki} = the element on the kth row and ith column of the modal matrix $\mathbf{\Phi}$
= kth entry of the right eigenvector $\boldsymbol{\phi}_i$
ψ_{ik} = the element on the ith row and kth column of the modal matrix $\mathbf{\Psi}$
= kth entry of the left eigenvector $\boldsymbol{\psi}_i$

The element $p_{ki}=\phi_{ki}\psi_{ik}$ is termed the *participation factor* [2]. It is a measure of the relative participation of the kth state variable in the ith mode, and vice versa.

Since ϕ_{ki} measures the *activity* of x_k in the ith mode and ψ_{ik} *weighs* the contribution of this activity to the mode, the product p_{ki} measures the *net participation*. The effect of multiplying the elements of the left and right eigenvectors is also to make p_{ki} dimensionless (i.e., independent of the choice of units).

In view of the eigenvector normalization, the sum of the participation factors associated with any mode ($\sum_{i=1}^{n} p_{ki}$) or with any state variable ($\sum_{k=1}^{n} p_{ki}$) is equal to 1.

From Equation 12.48, we see that the participation factor p_{ki} is actually equal to the sensitivity of the eigenvalue λ_i to the diagonal element a_{kk} of the state matrix **A**

$$p_{ki} = \frac{\partial \lambda_i}{\partial a_{kk}} \tag{12.50}$$

As we will see in a number of examples in this chapter, the participation factors are generally indicative of the relative participations of the respective states in the corresponding modes.

12.2.6 Controllability and Observability

In Section 12.1.3 the system response in the presence of input was given as Equations 12.8 and 12.9 and is repeated here for reference.

$$\Delta\dot{\mathbf{x}} = \mathbf{A}\Delta\mathbf{x} + \mathbf{B}\Delta\mathbf{u} \tag{12.8}$$

$$\Delta\mathbf{y} = \mathbf{C}\Delta\mathbf{x} + \mathbf{D}\Delta\mathbf{u} \tag{12.9}$$

Expressing them in terms of the transformed variables $\mathbf{z}$ defined by Equation 12.31 yields

$$\mathbf{\Phi}\dot{\mathbf{z}} = \mathbf{A}\mathbf{\Phi}\mathbf{z} + \mathbf{B}\Delta\mathbf{u}$$

$$\Delta\mathbf{y} = \mathbf{C}\mathbf{\Phi}\mathbf{z} + \mathbf{D}\Delta\mathbf{u}$$

The state equations in the "normal form" (decoupled) may therefore be written as

$$\dot{\mathbf{z}} = \mathbf{\Lambda z} + \mathbf{B}'\Delta\mathbf{u} \tag{12.51}$$

$$\Delta\mathbf{y} = \mathbf{C}'\mathbf{z} + \mathbf{D}\Delta\mathbf{u} \tag{12.52}$$

where

$$\mathbf{B}' = \mathbf{\Phi}^{-1}\mathbf{B} \tag{12.53}$$

$$\mathbf{C}' = \mathbf{C\Phi} \tag{12.54}$$

Referring to Equation 12.51, if the ith row of matrix $\mathbf{B}'$ is zero, the inputs have no effect on the ith mode. In such a case, the ith mode is said to be *uncontrollable*.

From Equation 12.52, we see that the ith column of the matrix $\mathbf{C}'$ determines whether or not the variable z_i contributes to the formation of the outputs. If the column is zero, then the corresponding mode is *unobservable*. This explains why some poorly damped modes are sometimes not detected by observing the transient response of a few monitored quantities.

The $n \times r$ matrix $\mathbf{B}' = \mathbf{\Phi}^{-1}\mathbf{B}$ is referred to as the *mode controllability matrix*, and the $m \times n$ matrix $\mathbf{C}' = \mathbf{C\Phi}$ as the *mode observability matrix*.

By inspecting $\mathbf{B}'$ and $\mathbf{C}'$ we can classify modes into controllable and observable; controllable and unobservable; uncontrollable and observable; uncontrollable and unobservable.[1]

12.2.7 The Concept of Complex Frequency

Consider the damped sinusoid

$$v = V_m e^{\sigma t}\cos(\omega t + \theta) \tag{12.55}$$

The unit of ω is radians per second and that of θ is radians. The dimensionless unit neper (Np) is commonly used for σt in honour of the mathematician John Napier (1550-1617) who invented logarithms. Thus the unit of σ is neper per second (Np/s).

For circuits in which the excitations and forced functions are damped sinusoids, such as that given by Equation 12.55, we can use phasor representations of damped sinusoids. This will work as well as the phasors of (undamped) sinusoids normally used in ac circuit analysis because the properties of sinusoids that make the phasors possible are shared by damped sinusoids. That is, the sum or difference of two or more damped sinusoids is a damped sinusoid and the derivative or indefinite

[1] This is referred to as *Kalman's canonical structure theorem*, since it was first proposed by R.E. Kalman in 1960.

integral of a damped sinusoid is also a damped sinusoid. In all these cases, V_m and θ may change; ω and σ are fixed.

Analogous to the form of phasor notation used for sinusoids, in the case of damped sinusoids, we may write

$$\begin{aligned} v &= V_m e^{\sigma t}\cos(\omega t+\theta) \\ &= \mathrm{Re}\left[V_m e^{\sigma t} e^{j(\omega t+\theta)}\right] \\ &= \mathrm{Re}\left[V_m e^{j\theta} e^{(\sigma+j\omega)t}\right] \end{aligned}$$

With $s=\sigma+j\omega$, we have

$$v = \mathrm{Re}\left(\tilde{V}e^{st}\right) \tag{12.56}$$

where $\tilde{V}$ is the phasor $(V_m\angle\theta)$ and is the same for both the undamped and damped sinusoids. Obviously, we may treat the damped sinusoids the same way we do undamped sinusoids by using s instead of $j\omega$.

Since s is a complex number, it is referred to as *complex frequency*, and $V(s)$ is called a *generalized phasor*.

All concepts such as impedance, admittance, Thevenin's and Norton's theorems, superposition, etc., carry over to the damped sinusoidal case.

It follows that, in the s-domain, the phasor current $I(s)$ and voltage $V(s)$, associated with a two-terminal network are related by

$$V(s) = Z(s)I(s)$$

where $Z(s)$ is the generalized impedance.

Similarly, input and output relations of dynamic devices can be expressed as

$$\frac{V_o(s)}{V_i(s)} = G(s) = \frac{b_m s^m + b_{m-1}s^{m-1} + \cdots + b_1 s + b_0}{a_n s^n + a_{n-1}s^{n-1} + \cdots + a_1 s + a_0}$$

In the factored form,

$$G(s) = \frac{b_m(s-z_1)(s-z_2)\cdots(s-z_m)}{a_n(s-p_1)(s-p_2)\cdots(s-p_n)}$$

The numbers $z_1, z_2, \ldots, z_m$ are called the *zeros* because they are values of s for which $G(s)$ becomes zero. The numbers $p_1, p_2, \ldots, p_n$ are called the *poles* of $G(s)$. The values

of poles and zeros, along with a_n and b_m, uniquely determine the system transfer function $G(s)$. Poles and zeros are useful in considering frequency domain properties of dynamic systems.

12.2.8 Relationship between Eigenproperties and Transfer Functions

The state-space representation is concerned not only with input and output properties of the system but also with its complete internal behaviour. In contrast, the transfer function representation specifies only the input/output behaviour. Hence, one can make an arbitrary selection of state variables when a plant is specified only by a transfer function. On the other hand, if a state-space representation of a system is known, the transfer function is uniquely defined. In this sense, the state-space representation is a more complete description of the system; it is ideally suited for the analysis of multi-variable multi-input and multi-output systems.

For small-signal stability analysis of power systems, we primarily depend on the eigenvalue analysis of the system state matrix. However, for control design we are interested in an open-loop transfer function between specific variables. To see how this is related to the state matrix and to the eigenproperties, let us consider the transfer function between the variables y and u. From Equations 12.8 and 12.9, we may write

$$\Delta\dot{\mathbf{x}} = \mathbf{A}\Delta\mathbf{x} + \mathbf{b}\Delta u \tag{12.57}$$

$$\Delta y = \mathbf{c}\Delta\mathbf{x} \tag{12.58}$$

where $\mathbf{A}$ is the state matrix, $\Delta\mathbf{x}$ is the state vector, Δu is a single input, Δy is a single output, $\mathbf{c}$ is a row vector and $\mathbf{b}$ is a column vector. We assume that y is not a direct function of u (i.e., $\mathbf{D}$=0).

The required transfer function is

$$G(s) = \frac{\Delta y(s)}{\Delta u(s)} = \mathbf{c}(s\mathbf{I}-\mathbf{A})^{-1}\mathbf{b} \tag{12.59}$$

This has the general form

$$G(s) = K\frac{N(s)}{D(s)} \tag{12.60}$$

If $D(s)$ and $N(s)$ can be factored, we may write

$$G(s) = K\frac{(s-z_1)(s-z_2)\cdots(s-z_l)}{(s-p_1)(s-p_2)\cdots(s-p_n)} \tag{12.61}$$

As discussed in Section 12.2.7, the n values of s, namely, $p_1, p_2, ..., p_n$, which make the denominator polynomial $D(s)$ zero are the *poles* of $G(s)$. The l values of s, namely, $z_1, z_2, ..., z_l$, are the *zeros* of $G(s)$.

Now, $G(s)$ can be expanded in partial fractions as

$$G(s) = \frac{R_1}{s-p_1} + \frac{R_2}{s-p_2} + \cdots + \frac{R_n}{s-p_n} \tag{12.62}$$

and R_i is known as the *residue* of $G(s)$ at pole p_i.

To express the transfer function in terms of the eigenvalues and eigenvectors, we express the state variables $\Delta\mathbf{x}$ in terms of the transformed variables $\mathbf{z}$ defined by Equation 12.31. Following the procedure used in Section 12.2.4, Equations 12.57 and 12.58 may be written in terms of the transformed variables as

$$\begin{aligned} \dot{\mathbf{z}} &= \mathbf{\Phi}^{-1}\mathbf{A}\mathbf{\Phi}\mathbf{z} + \mathbf{\Phi}^{-1}\mathbf{b}\Delta u \\ &= \mathbf{\Lambda}\mathbf{z} + \mathbf{\Phi}^{-1}\mathbf{b}\Delta u \end{aligned} \tag{12.63}$$

and

$$\Delta y = \mathbf{c}\mathbf{\Phi}\mathbf{z} \tag{12.64}$$

Hence,

$$\begin{aligned} G(s) &= \frac{\Delta y(s)}{\Delta u(s)} \\ &= \mathbf{c}\mathbf{\Phi}[s\mathbf{I} - \mathbf{\Lambda}]^{-1}\mathbf{\Psi}\mathbf{b} \end{aligned} \tag{12.65}$$

Since $\mathbf{\Lambda}$ is a diagonal matrix, we may write

$$G(s) = \sum_{i=1}^{n} \frac{R_i}{s-\lambda_i} \tag{12.66}$$

where

$$R_i = \mathbf{c}\boldsymbol{\phi}_i\boldsymbol{\psi}_i\mathbf{b} \tag{12.67}$$

We see that the poles of $G(s)$ are given by the eigenvalues of $\mathbf{A}$. Equation 12.67 gives the residues in terms of the eigenvectors. The zeros of $G(s)$ are given by the solution of

$$\sum_{i=1}^{n} \frac{R_i}{s-\lambda_i} = 0 \tag{12.68}$$

Example 12.1

In this example we will study a second-order linear system. Such a system is easy to analyze and is helpful in understanding the behaviour of higher-order systems. The performance of high-order systems is often viewed in terms of a dominant set of second-order poles or eigenvalues. Therefore, a thorough understanding of the characteristics of a second-order system is essential before we study complex systems.

Figure E12.1 shows the familiar *RLC* circuit, which represents a second-order system. Study the eigenproperties of the state matrix of the system and examine its modal characteristics.

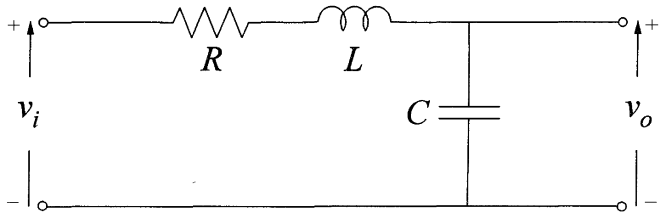


Figure E12.1

Solution

The differential equation relating v_o to v_i is

$$LC\frac{d^2v_o}{dt^2} + RC\frac{dv_o}{dt} + v_o = v_i \tag{E12.1}$$

This may be written in the standard form

$$\frac{d^2v_o}{dt^2} + (2\zeta\omega_n)\frac{dv_o}{dt} + \omega_n^2 v_o = \omega_n^2 v_i \tag{E12.2}$$

where

$\omega_n = 1/\sqrt{LC}$ = undamped natural frequency

$\zeta = (R/2)/\sqrt{L/C}$ = damping ratio

In order to develop the state-space representation, we define the following state, input and output variables:

$$\begin{aligned} x_1 &= v_o \\ x_2 &= \frac{dv_o}{dt} \\ u &= v_i \\ y &= v_o = x_1 \end{aligned} \tag{E12.3}$$

Using the above quantities, Equation E12.2 can be expressed in terms of two first-order equations:

$$\frac{dx_1}{dt} = x_2 \tag{E12.4}$$

$$\frac{dx_2}{dt} = -\omega_n^2 x_1 - (2\zeta\omega_n)x_2 + \omega_n^2 u \tag{E12.5}$$

In matrix form,

$$\begin{bmatrix} \dot{x}_1 \\ \dot{x}_2 \end{bmatrix} = \begin{bmatrix} 0 & 1 \\ -\omega_n^2 & -2\zeta\omega_n \end{bmatrix} \begin{bmatrix} x_1 \\ x_2 \end{bmatrix} + \begin{bmatrix} 0 \\ \omega_n^2 \end{bmatrix} u \tag{E12.6}$$

The output variable is given by

$$y = [1 \;\; 0] \begin{bmatrix} x_1 \\ x_2 \end{bmatrix} + 0u \tag{E12.7}$$

These have the standard state-space form:

$$\begin{aligned} \dot{\mathbf{x}} &= \mathbf{A}\mathbf{x} + \mathbf{b}u \\ y &= \mathbf{c}\mathbf{x} + du \end{aligned}$$

The eigenvalues of **A** are given by

$$\begin{vmatrix} -\lambda & 1 \\ -\omega_n^2 & -2\zeta\omega_n - \lambda \end{vmatrix} = 0$$

Hence,

$$\lambda^2 + 2\zeta\omega_n\lambda + \omega_n^2 = 0 \tag{E12.8}$$

Solving for the eigenvalues, we have

$$\begin{aligned}\lambda_1 &= -\zeta\omega_n+\omega_n\sqrt{\zeta^2-1}\\ \lambda_2 &= -\zeta\omega_n-\omega_n\sqrt{\zeta^2-1}\end{aligned} \tag{E12.9}$$

The right eigenvectors are given by

$$(\mathbf{A}-\lambda\mathbf{I})\boldsymbol{\phi} = 0$$

Therefore,

$$\begin{bmatrix}-\lambda_i & 1\\ -\omega_n^2 & -2\zeta\omega_n-\lambda_i\end{bmatrix}\begin{bmatrix}\phi_{1i}\\ \phi_{2i}\end{bmatrix} = \begin{bmatrix}0\\ 0\end{bmatrix}$$

This may be rewritten as

$$\begin{aligned}-\lambda_i\phi_{1i}+\phi_{2i} &= 0\\ -\omega_n^2\phi_{1i}-(2\zeta\omega_n+\lambda_i)\phi_{2i} &= 0\end{aligned} \tag{E12.10}$$

If we attempt to solve the above equations for ϕ_{1i} and ϕ_{2i}, we realize that they are not independent. As discussed earlier, this is true in general; for an nth order system, the equation $(\mathbf{A}-\lambda\mathbf{I})\boldsymbol{\phi}=0$ gives only $n-1$ independent equations for the n components of eigenvectors. One component of the eigenvector may be fixed arbitrarily and then the other components can be determined from the $n-1$ independent equations. It should, however, be noted that the eigenvectors themselves are linearly independent if eigenvalues are distinct.

For the second-order system, we can fix $\phi_{1i}=1$ and determine ϕ_{2i}, from one of the two relationships in Equation E12.10, for each eigenvalue.

The eigenvector corresponding to λ_1 is

$$\boldsymbol{\phi}_1 = \begin{bmatrix}\phi_{11}\\ \phi_{21}\end{bmatrix} = \begin{bmatrix}1\\ \lambda_1\end{bmatrix} = \begin{bmatrix}1\\ -\zeta\omega_n+\omega_n\sqrt{\zeta^2-1}\end{bmatrix} \tag{E12.11}$$

and the eigenvector corresponding to λ_2 is

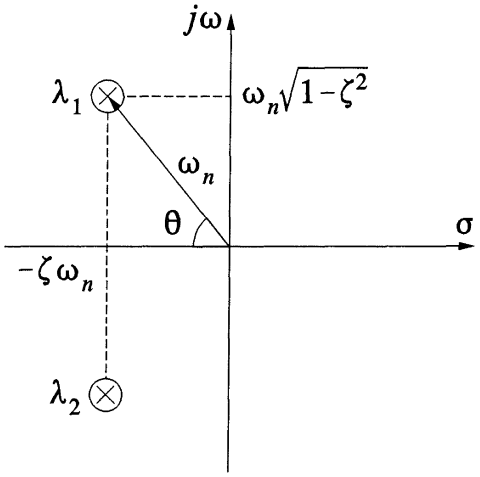
$$\boldsymbol{\phi}_2 = \begin{bmatrix}\phi_{12}\\ \phi_{22}\end{bmatrix} = \begin{bmatrix}1\\ \lambda_2\end{bmatrix} = \begin{bmatrix}1\\ -\zeta\omega_n-\omega_n\sqrt{\zeta^2-1}\end{bmatrix} \tag{E12.12}$$

The nature of the system response depends almost entirely on the damping ratio ζ. The value of ω_n has the effect of simply adjusting the time scale.

If ζ is greater than 1, both eigenvalues are real and negative; if ζ is equal to 1, both eigenvalues are equal to $-\omega_n$; and if ζ is less than 1, eigenvalues are complex conjugates, given as

$$\begin{aligned}\lambda &= -\zeta\omega_n \pm j\omega_n\sqrt{1-\zeta^2} \\ &= \sigma \pm j\omega\end{aligned} \tag{E12.13}$$

The location of the eigenvalues in the complex plane with respect to ζ and ω_n is indicated in Figure E12.2.



Damping angle θ

$$= \cos^{-1}\zeta$$

$$= \tan^{-1}\left(\frac{\sqrt{1-\zeta^2}}{\zeta}\right)$$

Figure E12.2

We will first examine the singularities of the second-order system and discuss the shape of the state trajectories near the singularity. We will then discuss in detail the case where both eigenvalues are real and negative, with λ_2 greater than λ_1, but with λ_1 and λ_2 not far different.

The state equations in the normal form are given by

$$\dot{z}_1 = \lambda_1 z_1 \tag{E12.14}$$

$$\dot{z}_2 = \lambda_2 z_2 \tag{E12.15}$$

Hence,

$$\frac{\dot{z}_2}{\dot{z}_1} = \frac{dz_2}{dz_1} = \frac{\lambda_2 z_2}{\lambda_1 z_1} \tag{E12.16}$$

By integration,

$$z_2 = cz_1^{\lambda_2/\lambda_1} \tag{E12.17}$$

where c is the arbitrary constant dependent upon initial conditions. Curves representing the above in the z_1–z_2 plane are generally parabolic, with the exact shape determined by the ratio λ_2/λ_1 and constant c. The slope of the curves is given by

$$\frac{dz_2}{dz_1} = c\frac{\lambda_2}{\lambda_1} z_1^{\lambda_2/\lambda_1 - 1} \tag{E12.18}$$

Near the origin, $dz_2/dz_1 \to 0$ as $z_1 \to 0$, since $\lambda_2/\lambda_1 > 1$.

Typical trajectories in the phase plane with "normal" coordinates are shown in Figure E12.3.

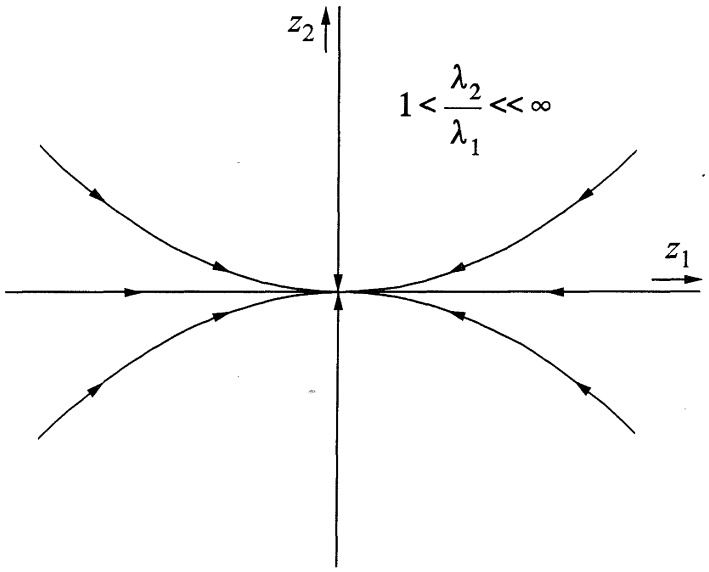


Figure E12.3

The curves represent loci of points determined by the corresponding values of z_1 and z_2. As the independent variable t increases, the point relating instantaneous values of z_1 and z_2 moves along the curve in the direction of the arrowheads. Initial conditions determine the value of c and the quadrant within which a particular solution lies. Since the roots are negative, both z_1 and z_2 decrease and ultimately reach zero as t increases. The singularity is referred to as a *stable node.*

If the initial conditions are such that one of the variables z_1 and z_2 is equal to zero, this variable remains zero, and the solution curve is on either the z_2 or z_1 axis. The axes then represent special cases of solution curves, corresponding to special initial conditions.

The corresponding plots in the x_1–x_2 plane are shown in Figure E12.4. The lines corresponding to z_1 and z_2 on this plane are skewed in accordance with the

transformation $\mathbf{x} = \mathbf{\Phi z}$.

If the input v_i is zero, and if the initial conditions are such that (x_1, x_2) is on one of the eigenvectors, the state vector will remain in the same direction but will vary in magnitude by the factor $e^{\lambda_1 t}$ or $e^{\lambda_2 t}$ as the case may be.

If the vector representing the initial condition is not an eigenvector, it can be represented by a linear combination of the two eigenvectors. The response of the circuit will be the sum of the two responses. As time increases, the component in the direction of the eigenvector $\boldsymbol{\phi}_2$ becomes less significant because $e^{\lambda_2 t}$ decays faster than $e^{\lambda_1 t}$. Thus the trajectories always approach the origin along the $\boldsymbol{\phi}_1$ direction unless the component of this eigenvector was initially zero. If the eigenvectors are not real, such a simple physical interpretation of eigenvectors is not possible.

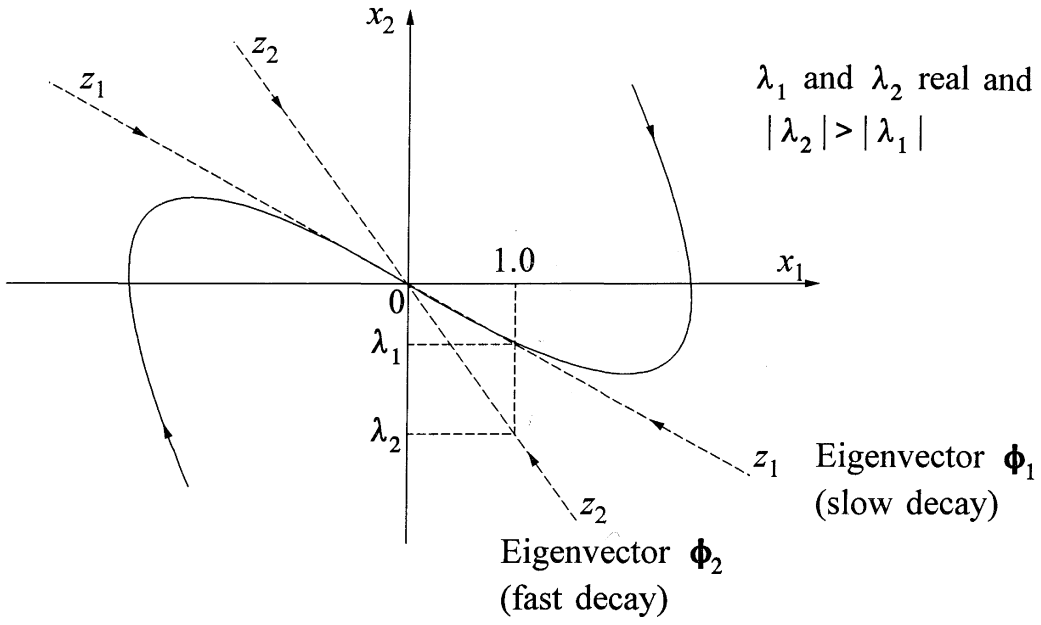


Figure E12.4 ■

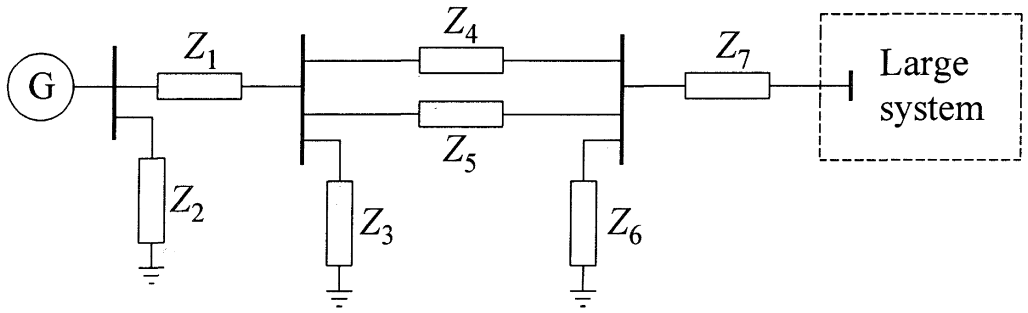
12.2.9 Computation of Eigenvalues

In the above example, we computed the eigenvalues by solving the characteristic equation of the system. This was possible because we were analyzing a simple second-order system. For higher-order systems with eigenvalues of widely differing magnitudes, this approach fails. The method that has been widely used for the computation of eigenvalues of real non-symmetrical matrices is the *QR* transformation method originally developed by J.G.F. Francis [3]. The method is numerically stable, robust, and converges rapidly. It is used in a number of very good general purpose commercial codes and has been successfully used for analyzing small-signal stability of power systems with several hundred states. The right eigenvectors may be computed by using the inverse iteration technique. A good description of the *QR* transformation and inverse iteration methods may be found in reference 4.

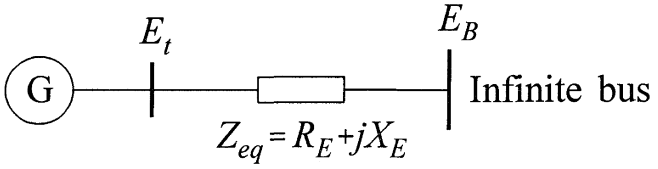
For large systems involving several thousand states, the *QR* method cannot be used for computing the eigenvalues. The reason for this and a description of special techniques for eigenvalue analysis of very large systems are presented in Section 12.8.

12.3 SMALL-SIGNAL STABILITY OF A SINGLE-MACHINE INFINITE BUS SYSTEM

In this section we will study the small-signal performance of a single machine connected to a large system through transmission lines. A general system configuration is shown in Figure 12.3(a). Analysis of systems having such simple configurations is extremely useful in understanding basic effects and concepts. After we develop an appreciation for the physical aspects of the phenomena and gain experience with the analytical techniques, using simple low-order systems, we will be in a better position to deal with large complex systems.



(a) General configuration



(b) Equivalent system

Figure 12.3 Single machine connected to a large system through transmission lines

For the purpose of analysis, the system of Figure 12.3(a) may be reduced to the form of Figure 12.3(b) by using Thévenin's equivalent of the transmission network external to the machine and the adjacent transmission. Because of the relative size of the system to which the machine is supplying power, dynamics associated with the machine will cause virtually no change in the voltage and frequency of Thévenin's

voltage E_B. Such a voltage source of constant voltage and constant frequency is referred to as an *infinite bus.*

For any given system condition, the magnitude of the infinite bus voltage E_B remains constant when the machine is perturbed. However, as the steady-state system conditions change, the magnitude of E_B may change, representing a changed operating condition of the external network.

In what follows we will analyze the small-signal stability of the system of Figure 12.3(b) with the synchronous machine represented by models of varying degrees of detail. We will begin with the classical model and gradually increase the model detail by accounting for the effects of the dynamics of the field circuit, excitation system, and amortisseurs. In each case, we will develop the expressions for the elements of the state matrix as explicit functions of system parameters. This will help make clear the effects of various factors associated with a synchronous machine on system stability. In addition to the state-space representation and modal analysis, we will use the block diagram representation and torque-angle relationships to analyze the system-stability characteristics. The block diagram approach was first used by Heffron and Phillips [5] and later by deMello and Concordia [6] to analyze the small-signal stability of synchronous machines. While this approach is not suited for a detailed study of large systems, it is useful in gaining a physical insight into the effects of field circuit dynamics and in establishing the basis for methods of enhancing stability through excitation control.

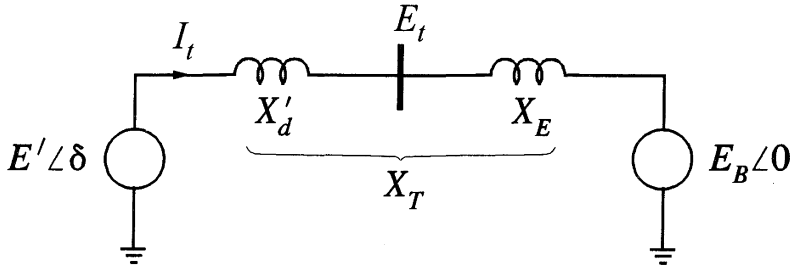
12.3.1 Generator Represented by the Classical Model

With the generator represented by the classical model (see Section 5.3.1) and all resistances neglected, the system representation is as shown in Figure 12.4.

Here E' is the voltage behind X'_d. Its magnitude is assumed to remain constant at the pre-disturbance value. Let δ be the angle by which E' leads the infinite bus voltage E_B. As the rotor oscillates during a disturbance, δ changes.

With E' as reference phasor,

$$\tilde{I}_t = \frac{E'\angle 0^\circ - E_B\angle -\delta}{jX_T} = \frac{E' - E_B(\cos\delta - j\sin\delta)}{jX_T} \tag{12.69}$$



$$\tilde{E}' = \tilde{E}_{t0} + jX'_d\tilde{I}_{t0}$$
$$X_T = X'_d + X_E$$

Figure 12.4

The complex power behind X'_d is given by

$$\begin{aligned} S' &= P+jQ' = \tilde{E}'\tilde{I}_t^* \\ &= \frac{E'E_B\sin\delta}{X_T} + j\frac{E'(E'-E_B\cos\delta)}{X_T} \end{aligned} \tag{12.70}$$

With stator resistance neglected, the air-gap power (P_e) is equal to the terminal power (P). In per unit, the air-gap torque is equal to the air-gap power (see Section 5.1.2). Hence,

$$T_e = P = \frac{E'E_B}{X_T}\sin\delta \tag{12.71}$$

Linearizing about an initial operating condition represented by $\delta=\delta_0$ yields

$$\Delta T_e = \frac{\partial T_e}{\partial\delta}\Delta\delta = \frac{E'E_B}{X_T}\cos\delta_0(\Delta\delta) \tag{12.72}$$

The equations of motion (Equations 3.209 and 3.210 of Chapter 3) in per unit are

$$p\Delta\omega_r = \frac{1}{2H}(T_m - T_e - K_D\Delta\omega_r) \tag{12.73}$$

$$p\delta = \omega_0\Delta\omega_r \tag{12.74}$$

where $\Delta\omega_r$ is the per unit speed deviation, δ is rotor angle[1] in electrical radians, ω_0 is the base rotor electrical speed in radians per second, and p is the differential operator d/dt with time t in seconds.

Linearizing Equation 12.73 and substituting for ΔT_e given by Equation 12.72, we obtain

$$p\Delta\omega_r = \frac{1}{2H}[\Delta T_m - K_S\Delta\delta - K_D\Delta\omega_r] \tag{12.75}$$

where K_S is the synchronizing torque coefficient given by

---

[1] As discussed in Section 5.3.1, for a classical generator model, the angle of E' with respect to a synchronously rotating reference phasor can be used as a measure of the rotor angle. Here we have chosen E_B as the reference, and the rotor angle δ is measured as the angle by which E' leads E_B.

$$K_S = \left(\frac{E'E_B}{X_T}\right)\cos\delta_0 \tag{12.76}$$

Linearizing Equation 12.74, we have

$$p\Delta\delta = \omega_0 \Delta\omega_r \tag{12.77}$$

Writing Equations 12.75 and 12.77 in the vector-matrix form, we obtain

$$\frac{d}{dt}\begin{bmatrix}\Delta\omega_r \\ \Delta\delta\end{bmatrix} = \begin{bmatrix}-\frac{K_D}{2H} & -\frac{K_S}{2H} \\ \omega_0 & 0\end{bmatrix}\begin{bmatrix}\Delta\omega_r \\ \Delta\delta\end{bmatrix} + \begin{bmatrix}\frac{1}{2H} \\ 0\end{bmatrix}\Delta T_m \tag{12.78}$$

This is of the form $\dot{\mathbf{x}} = \mathbf{A}\mathbf{x} + \mathbf{b}u$. The elements of the state matrix **A** are seen to be dependent on the system parameters K_D, H, X_T, and the initial operating condition represented by the values of E' and δ_0. The block diagram representation shown in Figure 12.5 can be used to describe the small-signal performance.

From the block diagram of Figure 12.5, we have

$$\begin{aligned}\Delta\delta &= \frac{\omega_0}{s}\left[\frac{1}{2Hs}\left(-K_S\Delta\delta - K_D\Delta\omega_r + \Delta T_m\right)\right] \\ &= \frac{\omega_0}{s}\left[\frac{1}{2Hs}\left(-K_S\Delta\delta - K_D s\frac{\Delta\delta}{\omega_0} + \Delta T_m\right)\right]\end{aligned} \tag{12.79}$$

Rearranging, we get

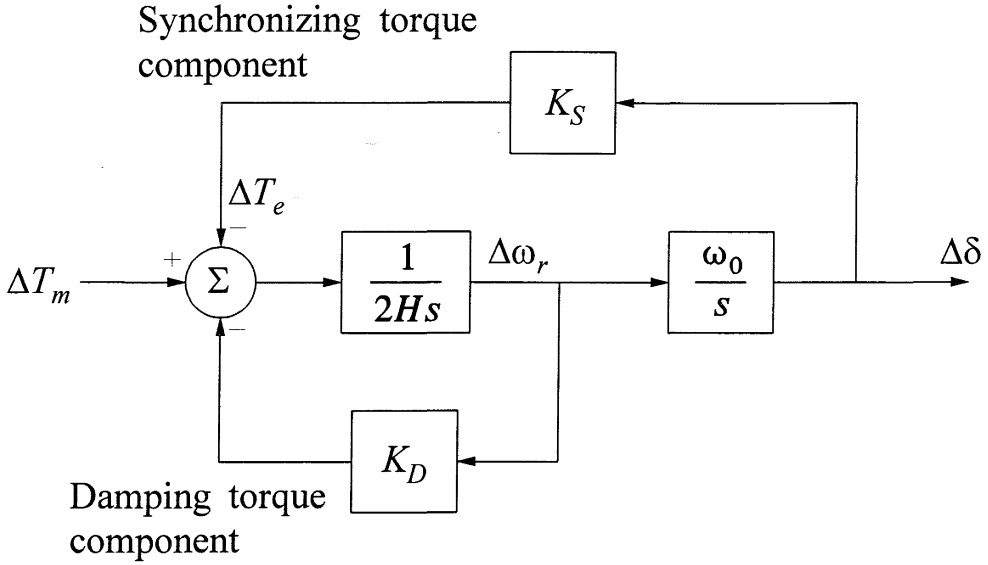
$$s^2(\Delta\delta) + \frac{K_D}{2H}s(\Delta\delta) + \frac{K_S}{2H}\omega_0(\Delta\delta) = \frac{\omega_0}{2H}\Delta T_m$$

Therefore, the characteristic equation is given by

$$s^2 + \frac{K_D}{2H}s + \frac{K_S\omega_0}{2H} = 0 \tag{12.80}$$

This is of the general form

$$s^2 + 2\zeta\omega_n s + \omega_n^2 = 0$$



K_S = synchronizing torque coefficient in pu torque/rad
K_D = damping torque coefficient in pu torque/pu speed deviation
H = inertia constant in MW·s/MVA
$\Delta\omega_r$ = speed deviation in pu = $(\omega_r-\omega_0)/\omega_0$
$\Delta\delta$ = rotor angle deviation in elec. rad
s = Laplace operator
ω_0 = rated speed in elec. rad/s = $2\pi f_0$
= 377 for a 60 Hz system

Figure 12.5 Block diagram of a single-machine infinite bus system with classical generator model

Therefore, the undamped natural frequency is

$$\omega_n = \sqrt{K_S \frac{\omega_0}{2H}} \quad \text{rad/s} \tag{12.81}$$

and the damping ratio is

$$\begin{aligned} \zeta &= \frac{1}{2}\frac{K_D}{2H\omega_n} \\ &= \frac{1}{2}\frac{K_D}{\sqrt{K_S 2H\omega_0}} \end{aligned} \tag{12.82}$$

As the synchronizing torque coefficient K_S increases, the natural frequency increases and the damping ratio decreases. An increase in damping torque coefficient K_D increases the damping ratio, whereas an increase in inertia constant decreases both ω_n and ζ.

Example 12.2

Figure E12.5 shows the system representation applicable to a thermal generating station consisting of four 555 MVA, 24 kV, 60 Hz units.

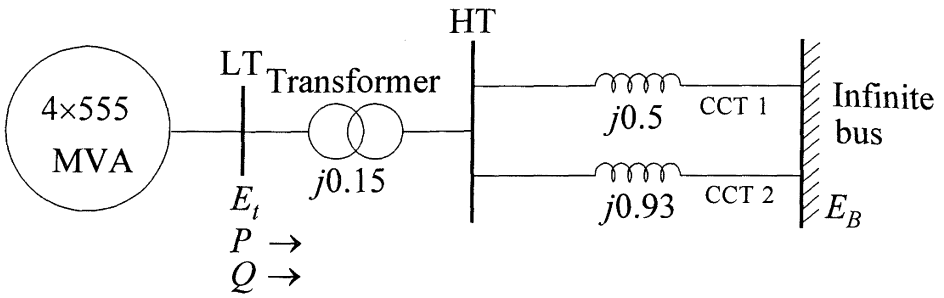


Figure E12.5

The network reactances shown in the figure are in per unit on 2220 MVA, 24 kV base (referred to the LT side of the step-up transformer). Resistances are assumed to be negligible.

The objective of this example is to analyze the small-signal stability characteristics of the system about the steady-state operating condition following the loss of circuit 2. The postfault system condition in per unit on the 2220 MVA, 24 kV base is as follows:

$$P = 0.9 \qquad Q = 0.3 \text{ (overexcited)} \qquad E_t = 1.0\angle 36° \qquad E_B = 0.995\angle 0°$$

The generators are to be modelled as a single equivalent generator represented by the classical model with the following parameters expressed in per unit on 2220 MVA, 24 kV base:

$$X'_d = 0.3 \qquad H = 3.5 \text{ MW·s/MVA}$$

(a) Write the linearized state equations of the system. Determine the eigenvalues, damped frequency of oscillation in Hz, damping ratio and undamped natural frequency for each of the following values of damping coefficient (in pu torque/pu speed):

(i) $K_D = 0$ (ii) $K_D = -10.0$ (iii) $K_D = 10.0$

(b) For the case with K_D=10.0, find the left and right eigenvectors, and participation matrix. Determine the time response if at t=0, $\Delta\delta$=5° and $\Delta\omega$=0.

Solution

(a) Figure E12.6 shows the circuit model representing the postfault steady-state operating condition with all parameters expressed in per unit on 2220 MVA base.

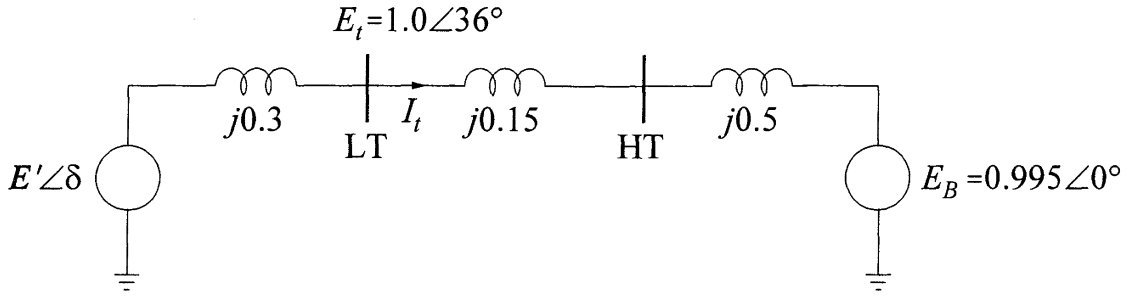


Figure E12.6

With E_t as reference phasor, the generator stator current is given by

$$\tilde{I}_t = \frac{(P+jQ)^*}{\tilde{E}_t^*} = \frac{0.9-j0.3}{1.0}$$
$$= 0.9-j0.3 \quad \text{pu}$$

The voltage behind the transient reactance is

$$\tilde{E}' = \tilde{E}_t + jX_d'\tilde{I}_t$$
$$= 1.0+j0.3(0.9-j0.3)$$
$$= 1.09+j0.27 = 1.123\angle 13.92° \quad \text{pu}$$

The angle by which E' leads E_B is

$$\delta_0 = 13.92° + 36° = 49.92°$$

The total system reactance is

$$X_T = 0.3+0.15+0.5 = 0.95 \quad \text{pu}$$

The corresponding synchronizing torque coefficient, from Equation 12.76, is

$$K_S = \frac{E'E_B}{X_T}\cos\delta_0$$
$$= \frac{1.123\times 0.995}{0.95}\cos 49.92°$$
$$= 0.757 \quad \text{pu torque/rad}$$

Linearized system equations are

$$\begin{bmatrix} \Delta\dot{\omega}_r \\ \Delta\dot{\delta} \end{bmatrix} = \begin{bmatrix} -\dfrac{K_D}{2H} & -\dfrac{K_S}{2H} \\ \omega_0 & 0 \end{bmatrix} \begin{bmatrix} \Delta\omega_r \\ \Delta\delta \end{bmatrix} + \begin{bmatrix} \dfrac{1}{2H} \\ 0 \end{bmatrix} \Delta T_m$$

$$= \begin{bmatrix} -0.143K_D & -0.108 \\ 377.0 & 0 \end{bmatrix} \begin{bmatrix} \Delta\omega_r \\ \Delta\delta \end{bmatrix} + \begin{bmatrix} 0.143 \\ 0 \end{bmatrix} \Delta T_m$$

The eigenvalues of the state matrix are given by

$$\begin{vmatrix} -0.143K_D - \lambda & -0.108 \\ 377.0 & -\lambda \end{vmatrix} = 0$$

or

$$\lambda^2 + 0.143K_D\lambda + 40.79 = 0$$

This is of the form

$$\lambda^2 + 2\zeta\omega_n\lambda + \omega_n^2 = 0$$

with

$$\omega_n = \sqrt{40.79} = 6.387 \text{ rad/s} = 1.0165 \text{ Hz}$$
$$\zeta = 0.143K_D/(2\times 6.387) = 0.0112K_D$$

The eigenvalues are

$$\lambda_1, \lambda_2 = -\zeta\omega_n \pm \omega_n\sqrt{1-\zeta^2}$$

The damped frequency is

$$\omega_d = \omega_n\sqrt{1-\zeta^2}$$

The following are the required results for different values of K_D.

K_D	0	10	-10
Eigenvalues λ	$0\pm j6.39$	$-0.714\pm j6.35$	$0.714\pm j6.36$
Damped frequency ω_d	1.0165 Hz	1.0101 Hz	1.0101 Hz
Damping ratio ζ	0	0.112	-0.112
Undamped natural frequency ω_n	1.0165 Hz	1.0165 Hz	1.0165 Hz

(b) The right eigenvectors are given by

$$(\mathbf{A}-\lambda\mathbf{I})\boldsymbol{\phi} = 0$$

For the given system, with K_D=10, the above equation becomes

$$\begin{bmatrix} -1.43-\lambda_i & -0.108 \\ 377.0 & -\lambda_i \end{bmatrix}\begin{bmatrix} \phi_{1i} \\ \phi_{2i} \end{bmatrix} = 0$$

For $\lambda=-0.714+j6.35$, the corresponding equations are

$$(0.714+j6.35)\phi_{11}+0.108\phi_{21} = 0$$

$$377.0\phi_{11}+(0.714-j6.35)\phi_{21} = 0$$

The above equations are not linearly independent. As discussed in Example 12.1, one of the eigenvectors corresponding to an eigenvalue has to be set arbitrarily. Therefore, let

$$\phi_{21} = 1.0$$

then

$$\phi_{11} = -0.0019+j0.0168$$

Similarly, eigenvectors corresponding to $\lambda_2=-0.714-j6.35$ are

$$\phi_{22} = 1.0 \qquad \phi_{12} = -0.0019-j0.0168$$

The right eigenvector modal matrix is

$$\boldsymbol{\Phi} = \begin{bmatrix} -0.0019+j0.0168 & -0.0019-j0.0168 \\ 1.0 & 1.0 \end{bmatrix}$$

The left eigenvectors normalized so that $\boldsymbol{\psi}_i \boldsymbol{\phi}_i = 1.0$ are given by

$$\boldsymbol{\Psi} = \boldsymbol{\Phi}^{-1} = \frac{\text{adj}(\boldsymbol{\Phi})}{|\boldsymbol{\Phi}|}$$

$$= \frac{\begin{bmatrix} 1.0 & -1.0 \\ 0.0019+j0.0168 & -0.0019+j0.0168 \end{bmatrix}^T}{(-0.0019+j0.0168+0.0019+j0.0168)}$$

$$= \begin{bmatrix} -j29.76 & 0.5-j0.056 \\ j29.76 & 0.5+j0.056 \end{bmatrix}$$

The participation matrix is

$$\mathbf{P} = \begin{bmatrix} \phi_{11}\psi_{11} & \phi_{12}\psi_{21} \\ \phi_{21}\psi_{12} & \phi_{22}\psi_{22} \end{bmatrix}$$

$$= \begin{bmatrix} 0.5+j0.056 & 0.5-j0.056 \\ 0.5-j0.056 & 0.5+j0.056 \end{bmatrix} = \begin{bmatrix} 0.503\angle 6.4^\circ & 0.503\angle -6.4^\circ \\ 0.503\angle -6.4^\circ & 0.503\angle 6.4^\circ \end{bmatrix}$$

The time response is given by

$$\begin{bmatrix} \Delta\omega_r(t) \\ \Delta\delta(t) \end{bmatrix} = \begin{bmatrix} \phi_{11} & \phi_{12} \\ \phi_{21} & \phi_{22} \end{bmatrix} \begin{bmatrix} c_1 e^{\lambda_1 t} \\ c_2 e^{\lambda_2 t} \end{bmatrix}$$

With $\Delta\delta = 5^\circ = 0.0873$ rad and $\Delta\omega_r = 0$ at $t=0$, we have

$$\begin{bmatrix} c_1 \\ c_2 \end{bmatrix} = \begin{bmatrix} \psi_{11} & \psi_{12} \\ \psi_{21} & \psi_{22} \end{bmatrix} \begin{bmatrix} \Delta\omega_r(0) \\ \Delta\delta(0) \end{bmatrix}$$

$$= \begin{bmatrix} -j29.76 & 0.5-j0.056 \\ j29.76 & 0.5-j0.056 \end{bmatrix} \begin{bmatrix} 0 \\ 0.0873 \end{bmatrix}$$

$$= \begin{bmatrix} 0.0436-j0.0049 \\ 0.0436+j0.0049 \end{bmatrix}$$

The time response of speed deviation is

$$\begin{aligned}\Delta\omega_r(t) &= \phi_{11}c_1e^{\lambda_1 t}+\phi_{12}c_2e^{\lambda_2 t}\\ &= (-0.0019+j0.0168)(0.0436-j0.0049)e^{(-0.714+j6.35)t}+\\ &\quad (-0.0019-j0.0168)(0.0436+j0.0049)e^{(-0.714-j6.35)t}\\ &= -0.0015e^{-0.714t}\sin(6.35t) \quad \text{pu}\end{aligned}$$

Similarly, the time response of rotor angle deviation is

$$\Delta\delta(t) = 0.088e^{-0.714t}\cos(6.35t-0.112) \quad \text{rad}$$

This is a second-order system with an oscillatory mode of response having a damped frequency of 6.35 rad/s or 1.0101 Hz. The oscillations decay with a time constant of 1/0.714 s. This corresponds to a damping ratio ζ of 0.112. As this is a rotor angle mode, $\Delta\omega_r$ and $\Delta\delta$ participate in it equally. ■

12.3.2 Effects of Synchronous Machine Field Circuit Dynamics

We now consider the system performance including the effect of field flux variations. The amortisseur effects will be neglected and the field voltage will be assumed constant (manual excitation control).

In what follows, we will develop the state-space model of the system by first reducing the synchronous machine equations to an appropriate form and then combining them with the network equations. We will express time in seconds, angles in electrical radians, and all other variables in per unit.

Synchronous machine equations

As in the case of the classical generator model, the acceleration equations are

$$p\Delta\omega_r = \frac{1}{2H}(T_m - T_e - K_D\Delta\omega_r) \tag{12.83}$$

$$p\delta = \omega_0\Delta\omega_r \tag{12.84}$$

where $\omega_0 = 2\pi f_0$ elec. rad/s. In this case, the rotor angle δ is the angle (in elec. rad) by which the q-axis leads the reference E_B. As shown in Figure 12.6, the rotor angle δ is the sum of the internal angle δ_i (see Section 3.6.3) and the angle by which E_t leads E_B. We need a convenient means of identifying the rotor position with respect to an appropriate reference and keeping track of it as the rotor oscillates. As discussed in

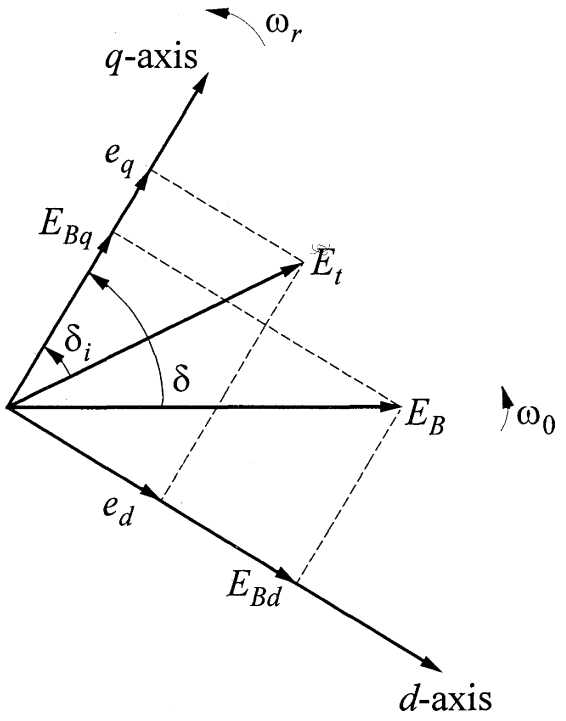


Figure 12.6

Chapter 3 (Section 3.6), the q-axis offers this convenience when the dynamics of rotor circuits are represented in the machine model. The choice of E_B as the reference for measuring rotor angle is convenient from the viewpoint of solution of network equations.

The per unit synchronous machine equations were summarized in Section 3.4.9 and the simplifications essential for large-scale stability studies were discussed in Section 5.1. From Equation 5.10, with time t in seconds instead of per unit, the field circuit dynamic equation is

$$\begin{aligned} p\psi_{fd} &= \omega_0(e_{fd} - R_{fd} i_{fd}) \\ &= \frac{\omega_0 R_{fd}}{L_{adu}} E_{fd} - \omega_0 R_{fd} i_{fd} \end{aligned} \tag{12.85}$$

where E_{fd} is the exciter output voltage defined in Section 8.6.1. Equations 12.83 to 12.85 describe the dynamics of the synchronous machine with $\Delta\omega_r$, δ, and ψ_{fd} as the state variables. However, the derivatives of these state variables appear in these equations as functions of T_e and i_{fd}, which are neither state variables nor input variables. In order to develop the complete system equations in the state-space form, we need to express i_{fd} and T_e in terms of the state variables as determined by the machine flux linkage equations and network equations.

With amortisseurs neglected, the equivalent circuits relating the machine flux linkages and currents are as shown in Figure 12.7.

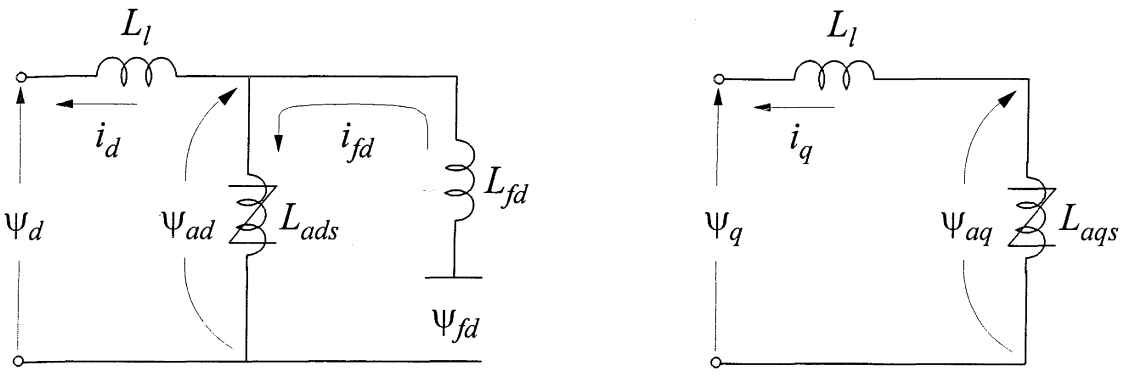


Figure 12.7

The stator and rotor flux linkages are given by

$$\begin{aligned}\psi_d &= -L_l i_d + L_{ads}(-i_d + i_{fd}) \\ &= -L_l i_d + \psi_{ad}\end{aligned} \tag{12.86}$$

$$\begin{aligned}\psi_q &= -L_l i_q + L_{aqs}(-i_q) \\ &= -L_l i_q + \psi_{aq}\end{aligned} \tag{12.87}$$

$$\begin{aligned}\psi_{fd} &= L_{ads}(-i_d + i_{fd}) + L_{fd} i_{fd} \\ &= \psi_{ad} + L_{fd} i_{fd}\end{aligned} \tag{12.88}$$

In the above equations ψ_{ad} and ψ_{aq} are the air-gap (mutual) flux linkages, and and L_{aqs} are the saturated values of the mutual inductances.

From Equation 12.88, the field current may be expressed as

$$i_{fd} = \frac{\psi_{fd} - \psi_{ad}}{L_{fd}} \tag{12.89}$$

The d-axis mutual flux linkage can be written in terms of ψ_{fd} and i_d as follows:

$$\begin{aligned}\psi_{ad} &= -L_{ads} i_d + L_{ads} i_{fd} \\ &= -L_{ads} i_d + \frac{L_{ads}}{L_{fd}}(\psi_{fd} - \psi_{ad}) \\ &= L'_{ads}\left(-i_d + \frac{\psi_{fd}}{L_{fd}}\right)\end{aligned} \tag{12.90}$$

where

$$L'_{ads} = \frac{1}{\frac{1}{L_{ads}} + \frac{1}{L_{fd}}} \tag{12.91}$$

Since there are no rotor circuits considered in the q-axis, the mutual flux linkage is given by

$$\psi_{aq} = -L_{aqs} i_q \tag{12.92}$$

The air-gap torque is

$$\begin{aligned} T_e &= \psi_d i_q - \psi_q i_d \\ &= \psi_{ad} i_q - \psi_{aq} i_d \end{aligned} \tag{12.93}$$

With $p\psi$ terms and speed variations neglected as discussed in Section 5.1, the stator voltage equations are

$$\begin{aligned} e_d &= -R_a i_d - \psi_q \\ &= -R_a i_d + (L_l i_q - \psi_{aq}) \end{aligned} \tag{12.94}$$

$$\begin{aligned} e_q &= -R_a i_q + \psi_d \\ &= -R_a i_q - (L_l i_d - \psi_{ad}) \end{aligned} \tag{12.95}$$

As a first step, we have expressed i_{fd} and T_e in terms of ψ_{fd}, i_d, i_q, ψ_{ad} and ψ_{aq}. In addition, e_d and e_q have been expressed in terms of these variables and will be used in conjunction with the network equations to provide expressions for i_d and i_q in terms of the state variables.

The advantages of using ψ_{ad} and ψ_{aq} as intermediate variables in the elimination process will be more apparent when we account for the effects of amortisseur circuits in Section 12.6.

Network equations

Since there is only one machine, the machine as well as network equations can be expressed in terms of one reference frame, i.e., the d-q reference frame of the machine. Referring to Figure 12.6, the machine terminal and infinite bus voltages in terms of the d and q components are

$$\tilde{E}_t = e_d + je_q \tag{12.96}$$

$$\tilde{E}_B = E_{Bd} + jE_{Bq} \tag{12.97}$$

The network constraint equation for the system of Figure 12.3(b) is

$$\begin{aligned} \tilde{E}_t &= \tilde{E}_B + (R_E + jX_E)\tilde{I}_t \\ (e_d + je_q) &= (E_{Bd} + jE_{Bq}) + (R_E + jX_E)(i_d + ji_q) \end{aligned} \tag{12.98}$$

Resolving into d and q components gives

$$e_d = R_E i_d - X_E i_q + E_{Bd} \tag{12.99}$$

$$e_q = R_E i_q + X_E i_d + E_{Bq} \tag{12.100}$$

where

$$E_{Bd} = E_B \sin\delta \tag{12.101}$$

$$E_{Bq} = E_B \cos\delta \tag{12.102}$$

Using Equations 12.94 and 12.95 to eliminate e_d, e_q in Equations 12.99 and 12.100, and using the expressions for ψ_{ad} and ψ_{aq} given by Equations 12.90 and 12.92, we obtain the following expressions for i_d and i_q in terms of the state variables ψ_{fd} and δ:

$$i_d = \frac{X_{Tq}\left[\psi_{fd}\left(\frac{L_{ads}}{L_{ads}+L_{fd}}\right) - E_B\cos\delta\right] - R_T E_B \sin\delta}{D} \tag{12.103}$$

$$i_q = \frac{R_T\left[\psi_{fd}\left(\frac{L_{ads}}{L_{ads}+L_{fd}}\right) - E_B\cos\delta\right] + X_{Td} E_B \sin\delta}{D} \tag{12.104}$$

where

$$\begin{aligned} R_T &= R_a + R_E \\ X_{Tq} &= X_E + (L_{aqs} + L_l) = X_E + X_{qs} \\ X_{Td} &= X_E + (L'_{ads} + L_l) = X_E + X'_{ds} \\ D &= R_T^2 + X_{Tq} X_{Td} \end{aligned} \tag{12.105}$$

The reactances X_{qs} and X'_{ds} are saturated values. In per unit they are equal to the corresponding inductances.

Equations 12.103 and 12.104, together with Equations 12.89, 12.90 and 12.92, can be used to eliminate i_{fd} and T_e from the differential equations 12.83 to 12.85 and express them in terms of the state variables. These equations are nonlinear and have to be linearized for small-signal analysis.

Linearized system equations

Expressing Equations 12.103 and 12.104 in terms of perturbed values, we may write

$$\Delta i_d = m_1 \Delta\delta + m_2 \Delta\psi_{fd} \tag{12.106}$$

$$\Delta i_q = n_1 \Delta\delta + n_2 \Delta\psi_{fd} \tag{12.107}$$

where

$$\begin{aligned} m_1 &= \frac{E_B (X_{Tq} \sin\delta_0 - R_T \cos\delta_0)}{D} \\ n_1 &= \frac{E_B (R_T \sin\delta_0 + X_{Td} \cos\delta_0)}{D} \\ m_2 &= \frac{X_{Tq}}{D} \frac{L_{ads}}{(L_{ads} + L_{fd})} \\ n_2 &= \frac{R_T}{D} \frac{L_{ads}}{(L_{ads} + L_{fd})} \end{aligned} \tag{12.108}$$

By linearizing Equations 12.90 and 12.92, and substituting in them the above expressions for Δi_d and Δi_q, we get

$$\begin{aligned}\Delta\psi_{ad} &= L'_{ads}\left(-\Delta i_d + \frac{\Delta\psi_{fd}}{L_{fd}}\right) \\ &= \left(\frac{1}{L_{fd}} - m_2\right)L'_{ads}\Delta\psi_{fd} - m_1 L'_{ads}\Delta\delta\end{aligned} \tag{12.109}$$

$$\begin{aligned}\Delta\psi_{aq} &= -L_{aqs}\Delta i_q \\ &= -n_2 L_{aqs}\Delta\psi_{fd} - n_1 L_{aqs}\Delta\delta\end{aligned} \tag{12.110}$$

Linearizing Equation 12.89 and substituting for $\Delta\psi_{ad}$ from Equation 12.109 gives

$$\begin{aligned}\Delta i_{fd} &= \frac{\Delta\psi_{fd} - \Delta\psi_{ad}}{L_{fd}} \\ &= \frac{1}{L_{fd}}\left(1 - \frac{L'_{ads}}{L_{fd}} + m_2 L'_{ads}\right)\Delta\psi_{fd} + \frac{1}{L_{fd}} m_1 L'_{ads}\Delta\delta\end{aligned} \tag{12.111}$$

The linearized form of Equation 12.93 is

$$\Delta T_e = \psi_{ad0}\Delta i_q + i_{q0}\Delta\psi_{ad} - \psi_{aq0}\Delta i_d - i_{d0}\Delta\psi_{aq}$$

Substituting for Δi_d, Δi_q, $\Delta\psi_{ad}$, and $\Delta\psi_{aq}$ from Equations 12.106 to 12.110, we obtain

$$\Delta T_e = K_1\Delta\delta + K_2\Delta\psi_{fd} \tag{12.112}$$

where

$$K_1 = n_1(\psi_{ad0} + L_{aqs} i_{d0}) - m_1(\psi_{aq0} + L'_{ads} i_{q0}) \tag{12.113}$$

$$K_2 = n_2(\psi_{ad0} + L_{aqs} i_{d0}) - m_2(\psi_{aq0} + L'_{ads} i_{q0}) + \frac{L'_{ads}}{L_{fd}} i_{q0} \tag{12.114}$$

By linearizing Equations 12.83 to 12.85 and substituting the expressions for Δi_{fd} and ΔT_e given by Equations 12.111 and 12.112, we obtain the system equations in the desired final form:

$$\begin{bmatrix} \Delta\dot{\omega}_r \\ \Delta\dot{\delta} \\ \Delta\dot{\psi}_{fd} \end{bmatrix} = \begin{bmatrix} a_{11} & a_{12} & a_{13} \\ a_{21} & 0 & 0 \\ 0 & a_{32} & a_{33} \end{bmatrix} \begin{bmatrix} \Delta\omega_r \\ \Delta\delta \\ \Delta\psi_{fd} \end{bmatrix} + \begin{bmatrix} b_{11} & 0 \\ 0 & 0 \\ 0 & b_{32} \end{bmatrix} \begin{bmatrix} \Delta T_m \\ \Delta E_{fd} \end{bmatrix} \tag{12.115}$$

where

$$\begin{aligned} a_{11} &= -\frac{K_D}{2H} \\ a_{12} &= -\frac{K_1}{2H} \\ a_{13} &= -\frac{K_2}{2H} \\ a_{21} &= \omega_0 = 2\pi f_0 \\ a_{32} &= -\frac{\omega_0 R_{fd}}{L_{fd}} m_1 L'_{ads} \\ a_{33} &= -\frac{\omega_0 R_{fd}}{L_{fd}} \left[1 - \frac{L'_{ads}}{L_{fd}} + m_2 L'_{ads} \right] \\ b_{11} &= \frac{1}{2H} \\ b_{32} &= \frac{\omega_0 R_{fd}}{L_{adu}} \end{aligned} \tag{12.116}$$

and ΔT_m and ΔE_{fd} depend on prime-mover and excitation controls. With constant mechanical input torque, ΔT_m=0; with constant exciter output voltage, ΔE_{fd}=0.

It is interesting to compare the above state-space equations with those derived in Section 12.3.1 by assuming the classical generator model (which is equivalent to assuming R_{fd}=0, R_a=0 and X_q=X'_d).

The mutual inductances L_{ads} and L_{aqs} in the above equations are saturated values. The method of accounting for saturation for small-signal analysis is described below.

Representation of saturation in small-signal studies

Since we are expressing small-signal performance in terms of perturbed values of flux linkages and currents, a distinction has to be made between *total saturation*

and *incremental saturation.*

Total saturation is associated with total values of flux linkages and currents. The method of accounting for total saturation was discussed in Section 3.8.

Incremental saturation is associated with perturbed values of flux linkages and currents. Therefore, the incremental slope of the saturation curve is used in computing the incremental saturation as shown in Figure 12.8.

Denoting the incremental saturation factor $K_{sd\,(incr)}$, we have

$$L_{ads\,(incr)} = K_{sd\,(incr)} L_{adu} \tag{12.117}$$

Based on the definitions of A_{sat}, B_{sat} and ψ_{T1} in Section 3.8.2, we can show that

$$K_{sd\,(incr)} = \frac{1}{1 + B_{sat} A_{sat} e^{B_{sat}(\psi_{at0} - \psi_{T1})}} \tag{12.118}$$

A similar treatment applies to q-axis saturation.

For computing the initial values of system variables (denoted by subscript 0), total saturation is used. For relating the perturbed values, i.e., in Equations 12.105, 12.108, 12.113, 12.114, and 12.116, the incremental saturation factor is used.

The method of computing the initial steady-state values of machine parameters was described in Section 3.6.5.

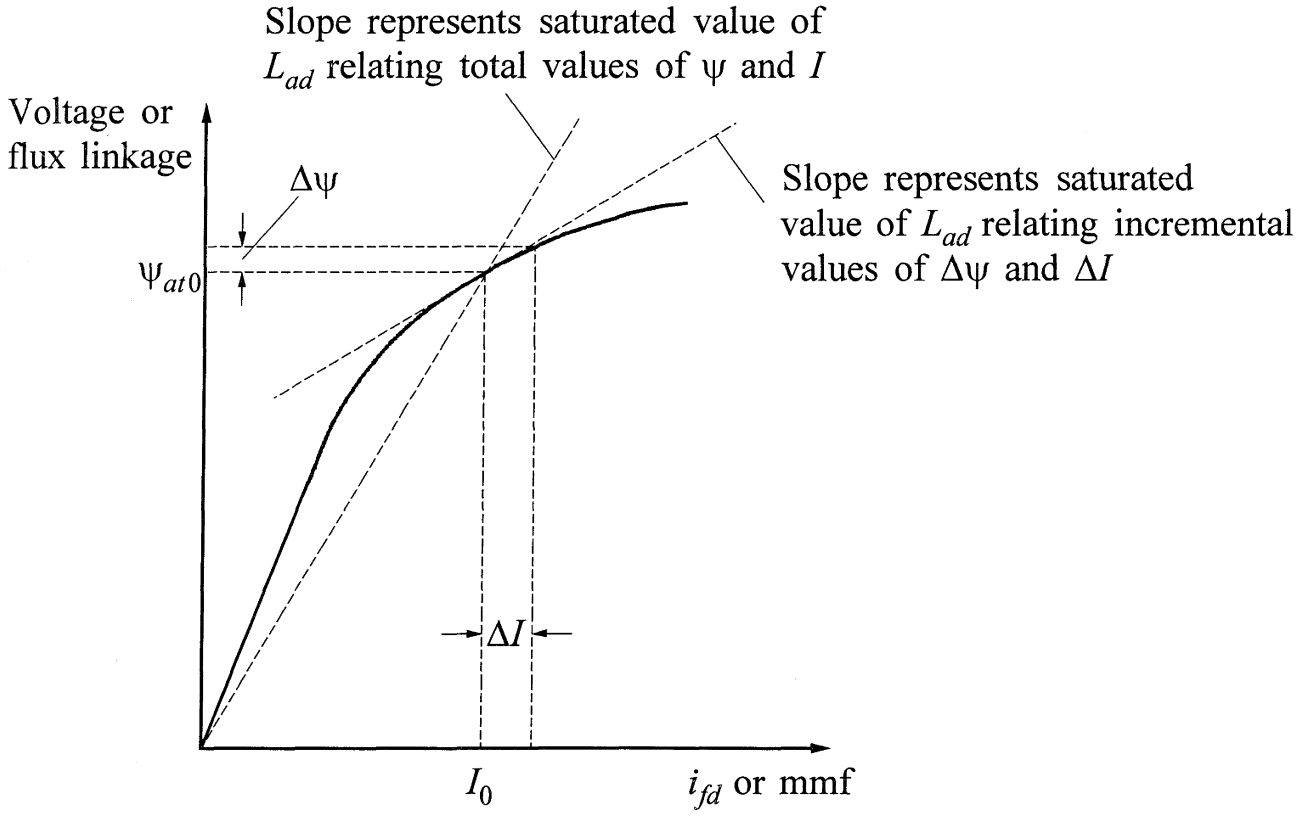


Figure 12.8 Distinction between incremental and total saturation

Summary of procedure for formulating the state matrix

(a) The following steady-state operating conditions, machine parameters and network parameters are given:

P_t Q_t E_t R_E X_E
L_d L_q L_l R_a L_{fd} R_{fd} A_{sat} B_{sat} ψ_{T1}

Alternatively E_B may be specified instead of Q_t or E_t.

(b) The first step is to compute the initial steady-state values of system variables:

I_t, power factor angle ϕ
Total saturation factors K_{sd} and K_{sq} (see Section 3.8)

$$X_{ds} = L_{ds} = K_{sd}L_{adu} + L_l$$
$$X_{qs} = L_{qs} = K_{sq}L_{aqu} + L_l$$
$$\delta_i = \tan^{-1}\left(\frac{I_t X_{qs}\cos\phi - I_t R_a \sin\phi}{E_t + I_t R_a \cos\phi + I_t X_{qs}\sin\phi}\right)$$
$$e_{d0} = E_t \sin\delta_i$$
$$e_{q0} = E_t \cos\delta_i$$
$$i_{d0} = I_t \sin(\delta_i + \phi)$$
$$i_{q0} = I_t \cos(\delta_i + \phi)$$
$$E_{Bd0} = e_{d0} - R_E i_{d0} + X_E i_{q0}$$
$$E_{Bq0} = e_{q0} - R_E i_{q0} - X_E i_{d0}$$
$$\delta_0 = \tan^{-1}\left(\frac{E_{Bd0}}{E_{Bq0}}\right)$$
$$E_B = \left(E_{Bd0}^2 + E_{Bq0}^2\right)^{1/2}$$
$$i_{fd0} = \frac{e_{q0} + R_a i_{q0} + L_{ds} i_{d0}}{L_{ads}}, \qquad E_{fd0} = L_{adu} i_{fd0}$$
$$\psi_{ad0} = L_{ads}(-i_{d0} + i_{fd0}), \qquad \psi_{aq0} = -L_{aqs} i_{q0}$$

(c) The next step is to compute incremental saturation factors and the corresponding saturated values of L_{ads}, L_{aqs}, L'_{ads}, and then

R_T, X_{Tq}, X_{Td}, D from Equation 12.105
m_1, m_2, n_1, n_2 from Equation 12.108
K_1, K_2 from Equations 12.113 and 12.114

(d) Finally, compute the elements of matrix **A** from Equation 12.116.

Block diagram representation

Figure 12.9 shows the block diagram representation of the small-signal performance of the system. In this representation, the dynamic characteristics of the system are expressed in terms of the so-called K constants [5]. The basis for the block diagram and the expressions for the associated constants are developed below.

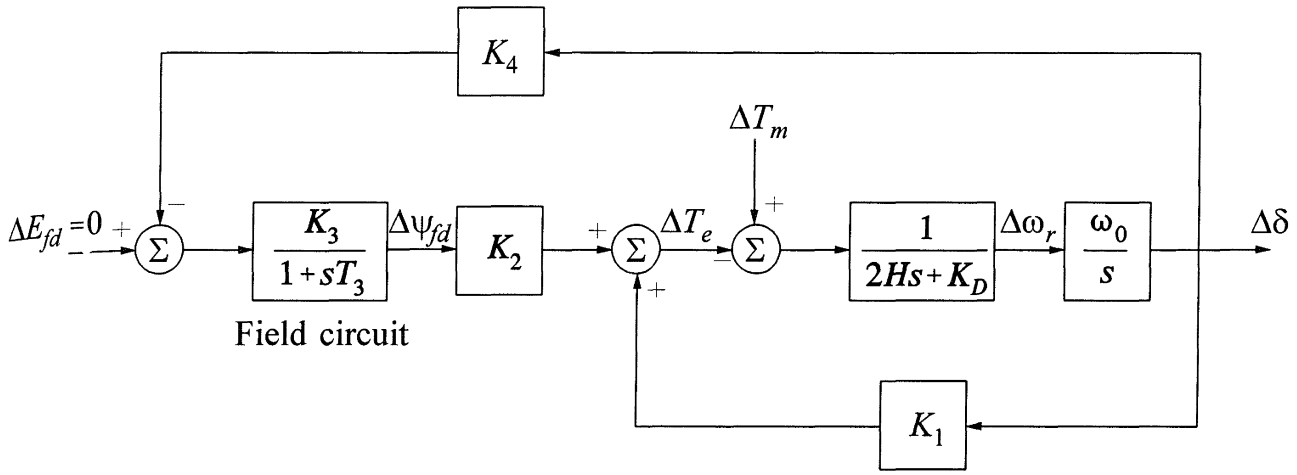


Figure 12.9 Block diagram representation with constant E_{fd}

From Equation 12.112, we may express the change in air-gap torque as a function of $\Delta\delta$ and $\Delta\psi_{fd}$ as follows:

$$\Delta T_e = K_1\Delta\delta + K_2\Delta\psi_{fd}$$

where

$K_1 = \Delta T_e/\Delta\delta$ with constant ψ_{fd}
$K_2 = \Delta T_e/\Delta\psi_{fd}$ with constant rotor angle δ

The expressions for K_1 and K_2 are given by Equations 12.113 and 12.114.

The component of torque given by $K_1\Delta\delta$ is in phase with $\Delta\delta$ and hence represents a synchronizing torque component.

The component of torque resulting from variations in field flux linkage is given by $K_2\Delta\psi_{fd}$.

The variation of ψ_{fd} is determined by the field circuit dynamic equation:

$$p\Delta\psi_{fd} = a_{32}\Delta\delta + a_{33}\Delta\psi_{fd} + b_{32}\Delta E_{fd}$$

By grouping terms involving $\Delta\psi_{fd}$ and rearranging, we get

$$\Delta\psi_{fd} = \frac{K_3}{1+pT_3}[\Delta E_{fd} - K_4\Delta\delta] \tag{12.119}$$

where

$$K_3 = -\frac{b_{32}}{a_{33}}$$

$$K_4 = -\frac{a_{32}}{b_{32}} \tag{12.120}$$

$$T_3 = -\frac{1}{a_{33}} = K_3 T'_{d0}\frac{L_{adu}}{L_{ffd}}$$

Equation 12.119, with s replacing p, accounts for the field circuit block in Figure 12.9.

Expression for the K constants in the expanded form

We have expressed the K constants in terms of the elements of matrix **A**. In the literature [5,6], they are usually expressed explicitly in terms of the various system parameters, as summarized below.

The constant K_1 was expressed in Equation 12.113 as

$$K_1 = n_1(\psi_{ad0} + L_{aqs}i_{d0}) - m_1(\psi_{aq0} + L'_{ads}i_{q0})$$

From Equation 12.95, the first term in parentheses in the above expression for K_1 may be written as

$$\psi_{ad0} + L_{aqs}i_{d0} = e_{q0} + R_a i_{q0} + X_{qs}i_{d0} = E_{q0} \tag{12.121}$$

where E_{q0} is the predisturbance value of the voltage behind $R_a + jX_q$. The second term in parentheses in the expression for K_1 may be written as

$$\begin{aligned}\psi_{aq0} + L'_{ads}i_{q0} &= -L_{aqs}i_{q0} + L'_{ads}i_{q0} \\ &= -(X_q - X'_d)i_{q0}\end{aligned} \tag{12.122}$$

Substituting for n_1, m_1 from Equation 12.108 and for the terms given by Equations 12.121 and 12.122 in the expression for K_1, yields

$$K_1 = \frac{E_B E_{q0}}{D}(R_T \sin\delta_0 + X_{Td}\cos\delta_0) + \frac{E_B i_{q0}}{D}(X_q - X'_d)(X_{Tq}\sin\delta_0 - R_T\cos\delta_0) \tag{12.123}$$

Similarly, the expanded form of the expression for the constant K_2 is

$$K_2 = \frac{L_{ads}}{L_{ads}+L_{fd}}\left[\frac{R_T}{D}E_{q0} + \left(\frac{X_{Tq}(X_q - X'_d)}{D} + 1\right) i_{q0}\right] \tag{12.124}$$

From Equations 12.91, 12.108, and 12.116, we may write

$$\begin{aligned} a_{33} &= -\omega_0 \frac{R_{fd}}{L_{fd}}\left[1 - \frac{L_{ads}}{L_{ads}+L_{fd}} + \frac{X_{Tq}}{D}\frac{L_{ads}}{(L_{ads}+L_{fd})}\frac{L_{ads}L_{fd}}{(L_{ads}+L_{fd})}\right] \\ &= -\omega_0 \frac{R_{fd}}{L_{ads}+L_{fd}}\left[1 + \frac{X_{Tq}}{D}\frac{L_{ads}^2}{(L_{ads}+L_{fd})}\right] \\ &= -\omega_0 \frac{R_{fd}}{L_{ads}+L_{fd}}\left[1 + \frac{X_{Tq}}{D}(X_d - X'_d)\right] \end{aligned} \tag{12.125}$$

Substitution of the above in the expression for K_3 and T_3 given by Equation 12.120 yields

$$K_3 = \frac{L_{ads}+L_{fd}}{L_{adu}}\frac{1}{1 + \frac{X_{Tq}}{D}(X_d - X'_d)} \tag{12.126}$$

$$\begin{aligned} T_3 &= \frac{L_{ads}+L_{fd}}{\omega_0 R_{fd}}\frac{1}{1 + \frac{X_{Tq}}{D}(X_d - X'_d)} \\ &= \frac{T'_{d0s}}{1 + \frac{X_{Tq}}{D}(X_d - X'_d)} \end{aligned} \tag{12.127}$$

where T'_{d0s} is the saturated value of T'_{d0}. Similarly, from Equations 12.91, 12.108 and

12.116, we may write

$$a_{32} = -\omega_0 \frac{R_{fd}}{L_{fd}} \frac{E_B}{D}(X_{Tq}\sin\delta_0 - R_T\cos\delta_0)\frac{L_{ads}L_{fd}}{L_{ads}+L_{fd}}$$

Substitution of the above in the expression for K_4 given by Equation 12.120 yields

$$K_4 = L_{adu}\frac{L_{ads}}{L_{ads}+L_{fd}}\frac{E_B}{D}(X_{Tq}\sin\delta_0 - R_T\cos\delta_0) \tag{12.128}$$

If the effect of saturation is neglected, this simplifies to

$$K_4 = \frac{E_B}{D}(X_d - X'_d)(X_{Tq}\sin\delta_0 - R_T\cos\delta_0) \tag{12.129}$$

If the elements of matrix **A** are available, the K constants may be computed directly from them. The expanded forms are derived here to illustrate the form of expressions used in the literature. An advantage of these expanded forms is that the dependence of the K constants on the various system parameters is more readily apparent. A disadvantage, however, is that some inconsistencies appear in representing saturation effects.

In the literature, $E'_q=(L_{ad}/L_{ffd})\psi_{fd}$ is often used as a state variable instead of ψ_{fd} (see Section 5.2). The effect of this is to remove the $L_{ad}/(L_{ad}+L_{fd})$ term from the expressions for K_2 and K_3. The product K_2K_3 would, however, remain the same.

Effect of field flux linkage variation on system stability

We see from the block diagram of Figure 12.9 that, with constant field voltage ($\Delta E_{fd}=0$), the field flux variations are caused only by feedback of $\Delta\delta$ through the coefficient K_4. This represents the demagnetizing effect of the armature reaction.

The change in air-gap torque due to field flux variations caused by rotor angle changes is given by

$$\left.\frac{\Delta T_e}{\Delta\delta}\right|_{\text{due to } \Delta\psi_{fd}} = -\frac{K_2K_3K_4}{1+sT_3} \tag{12.130}$$

The constants K_2, K_3, and K_4 are usually positive. The contribution of $\Delta\psi_{fd}$ to synchronizing and damping torque components depends on the oscillating frequency as discussed below.

(a) In the steady state and at very low oscillating frequencies ($s=j\omega\rightarrow 0$):

$$\Delta T_e \text{ due to } \Delta\psi_{fd} = -K_2 K_3 K_4 \Delta\delta$$

The field flux variation due to $\Delta\delta$ feedback (i.e., due to armature reaction) introduces a negative synchronizing torque component. The system becomes monotonically unstable when this exceeds $K_1\Delta\delta$. The steady-state stability limit is reached when

$$K_2 K_3 K_4 = K_1$$

(b) At oscillating frequencies much higher than $1/T_3$:

$$\Delta T_e \approx -\frac{K_2 K_3 K_4}{j\omega T_3}\Delta\delta$$

$$= \frac{K_2 K_3 K_4}{\omega T_3} j\Delta\delta$$

Thus, the component of air-gap torque due to $\Delta\psi_{fd}$ is 90° ahead of $\Delta\delta$ or in phase with $\Delta\omega$. Hence, $\Delta\psi_{fd}$ results in a positive damping torque component.

(c) At typical machine oscillating frequencies of about 1 Hz (2π rad/s), $\Delta\psi_{fd}$ results in a positive damping torque component and a negative synchronizing torque component. The net effect is to reduce slightly the synchronizing torque component and increase the damping torque component.

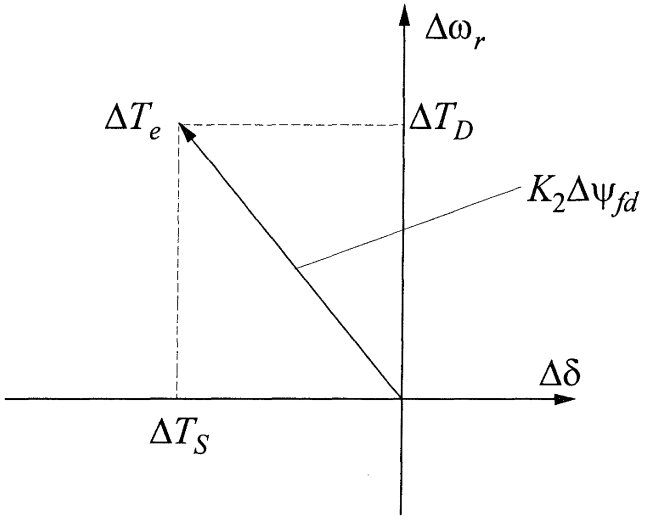


Figure 12.10 Positive damping torque and negative synchronizing torque due to $K_2\Delta\psi_{fd}$

Special situations with K_4 negative:

The coefficient K_4 is normally positive. As long as it is positive, the effect of field flux variation due to armature reaction ($\Delta\psi_{fd}$ with constant E_{fd}) is to introduce a positive damping torque component. However, there can be situations where K_4 is negative. From the expression given by Equation 12.128, K_4 is negative when $(X_E+X_q)\sin\delta_0-(R_a+R_E)\cos\delta_0$ is negative. This is the situation when a hydraulic generator without damper windings is operating at light load and is connected by a line of relatively high resistance to reactance ratio to a large system. This type of situation was reported in reference 7.

Also K_4 can be negative when a machine is connected to a large local load, supplied partly by the generator and partly by the remote large system [8]. Under such conditions, the torques produced by induced currents in the field due to armature reaction have components out of phase with $\Delta\omega$, and produce negative damping.

Example 12.3

In this example we analyze the small-signal stability of the system of Figure E12.5 (considered in Example 12.2) including the effects of the generator field circuit dynamics. The parameters of each of the four generators of the plant in per unit on its rating are as follows:

$X_d = 1.81$	$X_q = 1.76$	$X'_d = 0.3$	$X_l = 0.16$
$R_a = 0.003$	$T'_{d0} = 8.0$ s	$H = 3.5$	$K_D = 0$

The above parameters are unsaturated values. The effect of saturation is to be represented by assuming that d and q axes have similar saturation characteristics with

$$A_{sat} = 0.031 \qquad B_{sat} = 6.93 \qquad \psi_{T1} = 0.8$$

The effects of the amortisseurs may be neglected. The excitation system is on manual control (constant E_{fd}), and transmission circuit 2 is out of service.

(a) If the plant output in per unit on 2220 MVA, 24 kV base is

$$P = 0.9 \qquad Q = 0.3 \text{ (overexcited)} \qquad E_t = 1.0$$

compute the following:

(i) The elements of the state matrix **A** representing the small-signal performance of the system.

(ii) The constants K_1 to K_4 and T_3 associated with the block diagram representation of Figure 12.9.

(iii) Eigenvalues of **A** and the corresponding eigenvectors and participation matrix; frequency and damping ratio of the oscillatory mode.

(iv) Steady-state synchronizing torque coefficient; damping and synchronizing torque coefficients at the rotor oscillating frequency.

(b) Determine the limiting value of P (within ±0.025 pu) and the corresponding value of the rotor angle δ beyond which the system is unstable, with

(i) Saturation effects neglected

(ii) Saturation effects included

Assume that $Q=P/3$ as P varies and $E_t=1.0$. Comment on the mode of instability and the effect of representing saturation.

Solution

The four units of the plant may be represented by a single generator whose parameters on 2220 MVA base are the same as those of each unit on its rating. The circuit model of the system in per unit on 2220 MVA base is shown in Figure E12.7.

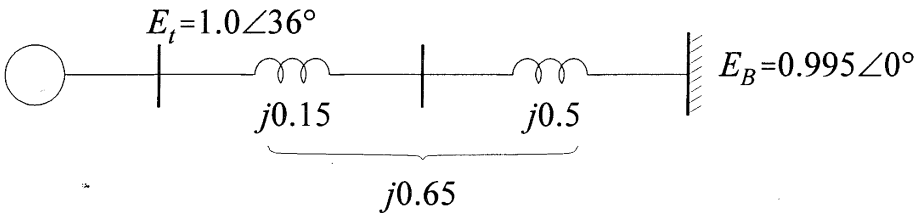


Figure E12.7

The generators of this example have the same characteristics as the generator considered in examples of Chapters 3 and 4, except for L_l.

The per unit fundamental parameters (elements of the d- and q-axis equivalent circuits) of the equivalent generator following the procedure used in Example 4.1 are

$L_{adu} = 1.65$ $L_{aqu} = 1.60$ $L_l = 0.16$
$R_a = 0.003$ $R_{fd} = 0.0006$ $L_{fd} = 0.153$

(a) (i) The initial steady-state values of the system variables are computed by using the procedure summarized earlier in this section.

$K_{sd} = K_{sq} = 0.8491$ $\delta_i = 43.13°$
$e_{d0} = 0.6836$ $e_{q0} = 0.7298$ $i_{d0} = 0.8342$ $i_{q0} = 0.4518$
$\delta_0 = 79.13°$ $E_{fd0} = 2.395$ $K_{sd(incr)} = K_{sq(incr)} = 0.434$

From Equation 12.108,

$$m_1 = 1.0437 \qquad m_2 = 0.8802 \qquad n_1 = 0.1268 \qquad n_2 = 0.0018$$

From Equation 12.116,

$$\mathbf{A} = \begin{bmatrix} 0 & -0.1092 & -0.1236 \\ 376.991 & 0 & 0 \\ 0 & -0.1938 & -0.4229 \end{bmatrix}$$

(ii) From Equations 12.113, 12.114, and 12.120, the constants of the block diagram of Figure 12.9 are

$$K_1 = 0.7643 \qquad K_2 = 0.8649$$
$$K_3 = 0.3230 \qquad K_4 = 1.4187 \qquad T_3 = 2.365$$

(iii) Eigenvalues computed by using a standard routine based on the QR transformation method are

$$\lambda_1, \lambda_2 = -0.11 \pm j6.41 \quad (\omega_d = 1.02 \text{ Hz}, \zeta = 0.017)$$
$$\lambda_3 = -0.204$$

The right eigenvector matrix is

$$\mathbf{\Phi} = \begin{bmatrix} 0.0169 - j0.0014 & 0.0169 + j0.0014 & 0.0004 \\ -0.0988 - j0.9945 & -0.0988 + j0.9945 & -0.7490 \\ 0.0301 - j0.0015 & 0.0301 + j0.0015 & 0.6625 \end{bmatrix}$$

The left eigenvector matrix normalized so that $\mathbf{\Psi\Phi} = \mathbf{I}$ is

$$\mathbf{\Psi} = \begin{bmatrix} 29.3884 + j1.9097 & -0.0410 + j0.4992 & -0.0643 + j0.5632 \\ 29.3884 - j1.9097 & -0.0410 - j0.4992 & -0.0643 - j0.5632 \\ -2.6820 & 0.0014 & 1.5126 \end{bmatrix}$$

The participation matrix is

$$\begin{array}{c} \\ \Delta\omega_r \\ \Delta\delta \\ \Delta\psi_{fd} \\ \\ \end{array} \begin{bmatrix} 0.501\angle -1.0^\circ & 0.501\angle 1.0^\circ & 0.001\angle 180^\circ \\ 0.501\angle -1.0^\circ & 0.501\angle 1.0^\circ & 0.001\angle 180^\circ \\ 0.017\angle 94^\circ & 0.017\angle -94^\circ & 1.002\angle 0^\circ \end{bmatrix} \begin{array}{c} \\ \\ \\ \\ \end{array}$$
$$\lambda_1 \qquad \lambda_2 \qquad \lambda_3$$

From the participation matrix, we see that $\Delta\omega_r$ and $\Delta\delta$ have a high participation in the oscillatory mode (corresponding to eigenvalues λ_1 and λ_2); the field flux linkage has a high participation in the non-oscillatory mode, represented by the eigenvalue λ_3.

(iv) The steady-state synchronizing torque coefficient due to $\Delta\psi_{fd}$ is

$$-K_2K_3K_4 = -0.8649\times0.323\times1.4187$$

$$= -0.3963$$

The total steady-state synchronizing torque coefficient is

$$K_S = K_1 - K_2K_3K_4$$

$$= 0.7643 - 0.3963 = 0.3679 \quad \text{pu torque/rad}$$

From the block diagram of Figure 12.9,

$$\left.\frac{\Delta T_e(s)}{\Delta\delta(s)}\right|_{\text{due to } \Delta\psi_{fd}} = \frac{-K_2K_3K_4}{1+sT_3} = \frac{-K_2K_3K_4(1-sT_3)}{1-s^2T_3^2}$$

Therefore, ΔT_e due to $\Delta\psi_{fd}$ is

$$\Delta T_e\,|\,\Delta\psi_{fd} = \frac{-K_2K_3K_4}{1-s^2T_3^2}\Delta\delta + \frac{K_2K_3K_4T_3}{1-s^2T_3^2}s\Delta\delta$$

$$= K_S(\Delta\psi_{fd})\,\Delta\delta + K_D(\Delta\psi_{fd})\,\Delta\omega_r\omega_0$$

From the eigenvalues, the complex frequency of rotor oscillation is $-0.11+j6.41$. Since the real component is much smaller than the imaginary component, we can compute K_S and K_D at the oscillation frequency by setting $s=j6.41$ without loss of much accuracy.

$$K_S(\Delta\psi_{fd}) = \frac{-K_2K_3K_4}{1-s^2T_3^2} = \frac{-0.3963}{1-(j6.41\times2.365)^2}$$

$$= -0.00172 \quad \text{pu torque/rad}$$

$$K_D(\Delta\psi_{fd}) = \frac{K_2K_3K_4T_3\omega_0}{1-s^2T_3^2} = \frac{0.3963\times2.365\times377}{1-(j6.41\times2.365)^2}$$

$$= 1.53 \quad \text{pu torque/pu speed change}$$

The effect of field flux variation (i.e., armature reaction) is thus to reduce the synchronizing torque slightly and to add a damping torque component.

The net synchronizing torque component is

$$K_S = K_1 + K_S(\Delta\psi_{fd}) = 0.7643 - 0.00172$$

$$= 0.7626 \quad \text{pu torque/rad}$$

The only source of damping is due to field flux variation. Hence, the net damping torque coefficient is

$$K_D = K_D(\Delta\psi_{fd}) = 1.53 \quad \text{pu torque/pu speed change}$$

From Equation 12.81, the undamped natural frequency is

$$\omega_n = \sqrt{\frac{K_S\omega_0}{2H}} = \sqrt{\frac{0.7626\times377}{2\times3.5}}$$

$$= 6.41 \quad \text{rad/s}$$

and from Equation 12.82, the damping ratio is

$$\zeta = \frac{1}{2}\frac{K_D}{\sqrt{K_S 2H\omega_0}} = \frac{1}{2}\frac{1.53}{\sqrt{0.7626\times2\times3.5\times377}}$$

$$= 0.0171$$

The above values of ω_n and ζ agree with those computed from the eigenvalues.

(b) The stability limit is determined by increasing P with $Q=P/3$ and $E_t=1.0$ pu (E_B is allowed to take appropriate values so as to satisfy the network equations). The results with and without saturation effects are as follows.

(i) With saturation effects:

The limiting P (within ±0.025 pu) and the corresponding system conditions in per unit are

$P = 1.3875$	$Q = 0.4625$	$E_t = 1.0$
$E_B = 1.1413$	$\delta = 102.6°$	$E_{fd} = 3.3$

The corresponding K constants are

$$K_1 = 0.4566 \quad K_2 = 0.960 \quad K_3 = 0.3028 \quad K_4 = 1.5749$$

Hence, the steady-state synchronizing torque coefficient is

$$K_S = K_1 - K_2K_3K_4 = -0.0014 \quad \text{pu torque/rad}$$

The eigenvalues of the system state matrix are

$$\lambda_1, \lambda_2 = -0.226 \pm j4.95 \quad (\omega_d = 0.79 \text{ Hz}, \zeta = 0.046)$$
$$\lambda_3 = +0.00142$$

The above represents conditions just past the stability limit. The system instability is due to lack of synchronizing torque. This is reflected in the real eigenvalue becoming slightly positive, representing a mode of instability through a non-oscillatory mode.

(ii) Without saturation effects:

The limiting value of P and the corresponding system conditions in this case are

$$P = 1.0375 \qquad Q = 0.3458 \qquad E_t = 1.0$$
$$E_B = 1.0275 \qquad \delta = 89.6° \qquad E_{fd} = 2.49$$

The K constants are

$$K_1 = 0.6862 \quad K_2 = 0.9956 \quad K_3 = 0.422 \quad K_4 = 1.633$$

The steady-state synchronizing torque coefficient is

$$K_S = K_1 - K_2K_3K_4 = 0.0001 \quad \text{pu torque/rad}$$

The eigenvalues are

$$\lambda_1, \lambda_2 = -0.162 \pm j6.08 \quad (\omega_d = 0.97 \text{ Hz}, \zeta = 0.027)$$
$$\lambda_3 = -0.00006$$

The system is on the verge of instability. The limiting rotor angle δ is very close to 90°. With constant E_{fd} and negligible saliency, the limiting rotor angle will be equal to 90° if the values of L_{ad} and L_{aq} used to compute the initial operating condition are the same as the values used to relate incremental flux linkages and currents.

In case (i), when we represented saturation, we made a distinction between total saturation and incremental saturation. Hence, the limiting rotor angle was about 102°, significantly higher than 90°. ■

12.4 EFFECTS OF EXCITATION SYSTEM

In this section, we will extend the state-space model and the block diagram developed in the previous section to include the excitation system. We will then examine the effect of the excitation system on the small-signal stability performance of the single-machine infinite bus system under consideration.

The input control signal to the excitation system is normally the generator terminal voltage E_t. In the generator model we implemented in the previous section, E_t is not a state variable. Therefore, E_t has to be expressed in terms of the state variables $\Delta\omega_r$, $\Delta\delta$, and $\Delta\psi_{fd}$.

In Section 3.6.2, we showed that $\tilde{E}_t$ may be expressed in complex form:

$$\tilde{E}_t = e_d + je_q$$

Hence,

$$E_t^2 = e_d^2 + e_q^2$$

Applying a small perturbation, we may write

$$(E_{t0} + \Delta E_t)^2 = (e_{d0} + \Delta e_d)^2 + (e_{q0} + \Delta e_q)^2$$

By neglecting second-order terms involving perturbed values, the above equation reduces to

$$E_{t0}\Delta E_t = e_{d0}\Delta e_d + e_{q0}\Delta e_q$$

Therefore,

$$\Delta E_t = \frac{e_{d0}}{E_{t0}}\Delta e_d + \frac{e_{q0}}{E_{t0}}\Delta e_q \tag{12.131}$$

In terms of the perturbed values, Equations 12.94 and 12.95 may be written as

$$\Delta e_d = -R_a\Delta i_d + L_l\Delta i_q - \Delta\psi_{aq}$$

$$\Delta e_q = -R_a\Delta i_q - L_l\Delta i_d + \Delta\psi_{ad}$$

Use of Equations 12.106, 12.107, 12.109, and 12.110 to eliminate Δi_d, Δi_q, $\Delta\psi_{ad}$ and $\Delta\psi_{aq}$ from the above equations in terms of the state variables and substitution of the

resulting expressions for Δe_d and Δe_q in Equation 12.131 yield

$$\Delta E_t = K_5 \Delta\delta + K_6 \Delta\psi_{fd} \tag{12.132}$$

where

$$K_5 = \frac{e_{d0}}{E_{t0}}\left[-R_a m_1 + L_l n_1 + L_{aqs} n_1\right] + \frac{e_{q0}}{E_{t0}}\left[-R_a n_1 - L_l m_1 - L'_{ads} m_1\right] \tag{12.133}$$

$$K_6 = \frac{e_{d0}}{E_{t0}}\left[-R_a m_2 + L_l n_2 + L_{aqs} n_2\right] + \frac{e_{q0}}{E_{t0}}\left[-R_a n_2 - L_l m_2 + L'_{ads}\left(\frac{1}{L_{fd}} - m_2\right)\right] \tag{12.134}$$

For the purpose of illustration and examination of the influence on small-signal stability, we will consider the excitation system model shown in Figure 12.11. It is representative of thyristor excitation systems classified as type ST1A in Chapter 8. The model shown in Figure 12.11, however, has been simplified to include only those elements that are considered necessary for representing a specific system. A high exciter gain, without transient gain reduction or derivative feedback, is used. Parameter T_R represents the terminal voltage transducer time constant.

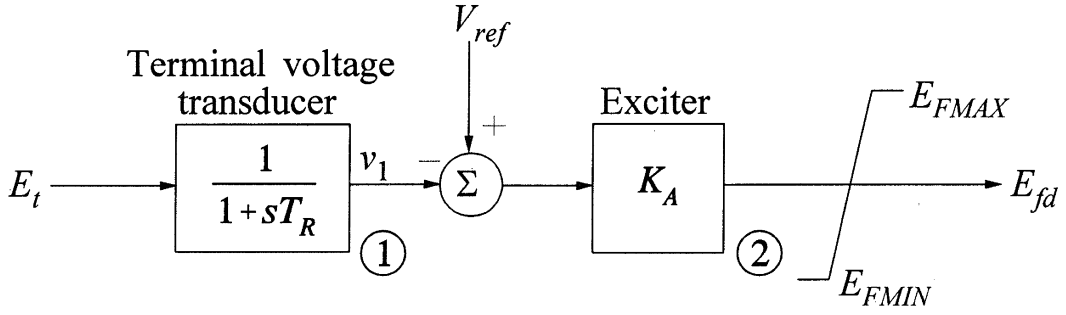


Figure 12.11 Thyristor excitation system with AVR

The only nonlinearity associated with the model is that due to the ceiling on the exciter output voltage represented by E_{FMAX} and E_{FMIN}. For small-disturbance studies, these limits are ignored as we are interested in a linearized model about an operating point such that E_{fd} is within the limits. Limiters and protective circuits (UEL, OXL, V/Hz) are not modelled as they do not affect small-signal stability.

From block 1 of Figure 12.11, using perturbed values, we have

$$\Delta v_1 = \frac{1}{1+pT_R}\Delta E_t$$

Hence

$$p\Delta v_1 = \frac{1}{T_R}(\Delta E_t - \Delta v_1)$$

Substituting for ΔE_t from Equation 12.132, we get

$$p\Delta v_1 = \frac{K_5}{T_R}\Delta\delta + \frac{K_6}{T_R}\Delta\psi_{fd} - \frac{1}{T_R}\Delta v_1 \tag{12.135}$$

From block 2 of Figure 12.11,

$$E_{fd} = K_A(V_{ref} - v_1)$$

In terms of perturbed values, we have

$$\Delta E_{fd} = K_A(-\Delta v_1) \tag{12.136}$$

The field circuit dynamic equation developed in the previous section, with the effect of excitation system included, becomes

$$p\Delta\psi_{fd} = a_{31}\Delta\omega_r + a_{32}\Delta\delta + a_{33}\Delta\psi_{fd} + a_{34}\Delta v_1 \tag{12.137}$$

where

$$a_{34} = -b_{32}K_A = -\frac{\omega_0 R_{fd}}{L_{adu}}K_A \tag{12.138}$$

The expressions for a_{31}, a_{32} and a_{33} remain unchanged and are given by Equation 12.116.

Since we have a first-order model for the exciter, the order of the overall system is increased by 1; the new state variable added is Δv_1.

From Equation 12.135,

$$p\Delta v_1 = a_{41}\Delta\omega_r + a_{42}\Delta\delta + a_{43}\Delta\psi_{fd} + a_{44}\Delta v_1 \tag{12.139}$$

where

$$\begin{aligned} a_{41} &= 0 \\ a_{42} &= \frac{K_5}{T_R} \\ a_{43} &= \frac{K_6}{T_R} \\ a_{44} &= -\frac{1}{T_R} \end{aligned} \tag{12.140}$$

and K_5 and K_6 are given by Equations 12.133 and 12.134.

Since $p\Delta\omega_r$ and $p\Delta\delta$ are not directly affected by the exciter,

$$a_{14} = a_{24} = 0$$

The complete state-space model for the power system, including the excitation system of Figure 12.11, has the following form:

$$\begin{bmatrix} \Delta\dot{\omega}_r \\ \Delta\dot{\delta} \\ \Delta\dot{\psi}_{fd} \\ \Delta\dot{v}_1 \end{bmatrix} = \begin{bmatrix} a_{11} & a_{12} & a_{13} & 0 \\ a_{21} & 0 & 0 & 0 \\ 0 & a_{32} & a_{33} & a_{34} \\ 0 & a_{42} & a_{43} & a_{44} \end{bmatrix} \begin{bmatrix} \Delta\omega_r \\ \Delta\delta \\ \Delta\psi_{fd} \\ \Delta v_1 \end{bmatrix} + \begin{bmatrix} b_1 \\ 0 \\ 0 \\ 0 \end{bmatrix} \Delta T_m \tag{12.141}$$

With constant mechanical torque input,

$$\Delta T_m = 0$$

Block diagram including the excitation system

Figure 12.12 shows the block diagram obtained by extending the diagram of Figure 12.9 to include the voltage transducer and AVR/exciter blocks. The

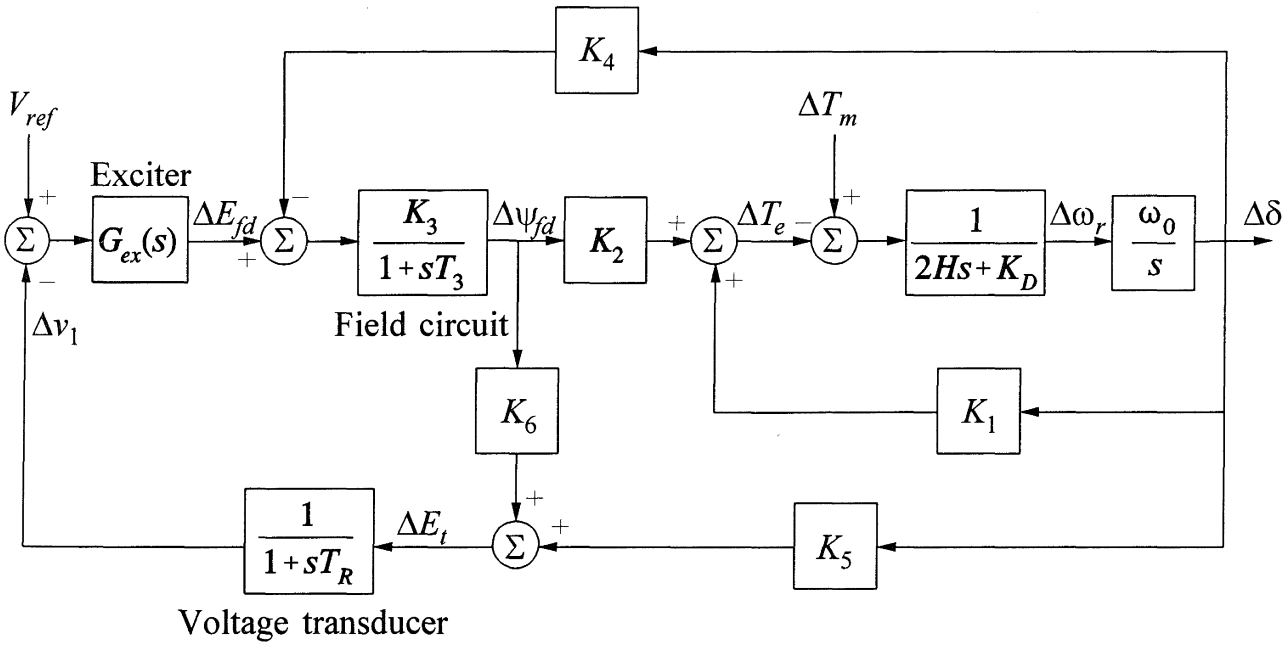


Figure 12.12 Block diagram representation with exciter and AVR

representation is applicable to any type of exciter, with $G_{ex}(s)$ representing the transfer function of the AVR and exciter. For a *thyristor exciter*,

$$G_{ex}(s) = K_A$$

The terminal voltage error signal, which forms the input to the voltage transducer block, is given by Equation 12.132:

$$\Delta E_t = K_5 \Delta\delta + K_6 \Delta\psi_{fd}$$

The coefficient K_6 is always positive, whereas K_5 can be either positive or negative, depending on the operating condition and the external network impedance $R_E + jX_E$. The value of K_5 has a significant bearing on the influence of the AVR on the damping of system oscillations as illustrated below.

Effect of AVR on synchronizing and damping torque components

With automatic voltage regulator action, the field flux variations are caused by the field voltage variations, in addition to the armature reaction. From the block diagram of Figure 12.12, we see that

$$\Delta\psi_{fd} = \frac{K_3}{1+sT_3}\left[-K_4\Delta\delta - \frac{G_{ex}(s)}{1+sT_R}(K_5\Delta\delta + K_6\Delta\psi_{fd})\right] \tag{12.142}$$

By grouping terms involving $\Delta\psi_{fd}$ and rearranging,

$$\Delta\psi_{fd} = \frac{-K_3[K_4(1+sT_R) + K_5 G_{ex}(s)]}{s^2 T_3 T_R + s(T_3+T_R) + 1 + K_3 K_6 G_{ex}(s)}\Delta\delta \tag{12.143}$$

The change in air-gap torque due to change in field flux linkage is

$$\Delta T_e\big|_{\Delta\psi_{fd}} = K_2 \Delta\psi_{fd} \tag{12.144}$$

As noted before, the constants K_2, K_3, K_4, and K_6 are usually positive; however, K_5 may take either positive or negative values. The effect of the AVR on damping and synchronizing torque components is therefore primarily influenced by K_5 and $G_{ex}(s)$. We will illustrate this by considering a specific case with parameters as follows:

$K_1 = 1.591$	$K_2 = 1.5$	$K_3 = 0.333$	$K_4 = 1.8$	$T_3 = 1.91$
$K_5 = -0.12$	$K_6 = 0.3$	$T_R = 0.02$	$G_{ex}(s) = K_A$	
$H = 3.0$	$K_D = 0.0$			

This represents a system with a thyristor exciter and system conditions such that K_5 is negative.

(a) Steady-state synchronizing torque coefficient:

From Equations 12.143 and 12.144, with $s=j\omega=0$, ΔT_e due to $\Delta\psi_{fd}$ is

$$\Delta T_e|_{\Delta\psi_{fd}} = \frac{-K_2K_3(K_4+K_5K_A)}{1+K_3K_6K_A}\Delta\delta$$

$$= \frac{-1.5\times0.333(1.8-0.12K_A)}{1+0.333\times0.3K_A}\Delta\delta$$

$$= \frac{0.06K_A-0.9}{1+0.1K_A}\Delta\delta$$

Hence, the synchronizing torque coefficient due to $\Delta\psi_{fd}$ is

$$K_{S(\Delta\psi_{fd})} = \frac{0.06K_A-0.9}{1+0.1K_A}$$

We see that the effect of the AVR is to increase the synchronizing torque component at steady state. With $K_A=0$ (i.e., constant E_{fd}), $K_{S(\Delta\psi_{fd})}=-0.9$. When $K_A=15$, the AVR compensates exactly for the demagnetizing effect of the armature reaction. With $K_A=200$, $K_{S(\Delta\psi_{fd})}=0.529$ and the total synchronizing torque coefficient is

$$K_S = K_1+K_{S(\Delta\psi_{fd})} = 1.591+0.529$$

$$= 2.12 \quad \text{pu torque/rad}$$

Here, we considered a case with K_5 negative. With a positive K_5 the AVR would have an effect opposite to the above; that is, the effect of the AVR would be to reduce the steady-state synchronizing torque component.

Although we have considered a thyristor exciter in our example, the above observations apply to any type of exciter with a steady-state exciter/AVR gain equal to K_A.

(b) Damping and synchronizing torque components at the rotor oscillation frequency:

Substitution of the numerical values applicable to the specific case under consideration in Equation 12.143 yields

$$\Delta\psi_{fd} = \frac{-0.6-0.333K_5K_A-0.012s}{0.0382s^2+1.93s+1+0.1K_A}\Delta\delta$$

From Equation 12.144,

$$\Delta T_e\big|_{\Delta\psi_{fd}} = K_2\Delta\psi_{fd}$$

$$= \frac{1.5(-0.6-0.333K_5K_A-0.012s)}{0.0382s^2+1.93s+1+0.1K_A}\Delta\delta$$

We will assume that the rotor oscillation frequency is 10 rad/s (1.6 Hz). With $s=j\omega=j10$,

$$\Delta T_e\big|_{\Delta\psi_{fd}} = \frac{-0.9-0.5K_5K_A-j0.18}{-2.82+0.1K_A+j19.3}\Delta\delta$$

With $K_5=-0.12$ and $K_A=200$,

$$\Delta T_e\big|_{\Delta\psi_{fd}} = \frac{11.1-j0.18}{17.18+j19.3}\Delta\delta$$

$$= 0.2804\Delta\delta - 0.3255(j\Delta\delta)$$

Thus the effect of the AVR is to increase the synchronizing torque component and decrease the damping torque component, when K_5 is negative.

The net synchronizing torque coefficient is

$$K_S = K_1+K_{S(\Delta\psi_{fd})} = 1.591+0.2804$$

$$= 1.8714 \quad \text{pu torque/rad}$$

The damping torque component due to $\Delta\psi_{fd}$ is

$$K_{D(\Delta\psi_{fd})} = -0.3255(j\Delta\delta)$$

Since $\Delta\omega_r=s\Delta\delta/\omega_0=j\omega\Delta\delta/\omega_0$,

$$K_{D(\Delta\psi_{fd})} = -\frac{0.3255\omega_0}{\omega}\Delta\omega_r$$

With ω=10 rad/s, the damping torque coefficient is

$$K_{D(\Delta\psi_{fd})} = -12.27 \quad \text{pu torque/pu speed change}$$

In the absence of any other source of damping, the total $K_D = K_{D(\Delta\psi_{fd})}$.

It is readily apparent that, with K_5 positive, the synchronizing and damping torque components due to $\Delta\psi_{fd}$ would be opposite to the above.

For the system under consideration, Table 12.1 summarizes the effect of the AVR on K_S and K_D at ω=10 rad/s for different values of K_A.

Table 12.1

K_A	$K_{S(\Delta\psi_{fd})}$	$K_S = K_1 + K_{S(\Delta\psi_{fd})}$	$K_{D(\Delta\psi_{fd})}$
0.0	-0.0025	1.5885	1.772
10.0	-0.0079	1.5831	0.614
15.0	-0.0093	1.5817	0.024
25.0	-0.0098	1.5812	-1.166
50.0	0.0029	1.5939	-4.090
100.0	0.0782	1.6692	-8.866
200.0	0.2804	1.8714	-12.272
400.0	0.4874	2.0784	-9.722
1000.0	0.5847	2.1757	-4.448
Infinity	0.6000	2.1910	0.000

With K_A=0, $\Delta\psi_{fd}$ is entirely due to armature reaction. The effect of the AVR is to decrease K_D for all positive values of K_A. The net damping is minimum (most negative) for K_A=200, and is zero for K_A=∞. For low values of K_A, the effect of the AVR is to decrease K_S very slightly, the net K_S being minimum at K_A of about 46. As K_A is increased beyond this value, K_S increases steadily. For infinite value of K_A, the torque due to $\Delta\psi_{fd}$ is in phase with $\Delta\delta$, and hence has no damping component.

We are normally interested in the performances of excitation systems with moderate or high responses. For such excitation systems, we can make the following general observations regarding the effects of the AVR:

- With K_5 *positive*, the effect of the AVR is to introduce a negative synchronizing torque and a positive damping torque component.

  The constant K_5 is positive for low values of external system reactance and low generator outputs.

  The reduction in K_S due to AVR action in such cases is usually of no particular concern, because K_1 is so high that the net K_S is significantly greater

than zero.

- With K_5 negative, the AVR action introduces a positive synchronizing torque component and a negative damping torque component. This effect is more pronounced as the exciter response increases.

  For high values of external system reactance and high generator outputs K_5 is negative. In practice, the situation where K_5 is negative are commonly encountered. For such cases, a high response exciter is beneficial in increasing synchronizing torque. However, in so doing it introduces negative damping. We thus have conflicting requirements with regard to exciter response. One possible recourse is to strike a compromise and set the exciter response so that it results in sufficient synchronizing and damping torque components for the expected range of system-operating conditions. This may not always be possible. It may be necessary to use a high-response exciter to provide the required synchronizing torque and transient stability performance. With a very high external system reactance, even with low exciter response the net damping torque coefficient may be negative.

An effective way to meet the conflicting exciter performance requirements with regard to system stability is to provide a power system stabilizer as described in the following section.

12.5 POWER SYSTEM STABILIZER

The basic function of a *power system stabilizer* (PSS) is to add damping to the generator rotor oscillations by controlling its excitation using auxiliary stabilizing signal(s). To provide damping, the stabilizer must produce a component of electrical torque in phase with the rotor speed deviations.

The theoretical basis for a PSS may be illustrated with the aid of the block diagram shown in Figure 12.13. This is an extension of the block diagram of Figure 12.12 and includes the effect of a PSS.

Since the purpose of a PSS is to introduce a damping torque component, a logical signal to use for controlling generator excitation is the speed deviation $\Delta\omega_r$.

If the exciter transfer function $G_{ex}(s)$ and the generator transfer function between ΔE_{fd} and ΔT_e were pure gains, a direct feedback of $\Delta\omega_r$ would result in a damping torque component. However, in practice both the generator and the exciter (depending on its type) exhibit frequency dependent gain and phase characteristics. Therefore, the PSS transfer function, $G_{PSS}(s)$, should have appropriate phase compensation circuits to compensate for the phase lag between the exciter input and the electrical torque. In the ideal case, with the phase characteristic of $G_{PSS}(s)$ being an exact inverse of the exciter and generator phase characteristics to be compensated, the PSS would result in a pure damping torque at all oscillating frequencies.

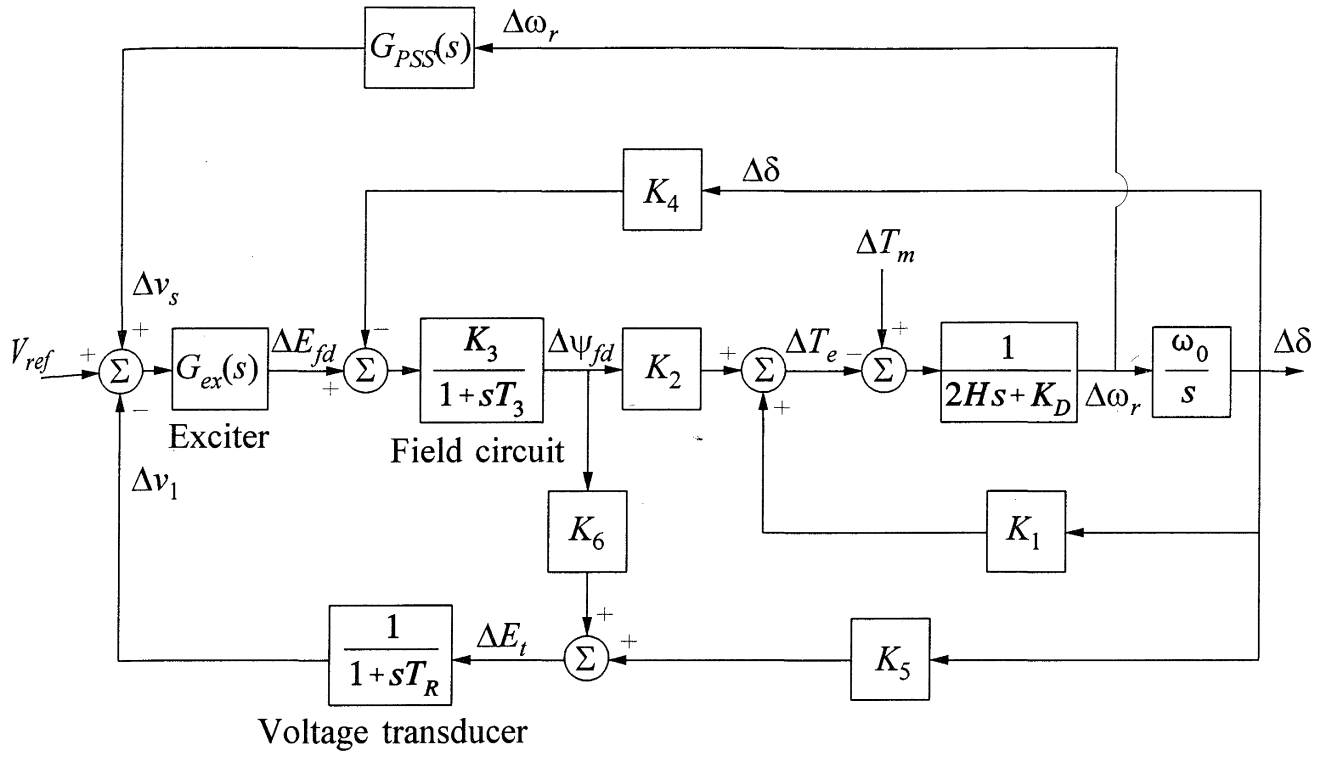


Figure 12.13 Block diagram representation with AVR and PSS

It should be recognized that the generator model assumed in the representation shown in Figure 12.13 neglects amortisseurs to simplify the system model and allow its representation in the form of a block diagram. However, amortisseurs could have a significant effect on the generator phase characteristics and should be considered in establishing the parameters of the PSS. Representation of amortisseur effects will be considered in Section 12.6.

We will illustrate the principle of PSS application by considering the system used in the previous section for examining the effect of the excitation system. The system parameters, as before, are

$K_1 = 1.591$ $K_2 = 1.5$ $K_3 = 0.333$ $K_D = 0.0$ $H = 3.0$
$T_3 = 1.91$ $K_5 = -0.12$ $K_6 = 0.3$ $G_{ex}(s) = K_A = 200$

Since T_R is very small in comparison to T_3, we will neglect its effect in examining the PSS performance. This simplifies the analysis without loss of accuracy.

From the block diagram of Figure 12.13, with T_R neglected, $\Delta\psi_{fd}$ due to PSS is given by

$$\Delta\psi_{fd} = \frac{K_3 K_A}{1+sT_3}(-K_6\Delta\psi_{fd}+\Delta v_s)$$

Therefore,

$$\frac{\Delta\psi_{fd}}{\Delta v_s} = \frac{K_3 K_A}{sT_3 + 1 + K_3 K_6 K_A}$$

$$= \frac{0.333 \times 200}{1.91s + 1 + 0.333 \times 0.3 \times 200}$$

$$= \frac{66.66}{1.91s + 21}$$

Let us examine the PSS phase compensation required to produce damping torque at a rotor oscillation frequency of 10 rad/s. With $s = j\omega = j10$,

$$\frac{\Delta\psi_{fd}}{\Delta v_s} = \frac{66.66}{21 + j19.1}$$

$$\Delta T_{PSS} = \Delta T_e \text{ due to PSS} = K_2(\Delta\psi_{fd} \text{ due to PSS})$$

Therefore, at a frequency of 10 rad/s,

$$\frac{\Delta T_{PSS}}{\Delta v_s} = K_2\left(\frac{66.66}{21 + j19.1}\right)$$

$$= \frac{1.5 \times 66.66}{21 + j19.1}$$

$$= 3.522\angle -42.3°$$

If ΔT_{PSS} has to be in phase with $\Delta\omega_r$ (i.e., a purely damping torque), the $\Delta\omega_r$ signal should be processed through a *phase-lead network* so that the signal is advanced by $\theta = 42.3°$ at a frequency of oscillation of 10 rad/s. The amount of damping introduced depends on the gain of PSS transfer function at that frequency. Therefore,

$$\Delta T_{PSS} = (\text{gain of PSS at } \omega = 10)(3.522)(\Delta\omega_r)$$

With the phase-lead network compensating exactly for the phase lag between ΔT_e and Δv_s, the above compensation is purely damping.

The damping torque coefficient due to PSS at $\omega = 10$ rad/s is equal to

$$K_D(\text{PSS}) = (\text{gain of PSS})(3.522)$$

In the previous section, K_D due to AVR action was found to equal −12.27. Therefore, the net K_D including the effects of AVR and PSS is

$$K_D = -12.27 + (\text{gain of PSS at } \omega = 10)(3.522)$$

With a gain of 12.27/3.522 =3.48, the PSS produces just enough damping to compensate for the negative damping due to AVR action. As the PSS gain is increased further, the amount of damping increases.

If the phase-lead network provides more compensation than the phase lag between ΔT_e and Δv_s, the PSS introduces, in addition to a damping component of torque, a negative synchronizing torque component. Conversely, with under-compensation a positive synchronizing torque component is introduced. Usually, the PSS is required to contribute to the damping of rotor oscillations over a range of frequencies, rather than a single frequency.

We will illustrate the basic structure, modelling, and performance of power system stabilizers by considering a thyristor excitation system. Figure 12.14 shows the block diagram of the excitation system, including the AVR and PSS. Since we are concerned with small-signal performance, stabilizer output limits and exciter output limits are not shown in the figure. The following is a brief description of the basis for the PSS configuration and considerations in the selection of the parameters.

The PSS representation in Figure 12.14 consists of three blocks: a phase compensation block, a signal washout block, and a gain block.

The *phase compensation* block provides the appropriate phase-lead characteristic to compensate for the phase lag between the exciter input and the generator electrical (air-gap) torque. The figure shows a single first-order block. In practice, two or more first-order blocks may be used to achieve the desired phase compensation. In some cases, second-order blocks with complex roots have been used.

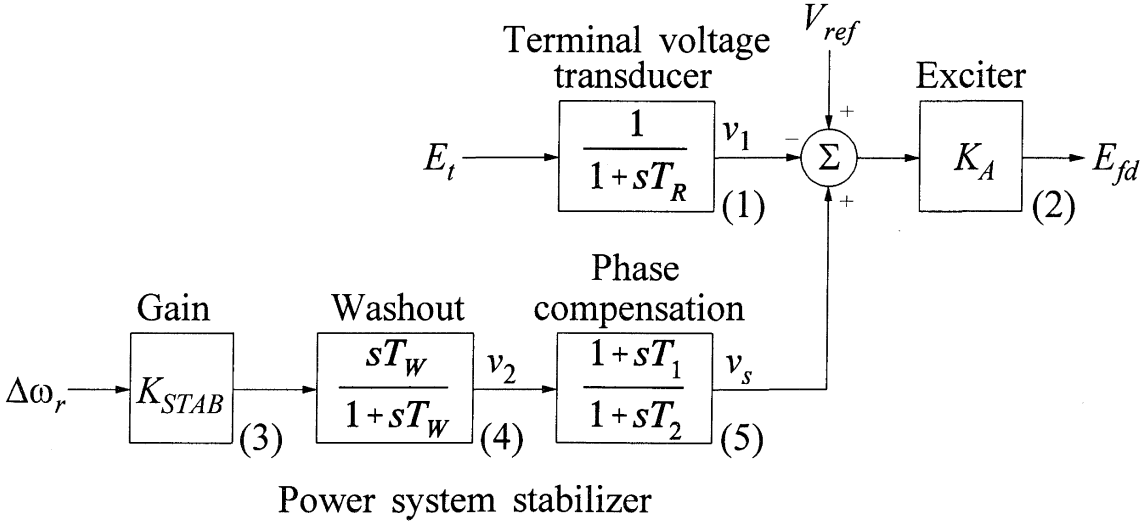


Figure 12.14 Thyristor excitation system with AVR and PSS

Normally, the frequency range of interest is 0.1 to 2.0 Hz, and the phase-lead network should provide compensation over this entire frequency range. The phase characteristic to be compensated changes with system conditions; therefore, a compromise is made and a characteristic acceptable for different system conditions is selected. Generally some undercompensation is desirable so that the PSS, in addition to significantly increasing the damping torque, results in a slight increase of the synchronizing torque.

The *signal washout* block serves as a high-pass filter, with the time constant T_W high enough to allow signals associated with oscillations in ω_r to pass unchanged. Without it, steady changes in speed would modify the terminal voltage. It allows the PSS to respond only to changes in speed. From the viewpoint of the washout function, the value of T_W is not critical and may be in the range of 1 to 20 seconds. The main consideration is that it be long enough to pass stabilizing signals at the frequencies of interest unchanged, but not so long that it leads to undesirable generator voltage excursions during system-islanding conditions.

The stabilizer gain K_{STAB} determines the amount of damping introduced by the PSS. Ideally, the gain should be set at a value corresponding to maximum damping; however, it is often limited by other considerations.

In applying the PSS, care should be taken to ensure that the overall system stability is enhanced, not just the small-signal stability [9]. The performance objectives of the PSS, alternative input signals, and a detailed description of the procedure for selection of its parameters so as to enhance overall system stability are presented in Chapter 17.

System state matrix including PSS

From block 4 of Figure 12.14, using perturbed values, we have

$$\Delta v_2 = \frac{pT_W}{1+pT_W}(K_{STAB}\Delta\omega_r)$$

Hence

$$p\Delta v_2 = K_{STAB}p\Delta\omega_r - \frac{1}{T_W}\Delta v_2$$

Substituting for $p\Delta\omega_r$ given by Equation 12.115, we obtain the following expression for $p\Delta v_2$ in terms of the state variables:

$$\begin{aligned} p\Delta v_2 &= K_{STAB}\left[a_{11}\Delta\omega_r + a_{12}\Delta\delta + a_{13}\Delta\psi_{fd} + \frac{1}{2H}\Delta T_m\right] - \frac{1}{T_W}\Delta v_2 \\ &= a_{51}\Delta\omega_r + a_{52}\Delta\delta + a_{53}\Delta\psi_{fd} + a_{55}\Delta v_2 + \frac{K_{STAB}}{2H}\Delta T_m \end{aligned} \tag{12.145}$$

where

$$a_{51} = K_{STAB} a_{11} \qquad a_{52} = K_{STAB} a_{12}$$
$$a_{53} = K_{STAB} a_{13} \qquad a_{55} = -\frac{1}{T_W} \tag{12.146}$$

Since $p\Delta v_2$ is not a function of Δv_1 and Δv_3, $a_{54}=a_{56}=0$.

From block 5,

$$\Delta v_s = \Delta v_2 \left(\frac{1+pT_1}{1+pT_2} \right)$$

Hence

$$p\Delta v_s = \frac{T_1}{T_2} p\Delta v_2 + \frac{1}{T_2} \Delta v_2 - \frac{1}{T_2} \Delta v_s$$

Substitution for $p\Delta v_2$, given by Equation 12.145, yields

$$p\Delta v_s = a_{61}\Delta\omega_r + a_{62}\Delta\delta + a_{63}\Delta\psi_{fd} + a_{64}\Delta v_1 + a_{65}\Delta v_2 + a_{66}\Delta v_s + \frac{T_1}{T_2}\frac{K_{STAB}}{2H}\Delta T_m \tag{12.147}$$

where

$$a_{61} = \frac{T_1}{T_2} a_{51} \qquad a_{62} = \frac{T_1}{T_2} a_{52}$$
$$a_{63} = \frac{T_1}{T_2} a_{53} \qquad a_{65} = \frac{T_1}{T_2} a_{55} + \frac{1}{T_2} \tag{12.148}$$
$$a_{66} = -\frac{1}{T_2}$$

From block 2 of Figure 12.14,

$$\Delta E_{fd} = K_A(\Delta v_s - \Delta v_1)$$

The field circuit equation, with PSS included, becomes

$$p\Delta\psi_{fd} = a_{32}\Delta\delta + a_{33}\Delta\psi_{fd} + a_{34}\Delta v_1 + a_{36}\Delta v_s \tag{12.149}$$

where

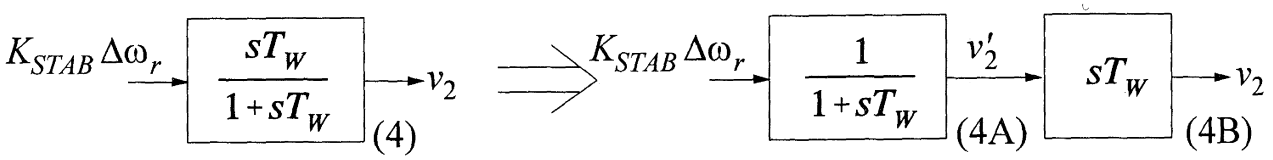
$$a_{36} = \frac{\omega_0 R_{fd}}{L_{adu}} K_A \tag{12.150}$$

The complete state-space model, including the PSS, has the following form (with $\Delta T_m = 0$):

$$\begin{bmatrix} \Delta\dot{\omega}_r \\ \Delta\dot{\delta} \\ \Delta\dot{\psi}_{fd} \\ \Delta\dot{v}_1 \\ \Delta\dot{v}_2 \\ \Delta\dot{v}_s \end{bmatrix} = \begin{bmatrix} a_{11} & a_{12} & a_{13} & 0 & 0 & 0 \\ a_{21} & 0 & 0 & 0 & 0 & 0 \\ 0 & a_{32} & a_{33} & a_{34} & 0 & a_{36} \\ 0 & a_{42} & a_{43} & a_{44} & 0 & 0 \\ a_{51} & a_{52} & a_{53} & 0 & a_{55} & 0 \\ a_{61} & a_{62} & a_{63} & 0 & a_{65} & a_{66} \end{bmatrix} \begin{bmatrix} \Delta\omega_r \\ \Delta\delta \\ \Delta\psi_{fd} \\ \Delta v_1 \\ \Delta v_2 \\ \Delta v_s \end{bmatrix} \tag{12.151}$$

Alternative methods of treating blocks 4 and 5:

Block 4 may be considered to be made up of two blocks:



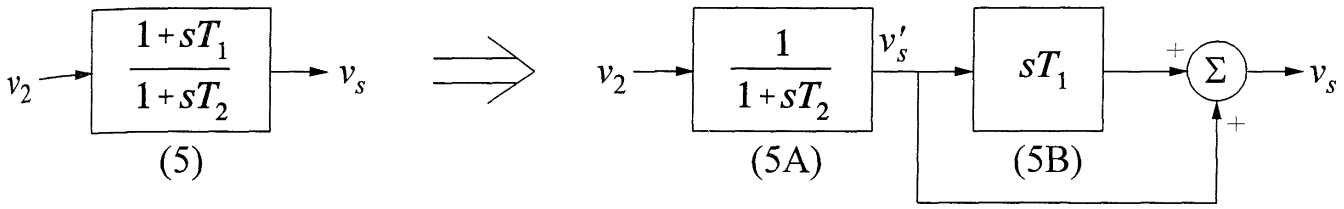
In this case, $\Delta v_2'$ becomes the state variable, with

$$p\Delta v_2' = \frac{1}{T_W}(K_{STAB}\Delta\omega_r - \Delta v_2')$$

and the output Δv_2 of the block is given by

$$\begin{aligned} \Delta v_2 &= T_W p\Delta v_2' \\ &= K_{STAB}\Delta\omega_r - \Delta v_2' \end{aligned}$$

The advantage of this approach is that the expression for the derivative of the input variable to the block is not required. This is important in situations where the input is not a state variable, in which case the expression for its derivative is not readily available. Similarly, block 5 may be treated as follows:



In this case, v_s' is the state variable, with

$$p\Delta v_s' = \frac{1}{T_2}(\Delta v_2 - \Delta v_s')$$

and the output Δv_s is given by

$$\begin{aligned}\Delta v_s &= T_1 p\Delta v_s' + \Delta v_s' \\ &= \frac{T_1}{T_2}\Delta v_2 + \left(1 - \frac{1}{T_2}\right)\Delta v_s'\end{aligned}$$

The disadvantage of this approach is that the output of the block is not a state variable and hence cannot be monitored directly by computing the state variable.

For excitation system models with higher-order transfer function blocks the following general procedure may be used.

Higher-order transfer function blocks:

Consider an *n*th order transfer function whose block diagram is shown in Figure 12.15.

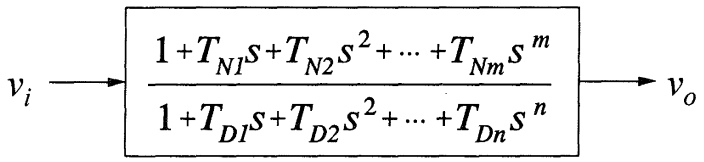


Figure 12.15

The above system has n poles and m zeros ($m<n$). The transfer function of Figure 12.15 may be divided into two parts:

$$G(s) = \frac{v_o(s)}{v_i(s)} = \frac{x_1(s)}{v_i(s)} \frac{v_o(s)}{x_1(s)} \tag{12.152}$$

Hence the nth order transfer function may be represented in terms of two blocks as shown in Figure 12.16.

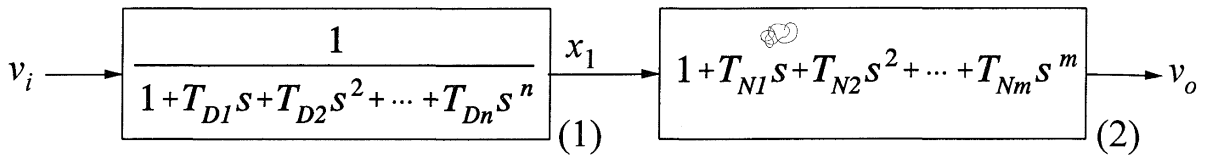


Figure 12.16

From block 1 of Figure 12.16,

$$x_1(1+T_{D1}s+T_{D2}s^2+\cdots+T_{Dn}s^n) = v_i \tag{12.153}$$

Let

$$\begin{aligned} x_2 &= \dot{x}_1 = \frac{dx_1}{dt} \\ x_3 &= \dot{x}_2 = \frac{dx_2}{dt} \\ &\cdots\ \cdots\ \cdots\ \cdots\ \cdots\ \cdots \\ x_n &= \dot{x}_{n-1} = \frac{dx_{n-1}}{dt} \end{aligned} \tag{12.154}$$

From Equation 12.153, in the time domain

$$x_1+T_{D1}x_2+T_{D2}x_3+\cdots+T_{D(n-1)}x_n+T_{Dn}\dot{x}_n = v_i$$

Therefore,

$$\dot{x}_n = \frac{1}{T_{Dn}}\left[v_i-x_1-T_{D1}x_2-\cdots-T_{D(n-1)}x_n\right] \tag{12.155}$$

Combining Equations 12.154 and 12.155, we have

$$\begin{bmatrix} \dot{x}_1 \\ \dot{x}_2 \\ \cdots \\ \dot{x}_{n-1} \\ \dot{x}_n \end{bmatrix} = \begin{bmatrix} 0 & 1 & 0 & \cdots & 0 \\ 0 & 0 & 1 & \cdots & 0 \\ \cdots & \cdots & \cdots & \cdots & \cdots \\ 0 & 0 & 0 & \cdots & 1 \\ -\dfrac{1}{T_{Dn}} & -\dfrac{T_{D1}}{T_{Dn}} & -\dfrac{T_{D2}}{T_{Dn}} & \cdots & -\dfrac{T_{D(n-1)}}{T_{Dn}} \end{bmatrix} \begin{bmatrix} x_1 \\ x_2 \\ \cdots \\ x_{n-1} \\ x_n \end{bmatrix} + \begin{bmatrix} 0 \\ 0 \\ \cdots \\ 0 \\ \dfrac{1}{T_{Dn}} \end{bmatrix} v_i \qquad (12.156)$$

From block 2 of Figure 12.16, the expression for the output is

$$\begin{aligned} v_o &= x_1 + T_{N1}x_2 + T_{N2}x_3 + \cdots + T_{Nm}x_{m+1} \\ &= \begin{bmatrix} 1 & T_{N1} & T_{N2} & \cdots & T_{Nm} & 0 & \cdots & 0 \end{bmatrix} \mathbf{x} + 0v_i \end{aligned} \qquad (12.157)$$

Equations 12.156 and 12.157 have the state-space form

$$\dot{\mathbf{x}} = \mathbf{A}\mathbf{x} + \mathbf{b}u$$

$$y = \mathbf{c}\mathbf{x} + du$$

The variables $x_1, x_2, \ldots, x_n$ defined above are referred to as *phase variables*. They are a particular set of state variables that consists of one variable and its n-1 derivatives.

Example 12.4

This example is an extension of the previous two examples which analyzed the small-signal stability of the system shown in Figure E12.5. Here we consider the effect of two alternative types of excitation control:

(a) A thyristor exciter with AVR as shown in Figure 12.11, with

$K_A = 200$ $T_R = 0.02$ s

(b) The above excitation system with PSS added as shown in Figure 12.13, with

$K_{STAB} = 9.5$ $T_W = 1.4$ s $T_1 = 0.154$ s $T_2 = 0.033$ s

The generator parameters and saturation data are as given in Example 12.3. With the transmission circuit 2 out of service, the plant output in per unit on 2220 MVA and 24 kV base is as follows:

$P = 0.9$ $Q = 0.3$ (overexcited)
$E_t = 1.0\angle 36°$ $E_B = 0.995\angle 0°$

Analyze the small-signal stability of the system with each of the two types of excitation control, by determining

(i) Elements of the state matrix

(ii) The constants of the block diagram of Figure 12.12

(iii) Eigenvalues of the state matrix, participation matrix, and frequency and damping ratio of each oscillatory mode

(iv) Synchronizing and damping torque coefficients at the rotor oscillation frequency

Compare with the results of Examples 12.2 and 12.3.

Solution

(i) From equations developed in Section 12.3.3, the state matrix of the system including the AVR and PSS is

$$\mathbf{A} = \begin{bmatrix} 0 & -0.1092 & -0.1236 & 0 & 0 & 0 \\ 376.99 & 0 & 0 & 0 & 0 & 0 \\ 0 & -0.1938 & -0.4229 & -27.3172 & 0 & 27.3172 \\ 0 & -7.3125 & 20.8391 & -50.0 & 0 & 0 \\ 0 & -1.0372 & -1.1738 & 0 & -0.7143 & 0 \\ 0 & -4.8404 & -5.4777 & 0 & 26.9697 & -30.3030 \end{bmatrix} \begin{matrix} \Delta\omega_r \\ \Delta\delta \\ \Delta\psi_{fd} \\ \Delta v_1 \\ \Delta v_2 \\ \Delta v_s \end{matrix}$$

States

With AVR only (i.e., without PSS), the last two rows and columns disappear.

(ii) The constants of the block diagram are

$K_1 = 0.7643$ $K_2 = 0.8649$ $K_3 = 0.3230$
$K_4 = 1.4187$ $K_5 = -0.1463$ $K_6 = 0.4168$
$T_3 = 2.365$ $T_R = 0.02$ $G_{ex}(s) = 200.0$

(iii) (a) With AVR only, the eigenvalues are

$\lambda_1, \lambda_2 = +0.504 \pm j7.23$ (ω_d=1.15 Hz, ζ=−0.07)
$\lambda_3 = -20.202$
$\lambda_4 = -31.230$

and the participation matrix is

$$\begin{array}{c} \left[\begin{array}{cccc} 0.474 & 0.474 & 0.077 & 0.024 \\ 0.474 & 0.474 & 0.077 & 0.024 \\ 0.065 & 0.065 & 2.524 & 1.633 \\ 0.010 & 0.010 & 1.677 & 2.681 \end{array}\right] \begin{array}{c} \Delta\omega_r \\ \Delta\delta \\ \Delta\psi_{fd} \\ \Delta v_1 \end{array} \\ \begin{array}{cccc} \lambda_1 & \lambda_2 & \lambda_3 & \lambda_4 \end{array} \end{array}$$

Only the magnitudes of the participation factors are shown above; the angles do not provide any useful information.

With AVR only, the system becomes unstable through an oscillatory mode of 1.15 Hz. From the participation factors, we see that this mode is associated primarily with the rotor angle and speed. The two non-oscillatory modes, both of which decay rapidly, are associated with the AVR and the field circuit.

(b) With AVR and PSS, the eigenvalues are

$$\begin{aligned} \lambda_1 &= -39.097 \\ \lambda_2, \lambda_3 &= -1.005 \pm j6.607 \qquad (\omega_d = 1.05 \text{ Hz}, \zeta = 0.15) \\ \lambda_4 &= -0.739 \\ \lambda_5, \lambda_6 &= -19.797 \pm j12.822 \qquad (\omega_d = 2.04 \text{ Hz}, \zeta = 0.84) \end{aligned}$$

and the participation matrix (magnitudes only) is

$$\begin{array}{c} \left[\begin{array}{cccccc} 0.004 & 0.528 & 0.525 & 0.035 & 0.013 & 0.013 \\ 0.004 & 0.528 & 0.528 & 0.035 & 0.013 & 0.013 \\ 0.188 & 0.073 & 0.073 & 0.002 & 0.984 & 0.984 \\ 0.908 & 0.025 & 0.025 & 0.000 & 0.527 & 0.527 \\ 0.012 & 0.160 & 0.160 & 1.072 & 0.094 & 0.094 \\ 0.300 & 0.052 & 0.052 & 0.001 & 0.417 & 0.417 \end{array}\right] \begin{array}{c} \Delta\omega_r \\ \Delta\delta \\ \Delta\psi_{fd} \\ \Delta v_1 \\ \Delta v_2 \\ \Delta v_s \end{array} \\ \begin{array}{cccccc} \lambda_1 & \lambda_2 & \lambda_3 & \lambda_4 & \lambda_5 & \lambda_6 \end{array} \end{array}$$

With the addition of the PSS, the system has become very stable. There are two oscillatory modes: one is the rotor angle mode with a frequency of 1.05 Hz; the other has a frequency of 2.04 Hz and is associated with the excitation system and field circuit. The two non-oscillatory modes are associated with the excitation system.

(iv) (a) *Synchronizing and Damping Torque Coefficients with AVR Only*

From the block diagram of Figure 12.12, field flux linkage change due to AVR and armature reaction (AR) is

$$\Delta\psi_{fd} = \frac{-K_3[K_4(1+sT_R)+K_AK_5]}{s^2T_3T_R+s(T_3+T_R)+(1+K_3K_6K_A)}\Delta\delta$$

Substituting the values of the constants summarized in (i) above and simplifying, we get

$$\Delta\psi_{fd} = \frac{8.993 - 0.0092s}{0.0473s^2 + 2.385s + 27.925}\Delta\delta$$

From the eigenvalue calculations, the complex frequency of rotor oscillation is $0.504 + j7.23$. With s equal to this complex frequency, the above expression for $\Delta\psi_{fd}$ simplifies to

$$\Delta\psi_{fd} = \frac{8.988 - j0.067}{26.67 + j17.59}\Delta\delta$$

Hence, ΔT_e due to $\Delta\psi_{fd}$ is

$$\Delta T_e\big|_{(\text{AVR+AR})} = K_2\Delta\psi_{fd} = 0.8649\,\Delta\psi_{fd}$$

$$= \frac{7.774 - j0.0573}{26.67 + j17.59}\Delta\delta$$

$$= 0.202\,\Delta\delta - 0.1354\,(j\Delta\delta)$$

Now,

$$\text{pu } \Delta\omega_r = \frac{s\Delta\delta}{\omega_0}$$

$$= \frac{(0.504 + j7.23)\,\Delta\delta}{377}$$

Hence,

$$j\Delta\delta = \frac{377}{7.23}\Delta\omega_r - \frac{0.504}{7.23}\Delta\delta$$

$$= 52.14\Delta\omega_r - 0.07\Delta\delta$$

Substituting for $j\Delta\delta$ in the expression for ΔT_e, we get

$$\Delta T_e\big|_{(\text{AVR+AR})} = 0.202\,\Delta\delta - 0.1354\,(52.14\,\Delta\omega_r - 0.07\,\Delta\delta)$$

$$= 0.2115\,\Delta\delta - 7.06\,\Delta\omega_r$$

Therefore,

$K_{S(\text{AVR+AR})} = 0.2115$ pu torque/rad
$K_{D(\text{AVR+AR})} = -7.06$ pu torque/pu speed change

The field flux linkage variation is due to armature reaction and AVR. In Example 12.3, we saw that the effect of the armature reaction alone is to decrease K_S by 0.00172 and increase K_D by 1.53 at the rotor oscillation frequency of 6.41 rad/s. The effect of AVR alone is therefore to increase K_S by nearly 0.2 and to decrease K_D by nearly 8.5.

The total synchronizing and damping torque coefficients are

$$K_S = K_1 + K_{S(\text{AVR+AR})} = 0.7643 + 0.2115$$

$$= 0.9758 \quad \text{pu torque/rad}$$

and

$$K_D = K_{D(\text{AVR+AR})} = -7.06 \quad \text{pu torque/pu speed change}$$

From Equation 12.82, the corresponding damping ratio is

$$\zeta = \frac{1}{2}\frac{K_D}{\sqrt{K_S 2H\omega_0}} = \frac{1}{2}\frac{-7.06}{\sqrt{0.9758\times 2\times 3.5\times 377}}$$

$$= -0.07$$

This agrees with ζ computed from the eigenvalues.

(b) *Synchronizing and Damping Torque Coefficients with PSS*

The complex frequency of rotor oscillation in this case is $-1.005 + j6.607$. From the block diagram of Figure 12.13, $\Delta\psi_{fd}$ due to PSS is

$$\Delta\psi_{fd}\big|_{\text{PSS}} = \frac{K_3 K_A}{1+sT_3}\left(\Delta v_s - \frac{K_6}{1+sT_R}\Delta\psi_{fd}\right)$$

with

$$\Delta v_s = K_{STAB}\frac{sT_W}{1+sT_W}\frac{1+sT_1}{1+sT_2}\Delta\omega_r$$

Therefore,

$$\Delta T_e\big|_{\text{PSS}} = K_2\,\Delta\psi_{fd}\big|_{\text{PSS}}$$

$$= \frac{K_{STAB}K_2K_3K_A(1+sT_R)(1+sT_1)sT_W}{[(1+sT_3)(1+sT_R)+K_3K_6K_A](1+sT_2)(1+sT_W)}\Delta\omega_r$$

Substituting the numerical values of the parameters, setting $s=-1.005+j6.607$, and simplifying, we get

$$\Delta T_e|_{\text{PSS}} = (24.0+j8.089)\,\Delta\omega_r$$

Now,

$$\begin{aligned} j\Delta\omega_r &= j\frac{s}{\omega_0}\Delta\delta = j\frac{-1.005+j6.607}{377}\Delta\delta \\ &= -0.01752\,\Delta\delta - \frac{1.005}{377}(j\Delta\delta) \\ &= -0.01752\,\Delta\delta - \frac{1.005}{377}\left(\frac{377}{6.607}\Delta\omega_r + \frac{1.005}{6.607}\Delta\delta\right) \\ &= -0.0179\,\Delta\delta - 0.1521\,\Delta\omega_r \end{aligned}$$

Hence,

$$\begin{aligned} \Delta T_e|_{\text{PSS}} &= 24.0\,\Delta\omega_r + 8.089(-0.0179\,\Delta\delta - 0.1521\,\Delta\omega_r) \\ &= -0.145\,\Delta\delta + 22.77\,\Delta\omega_r \end{aligned}$$

The synchronizing and damping torque coefficients due to PSS are

$$\begin{aligned} K_{S(\text{PSS})} &= -0.145 \quad \text{pu torque/rad} \\ K_{D(\text{PSS})} &= 22.77 \quad \text{pu torque/pu speed change} \end{aligned}$$

and K_S and K_D due to AVR and armature reaction (AR) must now also be evaluated at $s=-1.005+j6.607$. Following the same procedure used before, we have

$$\begin{aligned} K_{S(\text{AVR+AR})} &= 0.21 \quad \text{pu torque/rad} \\ K_{D(\text{AVR+AR})} &= -8.69 \quad \text{pu torque/pu speed change} \end{aligned}$$

The total synchronizing and damping torque coefficients are

$$\begin{aligned} K_S &= K_1 + K_{S(\text{AVR+AR})} + K_{S(\text{PSS})} \\ &= 0.7643 + 0.21 - 0.145 \\ &= 0.8293 \quad \text{pu torque/rad} \end{aligned}$$

$$\begin{aligned} K_D &= K_{D(\text{AVR+AR})} + K_{D(\text{PSS})} \\ &= -8.69 + 22.77 \\ &= 14.08 \quad \text{pu torque/pu speed change} \end{aligned}$$

From Equation 12.81, the undamped natural frequency is

$$\omega_n = \sqrt{\frac{K_S \omega_0}{2H}} = \sqrt{\frac{0.8293 \times 377}{2 \times 3.5}} = 6.683 \quad \text{rad/s}$$

$$\zeta = \frac{1}{2} \frac{K_D}{\sqrt{K_S 2H\omega_0}} = \frac{1}{2} \frac{14.08}{\sqrt{0.8293 \times 7.0 \times 377}} = 0.15$$

$$\omega_d = \omega_n \sqrt{1-\zeta^2} = 6.683\sqrt{1-0.15^2} = 6.607 \quad \text{rad/s}$$

The above results agree with ζ and ω_d computed from the eigenvalues.

We see that the PSS has increased K_D by 22.77 and reduced K_S by 0.145. The reduction in K_S indicates that phase lead compensation used results in slight overcompensation at the rotor oscillation frequency of 6.61 rad/s. By adjusting T_1 and/or T_2, the compensation may be altered to give zero or even positive synchronizing torque component.

The following is a summary of frequency of rotor oscillation, damping ratio, K_S and K_D with different types of excitation control and with classical model, based on the results of this and the previous two examples.

Model	Classical Model (K_D=0)	Constant E_{fd}	AVR only	AVR and PSS
ω_d	1.02 Hz	1.07 Hz	1.15 Hz	1.05 Hz
ζ	0	0.017	-0.07	0.15
K_S	0.757	0.763	0.976	0.829
K_D	0	1.53	-7.06	14.08

■

12.6 SYSTEM STATE MATRIX WITH AMORTISSEURS

When generator amortisseurs are included, the system equations developed in Section 12.3.2 change as follows. We will assume that the model includes one d-axis amortisseur and two q-axis amortisseurs, as shown in Figure 12.17.

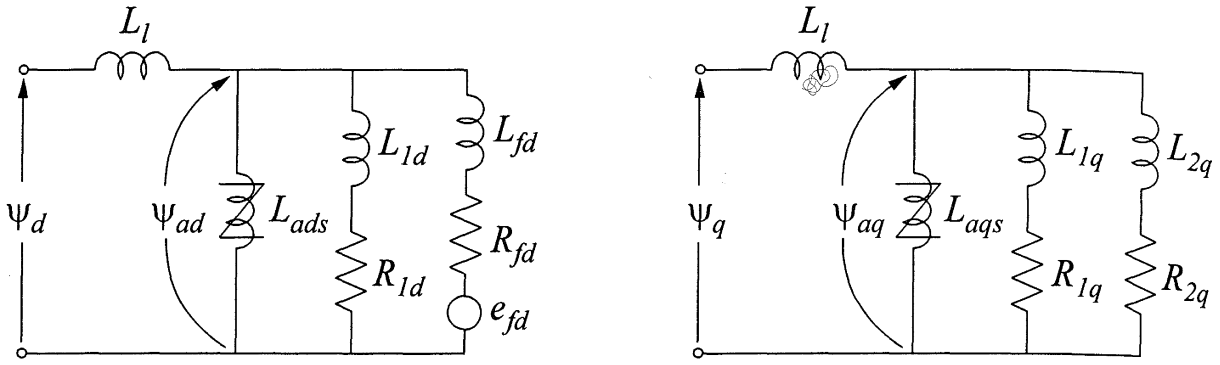


Figure 12.17 Synchronous machine equivalent circuits

Rotor circuit equations

$$\begin{aligned} p\psi_{fd} &= \frac{\omega_0 R_{fd}}{L_{adu}} E_{fd} - \omega_0 R_{fd} i_{fd} \\ p\psi_{1d} &= -\omega_0 R_{1d} i_{1d} \\ p\psi_{1q} &= -\omega_0 R_{1q} i_{1q} \\ p\psi_{2q} &= -\omega_0 R_{2q} i_{2q} \end{aligned} \tag{12.158}$$

The rotor currents are given by

$$\begin{aligned} i_{fd} &= \frac{1}{L_{fd}}(\psi_{fd} - \psi_{ad}) \\ i_{1d} &= \frac{1}{L_{1d}}(\psi_{1d} - \psi_{ad}) \\ i_{1q} &= \frac{1}{L_{1q}}(\psi_{1q} - \psi_{aq}) \\ i_{2q} &= \frac{1}{L_{2q}}(\psi_{2q} - \psi_{aq}) \end{aligned} \tag{12.159}$$

The d- and q-axis mutual flux linkages are given by

$$\begin{aligned}\psi_{ad} &= -L_{ads}i_d + L_{ads}i_{fd} + L_{ads}i_{1d} \\ &= L''_{ads}\left(-i_d + \frac{\psi_{fd}}{L_{fd}} + \frac{\psi_{1d}}{L_{1d}}\right)\end{aligned} \tag{12.160}$$

$$\psi_{aq} = L''_{aqs}\left(-i_q + \frac{\psi_{1q}}{L_{1q}} + \frac{\psi_{2q}}{L_{2q}}\right) \tag{12.161}$$

where

$$L''_{ads} = \frac{1}{\frac{1}{L_{ads}} + \frac{1}{L_{fd}} + \frac{1}{L_{1d}}} \tag{12.162}$$

$$L''_{aqs} = \frac{1}{\frac{1}{L_{aqs}} + \frac{1}{L_{1q}} + \frac{1}{L_{2q}}} \tag{12.163}$$

The expressions for i_d and i_q (corresponding to Equations 12.103 and 12.104) become

$$\begin{aligned} i_d &= \frac{X_{Tq}E_{qN} - R_T E_{dN}}{D} \\ i_q &= \frac{R_T E_{qN} + X_{Td}E_{dN}}{D} \end{aligned} \tag{12.164}$$

where

$$\begin{aligned} E_{dN} &= E''_d + E_B \sin\delta & E_{qN} &= E''_q - E_B \cos\delta \\ E''_d &= \bar{\omega}L''_{aqs}\left(\frac{\psi_{1q}}{L_{1q}} + \frac{\psi_{2q}}{L_{2q}}\right) & E''_q &= \bar{\omega}L''_{ads}\left(\frac{\psi_{fd}}{L_{fd}} + \frac{\psi_{1d}}{L_{1d}}\right) \\ X_{Td} &= X_E + \bar{\omega}(L''_{ads} + L_l) & X_{Tq} &= X_E + \bar{\omega}(L''_{aqs} + L_l) \\ &= X_E + X''_{ds} & &= X_E + X''_{qs} \\ R_T &= R_a + R_E & D &= R_T^2 + X_{Td}X_{Tq} \end{aligned} \tag{12.165}$$

As discussed in Chapter 5, $\bar{\omega}$ is assumed to be 1.0 pu to counterbalance the effects of neglecting stator transients.

Expressing Equations 12.164 and 12.165 in terms of perturbed values, we get

$$\begin{aligned}\Delta i_d &= m_1\Delta\delta + m_2\Delta\psi_{fd} + m_3\Delta\psi_{1d} + m_4\Delta\psi_{1q} + m_5\Delta\psi_{2q}\\ \Delta i_q &= n_1\Delta\delta + n_2\Delta\psi_{fd} + n_3\Delta\psi_{1d} + n_4\Delta\psi_{1q} + n_5\Delta\psi_{2q}\end{aligned} \tag{12.166}$$

with

$$\begin{aligned}m_1 &= \frac{E_B}{D}(X_{Tq}\sin\delta_0 - R_T\cos\delta_0)\\ m_2 &= \frac{X_{Tq}}{D}\frac{L''_{ads}}{L_{fd}} \qquad m_3 = \frac{X_{Tq}}{D}\frac{L''_{ads}}{L_{1d}}\\ m_4 &= -\frac{R_T}{D}\frac{L''_{aqs}}{L_{1q}} \qquad m_5 = -\frac{R_T}{D}\frac{L''_{aqs}}{L_{2q}}\\ n_1 &= \frac{E_B}{D}(R_T\sin\delta_0 + X_{Td}\cos\delta_0)\\ n_2 &= \frac{R_T}{D}\frac{L''_{ads}}{L_{fd}} \qquad n_3 = \frac{R_T}{D}\frac{L''_{ads}}{L_{1d}}\\ n_4 &= \frac{X_{Td}}{D}\frac{L''_{aqs}}{L_{1q}} \qquad n_5 = \frac{X_{Td}}{D}\frac{L''_{aqs}}{L_{2q}}\end{aligned} \tag{12.167}$$

The expressions for $\Delta\psi_{ad}$ and $\Delta\psi_{aq}$ are given by

$$\begin{aligned}\Delta\psi_{ad} &= L''_{ads}\left(-\Delta i_d + \frac{\Delta\psi_{fd}}{L_{fd}} + \frac{\Delta\psi_{1d}}{L_{1d}}\right)\\ &= (-m_1 L''_{ads})\Delta\delta + L''_{ads}\left(\frac{1}{L_{fd}} - m_2\right)\Delta\psi_{fd} + L''_{ads}\left(\frac{1}{L_{1d}} - m_3\right)\Delta\psi_{1d} +\\ &\quad (-m_4 L''_{ads})\Delta\psi_{1q} + (-m_5 L''_{ads})\Delta\psi_{2q}\end{aligned} \tag{12.168}$$

$$\begin{aligned}\Delta\psi_{aq} &= (-n_1 L''_{aqs})\Delta\delta + (-n_2 L''_{aqs})\Delta\psi_{fd} + (-n_3 L''_{aqs})\Delta\psi_{1d} +\\ &\quad L''_{aqs}\left(\frac{1}{L_{1q}} - n_4\right)\Delta\psi_{1q} + L''_{aqs}\left(\frac{1}{L_{2q}} - n_5\right)\Delta\psi_{2q}\end{aligned} \tag{12.169}$$

The expression for ΔT_e (corresponding to Equation 12.112) is given by

$$\begin{aligned}\Delta T_e &= \psi_{ad0}\Delta i_q + i_{q0}\Delta\psi_{ad} - \psi_{aq0}\Delta i_d - i_{d0}\Delta\psi_{aq} \\ &= K_1\Delta\delta + K_2\Delta\psi_{fd} + K_{21}\Delta\psi_{1d} + K_{22}\Delta\psi_{1q} + K_{23}\Delta\psi_{2q}\end{aligned} \tag{12.170}$$

where

$$\begin{aligned}K_1 &= n_1(\psi_{ad0} + L''_{aqs} i_{d0}) - m_1(\psi_{aq0} + L''_{ads} i_{q0}) \\ K_2 &= n_2(\psi_{ad0} + L''_{aqs} i_{d0}) - m_2(\psi_{aq0} + L''_{ads} i_{q0}) + \frac{L''_{ads}}{L_{fd}} i_{q0} \\ K_{21} &= n_3(\psi_{ad0} + L''_{aqs} i_{d0}) - m_3(\psi_{aq0} + L''_{ads} i_{q0}) + \frac{L''_{ads}}{L_{1d}} i_{q0} \\ K_{22} &= n_4(\psi_{ad0} + L''_{aqs} i_{d0}) - m_4(\psi_{aq0} + L''_{ads} i_{q0}) - \frac{L''_{aqs}}{L_{1q}} i_{d0} \\ K_{23} &= n_5(\psi_{ad0} + L''_{aqs} i_{d0}) - m_5(\psi_{aq0} + L''_{ads} i_{q0}) - \frac{L''_{aqs}}{L_{2q}} i_{d0}\end{aligned} \tag{12.171}$$

From Equations 12.83 and 12.170

$$\begin{aligned}p\Delta\omega_r &= \frac{1}{2H}[\Delta T_M - \Delta T_e - K_D\Delta\omega_r] \\ &= \frac{1}{2H}[\Delta T_m - K_1\Delta\delta - K_2\Delta\psi_{fd} - K_{21}\Delta\psi_{1d} - \\ &\qquad K_{22}\Delta\psi_{1q} - K_{23}\Delta\psi_{2q} - K_D\Delta\omega_r] \\ &= a_{11}\Delta\omega_r + a_{12}\Delta\delta + a_{13}\Delta\psi_{fd} + a_{14}\Delta\psi_{1d} + \\ &\qquad a_{15}\Delta\psi_{1q} + a_{16}\Delta\psi_{2q} + b_{11}\Delta T_m\end{aligned} \tag{12.172}$$

where

$$\begin{aligned}a_{11} &= -\frac{K_D}{2H} \qquad a_{12} = -\frac{K_1}{2H} \qquad a_{13} = -\frac{K_2}{2H} \\ a_{14} &= -\frac{K_{21}}{2H} \qquad a_{15} = -\frac{K_{22}}{2H} \qquad a_{16} = -\frac{K_{23}}{2H} \\ b_{11} &= \frac{1}{2H}\end{aligned} \tag{12.173}$$

As before,

$$p\Delta\delta = a_{21}\Delta\omega_r \tag{12.174}$$

where

$$a_{21} = \omega_0 = 2\pi f_0 \tag{12.175}$$

From Equations 12.158, 12.159, and 12.168,

$$\begin{aligned} p\Delta\psi_{fd} &= a_{31}\Delta\omega_r + a_{32}\Delta\delta + a_{33}\Delta\psi_{fd} + a_{34}\Delta\psi_{1d} \\ &\quad a_{35}\Delta\psi_{1q} + a_{36}\Delta\psi_{2q} + b_{32}\Delta e_{fd} \end{aligned} \tag{12.176}$$

where

$$\begin{aligned} a_{31} &= 0 & a_{32} &= -\frac{\omega_0 R_{fd}}{L_{fd}} m_1 L''_{ads} \\ a_{33} &= -\frac{\omega_0 R_{fd}}{L_{fd}}\left(1 - \frac{L''_{ads}}{L_{fd}} + m_2 L''_{ads}\right) \\ a_{34} &= -\frac{\omega_0 R_{fd}}{L_{fd}}\left(m_3 L''_{ads} - \frac{L''_{ads}}{L_{fd}}\right) \\ a_{35} &= -\frac{\omega_0 R_{fd}}{L_{fd}} m_4 L''_{ads} & a_{36} &= -\frac{\omega_0 R_{fd}}{L_{fd}} m_5 L''_{ads} \\ b_{32} &= \frac{\omega_0 R_{fd}}{L_{adu}} \end{aligned} \tag{12.177}$$

Similarly,

$$\begin{aligned} p\Delta\psi_{1d} &= -\omega_0 R_{1d}\Delta i_{1d} \\ &= a_{41}\Delta\omega_r + a_{42}\Delta\delta + a_{43}\Delta\psi_{fd} + a_{44}\Delta\psi_{1d} + a_{45}\Delta\psi_{1q} + a_{46}\Delta\psi_{2q} \end{aligned} \tag{12.178}$$

where

$$a_{41} = 0 \qquad a_{42} = -\frac{\omega_0 R_{1d}}{L_{1d}} m_1 L''_{ads}$$

$$a_{43} = -\frac{\omega_0 R_{1d}}{L_{1d}}\left(m_2 L''_{ads} - \frac{L''_{ads}}{L_{fd}}\right)$$

$$a_{44} = -\frac{\omega_0 R_{1d}}{L_{1d}}\left(1 - \frac{L''_{ads}}{L_{fd}} + m_3 L''_{ads}\right) \tag{12.179}$$

$$a_{45} = -\frac{\omega_0 R_{1d}}{L_{1d}} m_4 L''_{ads} \qquad a_{46} = -\frac{\omega_0 R_{1d}}{L_{1d}} m_5 L''_{ads}$$

$$\begin{aligned} p\Delta\psi_{1q} &= -\omega_0 R_{1q}\Delta i_{1q} \\ &= a_{51}\Delta\omega_r + a_{52}\Delta\delta + a_{53}\Delta\psi_{fd} + a_{54}\Delta\psi_{1d} + a_{55}\Delta\psi_{1q} + a_{56}\Delta\psi_{2q} \end{aligned} \tag{12.180}$$

where

$$a_{51} = 0 \qquad a_{52} = -\frac{\omega_0 R_{1q}}{L_{1q}} n_1 L''_{aqs}$$

$$a_{53} = -\frac{\omega_0 R_{1q}}{L_{1q}} n_2 L''_{aqs} \qquad a_{54} = -\frac{\omega_0 R_{1q}}{L_{1q}} n_3 L''_{aqs}$$

$$a_{55} = -\frac{\omega_0 R_{1q}}{L_{1q}}\left(1 - \frac{L''_{aqs}}{L_{1q}} + n_4 L''_{aqs}\right) \tag{12.181}$$

$$a_{56} = -\frac{\omega_0 R_{1q}}{L_{1q}}\left(n_5 L''_{aqs} - \frac{L''_{aqs}}{L_{2q}}\right)$$

$$\begin{aligned} p\Delta\psi_{2q} &= -\omega_0 R_{2q}\Delta i_{2q} \\ &= a_{61}\Delta\omega_r + a_{62}\Delta\delta + a_{63}\Delta\psi_{fd} + a_{64}\Delta\psi_{1d} + a_{65}\Delta\psi_{1q} + a_{66}\Delta\psi_{2q} \end{aligned} \tag{12.182}$$

where

$$a_{61} = 0 \qquad a_{62} = -\frac{\omega_0 R_{2q}}{L_{2q}} n_1 L''_{aqs}$$

$$a_{63} = -\frac{\omega_0 R_{2q}}{L_{2q}} n_2 L''_{aqs} \qquad a_{64} = -\frac{\omega_0 R_{2q}}{L_{2q}} n_3 L''_{aqs} \tag{12.183A}$$

$$a_{65} = -\frac{\omega_0 R_{2q}}{L_{2q}}\left(n_4 L''_{aqs} - \frac{L''_{aqs}}{L_{1q}}\right)$$

$$a_{66} = -\frac{\omega_0 R_{2q}}{L_{2q}}\left(1 - \frac{L''_{aqs}}{L_{2q}} + n_5 L''_{aqs}\right) \tag{12.183B}$$

The complete state equation is given by

$$\begin{bmatrix} \Delta\dot{\omega}_r \\ \Delta\dot{\delta} \\ \Delta\dot{\psi}_{fd} \\ \Delta\dot{\psi}_{1d} \\ \Delta\dot{\psi}_{1q} \\ \Delta\dot{\psi}_{2q} \end{bmatrix} = \begin{bmatrix} a_{11} & a_{12} & a_{13} & a_{14} & a_{15} & a_{16} \\ a_{21} & 0 & 0 & 0 & 0 & 0 \\ 0 & a_{32} & a_{33} & a_{34} & a_{35} & a_{36} \\ 0 & a_{42} & a_{43} & a_{44} & a_{45} & a_{46} \\ 0 & a_{52} & a_{53} & a_{54} & a_{55} & a_{56} \\ 0 & a_{62} & a_{63} & a_{64} & a_{65} & a_{66} \end{bmatrix} \begin{bmatrix} \Delta\omega_r \\ \Delta\delta \\ \Delta\psi_{fd} \\ \Delta\psi_{1d} \\ \Delta\psi_{1q} \\ \Delta\psi_{2q} \end{bmatrix} + \begin{bmatrix} b_{11} & 0 \\ 0 & 0 \\ 0 & b_{32} \\ 0 & 0 \\ 0 & 0 \\ 0 & 0 \end{bmatrix} \begin{bmatrix} \Delta T_m \\ \Delta E_{fd} \end{bmatrix} \tag{12.184}$$

With constant input torque, $\Delta T_m = 0$. Similarly, with constant field voltage, $\Delta E_{fd} = 0$.

If AVR action is to be represented, we need the expression for ΔE_t. Following the procedure used in Section 12.3.3,

$$\Delta E_t = \frac{e_{d0}}{E_{t0}}\Delta e_d + \frac{e_{q0}}{E_{t0}}\Delta e_q$$

with

$$\Delta e_d = -R_a \Delta i_d + L_l \Delta i_q - \Delta\psi_{ad}$$

$$\Delta e_q = -R_a \Delta i_q - L_l \Delta i_d + \Delta\psi_{aq}$$

By using Equations 12.166, 12.168, and 12.169, the perturbed value of the terminal voltage may be expressed in the following form:

$$\Delta E_t = K_5 \Delta\delta + K_6 \Delta\psi_{fd} + K_{61}\Delta\psi_{1d} + K_{62}\Delta\psi_{1q} + K_{63}\Delta\psi_{2q} \tag{12.185}$$

It is left to the reader as an exercise to develop the expressions for the K constants of the above equation in terms of system parameters.

Example 12.5

In this example, we extend the analysis presented in Examples 12.3 and 12.4 by including the effects of generator amortisseurs. In addition, we examine the effects of varying the exciter gain and stabilizer gain to provide additional insight into how the AVR and PSS influence the small-signal dynamic characteristic.

The per unit generator parameters related to the amortisseurs are as follows:

$X'_q = 0.65$ $X''_d = 0.23$ $X''_q = 0.25$
$T'_{q0} = 1.0$ s $T''_{d0} = 0.03$ s $T''_{q0} = 0.07$ s

All other data (including generator and excitation system parameters, and system conditions) are as considered in Example 12.4.

(a) With the excitation system on manual control, determine the state matrix and its eigenvalues. Identify the state variable with the highest participation for each mode.

(b) With AVR in service and PSS out of service, examine the effect of varying the exciter gain K_A on the eigenvalues. Assume T_R=0.02 s.

(c) With AVR and PSS in service, examine the effect of varying the stabilizer gain K_{STAB} on the eigenvalues. Assume all other parameters of the excitation system are fixed at values given in Example 12.4.

Solution

(a) The per unit values of the leakage inductances and resistances of the amortisseur circuits are computed following the procedure used in Example 4.1 as follows:

$L_{1d} = 0.1400$ $L_{1q} = 0.7063$ $L_{2q} = 0.1102$
$R_{1d} = 0.0248$ $R_{1q} = 0.0061$ $R_{2q} = 0.0227$

Based on equations developed in Section 12.6, the state matrix of the system including amortisseurs, but with constant E_{fd}, is

$$\mathbf{A} = \begin{bmatrix} 0 & -0.121 & -0.069 & -0.076 & -0.003 & -0.023 \\ 377 & 0 & 0 & 0 & 0 & 0 \\ 0 & -0.109 & -0.883 & 0.645 & 0 & 0.0003 \\ 0 & -4.928 & 26.72 & -37.47 & 0.002 & 0.013 \\ 0 & -0.058 & -0.0005 & -0.0005 & -2.914 & 2.250 \\ 0 & -1.39 & -0.011 & -0.012 & 8.367 & -24.18 \end{bmatrix}$$

The eigenvalues of **A** and the corresponding state variable with highest participation are

Eigenvalues		Dominant State(s)	ω_d	ζ
λ_1, λ_2	$-0.171 \pm j6.47$	$\Delta\omega_r, \Delta\delta$	1.03 Hz	0.0265
λ_3	-0.200	$\Delta\psi_{fd}$		
λ_4	-2.045	$\Delta\psi_{1q}$		
λ_5	-25.01	$\Delta\psi_{2q}$		
λ_6	-37.85	$\Delta\psi_{1d}$		

Comparing with the results of Example 12.3, we see that the effect of the amortisseurs is to increase the damping ratio from 0.017 to 0.0265 and to increase the frequency very slightly from 1.02 to 1.03 Hz.

(b) Table E12.1 shows the effect of varying K_A on the eigenvalues of the state matrix with PSS out of service. The table also indicates for each mode the state variable with highest participation as well as any other state with significant participation.

Table E12.1

K_A	Eigenvalues					
	λ_1, λ_2	λ_3	λ_4	λ_5	λ_6	λ_7
–	$-0.171 \pm j6.47$	-0.20	-37.85	-25.01	-2.04	–
0.1	$-0.170 \pm j6.47$	-0.20	-37.84	-25.01	-2.05	-50.00
5.0	$-0.112 \pm j6.46$	-0.59	-37.34	-25.02	-2.06	-50.22
10.0	$-0.050 \pm j6.46$	-0.98	-36.83	-25.02	-2.10	-50.42
15.0	$0.011 \pm j6.46$	-1.34	-36.34	-25.02	-2.16	-50.79
30.0	$0.182 \pm j6.50$	-2.94	-34.86	-25.03	-1.86	-51.12
50.0	$0.357 \pm j6.62$	-4.60	-32.87	-25.06	-1.94	-51.70
100.0	$0.552 \pm j6.95$	-9.40	-26.81	-25.54	-1.96	-52.84
110.0	$0.564 \pm j7.01$	-10.64	$-25.47 \pm j0.96$		-1.97	
125.0	$0.573 \pm j7.09$	-13.03	$-24.15 \pm j0.88$		-1.97	-53.30
130.0	$0.574 \pm j7.11$	-14.14	-22.92	-24.18	-1.97	
150.0	$0.570 \pm j7.21$	$-18.09 \pm j5.09$		-24.72	-1.97	-53.71
200.0	$0.528 \pm j7.38$	$-17.63 \pm j11.33$		-24.86	-1.97	-54.41
400.0	$0.315 \pm j7.66$	$-16.40 \pm j22.63$		-24.92	-1.98	-56.38
Dominant States	$\Delta\omega_r, \Delta\delta$	$\Delta\psi_{fd}, \Delta\psi_{1d}$		$\Delta\psi_{2q}$	$\Delta\psi_{1q}$	Δv_1
Significant States		Δv_1				$\Delta\psi_{1d}$

We see that the effect of the AVR is to introduce negative damping. For values of K_A higher than about 14, the system is unstable. The system is most unstable for a K_A of about 125; as K_A is increased further, the system becomes less and less unstable.

With K_A of about 110, two real eigenvalues (λ_4 and λ_5) merge to become a complex pair of eigenvalues. At K_A of about 130, these eigenvalues become real again. For K_A of about 150 and higher, the real eigenvalues λ_3 and λ_4 merge to form a complex pair. The oscillatory mode represented by these eigenvalues is restricted to the field circuit, *d*-axis amortisseur, and the AVR.

(c) Table E12.2 shows the effect of varying the stabilizer gain K_{STAB}, with K_A=200.

Table E12.2

K_{STAB}	Eigenvalues						
	λ_1, λ_2	λ_3, λ_4	λ_5	λ_6	λ_7	λ_8	λ_9
-	0.53±*j*7.4	-17.6±*j*11.3	-24.9	-1.97	-54.4	-	-
0.1	0.51±*j*7.4	-17.6±*j*11.4	-24.9	-1.97	-54.4	-30.4	-0.71
1.0	0.34±*j*7.4	-17.1±*j*11.8	-24.9	-1.97	-54.4	-30.9	-0.72
3.0	-0.01±*j*7.4	-16.2±*j*12.7	-24.9	-1.97	-54.5	-31.9	-0.72
5.0	-0.37±*j*7.2	-15.4±*j*13.6	-24.9	-1.97	-54.5	-32.8	-0.73
9.5	-1.08±*j*6.8	-13.9±*j*15.5	-25.0	-1.96	-54.5	-34.3	-0.74
15.0	-1.75±*j*6.2	-12.5±*j*17.7	-25.0	-1.95	-54.6	-35.6	-0.76
21.0	-2.20±*j*5.5	-11.4±*j*20.0	-25.0	-1.94	-54.7	-36.7	-0.78
Dominant States	$\Delta\omega_r$, $\Delta\delta$	$\Delta\psi_{fd}$, $\Delta\psi_{1d}$	$\Delta\psi_{2q}$	$\Delta\psi_{1q}$	Δv_1	Δv_2	Δv_s

From the results summarized in Table E12.2, we see that as K_{STAB} is increased the damping of rotor angle mode increases and the frequency decreases slightly. The reduction in frequency is indicative of reduction in synchronizing torque; this is due to the PSS phase lead circuit providing overcompensation at the rotor oscillating frequency. The frequency of the second oscillatory mode increases and its damping decreases as K_{STAB} is increased. This mode is associated with the field circuit. All other modes are not affected by the variation of K_{STAB}. ■

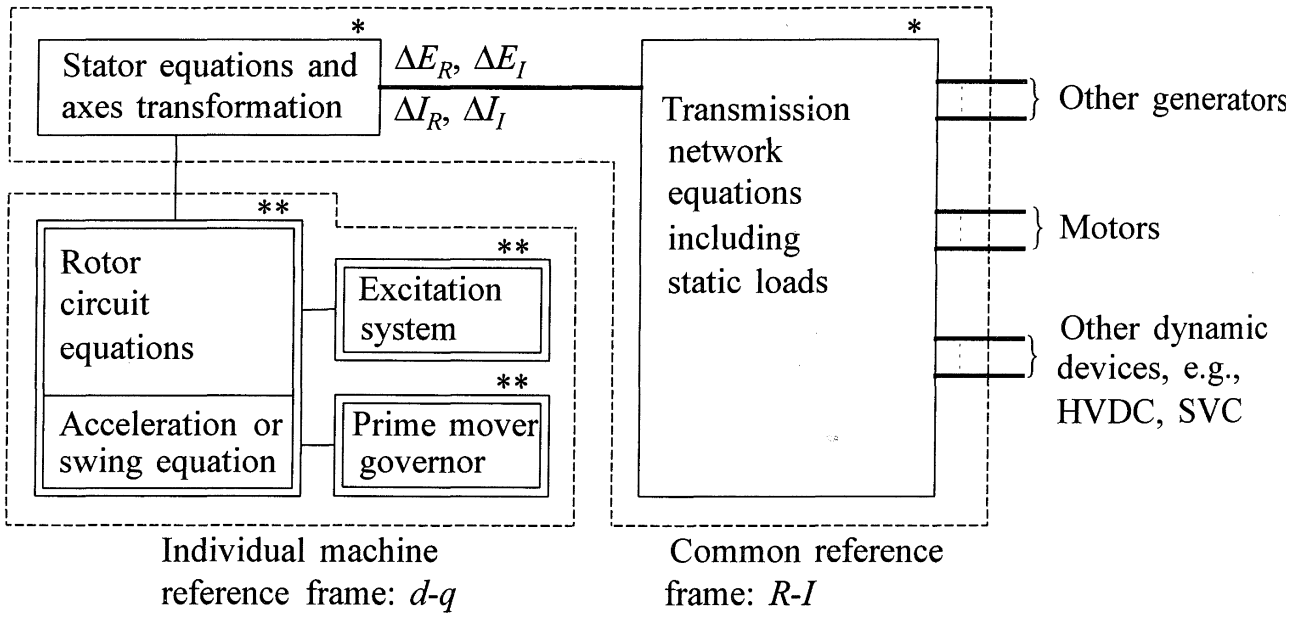
12.7 SMALL-SIGNAL STABILITY OF MULTIMACHINE SYSTEMS

Analysis of practical power systems involves the simultaneous solution of equations representing the following:

- Synchronous machines, and the associated excitation systems and prime movers
- Interconnecting transmission network
- Static and dynamic (motor) loads
- Other devices such as HVDC converters, static var compensators

Figure 12.18 shows the general structure of the complete system model.

As discussed in Chapter 5, for system stability studies it is appropriate to neglect the transmission network and machine stator transients. The dynamics of machine rotor circuits, excitation systems, prime mover and other devices are represented by differential equations. The result is that the complete system model consists of a large number of ordinary differential and algebraic equations.

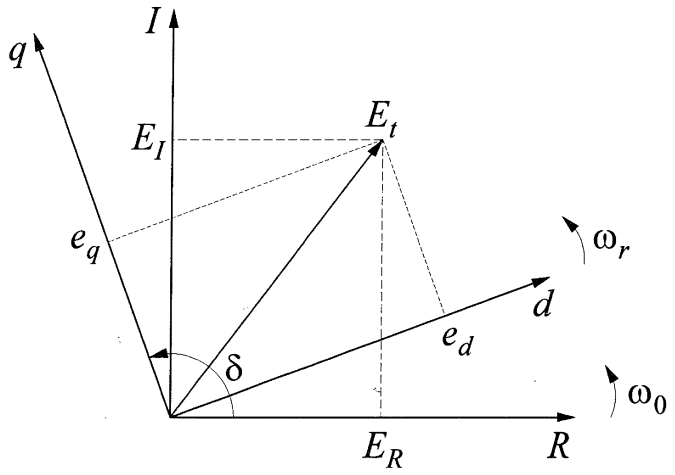


* Algebraic equations
** Differential equations

Figure 12.18 Structure of the complete power system model

Each machine model is expressed in its own *d-q* reference frame which rotates with its rotor. For the solution of interconnecting network equations, all voltages and currents must be expressed in a common reference frame. Usually a reference frame rotating at synchronous speed is used as the common reference. Axis transformation equations are used to transform between the individual machine (*d-q*) reference frames and the common (*R-I*) reference frame as shown in Figure 12.19. For convenience in the organization of the complete set of algebraic equations, the machine stator equations are also expressed in the common reference frame.

The *R*-axis of the common reference frame is usually used as the reference for measuring the machine rotor angle. For a machine represented in detail including dynamics of one or more rotor circuits, the rotor angle δ is defined as the angle by which the machine *q*-axis leads the *R*-axis, as shown in Figure 12.19. For a machine represented by a classical model, the rotor angle is the angle by which the voltage *E'* leads the *R*-axis. Under dynamic conditions, the angle δ changes with rotor speed.



$$e_d = E_R \sin\delta - E_I \cos\delta$$

$$e_q = E_I \sin\delta + E_R \cos\delta$$

$$E_R = e_d \sin\delta + e_q \cos\delta$$

$$E_I = e_q \sin\delta - e_d \cos\delta$$

Figure 12.19 Reference frame transformation

The formulation of the state equations for small-signal analysis involves the development of linearized equations about an operating point and elimination of all variables other than the state variables. The general procedure is similar to that used for a single-machine infinite bus system in the previous sections. However, the need to allow for the representation of extensive transmission networks, loads, a variety of excitation systems and prime mover models, HVDC links, and static var compensators makes the process very complex. Therefore, the formulation of the state equations requires a systematic procedure for treating the wide range of devices. The following is a description of one such procedure [10,11,12].

Formulation of the state equations

The linearized model of each dynamic device is expressed in the following form:

$$\dot{\mathbf{x}}_i = \mathbf{A}_i \mathbf{x}_i + \mathbf{B}_i \Delta \mathbf{v} \tag{12.186}$$

$$\Delta \mathbf{i}_i = \mathbf{C}_i \mathbf{x}_i - \mathbf{Y}_i \Delta \mathbf{v} \tag{12.187}$$

where

$\mathbf{x}_i$ are the perturbed values of the individual device state variables
$\mathbf{i}_i$ is the current injection into the network from the device
$\mathbf{v}$ is the vector of the network bus voltages

In Equations 12.186 and 12.187, $\mathbf{B}_i$ and $\mathbf{Y}_i$ have non-zero elements corresponding only to the terminal voltage of the device and any remote bus voltages used to control the device. The current vector $\mathbf{i}_i$ has two elements corresponding to the real and imaginary components. Similarly, the voltage vector $\mathbf{v}$ has two elements per bus associated with the device. Such state equations for all the dynamic devices in the system may be combined into the form

$$\dot{\mathbf{x}} = \mathbf{A}_D \mathbf{x} + \mathbf{B}_D \Delta \mathbf{v} \tag{12.188}$$

$$\Delta \mathbf{i} = \mathbf{C}_D \mathbf{x} - \mathbf{Y}_D \Delta \mathbf{v} \tag{12.189}$$

where $\mathbf{x}$ is the state vector of the complete system, and $\mathbf{A}_D$ and $\mathbf{C}_D$ are block diagonal matrices composed of $\mathbf{A}_i$ and $\mathbf{C}_i$ associated with the individual devices.

As described in Chapter 6, the interconnecting transmission network is represented by the node equation:

$$\Delta \mathbf{i} = \mathbf{Y}_N \Delta \mathbf{v} \tag{12.190}$$

The elements of $\mathbf{Y}_N$ include the effects of nonlinear static loads as shown later in this section.

Equating Equation 12.189 associated with the devices and Equation 12.190 associated with the network, we obtain

$$\mathbf{C}_D \mathbf{x} - \mathbf{Y}_D \Delta \mathbf{v} = \mathbf{Y}_N \Delta \mathbf{v}$$

Hence,

$$\Delta \mathbf{v} = (\mathbf{Y}_N + \mathbf{Y}_D)^{-1} \mathbf{C}_D \mathbf{x}$$

Substituting the above expression for $\Delta \mathbf{v}$ in Equation 12.188 yields the overall system state equation:

$$\begin{aligned}\dot{\mathbf{x}} &= \mathbf{A}_D\mathbf{x} + \mathbf{B}_D(\mathbf{Y}_N + \mathbf{Y}_D)^{-1}\mathbf{C}_D\mathbf{x} \\ &= \mathbf{A}\mathbf{x}\end{aligned} \tag{12.191}$$

where the state matrix $\mathbf{A}$ of the complete system is given by

$$\mathbf{A} = \mathbf{A}_D + \mathbf{B}_D(\mathbf{Y}_N + \mathbf{Y}_D)^{-1}\mathbf{C}_D \tag{12.192}$$

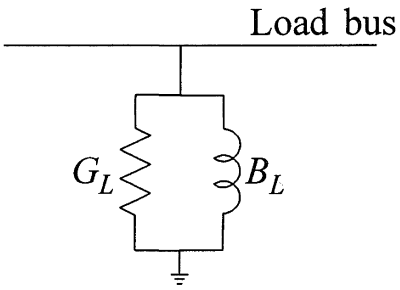
The method of building $\mathbf{A}_i$, $\mathbf{B}_i$, $\mathbf{C}_i$, and $\mathbf{Y}_i$ matrices for the synchronous machine and the associated controls can follow the general approach described in the previous sections. Motor loads can be treated in a similar way. Reference 12 gives details of treating HVDC links and SVCs.

The MASS (*Multi-Area Small-signal Stability*) computer program described in references 10 and 11 uses the above general approach for formulating the system state matrix. The program computes all eigenvalues of the matrix by using the *QR* transformation method discussed in Section 12.2.9. Since this approach cannot exploit sparsity, it cannot be used for analysis of very large systems. Depending on the capability of the computer used, the maximum system size is limited to a few hundred states. This is satisfactory for the analysis of stability of small systems or local stability problems in large systems. Since all modes of the system are computed, it is also ideally suited for the design and coordination of controls. In the next section, we will describe techniques for the analysis of global problems in very large systems.

Representation of static loads

(a) Constant impedance (linear) load:

The shunt admittance to ground representing the load is computed as



$$G_L = \frac{P_{L0}}{V_0^2} \qquad B_L = -\frac{Q_{L0}}{V_0^2} \tag{12.193}$$

Figure 12.20

where

P_{L0} = initial value of the active component of load
Q_{L0} = initial value of the reactive component of load
V_0 = initial value of the bus voltage magnitude

(b) Nonlinear load:

Let us consider the load whose voltage dependent characteristics are represented as

$$P_L = P_{L0}\left(\frac{V}{V_0}\right)^m$$
$$Q_L = Q_{L0}\left(\frac{V}{V_0}\right)^n \tag{12.194}$$

where V is the magnitude of the bus voltage given by

$$V = \sqrt{v_R^2 + v_I^2}$$

The R and I components of the load current are

$$i_R = P_L\frac{v_R}{V^2} + Q_L\frac{v_I}{V^2}$$
$$i_I = P_L\frac{v_I}{V^2} - Q_L\frac{v_R}{V^2}$$

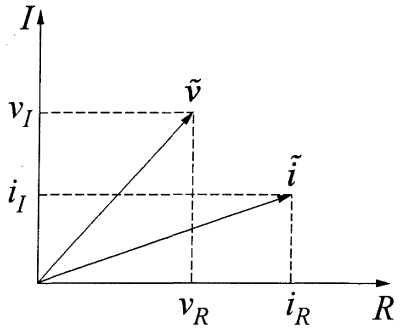


Figure 12.21

Linearizing, we find

$$\Delta i_R = \frac{v_{R0}}{V_0^2}\Delta P_L + \frac{v_{I0}}{V_0^2}\Delta Q_L + \frac{P_{L0}}{V_0^2}\Delta v_R + \frac{Q_{L0}}{V_0^2}\Delta v_I + (P_{L0}v_{R0} + Q_{L0}v_{I0})\left(-\frac{2}{V_0^3}\right)\Delta V$$
$$\Delta i_I = \frac{v_{I0}}{V_0^2}\Delta P_L - \frac{v_{R0}}{V_0^2}\Delta Q_L + \frac{P_{L0}}{V_0^2}\Delta v_I - \frac{Q_{L0}}{V_0^2}\Delta v_R + (P_{L0}v_{I0} - Q_{L0}v_{R0})\left(-\frac{2}{V_0^3}\right)\Delta V \tag{12.195}$$

where

$$\Delta V = \frac{v_{R0}}{V_0}\Delta v_R + \frac{v_{I0}}{V_0}\Delta v_I \tag{12.196}$$

Now,

$$\begin{aligned} \Delta P_L &= m\frac{P_{L0}}{V_0}\Delta V \\ \Delta Q_L &= n\frac{Q_{L0}}{V_0}\Delta V \end{aligned} \tag{12.197}$$

Substitution of Equations 12.196 and 12.197 in Equation 12.195 yields

$$\begin{bmatrix} \Delta i_R \\ \Delta i_I \end{bmatrix} = \begin{bmatrix} G_{RR} & B_{RI} \\ -B_{IR} & G_{II} \end{bmatrix} \begin{bmatrix} \Delta v_R \\ \Delta v_I \end{bmatrix} \tag{12.198}$$

where

$$\begin{aligned} G_{RR} &= \frac{P_{L0}}{V_0^2}\left((m-2)\frac{v_{R0}^2}{V_0^2}+1\right) + \frac{Q_{L0}}{V_0^2}\left((n-2)\frac{v_{R0}v_{I0}}{V_0^2}\right) \\ B_{RI} &= \frac{Q_{L0}}{V_0^2}\left((n-2)\frac{v_{I0}^2}{V_0^2}+1\right) + \frac{P_{L0}}{V_0^2}\left((m-2)\frac{v_{R0}v_{I0}}{V_0^2}\right) \\ B_{IR} &= \frac{Q_{L0}}{V_0^2}\left((n-2)\frac{v_{R0}^2}{V_0^2}+1\right) - \frac{P_{L0}}{V_0^2}\left((m-2)\frac{v_{R0}v_{I0}}{V_0^2}\right) \\ G_{II} &= \frac{P_{L0}}{V_0^2}\left((m-2)\frac{v_{I0}^2}{V_0^2}+1\right) - \frac{Q_{L0}}{V_0^2}\left((n-2)\frac{v_{R0}v_{I0}}{V_0^2}\right) \end{aligned} \tag{12.199}$$

As an example, consider a load such that

P_{L0} = 5.0 pu $\qquad$ Q_{L0} = 2.0 pu $\qquad$ $\tilde{v}_0 = 1.0\angle 20°$

The real and imaginary components of the initial bus voltage are

$$v_{R0} = 1.0\cos 20^\circ = 0.94 \quad \text{pu}$$
$$v_{I0} = 1.0\sin 20^\circ = 0.342 \quad \text{pu}$$

From Equation 12.199, with constant impedance characteristic (m=n=2.0),

$$G_{RR} = 5.0 \qquad B_{RI} = 2.0$$
$$-B_{IR} = -2.0 \qquad G_{II} = 5.0$$

Similarly, with constant current characteristic (m=n=1.0),

$$G_{RR} = -0.06 \qquad B_{RI} = 0.16$$
$$-B_{IR} = -1.84 \qquad G_{II} = 5.06$$

and with constant MVA characteristic (m=n=0.0),

$$G_{RR} = -5.12 \qquad B_{RI} = -1.68$$
$$-B_{IR} = -1.68 \qquad G_{II} = 5.12$$

The equivalent admittance matrix of Equation 12.198 representing a static load may be directly implemented in the network admittance matrix. However, as evident from the above example, the equivalent admittance matrix representing nonlinear loads is not symmetrical and does not represent a simple shunt admittance to ground as in the case of a constant impedance load.

Redundant state variables

The formulation of the system state equations described above uses absolute changes in machine rotor speed and angle as state variables. With such a formulation, the state matrix of a system which does not contain an infinite bus will have one or two zero eigenvalues [13].

One of these zero eigenvalues is associated with the lack of uniqueness of absolute rotor angle. In other words, if rotor angles of all machines are increased by a constant value, the system stability is not affected. The redundancy in rotor angle states can be eliminated by choosing one of the machines as a reference and expressing angle changes of all other machines with respect to this reference as follows.

For the reference machine R,

$$p\Delta\delta_R = 0$$

for any other machine i (i=1, ..., n; $i \neq R$),

$$p\Delta\delta_i = (\Delta\omega_r \text{ of machine } i) - (\Delta\omega_r \text{ of machine } R)$$

The second zero eigenvalue exists if all the generator torques are assumed to be independent of speed deviations, i.e., if a damping term represented by K_D is not included in the swing equation and a speed governor is not represented. This zero eigenvalue can also be avoided by measuring speed deviations with respect to that of a reference machine. Mathematically, the process of referring rotor angles or speed deviations to a reference machine is equivalent to a similarity transformation.

The zero eigenvalues, however, may not be computed exactly because of mismatches in the power flow solution and the limited accuracy of eigenvalue calculation routines. They may therefore appear as small eigenvalues.

12.8 SPECIAL TECHNIQUES FOR ANALYSIS OF VERY LARGE SYSTEMS

Analysis of interarea oscillations in a large interconnected power system requires a detailed modelling of the entire system. System representations with as many as 2,000 dynamic devices and 12,000 buses are not uncommon for such studies. With an average of 15 states per device, the number of state variables required for modal analysis may thus be on the order of 30,000. This is well outside the range of the conventional eigenvalue analysis methods. Special techniques have therefore been developed that focus on evaluating a *selected subset of eigenvalues* associated with the complete system response.

One such technique is the AESOPS algorithm originally presented in reference 14. It uses a novel frequency response approach to calculate the eigenvalues associated with the rotor angle modes. References 10 and 15 describe improved implementation of the AESOPS algorithm.

Several powerful methods for the computation of eigenvalues associated with a small number of selected modes of oscillation have been published in the literature on power system stability. Reference 16 describes the application of two sparsity-based eigenvalue techniques: simultaneous iterations and modified Arnoldi methods. The S-method described in reference 17 is particularly suited for finding the unstable modes. The *selective modal analysis* (SMA) approach described in references 2 and 18 computes eigenvalues associated with selected modes of interest by using special techniques to identify variables that are relevant to the selected modes, and then constructing a reduced-order model that involves only the relevant variables.

The PEALS (*Program for Eigenvalue Analysis of Large Systems*) described in references 10 and 11 uses two of these techniques: the AESOPS algorithm and the modified Arnoldi method. These two methods have been found to be efficient and reliable, and they complement each other in meeting the requirements of small-signal stability analysis of large complex power systems. The following is a description of these two techniques:

(a) The AESOPS algorithm

The acronym AESOPS stands for the *Analysis of Essentially Spontaneous Oscillations in Power Systems* [14]. It is based on an ingenious approach developed using sound engineering judgement rather than a rigorous mathematical procedure.

The algorithm computes eigenvalues associated *only with rotor angle modes*, one complex conjugate pair of eigenvalues at a time. The eigenvalues are determined by applying to the rotor of a selected generator an external torque having a complex sinusoidal form, expressed in terms of an initial estimate of an eigenvalue. Under steady-state conditions, all incremental variables of the linear system model will be complex sinusoids similar in form to the external torque. The complex frequency response of the system is calculated by solving an appropriate set of complex *algebraic equations*. A revised estimate of the eigenvalue is determined from the linear system response, and the process is repeated until successive estimates converge within a desired tolerance. The resulting eigenvalue represents a mode of oscillation in which the selected generator participates significantly. If the generator has several dominant modes of rotor oscillations, the eigenvalue computed depends on the initial estimate.

The procedure may be applied to different generators to compute the eigenvalues associated with the modes in which the generators have significant participation.

The AESOPS algorithm is derived from the linearized equation of motion of a generator:

$$\begin{aligned} 2H\frac{d\Delta\omega_r}{dt} &= \Delta T_m - \Delta T_e \\ &= \Delta T_m - (K_S\Delta\delta + K_D\Delta\omega_r) \end{aligned}$$

Taking the Laplace transform, we get

$$2Hs\Delta\omega_r = \Delta T_m - \left[K_S(s)\frac{\Delta\omega_r}{s} + K_D(s)\Delta\omega_r\right] \tag{12.200}$$

The above equation recognizes that synchronizing and damping torque coefficients K_S and K_D are functions of the frequency of oscillation.

Rearranging Equation 12.200, we have

$$\Delta T_m = \left[2Hs + K_D(s) + \frac{K_S(s)}{s}\right]\Delta\omega_r \tag{12.201}$$

The characteristic values (eigenvalues) of the system are given by the zeros of

$$2Hs + K_D(s) + \frac{K_S(s)}{s} = 0 \tag{12.202}$$

The characteristic values are thus those values of s which force ΔT_m to be zero, provided $\Delta\omega_r$ is not zero. This is used by the AESOPS algorithm to determine zeros of Equation 12.202.

With a finite external torque, the magnitude of system variables tends to be unbounded at complex frequencies close to an eigenvalue. From a computational viewpoint, it is preferable to limit the extent of system response and allow the magnitude of external torque to go to zero at an eigenvalue. This is achieved by setting the complex speed deviation of the perturbed generator to $1.0+j0.0$ per unit. The external torque ΔT_m is determined in the solution process. As iterations converge, the magnitude of the external torque tends to zero and provides an indication of the accuracy of the eigenvalue.

In practice, the model representing the system has poles as well as zeros. Zeros close to a pole prevent the AESOPS algorithm from converging to the corresponding eigenvalues. Poles associated with modes in which the machine has a significant participation are not cancelled by zeros. Thus, for each generator in the system, a subset of the overall system modes may be determined.

Iterative Procedure: The zeros of $\Delta T_m(s)$ may be determined by using Newton's method. This requires the derivative of ΔT_m with respect to s. From Equation 12.201,

$$\frac{\partial \Delta T_m}{\partial s} = \left[2H + \frac{\partial K_D(s)}{\partial s} + \frac{1}{s}\frac{\partial K_S(s)}{\partial s} - \frac{K_S(s)}{s^2}\right]\Delta\omega_r \tag{12.203}$$

This can be simplified by making the following approximations.

Close to a system eigenvalue, from Equation 12.202,

$$\frac{K_S(s)}{s^2} + \frac{K_D(s)}{s} = -2H \tag{12.204}$$

If $K_D(s)$ is small,

$$\frac{K_S(s)}{s^2} \approx -2H \tag{12.205}$$

Therefore,

$$\frac{\partial \Delta T_m}{\partial s} \approx \left[4H + \frac{\partial K_D(s)}{\partial s} + \frac{1}{s}\frac{\partial K_S(s)}{\partial s}\right]\Delta\omega_r \tag{12.206}$$

Further, $\frac{\partial K_D}{\partial s}$ and $\frac{\partial K_S}{\partial s}$ are small compared to $4H$. Therefore,

$$\frac{\partial \Delta T_m}{\partial s} \approx 4H\Delta\omega_r \tag{12.207}$$

The nth iteration of Newton's method for computing the eigenvalues, i.e., the values of s, is given by

$$s_{n+1} = s_n - \frac{\Delta T_m(s)}{\left[\frac{\partial \Delta T_m}{\partial s}\right]_{s=s_n}}$$

$$= s_n - \left[\frac{\Delta T_m(s)}{4H\Delta\omega_r}\right]_{s=s_n}$$

The momentum of the disturbed machine is

$$M_n = J\Delta\omega_r = 2H\Delta\omega_r$$

Hence,

$$s_{n+1} = s_n - \left[\frac{\Delta T_m(s)}{2M_n}\right]_{s=s_n} \tag{12.208}$$

For modes that involve many machines, this makes too large a change in the eigenvalue at each iteration. In such cases, $\partial K_S/\partial s$ and $\partial K_D/\partial s$ are not small. Therefore, a modified momentum is used based on an equivalent inertia defined so that kinetic energy associated with the change in speed at all machines in the system is equal to the equivalent inertia multiplied by the square of the speed change of the disturbed machine. The equivalent inertia is given by

$$H_e = \sum_{i=1}^{N_m} H_i |\Delta\omega_{ri}|^2 \tag{12.209}$$

with N_m = number of machines. Equation 12.208 is then modified to

$$s_{n+1} = s_n - \left[\frac{\Delta T_m(s)}{4H_e\Delta\omega_r}\right]_{s=s_n}$$

If as discussed earlier $\Delta\omega_r$ is set to $1.0+j0.0$ pu,

$$s_{n+1} = s_n - \frac{\Delta T_m(s_n)}{4H_e} \tag{12.210}$$

Implementation of the AESOPS algorithm in PEALS

The application of the AESOPS algorithm as developed above requires the calculation of

(a) The torque necessary to keep the speed change of a chosen disturbed machine equal to $1.0+j0.0$ per unit; and

(b) Speed changes of all the other machines and the equivalent inertia H_e.

These depend on Equation 12.186 of each dynamic device and Equation 12.190 of the interconnecting network.

We will first organize the device equations in a suitable form to perform the above calculations. From Equation 12.186, for any complex frequency s, for each dynamic device, we may write

$$s\mathbf{x}_i = \mathbf{A}_i\mathbf{x}_i + \mathbf{B}_i\Delta\mathbf{v}$$

Therefore,

$$\mathbf{x}_i = (s\mathbf{I}-\mathbf{A}_i)^{-1}\mathbf{B}_i\Delta\mathbf{v} \tag{12.211}$$

Substitution of the above in Equation 12.187, and expressing in the s domain yields

$$\begin{aligned}\Delta\mathbf{i}_i &= \mathbf{C}_i(s\mathbf{I}-\mathbf{A}_i)^{-1}\mathbf{B}_i\Delta\mathbf{v}-\mathbf{Y}_i\Delta\mathbf{v}\\ &= -\mathbf{Y}_{ie}(s)\Delta\mathbf{v}\end{aligned} \tag{12.212}$$

where

$$\begin{aligned}\mathbf{Y}_{ie}(s) &= \left[\mathbf{Y}_i-\mathbf{C}_i(s\mathbf{I}-\mathbf{A}_i)^{-1}\mathbf{B}_i\right]\\ &= \left[\mathbf{Y}_i-\mathbf{C}_i\mathbf{\Phi}_i(s\mathbf{I}-\Lambda_i)^{-1}\mathbf{\Phi}_i^{-1}\mathbf{B}_i\right]\end{aligned} \tag{12.213}$$

with

$\mathbf{\Lambda}_i$ = diagonal matrix of eigenvalues of $\mathbf{A}_i$ of the device
$\mathbf{\Phi}_i$ = corresponding eigenvector matrix

Computation of $\mathbf{Y}_{ie}(s)$ using Equation 12.213 is simplified due to $s\mathbf{I}-\mathbf{\Lambda}_i$ being diagonal.

For the machine k selected for applying the external torque, the dynamic equations, including the effect of the applied torque ΔT_m, may be written in the partitioned form:

$$\begin{bmatrix} \Delta\dot{\omega}_r \\ \Delta\dot{\delta} \\ \dot{\mathbf{x}}_r \end{bmatrix} = \begin{bmatrix} a_{11} & a_{12} & \mathbf{a}_{1r} \\ \omega_0 & 0 & 0 \\ \mathbf{a}_{r1} & \mathbf{a}_{r2} & \mathbf{A}_{rr} \end{bmatrix} \begin{bmatrix} \Delta\omega_r \\ \Delta\delta \\ \mathbf{x}_r \end{bmatrix} + \begin{bmatrix} \mathbf{b}_1 \\ 0 \\ \mathbf{B}_r \end{bmatrix} \Delta\mathbf{v} + \begin{bmatrix} \dfrac{1}{2H} \\ 0 \\ 0 \end{bmatrix} \Delta T_m \tag{12.214}$$

$$\Delta\mathbf{i}_k = [\ \mathbf{c}_1\ \mathbf{c}_2\ \mathbf{C}_r\ ] \begin{bmatrix} \Delta\omega_r \\ \Delta\delta \\ \mathbf{x}_r \end{bmatrix} - \mathbf{Y}_k \Delta\mathbf{v} \tag{12.215}$$

where $\mathbf{x}_r$ is a vector representing all state variables of the machine, except for $\Delta\omega_r$ and $\Delta\delta$. For the disturbed machine, $\Delta\omega_r$ is assumed to be equal to 1.0 pu, and hence $\Delta\delta = \omega_0/s$.

By manipulation and rearrangement of Equations 12.214 and 12.215 to eliminate $\Delta\delta$ and $\mathbf{x}_r$ in terms of $\Delta\omega_r$, and by setting $\Delta\omega_r$ to 1.0 pu, we obtain the following expressions for ΔT_m and $\Delta\mathbf{i}_k$ as functions of $\Delta\mathbf{v}$:

$$\Delta T_M = 2H\left[s - a_{11} - \frac{a_{12}\omega_0}{s} - \mathbf{a}_{1r}(s\mathbf{I}-\mathbf{A}_{rr})^{-1}\left(\mathbf{a}_{r1} + \frac{\mathbf{a}_{r2}\omega_0}{s}\right)\right] - 2H\left[\mathbf{b}_1 + \mathbf{a}_{1r}(s\mathbf{I}-\mathbf{A}_{rr})^{-1}\mathbf{B}_r\right]\Delta\mathbf{v} \tag{12.216}$$

$$\Delta\mathbf{i}_k = \Delta\mathbf{I}_{ke}(s) - \mathbf{Y}_{ke}(s)\,\Delta\mathbf{v} \tag{12.217}$$

where

$$\Delta\mathbf{I}_{ke}(s) = \left[\mathbf{c}_1 + \frac{\mathbf{c}_2\omega_0}{s} + \mathbf{C}_r(s\mathbf{I}-\mathbf{A}_{rr})^{-1}\left(\mathbf{a}_{r1} + \frac{\mathbf{a}_{r2}\omega_0}{s}\right)\right] \tag{12.218}$$

$$\mathbf{Y}_{ke}(s) = \mathbf{Y}_k - \mathbf{C}_r(s\mathbf{I}-\mathbf{A}_{rr})^{-1}\mathbf{B}_r \tag{12.219}$$

As in Equation 12.213, computations associated with the above equations are simplified by expressing $(s\mathbf{I}-\mathbf{A}_{rr})^{-1}$ in diagonal form in terms of the eigenvalues of $\mathbf{A}_{rr}$.

The current injections into the network are given by Equation 12.217 for the disturbed machine and by Equation 12.212 for all other machines and dynamic devices. The equivalent device admittances $\mathbf{Y}_{ie}(s)$ and the equivalent current source $\Delta\mathbf{i}_{ke}(s)$ for the disturbed machine are functions of the parameters of the devices, initial operating condition, and the complex frequency s.

The interconnecting network equations may be written as

$$\begin{bmatrix}\Delta\mathbf{i}_D\\ 0\end{bmatrix}=\begin{bmatrix}\mathbf{Y}_{DD} & \mathbf{Y}_{DL}\\ \mathbf{Y}_{LD} & \mathbf{Y}_{LL}\end{bmatrix}\begin{bmatrix}\Delta\mathbf{v}_D\\ \Delta\mathbf{v}_L\end{bmatrix} \tag{12.220}$$

where subscript D refers to buses with dynamic devices and the subscript L refers to buses with static loads, i.e., buses with no dynamic devices.

Combining the device equations 12.212 and 12.217 and the network equation 12.220 yields

$$\begin{bmatrix}\Delta\mathbf{I}_{De}(s)\\ 0\end{bmatrix}=\begin{bmatrix}\mathbf{Y}_{DD}+\mathbf{Y}_{De}(s) & \mathbf{Y}_{DL}\\ \mathbf{Y}_{LD} & \mathbf{Y}_{LL}\end{bmatrix}\begin{bmatrix}\Delta\mathbf{v}_D\\ \Delta\mathbf{v}_L\end{bmatrix} \tag{12.221}$$

where $\mathbf{Y}_{De}(s)$ is a block diagonal matrix of the device equivalent admittance matrix $\mathbf{Y}_{ie}(s)$, and $\Delta\mathbf{I}_{De}(s)$ is the device current source vector with non-zero element only for the disturbed machine given by Equation 12.218.

Equation 12.221 is solved for bus voltages $\Delta\mathbf{v}$. The network matrix is very large and sparse. PEALS exploits this by using an efficient sparsity-based network solution technique.

The following is a summary of the computation steps associated with the AESOPS algorithm:

1. Form the device models: $\mathbf{A}_i$, $\mathbf{B}_i$, $\mathbf{C}_i$, $\mathbf{Y}_i$; compute eigenvalues and eigenvectors of $\mathbf{A}_i$ using the *QR* transformation method.

2. Set the initial value of complex frequency s equal to the specified initial estimate of the eigenvalue.

3. Compute $\Delta\mathbf{I}_{ke}(s)$ and $\mathbf{Y}_{ke}(s)$ associated with the disturbed machine, using Equations 12.218 and 12.219, and $\mathbf{Y}_{ie}(s)$ for all other dynamic devices, using Equation 12.213.

4. Solve Equation 12.221 to compute bus voltage $\Delta\mathbf{v}$.

5. Compute ΔT_m for the disturbed machine, using Equation 12.216; $\Delta\omega_r$ for all machines, using Equation 12.211; H_e, using Equation 12.209.

6. Compute next estimate of s, using Equation 12.210.

7. If Δs between successive iterations is within the specified tolerance, set eigenvalue to s and stop; otherwise, go to step 3 and repeat the process.

The above approach to the calculation of eigenvalues corresponding to rotor angle modes involves the solution of only the algebraic Equations 12.221. It does not require the formation of the state matrix **A** of the overall system. Instead, the state equations for each dynamic device are formed and treated as a small eigenvalue problem to form the equivalent admittance matrix $\mathbf{Y}_{ie}(s)$. The overall admittance matrix of Equation 12.221 is highly sparse. Hence, with the use of efficient sparsity-based solution techniques, this approach has been applied to power systems with over 2,000 dynamic devices and 12,000 buses [10].

One of the limitations of the AESOPS algorithm is that, unless the general characteristics of critical modes are known *a priori*, a considerable amount of searching is required to find all the critical modes. In fact, there is never any assurance that all critical modes have been identified. The method is best suited for tracking changes in specific modes as system conditions change. The modified Arnoldi method described next overcomes these limitations of the AESOPS method.

Calculation of eigenvectors:

In the AESOPS approach, the speed deviations $\Delta\omega_r$ for all the machines computed in the last iteration directly give the corresponding component of the right eigenvector.

The left eigenvector is calculated by using the transposed system dynamic model of Equations 12.188 and 12.189:

$$\dot{\mathbf{y}} = \mathbf{A}_D^T\mathbf{y} + \mathbf{C}_D^T\Delta\mathbf{u}$$

$$\Delta\mathbf{j} = \mathbf{B}_D^T\mathbf{y} - \mathbf{Y}_D^T\Delta\mathbf{u}$$

and the transposed network model of Equation 12.190:

$$\Delta\mathbf{j} = \mathbf{Y}_N^T\Delta\mathbf{u}$$

It can be readily shown that the AESOPS algorithm when applied to the above model will converge to a system eigenvalue and the corresponding left eigenvector. With the initial eigenvalue estimate equal to the correct value, one iteration is usually sufficient for the algorithm to converge to the left eigenvector.

Frequency response calculation:

The frequency response can be calculated directly from the system equations in the form used by the AESOPS algorithm with s replaced by $j\omega$. The overall system has the general form of Equation 12.221. Instead of applying an external torque as input to one of the machines, the input signal may be applied to any device and the outputs monitored at the desired locations. Since the network equations are retained explicitly, the input and outputs may be associated with the network as well as the dynamic devices.

(b) The modified Arnoldi method (MAM)

The Arnoldi method was first presented in reference 19. However, in the original form it had poor numerical properties, the main problems being loss of orthogonality and slow convergence if several dominant eigenvalues are needed. These problems were solved in reference 20 by using complete reorthogonalization and an iterative process. The following is a description of the method as implemented in PEALS [10,11].

The modified Arnoldi method is based on a reduction technique in which the matrix **A**, whose eigenvalues are to be computed, is reduced to an upper Hessenberg matrix by the recurrence:

$$h_{i+1,i}\mathbf{v}_{i+1} = \mathbf{A}\mathbf{v}_i - \sum_{j=1}^{i} h_{j,i}\mathbf{v}_j \qquad i = 1,\ldots,m \tag{12.222}$$

where

$h_{j,i} = \mathbf{v}_j^H \mathbf{A}\mathbf{v}_i$ (superscript H denotes conjugate transpose)

and

$\mathbf{v}_1$ is an arbitrary starting vector with $\|\mathbf{v}_1\|_2 = 1$
$h_{i+1,i}$ is a scaling factor to make $\|\mathbf{v}_{i+1}\|_2 = 1$
m is a prespecified order of the reduced Hessenberg matrix

Equation 12.222 can be rearranged and assembled for all m equations to give

$$\mathbf{A}\mathbf{V}_m = \mathbf{V}_m\mathbf{H}_m + h_{m+1,m}\mathbf{v}_{m+1}\mathbf{e}_m^T \tag{12.223}$$

where

$$\mathbf{V}_m = [\,\mathbf{v}_1 \cdots \mathbf{v}_m\,]$$

$$\mathbf{H}_m = \begin{bmatrix} h_{1,1} & h_{1,2} & \cdots & h_{1,m} \\ h_{2,1} & h_{2,2} & \cdots & h_{2,m} \\ \cdots & \cdots & \cdots & \cdots \\ 0 & \cdots & h_{m,m-1} & h_{m,m} \end{bmatrix}$$

$$\mathbf{e}_m^T = [\, 0 \cdots 0 \; 1 \,]$$

Here $\mathbf{H}_m$ is an upper Hessenberg matrix. We can show that ideally the vector sequence $\mathbf{v}_i$ generated by Equation 12.222 is orthonormal. Therefore, if $m=N$ (the order of $\mathbf{A}$), we have

$$h_{N+1,N} = 0$$

and Equation 12.223 becomes

$$\mathbf{A}\mathbf{V}_N = \mathbf{V}_N\mathbf{H}_N \tag{12.224}$$

Thus $\mathbf{A}$ is reduced to the upper Hessenberg matrix $\mathbf{H}_N$ whose eigenvalues are the eigenvalues of $\mathbf{A}$. An important feature of the method is that the values of $h_{m+1,m}$, the subdiagonal elements of $\mathbf{H}_m$, decrease very rapidly as m increases; therefore, a good approximation can be made for $m \ll N$ by dropping out the second term in Equation 12.223:

$$\mathbf{A}\mathbf{V}_m \approx \mathbf{V}_m\mathbf{H}_m \tag{12.225}$$

The eigenvalues of $\mathbf{H}_m$, which is of a very low order, approximate a subset of the eigenvalues of $\mathbf{A}$. The corresponding eigenvectors of $\mathbf{A}$ are given by

$$\mathbf{W} \approx \mathbf{V}_m\mathbf{P} \tag{12.226}$$

where $\mathbf{P}$ is the eigenvector matrix of $\mathbf{H}_m$. To improve the accuracy of the eigenvalues of $\mathbf{A}$, the above procedure can be iterated with a new starting vector $\mathbf{v}_1^{new}$ derived from a linear combination of the columns of $\mathbf{V}_m$:

$$\mathbf{v}_1^{new} = \sum_{i=1}^{m} \alpha_i \mathbf{v}_i \tag{12.227}$$

where α_i are coefficients calculated from the modal properties of $\mathbf{H}_m$ [16].

Equation 12.225 holds only if the vector sequence $\mathbf{v}_i$ is kept orthogonal at each step of calculation [20]. In practice, the orthogonality may be lost rapidly due to numerical cancellation and roundoff errors. The remedy is to introduce a reorthogonalization process [16] after the calculation of each $\mathbf{v}_i$ from Equation 12.222.

An important property of the method is that the eigenvalues of $\mathbf{H}_m$ in Equation 12.225 usually converge to those eigenvalues of $\mathbf{A}$ which have largest (and smallest) modulus. Thus, if eigenvalues of $\mathbf{A}$ around a specified point λ_t are desired, the transformation

$$\mathbf{A}_t = (\mathbf{A}-\lambda_t\mathbf{I})^{-1} \tag{12.228}$$

can be used to magnify the eigenvalues of $\mathbf{A}$ close to λ_t, since

$$\lambda_{ti} = \frac{1}{\lambda_i-\lambda_t} \tag{12.229}$$

where λ_i is an eigenvalue of $\mathbf{A}$, and λ_{ti} is the corresponding eigenvalue of $\mathbf{A}_t$. Then $\mathbf{A}_t$ is the suitable matrix to which the method can be applied in order to find the set of eigenvalues of $\mathbf{A}$ close to λ_t, which is termed the *shift point*.

With the transformation 12.228, the only computation involving $\mathbf{A}$ in constructing the vector sequence $\mathbf{v}_i$ is the solution of the equation

$$(\mathbf{A}-\lambda_t\mathbf{I})\mathbf{u}_i = \mathbf{v}_i \tag{12.230}$$

Equation 12.222 may be written in terms of $\mathbf{u}_i$, as

$$h_{i+1,i}\mathbf{v}_{i+1} = \mathbf{u}_i - \sum_{j=1}^{i} h_{j,i}\mathbf{v}_j \qquad i=1,\cdots,m \tag{12.231}$$

and the upper triangular elements in $\mathbf{H}_m$ become

$$h_{j,i} = \mathbf{v}_j^H\mathbf{u}_i \qquad j \le i \tag{12.232}$$

Application of the MAM to power system model:

Substituting the expression for the state matrix $\mathbf{A}$ of a power system given by Equation 12.192 in Equation 12.230, we get

$$(\mathbf{A}_D-\lambda_t\mathbf{I})\mathbf{u}_i+\mathbf{B}_D(\mathbf{Y}_N+\mathbf{Y}_D)^{-1}\mathbf{C}_D\mathbf{u}_i = \mathbf{v}_i$$

This may be written as

$$(\mathbf{A}_D-\lambda_t\mathbf{I})\mathbf{u}_i+\mathbf{B}_D\mathbf{q}_i = \mathbf{v}_i \tag{12.233}$$

where

$$\mathbf{q}_i = (\mathbf{Y}_N+\mathbf{Y}_D)^{-1}\mathbf{C}_D\mathbf{u}_i$$

Rearranging,

$$\mathbf{C}_D\mathbf{u}_i-(\mathbf{Y}_N+\mathbf{Y}_D)\mathbf{q}_i = 0 \tag{12.234}$$

Equations 12.233 and 12.234 may be combined to give the matrix equation

$$\begin{bmatrix}(\mathbf{A}_D-\lambda_t\mathbf{I}) & \mathbf{B}_D\\ \mathbf{C}_D & -(\mathbf{Y}_N+\mathbf{Y}_D)\end{bmatrix}\begin{bmatrix}\mathbf{u}_i\\ \mathbf{q}_i\end{bmatrix} = \begin{bmatrix}\mathbf{v}_i\\ 0\end{bmatrix} \tag{12.235}$$

The following are the computational steps associated with the MAM:

1. Form the device models $\mathbf{A}_i$, $\mathbf{B}_i$, $\mathbf{C}_i$, $\mathbf{Y}_i$.

2. Compute the device admittance matrix corresponding to the chosen shift point λ_t:

$$\mathbf{Y}_{De}(\lambda_t) = \mathbf{Y}_D-\mathbf{C}_D(\lambda_t\mathbf{I}-\mathbf{A}_D)^{-1}\mathbf{B}_D \tag{12.236}$$

3. Solve for $\mathbf{q}_i$:

$$[\mathbf{Y}_N+\mathbf{Y}_{De}(\lambda_t)]\mathbf{q}_i = -\mathbf{C}_D(\lambda_t\mathbf{I}-\mathbf{A}_D)^{-1}\mathbf{v}_i \tag{12.237}$$

4. Calculate $\mathbf{u}_i$:

$$\mathbf{u}_i = (\lambda_t\mathbf{I}-\mathbf{A}_D)^{-1}(\mathbf{B}_D\mathbf{q}_i-\mathbf{v}_i) \tag{12.238}$$

5. Compute $\mathbf{v}_{i+1}$ using Equation 12.231 and the related elements in $\mathbf{H}_m$ using Equation 12.232, with the order m equal to the specified value. Repeat steps 3 to 5 to form the complete $\mathbf{V}_m$ and $\mathbf{H}_m$.

6. Compute eigenvalues of $\mathbf{H}_m$ using the *QR* transformation method. If the desired set of eigenvalues has converged within the specified tolerance, stop; otherwise, compute a new starting vector $\mathbf{v}_1^{new}$ using Equation 12.227, and go to step 3 for the next iteration.

The factorization of the network equivalent admittance matrix $\mathbf{Y}_N+\mathbf{Y}_{De}(\lambda_t)$ in Equation 12.237 needs to be performed only once since λ_t does not change during the iteration process; this adds to the efficiency of the method. As the admittance matrix is very sparse, the method can be applied to very large systems by using sparsity-based techniques for solution of algebraic equations.

The MAM, unlike the AESOPS algorithm, can compute eigenvalues associated with any system mode, not just the rotor angle mode. In addition, it does not require *a priori* knowledge about the mode characteristics of the system. Normally, the shift point λ_t is given in order to compute a particular set of eigenvalues close to it. By slightly modifying the algorithm, the method can be adopted to provide the capability for scanning eigenvalues over a frequency range on the complex plane with assurance that all critical eigenvalues within the specified range have been computed.

Calculation of eigenvectors:

The right eigenvectors are given directly by Equation 12.226 from the last iteration. The left eigenvectors are calculated by inverse iteration. This requires the solution of Equation 12.235 transposed as follows:

$$\begin{bmatrix} \mathbf{A}_D^T-\lambda_t\mathbf{I} & \mathbf{C}_D^T \\ \mathbf{B}_D^T & -(\mathbf{Y}_N+\mathbf{Y}_D)^T \end{bmatrix} \begin{bmatrix} \mathbf{y} \\ \mathbf{q} \end{bmatrix} = \begin{bmatrix} \mathbf{y}_0 \\ 0 \end{bmatrix}$$

with the computed eigenvalue λ_t and an arbitrary vector $\mathbf{y}_0$. Normally, one iteration is sufficient to give the left eigenvector.

Comparison of results

Table 12.2 compares the eigenvalue calculations using the *QR* transformation, AESOPS, and MAM. The test system consisted of 94 generators and about 1,400 buses. Eighteen of the generators were represented by detailed models and the other generators were represented by the classical model. This resulted in a system model with 366 states. The MASS and PEALS referred to above were used to compute the eigenvalues.

Table 12.2

Mode	*QR* Method	AESOPS	MAM
A	$-0.122\pm j1.650$	$-0.121\pm j1.650$	$-0.121\pm j1.650$
B	$-0.117\pm j3.073$	$-0.117\pm j3.073$	$-0.117\pm j3.073$
C	$-0.276\pm j5.212$	$-0.276\pm j5.212$	$-0.276\pm j5.212$

All eigenvalues of the state matrix and the corresponding participation factors were first computed using the MASS program, which uses the *QR* transformation method. Then three pairs of complex eigenvalues associated with rotor angle modes were selected for comparison with AESOPS and MAM. The initial estimates of the eigenvalues for both methods were set so that they deviated from the true values by about 10%. From Table 12.2, we see that all three methods give practically identical results. This is particularly reassuring in view of the widely differing theories on which the three methods are based.

As a further validation of the above results, frequency response was computed using PEALS with the change in mechanical torque of a large generator (with high participation in the three modes) as the input signal and the speed change of the same generator as the output signal. Figure 12.22 shows a plot of the computed frequency response, which exhibits resonant frequencies at about 0.26 Hz, 0.49 Hz, and 0.83 Hz. These are in agreement with the frequencies of the selected modes.

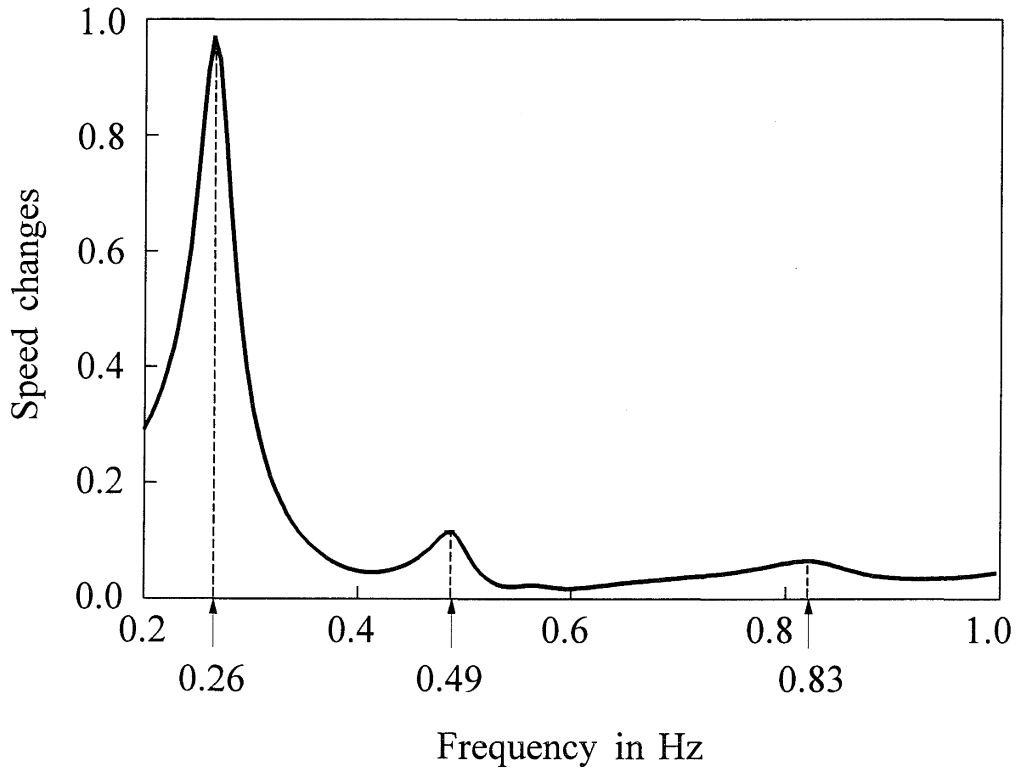


Figure 12.22 Frequency response

Example 12.6

In this example, we will analyze the small-signal stability of a simple two-area system shown in Figure E12.8. This system is similar in structure to the one used in references 23 and 24 to study the fundamental nature of interarea oscillations.

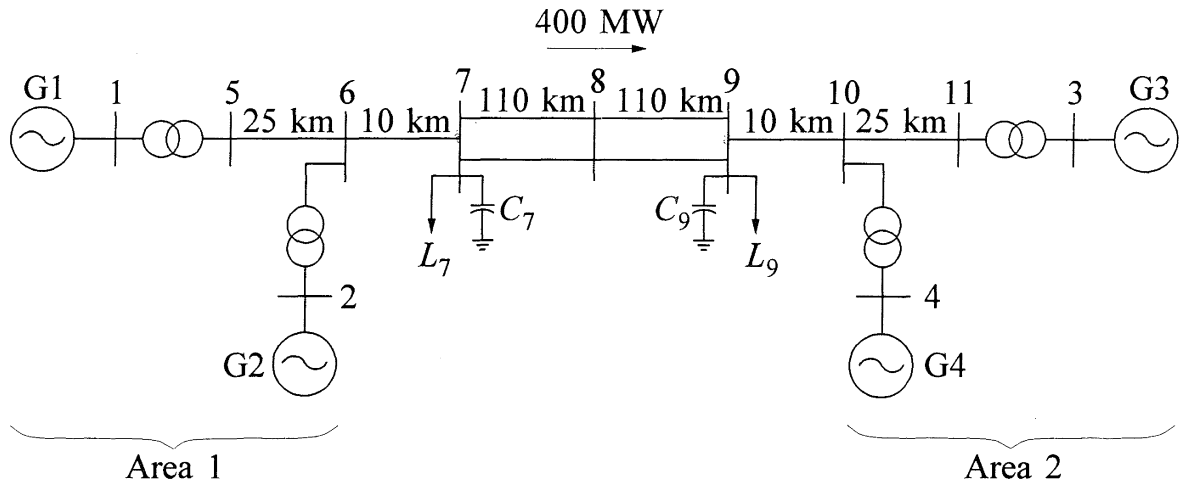


Figure E12.8 A simple two-area system

The system consists of two similar areas connected by a weak tie. Each area consists of two coupled units, each having a rating of 900 MVA and 20 kV. The generator parameters in per unit on the rated MVA and kV base are as follows:

$X_d = 1.8$	$X_q = 1.7$	$X_l = 0.2$	$X'_d = 0.3$	$X'_q = 0.55$
$X''_d = 0.25$	$X''_q = 0.25$	$R_a = 0.0025$	$T'_{d0} = 8.0$ s	$T'_{q0} = 0.4$ s
$T''_{d0} = 0.03$ s	$T''_{q0} = 0.05$ s	$A_{Sat} = 0.015$	$B_{Sat} = 9.6$	$\psi_{T1} = 0.9$
$H = 6.5$ (for G1 and G2)		$H = 6.175$ (for G3 and G4)		$K_D = 0$

Each step-up transformer has an impedance of $0+j0.15$ per unit on 900 MVA and 20/230 kV base, and has an off-nominal ratio of 1.0.

The transmission system nominal voltage is 230 kV. The line lengths are identified in Figure E12.8. The parameters of the lines in per unit on 100 MVA, 230 kV base are

$$r = 0.0001 \text{ pu/km} \qquad x_L = 0.001 \text{ pu/km} \qquad b_C = 0.00175 \text{ pu/km}$$

The system is operating with area 1 exporting 400 MW to area 2, and the generating units are loaded as follows:

G1:	$P = 700$ MW,	$Q = 185$ MVAr,	$E_t = 1.03\angle 20.2°$
G2:	$P = 700$ MW,	$Q = 235$ MVAr,	$E_t = 1.01\angle 10.5°$
G3:	$P = 719$ MW,	$Q = 176$ MVAr,	$E_t = 1.03\angle -6.8°$
G4:	$P = 700$ MW,	$Q = 202$ MVAr,	$E_t = 1.01\angle -17.0°$

The loads and reactive power supplied (Q_C) by the shunt capacitors at buses 7 and 9 are as follows:

Bus 7: P_L = 967 MW, Q_L = 100 MVAr, Q_C = 200 MVAr
Bus 9: P_L = 1,767 MW, Q_L = 100 MVAr, Q_C = 350 MVAr

(a) If all four generators are on manual excitation control (constant E_{fd}), compute the eigenvalues of the system state matrix representing the small-signal performance of the system about the initial operating condition. For each eigenvalue, identify the system state variables with high participation. Determine the frequencies, damping ratios, and mode shapes of the rotor oscillation modes. Assume that the active components of loads have constant current characteristics, and reactive components of loads have constant impedance characteristics.

(b) Determine the eigenvalues, frequencies, and damping ratios of rotor oscillation modes when all four generators are equipped with the following types of excitation control:

(i) Self-excited dc exciter (see Figures 8.38 and 8.40):

K_A = 20.0 T_A = 0.055 T_E = 0.36 K_F = 0.125
T_F = 1.8 A_{ex} = 0.0056 B_{ex} = 1.075 T_R = 0.05
T_B, T_C, R_C, and X_C are not used

(ii) Thyristor exciter with a high transient gain:

K_A = 200.0 T_R = 0.01

(iii) Thyristor exciter with a transient gain reduction (TGR):

K_A = 200.0 T_R = 0.01 T_A = 1.0 T_B = 10.0

(iv) Thyristor exciter with high transient gain and PSS:

K_A = 200.0 T_R = 0.01 K_{STAB} = 20.0 T_W = 10.0
T_1 = 0.05 T_2 = 0.02 T_3 = 3.0 T_4 = 5.4

The block diagram of thyristor excitation system with PSS is shown in Figure E12.9.

Solution

(a) *System modes with generators on manual excitation control:*

Table E12.3 summarizes the eigenvalues of the system state matrix and the state variables that have high participation in each mode. The first two eigenvalues represent the *zero eigenvalues* due to the redundant state variables. As described in Section 12.7, one of these zero eigenvalues is due to lack of uniqueness of absolute rotor angle (there is no infinite bus, and the rotor angles are referred to a common reference frame). The other zero eigenvalue is due to the assumption that the generator torques are independent of speed deviation (speed governors are not modelled and K_D=0).

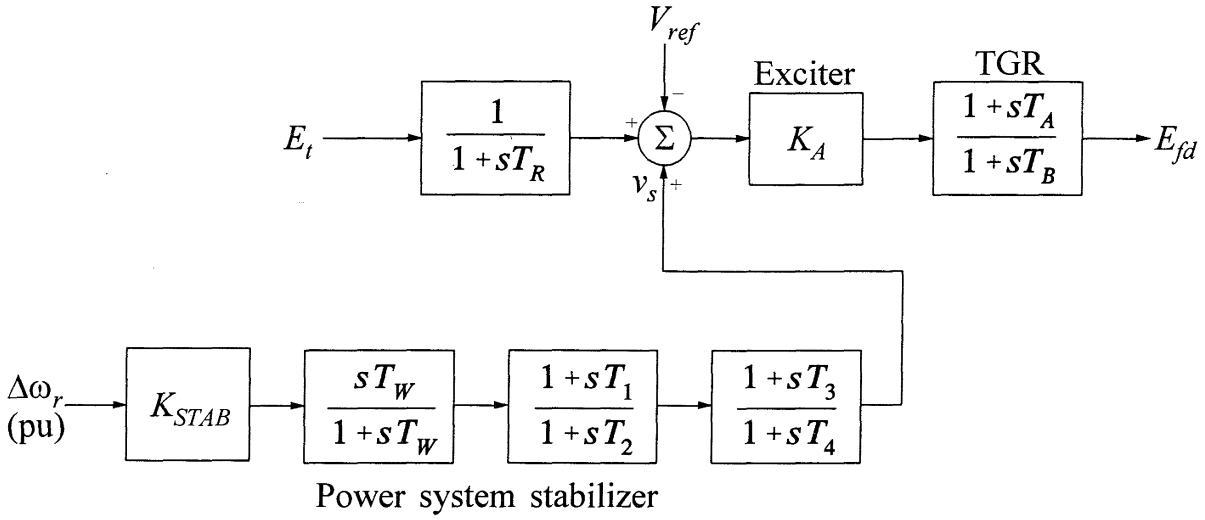
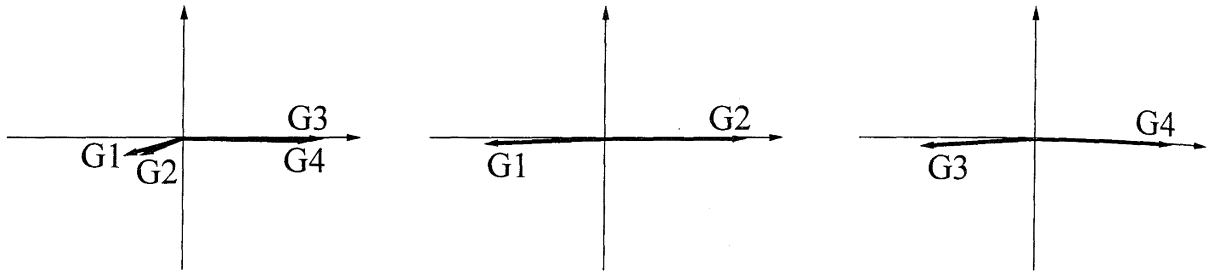


Figure E12.9 Thyristor excitation system with PSS

Table E12.3 System modes with manual excitation control

Eigenvalues			Frequency (Hz)	Damping Ratio	Dominant States
No.	Real	Imaginary			
1,2	-0.76E-3	±0.22E-2	0.0003	0.331	Δω and Δδ of G1, G2, G3, G4
3	-0.96E-1	–	–	–	"
4,5	-0.111	±3.43	0.545	0.032	"
6	-0.117	–	–	–	"
7	-0.265	–	–	–	$\Delta\psi_{fd}$ of G3 and G4
8	-0.276	–	–	–	$\Delta\psi_{fd}$ of G1 and G2
9,10	-0.492	±6.82	1.087	0.072	Δω and Δδ of G1 and G2
11,12	-0.506	±7.02	1.117	0.072	Δω and Δδ of G3 and G4
13	-3.428	–	–	–	*d* and *q* axis amortisseur flux linkages
14	-4.139	–	–	–	
15	-5.287	–	–	–	
16	-5.303	–	–	–	
17	-31.03	–	–	–	
18	-32.45	–	–	–	
19	-34.07	–	–	–	
20	-35.53	–	–	–	
21,22	-37.89	±0.142	0.023	≈1.0	
23,24	-38.01	±0.38E-1	0.006	≈1.0	

From the table, we see that the system is stable. There are three rotor angle modes of oscillation. Their mode shapes (normalized eigenvector components corresponding to rotor speeds of the four machines) are shown in Figure E12.10. From the mode shapes we see that the 0.55 Hz mode is the interarea mode, with generators G1 and G2 of area 1 swinging against generators G3 and G4 of area 2. The 1.09 Hz mode is the intermachine oscillation local to area 1, with G1 swinging against G2. The third rotor angle mode, with a frequency of 1.12 Hz, is the intermachine mode local to area 2.



(a) Interarea mode f=0.545 Hz, ζ=0.032

(b) Area 1 local mode f=1.087 Hz, ζ=0.072

(c) Area 2 local mode f=1.117 Hz, ζ=0.072

Figure E12.10 Mode shapes of rotor angle modes with manual excitation control

(b) *Rotor angle modes with different types of excitation control:*

Table E12.4 summarizes the eigenvalues, frequencies, and damping ratios associated with the rotor oscillation modes for the four alternative forms of excitation control.

We see that the local intermachine modes of oscillation have the same degree of damping with the dc exciter and thyristor exciter (with and without TGR). The interarea mode has a small positive damping with the dc exciter. It is unstable with high gain thyristor exciters. The TGR makes the interarea mode more unstable. The interarea mode as well as the local modes are very well damped when power system stabilizers are added to the thyristor exciters.

Table E12.4 Effects of excitation control on rotor oscillation modes

Type of Excitation Control	Eigenvalue/(Frequency in Hz, Damping Ratio)		
	Interarea Mode	Area 1 Local Mode	Area 2 Local Mode
(i) DC exciter	$-0.018\pm j3.27$ (f=0.52, ζ=0.005)	$-0.485\pm j6.81$ (f=1.08, ζ=0.07)	$-0.500\pm j7.00$ (f=1.11, ζ=0.07)
(ii) Thyristor with high gain	$+0.031\pm j3.84$ (f=0.61, ζ=−0.008)	$-0.490\pm j7.15$ (f=1.14, ζ=0.07)	$-0.496\pm j7.35$ (f=1.17, ζ=0.07)
(iii) Thyristor with TGR	$+0.123\pm j3.46$ (f=0.55, ζ=−0.036)	$-0.450\pm j6.86$ (f=1.09, ζ=0.06)	$-0.462\pm j7.05$ (f=1.12, ζ=0.06)
(iv) Thyristor with PSS	$-0.501\pm j3.77$ (f=0.60, ζ=0.13)	$-1.826\pm j8.05$ (f=1.28, ζ=0.22)	$-1.895\pm j8.35$ (f=1.33, ζ=0.22)

■

12.9 CHARACTERISTICS OF SMALL-SIGNAL STABILITY PROBLEMS

In large power systems, small-signal stability problems may be either local or global in nature.

Local problems

Local problems involve a small part of the system. They may be associated with rotor angle oscillations of a single generator or a single plant against the rest of the power system. Such oscillations are called *local plant mode oscillations*. The stability problems related to such oscillations are similar to those of a single-machine infinite bus system as studied in Sections 12.3 to 12.6. Most commonly encountered small-signal stability problems are of this category.

Local problems may also be associated with oscillations between the rotors of a few generators close to each other. Such oscillations are called *intermachine or interplant mode oscillations*. Usually, the local plant mode and interplant mode oscillations have frequencies in the range of 0.7 to 2.0 Hz.

Other possible local problems include instability of modes associated with controls of equipment such as generator excitation systems, HVDC converters, and static var compensators. The problems associated with *control modes* are due to inadequate tuning of the control systems [21]. In addition, these controls may interact with the dynamics of the turbine-generator shaft system, causing instability of *torsional mode oscillations* [22]. Torsional oscillation problems are described in Chapter 15.

Analysis of local small-signal stability problems requires a detailed representation of a small portion of the complete interconnected power system. The rest of the system representation may be appropriately simplified by use of simple models and system equivalents. Usually, the complete system may be adequately represented by a model having several hundred states at most.

Global problems

Global small-signal stability problems are caused by interactions among large groups of generators and have widespread effects. They involve oscillations of a group of generators in one area swinging against a group of generators in another area. Such oscillations are called *interarea mode oscillations*.

Large interconnected systems usually have two distinct forms of interarea oscillations:

(a) A very low frequency mode involving all the generators in the system. The system is essentially split into two parts, with generators in one part swinging against machines in the other part. The frequency of this mode of oscillation

is on the order of 0.1 to 0.3 Hz.

(b) Higher frequency modes involving subgroups of generators swinging against each other. The frequency of these oscillations is typically in the range of 0.4 to 0.7 Hz.

Illustration of global problems

We will consider two large systems with distinct characteristics to illustrate the two forms of interarea oscillations.

Test system A

This test system consists of 2,310 buses, 375 generators, and 3 HVDC links. The 3 dc links and 291 generators are modelled in detail. The remaining 84 generators represent equivalent machines and are modelled by the classical model.

To identify the critical modes of interarea oscillation, eigenvalues of system modes with frequencies in the range of 0.2 to 1.0 Hz are scanned, using the modified Arnoldi method. Table 12.3 lists the eigenvalues, frequencies, and damping ratios of the modes identified by this mode search. Figure 12.23 shows a plot of these eigenvalues on a complex plane. Box A in the figure represents the region on the complex plane within which all eigenvalues have been computed; outside this area, there may exist eigenvalues other than those shown on the complex plane.

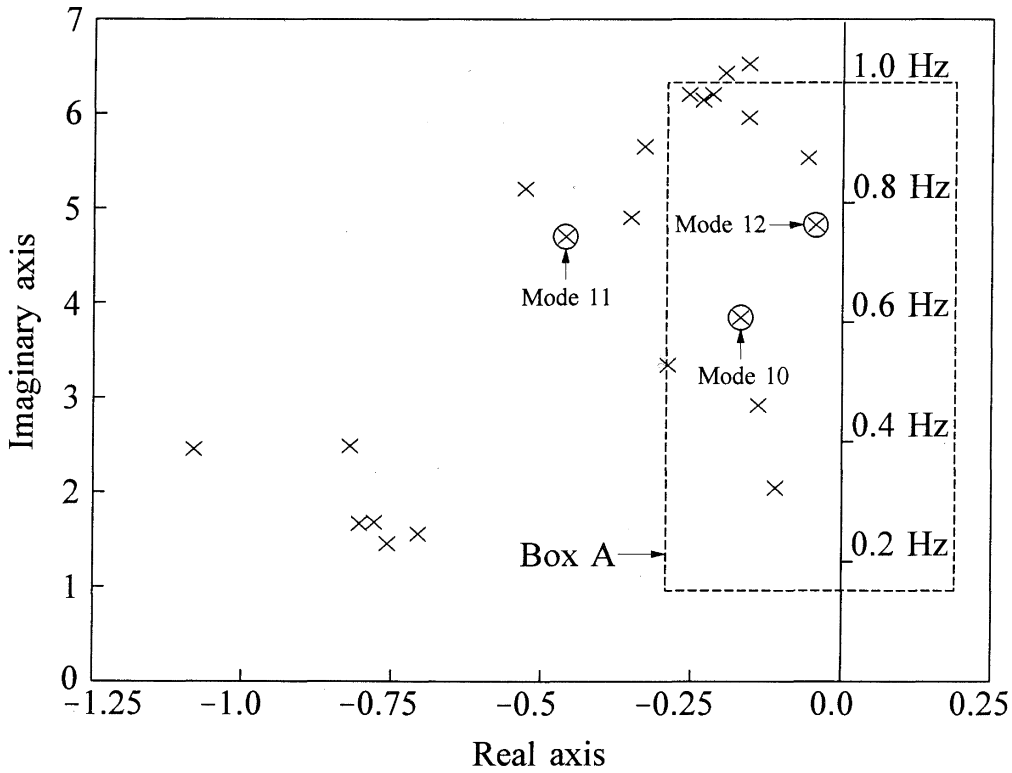


Figure 12.23 Eigenvalues computed by frequency scan using MAM

Table 12.3 Modes of system A computed by using frequency scanning technique

Mode no.	Eigenvalue	Frequency (Hz)	Damping Ratio
1	$-0.7567\pm j1.4163$	0.2254	0.4712
2	$-0.7193\pm j1.4605$	0.2324	0.4419
3	$-0.7999\pm j1.5623$	0.2486	0.4558
4	$-0.7806\pm j1.5776$	0.2511	0.4435
5	$-0.1265\pm j1.9894$	0.3166	0.0634
6	$-0.8248\pm j2.3509$	0.3742	0.3311
7	$-1.0698\pm j2.3642$	0.3763	0.4123
8	$-0.1434\pm j2.7826$	0.4429	0.0515
9	$-0.2871\pm j3.2495$	0.5172	0.0880
10	$-0.1609\pm j3.7797$	0.6016	0.0425
11	$-0.4382\pm j4.6754$	0.7441	0.0933
12	$-0.0470\pm j4.7439$	0.7550	0.0099
13	$-0.3336\pm j4.8262$	0.7681	0.0689
14	$-0.5420\pm j5.2074$	0.8288	0.1035
15	$-0.0551\pm j5.4200$	0.8626	0.0102
16	$-0.3116\pm j5.6159$	0.8938	0.0554
17	$-0.1451\pm j5.8825$	0.9362	0.0247
18	$-0.2385\pm j6.1228$	0.9745	0.0389
19	$-0.2243\pm j6.1745$	0.9827	0.0363
20	$-0.2552\pm j6.1814$	0.9838	0.0412
21	$-0.1961\pm j6.3504$	1.0107	0.0309
22	$-0.1457\pm j6.4356$	1.0243	0.0226

The 22 modes represented by the eigenvalues shown in Figure 12.23 and Table 12.3 can be divided, based on mode shapes, into three categories:

(a) Interarea modes. Examples are modes 5 and 8 to 12.

(b) Local plant modes. Examples are modes 13, 21, and 22.

(c) Control modes. Examples are modes 1 to 4, and 6.

Modes 10, 11, and 12 represent the critical interarea modes. These modes have frequencies in the 0.6 to 0.75 Hz range. Each represents oscillation of a subgroup of generators swinging against another subgroup of generators across a weak or heavily loaded transmission interface. Figure 12.24 shows how the interfaces associated with the three critical interarea modes geographically divide the overall system. The stability characteristics of each interarea mode of oscillation depend on the power transfer across its interface and on the controls associated with the subgroups of generating units on the two sides of the interface.

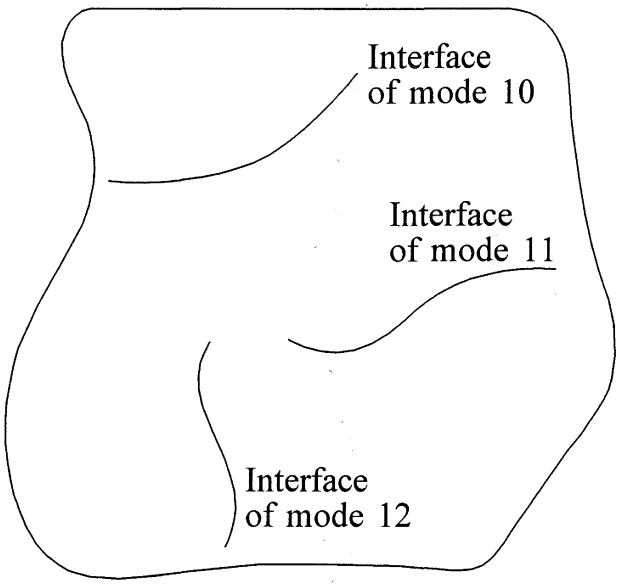


Figure 12.24 Interfaces of critical interarea modes of oscillation of system A

Test system B

This system consists of nearly 3,000 buses and 300 generators. It has a dominant 0.2 Hz interarea mode in which practically all the generators in the system participate. The mode shape of the interarea mode is such that its interface splits the system into two parts as depicted in Figure 12.25. When the system is perturbed, the generating units on the two sides of the interface swing against each other with a frequency of about 0.2 Hz.

Table 12.4 summarizes the results of analysis carried out to investigate the effects of excitation control of the generators at a large thermal plant having a high participation in the interarea mode. This plant is identified as GS "D" in Figure 12.25 and has a thyristor excitation system.

We see from the results that the control of excitation of generators at the thermal plant has a very significant effect on the stability of the 0.2 Hz interarea mode of oscillation. With a high gain thyristor exciter, for the system conditions considered,

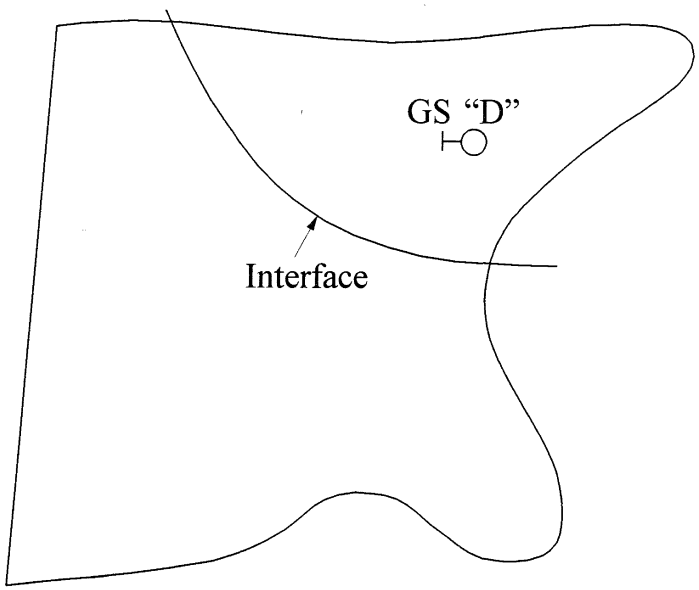


Figure 12.25 Interface of 0.2 Hz interarea mode of oscillation of system B

Table 12.4 Effect of excitation control of generating units at GS "D" on the stability of interarea mode

Type of Excitation Control	Interarea Mode	
	Frequency (Hz)	Damping Ratio
(a) Thyristor exciter with high transient gain	0.192	0.009
(b) Thyristor exciter with transient gain reduction	0.187	-0.057
(c) Thyristor exciter with power system stabilizer	0.179	0.122

the interarea mode has a small positive damping (ζ=0.009). With a transient gain reduction, the interarea mode actually becomes unstable (ζ=-0.057). When a power system stabilizer (designed as described in reference 9) is added, the damping increases significantly (ζ=0.122).

Factors influencing interarea modes of oscillation

The characteristics of interarea modes of oscillation are very complex and in some respects significantly differ from the characteristics of local plant modes. Load characteristics, in particular, have a major effect on the stability of interarea modes.

The manner in which excitation systems affect interarea oscillations depends on the types and locations of the exciters, and on the characteristics of loads [23].

Speed-governing systems normally do not have a very significant effect on interarea oscillations. However, if they are not properly tuned, they may decrease damping of the oscillations slightly. In extreme situations, this may be sufficient to aggravate the situation significantly. In the absence of any other convenient means of increasing the damping, adjustment or blocking of the governors may provide some relief [26].

A mode of oscillation in one part of the system may interact with a mode of oscillation in a remote part due to mode coupling. This occurs when the frequencies of the two modes are nearly equal [24,25]. Care should be exercised in interpreting results of analysis in such cases.

The controllability of interarea modes with PSS is a complex function of many factors:

- Location of unit with PSS
- Characteristics and location of loads
- Types of exciters on other units

On some units, the PSS does not have the desired effect on the damping of interarea oscillations. Reference 24 presents results of a detailed study of factors influencing PSS performance in damping interarea and interplant modes of oscillation.

Other effective means of stabilizing interarea modes of oscillation include modulation of HVDC converter controls and static var compensator controls.

Analysis of interarea oscillations requires detailed representation of the entire interconnected power system. Models for excitation systems and loads, in particular, should be accurate, and the same level of modelling detail should be used throughout the system.

Reference 27 provides a detailed account of a comprehensive study of the interarea oscillation problems, including the fundamental nature of the problem, methods of analysis, and control design procedures to mitigate the problem.

Enhancement of small-signal stability is discussed in Chapter 17.

REFERENCES

[1] A.M. Lyapunov, *Stability of Motion*, English translation, Academic Press, Inc., 1967.

[2] G.C. Verghese, I.J. Perez-Arriaga, and F.C. Schweppe, "Selective Modal Analysis with Application to Electric Power Systems, Part I: Heuristic Introduction, Part II: The Dynamic Stability Problem," *IEEE Trans.*, Vol., PAS-101, No. 9, pp. 3117-3134, September 1982.

[3] J.G.F. Francis, "The QR Transformation - A Unitary Analogue to the LR Transformation," Parts 1 and 2, *The Computer Journal*, Vol. 4, pp. 265-271, 1961; pp. 332-345, 1962.

[4] J.H. Wilkinson, *The Algebraic Eigenvalue Problem*, Clarendon Press, Oxford, 1965.

[5] W.G. Heffron and R.A. Phillips, "Effects of Modern Amplidyne Voltage Regulator in Underexcited Operation of Large Turbine Generators," *AIEE Trans.*, Vol. PAS-71, pp. 692-697, August 1952.

[6] F.P. deMello and C. Corcordia, "Concepts of Synchronous Machine Stability as Affected by Excitation Control," *IEEE Trans.*, Vol. PAS-88, pp. 316-329, April 1969.

[7] S.B. Crary, *Power System Stability*, Vol. II, John Wiley & Sons, Inc., 1955.

[8] F.P. DeMello and T.F. Laskoswski, "Concepts of Power System Dynamic Stability," *IEEE Trans.*, Vol. PAS-94, pp. 827-833, May/June 1975.

[9] P. Kundur, M. Klein, G.J. Rogers, and M.S. Zywno, "Application of Power System Stabilizer for Enhancement of Overall System Stability," *IEEE Trans.*, Vol. PWRS-4, pp. 614-626, May 1989.

[10] P. Kundur, G.J. Rogers, D.Y. Wong, L. Wang, and M.G. Lauby, "A Comprehensive Computer Program for Small Signal Stability Analysis of Power Systems," *IEEE Trans.*, Vol. PWRS-5, pp. 1076-1083, November 1990.

[11] EPRI Report EL-5798, "The Small Signal Stability Program Package," Vol. 1, Final Report of Project 2447-1, Prepared by Ontario Hydro, May 1988.

[12] S. Arabi, G.J. Rogers, D.Y. Wong, P. Kundur, and M.G. Lauby, "Small Signal Stability Program Analysis of SVC and HVDC in AC Power Systems," *IEEE Trans.*, Vol. PWRS-6, pp. 1147-1153, August 1991.

[13] N. Martins and L.T.G. Lima, "Eigenvalue and Frequency Domain Analysis of Small Signal Electromechanical Stability Problems," *Eigenanalysis and Frequency Domain Methods for System Dynamic Performance*, IEEE publication 90TH0292-3-PWR.

[14] R.T. Byerly, R.J. Bennon, and D.E. Sherman, "Eigenvalue Analysis of Synchronizing Power Flow Oscillations in Large Electric Power Systems," *IEEE Trans.*, Vol. PAS-101, pp. 235-243, January 1982.

[15] N. Martins, "Efficient Eigenvalue and Frequency Response Methods Applied to Power System Small-Signal Stability Studies," *IEEE Trans.*, Vol. PWRS-1, pp. 217-225, February 1986.

[16] L. Wang and A. Semlyen, "Application of Sparse Eigenvalue Techniques to the Small Signal Stability Analysis of Large Power Systems," *IEEE Trans.*, Vol. PWRS-6, pp. 635-642, November 1990.

[17] N. Uchida and T. Nagao, "A New Eigen-Analysis Method of Steady-State Stability Studies for Large Power Systems: S Matrix Method," *IEEE Trans.*, Vol. PWRS-3, pp. 706-714, May 1988.

[18] F.L. Pagola, L. Rouco, and I.J. Perez-Arriaga, "Analysis and Control of Small-Signal Stability in Electric Power Systems by Selective Modal Analysis," *Eigenanalysis and Frequency Domain Methods for System Dynamic Performance*, IEEE publication 90TH0292-3-PWR.

[19] W.E. Arnoldi, "The Principle of Minimized Iterations in the Solution of the Matrix Eigenvalue Problem," *Quart. Appl. Math.*, Vol. 9, pp. 17-29, 1951.

[20] Y. Saad, "Variations on Arnoldi's Method for Computing Eigenelements of Large Unsymmetric Matrices," *Linear Algebra and Its Applications*, Vol. 34, pp. 184-198, June 1981.

[21] P. Kundur, D.C. Lee, and H.M. Zein El-Din, "Power System Stabilizers for Thermal Units: Analytical Techniques and On-site Validation," *IEEE Trans.*, Vol. PAS-100, pp. 81-95, January 1981.

[22] P. Kundur and P.L. Dandeno, "Practical Application of Eigenvalue Techniques in the Analysis of Power System Dynamic Stability Problems," *Proceedings of Fifth Power System Computation Conference*, Cambridge, England, September 1975.

[23] M. Klein, G.J. Rogers, and P. Kundur, "A Fundamental Study of Inter-Area Oscillations," *IEEE Trans.*, Vol. PWRS-6, No. 3, pp. 914-921, August 1991.

[24] M. Klein, G.J. Rogers, S. Moorty, and P. Kundur, "Analytical Investigation of Factors Influencing Power System Stabilizers Performance," Paper 92WM016-6EC, Presented at the IEEE PES Winter Meeting, New York, January 1992.

[25] D.K. Mugwanya and J.E. Van Ness, "Mode Coupling in Power Systems," *IEEE Trans.*, Vol. PWRS-2, pp. 264-270, May 1987.

[26] O.W. Hanson, C.J. Goodwin, and P.L. Dandeno, "Identification of Excitation and Speed Control Parameters in Stabilizing Inter-System Oscillation," *IEEE Trans.*, Vol. PAS-87, pp. 1306-1313, May 1968.

[27] Canadian Electrical Association Report, "Investigation of Low Frequency Inter-area Oscillation Problems in Large Interconnected Power Systems," Report of Research Project 294T622, prepared by Ontario Hydro, 1993.

Chapter 13

Transient Stability

Transient stability, as described in Chapter 2, is the ability of the power system to maintain synchronism when subjected to a severe transient disturbance such as a fault on transmission facilities, loss of generation, or loss of a large load. The system response to such disturbances involves large excursions of generator rotor angles, power flows, bus voltages, and other system variables. Stability is influenced by the nonlinear characteristics of the power system. If the resulting angular separation between the machines in the system remains within certain bounds, the system maintains synchronism. Loss of synchronism because of transient instability, if it occurs, will usually be evident within 2 to 3 seconds of the initial disturbance.

This chapter illustrates the nature of transient stability problems, identifies factors influencing them, and describes modelling considerations and analytical techniques applicable to transient stability analysis.

13.1 AN ELEMENTARY VIEW OF TRANSIENT STABILITY [1-3]

Consider the system shown in Figure 13.1, consisting of a generator delivering power to a large system represented by an infinite bus through two transmission circuits. An infinite bus, as described in Chapter 12 (Section 12.3), represents a voltage source of constant voltage magnitude and constant frequency.

We will present fundamental concepts and principles of transient stability by analyzing the system response to large disturbances, using very simple models. All resistances are neglected. The generator is represented by the classical model (see Chapter 5, Section 5.3.1) and the speed governor effects are neglected. The corresponding system representation is shown in Figure 13.2(a). The voltage behind

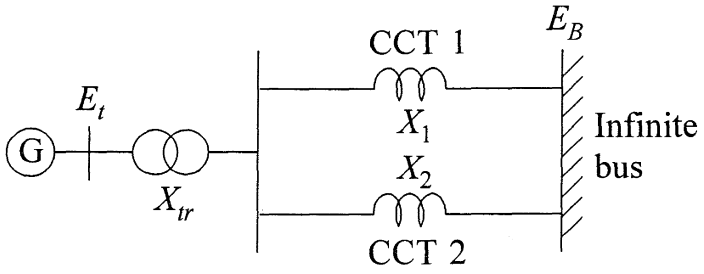
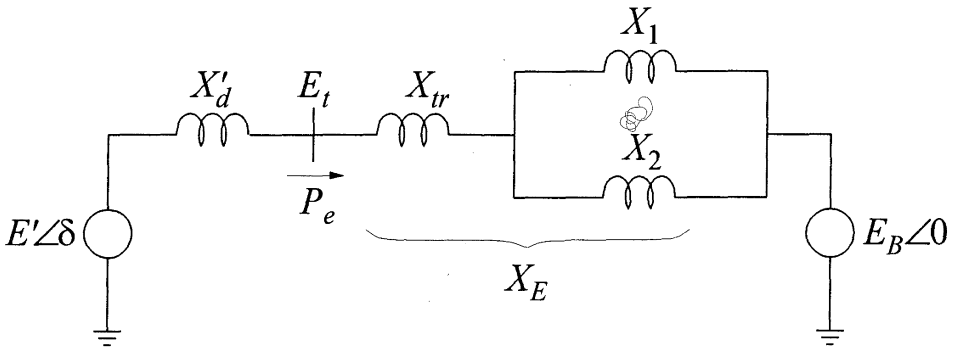
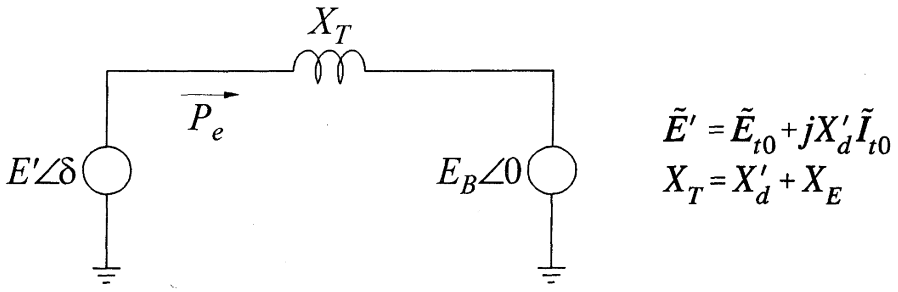


Figure 13.1 Single-machine infinite bus system



(a) Equivalent circuit



(b) Reduced equivalent circuit

Figure 13.2 System representation with generator represented by classical model

the transient reactance (X'_d) is denoted by E'. The rotor angle δ represents the angle by which E' leads E_B. When the system is perturbed, the magnitude of E' remains constant at its predisturbance value and δ changes as the generator rotor speed deviates from synchronous speed ω_0.

The system model can be reduced to the form shown in Figure 13.2(b). It can be analyzed by using simple analytical methods and is helpful in acquiring a basic understanding of the transient stability phenomenon. This model is identical to that shown in Figure 12.4 of Chapter 12. From Equation 12.71, the generator's electrical power output is

$$P_e = \frac{E'E_B}{X_T}\sin\delta = P_{max}\sin\delta \tag{13.1}$$

where

$$P_{max} = \frac{E'E_B}{X_T} \tag{13.2}$$

Since we have neglected the stator resistance, P_e represents the air-gap power as well as the terminal power. The power-angle relationship with both transmission circuits in service (I/S) is shown graphically in Figure 13.3 as curve 1. With a mechanical power input of P_m, the steady-state electrical power output P_e is equal to P_m, and the operating condition is represented by point a on the curve. The corresponding rotor angle is δ_a.

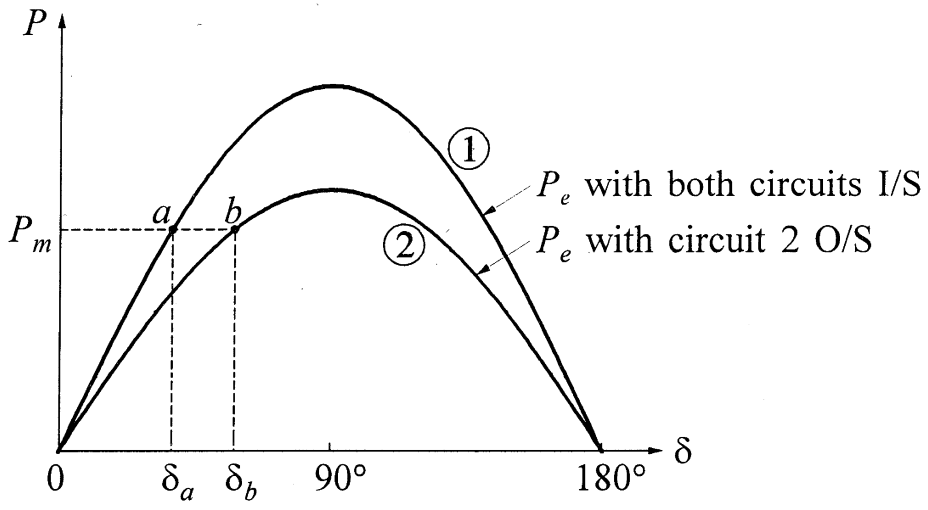


Figure 13.3 Power-angle relationship

If one of the circuits is out of service (O/S), the effective reactance X_T is higher. The power-angle relationship with circuit 2 out of service is shown in Figure 13.3 as curve 2. The maximum power is now lower. With a mechanical power input of P_m, the rotor angle is now δ_b corresponding to the operating point b on curve 2; with a higher reactance, the rotor angle is higher in order to transmit the same steady-state power.

During a disturbance, the oscillation of δ is superimposed on the synchronous speed ω_0, but the speed deviation ($\Delta\omega_r = d\delta/dt$) is very much smaller than ω_0. Therefore, the generator speed is practically equal to ω_0, and the per unit (pu) air-gap torque may be considered to be equal to the pu air-gap power. We will therefore use torque and power interchangeably when referring to the swing equation.

The *equation of motion* or the *swing equation* (see Chapter 3, Section 3.9) may be written as

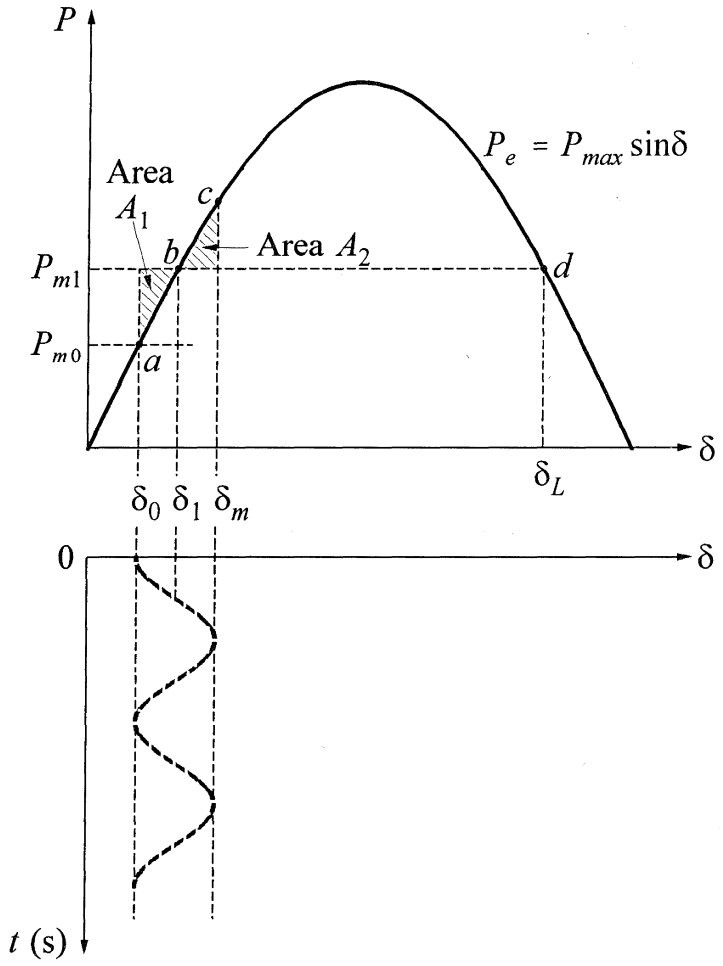
$$\frac{2H}{\omega_0}\frac{d^2\delta}{dt^2} = P_m - P_{max}\sin\delta \tag{13.3}$$

where

P_m = mechanical power input, in pu
P_{max} = maximum electrical power output, in pu
H = inertia constant, in MW·s/MVA
δ = rotor angle, in elec. rad
t = time, in s

Response to a step change in P_m

Let us now examine the transient behaviour of the system, with both circuits in service, by considering a sudden increase in the mechanical power input from an initial value of P_{m0} to P_{m1} as shown in Figure 13.4(a). Because of the inertia of the



(a) Power-angle variations

(b) Rotor angle time response

Figure 13.4 Response to a step change in mechanical power input

rotor, the rotor angle cannot change instantly from the initial value of δ_0 to δ_1 corresponding to the new equilibrium point b at which $P_e=P_{m1}$. The mechanical power is now in excess of the electrical power. The resulting accelerating torque causes the rotor to accelerate from the initial operating point a toward the new equilibrium point b, tracing the P_e-δ curve at a rate determined by the swing equation. The difference between P_{m1} and P_e at any instant represents the accelerating power.

When point b is reached, the accelerating power is zero, but the rotor speed is higher than the synchronous speed ω_0 (which corresponds to the frequency of the infinite bus voltage). Hence, the rotor angle continues to increase. For values of δ higher than δ_1, P_e is greater than P_{m1} and the rotor decelerates. At some peak value δ_m, the rotor speed recovers to the synchronous value ω_0, but P_e is higher than P_{m1}. The rotor continues to decelerate with the speed dropping below ω_0; the operating point retraces the P_e-δ curve from c to b and then to a. The rotor angle oscillates indefinitely about the new equilibrium angle δ_1 with a constant amplitude as shown by the time plot of δ in Figure 13.4(b).

In our representation of the power system in the above analysis, we have neglected all resistances and the classical model is used to represent the generator. In effect, this neglects all sources of damping. Therefore, the rotor oscillations continue unabated following the perturbation. In practice, as discussed in Chapter 12, there are many sources of positive damping including field flux variations and rotor amortisseur circuits. In a system which is small-signal stable, the oscillations damp out.

Equal-area criterion

For the system model considered above, it is not necessary to formally solve the swing equation to determine whether the rotor angle increases indefinitely or oscillates about an equilibrium position. Information regarding the maximum angle excursion (δ_m) and the stability limit may be obtained graphically by using the power-angle diagram shown in Figure 13.4. Although this method is not applicable to multimachine systems with detailed representation of synchronous machines, it helps in understanding basic factors that influence the transient stability of any system.

From Equation 13.3, we have the following relationship between the rotor angle and the accelerating power:

$$\frac{d^2\delta}{dt^2} = \frac{\omega_0}{2H}(P_m - P_e) \tag{13.4}$$

Now P_e is a nonlinear function of δ, and therefore the above equation cannot be solved directly. If both sides are multiplied by $2d\delta/dt$, then

$$2\frac{d\delta}{dt}\frac{d^2\delta}{dt^2} = \frac{\omega_0(P_m - P_e)}{H}\frac{d\delta}{dt}$$

or

$$\frac{d}{dt}\left[\frac{d\delta}{dt}\right]^2 = \frac{\omega_0(P_m - P_e)}{H}\frac{d\delta}{dt} \tag{13.5}$$

Integrating gives

$$\left[\frac{d\delta}{dt}\right]^2 = \int \frac{\omega_0(P_m - P_e)}{H} d\delta \tag{13.6}$$

The speed deviation $d\delta/dt$ is initially zero. It will change as a result of the disturbance. For stable operation, the deviation of angle δ must be bounded, reaching a maximum value (as at point c in Figure 13.4) and then changing direction. This requires the speed deviation $d\delta/dt$ to become zero at some time after the disturbance. Therefore, from Equation 13.6, as a criterion for stability we may write

$$\int_{\delta_0}^{\delta_m} \frac{\omega_0}{H}(P_m - P_e)d\delta = 0 \tag{13.7}$$

where δ_0 is the initial rotor angle and δ_m is the maximum rotor angle, as illustrated in Figure 13.4. Thus, the area under the function $P_m - P_e$ plotted against δ must be zero if the system is to be stable. In Figure 13.4, this is satisfied when area A_1 is equal to area A_2. Kinetic energy is gained by the rotor during acceleration when δ changes from δ_0 to δ_1. The energy gained is

$$E_1 = \int_{\delta_0}^{\delta_1} (P_m - P_e)d\delta = \text{area } A_1 \tag{13.8}$$

The energy lost during deceleration when δ changes from δ_1 to δ_m is

$$E_2 = \int_{\delta_1}^{\delta_m} (P_e - P_m)d\delta = \text{area } A_2 \tag{13.9}$$

As we have not considered any losses, the energy gained is equal to the energy lost; therefore, area A_1 is equal to area A_2. This forms the basis for the equal-area criterion. It enables us to determine the maximum swing of δ and hence the stability of the system without computing the time response through formal solution of the swing equation.

The criterion can be readily used to determine the maximum permissible increase in P_m for the system of Figure 13.1. The stability is maintained only if an area A_2 at least equal to A_1 can be located above P_{m1}. If A_1 is greater than A_2, then $\delta_m > \delta_L$, and stability will be lost. This is because, for $\delta > \delta_L$, P_{m1} is larger than P_e and the net torque is accelerating rather than decelerating.

We will examine the mechanism of transient instability by considering next the system response to a short-circuit fault on the transmission system, which is a more common form of a disturbance considered in transient stability studies.

Response to a short-circuit fault

Let us consider the response of the system to a three-phase fault at location F on transmission circuit 2, as shown in Figure 13.5(a). The corresponding equivalent circuit, assuming a classical generator model, is shown in Figure 13.5(b). The fault is cleared by opening circuit breakers at both ends of the faulted circuit, the fault-clearing time depending on the relaying time and breaker time (see Section 13.5.2).

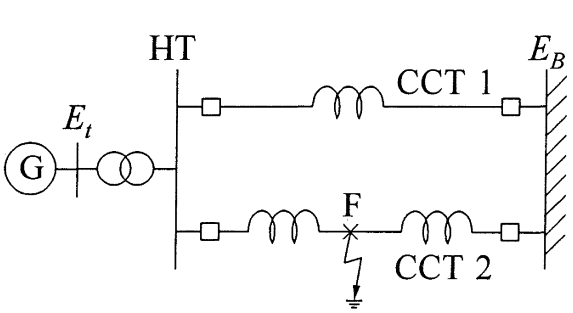
If the fault location F is at the sending end (HT bus) of the faulted circuit, no power is transmitted to the infinite bus. The short-circuit current from the generator flows through pure reactances to the fault. Hence, only reactive power flows and the active power P_e and the corresponding electrical torque T_e at the air-gap are zero during the fault. If we had included generator stator and transformer resistances in our model, P_e would have a small value, representing the corresponding resistive losses.

If the fault location F is at some distance away from the sending end as shown in Figures 13.5(a) and (b), some active power is transmitted to the infinite bus while the fault is still on.

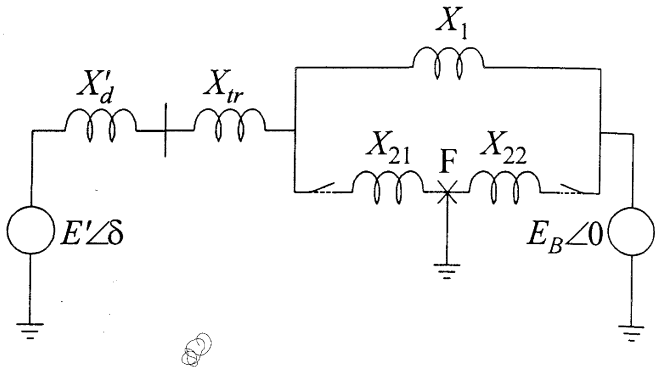
Figures 13.5(c) and (d) show P_e-δ plots for the three network conditions: (i) prefault (both circuits in service), (ii) with a three-phase fault on circuit 2 at a location some distance from the sending end, and (iii) postfault (circuit 2 out of service). Figure 13.5(c) considers the system performance with a fault-clearing time of t_{c1} and represents a stable case. Figure 13.5(d) considers a longer fault-clearing time (t_{c2}) such that the system is unstable. In both cases P_m is assumed to be constant.

Let us examine the stable case depicted by Figure 13.5(c). Initially, the system is operating with both circuits in service such that $P_e = P_m$ and $\delta = \delta_0$. When the fault occurs, the operating point suddenly changes from *a* to *b*. Owing to inertia, angle δ cannot change instantly. Since P_m is now greater than P_e, the rotor accelerates until the operating point reaches *c*, when the fault is cleared by isolating circuit 2 from the system. The operating point now suddenly shifts to *d*. Now P_e is greater than P_m, causing deceleration of the rotor. Since the rotor speed is greater than the synchronous speed ω_0, δ continues to increase until the kinetic energy gained during the period of acceleration (represented by area A_1) is expended by transferring the energy to the system. The operating point moves from *d* to *e*, such that area A_2 is equal to area A_1. At point *e*, the speed is equal to ω_0 and δ has reached its maximum value δ_m. Since P_e is still greater than P_m, the rotor continues to retard, with the speed dropping below ω_0. The rotor angle δ decreases, and the operating point retraces the path from *e* to

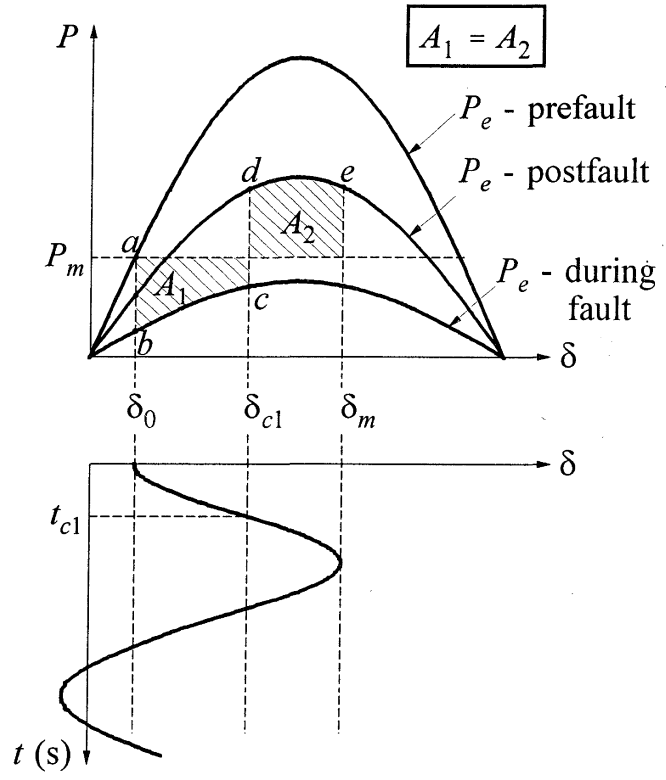
d and follows the P_e-δ curve for the postfault system farther down. The minimum value of δ is such that it satisfies the equal-area criterion for the postfault system. In the absence of any source of damping, the rotor continues to oscillate with constant amplitude.



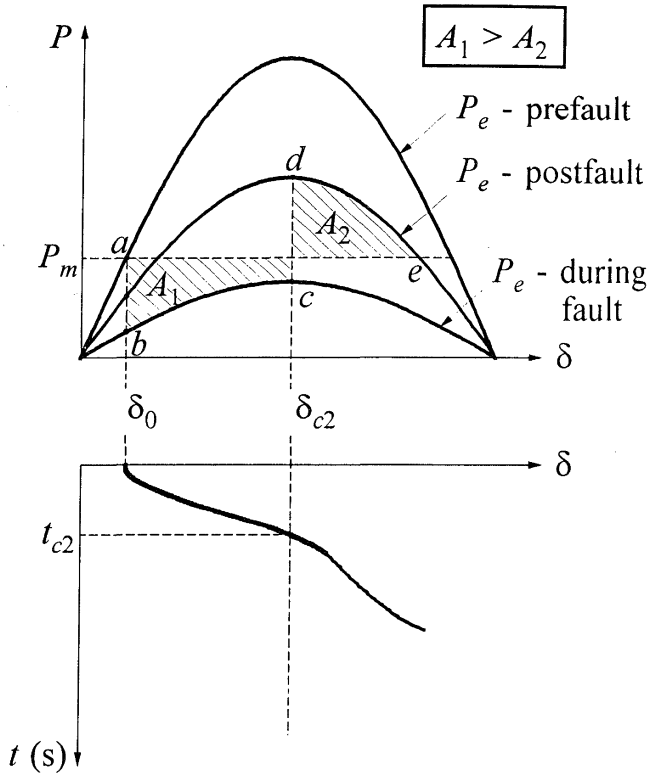
(a) Single-line diagram



(b) Equivalent circuit



(c) Response to a fault cleared in t_{c1} seconds - stable case



(d) Response to a fault cleared in t_{c2} seconds - unstable case

Figure 13.5 Illustration of transient stability phenomenon

With a delayed fault clearing, as shown in Figure 13.5(d), area A_2 above P_m is less than A_1. When the operating point reaches e, the kinetic energy gained during the accelerating period has not yet been completely expended; consequently, the speed is still greater than ω_0 and δ continues to increase. Beyond point e, P_e is less than P_m, and the rotor begins to accelerate again. The rotor speed and angle continue to increase, leading to *loss of synchronism*.

Factors influencing transient stability

From the above discussions, and referring to Figure 13.5, we can conclude that transient stability of the generator is dependent on the following:

(a) How heavily the generator is loaded.

(b) The generator output during the fault. This depends on the fault location and type.

(c) The fault-clearing time.

(d) The postfault transmission system reactance.

(e) The generator reactance. A lower reactance increases peak power and reduces initial rotor angle.

(f) The generator inertia. The higher the inertia, the slower the rate of change in angle. This reduces the kinetic energy gained during fault; i.e., area A_1 is reduced.

(g) The generator internal voltage magnitude (E'). This depends on the field excitation.

(h) The infinite bus voltage magnitude E_B.

As a means of introducing basic concepts, we have considered a system having a simple configuration and represented by a simple model. This has enabled the analysis of stability by using a graphical approach. Although rotor angle plots as a function of time are shown in Figures 13.4 and 13.5, we have not actually computed them, and hence the time scales have not been defined for these plots. Practical power systems have complex network structures. Accurate analysis of their transient stability requires detailed models for generating units and other equipment. *At present, the most practical available method of transient stability analysis is time-domain simulation in which the nonlinear differential equations are solved by using step-by-step numerical integration techniques.* This leads us to the next section in which some of the commonly used numerical integration methods are described.

13.2 NUMERICAL INTEGRATION METHODS [4-6]

The differential equations to be solved in power system stability analysis are nonlinear ordinary differential equations with known initial values:

$$\frac{d\mathbf{x}}{dt} = \mathbf{f}(\mathbf{x},t) \tag{13.10A}$$

where $\mathbf{x}$ is the state vector of n dependent variables and t is the independent variable (time). Our objective is to solve $\mathbf{x}$ as a function of t, with the initial values of $\mathbf{x}$ and t equal to $\mathbf{x}_0$ and t_0, respectively.

In this section we provide a general description of numerical integration methods applicable to the solution of equations of the above form. In describing these methods, without loss of generality, we will treat Equation 13.10A as if it were a first-order differential equation. This simplifies presentation and makes it easier for a novice reader to comprehend the special features of each method.

We will first describe the Euler method, which by virtue of its simplicity serves as a good introduction to numerical integration, and then we discuss more advanced methods.

13.2.1 Euler Method

Consider the first-order differential equation

$$\frac{dx}{dt} = f(x,t) \tag{13.10B}$$

with $x=x_0$ at $t=t_0$. Figure 13.6 illustrates the principle of applying the Euler method.

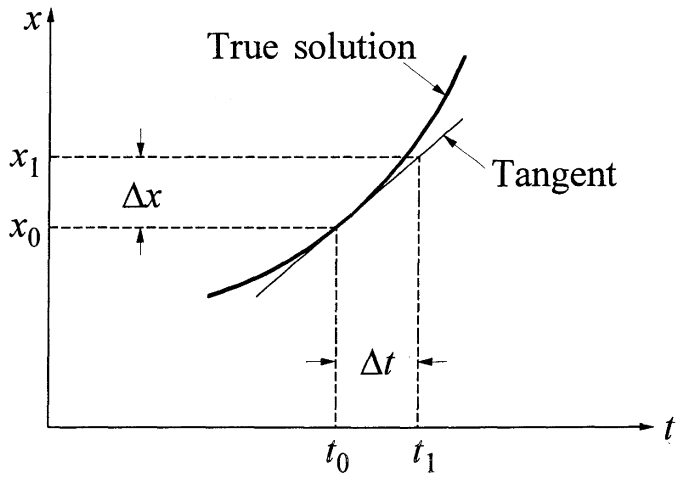


Figure 13.6

At $x=x_0$, $t=t_0$ we can approximate the curve representing the true solution by its tangent having a slope

$$\left.\frac{dx}{dt}\right|_{x=x_0} = f(x_0,t_0)$$

Therefore,

$$\Delta x = \left.\frac{dx}{dt}\right|_{x=x_0} \cdot \Delta t$$

The value of x at $t=t_1=t_0+\Delta t$ is given by

$$x_1 = x_0+\Delta x = x_0+\left.\frac{dx}{dt}\right|_{x=x_0} \cdot \Delta t \tag{13.11}$$

The Euler method is equivalent to using the first two terms of the Taylor series expansion for x around the point (x_0,t_0):

$$x_1 = x_0+\Delta t(\dot{x}_0)+\frac{\Delta t^2}{2!}(\ddot{x}_0)+\frac{\Delta t^3}{3!}(\dddot{x}_0)+\cdots \tag{13.12}$$

After using the Euler technique for determining $x=x_1$ corresponding to $t=t_1$, we can take another short time step Δt and determine x_2 corresponding to $t_2=t_1+\Delta t$ as follows:

$$x_2 = x_1+\left.\frac{dx}{dt}\right|_{x=x_1} \cdot \Delta t \tag{13.13}$$

By applying the technique successively, values of x can be determined corresponding to different values of t.

The method considers only the first derivative of x and is, therefore, referred to as a *first-order* method. To give sufficient accuracy for each step, Δt has to be small. This will increase round-off errors, and the computational effort required will be very high.

In the application of numerical integration methods, it is very important to consider the *propagation of error*, which may cause slight errors made early in the process to be magnified at later steps. *Numerical stability* depends on the propagation of error. If early errors carry through but cause no significant further errors later, the method is said to be numerically stable. If, on the other hand, early errors cause other large errors later, the method is said to be numerically unstable.

13.2.2 Modified Euler Method

The standard Euler method results in inaccuracies because it uses the derivative at the beginning of the interval as though it applied throughout the interval. The modified Euler method tries to overcome this problem by using the average of the derivatives at the two ends.

The modified Euler method consists of the following steps:

(a) *Predictor step.* By using the derivative at the beginning of the step, the value at the end of the step is *predicted*

$$x_1^p = x_0 + \left.\frac{dx}{dt}\right|_{x=x_0} \cdot \Delta t \tag{13.14}$$

(b) *Corrector step.* By using the predicted value of x_1^p, the derivative at the end of the step is computed and the average of this derivative and the derivative at the beginning of the step is used to find the *corrected value*

$$x_1^c = x_0 + \frac{1}{2}\left(\left.\frac{dx}{dt}\right|_{x=x_0} + \left.\frac{dx}{dt}\right|_{x=x_1^p} \right) \Delta t \tag{13.15}$$

If desired, a more accurate value of the derivative at the end of the step can be calculated, again by using $x=x_1^c$. This derivative can be used to calculate a more accurate value of the average derivative which is in turn used to apply the corrector step again. This process can be used repeatedly until successive steps converge with the desired accuracy.

The modified Euler method is the simplest of *predictor-corrector* (P-C) methods. Among the well known higher order P-C methods are the Adams-Bashforth method, Milne method, and Hamming method [4]. The applicability of these methods to power system stability analysis has been investigated in reference 7 and has been found to suffer from a number of limitations. They are not self-starting, need more computer storage and require smaller time steps than the Runge-Kutta methods described below.

13.2.3 Runge-Kutta (R-K) Methods [4,5]

The R-K methods approximate the Taylor series solution; however, unlike the formal Taylor series solution, the R-K methods do not require explicit evaluation of derivatives higher than the first. The effects of higher derivatives are included by several evaluations of the first derivative. Depending on the number of terms effectively retained in the Taylor series, we have R-K methods of different orders.

Second-order R-K method

Referring to the differential equation 13.10B, the second-order R-K formula for the value of x at $t=t_0+\Delta t$ is

$$x_1 = x_0+\Delta x = x_0+\frac{k_1+k_2}{2}$$

where

$$k_1 = f(x_0,t_0)\Delta t$$

$$k_2 = f(x_0+k_1,t_0+\Delta t)\Delta t$$

This method is equivalent to considering first and second derivative terms in the Taylor series; error is on the order of Δt^3.

A general formula giving the value of x for the $(n+1)^{st}$ step is

$$x_{n+1} = x_n+\frac{k_1+k_2}{2}$$

where

$$k_1 = f(x_n,t_n)\Delta t$$

$$k_2 = f(x_n+k_1,t_n+\Delta t)\Delta t$$

Fourth-order R-K method

The general formula giving the value of x for the $(n+1)^{st}$ step is

$$x_{n+1} = x_n+\frac{1}{6}(k_1+2k_2+2k_3+k_4) \tag{13.16}$$

where

$$k_1 = f(x_n,t_n)\Delta t$$

$$k_2 = f\left(x_n+\frac{k_1}{2},t_n+\frac{\Delta t}{2}\right)\Delta t$$

$$k_3 = f\left(x_n+\frac{k_2}{2},t_n+\frac{\Delta t}{2}\right)\Delta t$$

$$k_4 = f(x_n+k_3,t_n+\Delta t)\Delta t$$

The physical interpretation of the above solution is as follows:

k_1 = (slope at the beginning of time step)Δt
k_2 = (first approximation to slope at midstep)Δt
k_3 = (second approximation to slope at midstep)Δt
k_4 = (slope at the end of step)Δt
$\Delta x = 1/6\,(k_1+2k_2+2k_3+k_4)$

Thus Δx is the incremental value of x given by the *weighted average* of estimates based on slopes at the beginning, midpoint, and end of the time step.

This method is equivalent to considering up to fourth derivative terms in the Taylor series expansion; it has an error on the order of Δt^5.

Gill's version of fourth order R-K method (R-K-G)

With x_0 as the initial value of x at the beginning of a step and by using j=1,2,3 and 4 to denote four stages, each stage of the Gill method can be described as follows [4]:

$$\begin{aligned} k_j &= a_j[f(x_{j-1},t)-b_j q_{j-1}] \\ x_j &= x_{j-1}+k_j\Delta t \\ q_j &= q_{j-1}+3k_j-c_j f(x_{j-1},t) \end{aligned} \tag{13.17}$$

The values of the *a, b,* and *c* coefficients are as follows:

$$a_1 = 1/2, \quad b_1 = 2, \quad c_1 = a_1; \quad a_2 = 1-\sqrt{0.5}, \quad b_2 = 1, \quad c_2 = a_2$$
$$a_3 = 1+\sqrt{0.5}, \quad b_3 = 1, \quad c_3 = a_3; \quad a_4 = 1/6, \quad b_4 = 2, \quad c_4 = 1/2$$

Solution at the end of a time step is given by x_4. Initially q_0=0, thereafter in advancing the solution, q_0 for the next step is equal to q_4 of the previous step.

The following are the advantages of Gill's version of the R-K method:

(a) Roundoff errors are minimized (variable q is used for this purpose).

(b) Storage requirements are less than for the original R-K method.

Care should be exercised in applying the R-K-G method when discontinuities or sudden changes in the rate of change of variables occur. Within a time step, a variable should not be limited, as a result of sharp nonlinearities; otherwise the variable q takes on incorrect values.

Richardson's formula for accuracy check

The accuracy of results obtained with the above numerical integration methods may be checked by using Richardson's formula which gives the accumulated truncation error *propagated* in the course of integration. The difference between the true value of a variable and the value obtained by a fourth-order Runge-Kutta method using a step length of Δt is given by [4,7]

$$x(\text{true}) - x(\Delta t) = \frac{x(\Delta t) - x(2\Delta t)}{15} \tag{13.18}$$

where

$x(\text{true})$ = true value of x
$x(\Delta t)$ = value computed with a step length of Δt
$x(2\Delta t)$ = value computed with a step length of $2\Delta t$

13.2.4 Numerical Stability of Explicit Integration Methods

Integration methods described in Sections 13.2.1 to 13.2.3 (i.e., the Euler, predictor-corrector, and R-K methods) are known as *explicit methods*. In these methods the value of the dependent variable $\mathbf{x}$ at any value of t is computed from knowledge of the values of $\mathbf{x}$ from the previous time steps. In other words, $\mathbf{x}_{n+1}$ for $(n+1)^{st}$ step is calculated explicitly by evaluating $\mathbf{f}(\mathbf{x},t)$ with known $\mathbf{x}$. These methods are easy to implement for the solution of a complex set of system state equations.

A significant limitation of the explicit integration methods is that they are not numerically A-stable [6]. Consequently, the length of the integration time step (Δt) is restricted by the small time constants of the system.

Numerical stability is related to the *stiffness* of the set of differential equations representing the system. The stiffness is associated with the range of time constants in the system model. It is measured by the ratio of the largest to smallest time constant, or more precisely by the ratio of the largest to smallest eigenvalues of the linearized system.

Stiffness in a transient stability simulation increases with modelling detail. In the overall system, not all the time constants may be readily apparent. Thus the stiffness may be hidden and can only be established by computing the eigenvalues of the linearized system.

Explicit integration methods have weak stability numerically; with stiff systems, the solution "blows up" unless a small step size is used. Even after the fast modes die out, small time steps continue to be required to maintain numerical stability.

13.2.5 Implicit Integration Methods

Consider the differential equation

$$\frac{dx}{dt} = f(x,t) \qquad \text{with } x=x_0 \text{ at } t=t_0$$

The solution for x at $t=t_1=t_0+\Delta t$ may be expressed in integral form as

$$x_1 = x_0 + \int_{t_0}^{t_1} f(x,\tau)\,d\tau \tag{13.19}$$

Implicit integration methods use interpolation functions for the expression under the integral. Interpolation implies that the functions must pass through the yet unknown points at time t_1.

The simplest implicit integration method is the *trapezoidal rule*. It uses linear interpolation. As shown in Figure 13.7, this implies that the area under the integral of Equation 13.19 is approximated by trapezoids; hence the name - trapezoidal rule.

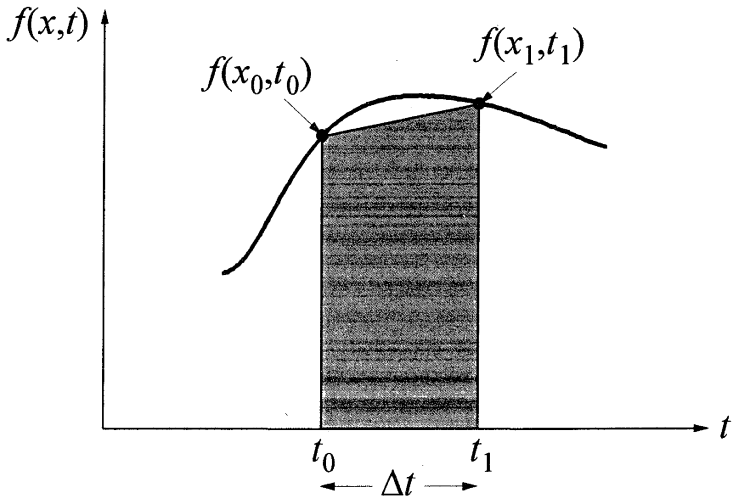


Figure 13.7

The trapezoidal rule for Equation 13.19 is given by

$$x_1 = x_0 + \frac{\Delta t}{2}[f(x_0,t_0)+f(x_1,t_1)] \tag{13.20}$$

A general formula giving the value of x at $t=t_{n+1}$ is

$$x_{n+1} = x_n + \frac{\Delta t}{2}[f(x_n, t_n) + f(x_{n+1}, t_{n+1})] \tag{13.21}$$

We see that x_{n+1} appears on both sides of Equation 13.21. This implies that the variable x is computed as a function of its value at the previous time step as well as the current value (which is unknown). Therefore, an implicit equation must be solved.

The trapezoidal rule is numerically A-stable [6]. The stiffness of the system being analyzed affects accuracy but not numerical stability. With larger time steps, high frequency modes and fast transients are filtered out, and the solutions for the slower modes is accurate. For systems involving simulations in which time steps are limited by numerical stability considerations rather than accuracy, implicit methods are generally better suited than explicit methods.

The trapezoidal rule is a second-order method. Implicit integration methods of higher order have been proposed in the literature on numerical methods. However, they have not been widely used for power system applications since they are more difficult to program and less numerically stable than the trapezoidal rule.

In the above description of different numerical integration methods, for simplicity we have considered a first-order differential equation. When applied to the analysis of power system stability, the system equations are organized as a set of first-order differential equations. The rate of change of each state variable depends on other state variables and is not an explicit function of time t. The following example serves as a simple illustration of the application of numerical integration as well as the equal-area criterion for transient stability analysis.

Example 13.1

In this example, we examine the transient stability of a thermal generating station consisting of four 555 MVA, 24 kV, 60 Hz units supplying power to an infinite bus through two transmission circuits as shown in Figure E13.1. This system is the same as the one considered in Example 12.2 of Chapter 12 in which we examined the small-signal performance.

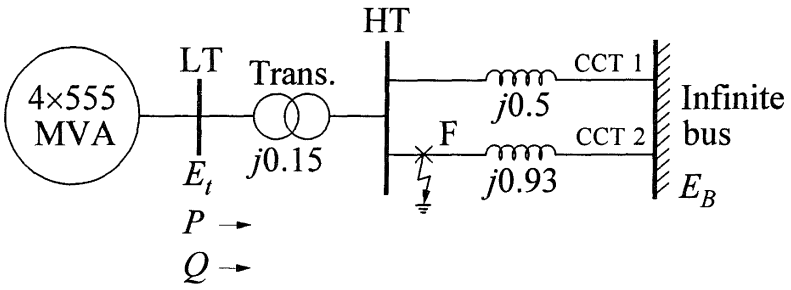


Figure E13.1

The network reactances shown in the figure are in per unit on 2220 MVA, 24 kV base (referred to the LT side of the step-up transformer). Resistances are assumed to be negligible.

The initial system-operating condition, with quantities expressed in per unit on 2220 MVA and 24 kV base, is as follows:

$$P=0.9 \qquad Q=0.436 \text{ (overexcited)} \qquad \tilde{E}_t=1.0\angle 28.34^\circ \qquad \tilde{E}_B=0.90081\angle 0$$

The generators are modelled as a single equivalent generator represented by the classical model with the following parameters expressed in per unit on 2220 MVA, 24 kV base:

$$X'_d=0.3 \qquad H=3.5 \text{ MW·s/MVA} \qquad K_D=0$$

Circuit 2 experiences a solid three-phase fault at point F, and the fault is cleared by isolating the faulted circuit.

(a) Determine the critical fault-clearing time and the critical clearing angle by computing the time response of the rotor angle, using numerical integration.

(b) Check the above value of critical clearing angle, using the equal-area criterion.

Solution

With the generator represented by the classical model, the system-equivalent circuit is as shown in Figure E13.2.

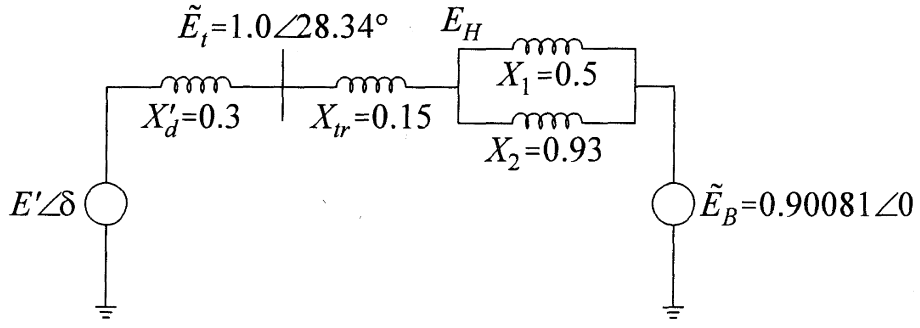


Figure E13.2 Equivalent circuit

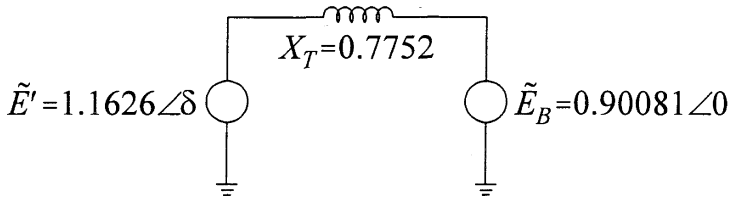
For the initial operating condition, the voltage behind X'_d is

$$\tilde{E}' = \tilde{E}_t + jX'_d\tilde{I}_t$$

$$= 1.0\angle 28.34^\circ + \frac{j0.3(0.9-j0.436)}{1.0\angle -28.34^\circ}$$

$$= 1.1626\angle 41.77^\circ$$

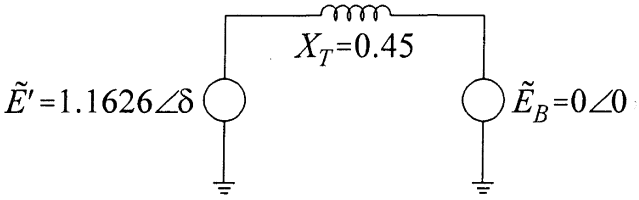
Figure E13.3 shows the reduced equivalent circuits representing the three system conditions: (i) prefault, (ii) during fault, and (iii) postfault. Also shown in the figure are the corresponding expressions for the electrical power output as a function of δ.



$$P_e = \frac{1.1626 \times 0.90081}{0.7752} \sin\delta$$

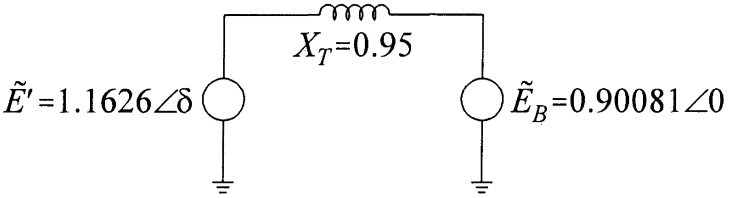
$$= 1.351 \sin\delta$$

(a) Prefault



$$P_e = 0$$

(b) During fault



$$P_e = \frac{1.1626 \times 0.90081}{0.95} \sin\delta$$

$$= 1.1024 \sin\delta$$

(c) Postfault

Figure E13.3 Reduced equivalent circuits and equations for power output

(a) Time response using numerical integration:

Equation 13.3 may be written in terms of the two first-order equations:

$$p(\Delta\omega_r) = \frac{1}{2H}(P_m - P_{max}\sin\delta)$$

$$= \frac{1}{7.0}(0.9 - P_{max}\sin\delta) \qquad \text{(E13.1)}$$

$$p(\delta) = \omega_0 \Delta\omega_r$$

$$= 377\,\Delta\omega_r \qquad \text{(E13.2)}$$

where

$$P_{max} = \begin{cases} 1.351 & \text{before the fault} \\ 0 & \text{during the fault} \\ 1.1024 & \text{after the fault} \end{cases}$$

The initial values of δ and $\Delta\omega_r$ are 41.77° and 0 pu, respectively.

Any of the numerical integration methods described in Section 13.2 may be used to solve Equations E13.1 and E13.2. For illustration, let us consider the second-order R-K method. The general formulas giving the values of $\Delta\omega_r$, δ, and t for the $(n+1)^{st}$ step of integration are as follows:

$$(\Delta\omega_r)_{n+1} = (\Delta\omega_r)_n + \frac{k_1' + k_2'}{2}$$

$$\delta_{n+1} = \delta_n + \frac{k_1'' + k_2''}{2}$$

$$t_{n+1} = t_n + \Delta t$$

where

$$k_1' = \left[0.1286 - \frac{P_{max}}{7.0}\sin(\delta)_n\right]\Delta t$$

$$k_1'' = [377(\Delta\omega_r)_n]\Delta t$$

$$k_2' = \left[0.1286 - \frac{P_{max}}{7.0}\sin(\delta_n + k_1'')\right]\Delta t$$

$$k_2'' = \{377[(\Delta\omega_r)_n + k_1']\}\,\Delta t$$

Figure E13.4 shows plots of δ as a function of time, for the three values of fault-clearing time (t_c): 0.07 s, 0.086 s, and 0.087 s. The corresponding values of clearing angle (δ_c) are 48.58°, 52.04°, and 52.30°, respectively. These results were computed using a time step (Δt) of 0.05 s throughout the solution. The time step was, however, adjusted near the fault-clearing time so as to give the exact switching instant.

From the results, we see that the system is stable with t_c=0.086 s (δ_c=52.04°), and is unstable with t_c=0.087 s (δ_c=52.30°); the critical clearing time is, therefore, 0.0865±0.0005 s, and the critical clearing angle is 52.17°±0.13°.

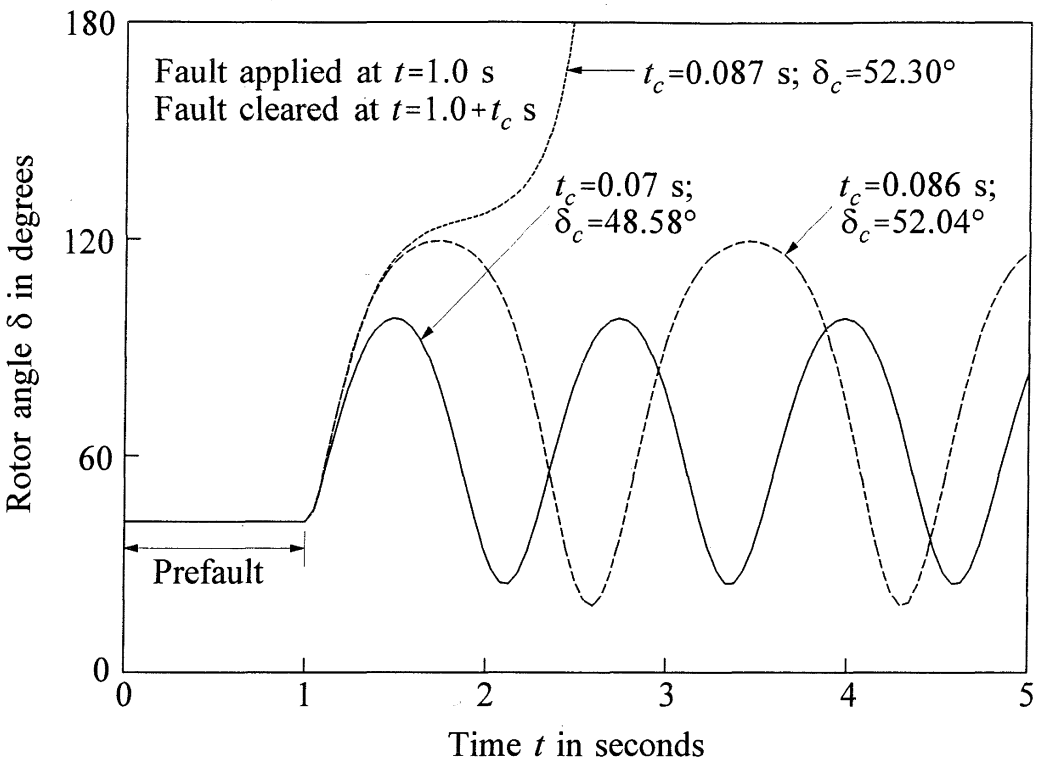


Figure E13.4 Rotor angle response for different values of fault-clearing time

(b) Equal-area criterion:

The power-angle diagrams for the three network conditions are shown in Figure E13.5. For the critically stable case, the maximum swing in δ is given by

$$1.1024\sin\delta_m = 0.9 \qquad \text{hence,} \quad \delta_m = 125.27°$$

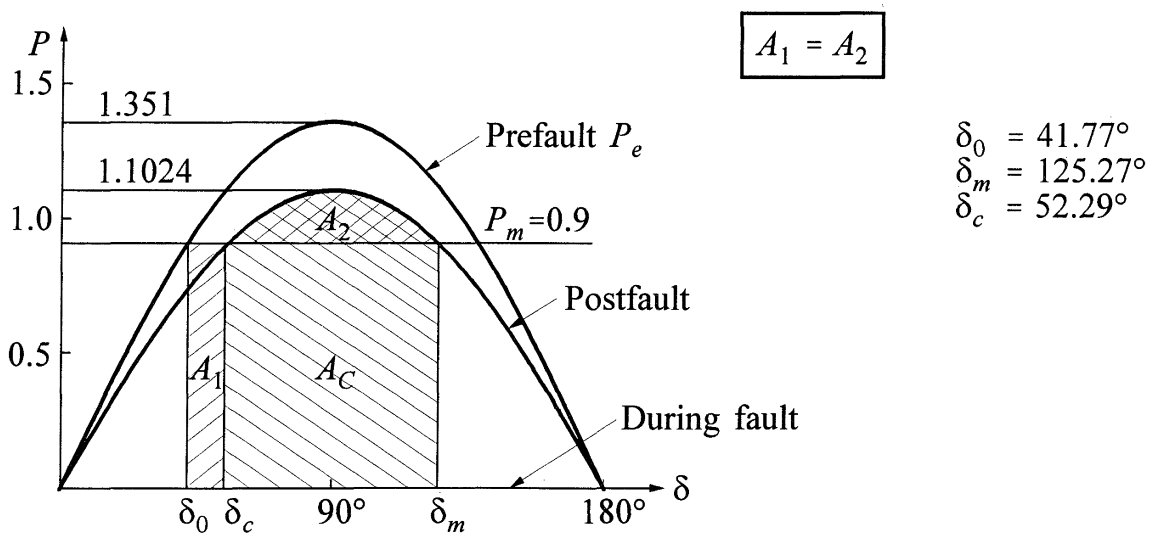


Figure E13.5 Power-angle diagram

From Figure E13.5, for critical clearing,

$$A_1 = A_2$$

or

$$A_1 + A_c = A_2 + A_c$$

Therefore, from the plots, we have

$$0.9(125.27 - 41.77)\frac{\pi}{180} = \int_{\delta_c}^{125.27} 1.1024 \sin\delta \, d\delta$$

$$1.3116 = 1.1024(\cos\delta_c + 0.5781)$$

Thus the critical clearing angle is

$$\delta_c = 52.29°$$

This agrees with the value determined from time responses. ■

13.3 SIMULATION OF POWER SYSTEM DYNAMIC RESPONSE

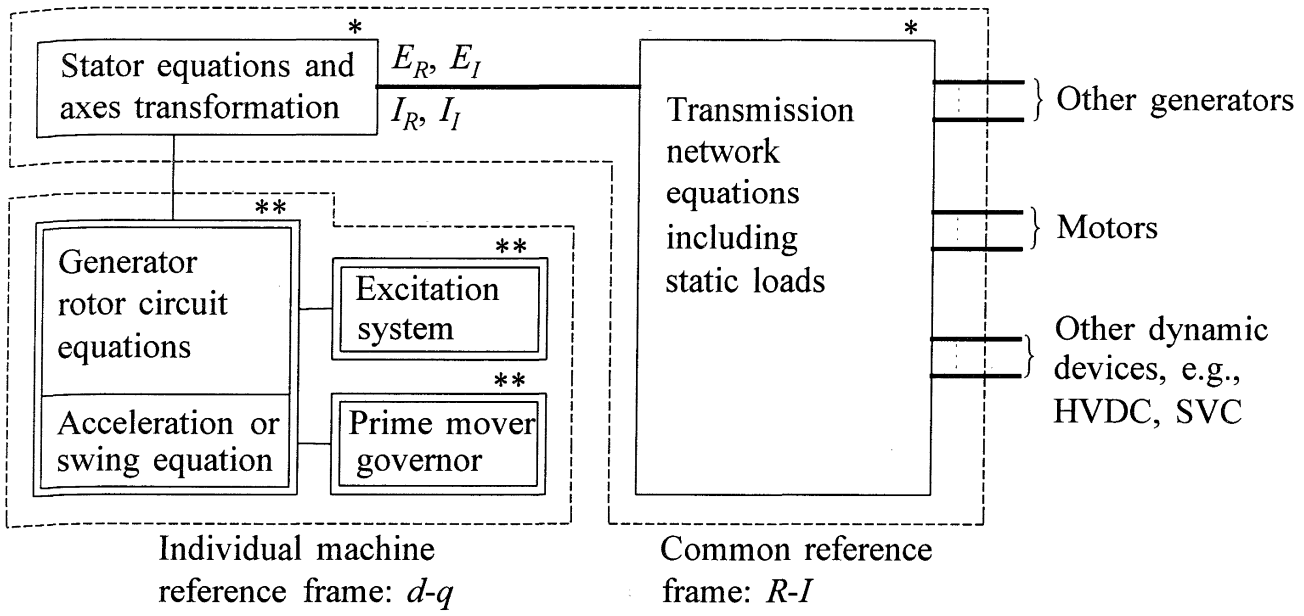
13.3.1 Structure of the Power System Model

Analysis of transient stability of power systems involves the computation of their nonlinear dynamic response to large disturbances, usually a transmission network fault, followed by the isolation of the faulted element by protective relaying.

Figure 13.8 depicts the general structure of the power system model applicable to transient stability analysis. This model structure is similar to that presented in Chapter 12 (Figure 12.18) for small-signal stability analysis. However, for transient stability analysis, nonlinear system equations are solved. In addition, large discontinuities due to faults and network switching, and small discontinuities due to limits on system variables, appear in the system model. Bus voltages, line flows, and performance of protection systems are of interest, in addition to the basic information related to the stability of the system.

As seen in Figure 13.8, the overall power system representation includes models for the following individual components:

- Synchronous generators, and the associated excitation systems and prime movers
- Interconnecting transmission network including static loads



* Algebraic equations
** Differential equations

Figure 13.8 Structure of the complete power system model for transient stability analysis

- Induction and synchronous motor loads
- Other devices such as HVDC converters and SVCs

The model used for each component should be appropriate for transient stability analysis, and the system equations must be organized in a form suitable for applying numerical methods.

As we will see in what follows, the complete system model consists of a large set of ordinary differential equations and large sparse algebraic equations. The transient stability analysis is thus a differential algebraic initial-value problem.

13.3.2 Synchronous Machine Representation [8]

Synchronous machine modelling is presented in Chapters 3 to 5. The per unit synchronous machine equations are summarized in Section 3.4.9. Modifications of these equations necessary for representation in stability studies are discussed in Section 5.1.

To illustrate the implementation of the generator model for transient stability analysis, we assume that the generator is represented by a model with one d-axis and two q-axis amortisseurs as shown in Figure 13.9. However, the equations presented here can be readily modified to account for a model with an arbitrary number of amortisseurs.

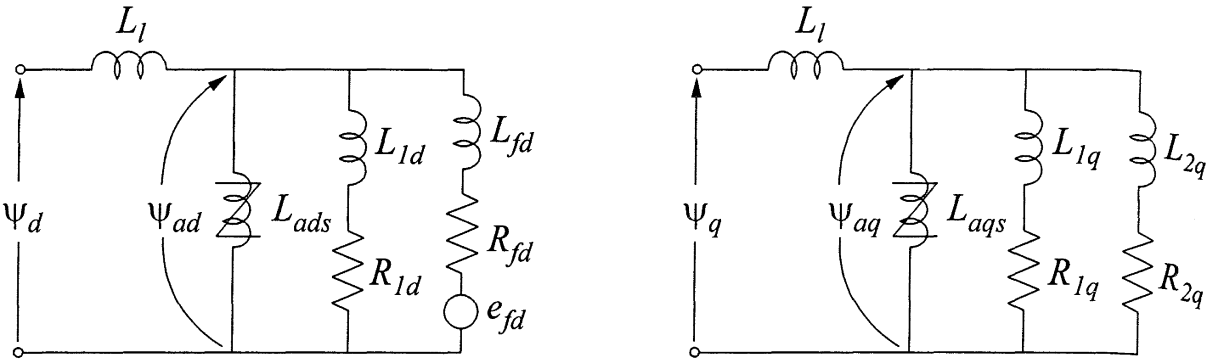


Figure 13.9 Synchronous machine equivalent circuits

The following is a summary of the synchronous machine equations as a set of first order differential equations, with time t in seconds, rotor angle δ in electrical radians, and all other quantities in per unit.

Equations of motion

$$\begin{aligned} p\Delta\omega_r &= \frac{1}{2H}(T_m - T_e - K_D\Delta\omega_r) \\ p\delta &= \omega_0\Delta\omega_r \end{aligned} \tag{13.22}$$

where

ω_0 = $2\pi f_0$ electrical rad/s
$\Delta\omega_r$ = pu rotor speed deviation
p = derivative operator d/dt

Rotor circuit equations

With rotor currents expressed in terms of rotor and mutual flux linkages (see Equation 12.159 of Chapter 12), the rotor circuit dynamic equations are

$$\begin{aligned} p\psi_{fd} &= \omega_0\left[e_{fd} + \frac{(\psi_{ad} - \psi_{fd})R_{fd}}{L_{fd}}\right] \\ p\psi_{1d} &= \omega_0\left(\frac{\psi_{ad} - \psi_{1d}}{L_{1d}}\right)R_{1d} \\ p\psi_{1q} &= \omega_0\left(\frac{\psi_{aq} - \psi_{1q}}{L_{1q}}\right)R_{1q} \\ p\psi_{2q} &= \omega_0\left(\frac{\psi_{aq} - \psi_{2q}}{L_{2q}}\right)R_{2q} \end{aligned} \tag{13.23}$$

The d- and q-axis mutual flux linkages are given by

$$\begin{aligned}\psi_{ad} &= -L_{ads}i_d + L_{ads}i_{fd} + L_{ads}i_{1d} \\ &= L''_{ads}\left(-i_d + \frac{\psi_{fd}}{L_{fd}} + \frac{\psi_{1d}}{L_{1d}}\right)\end{aligned} \tag{13.24}$$

$$\psi_{aq} = L''_{aqs}\left(-i_q + \frac{\psi_{1q}}{L_{1q}} + \frac{\psi_{2q}}{L_{2q}}\right) \tag{13.25}$$

where

$$\begin{aligned}L''_{ads} &= \frac{1}{\frac{1}{L_{ads}} + \frac{1}{L_{fd}} + \frac{1}{L_{1d}}} \\ L''_{aqs} &= \frac{1}{\frac{1}{L_{aqs}} + \frac{1}{L_{1q}} + \frac{1}{L_{2q}}}\end{aligned} \tag{13.26}$$

Here L_{ads} and L_{aqs} are saturated values of the d- and q-axis mutual inductances given by

$$\begin{aligned}L_{ads} &= K_{sd}L_{adu} \\ L_{aqs} &= K_{sq}L_{aqu}\end{aligned} \tag{13.27}$$

and K_{sd} and K_{sq} are computed as a function of the air-gap flux linkage ψ_{at} as described in Chapter 3 (Section 3.8.2).

Stator voltage equations

With stator transients ($p\psi_d$, $p\psi_q$) and speed variations (ω/ω_0) neglected as discussed in Chapter 5 (Section 5.1), the stator voltage may be written as follows:

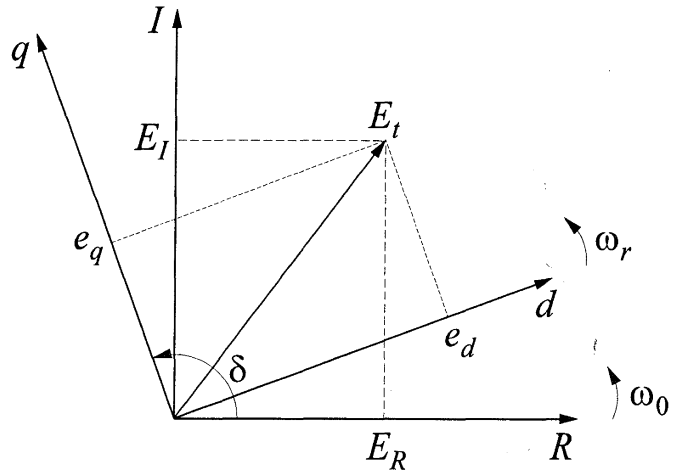
$$\begin{aligned}e_d &= -R_a i_d + (\bar{\omega}L''_q)i_q + E''_d \\ e_q &= -R_a i_q - (\bar{\omega}L''_d)i_d + E''_q\end{aligned} \tag{13.28}$$

with

$$E''_d = -\bar{\omega}L''_{aqs}\left(\frac{\psi_{1q}}{L_{1q}} + \frac{\psi_{2q}}{L_{2q}}\right)$$
$$E''_q = \bar{\omega}L''_{ads}\left(\frac{\psi_{fd}}{L_{fd}} + \frac{\psi_{1d}}{L_{1d}}\right) \tag{13.29}$$

$$L''_d = L_l + L''_{ads}$$
$$L''_q = L_l + L''_{aqs} \tag{13.30}$$

Since we have neglected the effect of speed variations on the stator voltage, $\bar{\omega} = \omega/\omega_0 = 1.0$ in the above equations. Consequently, $\bar{\omega}L''_d = X''_d$ and $\bar{\omega}L''_q = X''_q$. The above equations are in the individual machine *d-q* reference frame which rotates with the machine's rotor. For the solution of the interconnecting transmission network equations, a synchronously rotating common *R-I* reference is used. The relationships shown in Figure 13.10 are used to transform variables from one reference frame to the other. The *R*-axis of the common reference frame also serves as the reference for measuring the rotor angle δ of each machine.



$$e_d = E_R\sin\delta - E_I\cos\delta$$
$$e_q = E_I\sin\delta + E_R\cos\delta$$
$$E_R = e_d\sin\delta + e_q\cos\delta \tag{13.31}$$
$$E_I = e_q\sin\delta - e_d\cos\delta$$

Figure 13.10 Reference frame transformation and definition of rotor angle δ

For convenience in the organization of the complete set of algebraic equations, the stator voltage equations are expressed in the common *R-I* reference frame as indicated in Figure 13.8. Use of Equations 13.31 to transform the stator voltage equations 13.28 yields

$$\begin{bmatrix} E_R \\ E_I \end{bmatrix} = \begin{bmatrix} -R_{RR} & X_{RI} \\ -X_{IR} & -R_{II} \end{bmatrix} \begin{bmatrix} I_R \\ I_I \end{bmatrix} + \begin{bmatrix} E''_R \\ E''_I \end{bmatrix} \tag{13.32}$$

The elements of the impedance matrix are given by

$$\begin{aligned} R_{RR} &= (X''_d - X''_q)\sin\delta\cos\delta + R_a \\ R_{II} &= (X''_q - X''_d)\sin\delta\cos\delta + R_a \\ X_{RI} &= X''_d\cos^2\delta + X''_q\sin^2\delta \\ X_{IR} &= X''_d\sin^2\delta + X''_q\cos^2\delta \end{aligned} \tag{13.33}$$

As noted earlier, $\bar{\omega}$ is assumed to be equal to 1.0 pu. The internal voltage components are given by

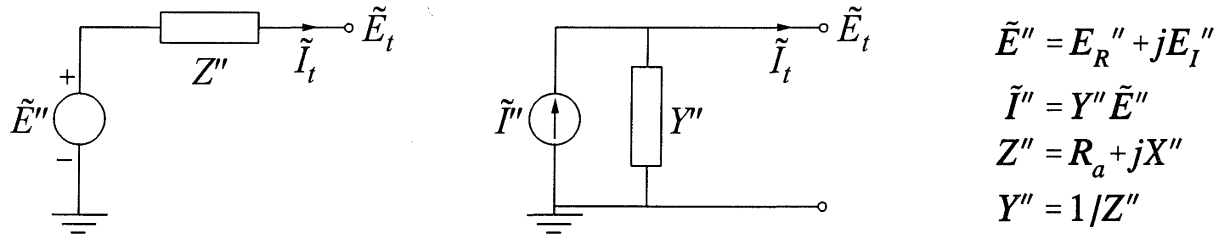
$$\begin{aligned} E''_R &= E''_d\sin\delta + E''_q\cos\delta \\ E''_I &= E''_q\sin\delta - E''_d\cos\delta \end{aligned} \tag{13.34}$$

If *subtransient saliency is negligible*, $L''_d = L''_q$. Then

$$R_{RR} = R_{II} = R_a$$

$$X_{RI} = X_{IR} = \bar{\omega}L''_d = X''_d = X''_q = X''$$

In this case, $E''_R + jE''_I$ represents the voltage behind the subtransient impedance $R_a + jX''$. For network solution, the generator may be represented by either of the simple equivalent circuits shown in Figure 13.11.



(a) Thevenin's equivalent (b) Norton's equivalent

Figure 13.11 Synchronous machine equivalent circuits with negligible subtransient saliency

Variations in L_{ads} and L_{aqs} due to saturation may introduce a small amount of subtransient saliency during a transient condition. This is usually insignificant and may be ignored, if it is desired to take advantage of the computational simplicity offered by the above equivalent circuits.

Active power and reactive power at the generator stator terminals are

$$P_t = e_d i_d + e_q i_q \tag{13.35}$$

$$Q_t = e_q i_d - e_d i_q \tag{13.36}$$

The air-gap torque required for the solution of the swing equation (13.22) is

$$\begin{aligned} T_e &= \psi_d i_q - \psi_q i_d \\ &= \psi_{ad} i_q - \psi_{aq} i_d \end{aligned} \tag{13.37A}$$

Since we have assumed $\bar{\omega} = \omega/\omega_0 = 1.0$ pu in the stator voltage equations, in per unit the air-gap torque is equal to the air-gap power (see Chapter 5, Section 5.1.2). Hence,

$$T_e = P_e = P_t + R_a I_t^2 \tag{13.37B}$$

The field current in the reciprocal per unit system is given by

$$i_{fd} = \frac{\psi_{fd} - \psi_{ad}}{L_{fd}} \tag{13.38}$$

The per unit exciter output current I_{fd} (see Chapter 8, Section 8.6) is

$$I_{fd} = L_{adu} i_{fd} \tag{13.39}$$

Here we have considered a generator model with one d-axis and two q-axis amortisseur circuits. For models with a different number of rotor circuits, changes to the above formulation of machine equations are straightforward. However, we have assumed equal mutual inductances between the armature and rotor circuits in each axis. Reference 8 provides a description of the implementation of a model with unequal mutual inductances for stability analysis, using the above general approach.

Initial values of generator variables:

As noted earlier, the transient stability analysis involves the solution of a large set of differential and algebraic equations with known initial values. Prefault power-flow analysis provides the initial values of network variables, including the active and reactive power outputs and voltages at the generator terminals.

The procedure for computing the initial values of the generator quantities for known terminal conditions is presented in Section 3.6.5 of Chapter 3.

Classical generator model and infinite bus

For a machine represented by the classical model, $X_{RI}=X_{IR}=X'_d$, and E'' is replaced by E'. The rotor angle δ is the angle by which E' leads the R-axis. The magnitude of E' is constant throughout the solution. The R and I components of E' change with δ, as determined by the solution of the swing equation.

For a node associated with an infinite bus, both the magnitude and angle of the node voltage remain constant.

13.3.3 Excitation System Representation

Models for different types of excitation systems in use are described in Chapter 8. We will illustrate the method of incorporating these models into a transient stability program by considering the excitation system model shown in Figure 13.12. It represents a bus-fed thyristor excitation system (classified as type ST1A in Chapter 8) with an *automatic voltage regulator* (AVR) and a *power system stabilizer* (PSS). A high exciter gain (K_A) without transient gain reduction or derivative feedback is used. The model of Figure 13.12 is identical to the excitation system model considered in Chapter 12 (see Figure 12.14), except that we also account for the limits on exciter and PSS outputs.

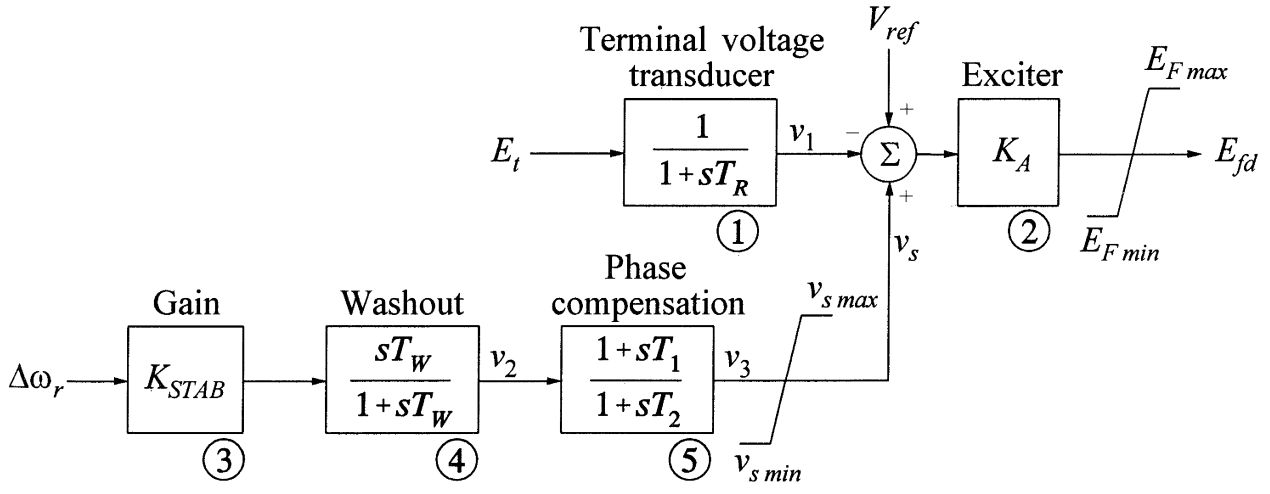


Figure 13.12 Thyristor excitation system with AVR and PSS

For a bus-fed (potential source) thyristor exciter, the voltages vary with the generator terminal voltage (E_t) and exciter output current (I_{fd}):

$$\begin{aligned} E_{Fmax} &= V_{Rmax}E_t - K_c I_{fd} \\ E_{Fmin} &= V_{Rmin}E_t \end{aligned} \tag{13.40}$$

From block 1 of Figure 13.12, we may write

$$pv_1 = \frac{1}{T_R}(E_t - v_1) \tag{13.41}$$

From blocks 3 and 4,

$$pv_2 = K_{STAB}p\Delta\omega_r - \frac{1}{T_W}v_2 \tag{13.42}$$

with $p\Delta\omega_r$ given by Equation 13.22. From block 5,

$$pv_3 = \frac{1}{T_2}[T_1 pv_2 + v_2 - v_3] \tag{13.43}$$

with pv_2 given by Equation 13.42. The stabilizer output v_s is

$$v_s = v_3 \tag{13.44A}$$

with

$$v_{smax} \geq v_s \geq v_{smin} \tag{13.44B}$$

From block 2, the exciter output voltage is

$$E_{fd} = K_A[V_{ref} - v_1 + v_s] \tag{13.45A}$$

with

$$E_{Fmax} \geq E_{fd} \geq E_{Fmin} \tag{13.45B}$$

Both limits considered here are *windup limits*. Modelling of *non-windup limits* is discussed in Chapter 8.

The generator field voltage e_{fd} in the reciprocal per unit system is related to exciter output voltage E_{fd} (see Chapter 8, Section 8.6) as follows:

$$e_{fd} = \frac{R_{fd}}{L_{adu}} E_{fd} \tag{13.46}$$

An alternative method of treating blocks 4 and 5, in which the derivatives of the input variables are not required, is described in Chapter 12, Section 12.3.4.

Initial values of excitation system variables:

For any given steady-state generator output, the field voltage e_{fd} is determined by the generator equations (see Section 13.3.2). The excitation system quantities are determined as follows:

$$E_{fd} = \frac{L_{adu}}{R_{fd}} e_{fd} \tag{13.47}$$

$$v_1 = E_t \qquad v_2 = 0 \qquad v_s = 0$$

The AVR reference is

$$V_{ref} = \frac{E_{fd}}{K_A} + v_1 \tag{13.48}$$

Thus V_{ref} takes a value appropriate to the generator loading condition prior to the disturbance.

Representation of field-shorting circuit [8]

In the case of an ac or static exciter, the exciter current usually cannot be negative. Therefore, a special field-shorting circuit in the form of a "crowbar" or a varistor is provided to bypass the exciter and allow negative field current to flow (see Chapter 8, Section 8.5.8).

The effects of field-shorting circuits are simulated by setting the field voltage to zero and increasing the field resistance (R_{fd}) appropriately during the period when the field current is negative. The resistance added is fixed for a crowbar. For a varistor the resistance is a nonlinear function of the applied voltage. Once the field current becomes positive, the field circuit resistance is restored to its normal value, and the field voltage is established by the exciter output.

13.3.4 Transmission Network and Load Representation

The transients associated with the transmission network decay very rapidly. In fact, network transients will have died out by the time the solution of the swing equation is advanced by one time step. Therefore, it is usually adequate to regard the network, during the electromechanical transient conditions, as though it were passing directly from one steady state to another. The fundamental frequency (50 or 60 Hz) variations may be regarded as microprocesses, and only the variations in the envelopes (amplitude modulation) of current and voltage waveforms are considered for stability analysis. For analysis of balanced conditions, a single-phase representation of the three phases is used. Unbalanced faults are simulated by using symmetrical components as described in Section 13.4.

Without the balanced steady-state representation of the transmission network, stability analysis of large practical power systems would be impractical. For special electromechanical problems requiring inclusion of transmission network and generator stator transients, and three-phase representation, a program such as the electromagnetic transients program (EMTP) may be used [9]. For conventional transient stability analysis, the network representation is similar to that for power-flow analysis. As described in Chapter 6 (Section 6.4.1.), the most convenient form of network representation is in terms of the node admittance matrix. The structure and formulation of this matrix are presented in Section 6.4.1.

The characteristics and modelling of loads are covered in Chapter 7. Dynamic loads are represented as induction or synchronous motors, and their treatment is similar to that of synchronous machines.

Static loads are represented as part of the network equations. Loads with constant impedance characteristics are the simplest to handle and are included in the node admittance matrix. Nonlinear loads are modelled as exponential or polynomial functions of bus voltage magnitude and frequency. The net effect is that a nonlinear static load model is treated as a current injection at the appropriate node in the network equation. The value of the node current from ground into the network is

$$\tilde{I}_L = -\frac{P_L - jQ_L}{\tilde{V}_L^*} \tag{13.49}$$

where $\tilde{V}_L^*$ is the conjugate of the load bus voltage, and P_L and Q_L are portions of the active and reactive components of the load which vary as nonlinear functions of V_L and frequency deviation. For an inductive load Q_L is positive.

The overall network/load representation comprises a large sparse nodal admittance matrix equation with a structure similar to that of the power-flow problem discussed in Chapter 6, Section 6.4. The network equation is identical to Equation 6.87, which in matrix notation may be written as

$$\tilde{\mathbf{I}} = \mathbf{Y}_N \tilde{\mathbf{V}} \tag{13.50}$$

The node admittance matrix $\mathbf{Y}_N$ is symmetrical, except for dissymmetry introduced by phase-shifting transformers (see Section 6.2.3). Within the time frame of transient stability simulations, transformer taps and phase-shift angles do not change. Therefore, the elements of the matrix are constant except for changes introduced by network-switching operations.

The effects of generators, nonlinear static loads, dynamic loads, and other devices such as HVDC converters and regulated var compensators are reflected as boundary conditions providing additional relationships between $\tilde{V}$ and $\tilde{I}$ at the respective nodes.

In contrast to power-flow analysis (See Chapter 6), tie line power-flow control, limits on generator reactive power output, and the slack bus make-up for the unknown losses need not be considered in transient stability analysis.

Simulation of faults:

A fault at or near a bus is simulated by appropriately changing the self-admittance of the bus.

Methods of simulating different types of fault will be discussed in Section 13.4.5. Depending on the type of fault, the equivalent negative- and zero-sequence impedances seen at the fault point are computed, combined appropriately, and inserted between the fault point and ground. This simply alters the self-admittance of the node representing the fault bus.

For a three-phase fault, the fault impedance is zero and the faulted bus has the same potential as the ground. This involves placing an infinite shunt admittance. In practice, a sufficiently high shunt admittance (i.e., a very small shunt impedance) is used so that the bus voltage is in effect zero. For example, a conductance G equal to 10^6 pu on 100 MVA base would effectively reduce the bus voltage to zero. The fault is removed by restoring the shunt admittance to the appropriate value depending on the postfault system configuration.

13.3.5 Overall System Equations

In Sections 13.3.2 and 13.3.3 we described the organization of synchronous generator and excitation system equations. Modelling of turbine governing systems is described in Chapter 9. Treatment of these models is similar to that of the excitation system.

Other devices whose dynamics are represented in transient stability studies include motors, HVDC converters and their controls, static var compensators, and synchronous condensers. Models of these devices are described in Chapters 7, 10, and 11.

Equations for each of the generating units and other dynamic devices may be expressed in the following form:

$$\dot{\mathbf{x}}_d = \mathbf{f}_d(\mathbf{x}_d, \mathbf{V}_d) \tag{13.51}$$

$$\mathbf{I}_d = \mathbf{g}_d(\mathbf{x}_d, \mathbf{V}_d) \tag{13.52}$$

where

$\mathbf{x}_d$ = state vector of individual device
$\mathbf{I}_d$ = R and I components of current injection from the device into the network
$\mathbf{V}_d$ = R and I components of bus voltage

The overall system equations, including the differential equations (13.51) for all the devices and the combined algebraic equations for the devices (13.52) and the network (13.50) are expressed in the following general form comprising a set of first-order differential equations

$$\dot{\mathbf{x}} = \mathbf{f}(\mathbf{x}, \mathbf{V}) \tag{13.53}$$

and a set of algebraic equations

$$\mathbf{I}(\mathbf{x}, \mathbf{V}) = \mathbf{Y}_N \mathbf{V} \tag{13.54}$$

with a set of known initial conditions $(\mathbf{x}_0, \mathbf{V}_0)$, where

$\mathbf{x}$ = state vector of the system
$\mathbf{V}$ = bus voltage vector
$\mathbf{I}$ = current injection vector

Time t does not appear explicitly in the above equations. A wide range of approaches has been reported in the literature for solving these equations, depending on the numerical methods and modelling details used. Reference 10 provides a review of these approaches. The many possible schemes for the solution of Equations 13.53 and 13.54 are characterized by the following factors:

(a) The manner of interface between the differential equations 13.53 and the algebraic equations 13.54. Either a *partitioned* approach or a *simultaneous* approach may be used.

(b) The integration method used, i.e., implicit method or explicit method.

(c) The method used for solving the algebraic equations. As in the case of power-flow analysis described in Chapter 6, one of the following methods may be used: (i) the Gauss-Seidal method based on admittance matrix formulation, (ii)

a direct solution using sparsity-oriented triangular factorization, and (iii) an iterative solution using the Newton-Raphson method.

All of the above approaches/methods have been successfully used in production-grade transient stability programs. In the next section, two basic solution schemes are described. One scheme uses a partitioned solution and an explicit integration method, and the other uses a simultaneous solution with an implicit integration method.

13.3.6 Solution of Overall System Equations

(a) Partitioned solution with explicit integration

In this approach, the algebraic and differential equations are solved separately. Initially, at $t=0^-$, the values of the state variables $\mathbf{x}$ and the network variables $\mathbf{V}$ and $\mathbf{I}$ are known, and they form a consistent set; that is, the system is in steady state and the time derivatives $\mathbf{f}(\mathbf{x}, \mathbf{V})$ are equal to zero.

Following a disturbance, usually a network fault, the state variables $\mathbf{x}$ cannot change instantly. The algebraic equations 13.54 are solved first to give $\mathbf{V}$ and $\mathbf{I}$, and the corresponding power flows and other non-state variables of interest at $t=0^+$. Then the time derivatives $\mathbf{f}(\mathbf{x}, \mathbf{V})$ are computed by using the known values of $\mathbf{x}$ and $\mathbf{V}$ in Equations 13.53. These then can be used to initiate the solution of the state variables $\mathbf{x}$ by using any of the explicit integration methods described in Section 13.2.

We will illustrate this by considering Gill's version of the fourth order R-K method. There are four stages ($j=1$ to 4) per time step Δt. Using the values of $\mathbf{f}(\mathbf{x}, \mathbf{V})$ computed at the beginning of a time step, $\mathbf{k}_1$, $\mathbf{x}_1$, and $\mathbf{q}_1$ are computed according to Equations 13.17 with $j=1$. Then the algebraic equations 13.54 are solved with $\mathbf{x}=\mathbf{x}_1$ to compute $\mathbf{V}_1$ and $\mathbf{I}_1$. These are in turn used in Equations 13.17 to compute $\mathbf{k}_2$, $\mathbf{x}_2$, and $\mathbf{q}_2$. This process, involving alternating solutions of algebraic and differential equations, is applied successively with $\mathbf{x}_4$ representing the solution at the end of each time step. During a switching operation, the network variables change instantly, but not the state variables.

Since the solution of differential equations requires values of network and state variables only from the previous step/stage, the differential equations may be partitioned in any way desired. For example, differential equations associated with each device may be solved independently. This offers considerable programming flexibility.

For solution of networks associated with large interconnected systems, the most efficient method is to use sparsity-oriented triangular factorization.

The partitioned approach with explicit integration is the traditional approach used widely in production-grade stability programs. Its advantages are programming flexibility and simplicity, reliability, and robustness. Its principal disadvantage is susceptibility to numerical instability. For a stiff system, a small time step is required throughout the solution period, as dictated by the smallest time constant (or eigenvalue).

(b) Simultaneous solution with implicit integration [14]

In this approach, the state variables and the network variables are solved simultaneously. We will illustrate this using the trapezoidal rule.

With $\mathbf{x}=\mathbf{x}_n$ and $\mathbf{V}=\mathbf{V}_n$ at $t=t_n$, the solution of $\mathbf{x}$ at $t=t_{n+1}=t_n+\Delta t$ is given by applying the trapezoidal rule (Equation 13.21) to solve Equation 13.53:

$$\mathbf{x}_{n+1} = \mathbf{x}_n + \frac{\Delta t}{2}[\mathbf{f}(\mathbf{x}_{n+1},\mathbf{V}_{n+1}) + \mathbf{f}(\mathbf{x}_n,\mathbf{V}_n)] \tag{13.55}$$

From Equation 13.54, the solution of $\mathbf{V}$ at $t=t_{n+1}$ is

$$\mathbf{I}(\mathbf{x}_{n+1},\mathbf{V}_{n+1}) = \mathbf{Y}_N\mathbf{V}_{n+1} \tag{13.56}$$

The vectors $\mathbf{x}_{n+1}$ and $\mathbf{V}_{n+1}$ are unknown. Let

$$\mathbf{F}(\mathbf{x}_{n+1},\mathbf{V}_{n+1}) = \mathbf{x}_{n+1} - \mathbf{x}_n - \frac{\Delta t}{2}[\mathbf{f}(\mathbf{x}_{n+1},\mathbf{V}_{n+1}) + \mathbf{f}(\mathbf{x}_n,\mathbf{V}_n)] \tag{13.57}$$

and

$$\mathbf{G}(\mathbf{x}_{n+1},\mathbf{V}_{n+1}) = \mathbf{Y}_N\mathbf{V}_{n+1} - \mathbf{I}(\mathbf{x}_{n+1},\mathbf{V}_{n+1}) \tag{13.58}$$

At solution,

$$\mathbf{F}(\mathbf{x}_{n+1},\mathbf{V}_{n+1}) = 0 \tag{13.59}$$

$$\mathbf{G}(\mathbf{x}_{n+1},\mathbf{V}_{n+1}) = 0 \tag{13.60}$$

Equations 13.59 and 13.60 are both *nonlinear algebraic* equations. Thus the differential equations have been made algebraic by using an implicit formula. These equations are very sparse; for computational efficiency it is necessary to take advantage of their special structure. Applying the Newton method (see Chapter 6) to solve Equations 13.59 and 13.60, we may write for the $(k+1)^{st}$ iteration

$$\begin{bmatrix} \mathbf{x}_{n+1}^{k+1} \\ \mathbf{V}_{n+1}^{k+1} \end{bmatrix} = \begin{bmatrix} \mathbf{x}_{n+1}^{k} \\ \mathbf{V}_{n+1}^{k} \end{bmatrix} + \begin{bmatrix} \Delta\mathbf{x}_{n+1}^{k} \\ \Delta\mathbf{V}_{n+1}^{k} \end{bmatrix} \tag{13.61}$$

The following equation is solved to obtain $\Delta\mathbf{x}_{n+1}^{k}$ and $\Delta\mathbf{V}_{n+1}^{k}$:

$$\begin{bmatrix} -\mathbf{F}(\mathbf{x}_{n+1}^k, \mathbf{V}_{n+1}^k) \\ -\mathbf{G}(\mathbf{x}_{n+1}^k, \mathbf{V}_{n+1}^k) \end{bmatrix} = \begin{bmatrix} \frac{\partial \mathbf{F}}{\partial \mathbf{x}} & \frac{\partial \mathbf{F}}{\partial \mathbf{V}} \\ \frac{\partial \mathbf{G}}{\partial \mathbf{x}} & \frac{\partial \mathbf{G}}{\partial \mathbf{V}} \end{bmatrix} \begin{bmatrix} \Delta \mathbf{x}_{n+1}^k \\ \Delta \mathbf{V}_{n+1}^k \end{bmatrix} \tag{13.62}$$

The Jacobian in the above equation is computed at $\mathbf{x}=\mathbf{x}_{n+1}^k$ and $\mathbf{V}=\mathbf{V}_{n+1}^k$. It has the following structure:

$$\mathbf{J} = \begin{bmatrix} \frac{\partial \mathbf{F}}{\partial \mathbf{x}} & \frac{\partial \mathbf{F}}{\partial \mathbf{V}} \\ \frac{\partial \mathbf{G}}{\partial \mathbf{x}} & \frac{\partial \mathbf{G}}{\partial \mathbf{V}} \end{bmatrix} = \begin{bmatrix} \mathbf{A}_D & \mathbf{B}_D \\ \mathbf{C}_D & (\mathbf{Y}_N + \mathbf{Y}_D) \end{bmatrix} \tag{13.63}$$

The matrices $\mathbf{A}_D$, $\mathbf{B}_D$, $\mathbf{C}_D$ and $\mathbf{Y}_D$ are associated with the models for the dynamic devices and nonlinear static loads. For a system with m such devices, they have the following structures:

$$\mathbf{A}_D = \begin{bmatrix} \mathbf{A}_{d1} & 0 & \cdots & 0 \\ 0 & \mathbf{A}_{d2} & \cdots & 0 \\ \vdots & \vdots & \ddots & \vdots \\ 0 & 0 & \cdots & \mathbf{A}_{dm} \end{bmatrix} \quad \mathbf{B}_D = \begin{bmatrix} \mathbf{B}_{d1} \\ \mathbf{B}_{d2} \\ \vdots \\ \mathbf{B}_{dm} \end{bmatrix} \quad \mathbf{Y}_D = \begin{bmatrix} \mathbf{Y}_{d1} & 0 & \cdots & 0 \\ 0 & \mathbf{Y}_{d2} & \cdots & 0 \\ \vdots & \vdots & \ddots & \vdots \\ 0 & 0 & \cdots & \mathbf{Y}_{dm} \end{bmatrix}$$

$$\mathbf{C}_D = \begin{bmatrix} \mathbf{C}_{d1} & \mathbf{C}_{d2} & \cdots & \mathbf{C}_{dm} \end{bmatrix}$$

The solutions of Equations 13.59 and 13.60 are given in terms of the above matrices by

$$\mathbf{A}_D \Delta \mathbf{x}_{n+1}^k + \mathbf{B}_D \Delta \mathbf{V}_{n+1}^k = -\mathbf{F}(\mathbf{x}_{n+1}^k, \mathbf{V}_{n+1}^k) \triangleq -\mathbf{F}_{n+1}^k \tag{13.64}$$

$$\mathbf{C}_D \Delta \mathbf{x}_{n+1}^k + (\mathbf{Y}_N + \mathbf{Y}_D) \Delta \mathbf{V}_{n+1}^k = -\mathbf{G}(\mathbf{x}_{n+1}^k, \mathbf{V}_{n+1}^k) \triangleq -\mathbf{G}_{n+1}^k \tag{13.65}$$

In the above equations, k is the iteration counter and good starting values $(\mathbf{x}_{n+1}^0, \mathbf{V}_{n+1}^0)$ are established by extrapolation. Also $\mathbf{F}_{n+1}^k$ and $\mathbf{G}_{n+1}^k$ are the residue vectors of the states and current injections, respectively.

From Equation 13.64, $\Delta \mathbf{x}_{n+1}^k$ can be expressed as a function of $\Delta \mathbf{V}_{n+1}^k$:

$$\Delta \mathbf{x}_{n+1}^k = -\mathbf{A}_D^{-1} [\mathbf{F}_{n+1}^k + \mathbf{B}_D \Delta \mathbf{V}_{n+1}^k] \tag{13.66}$$

Substitution of Equation 13.66 into Equation 13.65 yields

$$(\mathbf{Y}_N + \mathbf{Y}_D - \mathbf{C}_D \mathbf{A}_D^{-1} \mathbf{B}_D) \Delta \mathbf{V}_{n+1}^k = -\mathbf{G}_{n+1}^k + \mathbf{C}_D \mathbf{A}_D^{-1} \mathbf{F}_{n+1}^k \tag{13.67}$$

Now $\Delta \mathbf{V}_{n+1}^k$ and $\Delta \mathbf{x}_{n+1}^k$ can be calculated by solving Equations 13.66 and 13.67. Then $\mathbf{x}_{n+1}^{k+1}$ and $\mathbf{V}_{n+1}^{k+1}$ are obtained from Equation 13.61.

Treatment of discontinuities:

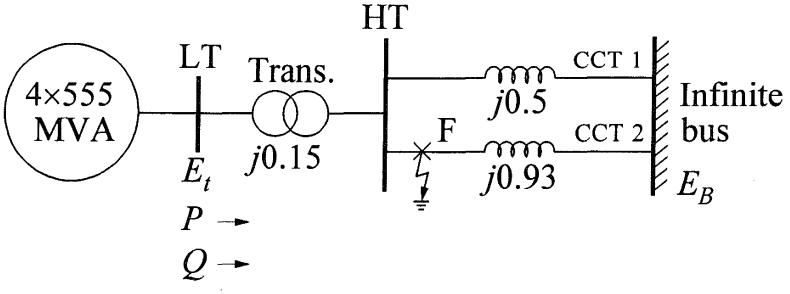
Equations 13.64 and 13.65 are valid only when the functions given by Equations 13.57 and 13.58 are continuous and differentiable. At points of discontinuity, such as network switching or limits on state variables, the exact formulation by the Newton method or any method requiring derivatives would be complicated [13]. This problem is dealt with in reference 14 as follows:

- For large network discontinuities, such as a network fault or switching operations, the integration method is temporarily changed to the fourth order Runge-Kutta method for one step at the point of discontinuity. This time step has a zero step size and is used only for the calculation of the postfault network conditions (the state vector is not updated). After this, the normal trapezoidal integration is resumed.

- For local non-differentiable functions, such as limits associated with controllers, the device Jacobians are computed by neglecting their effect. This is acceptable since they have only local impact and the overall convergence will not be significantly affected.

Example 13.2

In this example, we analyze the transient stability of the system of Figure E13.1 (considered in Example 13.1) including the effects of rotor circuit dynamics and excitation control. The system diagram is reproduced here as Figure E13.6 for reference.



Network reactances in pu on 2220 MVA base

Figure E13.6

Generator parameters:

The four generators of the plant are represented by an equivalent generator whose parameters in per unit on 2220 MVA base are as follows:

$X_d = 1.81$	$X_q = 1.76$	$X'_d = 0.30$	$X'_q = 0.65$
$X''_d = 0.23$	$X''_q = 0.25$	$X_l = 0.15$	$R_a = 0.003$
$T'_{d0} = 8.0$ s	$T'_{q0} = 1.0$ s	$T''_{d0} = 0.03$ s	$T''_{q0} = 0.07$ s
$H = 3.5$	$K_D = 0$		

The above parameters are unsaturated values. The effect of saturation is to be represented by assuming that *d*- and *q*-axes have similar saturation characteristics with

$A_{sat} = 0.031$	$B_{sat} = 6.93$	$\psi_{T1} = 0.8$	$\psi_{T2} = \infty$

Excitation system parameters:

The generators are equipped with thyristor exciters with AVR and PSS as shown in Figure 13.12, with parameters as follows:

$K_A = 200$	$T_R = 0.015$ s	$E_{F\,max} = 7.0$	$E_{F\,min} = -6.4$
$K_{STAB} = 9.5$	$T_W = 1.41$ s	$T_1 = 0.154$ s	$T_2 = 0.033$ s
$v_{s\,max} = 0.2$	$v_{s\,min} = -0.2$		

The exciter is assumed to be alternator supplied; therefore, $E_{F\,max}$ and $E_{F\,min}$ are independent of E_t.

Prefault system condition in pu on 2220 MVA, 24 kV base:

$P = 0.9$	$Q = 0.436$ (overexcited)
$\tilde{E}_t = 1.0\angle 28.34°$	$\tilde{E}_B = 0.90081\angle 0$

Disturbance:

A three-phase fault on circuit 2 at point F cleared by isolating the faulted circuit simultaneously at both ends.

Examine the stability of the system with the following alternative forms of excitation control:

(i) Manual control, i.e., constant E_{fd}

(ii) AVR with no PSS

(iii) AVR with PSS

Consider the following alternative fault-clearing times:

(a) 0.07 s

(b) 0.10 s

Solution

The generators of this example have the same characteristics as the generator considered in examples of Chapters 3 and 4.

The per unit fundamental parameters as determined in Example 4.1 are as follows:

L_{adu} = 1.66	L_{aqu} = 1.61	L_l = 0.15	R_a=0.003
L_{fd} = 0.165	R_{fd} = 0.0006	L_{1d} = 0.1713	R_{1d} = 0.0284
L_{1q} = 0.7252	R_{1q} = 0.0062	L_{2q} = 0.125	R_{2q} = 0.0237

The initial per unit values of generator variables based on the results of Examples 3.2 and 3.3 are as follows:

$K_{sd} = K_{sq}$ = 0.835		δ_i = 39.1°	
e_d = 0.631	e_q = 0.776	i_d = 0.906	i_q = 0.423
i_{fd} = 1.565	e_{fd} = 0.000939		

The initial per unit values of exciter output current and voltages are

$$I_{fd} = L_{adu} i_{fd} = 1.66 \times 1.565 = 2.598$$

$$E_{fd} = (L_{adu}/R_{fd}) e_{fd} = (1.66/0.0006) \times 0.000939 = 2.598$$

With E_B assumed to be in phase with the R-axis, the initial value of the rotor angle is

$$\delta = \delta_i + 28.34° = 39.1° + 28.34° = 67.44°$$

(a) Transient response with the fault-clearing time t_c equal to 0.07 s:

The results of time responses computed with the three alternative excitation controls are shown in Figures E13.7(a) to (d), which show time responses of δ, P_e, E_t and E_{fd}, respectively. These results were computed by using Gill's version of the R-K integration method with a time step of 0.02 s.

From Figure E13.7(a), we see that with constant E_{fd}, the system is transiently stable; however, the level of damping of oscillations is low.

With a fast-acting AVR and a high exciter ceiling voltage, the first rotor angle swing is significantly reduced. However, the subsequent swings are negatively damped; the system loses synchronism in the third swing.

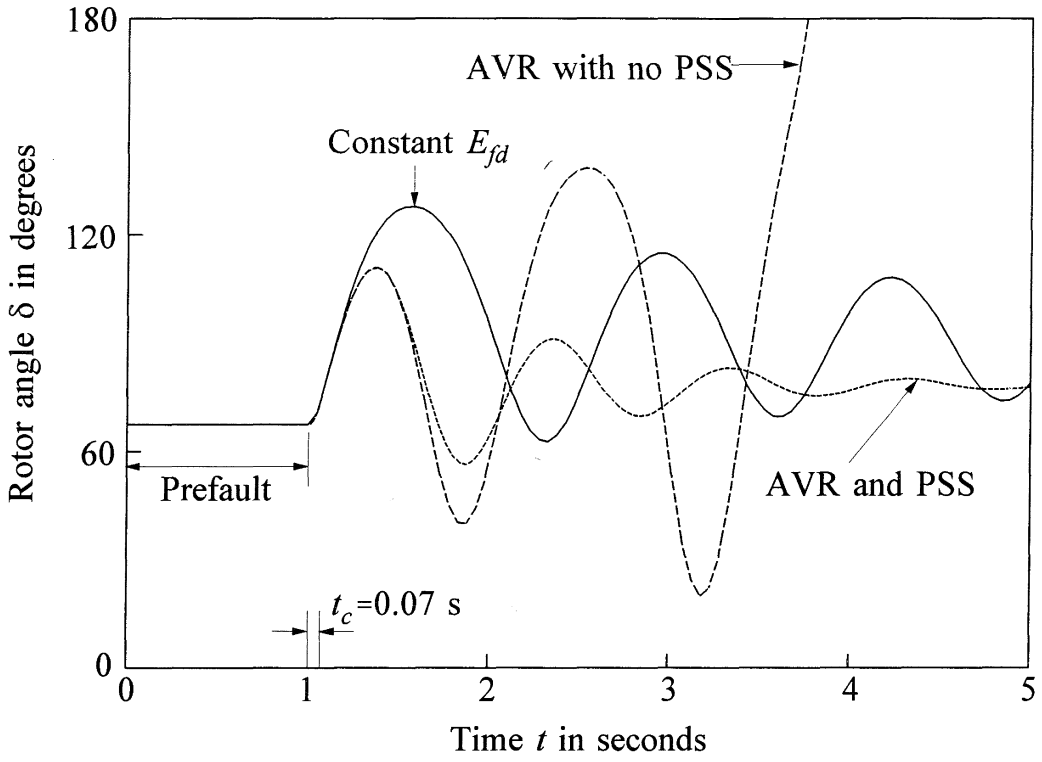


Figure E13.7 (a) Rotor angle response with fault cleared in 0.07 s

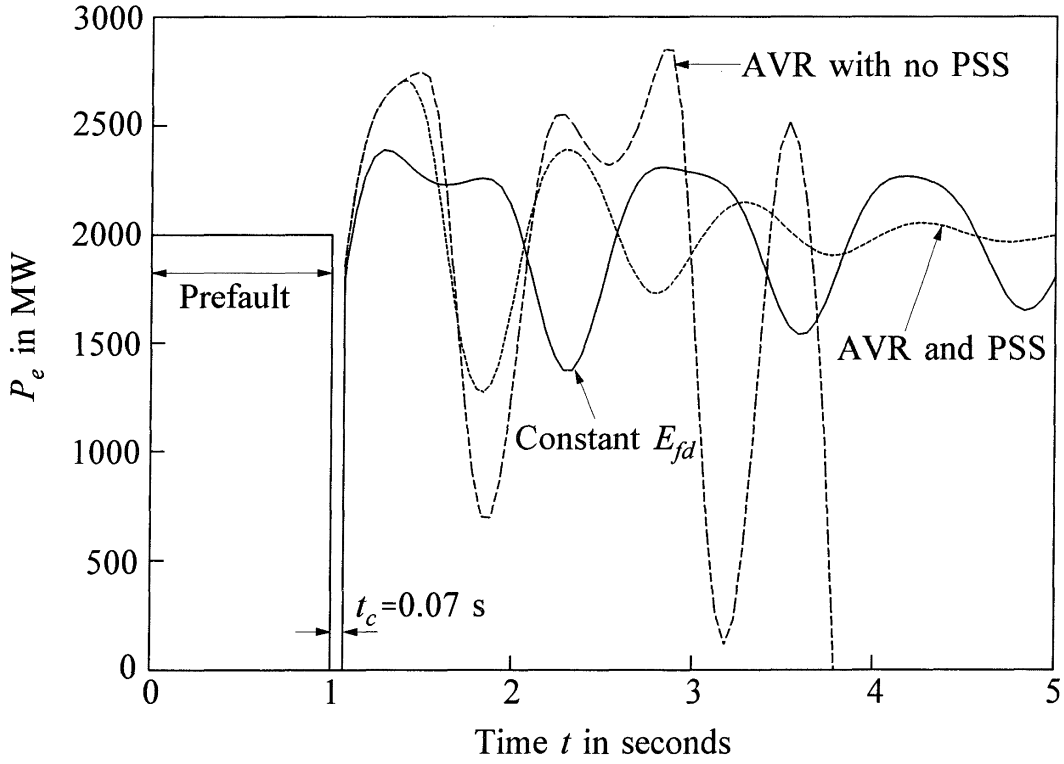


Figure E13.7 (b) Active power response with fault cleared in 0.07

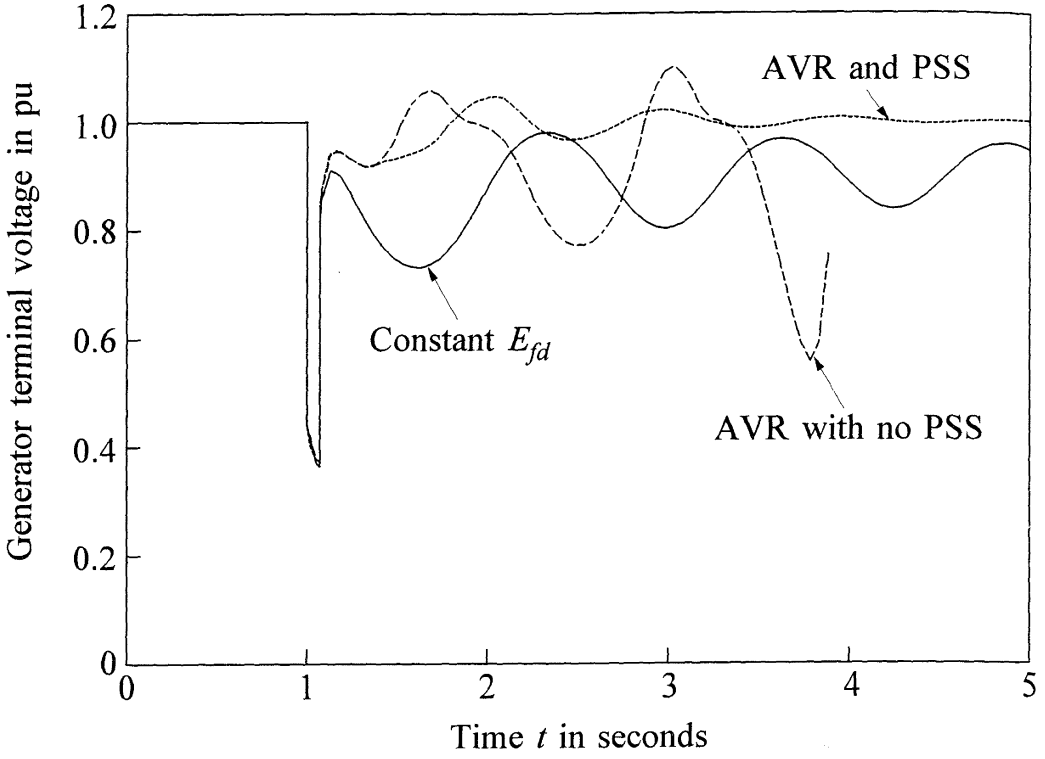


Figure E13.7 (c) Terminal voltage response with fault cleared in 0.07 s

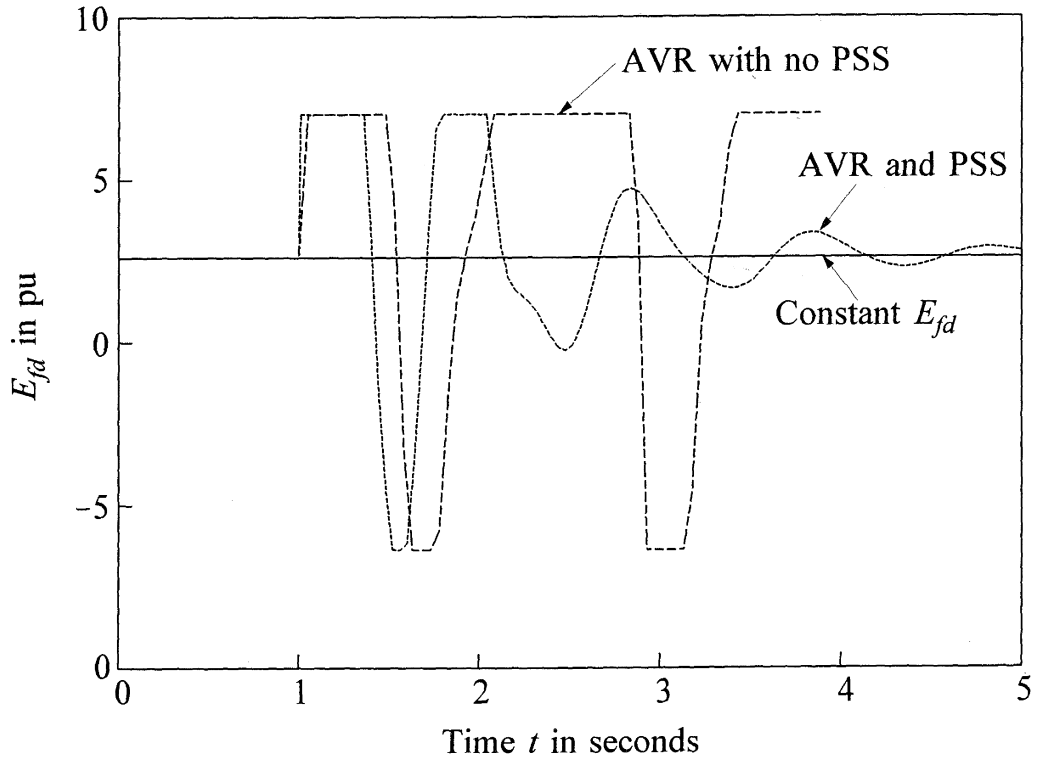


Figure E13.7 (d) Exciter output voltage response with fault cleared in 0.07 s

With the PSS, the rotor oscillations are very well damped without compromising the first-swing stability.

The results with regard to oscillatory stability (i.e., damping of rotor oscillations) are consistent with those of Examples 12.4 and 12.5 of Chapter 12.

(b) Transient response with the fault-clearing time t_c equal to 0.1 s:

The transient responses of rotor angle δ with the three alternative forms of excitation control are shown in Figure E13.8. With constant E_{fd}, the generator is first-swing unstable. With a fast-acting exciter and AVR, the generator maintains first-swing stability but loses synchronism during the second swing. The addition of a PSS contributes to the damping of second and subsequent swings.

It is evident from these results that the use of a fast exciter having a high-ceiling voltage and equipped with a PSS contributes to the enhancement of the overall system stability.

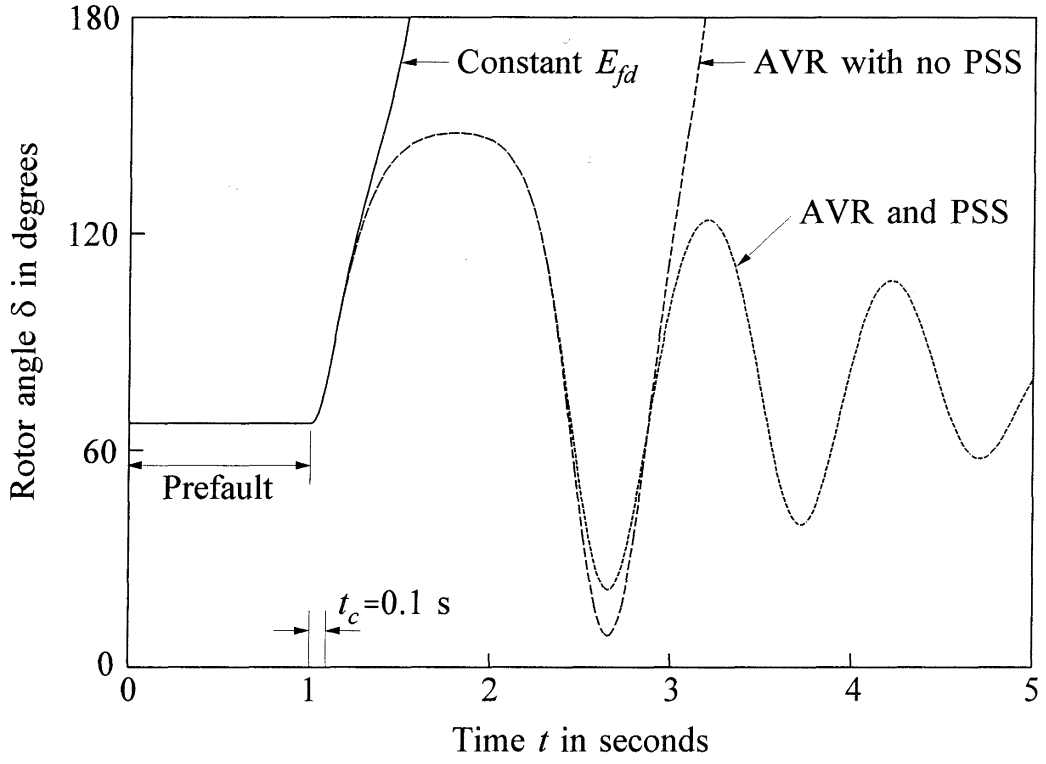


Figure E13.8 Rotor angle response with fault cleared in 0.1 s ■

Example 13.3

For the system considered in Example 13.2, examine the accuracy and numerical stability of Gill's version of the fourth order R-K method and the trapezoidal rule. Consider the case with AVR and PSS, and the fault cleared in 0.07 s.

Solution

The system considered here includes the effects of rotor circuit dynamics and a fast exciter with a PSS. This represents a very stiff system as is evident from the eigenvalues computed in Example 12.5 of Chapter 12 (see Table E12.2).

R-K method:

Figure E13.9 shows plots of rotor angle transient responses computed by using four different values of time step (Δt): 0.01 s, 0.03 s, 0.04 s, and 0.043 s.

With time steps of 0.01 s and 0.03 s, the results are practically identical. When the time step is increased to 0.04 s, errors become noticeable. With a step size of 0.043 s, the solution is numerically unstable.

In Table E13.1, the accuracy of results obtained with the R-K method is checked by applying Richardson's formula (see Equation 13.18) to the results obtained with step sizes of 0.01 s and 0.02 s. The magnitude of the error is seen never to exceed 0.05°. The table indicates the manner in which the error propagates. It is evident that the accumulated error oscillates, becoming alternately positive and negative.

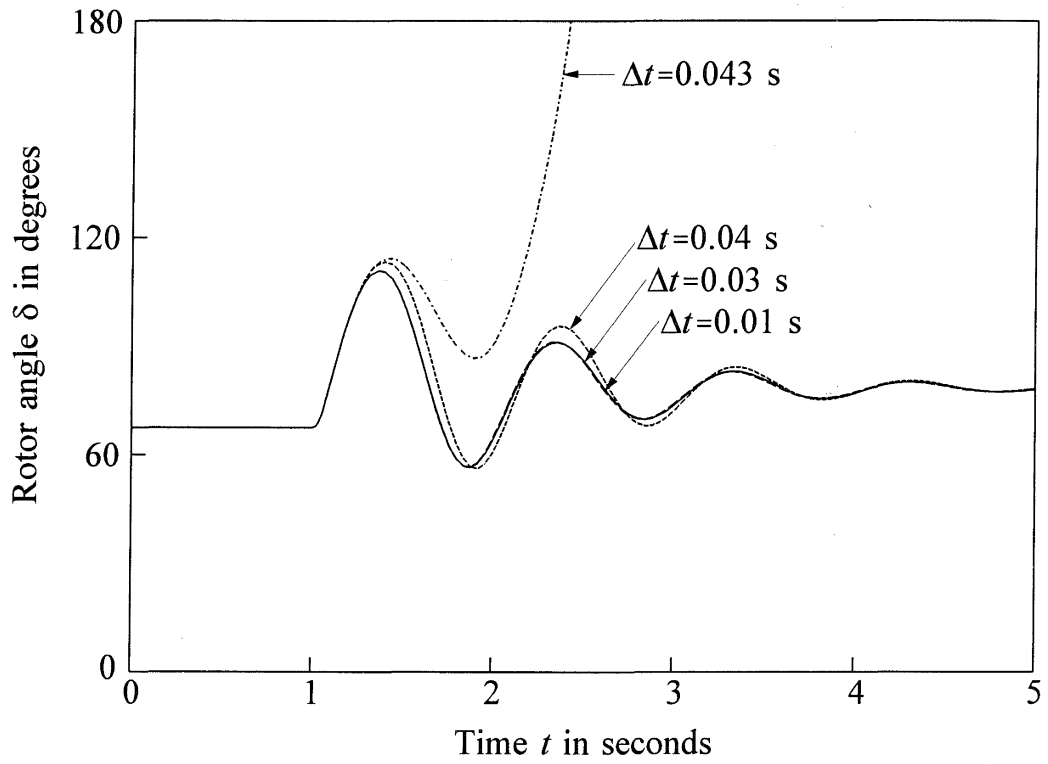


Figure E13.9 Effect of integration step size on the results of R-K method

Table E13.1 Accuracy of results obtained with R-K method

Time (seconds)	Rotor Angle (degrees)		Accumulated Error (degrees)
	Δt = 0.01 s	Δt = 0.02 s	
1.4	110.4577	110.4607	−0.0002
1.6	87.2801	87.1575	+0.0082
1.8	58.7696	58.6709	+0.0066
2.0	63.7337	64.1752	−0.0294
2.2	84.8016	85.4362	−0.0423
2.4	90.5653	90.5292	+0.0024
2.6	79.5231	78.9659	+0.0371
2.8	70.0900	69.9465	+0.0096
3.0	73.5296	73.9370	−0.0272
3.2	81.1694	81.4342	−0.0176
3.4	82.5907	82.3862	+0.0136
3.6	78.2763	77.9735	+0.0202
3.8	75.3601	75.3947	−0.0023
4.0	76.9479	77.1938	−0.0164
4.2	79.5847	79.6669	−0.0055
4.4	79.7843	79.6378	+0.0098
4.6	78.1531	78.0250	+0.0085
4.8	77.2835	77.3357	−0.0035
5.0	77.9709	78.0883	−0.0078

$$\text{Accumulated error} = \frac{1}{15}[\delta(\Delta t = 0.01) - \delta(\Delta t = 0.02)]$$

Trapezoidal rule:

The results obtained with step sizes of 0.01 s, 0.059 s, 0.09 s, and 0.093 s are shown in Figure E13.10.

With step sizes of 0.01 s and 0.059 s, the results are practically identical. When the step size is increased to 0.09 s, significant errors result; however, the general characteristics of the overall response are still retained. With a step size of 0.093 s, the errors become so large that the solution blows up after about 1.7 s.

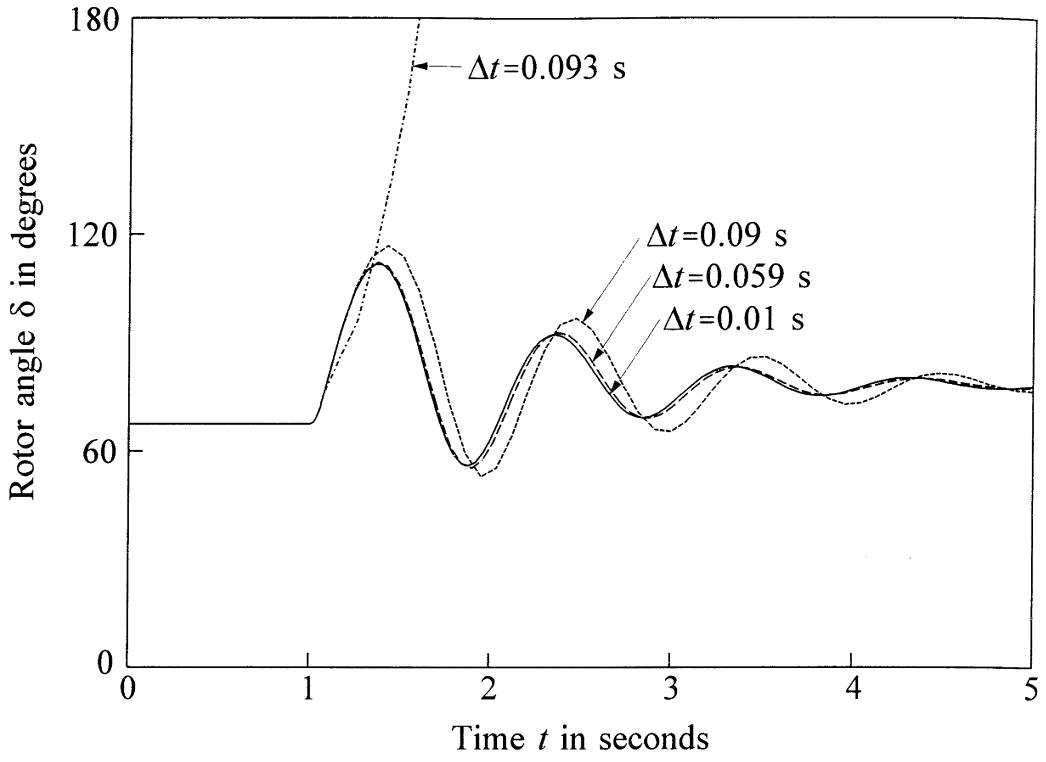


Figure E13.10 Effect of integration step size on the results of trapezoidal rule ■

13.4 ANALYSIS OF UNBALANCED FAULTS

So far, we have considered only balanced operation of the power system; this allowed for analysis of system performance by solving for the variables in only one of the phases in a manner similar to single-phase circuits. The solution of unbalanced three-phase circuits does not permit this simplification. A three-phase representation can be used instead, but it complicates the problem enormously. The method of symmetrical components is preferred because it offers considerable simplicity in the analysis of power system stability problems involving unbalanced faults.

13.4.1 Introduction to Symmetrical Components [15-18]

The general concept of symmetrical components was first developed by C.L. Fortescue in 1918 [19]. He showed that an unbalanced system of n related phasors can be resolved into n systems of balanced phasors called symmetrical components of the original phasors.

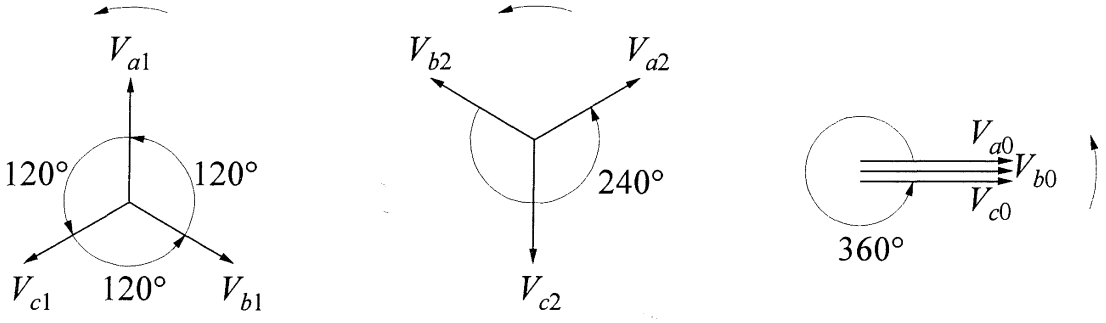
In a three-phase system, a set of three unbalanced phasors can be resolved into three balanced systems of phasors as follows:

(a) *Positive-sequence components* consisting of a balanced system of three phasors having the same phase sequence as the original phasors.

(b) *Negative-sequence components* consisting of a balanced system of three phasors having a phase sequence opposite to that of the original phasors.

(c) *Zero-sequence components* consisting of three phasors equal in magnitude and phase.

Figure 13.13 shows the three sets of balanced phasors that form the symmetrical components of three unbalanced phasors.



(a) Positive-sequence components

$V_{b1} = a^2 V_{a1}$
$V_{c1} = aV_{a1}$

(denoted by subscript 1)

(b) Negative-sequence components

$V_{b2} = aV_{a2}$
$V_{c2} = a^2 V_{a2}$

(denoted by subscript 2)

(c) Zero-sequence components

$V_{b0} = V_{a0}$
$= V_{c0}$

(denoted by subscript 0)

Figure 13.13 Symmetrical components of three balanced phasors

Definition of operator a

The operator a denotes 120° phase shift. It is equal to the unit vector $e^{j120°}$. Recalling that $e^{j\theta} = \cos\theta + j\sin\theta$, the unit vector representing a is given by

$$a = e^{j120°} = \cos 120° + j\sin 120°$$

$$= -0.5 + j0.866$$

The operators a^2 and a^3 represent phase shifts of 240° and 360°, respectively. Thus,

$$a^2 = e^{j240°} = -0.5 - j0.866$$

and

$$a^3 = e^{j360^\circ} = 1.0+j0.0$$

Relationship between the original unbalanced phasors and their symmetrical components

The total voltage of any phase is equal to the sum of the corresponding components of the different sequences in that phase. Thus,

$$\begin{aligned} V_a &= V_{a1}+V_{a2}+V_{a0} \\ V_b &= V_{b1}+V_{b2}+V_{b0} \\ &= a^2V_{a1}+aV_{a2}+V_{a0} \\ V_c &= V_{c1}+V_{c2}+V_{c0} \\ &= aV_{a1}+a^2V_{a2}+V_{a0} \end{aligned} \tag{13.68}$$

In matrix form,

$$\begin{bmatrix} V_a \\ V_b \\ V_c \end{bmatrix} = \begin{bmatrix} 1 & 1 & 1 \\ 1 & a^2 & a \\ 1 & a & a^2 \end{bmatrix} \begin{bmatrix} V_{a0} \\ V_{a1} \\ V_{a2} \end{bmatrix} \tag{13.69}$$

or

$$\mathbf{V}_{abc} = \mathbf{T}\mathbf{V}_{012} \tag{13.70}$$

Figure 13.14 depicts graphically the synthesis of a set of three unbalanced phasors in accord with the above equations.

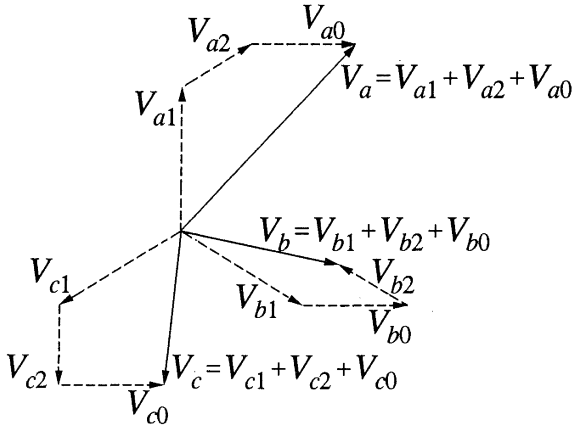


Figure 13.14 Unbalanced set of phasors reconstituted from sequence components

The inverse transformation is given by

$$\begin{bmatrix} V_{a0} \\ V_{a1} \\ V_{a2} \end{bmatrix} = \frac{1}{3}\begin{bmatrix} 1 & 1 & 1 \\ 1 & a & a^2 \\ 1 & a^2 & a \end{bmatrix}\begin{bmatrix} V_a \\ V_b \\ V_c \end{bmatrix} \tag{13.71}$$

Similar transformations apply to currents. The sum of the three line currents is equal to the neutral current. Thus,

$$I_a + I_b + I_c = I_n \tag{13.72}$$

Hence,

$$I_n = 3I_{a0} \tag{13.73}$$

Effect of transformation on impedances

The impedances of system elements satisfy the equation

$$\mathbf{V}_{abc} = \mathbf{Z}_{abc}\mathbf{I}_{abc} \tag{13.74}$$

where $\mathbf{Z}_{abc}$ is the impedance matrix giving self- and mutual impedances in and between phases.

By using the transformation of Equation 13.70, Equation 13.74 can be expressed in terms of the sequence components of voltages and currents:

$$\mathbf{T}\mathbf{V}_{012} = \mathbf{Z}_{abc}\mathbf{T}\mathbf{I}_{012} \tag{13.75}$$

or

$$\begin{aligned} \mathbf{V}_{012} &= \mathbf{T}^{-1}\mathbf{Z}_{abc}\mathbf{T}\mathbf{I}_{012} \\ &= \mathbf{Z}_{012}\mathbf{I}_{012} \end{aligned} \tag{13.76}$$

For typical power systems $\mathbf{Z}_{abc}$ is not diagonal but does possess certain *symmetries*. These symmetries are such that the sequence impedance matrix $\mathbf{Z}_{012}$ is *diagonal*, either exactly or approximately. Sequence impedances of different types of system elements will be discussed in Section 13.4.2.

Expression for power in terms of sequence components

Complex three-phase power is given by

$$\begin{aligned} S_{3\,\text{phase}} &= V_a I_a^* + V_b I_b^* + V_c I_c^* \\ &= \mathbf{V}_{\text{abc}}^{\text{T}} \mathbf{I}_{\text{abc}}^* \\ &= \left(\mathbf{T}\mathbf{V}_{012}\right)^{\text{T}} \left(\mathbf{T}\mathbf{I}_{012}\right)^* \\ &= \mathbf{V}_{012}^{\text{T}} \mathbf{T}^{\text{T}} \mathbf{T}^* \mathbf{I}_{012}^* \\ &= 3\mathbf{V}_{012}^{\text{T}} \mathbf{I}_{012}^* \\ &= 3\left(V_{a0} I_{a0}^* + V_{a1} I_{a1}^* + V_{a2} I_{a2}^*\right) \end{aligned} \tag{13.77}$$

In the above, the currents are line values and the voltages are line-to-neutral values. It is interesting to note that there are no "cross" terms or components caused by interaction between voltages of one sequence and currents of another sequence. The factor 3 is reasonable when we think in terms of 9 components. This also means that the transformation is not power invariant.

Why symmetrical components?

The resolution of three unbalanced phasors into symmetrical components results in three balanced systems. In symmetrical power systems (systems in which the three phases are identical), currents and voltages of different sequences do not react to each other; that is, currents of one sequence induce voltage drops of like sequence only.

Most of the apparatus used in practice is of the symmetrical type. This results in considerable simplification of many types of unbalanced problems, such as those introduced by unbalanced faults or the opening of one phase.

Since in a symmetrical system there is no interaction between quantities of different sequences, currents of any one sequence may be considered to flow in an independent network associated with that sequence only. The single-phase equivalent circuit composed of the impedances to currents of any one sequence is called the *sequence network* for that particular sequence. To analyze the system performance where there is an unbalanced fault, the sequence networks are interconnected at the fault location to represent the interaction between quantities of different sequences due to unbalance created by the fault.

The resolution of the problem into the sequence components has a further advantage in that it *isolates the quantities into components which represent a better*

criterion of the controlling factors in certain phenomena. For example, in stability investigations the synchronizing force between machines is affected principally by the positive-sequence quantities, the heating effects due to unbalanced currents depend on negative-sequence currents, and the ground relays and grounding phenomena are very closely associated with zero-sequence components. Thus, the analysis of many problems is not only simpler, but the results are resolved into factors which may be investigated separately.

Sequence impedances

The impedance of a circuit when positive-sequence currents alone are flowing is called the impedance to positive-sequence currents or *positive-sequence impedance*. Similarly, impedance to negative-sequence currents is called *negative-sequence impedance*, and the impedance to zero-sequence currents the *zero-sequence impedance*.

A knowledge of the sequence impedances of the power system elements is essential for the analysis of system performance during unbalanced faults.

13.4.2 Sequence Impedances of Synchronous Machines [15]

Positive-sequence impedance

In Section 13.3.2, we discussed the detailed representation of synchronous machines in the positive-sequence network appropriate for stability studies. Such a model is accurate for the entire study period, including the subtransient, transient, and steady-state conditions.

Figure 13.15 shows the simplified positive-sequence equivalent circuit of a synchronous machine. As discussed in Chapter 5 (Section 5.3.3), the value of the *positive-sequence reactance* X_1 depends on the time frame of interest: subtransient, transient, and steady state.

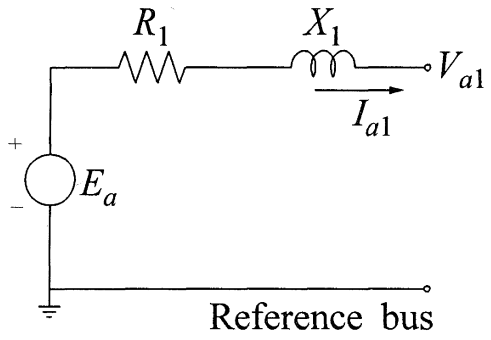


Figure 13.15 Positive-sequence equivalent circuit of synchronous machine

For the time frame representing

- the initial subtransient condition, $X_1 = X_d''$;
- the initial transient condition, $X_1 = X_d'$;
- the steady-state condition, $X_1 = X_d$.

The above assumes that saliency effects are negligible.

The *positive-sequence resistance* R_1 is the ac resistance of the armature.

The equivalent circuit of Figure 13.15 represents one phase of the balanced positive-sequence circuits. Its reference bus is the neutral of the generator.

Negative-sequence impedance

Negative-sequence reactance (X_2):

When fundamental frequency negative-sequence (reverse phase sequence) currents are applied to the armature windings of a machine, with the rotor running at synchronous speed and the field winding shorted through the exciter, the ratio of the resulting negative-sequence fundamental frequency voltages to the currents gives the negative-sequence impedance. The reactive part of this impedance is the negative-sequence reactance X_2.

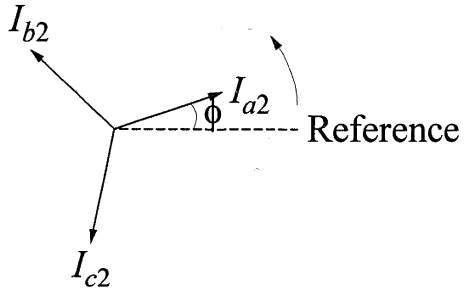
In what follows, we will show that the negative-sequence reactance X_2 is equal to the mean between the *d*- and *q*-axis subtransient reactances, X_d'' and X_q''. Saliency effects result in somewhat different values of X_2 depending on whether sinusoidal currents are circulated or sinusoidal voltages are applied.

With time t in seconds, the negative-sequence currents may be expressed as

$$i_{a2} = I_{a2}\cos(\omega t + \phi)$$

$$i_{b2} = I_{a2}\cos\left(\omega t + \phi + \frac{2\pi}{3}\right)$$

$$i_{c2} = I_{a2}\cos\left(\omega t + \phi - \frac{2\pi}{3}\right)$$



Transforming into *d*, *q*, 0 components (see Chapter 3, Section 3.3), we have

$$i_d = I_{a2}\cos(2\omega t + \phi)$$

$$i_q = -I_{a2}\sin(2\omega t + \phi)$$

$$i_0 = 0$$

The resulting field due to the negative-sequence stator currents rotates at synchronous speed opposite to the direction of the rotor. Therefore, as viewed from the rotor, the stator currents appear to be double frequency currents i_d and i_q. Currents of twice the rated frequency are induced in the rotor circuits, keeping the flux linkages of the rotor circuits almost constant (since resistance is considerably smaller than inductance). The flux due to the stator currents is forced into paths of low permeance which do not link with any rotor circuit. These flux paths are the same as those encountered in evaluating subtransient inductances. Therefore, the d- and q-axis components of stator currents at 120 Hz encounter subtransient inductances L_d'' and L_q'' (see Chapter 4, Section 4.2). The corresponding per unit stator flux linkages are

$$\psi_d = -L_d'' i_d = -X_d'' i_d$$

$$\psi_q = -L_q'' i_q = -X_q'' i_q$$

Neglecting the stator resistance, with time t in seconds and ω_r equal to 1.0 pu, the per unit stator voltages are given by the following equations:

$$\begin{aligned} e_d &= \frac{1}{\omega_0}\frac{d\psi_d}{dt} - \psi_q \\ &= \frac{1}{\omega_0}\frac{d}{dt}\left[-X_d'' I_{a2}\cos(2\omega t+\phi)\right] - X_q'' I_{a2}\sin(2\omega t+\phi) \\ &= 2\frac{\omega}{\omega_0} X_d'' I_{a2}\sin(2\omega t+\phi) - X_q'' I_{a2}\sin(2\omega t+\phi) \end{aligned}$$

For fundamental frequency negative-sequence currents, $\omega = \omega_0$. Hence,

$$e_d = (2X_d'' - X_q'')I_{a2}\sin(2\omega_0 t+\phi)$$

Similarly,

$$e_q = (2X_q'' - X_d'')I_{a2}\cos(2\omega_0 t+\phi)$$

and

$$e_0 = 0$$

The corresponding phase voltages (negative sequence) may be determined by applying the inverse Park's transformation (see Chapter 3, Section 3.3):

$$e_a = e_d\cos\theta + e_q(-\sin\theta) + e_0$$

Denoting the negative-sequence stator voltage by e_{a2} and noting that $\theta=\omega t$ at synchronous speed, we have

$$e_{a2} = e_d\cos(\omega t) - e_q\sin(\omega t) + 0$$

$$= \underbrace{\frac{X_d'' + X_q''}{2} I_{a2}\sin(\omega t+\phi)}_{\text{Fundamental frequency}} + \underbrace{\frac{3}{2}(X_d'' - X_q'')I_{a2}\sin(3\omega t+\phi)}_{\text{Third harmonic}}$$

Similarly,

$$e_{b2} = \frac{X_d'' + X_q''}{2} I_{a2}\sin(\omega t+120^\circ+\phi) + \frac{3}{2}(X_d'' - X_q'')I_{a2}\sin(3\omega t+\phi)$$

$$e_{c2} = \frac{X_d'' + X_q''}{2} I_{a2}\sin(\omega t-120^\circ+\phi) + \frac{3}{2}(X_d'' - X_q'')I_{a2}\sin(3\omega t+\phi)$$

We see that the voltages have a *third harmonic* negative-sequence component which is a function of subtransient saliency $(X_d''-X_q'')$. This component is small; unless the system resonates near this harmonic, it may be neglected. As far as the fundamental frequency negative-sequence currents are concerned, the reactance is equal to the average of the subtransient reactances:

$$X_2 = \frac{X_d'' + X_q''}{2} \tag{13.78}$$

Since the mmf wave due to negative-sequence stator currents moves at twice the synchronous speed with respect to the rotor, it alternately meets permeances of the two rotor axes, corresponding to X_d'' and X_q''. Hence the value of X_2 lies between X_d'' and X_q''. *With sinusoidal negative-sequence currents applied*, the negative-sequence reactance is the *arithmetic mean* of X_d'' and X_q''. This would apply when the external circuit has a large reactance in series.

If *sinusoidal negative-sequence voltages are applied* to the stator, the resulting currents in the stator windings can be shown to have a fundamental frequency component proportional to $\frac{1}{2}\left(\frac{1}{X_d''} + \frac{1}{X_q''}\right)$ and a third harmonic component

proportional to $\frac{3}{2}\left(\frac{1}{X_d''}-\frac{1}{X_q''}\right)$. If only the fundamental is considered, the effective negative-sequence reactance is

$$X_2 = 2\frac{X_d'' X_q''}{X_d'' + X_q''} \tag{13.79}$$

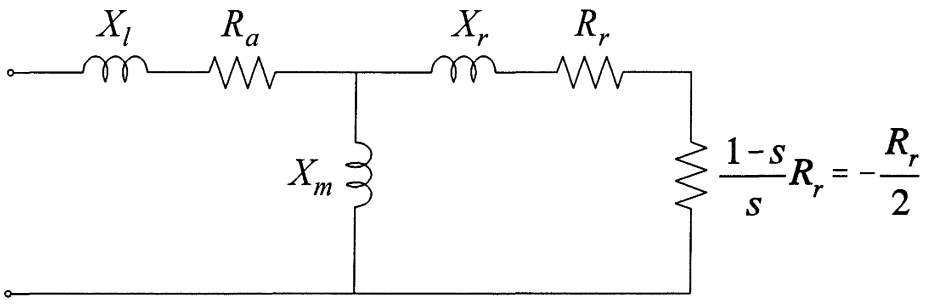
When $X_d''=X_q''$, there is no third harmonic component. In this case, the voltages and currents would have only fundamental frequency components, and $X_2=X_d''=X_q''$.

Negative-sequence resistance (R_2):

The power associated with the negative-sequence current may be expressed as a resistance times the square of the current. This resistance is designated as the negative-sequence resistance R_2.

As far as the negative-sequence stator currents are concerned, the rotor circuits appear as short-circuited windings. The situation is similar to that of an induction machine. Therefore, the physical nature of the negative-sequence resistance is best visualized by analyzing the performance of an induction motor. Figure 13.16 shows the equivalent circuit of an induction machine with symmetry in both axes. For the case with asymmetry in the two axes, the circuit represents the average of the two axes. With negative-sequence stator currents, slip $s=2$. Therefore, the equivalent resistance representing power transfer from rotor to shaft is $R_r(1-s)/s=-R_r/2$.

The total rotor copper loss is represented by R_r. *Half of the rotor loss is supplied from the stator and the other half by the shaft torque (represented by $-R_r/2$) through the rotor by conversion of mechanical power.*



X_m = magnetizing reactance
X_r = rotor leakage reactance
R_a = stator resistance
X_l = stator leakage reactance
R_r = rotor resistance
s = slip

Figure 13.16 Induction motor equivalent circuit

The real part of the equivalent impedance seen from the stator terminals is the negative-sequence resistance R_2. Since X_m is large, it may be neglected. Hence,

$$R_2 \approx R_a + \frac{R_r}{2} \tag{13.80}$$

Figure 13.17 shows the equivalent circuit of a synchronous machine appropriate for use in negative-sequence networks. Since the generated voltages in the machine are of positive sequence only, the negative-sequence equivalent circuit contains no emf, but is represented by the impedance $(R_2 + jX_2)$ offered to the flow of negative-sequence currents. The reference bus of the equivalent circuit is the neutral of the generator.

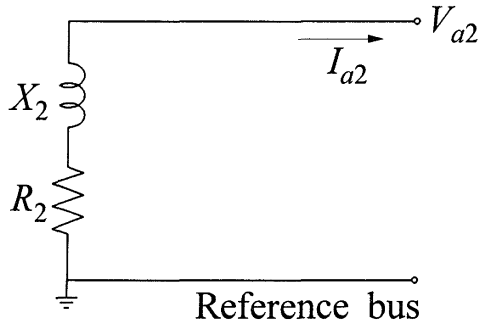


Figure 13.17 Negative-sequence equivalent circuit of a synchronous machine

Zero-sequence impedance

The machine must be star-connected; otherwise, the term zero-sequence impedance has no significance as no zero-sequence current can flow.

Zero-sequence reactance (X_0):

When zero-sequence currents are applied to the armature, the instantaneous values of currents in the three phases are equal. With the armature windings infinitely distributed so that each phase produces a sinusoidal spatial distribution of the mmf, the net field produced by the three phases with equal instantaneous currents is zero. No flux is produced across the air-gap. The only reactance associated with any phase winding is due to slot leakage flux and end-winding leakage flux. However, in an actual machine, the winding distribution is not perfectly sinusoidal, and the flux due to the three phases will have a small value. Therefore, the actual X_0 is slightly higher than for the ideal case and depends on pitch and breadth factors of the winding.

Zero-sequence resistance (R_0):

The zero-sequence resistance of a synchronous machine is somewhat larger than the positive-sequence resistance for reasons discussed below.

The spatial distribution of stator windings is usually not purely sinusoidal, but consists of higher harmonics. The spatial third harmonic contribution to the mmf due to stator currents i_a, i_b, i_c is

$$MMF = K[i_a \cos 3\theta + i_b \cos 3(\theta - 120°) + i_c \cos 3(\theta + 120°)]$$

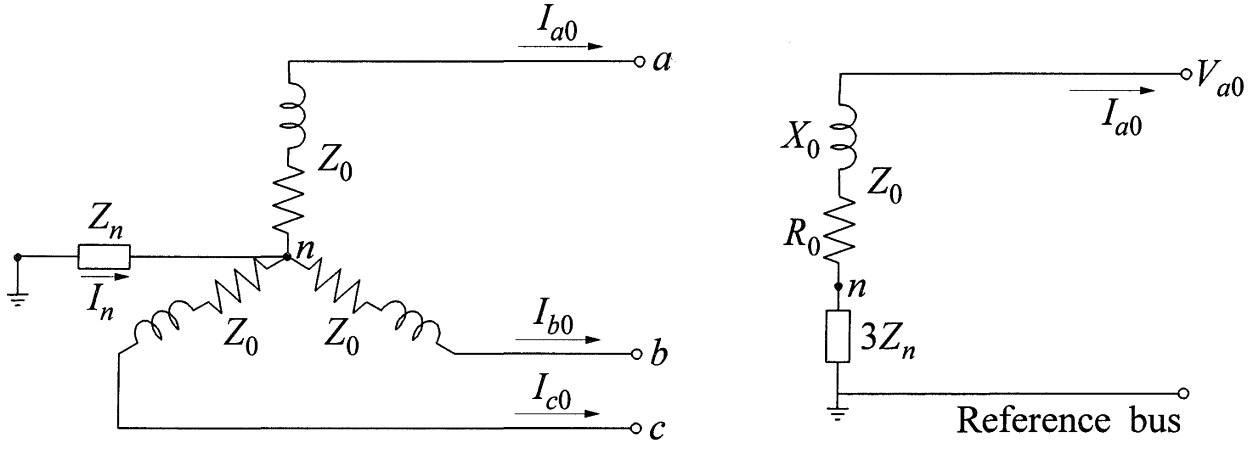
When the stator currents form a balanced set, such as the positive- or negative-sequence, the net mmf due to spatial winding distribution harmonics is zero. However, for zero-sequence currents, with $i_a = i_b = i_c = I_m \cos\omega t$ and the rotor travelling at synchronous speed ($\theta = \omega t$), the mmf due to third harmonic spatial distribution is

$$MMF = \frac{3}{2} I_m [\cos(3\theta + \omega t) + \cos(3\theta - \omega t)]$$

$$= \frac{3}{2} I_m [\cos(4\omega t) + \cos(2\omega t)]$$

Thus the mmf due to third harmonic spatial winding distribution, when zero-sequence currents flow in the stator windings, consists of second and fourth harmonic components. These induce currents in the rotor and cause rotor heating. Therefore, the zero-sequence resistance (R_0) is slightly higher than the positive-sequence resistance (R_1). The difference is usually not significant.

Figure 13.18(a) shows the flow of zero-sequence currents in the three phases and the neutral of the synchronous machine. The corresponding (single-phase) equivalent circuit is shown in Figure 13.18(b).



$$I_n = I_{a0} + I_{b0} + I_{c0} = 3I_{a0}$$

(a) Current paths (b) Equivalent circuit

Figure 13.18 Zero-sequence current paths and equivalent circuit of a synchronous machine

The neutral impedance Z_n carries a current equal to the sum of the zero-sequence currents in the three phases. This is reflected as $3Z_n$ in the equivalent circuit of Figure 13.18(b), which represents only one phase. The reference bus for the zero-sequence equivalent circuit is the ground at the generator. If the neutral is isolated from the ground, $Z_n=\infty$ and $I_{ao}=0$.

13.4.3 Sequence Impedances of Transmission Lines

Positive- and negative-sequence impedances

In a symmetrical three-phase static circuit, the positive- and negative-sequence impedances are identical because the impedance of such a circuit is independent of the phase order of the applied voltages. The equivalent circuits of transmission lines developed in Chapter 6 are applicable to the positive-sequence as well as the negative-sequence networks.

Zero-sequence impedance

When only zero-sequence currents flow in a transmission line, the currents in the three phases are identical. The sum of these currents returns through the ground and/or overhead ground wires. Since the three-phase currents are in phase, the magnetic field produced is very different from that produced by positive- or negative-sequence currents. It requires consideration of the current distribution in the earth. The net effect is that the zero-sequence reactance of transmission lines tends to be 2 to 3 times the positive-sequence reactance [15-17].

Zero-sequence currents flowing through ground result in voltage drops due to the impedance of the ground. Evidently, the ground is not necessarily at the same potential at all points. The reference bus of the zero-sequence network does not represent the ground potential at any particular point but is the reference ground for zero-sequence voltages throughout the system. Therefore, the impedances of the ground and ground wires are included in zero-sequence impedances of the transmission lines. This ensures that the zero-sequence voltages at the terminals are correctly given when referred to the reference bus.

13.4.4 Sequence Impedances of Transformers

Positive- and negative-sequence impedances

Transformers, like transmission lines, are non-rotative or static. With the assumption that symmetry exists between different phases, the impedances to balanced three-phase currents do not depend on the phase sequence. Therefore, the equivalent circuits and the associated impedances derived in Chapter 6 for the two-winding and three-winding transformers are equally valid for the positive-sequence and the negative-sequence networks.

Zero-sequence impedances

The impedance offered by a transformer to the flow of zero-sequence currents depends on the winding connections. Figure 13.19 gives the zero-sequence equivalent circuits for different winding connections applicable to two-winding and three-winding transformers.

For zero-sequence currents to flow through windings on one side of the transformer and into the connected lines, a return path must exist through which a completed circuit is provided. Additionally, there must be a path for the corresponding current in the coupled windings on the other side.

For illustration, let us consider the winding connections for case 1 in Figure 13.19. The Y-connected primary (P) windings with the neutral grounded provide a path to the ground. The Δ-connected secondary (S) windings provide a path for the zero-sequence currents, which circulate within the Δ. This serves to balance the currents in the primary windings; however, the zero-sequence currents circulating within the secondary windings cannot flow in the lines connected to them. The impedance Z_0 represents the total per-phase leakage reactances and resistances of the primary and secondary windings and is equal to the positive-sequence impedance. The neutral of the Y-connected primary is grounded through an impedance Z_n; therefore, the effective zero-sequence impedance as seen from the primary side is Z_0+3Z_n. Since a Δ-connected circuit provides no path for zero-sequence currents flowing in the line, the impedance as seen from the secondary side is infinite.

If the windings on one side are Y-connected with neutral ungrounded (as in cases 2 and 5), zero-sequence currents cannot flow in the windings on either side. Viewed from either the primary side or the secondary side, the zero-sequence impedance is infinite.

Cases 6 to 8 in Figure 13.19 consider three-winding transformers where the effects of the leakage reactances and resistances of the three windings are represented by a star-connected equivalent (see Chapter 6). Connection of this equivalent to the primary (P), secondary (S), and tertiary (T) terminals, and the reference bus depends on the winding connections as shown in the figure.

13.4.5 Simulation of Different Types of Faults

In this section, we consider the simulation of a power system that is essentially symmetrical but is rendered unbalanced by a fault at a particular location on the system. Such faults can be analyzed by appropriately interconnecting the positive-, negative-, and zero-sequence networks at the fault point as described below.

Figure 13.20 identifies the fault currents and voltages at fault location F. The *currents flowing into the fault* from the three phases *a*, *b*, and *c* are represented by I_a, I_b, and I_c, respectively; V_a, V_b and V_c represent *voltages to ground* at F.

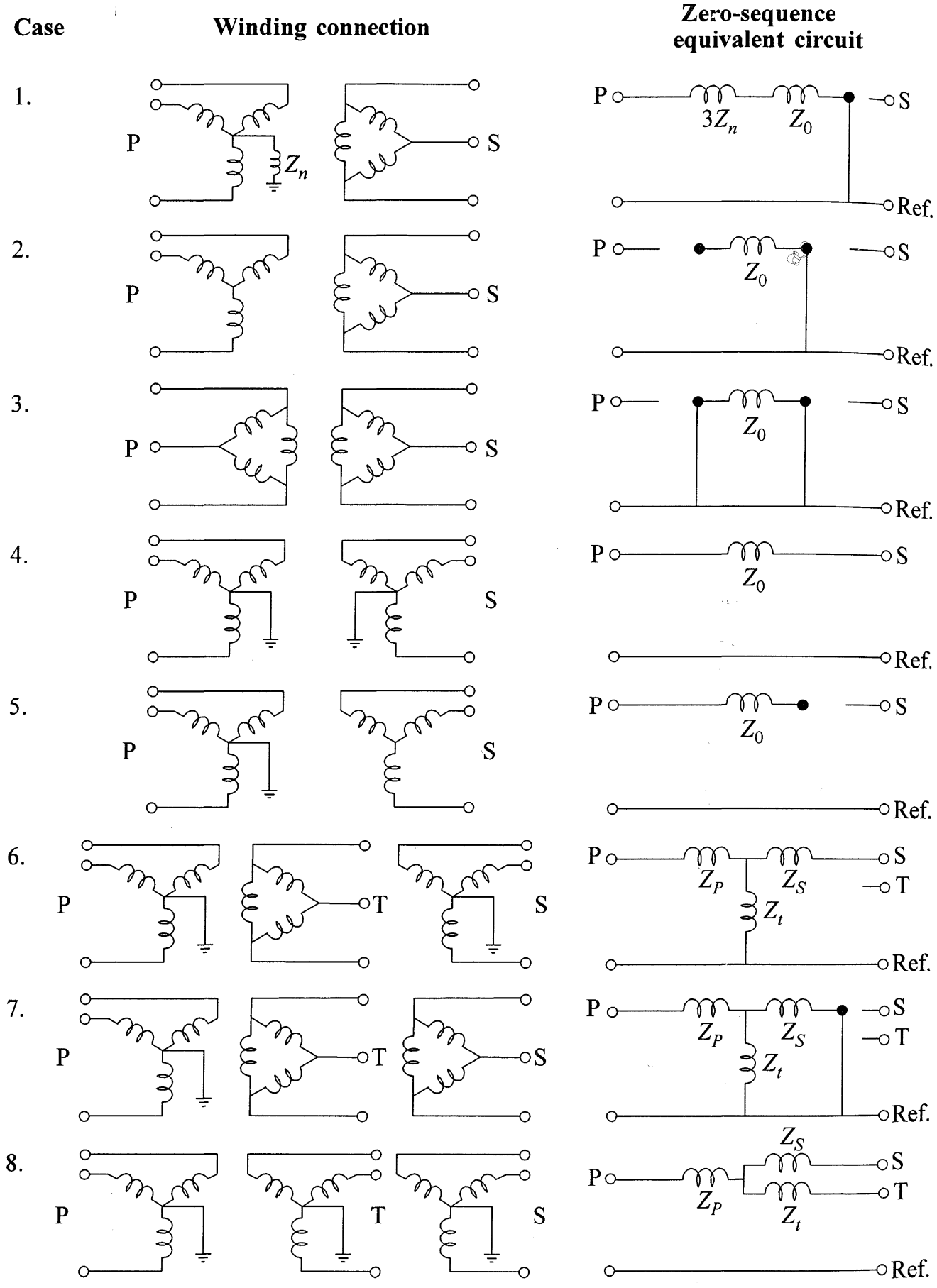


Figure 13.19 Zero-sequence equivalent of three-phase two-winding and three-winding transformer banks

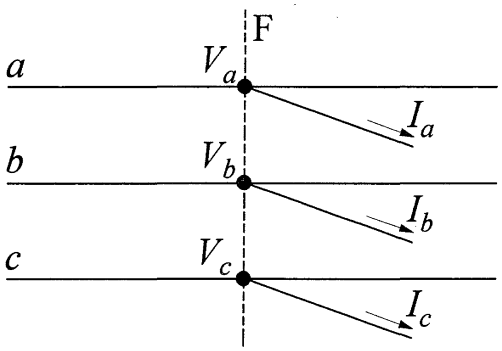


Figure 13.20 Designation of fault currents and voltages

(a) Single line-to-ground fault

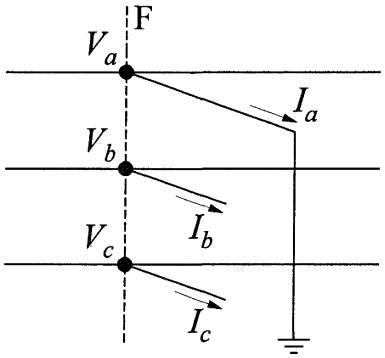
Let us assume that phase *a* is shorted to ground at the fault point F, as shown in Figure 13.21(a). From the figure, we see that

$$V_a = 0 \qquad I_b = I_c = 0$$

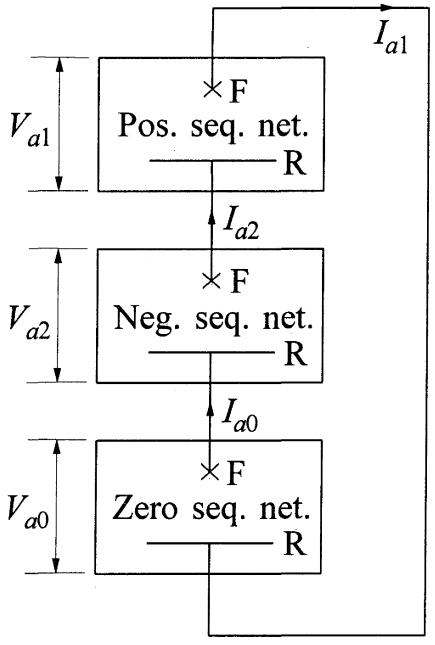
In terms of the symmetrical components (see Equations 13.69 and 13.71), we have

$$V_{a1} + V_{a2} + V_{a0} = V_a = 0$$

$$I_{a1} = I_{a2} = I_{a0} = \frac{I_a}{3}$$



(a) Fault schematic



(b) Sequence network connection

Figure 13.21 Simulation of a single line-to-ground fault

The connection of the sequence networks to satisfy the above relationships is shown in Figure 13.21(b). The three sequence networks are connected at the fault point (F) and the reference bus (R) of each sequence network so as to form a series connection.

(b) Line-to-line fault

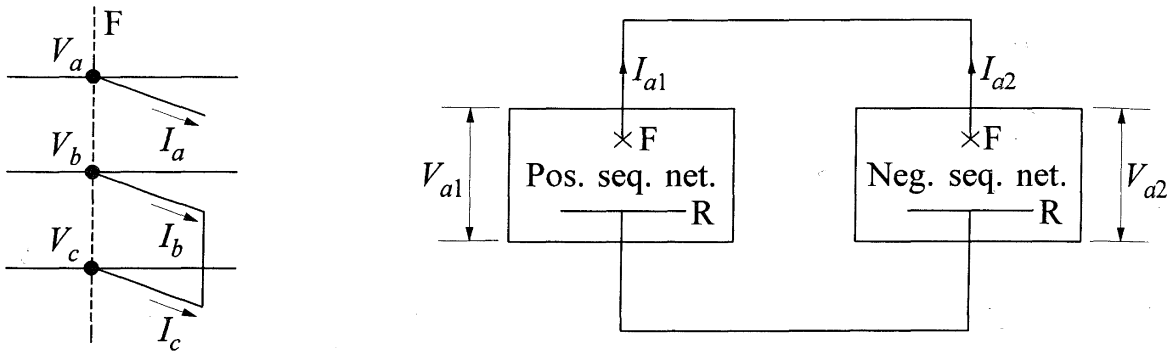
From Figure 13.22(a),

$$V_b = V_c \qquad I_a = 0 \qquad I_b + I_c = 0$$

In terms of symmetrical components,

$$V_{a1} = V_{a2} \qquad I_{a1} + I_{a2} = 0 \qquad I_{a0} = 0$$

The sequence network connection reflecting the above relationships is shown in Figure 13.22(b). Since the fault does not involve ground, the zero-sequence network is absent.



(a) Fault schematic (b) Sequence network connection

Figure 13.22 Simulation of a line-to-line fault

(c) Double line-to-ground fault

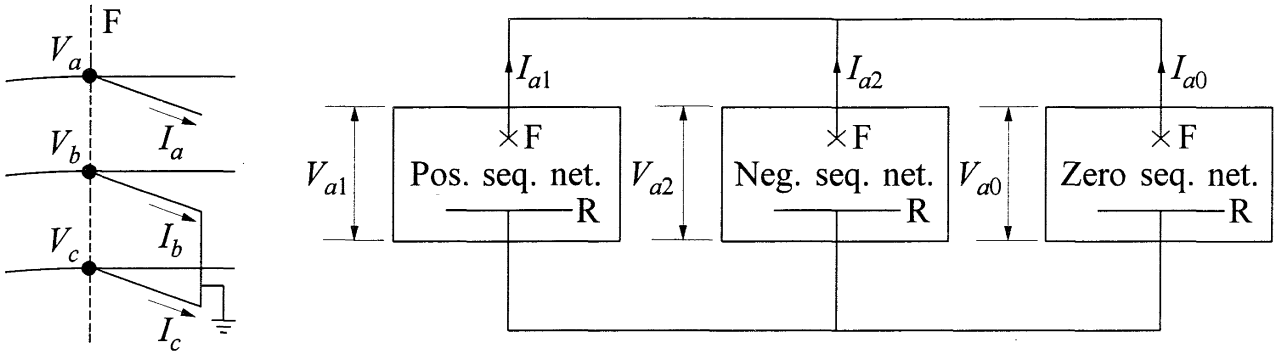
From Figure 13.23(a),

$$V_b = V_c = 0 \qquad I_a = 0$$

In terms of symmetrical components,

$$V_{a1} = V_{a2} = V_{a0}$$

$$I_{a1} + I_{a2} + I_{a0} = 0$$



(a) Fault schematic (b) Sequence network connection

Figure 13.23 Simulation of a double line-to-ground fault

The corresponding sequence network connection is shown in Figure 13.23(b).

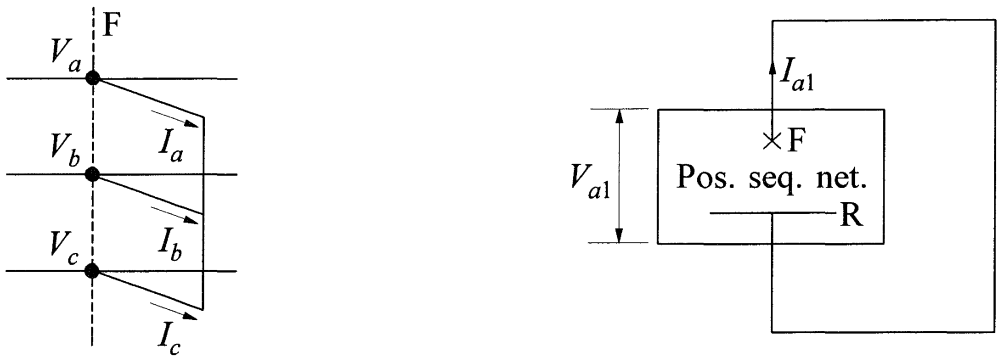
(d) Three-phase fault

To complete the picture with regard to simulation of different types of faults in terms of sequence networks, let us examine a symmetrical three-phase fault as shown in Figure 13.24(a).

From Figure 13.24,

$$V_a = V_b = V_c = 0$$

$$I_a + I_b + I_c = 0$$



(a) Fault schematic (b) Sequence network connection

Figure 13.24 Simulation of a three-phase fault

In terms of symmetrical components,

$$I_{a0} = 0$$

$$V_{a1} = V_{a2} = V_{a0} = 0$$

There are no zero-sequence or negative-sequence emf's, and the voltages V_{a0} and V_{a2} at the fault point F are each equal to zero. Therefore, zero- and negative-sequence currents do not flow anywhere in the system. As expected, only the positive-sequence network is involved. The fault is simulated by shorting the fault point F and the reference bus R of the positive-sequence network, as shown in Figure 13.24(b).

Formation of sequence networks

We see from the above analyses that a fault on a power system can be analyzed by appropriately interconnecting the sequence networks of the system. The solution of the resulting network gives the symmetrical components of voltages and currents throughout the system.

The positive-, negative-, and zero-sequence systems represent symmetrical systems. Therefore, each of these systems may be represented by an equivalent single-phase network. Each element of the power system is represented by a model with an appropriate degree of precision.

In each sequence network, the sequence voltages are referred to the reference (or zero potential) bus for the network. In the positive- or negative-sequence systems, all neutral points are at the same potential. Therefore, the neutrals of each of these systems can be connected to a common bus which is the reference or zero-potential bus for its sequence network.

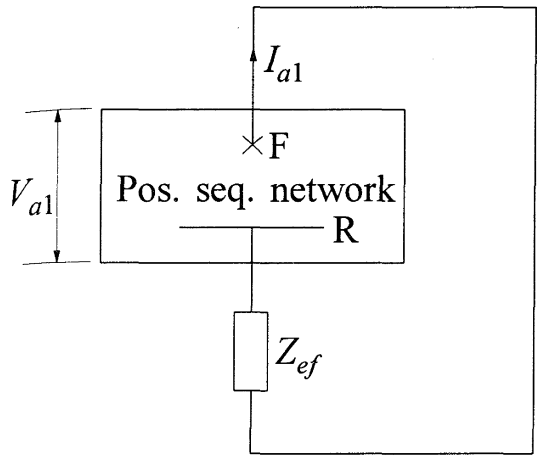
As stated earlier, the ground is not necessarily at the same potential at all points in the system. Therefore, the reference bus for the zero-sequence network is not representative of the ground at any particular point; instead, the reference bus serves as a reference for zero-sequence voltages at all points of the system. The individual equipment models are so constructed that the zero-sequence voltages to ground are correctly represented when referred to the reference bus of the network.

Representation in stability studies

The positive-sequence network is represented in detail with equipment models as described in Chapters 3 to 11.

The negative- and zero-sequence voltages and currents throughout the system are usually not of interest in stability studies. Therefore, it is unnecessary to simulate the complete negative- and zero-sequence networks in system stability simulations. Their effects may be represented by equivalent impedances (Z_2 and Z_0) as viewed at the fault point F. These impedances are combined appropriately depending on the type

of fault and inserted as the effective fault impedance Z_{ef} in the positive-sequence network as shown in Figure 13.25.



Fault type	Z_{ef}
Line-to-ground	Z_2+Z_0
Line-to-line	Z_2
Double line-to-ground	$\dfrac{Z_2 Z_0}{Z_2+Z_0}$
Three-phase	0

Figure 13.25 Representation of faults in system stability studies

This representation gives the correct voltages and currents in the positive-sequence network.

There are no negative- or zero-sequence voltages generated in the system. The negative- and zero-sequence currents that flow during unbalanced faults are driven by the positive-sequence voltage sources. The positive-sequence power outputs computed represent the actual power supplied electrically by the machines. This includes all negative- and zero-sequence resistance losses supplied electrically.

Negative-sequence braking torque

As discussed in Section 13.4.2, only half of the negative-sequence rotor losses in synchronous machines are supplied electrically. The other half are supplied mechanically by the shaft power or torque. This represents the component of the total mechanical torque that is converted to supply rotor losses. It acts to decelerate the rotor and is called the negative-sequence braking torque. This effect could be significant for machines close to a fault, particularly those with solid rotors or salient pole rotors with high-resistance damper windings. The method of accounting for this braking torque is described below.

Referring to Figure 13.16, with the magnetizing reactance X_m neglected, the negative-sequence braking torque is

$$T_{b2} = \frac{R_r}{2} I_{a2}^2 = (R_2 - R_a) I_{a2}^2 \tag{13.81}$$

where R_2 is the negative-sequence resistance of the machine and R_a is its stator resistance.

The machine negative-sequence current I_{a2} can be determined from the negative-sequence network. Depending on the network configuration, I_{a2} can be estimated as a fraction of the machine positive-sequence current [20].

The total accelerating torque acting on the rotor is

$$T_a = T_m - T_e - K_D \Delta\omega_r - T_{b2}$$

The swing equation (Equation 13.22) is appropriately modified to include T_{b2}.

Example 13.4

Figure E13.11 shows the system representation applicable to a 1,000 MVA, 20 kV, 60 Hz generating unit.

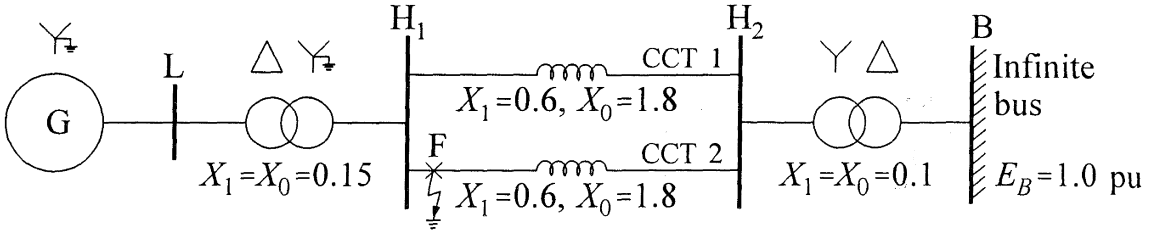


Figure E13.11

The transmission data shown on the figure are in per unit on 1,000 MVA, 20 kV base. Network resistances are assumed to be negligible.

The generator data in per unit on the rating of the unit are as follows:

$X_d = 1.81$	$X_q = 1.76$	$X'_d = 0.3$	$X'_q = 0.65$
$X''_d = X''_q = 0.25$	$X_2 = 0.25$	$X_0 = 0.04$	$R_a = 0.003$
$R_2 = 0.063$	$R_0 = 0.005$	$T'_{d0} = 8.0$ s	$T'_{q0} = 1.0$ s
$T''_{d0} = 0.03$ s	$T''_{q0} = 0.07$ s	$H = 3.5$	$K_D = 0$

The neutrals of the generator stator and the step-up transformer HT windings are solidly grounded. The neutral of the star-connected winding of the transformer near the infinite bus is ungrounded.

(a) A double line-to-ground (LLG) fault occurs on circuit 2 at point F as shown in Figure E13.11.

(i) Neglecting all resistances, find the value of the effective fault impedance Z_{ef} which, when inserted in the positive-sequence network, represents the unbalanced fault.

(ii) If the initial generator output conditions are

$$P_0 = 0 \qquad Q_0 = 0 \qquad E_t = 1.0$$

compute the magnitudes of positive-, negative-, and zero-sequence currents throughout the network immediately after the fault occurs, neglecting the effect of generator resistance.

(iii) Compute the negative-sequence braking torque corresponding to the above condition.

(b) How would the above results change if a line-to-ground fault or a line-to-line fault were to occur at point F?

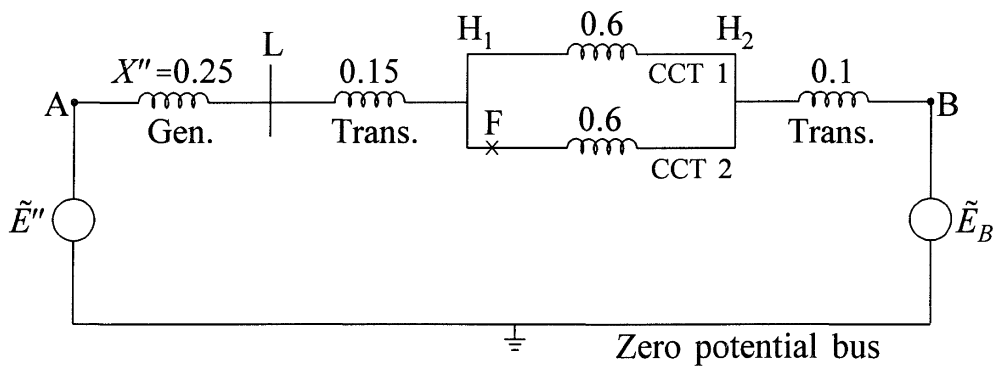
Solution

For conditions immediately after the fault occurs, the effective positive-sequence machine reactance is $X''=X_d''=X_q''$.

The three-sequence networks of the system are shown in Figure E13.12. Since $X_d''=X_q''=X_2$, the negative- and positive-sequence reactances are equal for each of the elements in the system.

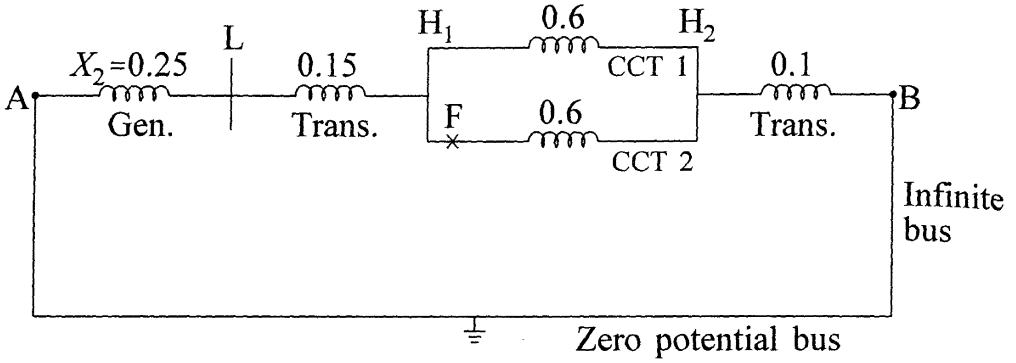
(a) Double line-to-ground fault

(i) Each sequence network represents a balanced system. The unbalanced effect introduced by the fault at location F is represented by interconnecting the sequence networks as shown in Figure E13.13.

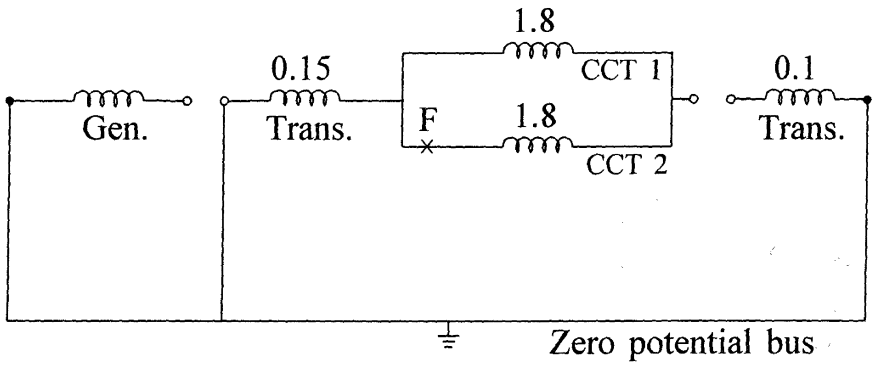


(a) Positive-sequence network

Figure E13.12 *(Continued on the next page)*



(b) Negative-sequence network



(c) Zero-sequence network

Figure E13.12 (*Continued*)

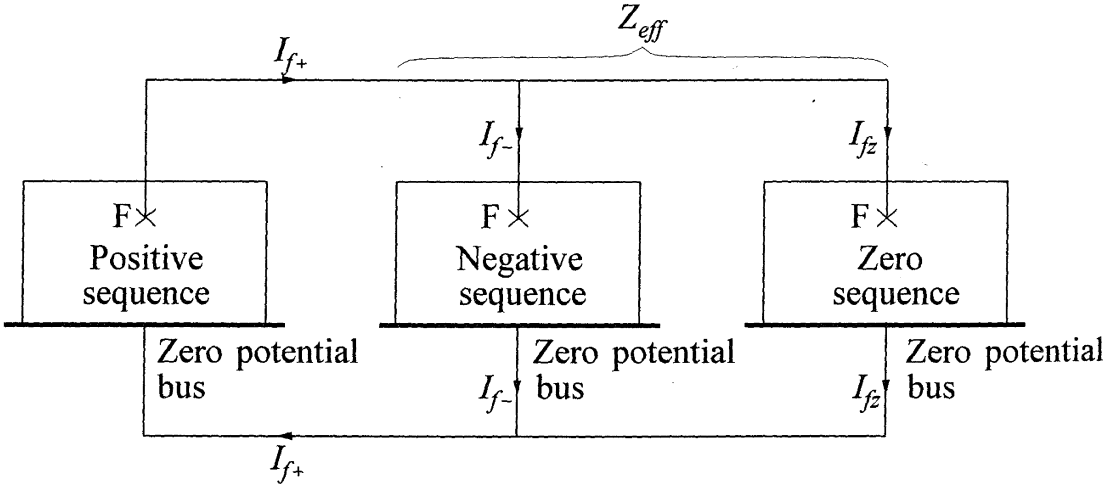
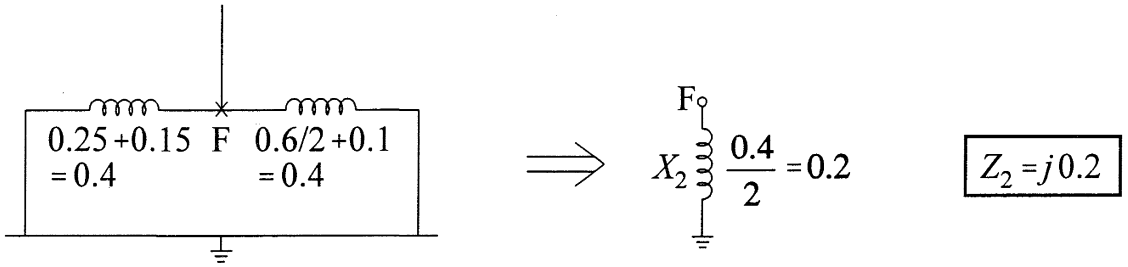
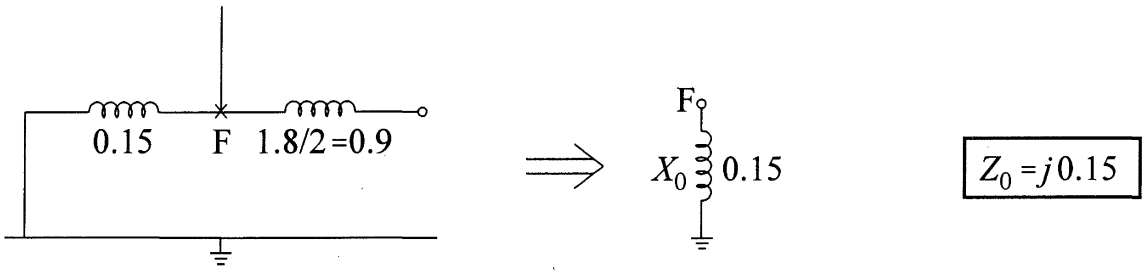


Figure E13.13

The effective negative-sequence and zero-sequence impedances as measured at point F are shown in Figure E13.14.



(a) Effective negative-sequence impedance



(b) Effective zero-sequence impedance

Figure E13.14

The effective fault impedance representing the L-L-G fault is

$$Z_{ef} = \frac{Z_2 Z_0}{Z_2 + Z_0}$$

$$= \frac{j(0.2 \times 0.15)}{0.35}$$

$$= j0.0857 \text{ pu}$$

(ii) Since prior to the fault $P=Q=0$,

$$E'' = E_t = E_B = 1.0 \text{ pu}$$

The positive-sequence network with the effective fault impedance inserted at F reduces to the form shown in Figure E13.15(a).

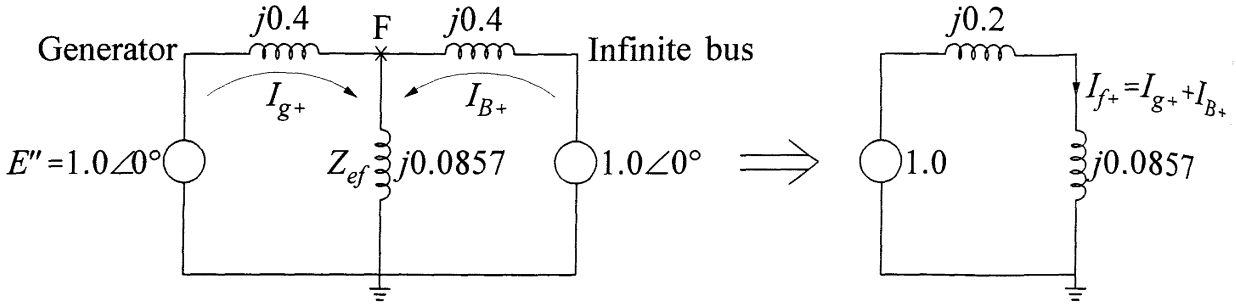
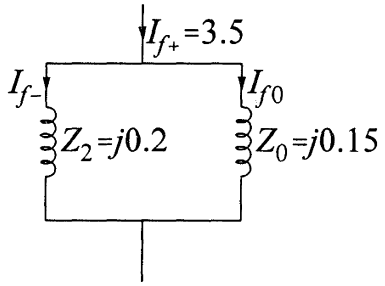


Figure E13.15 (a)

Because of network symmetry the solution is considerably simplified. The positive-sequence component of the fault current is

$$I_{f+} = \frac{1.0}{j0.2857} = -j3.5 \quad \text{pu}$$

The total positive-sequence fault current splits into negative- and zero-sequence components as shown in Figure E13.15(b).



$$I_{f-} = \frac{0.15\times 3.5}{0.35} = 1.5 \quad \text{pu}$$

$$I_{f0} = I_{f+} - I_{f-} = 3.5 - 1.5 = 2.0 \quad \text{pu}$$

Figure E13.15 (b)

Because of the network symmetry about the point F, one-half of the fault current of each sequence component flows from the generator, and the other half from the infinite bus. Owing to the generator step-up transformer winding connections, the zero-sequence current is restricted to the transformer; no zero-sequence current flows through the generator. Figure E13.16 shows current flows in different parts of the sequence networks.

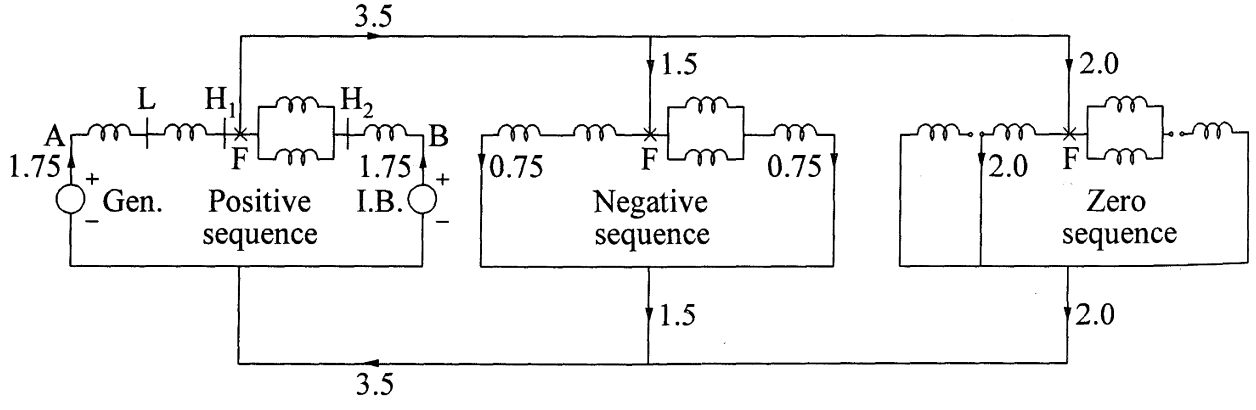


Figure E13.16

(iii) The negative-sequence braking torque is given by

$$T_{b2} = (R_2 - R_a) I_{g2}^2$$

$$= (0.063 - 0.003)0.75^2 = 0.034 \quad \text{pu}$$

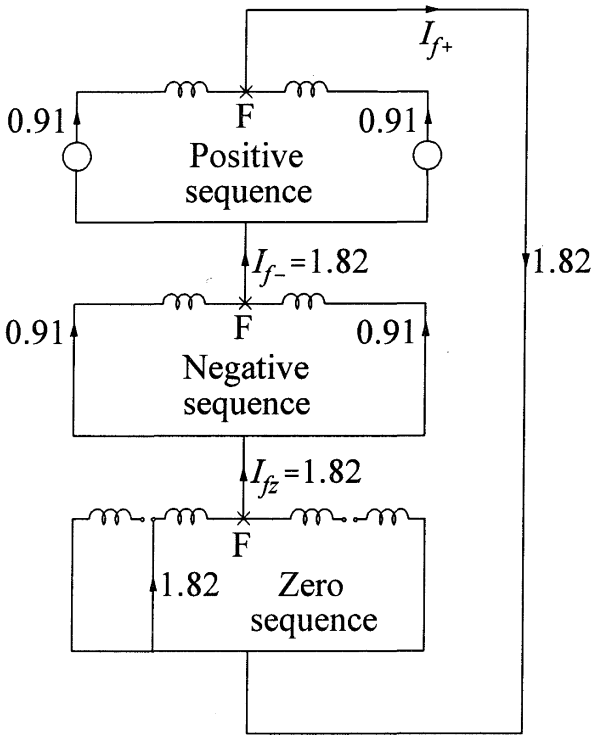
(b) Line-to-ground fault

(i) The effective fault impedance is

$$Z_{ef} = Z_2 + Z_0 = j(0.2 + 0.15)$$

$$= j0.35 \quad \text{pu}$$

(ii) Figure E13.17 shows current flows in different parts of the sequence networks.



$$I_{f+} = I_{f-} = I_{fz}$$

$$= \frac{1.0}{Z_1 + Z_2 + Z_0}$$

$$= \frac{1.0}{j(0.2 + 0.2 + 0.15)}$$

$$= -j1.82 \quad \text{pu}$$

Figure E13.17

(iii) The negative-sequence braking torque is

$$T_{b2} = (R_2 - R_a) I_2^2$$

$$= (0.063 - 0.003)0.91^2$$

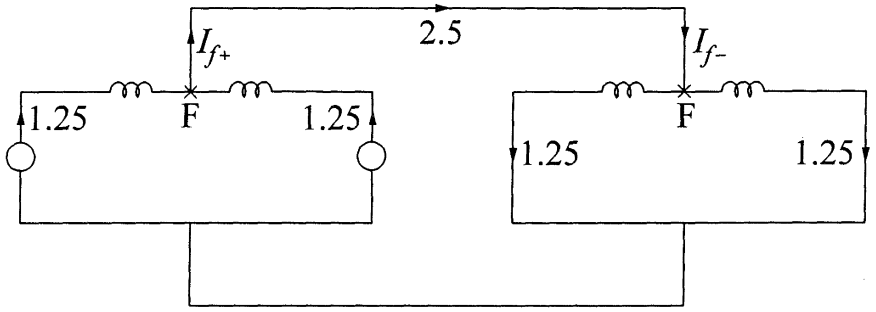
$$= 0.05 \quad \text{pu}$$

Line-to-line fault

(i) The effective fault impedance is

$$Z_{ef} = Z_2 = j0.2$$

(ii) Figure E13.18 shows current flows in the sequence network.



$$I_{f+} = -I_{f-} = \frac{1.0}{Z_1 + Z_2}$$

$$= \frac{1.0}{j0.4} = -j2.5 \text{ pu}$$

Figure E13.18

(iii) The negative-sequence braking torque is

$$T_{b2} = (R_2 - R_a) I_2^2 = (0.063 - 0.003)\, 1.25^2$$

$$= 0.094 \text{ pu}$$

■

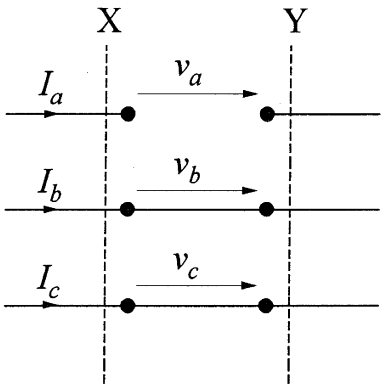
13.4.6 Representation of Open-Conductor Conditions

Open-conductor conditions may be caused by broken conductors or a deliberate single-phase switching operation. Such faults may involve the opening of one phase or two phases of a three-phase circuit.

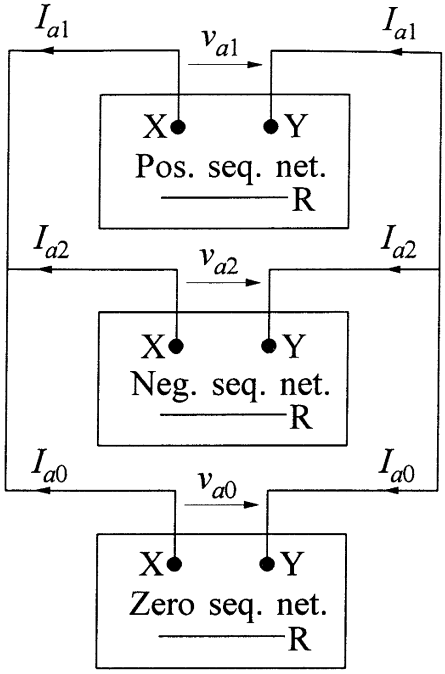
(a) One open conductor

Figure 13.26(a) shows a section of a three-phase system with phase *a* open between points X and Y. Let v_a, v_b, and v_c be series voltage drops in phases between X and Y in phases *a*, *b*, *c*, respectively; I_a, I_b and I_c are the line currents. From Figure 13.26(a),

$$v_b = v_c = 0 \qquad I_a = 0$$



(a) Schematic diagram



(b) Connection of sequence networks

Figure 13.26 Simulation of one open-conductor condition

In terms of symmetrical components,

$$v_{a1} = v_{a2} = v_{a0} = \frac{1}{3}v_a$$

$$I_{a1}+I_{a2}+I_{a0} = 0$$

The connections of sequence networks so as to satisfy the above equations are shown in Figure 13.26(b).

(b) Two open conductors

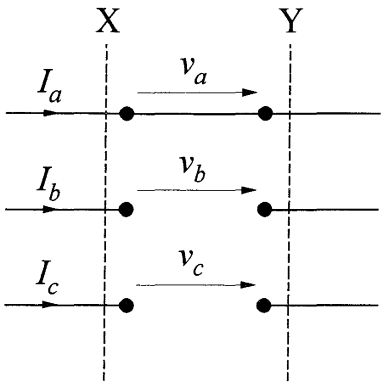
We now consider the condition with phases *b* and *c* open between points X and Y as shown in Figure 13.27(a). The applicable equations are

$$v_a = 0 \qquad I_b = I_c = 0$$

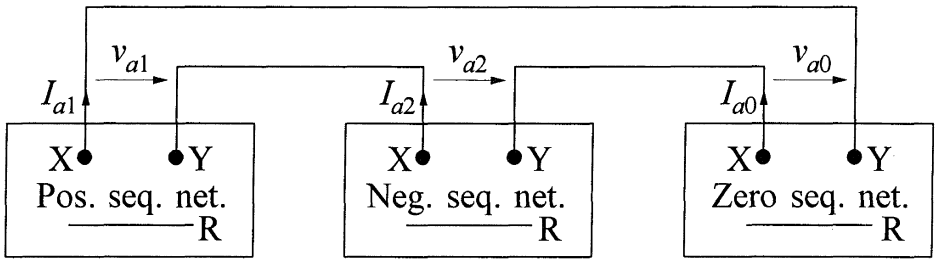
In terms of symmetrical components,

$$v_{a1}+v_{a2}+v_{a0} = 0$$

$$I_{a1} = I_{a2} = I_{a0} = \frac{1}{3}I_a$$



(a) Schematic diagram



(b) Connection of sequence networks

Figure 13.27 Simulation of two-open-conductors condition

The sequence network connections that satisfy the above equations are shown in Figure 13.27(b).

From Figure 13.26 we see that, for the one-phase open-circuited condition, the three-sequence networks are connected in parallel at points X and Y; therefore, even if the zero-sequence circuit as seen from X and Y has infinite impedance, some power is transferred through the line between X and Y.

For the case with two phases open-circuited as in Figure 13.27, the three-sequence networks are connected in series; unless the zero-sequence circuit provides a path having finite impedance, no power can be transferred through the line.

Example 13.5

The system shown in Figure E13.11 (Example 13.4) is subjected to a single line-to-ground fault at point F on circuit 2. The fault is cleared by single-phase switching which disconnects the faulted conductor at both ends simultaneously. Show how the network may be represented in stability studies during the period when one conductor of circuit 2 is switched out.

Solution

This situation differs slightly from that depicted in Figure 13.26. As shown in Figure E13.19, the impedances of conductors of phases *b* and *c* need to be accounted for. This is achieved by including the impedances associated with circuit 2 in the sequence networks.

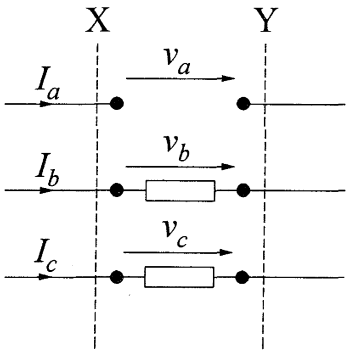


Figure E13.19

Figure E13.20 shows the sequence networks of the system of Figure E13.11 and their interconnection to represent the condition with one phase of circuit 2 open at both ends.

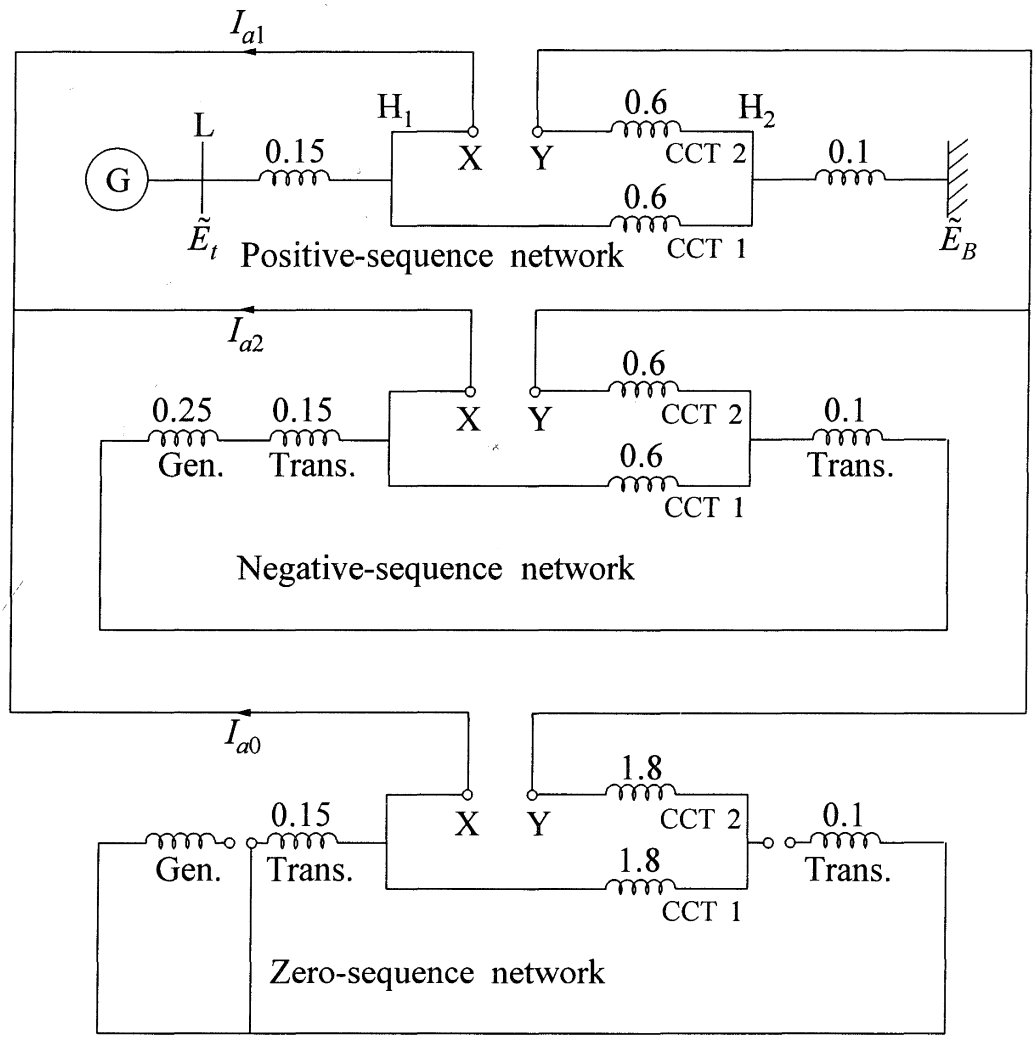
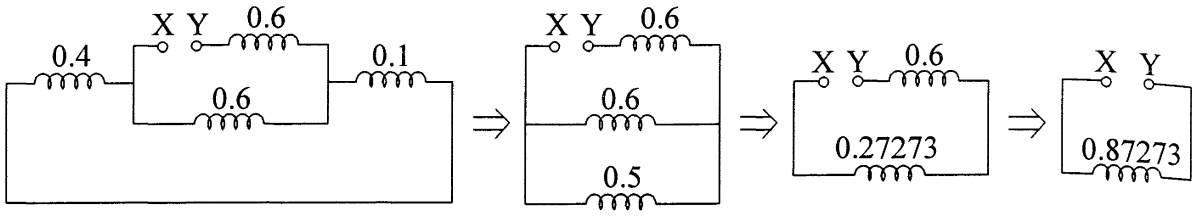
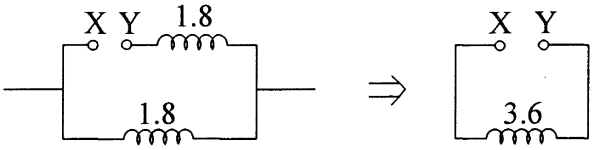


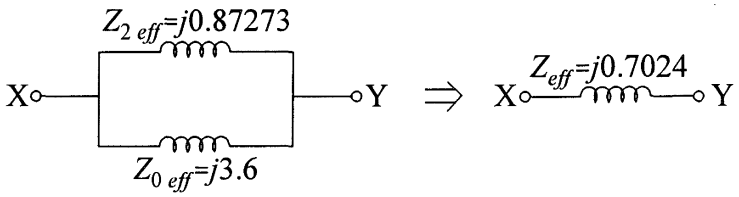
Figure E13.20



(a) Reduction of negative-sequence network



(b) Reduction of zero-sequence network



(c) Total effective series impedance

Figure E13.21 Reduction of negative- and zero-sequence networks

As shown in Figure E13.21, the effective negative- and zero-sequence impedances as viewed from points X and Y are

$$Z_{2eff} = j0.87273 \quad \text{pu}$$

$$Z_{0eff} = j3.6 \quad \text{pu}$$

and the net effective impedance that has to be inserted between points X and Y of the positive sequence network is

$$Z_{eff} = j0.7024 \quad \text{pu}$$

Thus, from the viewpoint of power transfer between the generator and the infinite bus, the effect of opening one phase of circuit 2 is the same as increasing the reactance of the circuit by 0.7024 pu. ■

13.5 PERFORMANCE OF PROTECTIVE RELAYING

Protective relays detect the existence of abnormal system conditions by monitoring appropriate system quantities, determine which circuit breakers should be opened, and energize trip circuits of those breakers. In order to perform their functions satisfactorily, relays should satisfy three basic requirements: selectivity, speed, and reliability.

Since transient stability is concerned with the ability of the power system to maintain synchronism when subjected to a severe disturbance, satisfactory performance of certain protection systems is of paramount importance in ensuring system stability. Protective relays must be able to distinguish among fault conditions, stable power swings and out-of-step conditions. While the relays should initiate circuit-breaker operations to clear faulted elements, it is important to ensure that there are no further relaying operations that cause unnecessary opening of unfaulted elements during stable power swings. Tripping of unfaulted elements would weaken the system further and could lead to system instability.

On the other hand, if the system is unstable we need to know how it separates and whether the point of separation is acceptable. Special relaying may be required to cause separation as desired.

One of the important aspects of transient stability analysis, then, is the evaluation of the performance of protective systems during the transient period, particularly the performance of relaying used for protection of transmission lines and generators.

13.5.1 Transmission Line Protection [21-23]

There are a variety of line protection schemes and practices used by utilities to meet particular system requirements. The following factors influence the choice of the protection scheme:

- Type of circuit: single line, parallel line, multiterminal, magnitude of fault current infeeds, etc.
- Function of line, its effect on service continuity, speed with which fault has to be cleared
- Coordination and matching requirements

Three basic types of relaying schemes are used for line protection: (a) overcurrent relaying, (b) distance relaying, and (c) pilot relaying [22].

(a) Overcurrent relaying

Overcurrent relaying is the simplest and cheapest form of line protection. Two basic forms of relays are used: instantaneous overcurrent relay and time overcurrent relay. They are difficult to apply where coordination, selectivity, and speed are important. Changes to their settings are usually required as the system configuration changes [22].

Overcurrent relaying cannot discriminate between load and fault currents; therefore, when used for phase-fault protection, it is applicable only when the minimum fault current exceeds the full load current.

Overcurrent relaying is used principally on subtransmission systems and radial distribution systems. Since faults on these systems usually do not affect system stability, high-speed protection is not required.

Overcurrent relaying schemes, which utilize communication channels to interchange intelligence between terminal stations, have been developed to overcome the above limitations. The two most common schemes are pilot wire relaying and phase-comparison relaying schemes.

(b) Distance relaying

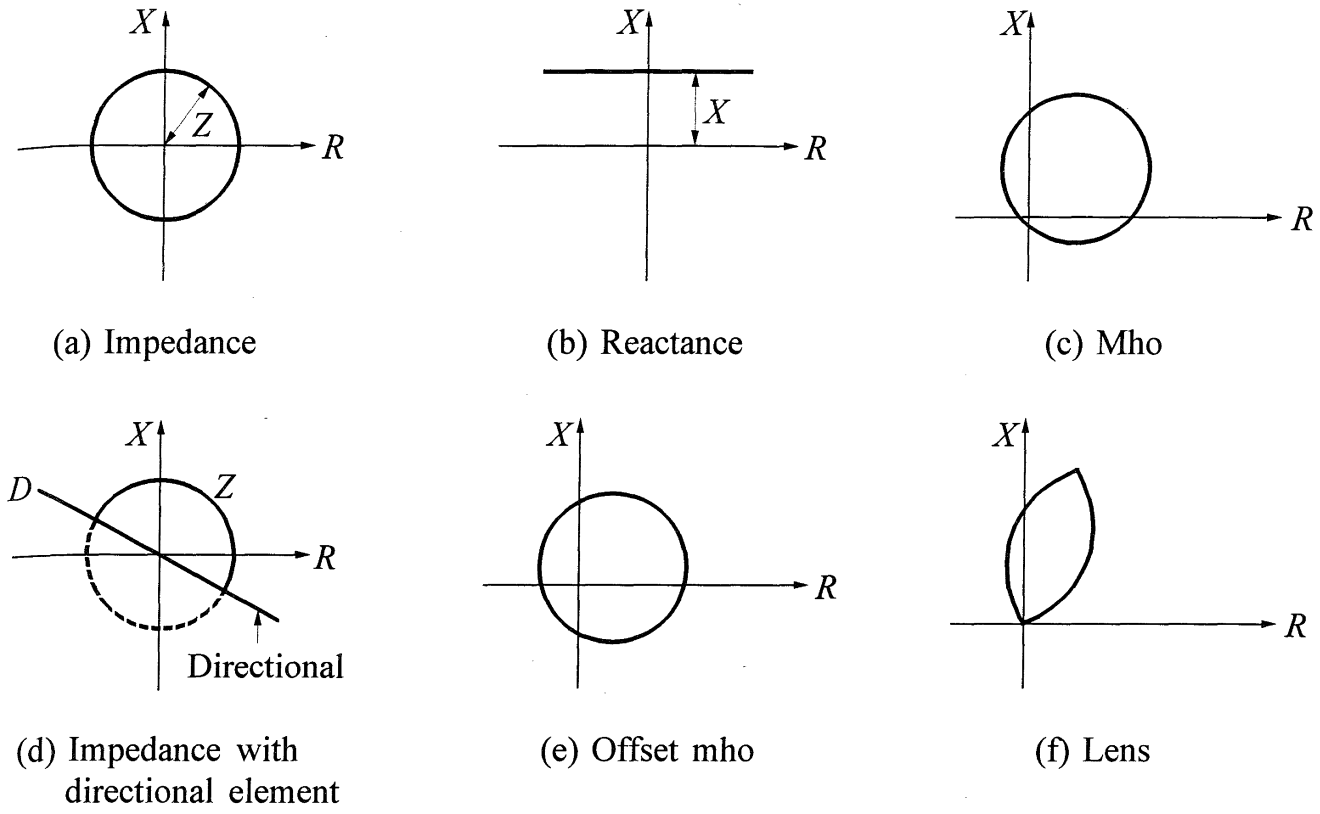
A distance relay responds to a ratio of measured voltage to measured current. The relay operates if the ratio, which represents the effective impedance of the network, is less than the relay setting. Impedance is a measure of distance along the transmission line and, therefore, the relay is known as a distance relay.

The impedance approach provides an excellent way of obtaining discrimination and selectivity, by limiting relay operation to a certain range of the impedance. The following are the different forms of distance relays:

- Impedance relay
- Reactance relay
- Mho relay
- Modified mho and impedance relays, and combinations thereof

The triggering characteristics of distance relays may be shown conveniently on a complex impedance (R-X) plane [24] as illustrated in Figure 13.28.

The impedance characteristic is a circle on the R-X plane; the reactance characteristic is a horizontal line on the R-X plane; the mho characteristic is a straight line on the G-B (admittance) plane, and a circle through origin on the R-X (impedance) plane. The relay operates when the impedance measured by the relay falls within the characteristic.



(a) Impedance (b) Reactance (c) Mho

(d) Impedance with directional element (e) Offset mho (f) Lens

Figure 13.28 Distance relay characteristics displayed on a coordinate system with resistance (R) as the abscissa and reactance (X) as the ordinate

The mho characteristic is inherently directional; i.e., it detects faults only in one direction. The reactance and impedance characteristics detects faults in all four quadrants. Therefore, some type of directional supervision is generally used with these relays. Combinations of similar elements with different settings and/or elements with different characteristics are used to provide selectivity and coordination.

Distance relaying is the most widely used form of protection for transmission lines. It is easy to apply and coordinate, provides fast protection, and is less affected by changes in system conditions.

Figure 13.29 illustrates the application of distance relaying. At each end of the line, three separate sets of relays are arranged to provide three protective zones as shown. The first and second protective zones provide *primary protection* for the protected line, and the third zone provides *remote backup* for the adjacent line.

For example, the first-zone relays at A are set to protect about 80% of line AB without any time delay. This ensures high-speed protection of the line section and provides about a 20% margin of safety to avoid incorrect relay operation caused by equipment errors for faults beyond the end of the line section.

The second-zone relays at A are set to reach beyond the end of the line, a typical setting being about 120% of the impedance of the protected line AB. This ensures protection of the remaining 20% of the line not protected by the first-zone relays. Since the second-zone relays will overreach line AB and operate for faults on

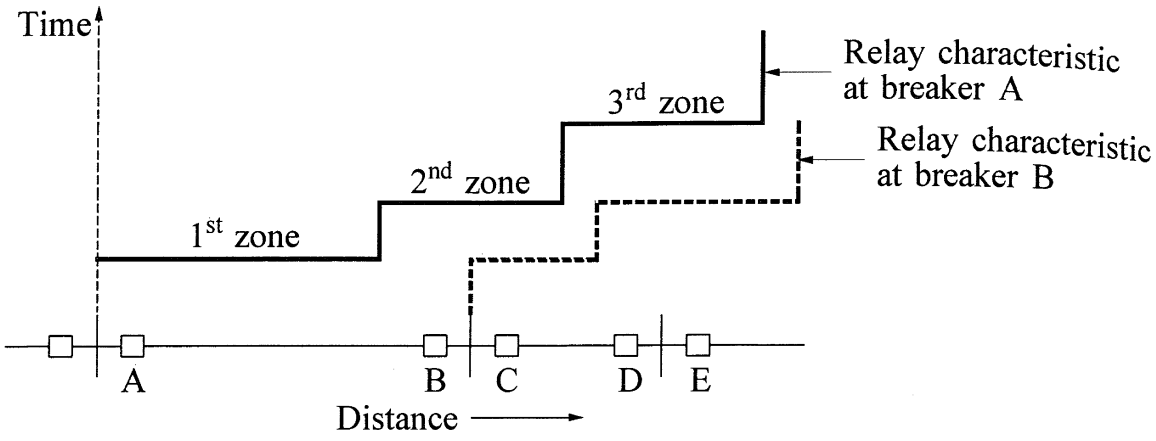


Figure 13.29 Distance relay characteristic

a section of the adjacent line CD, they are set to trip after a time delay (typically 0.3 to 0.5 seconds) thereby providing time coordination with the first-zone relays at C protecting the adjacent line CD.

The third-zone relays at A provide *backup protection* for the adjacent line CD. They are set to reach beyond line CD, so that relay operation is assured for faults on the line. Time coordination with primary protection of line CD is achieved by having a time delay of about 2 seconds for the third-zone protection.

A protection scheme similar to that at A is provided at B, but set to reach in the opposite direction. Thus a fault on line AB opens breakers at both ends of the line.

The number of relays at each end of a line is determined by the requirement that three-phase, phase-to-phase, phase-to-ground, and double phase-to-ground faults be covered. Usually, two sets of relays are provided: one set for phase faults and the other for ground faults.

The reactance type relays are used for short lines, and the mho type relays for long lines. Lens type relays are used when needed to restrict the tripping area of mho units for protection of long lines.

Straight-distance relaying provides adequate protection for many situations. However, it is not satisfactory when simultaneous high-speed tripping of both ends of the line is critical to maintain system stability. Pilot-relaying schemes, described below, are better suited for such applications.

(c) Pilot-relaying schemes

Pilot-relaying schemes utilize communication channels (pilots) between the terminals of the line that they protect. Relays located at each of the terminals determine whether the fault is internal or external to the protected line, and this information is transmitted between the line terminals through the communication channel. For an internal fault, circuit breakers at all terminals of the protected line are tripped; for an external fault the tripping is blocked.

The *communication medium* for transmitting signals between terminals may be pilot wire (metallic wires), power-line carrier, microwave, or fibre optics.

The pilot relay systems can be categorized by the manner in which the transmitted signal is used and by the fault detector principle:

- The transmitted signal may be used for blocking, unblocking, or transfer trip operations. In a *blocking system*, the transmitted signal blocks the tripping function of local relays that are normally set to trip a breaker. In a *transfer trip system*, a signal is sent by relays at one end of the line to either cause or permit the breakers at the other end to trip. An *unblocking system* is a combination of the above two systems. In this system, the tripping function of the local relays is normally blocked; the signal transmitted from the remote terminal unblocks them when tripping is required. In the event that the communication channel is lost for any reason, local relays are permitted to trip, thus protecting against a fault that may occur during this period.

- The detection of the fault location (i.e., internal or external to the protected line) may be based on either the directional comparison or the phase comparison principle, depending on the type of sensing relay used.

  In a scheme using the *directional comparison* principle, distance relays and directional relays are used to detect internal and external faults.

  In a scheme using the *phase comparison* principle, the fault location (i.e., whether the fault is internal or external) is detected by comparison of the relative phase displacement of currents entering and leaving the protected line.

Several different pilot-relaying schemes using a combination of the above categories are possible. We will describe here two such commonly used schemes. For simplicity we will consider only two terminal lines.

Permissive overreaching scheme:

Figure 13.30 illustrates the principle of operation of this scheme.

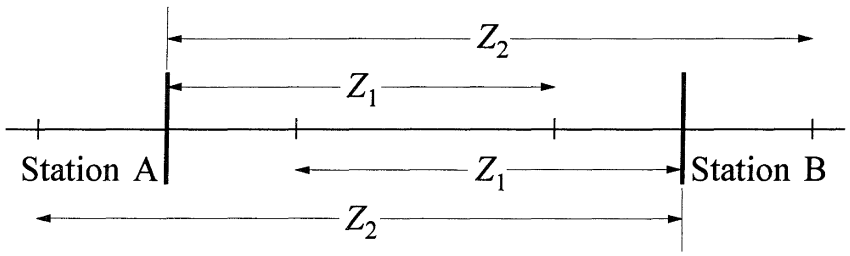


Figure 13.30 Permissive overreaching relay

Each terminal station of the line has the following relays:

- *Underreaching zone 1* phase and ground directional distance relays covering about 80% of the impedance of the protected line. Operation of these relays results in tripping of local breakers. These relays operate instantaneously with no communication required from the remote end.

- *Overreaching zone 2* phase and ground directional distance relays covering about 120% of the impedance of the protected line.

  Operation of these relays results in a permissive signal being sent to the remote end. Provided a permissive trip signal is received from the remote end, a zone 2 operation also results in the local breakers being tripped and a transfer trip signal being sent to the remote end.

  If the apparent impedance remains inside the zone 2 relay characteristic for a fixed time (typically 0.4 seconds), local breakers will be tripped without receiving a permissive trip signal. In this case no transfer trip signal is sent.

Typical zone 1 and zone 2 relay characteristics at each station are shown in Figure 13.31. If the apparent impedance measured by the relays at a station is within zone 1 characteristics, then breakers at that station are tripped instantaneously.

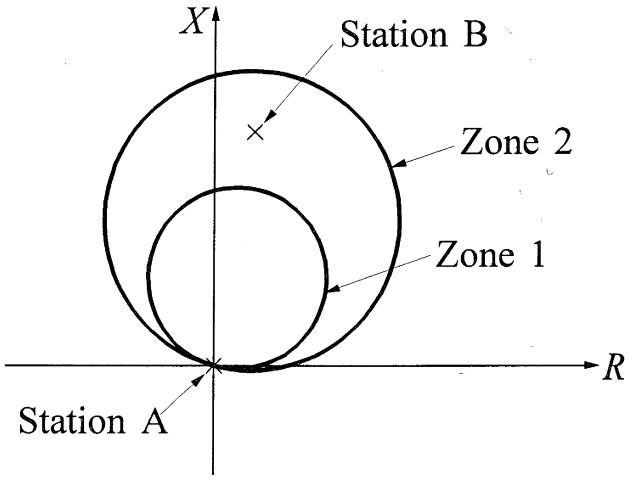


Figure 13.31 Relay characteristic at station A

If the apparent impedances measured by the relays at both ends are within zone 2 characteristics, then breakers at both ends open at high speed.

If the apparent impedance is within zone 2 characteristics of the relays at only one station, the breakers at that station are tripped with a time delay of 0.4 seconds, provided the impedance remains within zone 2 for 0.4 seconds.

To illustrate how this scheme operates, consider the faults F_1, F_2, and F_3 as shown in Figure 13.32.

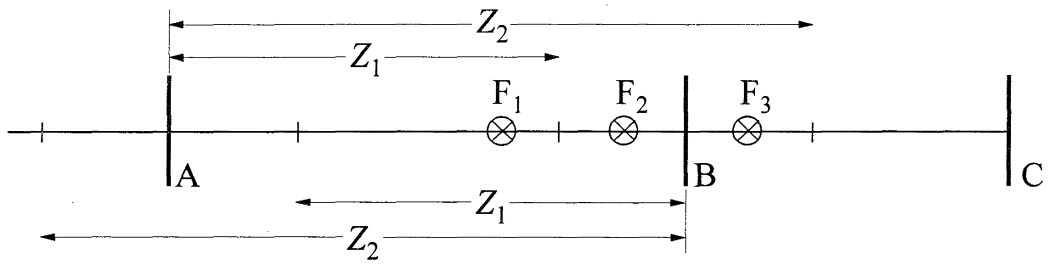


Figure 13.32 Fault locations F_1, F_2 and F_3

For the fault at F_1 within the zone 1 characteristics of the relays at both ends, breakers at the two ends are tripped without intentional time delay. For the fault at F_2 within zone 1 characteristic of the relay at B and zone 2 characteristic (but outside zone 1) of the relay at A, breakers at B trip instantaneously; the zone 2 relays at both ends are picked up and they send a permissive signal to each other. The zone 2 relay at A, upon receiving permissive signal from B (channel time not more than 20 ms), trips the breakers at A.

For the fault at F_3 (outside of the line section), the zone 2 relay at A is picked up. As the zone 2 relay at B is not picked up, no tripping occurs at B and no permissive signal is sent to A. The zone 2 relay at A trips the breakers only if the fault is not cleared by the protective relays of line section BC within 0.4 seconds.

Directional comparison scheme:

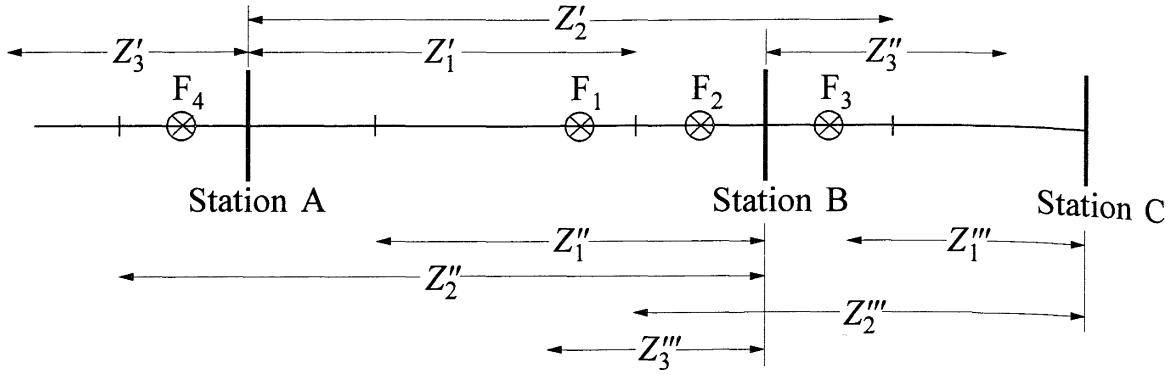
The principle of operation of a directional comparison scheme with a blocking-type pilot is illustrated in Figure 13.33. The pilot channel is used to block tripping for faults external to the protected line.

Each terminal station of the line has three sets of relays:

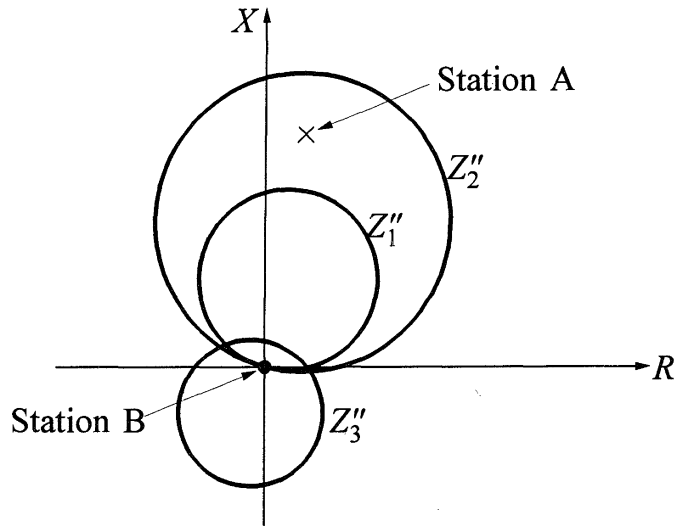
- *Underreaching zone 1* phase and ground directional distance relays covering about 80% of the impedance of the line. These relays operate instantaneously to trip the local breakers.

- *Overreaching zone 2* phase and ground directional distance relays set to reach beyond the remote terminal so as to cover about 120% of the line impedance. This ensures that all internal faults are detected. These relays trip local breakers after a delay of about 25 ms (pickup time of the coordinator timer), if no blocking signal is received from the remote terminal. Zone 2 relays trip local breakers if the fault is not cleared in about 0.4 s, irrespective of any blocking signal received from the remote end.

- *Zone 3 reverse blocking* directional distance relays set in a direction opposite to the protected line. They detect external faults and send a blocking signal to the remote end to prevent tripping.



(a) Protective zones of relays at stations A and B, protecting line AB, and at station C protecting line BC



(b) Relay characteristics at station B, protecting line from B to A

Figure 13.33 Directional comparison relaying scheme

Let us examine the operation of this scheme for four different fault locations F_1, F_2, F_3 and F_4 identified in Figure 13.33(a). For a fault at location F_1 identified in Figure 13.33, zone 1 relays at both stations A and B operate and trip breakers at the two ends with no delay.

For a fault at F_2, the zone 1 relays (Z_1'') at station B trip the local breakers instantaneously; the zone 2 relays at station A, having received no blocking signal from the zone 3 relays (Z_3'') at station B, trip the breakers at A after a short time delay of about 25 ms associated with the coordinating timer. This time delay is the waiting period in case a blocking signal is sent from the other end. The zone 2 relays (Z_2''') at station C also detect the fault at F_2, but are prevented from tripping at high speed by the blocking signal received from the reverse sensing zone 3 relays (Z_3''') at station

B. However, a local timed trip results, if the fault is not cleared and the zone 2 relay at station C continues to detect the fault after about 0.4 s.

For a fault at F_3, the zone 2 relays (Z_2') at station A detect the fault but are prevented from tripping by the blocking signal received from the zone 3 relays (Z_3'') at station B. Similarly, a fault at F_4 is detected by the zone 2 relays (Z_2'') at station B, but is blocked by signals from the zone 3 relays (Z_3') at A.

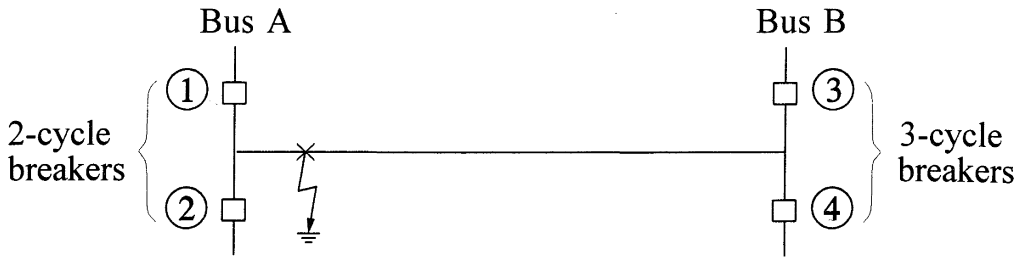
13.5.2 Fault-Clearing Times

The removal of a faulted element requires a protective relay system to detect that a fault has occurred and to initiate the opening of circuit breakers which will isolate the faulted element from the system. The total fault-clearing time is, therefore, made up of the relay time and breaker-interrupting time. The relay time is the time from the initiation of the short-circuit current to the initiation of the trip signal to the circuit breaker. The interrupting time is the time from the initiation of the trip signal to the interruption of the current through the breaker. On high voltage (HV) and extra-high voltage (EHV) transmission systems, the normal relay times range from 15 to 30 ms (1 to 2 cycles) and circuit-breaker interrupting times range from 30 to 70 ms (2 to 4 cycles).

Local breaker failure backup protection is usually provided on each breaker on critical high-voltage transmission systems. If a breaker fails to operate at a local station, infeed to a fault through the stuck (failed) breaker will be interrupted by sending trip signals to adjacent zone breakers and transferring trip signals to remote end breakers.

An example of a *normally cleared fault* is given in Figure 13.34. Bus A has 2-cycle air-blast breakers, and bus B has 3-cycle oil breakers. The system nominal frequency is 60 Hz and the communication medium is microwave. A fault within zone 1 characteristic of the relay at bus A and within zone 2 (but outside zone 1) characteristic of the relay at bus B is considered. With the typical relaying times shown in Figure 13.34, the fault is cleared from bus A in 64 ms and from bus B in 104 ms.

An example of a *stuck breaker fault* cleared by backup protection is given in Figure 13.35. A fault on line BC within zone 1 characteristic of the relay at bus B and within zone 2 (but outside zone 1) characteristic of the relay at bus C is considered. Breaker 4 at bus B fails to operate, and the fault is cleared from bus B by sending trip signals to breaker 3 at bus B (local backup) and to breakers 1 and 2 at bus A (remote backup). With the typical breaker-interrupting and relaying times shown in Figure 13.35, the fault is cleared from bus C in 104 ms, from bus B in 157 ms, and from bus A in 180 ms. We see from this example that the effect of a breaker-failure is not only to delay fault-clearing, but to isolate from the system additional elements adjacent to the faulted element.



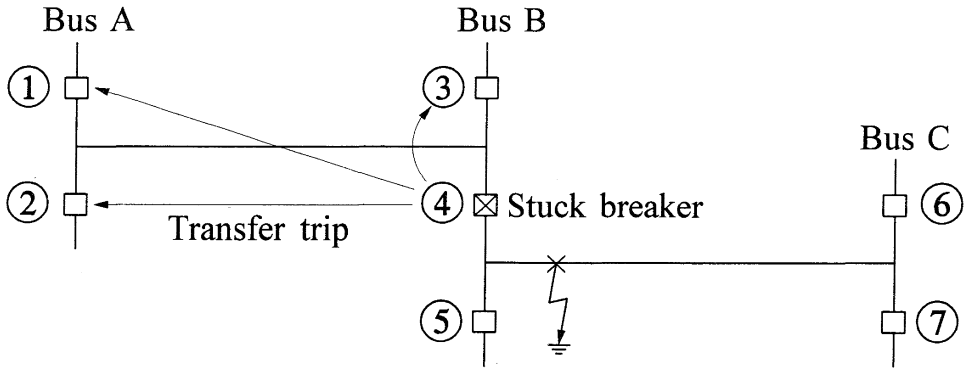
	Local (bus A) breakers 1 and 2	Remote (bus B) breakers 3 and 4
Primary relay time (fault detection)	25 ms	25 ms
Auxiliary relay(s) time	3 ms	9 ms
Communication time	–	17 ms (microwave)
Breaker trip module	3 ms	3 ms
Breaker-clearing time	33 ms (2 cycles)	50 ms (3 cycles)
Total time	64 ms	104 ms

Fault cleared from bus A in 64 ms
Fault cleared from bus B in 104 ms

Notes: (i) For purposes of illustration, 2-cycle breakers have been assumed at A and 3-cycle breakers at B.

(ii) Communication time depends on channel medium used. With power line carrier the time may be longer.

Figure 13.34 Typical fault-clearing times for a normally cleared fault



Breaker 4 assumed to be stuck
Breakers 1, 2, 3, 4, and 5 assumed to be 2-cycle air-blast breakers (33 ms)
Breakers 6 and 7 assumed to be 3-cycle oil breakers (50 ms)

	Local breaker 5	Remote breakers 6 and 7	Local backup breaker 3	Remote backup breakers 1 and 2
Primary relay time (at bus B)	25 ms	25 ms	25 ms	25 ms
Auxiliary relay(s) time	3 ms	9 ms	6 ms	12 ms
Communication channel time	–	17 ms	–	17 ms
Breaker failure timer setting	–	–	90 ms	90 ms
Breaker-tripping module time	3 ms	3 ms	3 ms	3 ms
Breaker time	33 ms (2 cyc.)	50 ms (3 cyc.)	33 ms	33 ms
Total time	64 ms	104 ms	157 ms	180 ms

Fault cleared from bus C in 104 ms
Fault cleared from bus B in 157 ms
Fault cleared from bus A in 180 ms

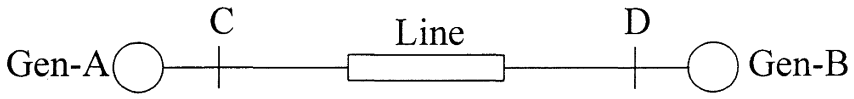
Notes: (i) Breaker failure timer setting has been assumed to be 90 ms for the 2-cycle breaker 4. This could vary from one application to another. For a 3-cycle oil breaker, a typical value is 150 ms.

(ii) Communication channel time depends on channel medium used.

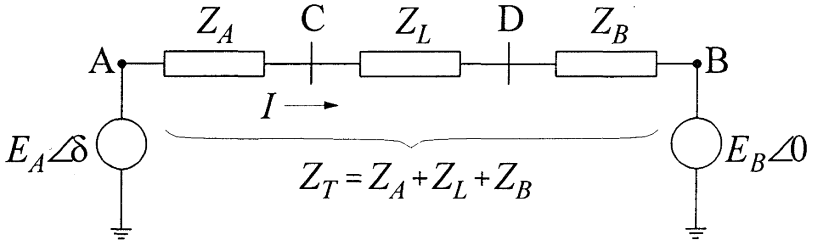
Figure 13.35 Typical fault-clearing times for a stuck breaker fault

13.5.3 Relaying Quantities during Swings

The performance of protective relaying schemes during swings (electromechanical oscillations) and out-of-step conditions may be illustrated by considering the simple two-machine system of Figure 13.36. The machines are assumed to be represented by voltages of constant magnitudes behind their transient impedances (Z_A and Z_B). The effect of swings on relaying quantities is analyzed by considering the voltage, current, and apparent impedance measured by a relay at bus C (terminal of machine A).



(a) Schematic diagram



(b) Equivalent circuit

Figure 13.36 Two-machine system

E_A and E_B are voltages behind the transient impedances of the two machines. E_B is assumed to be the reference phasor, and δ represents the angle by which E_A leads E_B.

The current I is given by

$$\tilde{I} = \frac{E_A\angle\delta - E_B\angle 0}{Z_T} \tag{13.82}$$

The voltage at bus C is

$$\tilde{E}_C = \tilde{E}_A - Z_A\tilde{I} \tag{13.83}$$

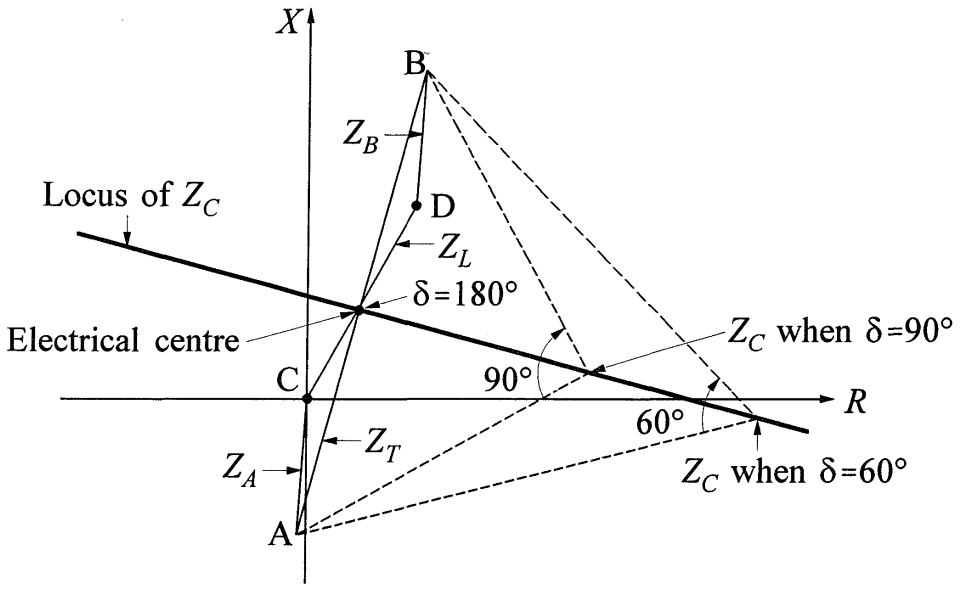
The apparent impedance measured by an impedance relay at C protecting line CD is given by

$$Z_C = \frac{\tilde{E}_C}{\tilde{I}} = \frac{\tilde{E}_A - Z_A\tilde{I}}{\tilde{I}} = -Z_A + Z_T\frac{E_A\angle\delta}{E_A\angle\delta - E_B\angle 0} \tag{13.84}$$

If $E_A = E_B = 1.0$ pu,

$$\begin{aligned} Z_C &= -Z_A + \frac{Z_T}{1\angle 0 - 1\angle -\delta} \\ &= -Z_A + Z_T\frac{1\angle 0 + 1\angle -\delta}{(1\angle 0 - 1\angle -\delta)(1\angle 0 + 1\angle -\delta)} \\ &= -Z_A + Z_T\frac{1+\cos\delta + j\sin\delta}{2j\sin\delta} \\ &= -Z_A + Z_T\left[\frac{1}{2} - j\left(\frac{1+\cos\delta}{2\sin\delta}\right)\right] \\ &= \left(\frac{Z_T}{2} - Z_A\right) - j\left(\frac{Z_T}{2}\cot\frac{\delta}{2}\right) \end{aligned} \tag{13.85}$$

During a swing, the angle δ changes. Figure 13.37 shows the locus of Z_C as a function of δ on an R-X diagram, when $E_A = E_B$.



Note: Origin is assumed to be at C, where the relay is located.

Figure 13.37 Locus of Z_C as a function of δ, with $E_A = E_B$

When the voltage magnitudes E_A and E_B are equal, the locus of Z_C is seen to be a straight line which is the perpendicular bisector of the total system impedance between A and B, i.e., of the impedance Z_T. The angle formed by lines from A and B to any point on the locus is equal to the corresponding angle δ.

When $\delta=0$, the current I is zero and Z_C is infinite. When $\delta=180°$, the voltage at the *electrical centre* (middle of total system impedance) is zero. Therefore, the relay at C in effect will see a three-phase fault at the electrical centre. The electrical centre and impedance centre coincide in this case.

If E_A is not equal to E_B, the apparent impedance loci are circles with their centres on extensions of the impedance line AB. When $E_A>E_B$, the electrical centre will be above the impedance centre; when $E_A<E_B$, the electrical centre will be below the impedance centre. Figure 13.38 illustrates the shape of the apparent impedance loci for three different values of the ratio E_A/E_B.

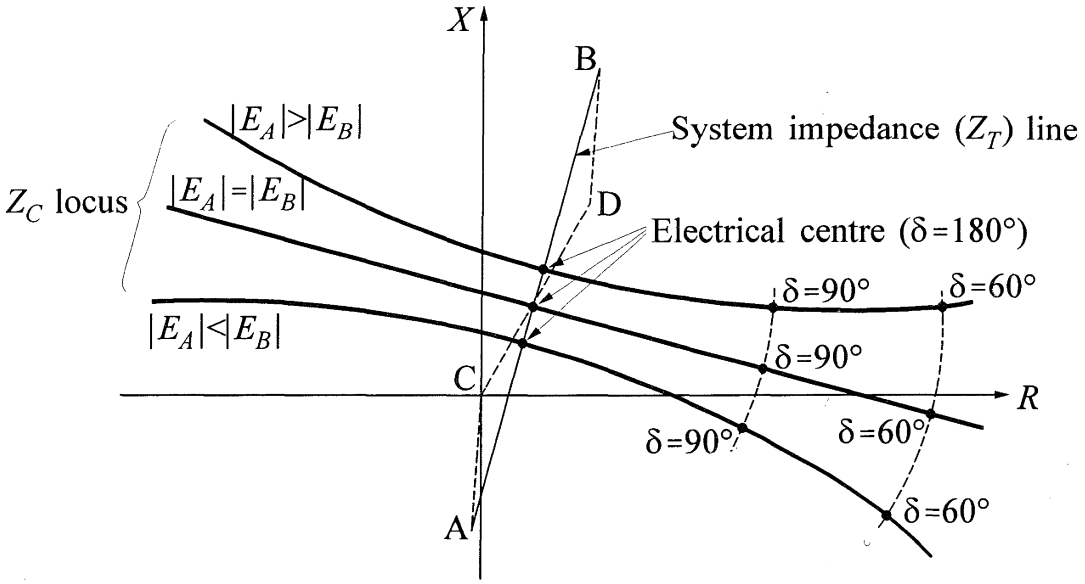


Figure 13.38 Loci of Z_C with different values of E_A/E_B

For generators connected to the main system through a *weak transmission system* (high external impedance), the electrical centre may appear on the transmission line. On the other hand, for the case where a generator is connected to the main system through a *strong transmission system*, the electrical centre will be in the step-up transformer or possibly within the generator itself.

We should recognize that the electrical centres are not fixed points since the effective machine reactance (assumed to be fixed at X'_d in our analysis) and the magnitudes of internal voltages vary during dynamic conditions.

The voltage at the electrical centre drops to zero as δ increases to 180° and then increases in magnitude as δ increases further until it reaches 360°. When δ reaches 180°, the generator will have *slipped a pole*; when δ reaches the initial value where the swing started, one slip cycle will have been completed.

After a system disturbance, the rates of change of the angle, voltage, and current are quite variable. At first the rotor angle changes quickly, slowing down as the peak angle is reached for a *stable* case; then the angle decreases and oscillates with smaller changes until equilibrium is reached. If the system is *unstable*, the angle increases gradually until it reaches 180°, when a pole is slipped. Unless the system is separated by protective systems, this is followed by repeated pole slips in rapid succession. The voltages and apparent impedances at points near the electrical centre oscillate rapidly during pole slipping.

Actual loci of apparent impedances measured by distance relays are more complex than for the idealized case we have considered; they depend on variations in internal machine voltages, voltage regulator and speed governor actions, and interactions between all the machines in the system as influenced by the interconnecting network. Such loci can be readily determined for any given situation by using a transient stability program. However, analysis of idealized cases involving simple-system configurations is helpful in understanding the results obtained with complex simulations.

Generalized impedance diagram

The concept of using the impedance diagrams for the analysis of distance relay performance was initially developed by C.R. Mason and J.H. Neher [25,26]. They considered the "swing line" on the *R-X* diagram for the case $E_A=E_B$ and analyzed the performance of different relays by plotting their characteristics on the same *R-X* diagram. This was indeed a pioneering step in understanding the performance of protective systems during power swings.

This concept was subsequently extended by other workers such as Edith Clarke [27] by developing impedance loci for various values of the ratio E_A/E_B. They showed that the impedance locus was a circle for each value of the ratio E_A/E_B, centred on the system impedance line with radii and offset determined by the values of the voltage ratio as shown in Figure 13.39. The specific case of $E_A/E_B=1$ is the limiting case with infinite radius and offset.

In reference 27, Edith Clarke also developed another family of curves representing apparent impedance loci for constant angular separation (δ). If the angle between E_A and E_B is held constant while the voltage-magnitude ratio is varied, the apparent impedance will trace a portion of a circle which passes through A and B, and whose centre lies on the perpendicular bisector of the system-impedance line. These characteristics are shown in Figure 13.40. Line AB is seen to be a portion of the circle (with infinite radius) which represents 0° and 180° angular separation. It also separates the right and left portions of each constant-δ circle into two characteristics such that the separation angle for the parts differs by 180°. For example, the 90° circle on the right becomes the 270° circle on the left.

The two families of characteristics shown in Figures 13.39 and 13.40 can be combined to form the generalized per-unit impedance diagram [24,27]. These characteristics are helpful in visualizing and analyzing how the apparent impedance varies in the general case when both the angular separation and the ratio of source voltages are varied.

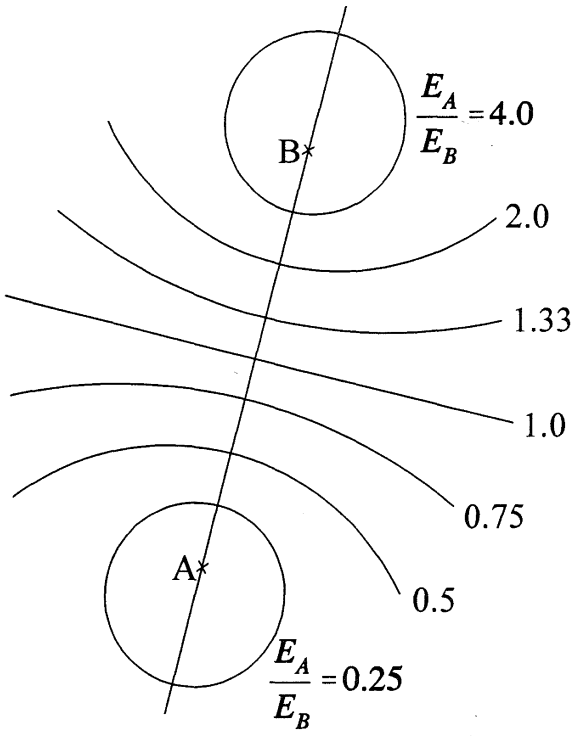


Figure 13.39 Impedance loci for constant voltage ratio

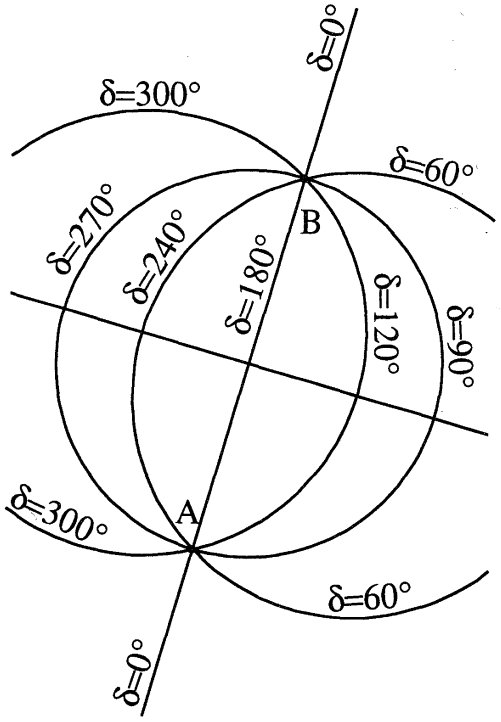


Figure 13.40 Loci of apparent impedance for constant angular separation

13.5.4 Evaluation of Distance Relay Performance during Swings

It is clear from the loci of apparent impedance derived in Section 13.5.3 that the impedance measured by a distance relay during electromechanical oscillations could be within the relay characteristics. The relay should, however, trip only for unstable conditions.

The performance of the relays during power swing conditions can be determined by calculating the impedances measured by the relays during the step-by-step stability simulations and comparing this with the operating characteristics of the relays.

For line pq of Figure 13.41, the apparent impedance measured by a relay at p is given by

$$Z_p = \frac{\tilde{E}_p}{\tilde{I}_{pq}} = \frac{\tilde{E}_p}{y_{pq}(\tilde{E}_p - \tilde{E}_q)}$$

For evaluating the performance of distance relays, the locus of apparent impedance so computed is plotted on the R-X diagram along with the relay characteristics as shown in Figure 13.42.

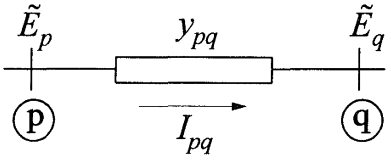


Figure 13.41

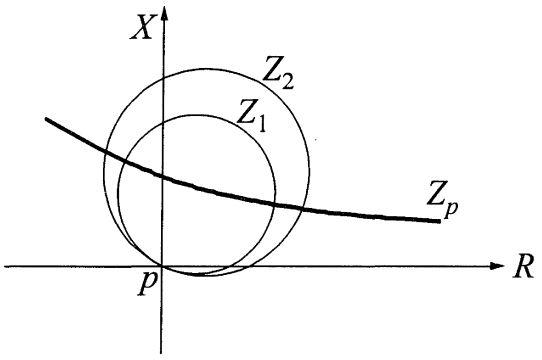


Figure 13.42

The performance of protective relaying, using a timed second zone and not using communication between line terminals, does not depend on relaying at the opposite end of the circuit. Tripping occurs if the impedance locus at either end remains in the second-zone characteristic sufficiently long to allow timed operation or if the first-zone characteristic is entered.

Performance of schemes using pilot relaying will depend on impedances measured at both ends.

13.5.5 Prevention of Tripping during Transient Conditions

Requirements for prevention of tripping during swing conditions generally fall into two categories:

(a) Prevention of tripping during stable swings while allowing tripping for unstable transients.

(b) Prevention of tripping during unstable transients and forcing of separation at another point.

Prevention of tripping during stable transients

The "mho" relays have smaller tripping characteristics than impedance and reactance relays set to reach the same distance. They may still cover too wide a range to avoid tripping of long lines during swings. If swings up to 120° are to be permitted, the mho relay characteristic is satisfactory for lines whose impedance is less than about half the total impedance of the two generators.

The angular range covered by the mho relay may be reduced by the use of two "ohm" units having linear characteristics as shown in Figure 13.43. The ohm units are similar to reactance units except that they respond to impedances at angles of +160° and −30° instead of +90°. These angles are chosen to make the characteristics of the ohm units parallel to the boundaries of fault area.

The mho unit controls the reach, and the ohm units control the angular range of tripping on swings. The ohm units are referred to as "blinders." If the line flow is only in one direction, it is sufficient to use only one blinder (O_2). Instead of using blinders, relays with shaped characteristics such as the "lens" characteristic shown in Figure 13.28 or the "peanut" characteristic shown in Figure 13.44 may be used for line protection. Such characteristics can be readily realized by using solid-state relays.

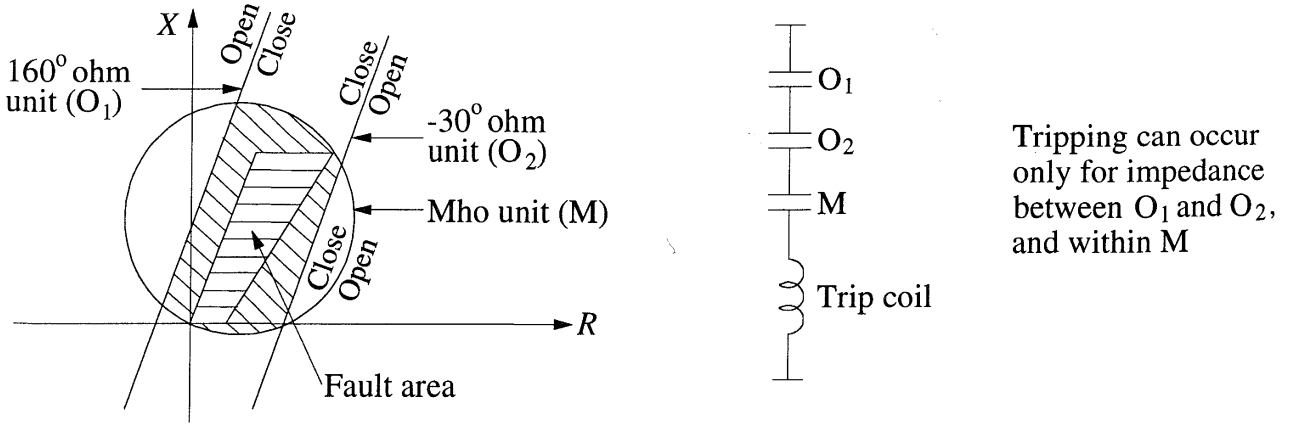


Figure 13.43 Reduction of mho relay angular range

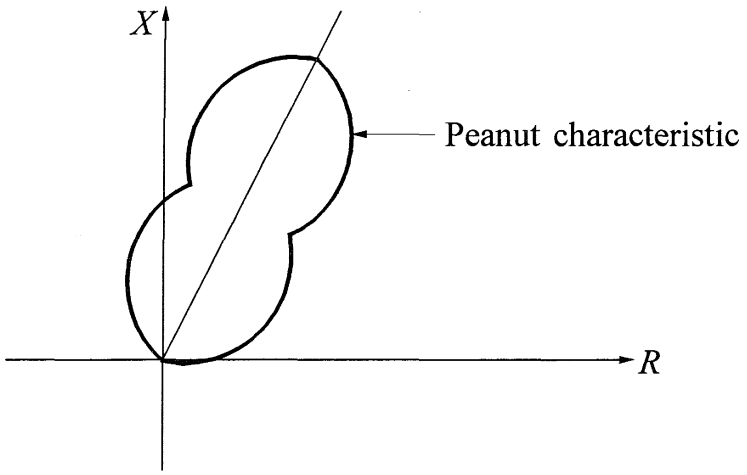


Figure 13.44

Out-of-step blocking and tripping relays

In some cases, it may be desirable to prevent tripping of lines at the natural separation point and choose the separation point so that (a) load and generation are better balanced on both sides, or (b) a critical load is protected, or (c) the separation is at a corporate boundary.

In certain instances, it may be desirable to trip faster in order to prevent the voltage from declining too far. Out-of-step relaying, either blocking or tripping, is used for this purpose.

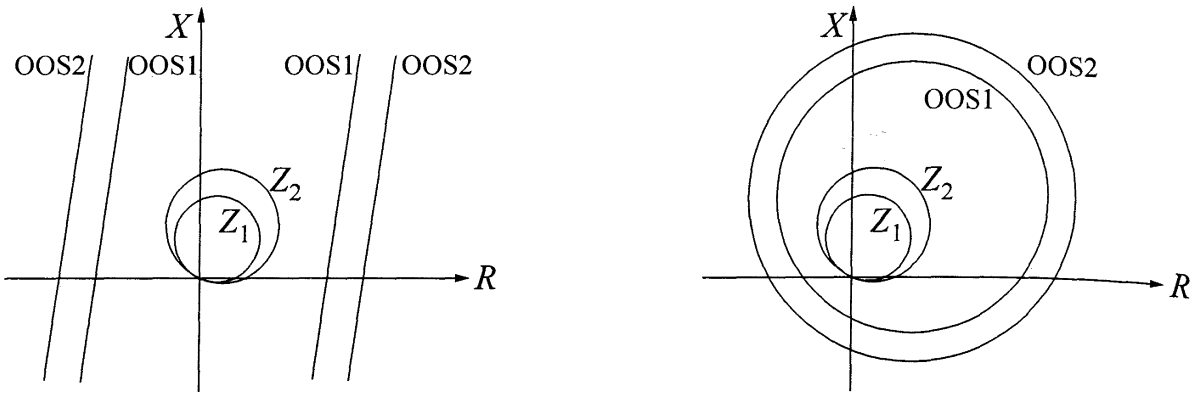
Principle of out-of-step relaying:

The movement of the apparent impedance under out-of-step conditions is slow compared to its movement when a line fault occurs. Therefore, a transient swing condition can be detected by using two relays having vertical or circular characteristics on an *R-X* plane as shown in Figure 13.45. If the time required to cross the two characteristics (OOS2, OOS1) exceeds a specified value, the out-of-step function is initiated.

In an *out-of-step tripping scheme*, local breakers would be tripped. Such a scheme could be used to

- Speed up tripping to limit voltage decline
- Ensure that a selected line is tripped instead of other circuits that may be more critical

The out-of-step tripping relays should not operate for stable swings. They must detect all unstable swings and must be set so that normal load conditions are not picked up.



(a) Vertical characteristics (b) Circular characteristics

Figure 13.45 Out-of-step relaying schemes

In an *out-of-step blocking scheme*, zone 2 and perhaps zone 1 relays are prevented from initiating tripping of the line monitored, and transfer trip signals are sent to open circuits at a remote location in order to cause system separation at a more preferable location.

The out-of-step blocking relays must detect the condition before the line protection operates. To ensure that line relaying is not blocked for fault conditions, the setting of the relays must be such that normal load conditions are not in the blocking area.

13.5.6 Automatic Line Reclosing

The majority (60 to 80%) of transmission line faults are of a transitory nature. An example of such a fault is an insulator flashover due to high transient voltages induced by lightning. After the line is de-energized long enough for the fault source to pass and the fault arc to de-ionize, the line may be reconnected. Therefore, common practice is to reclose the circuit breakers automatically to improve service continuity.

Reclosing may be either single-shot (one attempt) or multishot (several attempts) with time delay between each attempt. If the fault persists after two or three attempts, the operator may attempt to reclose manually after some delay. If this fails, it is indicative of a permanent fault and the line is taken out of service for repair. The first attempt to reclose may be either high-speed or with time delay.

High-speed reclosure refers to the closing of circuit breakers after a time just long enough to permit fault-arc de-ionization. The reclosure can be completed in less than 1 second. The following are the benefits of high-speed reclosure:

- Reduction of the likelihood of system difficulties resulting from several outages in rapid succession, usually caused by severe lightning, wind, or icing, by speeding up restoration of the system to the prior level of security.

- Minimization of the effect of line outage on critical load areas and restoration of normal voltages.

However, high-speed reclosure may not be acceptable in all cases. Reclosure into a permanent fault may cause system instability. Many utilities operate on the premise that all circuit faults are permanent and therefore the system must successfully withstand reclosing into a fault. In such cases, high-speed reclosure does not contribute to increased flexibility of system operation.

In addition, high-speed reclosure of lines close to steam turbine generating units may increase shaft fatigue. This is discussed further in Chapter 15.

In view of the above considerations, *timed and supervised reclosure* is often used on the bulk transmission system. This ensures that specific conditions are satisfied and a preferred sequence of reclosing of circuit breakers is followed. The general procedure is as follows:

- Potential is applied by closing one pre-selected breaker at one terminal after a time delay of 5 to 10 seconds.

- At terminals where out-of-synchronism conditions are a significant probability (e.g., at points in the system with few lines), the other circuit breakers associated with the line are automatically closed after the line has successfully remained on potential with acceptable angles across open breakers (measured by synchrocheck relays) for a period of at least 1 second.

  Where the probability of an out-of-synchronism condition existing between terminals is minimal, the circuit is automatically placed back on load by closing all remaining breakers associated with the circuit after it has successfully remained on potential for about 0.5 seconds.

13.5.7 Generator Out-of-Step Protection

For situations where the electrical centre is out in the transmission system, the detection of an out-of-step condition and the isolation of unstable generator(s) are accomplished by line protection.

However, for situations where the electrical centre is within the generator or step-up transformer, a special relay must be provided at the generator. Such a situation occurs when a generator pulls out of synchronism in a system with strong transmission. A low excitation level on the generator ($E_A < E_B$) also tends to contribute to such a condition.

Effect of generators operating in out-of-step condition

During an out-of-step condition, there are large cyclic variations in currents and voltages of the affected machine with the frequency being a function of the rate

of slip of its poles. The high amplitude currents and off-nominal frequency operation could result in winding stresses and pulsating torques that can excite potentially damaging mechanical vibrations. There is also a risk of losing the auxiliaries of the affected unit as well as the auxiliaries of nearby stable units.

In order to avoid these adverse effects on the unit and the rest of the system, it is desirable to have an out-of-step relay that will trip the unit; the tripping should be restricted to disconnection of the machine from the system by tripping the generator breaker, rather than initiating a complete shutdown of the unit. This allows resynchronization of the generator as soon as conditions stabilize.

Relays for out-of-step tripping of generators

The basic schemes available are similar to those used to detect out-of-step conditions on the transmission system. There are, however, no industry standards or commonly used practices with regard to generator out-of-step protection. Reference 28 provides the results of a survey of utility practices and a description of different possible schemes. We will discuss two of the schemes here.

(a) Mho element scheme:

The principle on which this scheme is based is illustrated in Figure 13.46. A mho relay monitors the apparent impedance (looking into the network) at the HT terminal (H) of the unit transformer and is set to reach into the local generator.

The relay will immediately trip the generator when the apparent impedance measured at the HT bus enters the offset mho characteristic. The setting objective (achieved by choosing the size of the circle) is to allow tripping only for unstable swings. Typically, the angle δ_C at the point where the swing impedance enters the relay characteristic is set to about 120°, the maximum angular separation of the machine from the system which may occur without loss of synchronism.

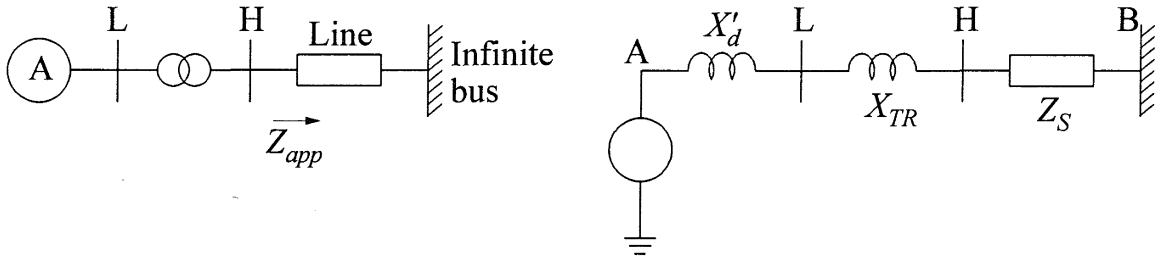
If the relay circle is too large, the protection may trip the generator for stable swings. If the relay circle is too small (δ_C large), the scheme may not trip the generator for unstable swings. In addition, if δ_C is too large the tripping can occur when the angular separation approaches 180°; this should be avoided since it subjects the circuit breaker to the maximum recovery voltage during interruption.

To minimize the probability of false tripping for a loss-of-potential condition, an overcurrent fault detector is sometimes used to supervise the mho characteristic.

(b) Blinder scheme:

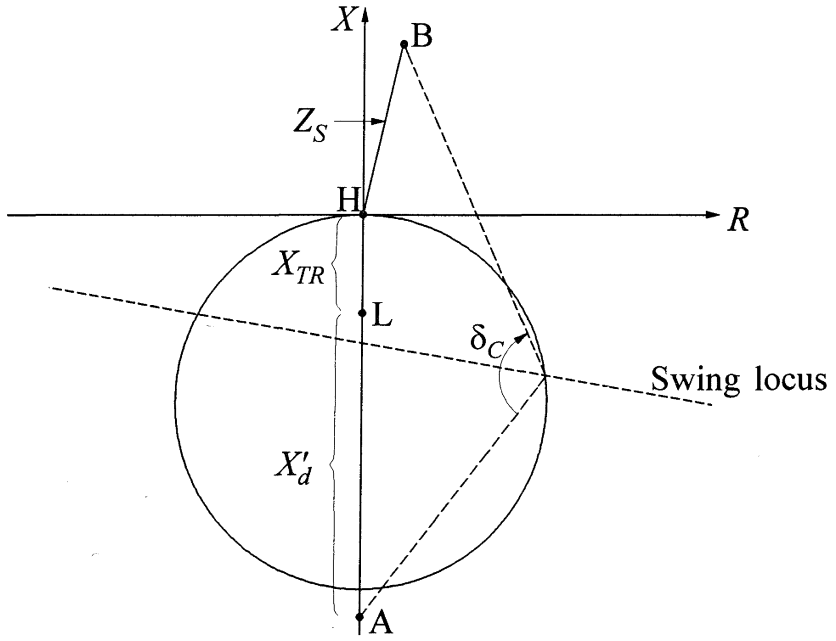
This scheme consists of two impedance elements, referred to as blinders, and a supervisory relay with an offset mho characteristic. The characteristics are shown in Figure 13.47.

There are many possible ways of applying blinders. In one scheme, the generator is tripped when the apparent impedance locus is within the mho



(a) System schematic

(b) System equivalent circuit



(c) Relay characteristic and swing locus as measured at the HV bus

Figure 13.46 Generator out-of-step protection using an mho element scheme

characteristic and crosses both blinders, the time for crossing being in excess of a set value (typically 0.15 s).

The scheme offers more selectivity than the simple mho element scheme. It is also easy to set the scheme so that circuit breaker operation is effected at a favourable swing angle. In view of the time delay involved in detecting the out-of-step condition, it is easy to coordinate with the transmission line protection; this permits the reach to extend into the system beyond the HT bus (H) of the step-up transformer, as depicted in Figure 13.47.

In Figure 13.47, the relay is assumed to be located at the HT bus of the step-up transformer. It may just as conveniently be located at the generator terminals, in which case the origin of the *R*-*X* diagram shifts to point L.

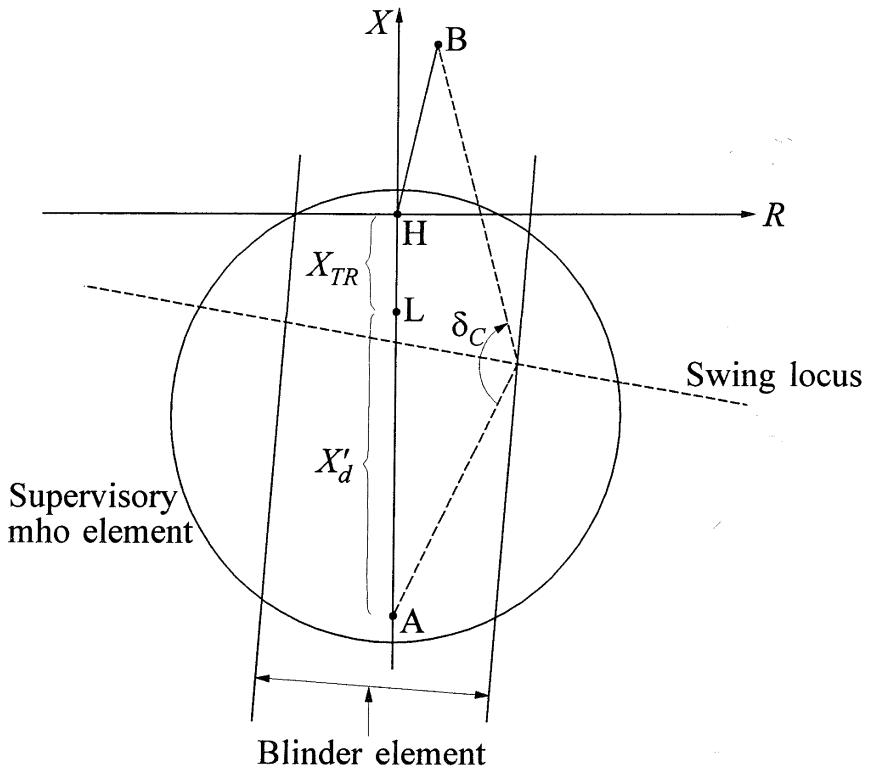


Figure 13.47 Generator out-of-step protection using a blinder scheme

Example 13.6

For the following unstable case simulated in Example 13.2, plot the apparent impedance measured by a distance relay located at the HT bus:

– Exciter on manual control (constant E_{fd}); fault duration equal to 0.1 s.

Identify the location of the electrical centre and compute the effective machine reactance.

Solution

Figure E13.22 shows the locus of apparent impedance computed during the time-domain simulation.

From the apparent impedance locus plot, we see that the electrical centre (C) lies between the HT bus (H) and the infinite bus (B). The reactance between points H and C, as measured on the plot, is equal to 0.055 pu. Therefore,

$$AC = BC$$

or

$$X_{eff} + 0.15 + 0.055 = 0.5 - 0.055$$

Solving, we get

$$X_{eff} = 0.5 - 0.15 - 2\times 0.055$$
$$= 0.24 \text{ pu}$$

This is equal to the average of $X''_d = 0.23$ and $X''_q = 0.25$.

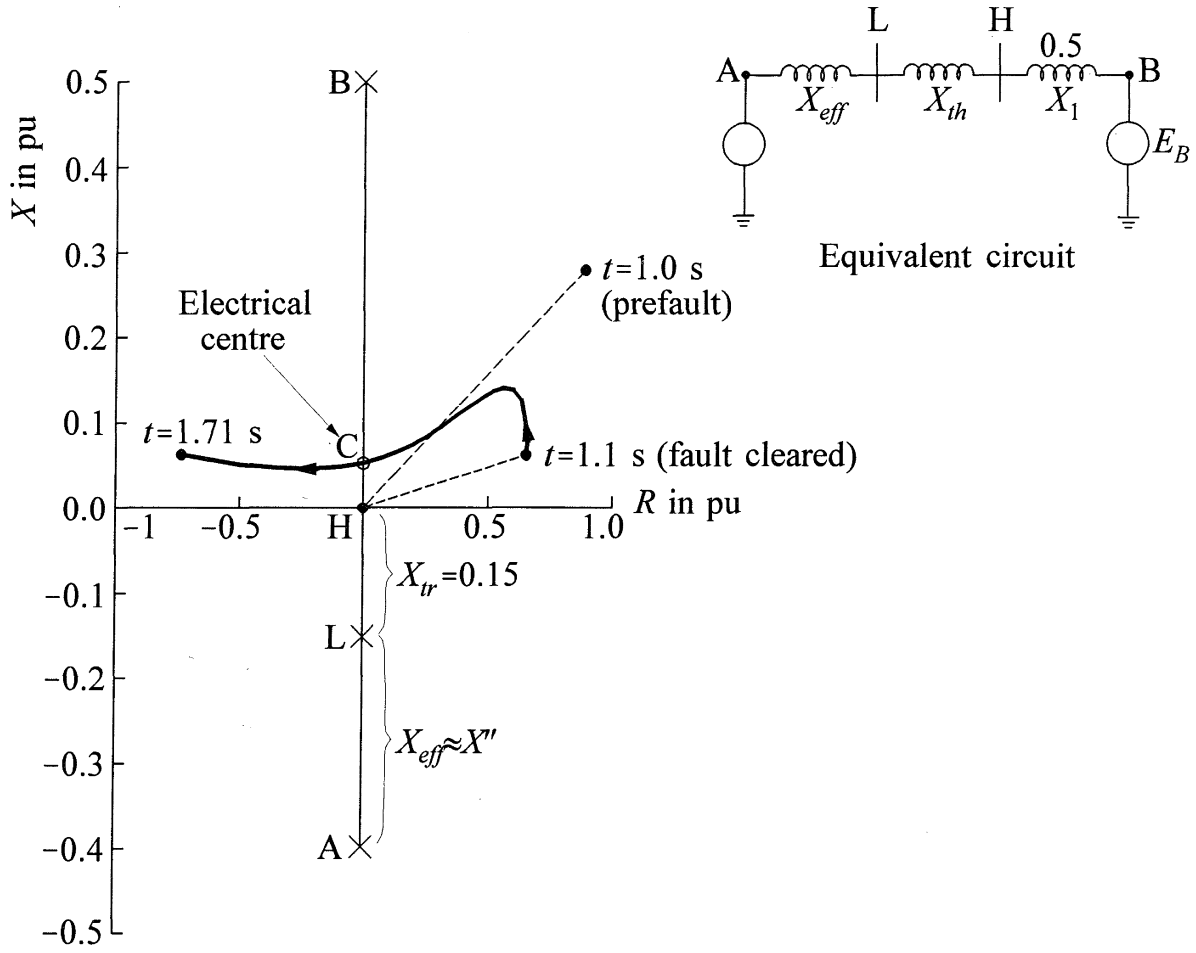


Figure E13.22 Apparent impedance locus ■

13.5.8 Loss-of-Excitation Protection

Loss of excitation of a synchronous machine can be caused by a wide variety of abnormal field circuit conditions. This may range from a complete short-circuit of the field winding to an effectively open-circuited field winding.

When a generator loses excitation, it operates as an induction generator, running above synchronous speed. The excitation is now supplied from the power system; hence, the machine draws reactive power from the system. This may cause severe system voltage reductions.

Continued operation of the machine as an induction generator may cause damage due to stator and rotor heating. The stator current may be as high as 2 to 3 times rated, depending on slip. The induced slip frequency rotor currents may cause

rotor overheating in steam-turbine generators. The time to reach dangerous overheating is on the order of several minutes, depending on the slip.

Loss of generator excitation may cause widespread voltage reduction if the power system to which the generator is connected is weak. This may, in turn, cause loss of load and loss of synchronism of other generators in the system. To prevent this, quick-acting loss-of-excitation relaying should be provided to trip the main and field breakers of the faulty generator.

The older loss-of-excitation protection consisted of undercurrent relays connected in the field circuit. Such relaying could not distinguish between purposely reduced excitation during light load conditions and accidental loss of excitation.

The relay equipment widely used now for loss-of-excitation protection is a directional-distance relay connected to the generator terminals. It is based on the principles developed by C.R. Mason in reference 29. In order to understand the basis for this relay, we need to first understand the loss-of-excitation characteristics of the generator.

Loss-of-excitation (LOE) characteristics [23,24,29]

The response of the machine following the loss of excitation depends on the initial loading condition.

Figure 13.48 shows the general shapes of the paths traced by the apparent impedance as measured at the generator terminal when the field circuit is short-circuited for three different initial power output conditions. The apparent impedance loci have been plotted on an *R-X* diagram on a per unit machine impedance base. Each characteristic is terminated just before the rotor angle δ is 180°. Beyond this point, the impedance changes become erratic due to pole slipping.

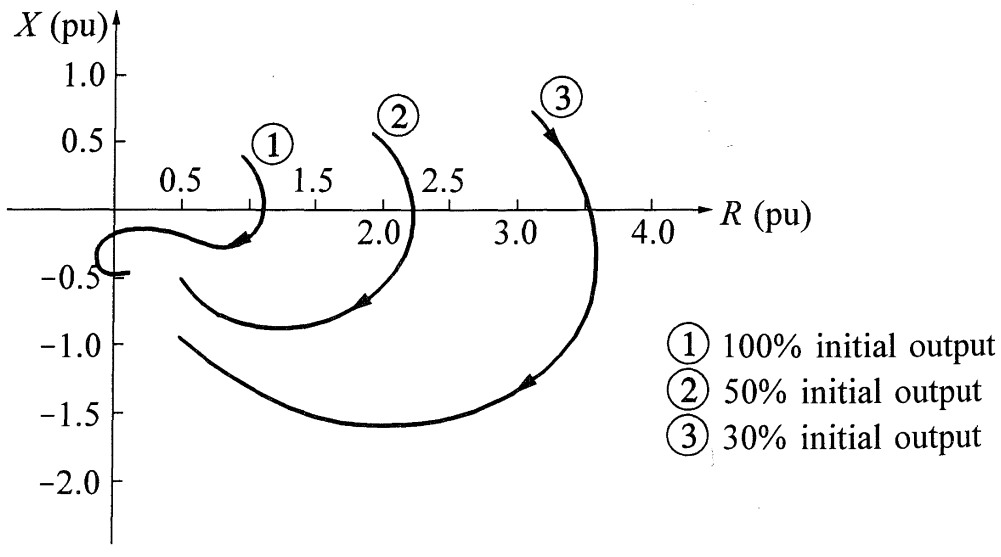


Figure 13.48 Typical LOE characteristics

When excitation is lost, the field flux linkage and the effective internal voltage gradually decrease depending on the field circuit time constant. This results in a gradual reduction in active power output, accompanied by an increase in rotor angle. In addition, the machine absorbs increasing amounts of reactive power as the field flux decays. Referring to the two-machine equivalent circuit of Figure 13.36, what we have is a situation where the internal voltage E_A is decreasing and the rotor angle δ is increasing. The loss-of-excitation characteristic is, therefore, some combination of the two families of curves shown in Figures 13.39 and 13.40. The actual path traced depends on the relative rates of variation in E_A and δ, which in turn depend on the initial generator output, transmission strength, and field circuit time constant. The overall effect on the apparent impedance at the machine terminals is as depicted in Figure 13.48.

With a high initial output, the rotor angle advances more rapidly and the endpoint shown in the figure is reached more quickly, typically within about 10 s. The slip is also relatively high, and therefore the impedance locus terminates at a value corresponding to the average of subtransient d- and q-axis reactances.

On the other hand, with a low initial output, the rotor angle advances slowly and the slip at the endpoint is small. The impedance locus terminates at a value corresponding to the average of d- and q-axis synchronous reactances.

The locus of the endpoints of the loss-of-excitation characteristic is shown in Figure 13.49. It ranges between the subtransient reactances and the synchronous reactances. Although these extreme values are not actually reached, they are helpful in identifying the LOE relay characteristic. By encompassing the locus of the endpoints as shown in Figure 13.49, the relay will operate before the generator first starts to slip poles.

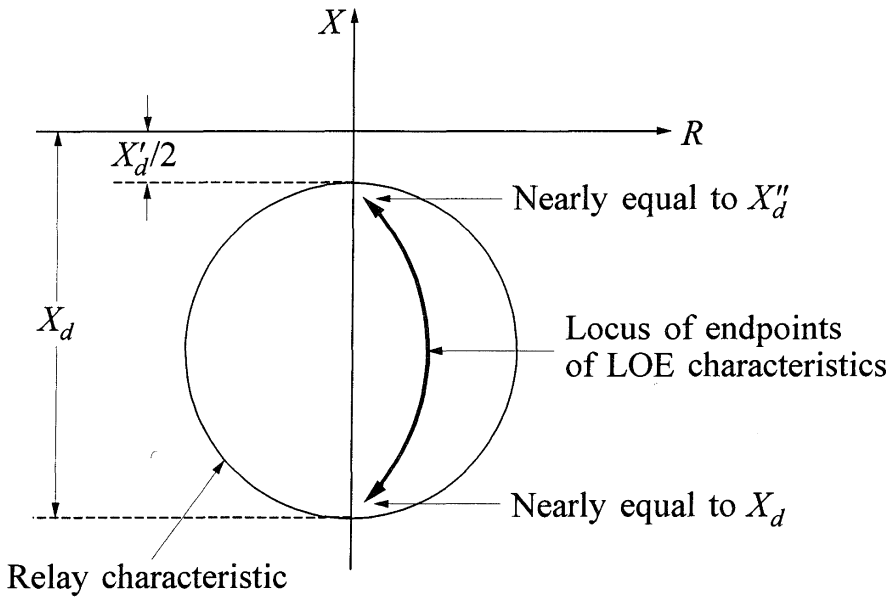


Figure 13.49 LOE relay and system characteristics

Loss-of-excitation relays

The characteristics of an LOE relay proposed by Mason in reference 29 are shown in Figure 13.49. It is an offset mho relay. The offset is equal to one-half of the transient reactance of the generator. The total reach of the relay is equal to the synchronous reactance X_d.

The offsetting of the relay characteristic from the origin provides selectivity against improper operation during power swings or out-of-step conditions. In an extreme case of zero external impedance, the electrical centre (intersection of the swing locus with the system impedance locus) is at the centre of the generator impedance X'_d. Therefore, the LOE relay characteristic is offset by $X'_d/2$.

The offset mho relay with the above characteristic has been widely used and has generally performed satisfactorily.

To provide greater selectivity against false operation during underexcited operation, stable transient swings, or system disturbances causing underfrequency operation, the use of two offset mho relays with characteristics as shown in Figure 13.50 is proposed by J. Berdy in reference 30.

Reference 31 describes a more discriminating relay developed at Ontario Hydro in 1978. This relay can prevent unit trip for recoverable excitation failures and trip the unit more rapidly for unrecoverable failures. The relay uses generator field and terminal voltages as inputs. It operates on the general principle that when the terminal voltage is high the field voltage should be low and, conversely, when the terminal voltage is low the field voltage should be high. For a detected excitation problem, the relay will initially try to transfer voltage control to an alternate AVR/exciter. If this does not rectify the problem, the relay trips the unit. Figure 13.51 shows a block diagram of the relay. The relay also includes selective overexcitation protection as shown by the dashed blocks in the figure.

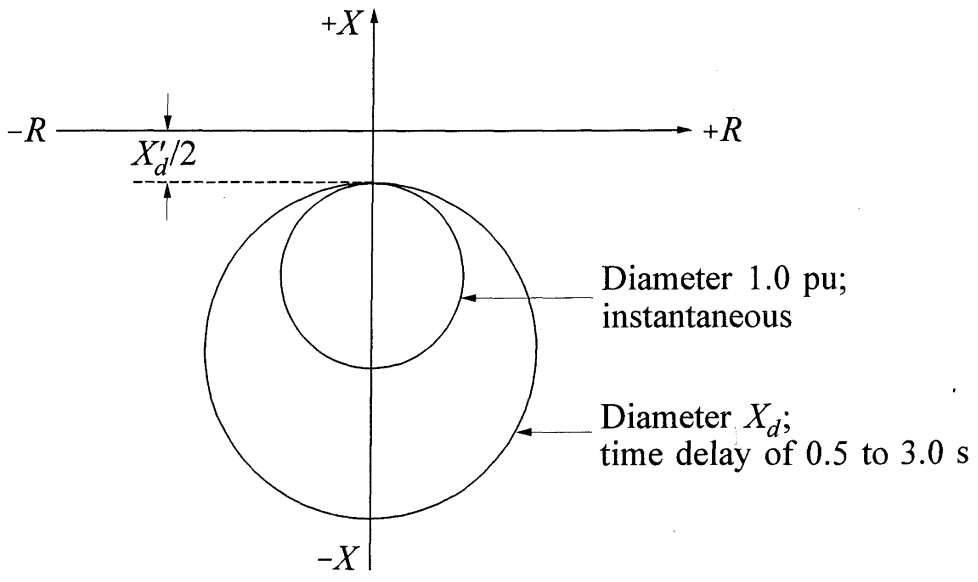


Figure 13.50 LOE protection with two mho relays

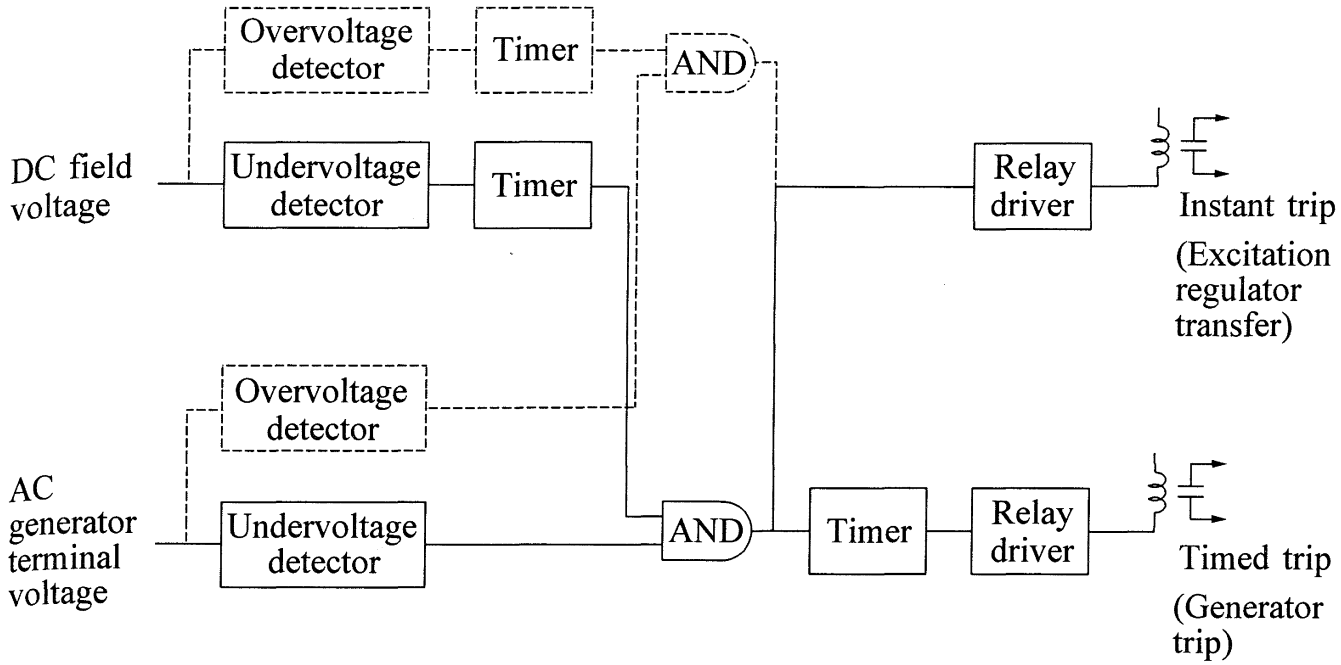


Figure 13.51 A discriminating loss-of-excitation relay [31]

Example 13.7

In this example, we examine the response of the system of Example 13.2 to loss of generator excitation.

(a) If the field of the equivalent generator representing the four units of the plant is suddenly shorted (directly, with zero external resistance), determine the locus of apparent impedance measured by an LOE relay located at the generator terminals. Assume that the LOE relay has a characteristic similar to that shown in Figure 13.49. Show the corresponding time responses of generator terminal voltage, active and reactive power outputs, and rotor angle.

(b) Determine the locus of apparent impedance if the field of only one of the four generators in the plant is shorted (directly). The other generators operate normally with excitation control.

Assume that in each of the above cases the initial system operating condition is the same as in Example 13.2.

Solution

(a) The apparent impedance locus computed by using a transient stability program is shown in Figure E13.23. The generator is represented in detail including amortisseur circuits, and shorting of the field is simulated by setting the field voltage E_{fd} to zero at t=1.0 s.

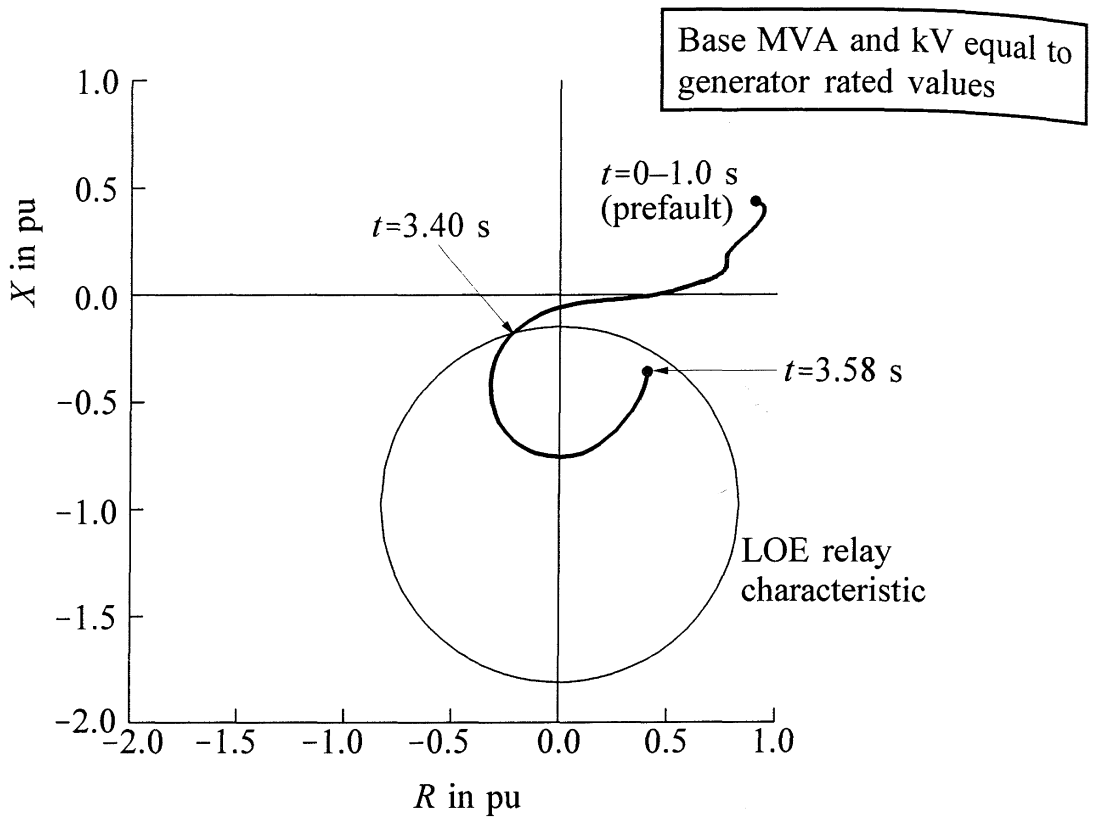


Figure E13.23 Apparent per unit Z measured by an LOE relay when field windings of all four units are shorted

The corresponding time response plots of E_t, P, Q and δ are shown in Figure E13.24. These plots are helpful in explaining the shape of the apparent impedance locus, if we note that

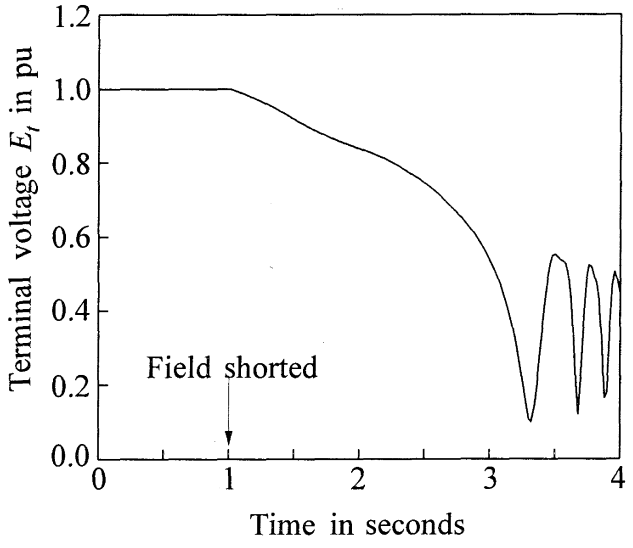
$$Z_{app} = \frac{\tilde{E}}{\tilde{I}_t} = R+jX$$

where

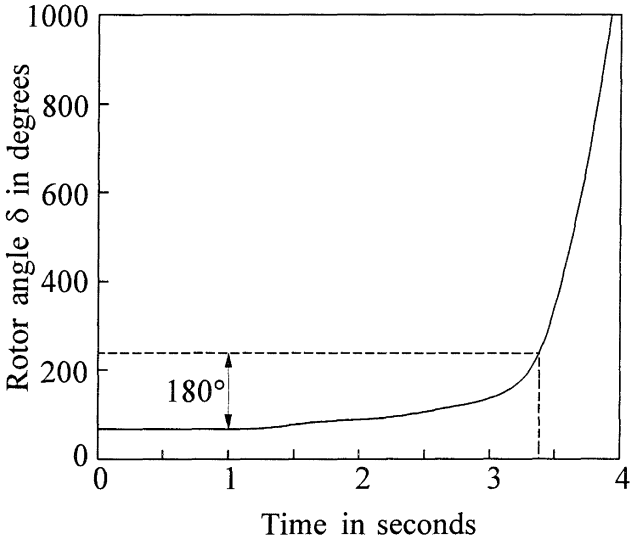
$$R = \frac{E_t^2 P}{P^2+Q^2} \qquad X = \frac{E_t^2 Q}{P^2+Q^2}$$

From Figure E13.23, we see that the apparent impedance locus enters the LOE characteristic at t=3.4 s, i.e., 2.4 s after the field is shorted. As we see in Figure E13.24(b), this corresponds to the time when the generator has slipped one complete cycle. As the generator continues to slip poles, P, Q, and E_t oscillate in rapid succession.

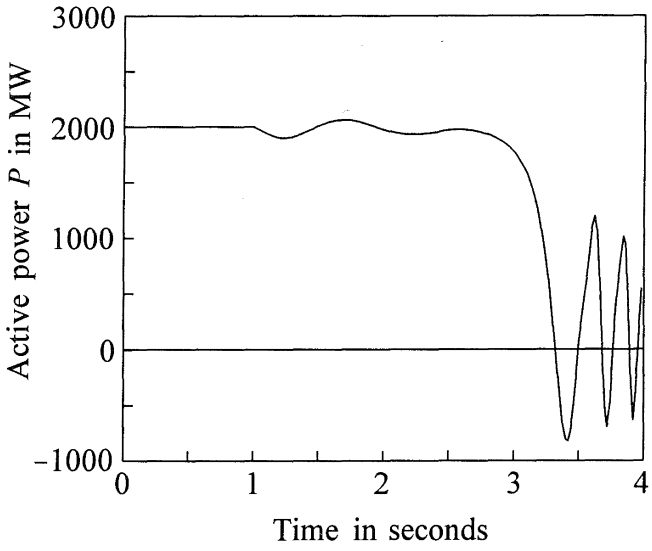
(b) Figure E13.25 shows the apparent impedance locus when the field of one of the generators is shorted. The other three generators continue to operate normally with AVR and PSS controlling their excitation.



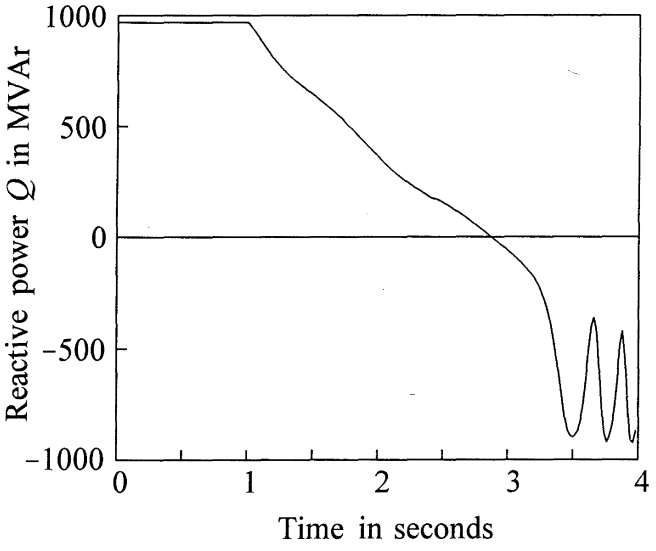
(a) Time response of terminal voltage E_t



(b) Time response of rotor angle δ



(c) Time response of active power P



(d) Time response of reactive power Q

Figure E13.24 Time responses of generator variables following shorting of field windings

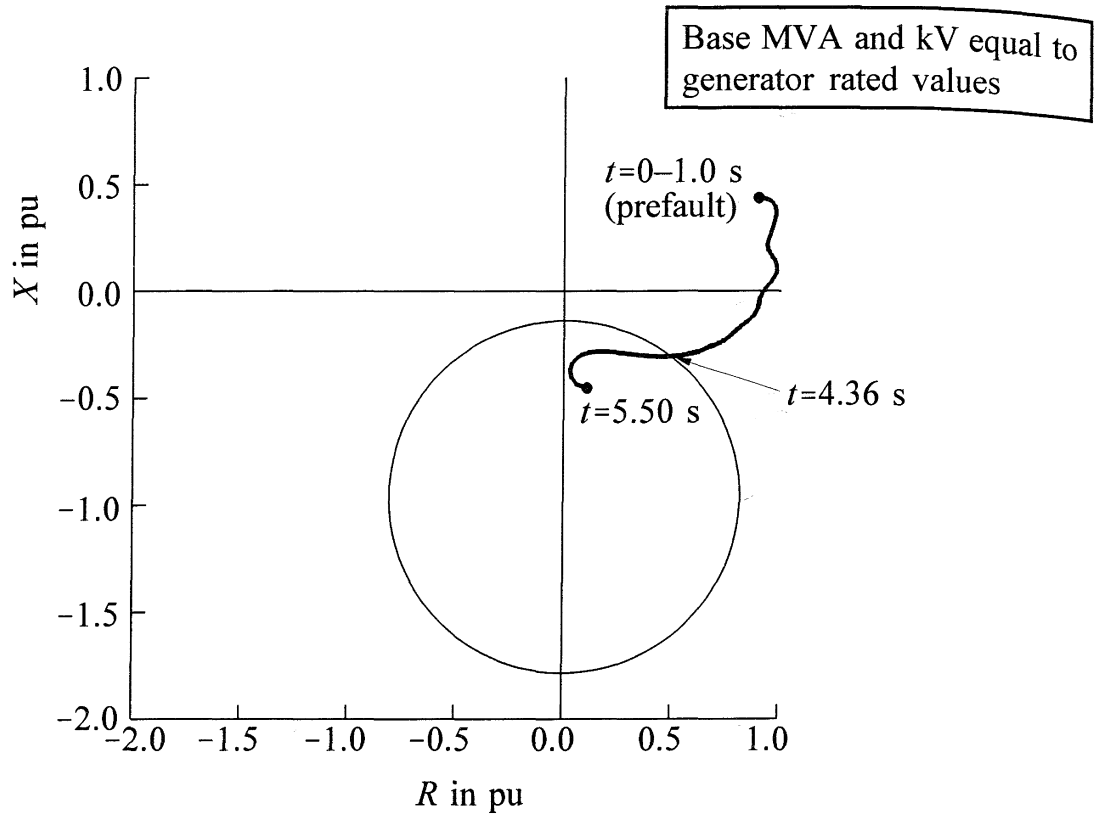


Figure E13.25 Apparent per unit Z measured by an LOE relay when the field winding of one of the generators is shorted ■

13.6 CASE STUDY OF TRANSIENT STABILITY OF A LARGE SYSTEM

This case study is intended to demonstrate the analysis of a large practical system for which a disturbance results in transient instability. The results show how the unstable portion of the system is isolated from the rest of the system through the actions of protective relaying. In addition, two possible methods of maintaining stability are illustrated.

The system

The area of interest for the system under study is shown in Figure 13.52. It consists of an 8 unit 7,000 MW nuclear plant connected to the rest of the system through two 500 kV double circuit lines and three 230 kV double circuit lines. The system model, which represents a portion of a large interconnected power system, consists of

- 2279 buses, 467 machines, and 6581 branches
- All machines and associated controls modeled in detail
- Loads modeled as voltage dependent (P=50%I+50%Z, Q=100%Z)

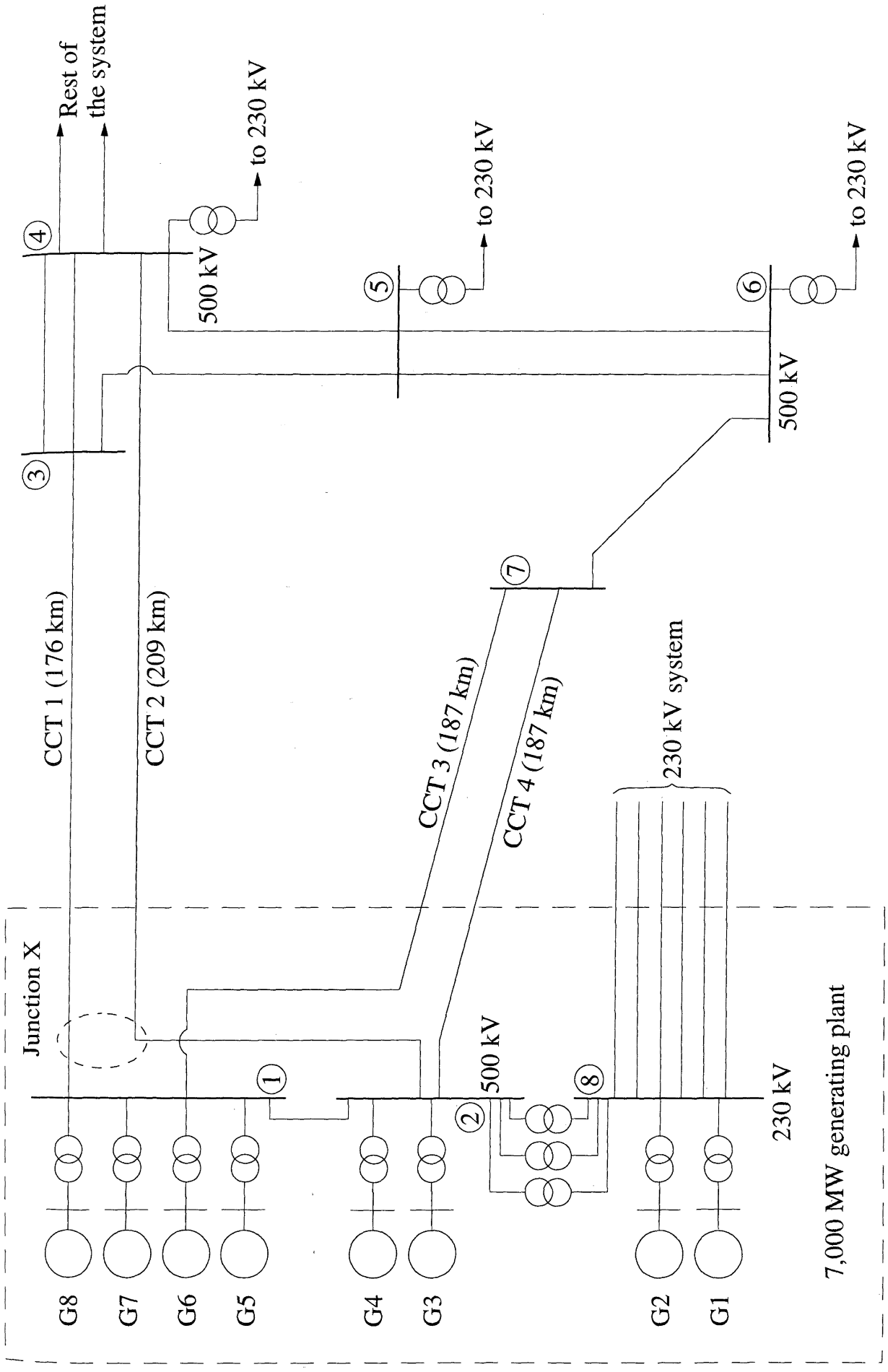


Figure 13.52 Diagram of system in the vicinity of a 7,000 MW plant

The contingency

A double line-to-ground (LLG) fault occurs on the 500 kV double-circuit line comprising circuits 1 and 2 in Figure 13.52. The location of the fault is shown in the figure as junction X, which represents the location nearest the plant where the two circuits share the same tower. The switching sequence is as follows:

Time (ms)	Event
0	No disturbance
100	Apply LLG fault at junction X on circuits 1 and 2
164	Local end clearing: Open breakers at bus 1 for circuit 1 Open breakers at bus 2 for circuit 2 This occurs 64 ms after the fault is applied, and this time is computed as the sum of fault detection time (25 ms), auxiliary relay time (6 ms), and breaker-clearing time (33 ms = 2 cycles). At this time, the fault remains connected on the ends of circuits 1 and 2 at junction X.
187	Remote end clearing: Open breakers at bus 4 for circuit 2 Open breakers at bus 3 for circuit 1 Clear fault (the line is isolated) This occurs 87 ms after the fault is applied, and the time is calculated as the sum of fault detection time (25 ms), auxiliary relay time (12 ms), communication time (17 ms; microwave), and breaker-clearing time (33 ms = 2 cycles)
5000	Terminate simulation

Simulation

The 5-second simulation was conducted using explicit numerical integration (fourth order R-K) and an integration time step of 0.01 second.

Figure 13.53 shows the absolute rotor angle plots for unit G3 and for a unit located in the external system. Absolute angle is measured relative to the synchronously rotating reference frame, and it is clear from plots that the external system unit remains synchronized while the unit G3 *loses synchronism and becomes monotonically unstable*. The responses of the other seven units at the nuclear plant is similar to that of G3. As units G1 to G8 become unstable, the rest of the system

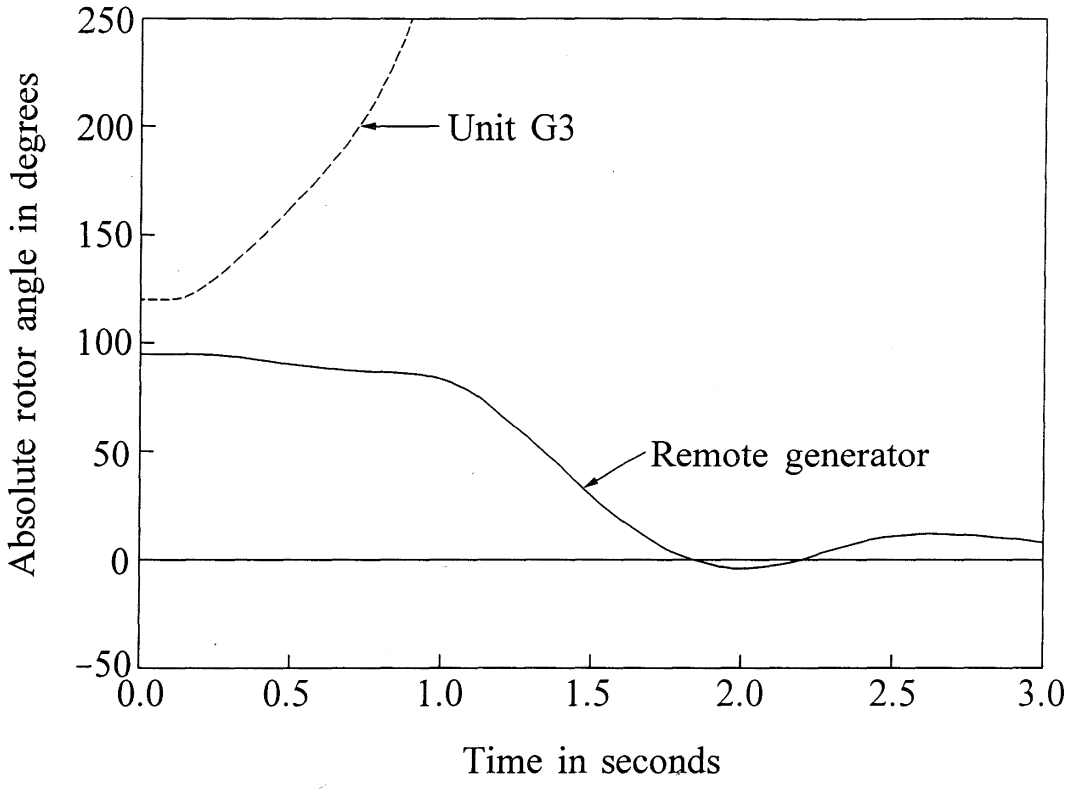


Figure 13.53 Rotor angle time response

becomes generation deficient, and hence the absolute angles of all machines in the system drift slightly. In this regard, using relative angles rather than absolute angles is often a better choice since it permits one to easily observe the relative motion of rotors between machines. The LLG fault results in the loss of one 500 kV double-circuit line, leaving the entire 7,000 MW plant connected to the system through a significantly weaker (i.e., higher impedance) path consisting of one double-circuit 500 kV line and three 230 kV double-circuit lines. The plant is unable to transfer full output through this path, and the resulting accelerating power leads to instability.

How does the system come apart as a result of instability?

Figure 13.54 shows the characteristic for the out-of-step protection on unit G3. The locus of the effective network impedance measured at the unit terminals is superimposed on the circle. We see that the impedance locus *does not enter the circle* except during the brief period when the fault is on; therefore, the protection *will not* trip the units. The point of system separation is clearly beyond the reach of the out-of-step protection.

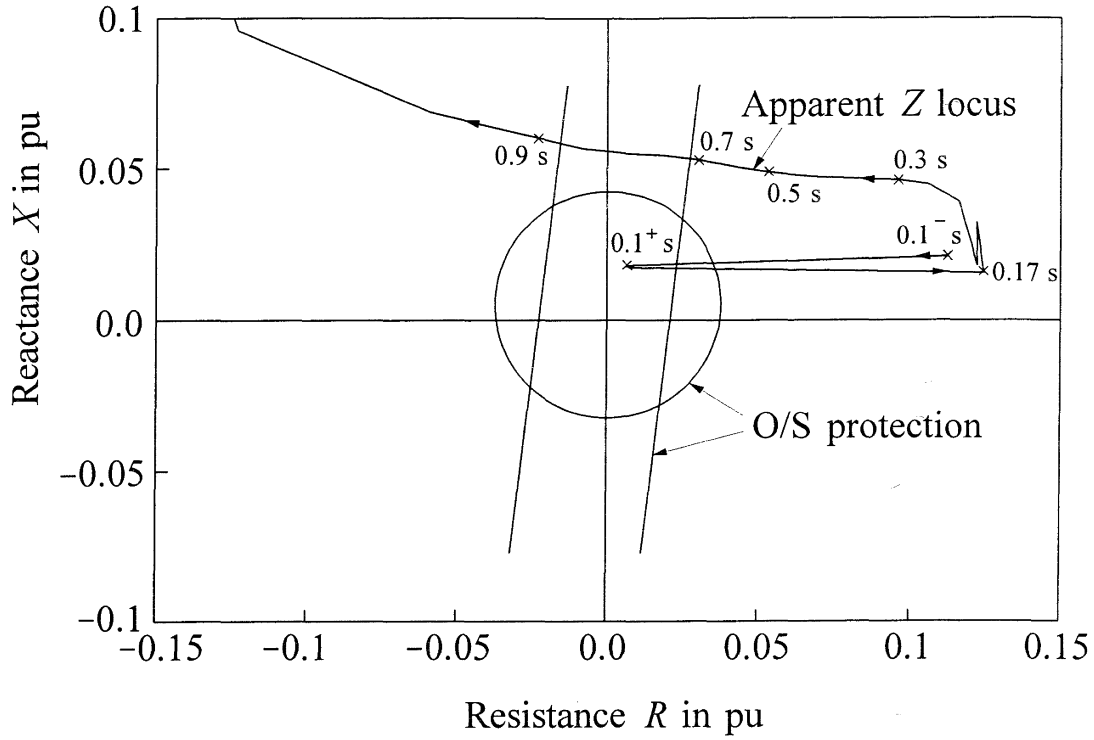


Figure 13.54 Unit G3 out-of-step protection

Figure 13.55 and Figure 13.56 show the line protection performance for relays on circuit 3 at buses 1 and 7, respectively. The apparent impedances measured at each end looking toward the opposite ends are shown on the plots. The relays are mho distance relays and have zone 1 coverage of about 75% of line length and zone 2 overreach of about 125% of line length. These plots show that the apparent impedance enters the zone 2 relays at bus 1 and enters the zone 1 and zone 2 relays at bus 7. The zone 1 relay at bus 7 would trip circuit 3 at bus 7 and send a transfer trip signal to the breakers at bus 1 which would then trip circuit 3 at bus 1. This logic also holds true for the companion 500 kV circuit (#4) which would be tripped in an identical manner. Following the loss of the 500 kV circuits (at approximately 0.8 s), the remaining 230 kV circuits would become extremely overloaded and would be lost through protection actions, thereby completely isolating the unstable plant from the system.

From Figure 13.55, we can determine that the impedance swing *crosses* the circuit at a point about 84% of the line length from bus 1. This point represents the *electrical centre* following the disturbance and is theoretically where separation occurs (although the entire circuit is tripped). Figure 13.57 shows plots of bus voltage measured at buses 1 and 7, and at the electrical centre. The voltage at the electrical centre leads the other voltages in collapsing as instability occurs.

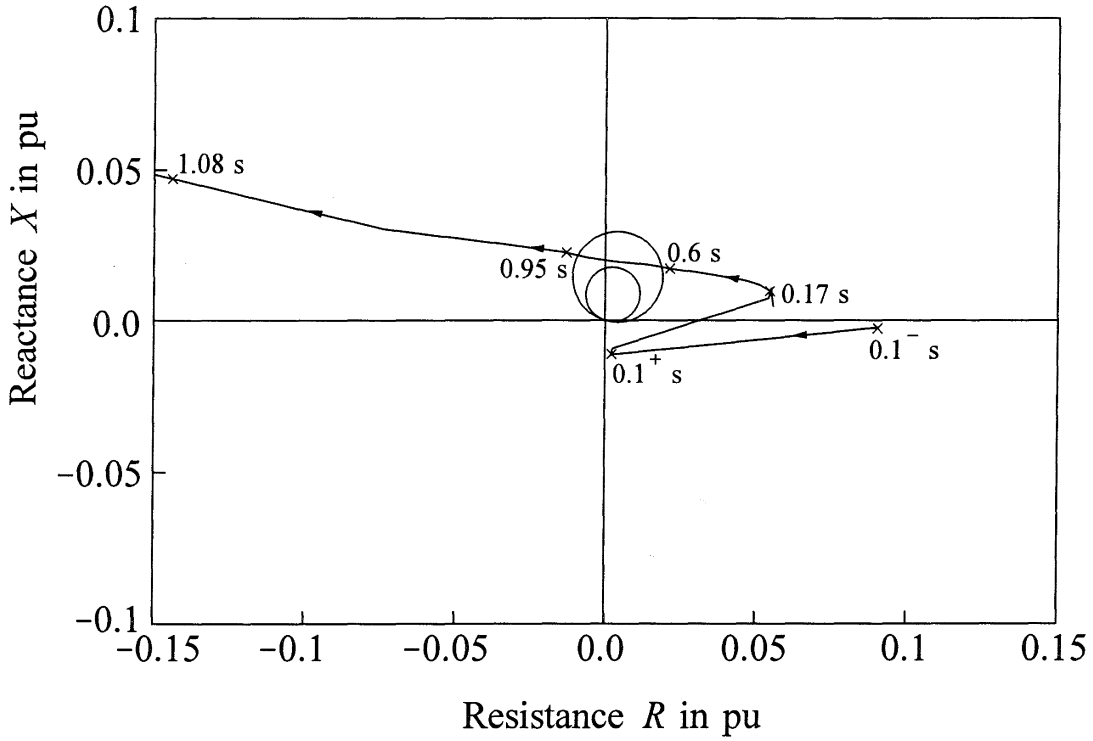


Figure 13.55 Line protection (circuit 3) at bus 1

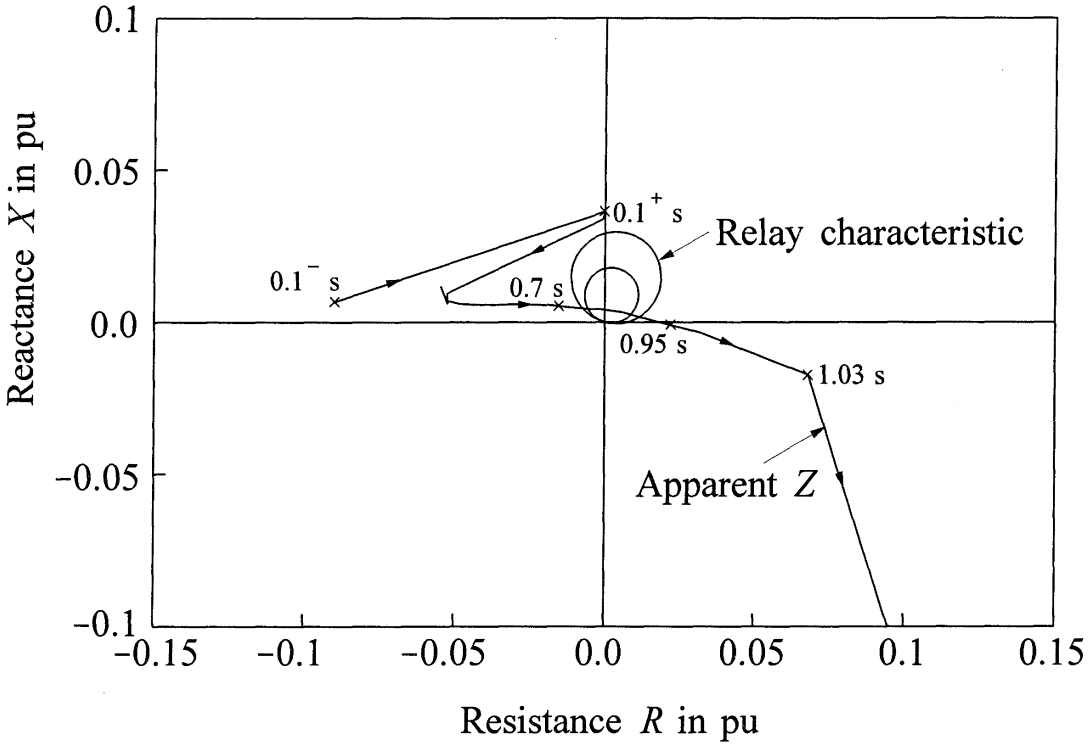


Figure 13.56 Line protection (circuit 3) at bus 7

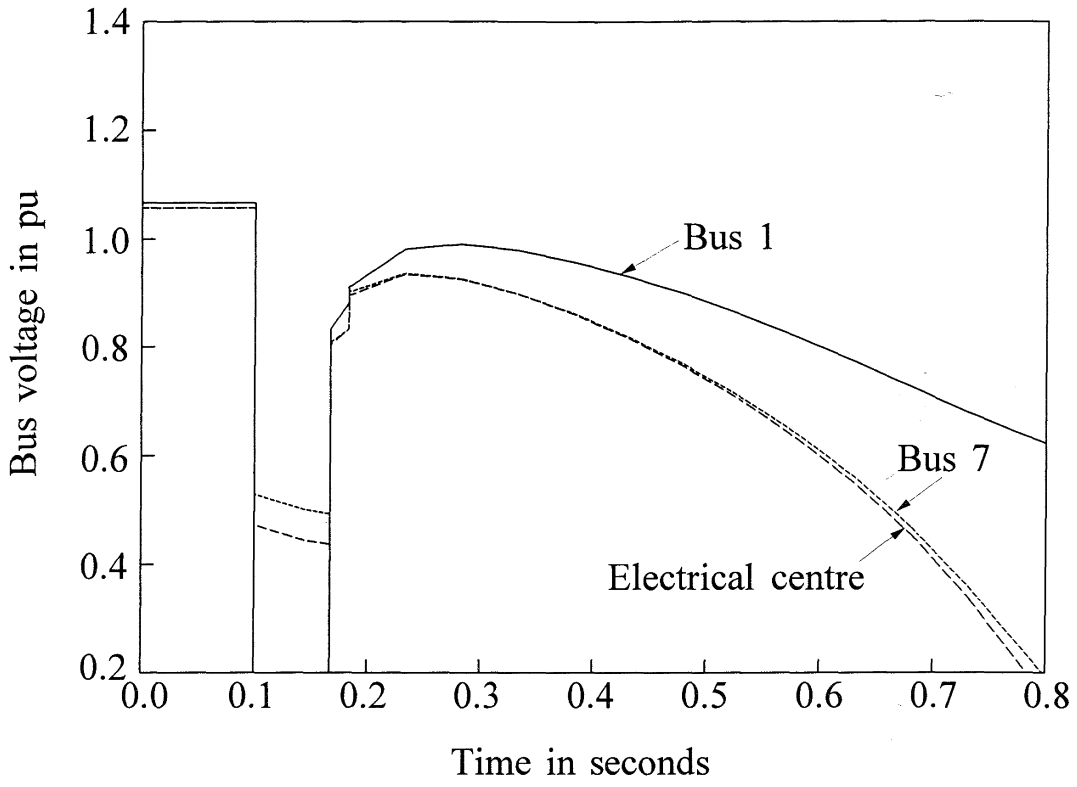


Figure 13.57

Methods of maintaining stability

As discussed in Chapter 17, there exist many possible ways of improving transient stability (including adding transmission facilities, fast-valving, faster fault clearing, etc.). Here, we consider the following two methods:

(a) *Reduction of the pre-contingency output of the plant.* If one unit is taken off line (with output redispatched to other units in the external system), the total plant output will be reduced sufficiently to ensure stability following the LLG fault. Curve 2 in Figure 13.58 shows the absolute rotor angle for unit G3 for this case. It shows that the plant remains in synchronism. This solution to instability is, however, generally costly because available energy is kept idle or *bottled* in the plant.

(b) *Rejection of generation following the disturbance.* If the output of the plant can be rapidly reduced following the contingency, the accelerating power can be reduced sufficiently to maintain synchronism. Curve 3 in Figure 13.58 shows the unit G3 rotor angle response with two units (G7 and G8) tripped at 173 ms (73 ms following fault application).

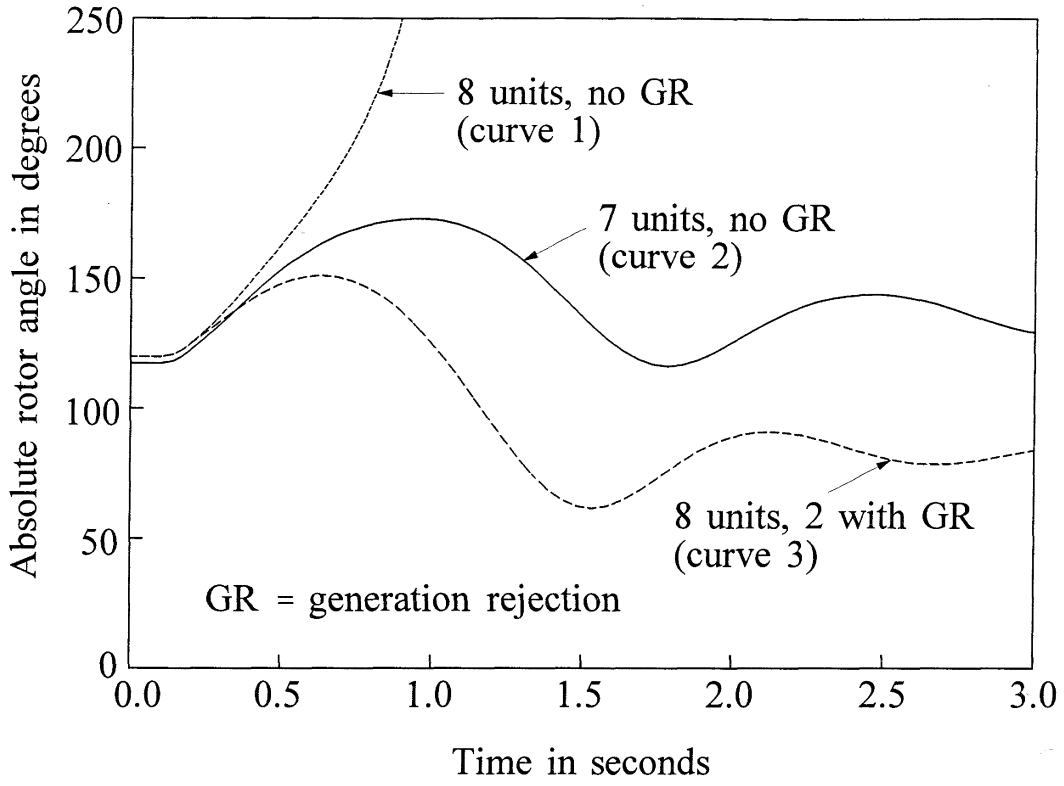


Figure 13.58 Unit G3 rotor angle responses with and without generation rejection

13.7 DIRECT METHOD OF TRANSIENT STABILITY ANALYSIS

The direct methods determine stability without explicitly solving the system differential equations. This approach is academically appealing and has received considerable attention since the early work of Magnusson [32] and Aylett [33] who used transient energy for assessment of transient stability. The energy-based methods are a special case of the more general Lyapunov's second method or the direct method (see Chapter 12, Section 12.1.4), the energy function being one possible Lyapunov function [34-37].

This section describes the basic concepts on which the direct methods are based. A detailed treatment of the subject is beyond the scope of this book. Interested readers may consult references 38 and 39, books dedicated entirely to the analysis of power system transient stability by the direct methods.

13.7.1 Description of the Transient Energy Function Approach

Rolling ball analogy [40,41]

The transient energy approach can be described by considering a ball rolling on the inner surface of a bowl as depicted in Figure 13.59. The area inside the bowl represents the region of stability, and the area outside is the region of instability. The

rim of the bowl is irregular in shape so that different points on the rim have different heights.

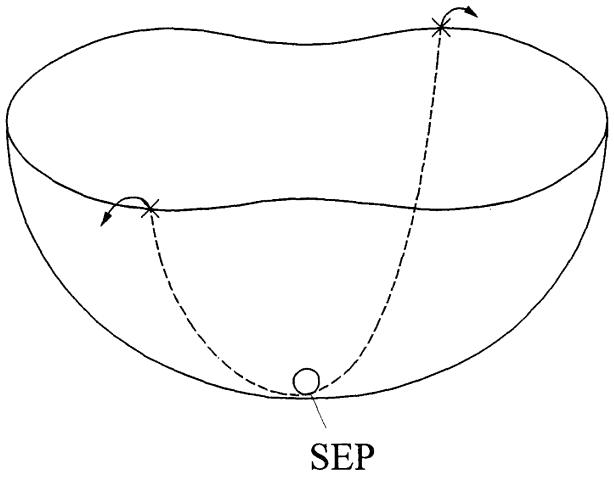


Figure 13.59 A ball rolling on the inner surface of a bowl

Initially the ball is resting at the bottom of the bowl, and this state is referred to as the *stable equilibrium point* (SEP). When some kinetic energy is injected into the ball, causing it to move in a particular direction, the ball will roll up the inside surface of the bowl along a path determined by the direction of initial motion. The point where the ball will stop is governed by the amount of kinetic energy initially injected. If the ball converts all its kinetic energy into potential energy before reaching the rim, then it will roll back and eventually settle down at the stable equilibrium point again. However, if the kinetic energy injected is high enough to cause the ball to go over the rim, then the ball will enter the region of instability and will not return to the stable equilibrium point. The surface inside the bowl represents the *potential energy surface*, and the rim of the bowl represents the *potential energy boundary surface* (PEBS).

Two quantities are required to determine if the ball will enter the instability region: (a) the initial kinetic energy injected and (b) the height of the rim at the crossing point. The location of the crossing point depends on the direction of the initial motion.

Application to power systems

The basis for the application of the TEF method to the analysis of power system stability is conceptually similar to that for a ball rolling in a bowl. Initially the system is operating at a stable equilibrium point. If a fault occurs, the equilibrium is disturbed and the synchronous machines accelerate. The power system gains kinetic and potential energy during the fault-on period and the system moves away from the SEP. After fault clearing, the kinetic energy is converted into potential energy in the

same manner as the ball rolling up the potential energy surface. To avoid instability, the system must be capable of absorbing the kinetic energy at a time when the forces on the generators tend to bring them toward new equilibrium positions. This depends on the potential energy-absorbing capability of the postdisturbance system. For a given postdisturbance network configuration, there is a maximum or critical amount of transient energy that the system can absorb. Consequently, assessment of transient stability requires

(a) Functions that adequately describe the transient energy responsible for separation of one or more synchronous machines from the rest of the system

(b) An estimate of the *critical energy* required for the machines to lose synchronism

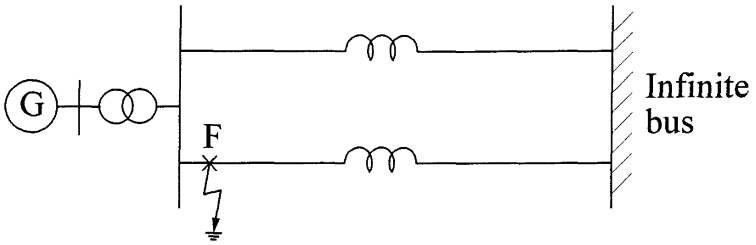
For a two-machine system the critical energy is uniquely defined, and the TEF analysis is equivalent to the equal-area criterion described in Section 13.1. This is illustrated in Figure 13.60, which shows two plots, both having rotor angle (δ) as the ordinate [40]. The upper plot illustrates the equal-area criterion in which the critical clearing angle (δ_c) is established by equality of areas A_1 and A_2. The lower plot illustrates the transient energy method which can be used to specify the critical clearing angle in terms of potential and kinetic energy. The kinetic energy gained during the fault-on period is added to the potential energy at the corresponding rotor angle, and the sum is compared to the critical potential energy to determine stability.

Given a disturbance, there is a stable equilibrium point for the postfault system. A region of attraction can be defined for this postfault SEP as shown in Figure 13.61. Any postfault system trajectory with the state of the system at fault clearing ($\mathbf{x}_{cl}$) inside this region of attraction will eventually converge to the SEP, and the system is said to be stable. On the other hand, if $\mathbf{x}_{cl}$ lies outside the region of attraction, the postfault system will not converge to the stable equilibrium point, and the system is said to be unstable.

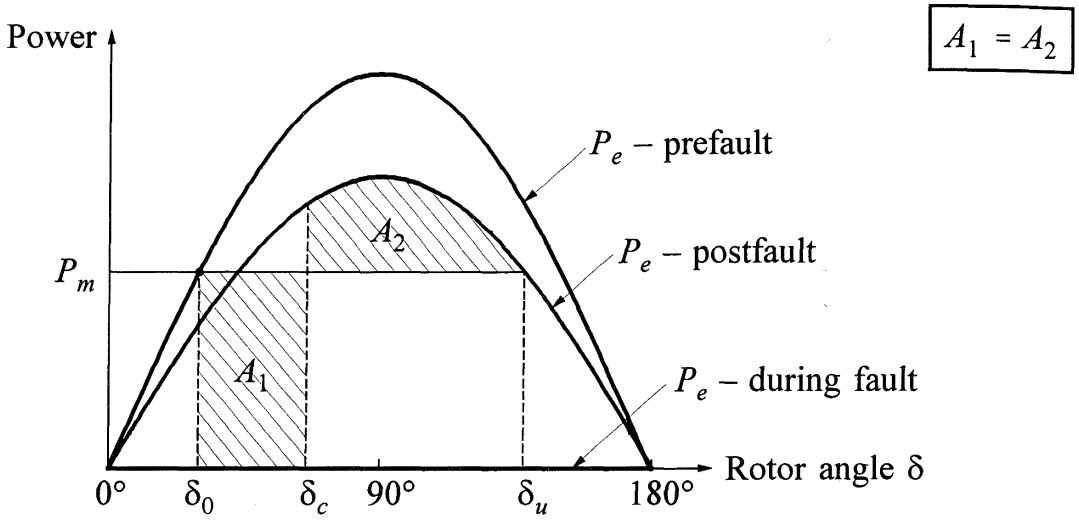
The state of the system at fault clearing ($\mathbf{x}_{cl}$) can be described by the value of the energy function evaluated at $\mathbf{x}_{cl}$, i.e., $V(\mathbf{x}_{cl})$. Hence the direct method solves the stability problem by comparing $V(\mathbf{x}_{cl})$ to the critical energy V_{cr}. The system is stable if $V(\mathbf{x}_{cl})$ is less than V_{cr} and the quantity $V_{cr}-V(\mathbf{x}_{cl})$ is a good measure of system relative stability. This quantity is defined as the *transient energy margin.*

The quantity $V(\mathbf{x}_{cl})$ measures the amount of transient energy injected into the system by the fault while the critical energy measures the strength of the postfault system. More precisely, the critical energy measures the energy-absorbing capability of the postfault system.

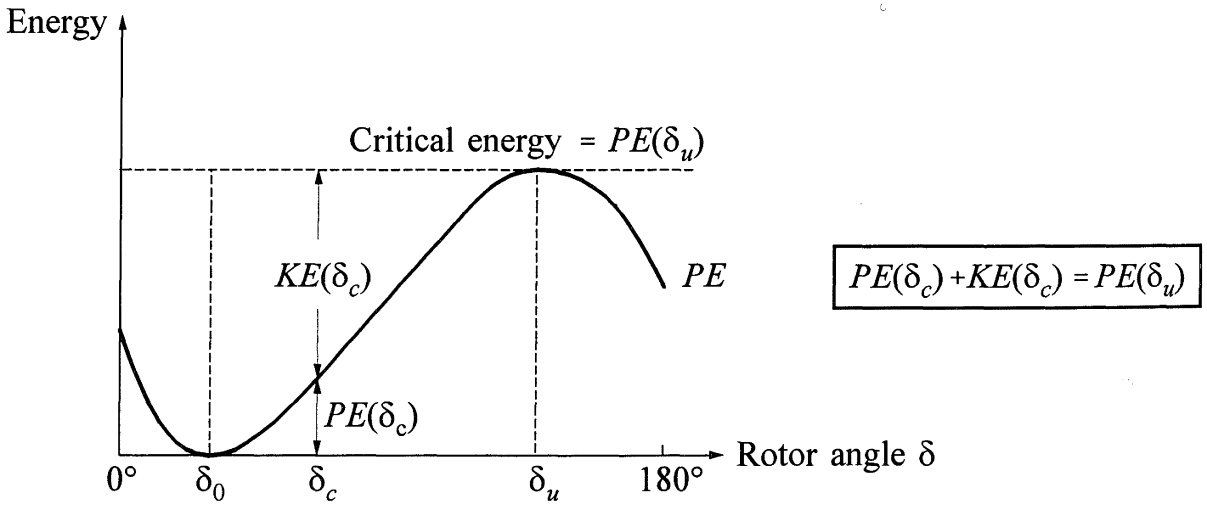
Referring to Figure 13.61, if the rotor oscillates within the range δ_{u1} to δ_{u2}, the system will remain transiently stable. If the rotor swings beyond this range, the system will become unstable. Hence the two points δ_{u1} and δ_{u2} on the potential energy curve form a boundary to all stable rotor angle trajectories. This boundary is called the *potential energy boundary surface* (PEBS) and the points on this boundary are local potential energy peaks.



(a) System configuration



(b) Power-angle relationships



(c) Energy-angle relationships

Figure 13.60 Illustration of equivalence of transient energy method and equal-area criterion

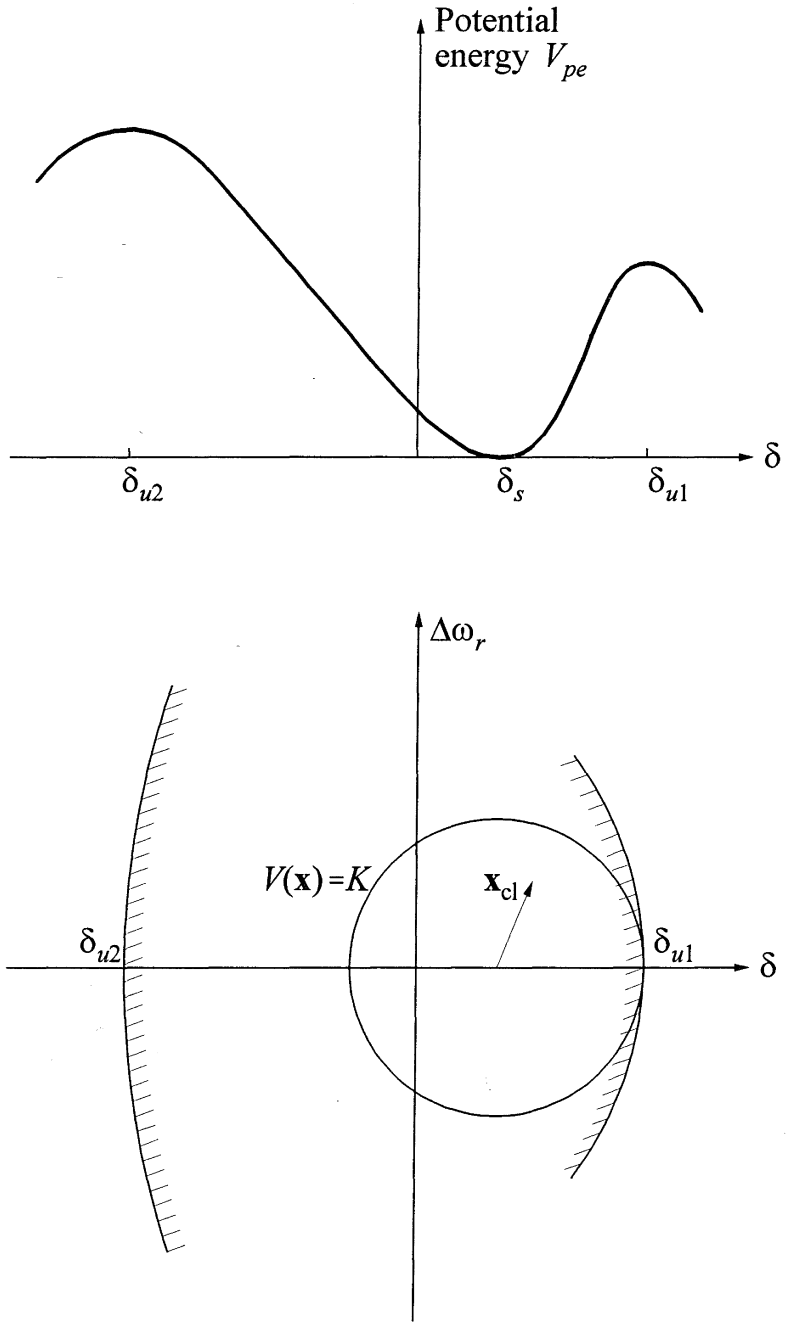


Figure 13.61 Region of stability and its local approximation

The boundary of the stability region is usually approximated locally by a constant energy surface $\{\mathbf{x} \mid V(\mathbf{x}) = K\}$ as shown in Figure 13.61, where K represents the critical energy V_{cr} of the postfault system.

13.7.2 Analysis of Practical Power Systems [40-49]

The application of the direct method to practical power systems is difficult. A number of simplifying assumptions are necessary. To date, the analysis has been mostly limited to power system representation with the generators represented by the classical model and loads modelled as constant impedances [42-45]. Recently, there

have been several attempts to extend the method to include more detailed models [46,47]. This, however, is still at a developmental stage and further research efforts are required to improve the accuracy and reliability of the method with detailed models. Here, we will limit our discussion to the simplified system models.

With the generator transient reactances and load admittances included in the node admittance matrix, we may write

$$\mathbf{I}_G = \mathbf{Y}_R \mathbf{E}_G \tag{13.86}$$

where $\mathbf{Y}_R$ is the reduced admittance matrix with all nodes other than the generator internal nodes eliminated, $\mathbf{E}_G$ is the generator internal source voltage vector, and $\mathbf{I}_G$ is the generator current vector.

Let the internal voltage of the i^{th} generator in phasor notation be given by

$$\tilde{E}_i = E_i \angle \delta_i$$

and the i^{th} row, j^{th} column element of $\mathbf{Y}_R$ by

$$y_{ij} = G_{ij} + jB_{ij}$$

For a system with n machines, the active output of the i^{th} generator is given by

$$\begin{aligned} P_i &= \mathrm{Re}(\tilde{E}_i \tilde{I}_i^*) \\ &= \mathrm{Re}(\tilde{E}_i \sum_{j=1}^{n} \tilde{y}_{ij}^* \tilde{E}_j^*) \\ &= E_i^2 G_{ii} + \sum_{\substack{j=1 \\ j \neq i}}^{n} E_i E_j \{B_{ij} \sin(\delta_i - \delta_j) + G_{ij} \cos(\delta_i - \delta_j)\} \end{aligned} \tag{13.87}$$

For the application of the TEF method, it is convenient to describe the transient behaviour of the system with the generator rotor angles expressed with respect to the inertial centre of all the generators. The position of the *centre of inertia* (COI) is defined as

$$\delta_{COI} \triangleq \frac{1}{H_T} \sum_{i=1}^{n} H_i \delta_i \tag{13.88}$$

where H_T is the sum of the inertia constants of all n generators in the system.

The motion of the COI is determined by

$$2H_T p(\Delta\omega_{COI}) = P_{COI} = \sum_{i=1}^{n} (P'_{mi} - P_{ei}) \tag{13.89}$$

and

$$p(\delta_{COI}) = (\Delta\omega_{COI})\omega_0 \tag{13.90}$$

with

$$P'_{mi} = P_{mi} - E_i^2 G_{ii} \tag{13.91}$$

$$P_{ei} = \sum_{\substack{j=1 \\ j \neq i}}^{n} [C_{ij}\sin(\delta_i - \delta_j) + D_{ij}(\delta_i - \delta_j)] \tag{13.92}$$

where

P_{mi} = mechanical input power of the i^{th} machine
$C_{ij} = E_i E_j B_{ij}$
$D_{ij} = E_i E_j G_{ij}$
ω_0 = synchronous speed in elec. rad/s
$\Delta\omega_{COI}$ = per unit speed deviation of COI from synchronous speed

The motion of the generators with respect to the COI can be expressed by defining

$$\theta_i = \delta_i - \delta_{COI} \quad \text{rad} \tag{13.93}$$

and

$$\omega_i = \frac{\dot{\theta}_i}{\omega_0} = \left(\frac{\dot{\delta}_i}{\omega_0} - \Delta\omega_{COI}\right) \quad \text{pu} \tag{13.94}$$

The equations of motion of the i^{th} machine in the COI reference frame are

$$2H_i p(\omega_i) = P'_{mi} - P_{ei} - \frac{H_i}{H_T} P_{COI} \tag{13.95}$$

$$p(\theta_i) = \omega_i \omega_0 \tag{13.96}$$

where ω_i is the pu speed of the i^{th} machine with respect to the COI.

The energy function V describing the total system transient energy for the postdisturbance system is defined as

$$V = \frac{1}{2}\sum_{i=1}^{n} J_i\omega_i^2 - \sum_{i=1}^{n} P'_{mi}(\theta_i - \theta_i^s) - \sum_{i=1}^{n-1}\sum_{j=i+1}^{n}\left[C_{ij}(\cos\theta_{ij} - \cos\theta_{ij}^s) - \int_{\theta_i^s+\theta_j^s}^{\theta_i+\theta_j} D_{ij}\cos\theta_{ij}\, d(\theta_i+\theta_j)\right] \tag{13.97}$$

where

θ_i^s = angle of bus i at the postdisturbance SEP
$J_i = 2H_i\omega_0$ = per unit moment of inertia of the i^{th} generator

The transient energy function is composed of the following four terms:

(a) $\frac{1}{2}\Sigma J_i\omega_i^2$: change in rotor kinetic energy of all generators in the COI reference frame

(b) $\Sigma P'_{mi}(\theta_i - \theta_i^s)$: change in rotor potential energy of all generators relative to COI

(c) $\Sigma\Sigma C_{ij}(\cos\theta_{ij} - \cos\theta_{ij}^s)$: change in stored magnetic energy of all branches

(d) $\Sigma\Sigma\int D_{ij}\cos\theta_{ij}\, d(\theta_i+\theta_j)$: change in dissipated energy of all branches

The first term is called the *kinetic energy* (V_{ke}) and is a function of only generator speeds. The sum of terms 2, 3, and 4 is called the *potential energy* (V_{pe}) and is a function of only generator angles.

The transient stability assessment involves the following steps:

1. Calculation of the critical energy V_{cr}
2. Calculation of the total system energy at the instant of fault-clearing V_{cl}
3. Calculation of stability index: $V_{cr} - V_{cl}$. The system is stable if the stability index is positive.

Time-domain simulation is run up to the instant of fault clearing to obtain the angles and speeds of all the generators. These are used to calculate the total system energy (V_{cl}) at fault clearing.

The calculation of V_{cr}, i.e., the boundary of the region of stability, is the most difficult step in applying the TEF method. Three different approaches are briefly described below.

(a) The closest unstable equilibrium point (UEP) approach

Early papers on the application of the TEF method for transient stability analysis used the following approach to determine the smallest V_{cr}:

Step 1: Determine all the UEPs. This is achieved by solving the postdisturbance system steady-state equations with different initial values of bus angles.

Step 2: Calculate system potential energy at each of the UEPs obtained in step 1. The critical energy V_{cr} is given by system energy at the UEP which results in the minimum potential energy.

Referring to the rolling ball analogy, the closest UEP is analogous to the lowest point on the rim of the bowl. The critical energy at the closest UEP is equal to the potential energy of the ball when it is at the lowest point on the rim. This assumes that the direction of initial motion is always toward the lowest point on the rim. Similarly, for a power system this approach computes the critical energy by implicitly assuming the worst fault location; hence, the results are very conservative.

(b) The controlling UEP approach [40, 48]

The degree of conservatism introduced by the closest UEP approach is such that the results are usually of little practical value. The controlling UEP approach removes much of this conservativeness by computing the critical energy dependent on the fault location. This approach is based on the observation that the system trajectories for all critically stable cases get near to those UEPs that are closely related to the boundary of system separation. The UEPs are called the controlling or relevant UEPs.

The computation process in this approach consists of two steps: (1) identification of the mode of disturbance and (2) calculation of the controlling UEP.

Mode of disturbance (MOD):

The mode of disturbance identifies the machines that are severely disturbed by a given disturbance. These machines are most likely to lose synchronism with the rest of the system if the disturbance is severe enough to cause system instability. One way to determine the MOD is to perform time-domain simulations and identify which machines go unstable. An automatic procedure for determining the MOD is described in reference 49 based on the normalized V_{pe}. This procedure requires a considerable amount of CPU time when detailed generator models are used.

Controlling UEP calculation:

The SEP or UEP is a solution of the power-flow equations (with i=1 to n):

$$f_i = P'_{mi} - P_{ei} - \frac{H_i}{H_T} P_{COI} = 0 \tag{13.98}$$

$$\omega_i = 0 \tag{13.99}$$

There are many solutions to the above equations, one of which is the SEP. All other solutions are UEPs. The controlling UEP is calculated by solving the following minimization problem:

$$\min\left\{F = \sum_{i=1}^{n} f_i\right\}$$

An approximate UEP based on the MOD is used as a starting point for the solution.

Numerical problems are sometimes encountered when one is solving for the controlling UEP based on the above approach. A robust procedure based on the potential energy boundary surface crossing point suggested in reference 44 is described below.

(c) The boundary of stability-region-based controlling UEP (BCU) method

Earlier CUEP methods face serious convergence problems when solving for the controlling UEP, especially when the system is highly stressed or highly unstressed, or the mode of system instability is complex. These problems usually arise if the starting point for the CUEP solution is not sufficiently close to the exact CUEP. Some of the convergence problems can be overcome by the BCU method which has the capability of producing a much better starting point for the CUEP solution.

In reference 44, the boundary of the stability region is defined as the union of the stable manifolds of the UEPs on the boundary. Any trajectory starting from a point on the boundary will converge to one of the UEPs as time increases. By making use of this property, the BCU method computes the controlling UEP of a power system through computing the CUEP of its associated reduced system.

The dynamic behaviour of a multimachine power system represented by classical generator models and constant impedance loads is described by Equations 13.95 and 13.96. The associated reduced system model for this multimachine power system is defined as

$$\dot{\theta}_i = P'_{mi} - P_{ei} - \frac{H_i}{H_T} P_{COI} = g_i \qquad i = 1, \ldots, n \tag{13.100}$$

The equilibrium points of the reduced system are the same as those of the original system. The BCU method computes the CUEP as follows:

(i) For a given system and a contingency, a sustained fault trajectory in time domain is simulated until it reaches the boundary of stability region of the reduced system (the PEBS). The system state at this time instant is referred to as the *exit point.*

(ii) Starting with the exit point, the reduced system is simulated in time domain until the quantity $\sum|g_i|$ reaches its first local minimum. The rotor angles at this point constitute the starting point for the CUEP solution.

(iii) The controlling UEP is computed using any robust numerical technique. The UEP so obtained is the controlling UEP relative to the fault-on trajectory.

The BCU method appears to be promising and can be easily extended to accommodate more detailed models. More testing is required to verify its accuracy and convergence characteristics. More importantly, the boundary of stability region for power systems modelled in detail needs to be investigated.

(d) Sustained-fault approach [42]

The calculation of the controlling UEP for large systems is very time-consuming. Under severe system conditions, the solution process may either fail to converge or converge to the wrong UEP. The sustained-fault approach was developed to avoid the calculation of the controlling UEP.

The critical energy is determined as follows:

1. A time domain simulation with a sustained fault is run until the system crosses the potential energy boundary surface (PEBS). The crossing of the PEBS is indicated by the potential energy reaching its maximum.

2. The potential energy at the crossing of the PEBS is taken as the critical energy for that particular fault location.

Example 13.8

In this example, we illustrate the use of the TEF method for transient stability analysis by considering the simple system of Example 13.1.

For the single-machine infinite bus system of Figure E13.1,

(a) Write the dynamic equations for the postdisturbance system corresponding to Equations 13.95 and 13.96.

(b) Write the expression for the system energy function.

(c) Calculate the postdisturbance system SEP, UEP, and the critical energy V_{cr}.

(d) Calculate the energy at fault clearing with t_c=0.07 s, 0.086 s, and 0.087 s. Determine the system stability for each of the three fault durations.

Solution

(a) The postdisturbance reduced equivalent circuit of the system is shown in Figure E13.26.

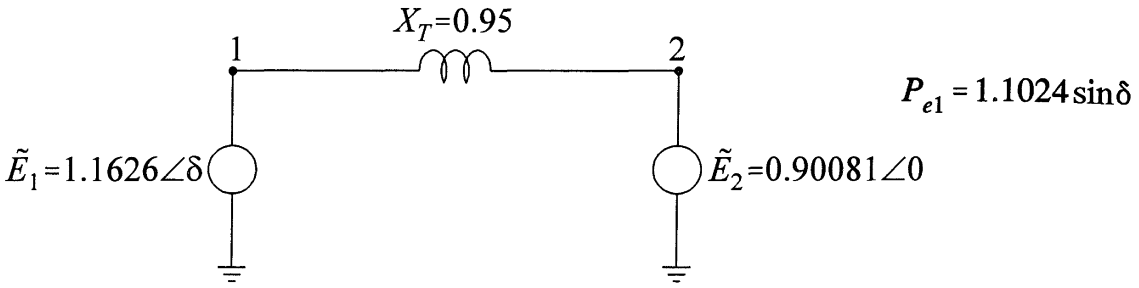


Figure E13.26 Postdisturbance equivalent circuit

Because bus 2 represents an infinite bus, $M_T=\infty$ and $\Delta\omega_{COI}=0$. Consequently, $\theta_1=\delta$ and $\omega_1=\dot{\theta}_1/\omega_0=\Delta\omega_r$.

Since G_{12}=0, D_{12}=0 and $P'_{m1}=P_{m1}$=0.9. The postdisturbance dynamic equations of the system, corresponding to Equations 13.95 and 13.96, are

$$2\times3.5p(\omega_1) = 0.9-1.1024\sin\theta_1$$

$$p(\theta_1) = 377\omega_1$$

(b) From Equation 13.97, the system transient energy function is

$$V = 3.5\times377\omega_1^2-0.9(\theta_1-\theta_1^s)-1.1024(\cos\theta_1-\cos\theta_1^s)$$

(c) At the postdisturbance SEP, we have

$$0.9-1.1024\sin\theta_1^s = 0$$

Hence,

$$\theta_1^s = 0.9552 \text{ rad} = 54.73°$$

For this simple system there is only one postdisturbance UEP, which is given by

$$\theta_1^u = \pi - \theta_1^s = 2.1864 \text{ rad} = 125.27°$$

The critical energy, which equals the system potential energy at the postdisturbance UEP, is

$$V_{cr} = -P'_{m1}(\theta_1^u - \theta_1^s) - C_{12}(\cos\theta_1^u - \cos\theta_1^s)$$

$$= -0.9(2.1864 - 0.9552) - 1.1024(-0.5775 - 0.5775)$$

$$= 0.1651$$

(d) To compute the energy at fault clearing, we will use the generator angles computed in Example 3.1.

(i) With t_c=0.07 s, θ_1^c=48.58°=0.8479 rad, and

$$\omega_c = \frac{0.9}{7} \times 0.07 = 0.009 \text{ pu}$$

The total energy at fault clearing is

$$V_{cl} = \frac{7}{2} \times 377 \times 0.09^2 - 0.9(0.8479 - 0.9552) - 1.1024(\cos 48.58° - \cos 54.73°)$$

$$= 0.1107$$

Since $V_{cl} < V_{cr}$, the system is stable; the stability margin is $V_{cr} - V_{cl}$= 0.1651 - 0.1107 = 0.0544.

(ii) With t_c=0.86 s, θ_1^c=52.04°=0.9083 rad, and

$$\omega_c = \frac{0.9}{7} \times 0.086 = 0.011057 \text{ pu}$$

The total energy at fault clearing is

$$V_{cl} = \frac{7}{2} \times 377 \times 0.011057^2 - 0.9(0.9083 - 0.9552) - 1.1024(\cos 52.04° - \cos 54.73°)$$

$$= 0.1620$$

The system is stable; however, the stability margin is now reduced to 0.1651 - 0.1620 = 0.0031.

(iii) With t_c=0.087 s, θ_1^c=52.3°=0.9128 rad, and ω_c=0.011186 pu. The total energy at fault clearing is

$$V_{cl} = \frac{7}{2}\times 377\times 0.011186^2 - 0.9(0.9128-0.9552) - 1.1024(\cos 52.3^\circ - \cos 54.73^\circ)$$

$$= 0.1657$$

Since $V_{cl} > V_{cr}$, the system is unstable.

The above results are consistent with the time-domain simulation results of Example 13.1. ■

13.7.3 Limitations of the Direct Methods

In spite of the many significant accomplishments in recent years in the application of the direct methods, modelling limitations and unreliability of computation techniques continue to be major impediments to their widespread practical use. The direct methods are vulnerable to numerical problems when one is solving stressed systems. The use of sophisticated and robust CUEP solution techniques usually imposes a heavy computational burden, making the method slower than the time-domain simulation.

The best course appears to be the use of a hybrid approach in which the transient energy calculation is incorporated into the conventional time-domain simulation [50-54]. This enhances the capability of time-domain simulations by computing the stability margin and minimizing the effort required in determining the stability limits.

REFERENCES

[1] W.D. Stevenson, *Elements of Power System Analysis*, 3rd Edition, McGraw-Hill, 1975.

[2] R.T. Byerly and E.W. Kimbark, *Stability of Large Electric Power Systems*, IEEE Press, 1974.

[3] E.R. Laithwaite and L.L. Freris, *Electric Energy: Its Generation, Transmission and Use*, McGraw-Hill (UK), 1980.

[4] A. Ralston and H.S. Wilf, *Mathematical Methods for Digital Computers*, John Wiley & Sons, 1962.

[5] B. Carnahan, H.A. Luther, and J.O. Wilkes, *Applied Numerical Methods*, John Wiley & Sons, 1969.

[6] C.W. Gear, *Numerical Initial Value Problems in Ordinary Differential Equations*, Prentice-Hall, 1971.

[7] Kundur Prabhashankar, *Digital Simulation and Analysis of Power System Dynamic Performance*, Ph.D. thesis, University of Toronto, 1967.

[8] P. Kundur and P.L. Dandeno, "Implementation of Advanced Generator Models into Power System Stability Programs," *IEEE Trans.*, Vol. PAS-102, pp. 2047-2052, July 1983.

[9] H.W. Dommel, "Digital Computer Solution of Electromagnetic Transients in Single and Multiphase Networks," *IEEE Trans.*, Vol. PAS-88, pp. 388-399, April 1969.

[10] B. Stott, "Power System Dynamic Response Calculations," *Proc. IEEE*, Vol. 67, pp. 219-241, February 1979.

[11] P.L. Dandeno and P. Kundur, "A Non-iterative Transient Stability Program Including the Effects of Variable Load-Voltage Characteristics," *IEEE Trans.*, Vol. PAS-92, pp. 1478-1484, September 1973.

[12] H.W. Dommel and N. Sato, "Fast Transient Stability Solutions," *IEEE Trans.*, Vol. PAS-91, pp. 1643-1650, July/August 1972.

[13] M. Stubbe, A. Bihain, J. Deuse, and J.C. Baader, "STAG - A New Unified Software Program for the Study of the Dynamic Behaviour of Electrical Power Systems," *IEEE Trans.*, Vol. PWRS-4, No. 1, pp. 129-138, 1989.

[14] EPRI Report, *Programmers Manual for ETMSP Version 3*, Prepared by Ontario Hydro, 1992.

[15] C.F. Wagner and R.D. Evans, *Symmetrical Components*, McGraw-Hill, 1933.

[16] Edith Clarke, *Circuit Analysis of AC Power Systems*, Vol. I, John Wiley & Sons, 1943.

[17] P.M. Anderson, *Analysis of Faulted Power Systems*, Iowa State Press, Ames, Iowa, 1973.

[18] Westinghouse Electric Corporation, *Electric Transmission and Distribution Reference Book*, East Pittsburgh, Pa., 1964.

[19] C.L. Fortescue, "Method of Symmetrical Coordinates Applied to the Solution of Polyphase Networks," *AIEE Trans.*, Vol. 37, Pt. II, pp. 1027-1140, 1918.

[20] T.M. O'Flaherty and A.S. Aldred, "Synchronous Machine Stability under Unsymmetrical Faults," *Proceedings IEE*, Vol. 109A, p. 431, 1962.

[21] Westinghouse Electric Corporation, *Applied Protective Relaying*, a new "Silent Sentinels" publication, Newark, 1976.

[22] H.M. Rustebakke (editor), *Electric Utility Systems and Practices*, John Wiley & Sons, 1983.

[23] C.R. Mason, *The Art and Science of Protective Relaying*, John Wiley & Sons, 1956.

[24] General Electric Company, *Use of the R-X Diagram in Relay Work*, Philadelphia, Pa., 1966.

[25] C.R. Mason, "Relay Operation during System Oscillations," *AIEE Trans.*, Vol. 56, pp. 823-832, 1937. Discussion by J.H. Neher, pp. 1513-1514. Closure by C.R. Mason, Vol. 57, pp. 111-114, 1938.

[26] J.H. Neher, "A Comprehensive Method of Determining the Performance of Distance Relays," *AIEE Trans.*, Vol. 56, pp. 833-844, 1937.

[27] Edith Clarke, "Impedances Seen by Relays during Power Swings with and without Faults," *AIEE Trans.*, Vol. 64, pp. 372-384, 1945. Discussion by A.J. McConnell, p. 472, June Supplement 1945.

[28] IEEE Working Group Report, "Out of Step Relaying for Generators," *IEEE Trans.*, Vol. PAS-96, pp. 1556-1564, September/October 1977.

[29] C.R. Mason, "A New Loss-of-Excitation Relay for Synchronous Generators," *AIEE Trans.*, Vol. 68, pp. 1240-1245, 1949.

[30] J. Berdy, "Loss of Excitation Protection for Modern Synchronous Generators," *IEEE Trans.*, Vol. PAS-94, pp. 1457-1463, September/October 1975.

[31] D.C. Lee, P. Kundur, and R.D, Brown, "A High Speed, Discriminating Generator Loss of Excitation Protection," *IEEE Trans.*, Vol. PAS-98, pp. 1895-1898, November/December 1979.

[32] P.C. Magnusson, "Transient Energy Method of Calculating Stability," *AIEE Trans.*, Vol. 66, pp. 747-755, 1947.

[33] P.D. Aylett, "The Energy Integral-Criterion of Transient Stability Limits of Power Systems," *Proc. IEE*, Vol. 105c, No. 8, pp. 527-536, September 1958.

[34] G.E. Gless, "Direct Method of Lyapunov Applied to Transient Power System Stability," *IEEE Trans.*, Vol. PAS-85, No. 2, pp. 159-168, February 1966.

[35] A.H. El-Abiad and K. Nagappan, "Transient Stability Regions of Multimachine Power Systems," *IEEE Trans.*, Vol. PAS-85, No. 2, pp. 169-178, February 1966.

[36] M. Ribbens-Pavella, "Critical Survey of Transient Stability Studies of Multi-Machine Power Systems by Lyapunov's Direct Method," *Proc. 9th Annual Allerton Conference on Circuits and System Theory*, pp. 751-767, October 1971.

[37] A.A. Fouad, "Stability Theory-Criteria for Transient Stability," *Proc. Engineering Foundation Conference on System Engineering for Power,* pp. 421-450, Henniker, N.H., 1975.

[38] M.A. Pai, *Energy Function Analysis for Power System Stability*, Kluwer Academic Press, 1989.

[39] A.A. Fouad and Vijay Vittal, *Power System Transient Stability Analysis Using the Transient Energy Function Method*, Prentice-Hall, 1992.

[40] T. Athay, V.R. Sherkat, R. Podmore, S. Virmani, and C. Puech, "Transient Energy Analysis," Final Report of U.S. Department of Energy Contract No. EX-76-C-01-2076, Prepared by Systems Control, Inc., June 1979.

[41] Chi-Keung Tang, "Evaluation of the Direct Method for Power System Transient Stability Analysis," M.Eng. degree thesis, University of Toronto, August 1984.

[42] N. Kakimoto, Y. Ohsawa, and M. Hayashi, "Transient Stability Analysis of Electric Power System Via Lure' Type Lyapunov Functions, Parts I and II," *Trans. IEE of Japan*, Vol. 98, No. 516, May/June 1978.

[43] A.A. Fouad and S.E. Stanton, "Transient Stability of Multimachine Power System, Parts I and II," *IEEE Trans.*, Vol. PAS-100, pp. 3408-3424, July 1981.

[44] H.D. Chiang, F.F. Wu, and P.P. Varaiya, "Foundations of the Potential Energy Boundary Surface Method for Power System Transient Stability Analysis," *IEEE Trans.*, Vol. CAS-35, pp. 712-728, June 1988.

[45] M.A. El-Kady, M.M. Abu-Elnaga, R.D. Findlay, and C.G. Bailey, "Sparse Formulation of the Direct Method of Transient Stability for Applications on Micro-Computers," *Proc. 29th Midwest Symposium on Circuits and Systems*, pp. 519-522, Lincoln, Neb., 1986.

[46] A.A. Fouad, V. Vittal, Y-X. Ni, H.M. Zein-Eldin, E. Vaahedi, H.R. Pota, K. Nodehi, and J. Kim, "Direct Transient Stability Assessment with Excitation Control," *IEEE Trans.*, Vol. PWRS-4, No. 1, pp. 75-82, February 1989.

[47] V. Vittal, N. Bhatia, A.A. Fouad, G.A. Maria, and H.M. Zein-Eldin, "Incorporation of Nonlinear Load Models in the Transient Energy Function Method," *IEEE Trans.*, Vol. PWRS-4, No. 3, pp. 1031-1036, August 1989.

[48] T. Athay, R. Podmore, and S. Virmani, "A Practical Method for the Direct Analysis of Transient Stability," *IEEE Trans.*, Vol. PAS-98, No. 2, pp. 573-584, March/April 1979.

[49] A.A. Fouad, V. Vittal, and Taekyoo Oh, "Critical Energy for Transient Stability Assessment of a Multimachine Power System," *IEEE Trans.*, Vol. PAS-103, pp. 2199-2206, 1984.

[50] P. Kundur, "A Practical View of the Applicability of the Direct Methods," Minipaper presented at the IEEE Panel Session on Application of Direct Methods to Transient Stability Analysis of Power Systems, *IEEE Trans.*, Vol. PAS-193, pp. 1634-1635, July 1984.

[51] P. Kundur, "Evaluation of Methods for Studying Power System Stability," *Proc. International Symposium on Power System Stability*, Ames, Iowa, 1985.

[52] B. Gao, "Assessment of Power System Transient Stability Using Energy Functions," M.A.Sc. thesis, University of Toronto, 1986.

[53] G. Maria, C. Tang, and J. Kim, "Hybrid Transient Stability Analysis," *IEEE Trans.*, Vol. PWRS-5, No. 2, pp. 384-393, May 1990.

[54] C.K. Tang, C.E. Graham, M. El-Kady, and R.T.H. Alden, "Transient Stability Index from Conventional Time Domain Simulation," Paper 93SM487-9PWRS, presented at the 1993 IEEE PES Summer Meeting, Vancouver, July 1993.

Chapter 14

Voltage Stability

Voltage control and stability problems are not new to the electric utility industry but are now receiving special attention in many systems. Once associated primarily with weak systems and long lines, voltage problems are now also a source of concern in highly developed networks as a result of heavier loadings. In recent years, voltage instability has been responsible for several major network collapses. The following are some examples [1,2]:

- New York Power Pool disturbances of September 22, 1970
- Florida system disturbance of December 28, 1982
- French system disturbances of December 19, 1978, and January 12, 1987
- Northern Belgium system disturbance of August 4, 1982
- Swedish system disturbance of December 27, 1983
- Japanese system disturbance of July 23, 1987

As a consequence, the terms "voltage instability" and "voltage collapse" are appearing more frequently in the literature and in discussions of system planning and operation.

Although low voltages can be associated with the process of rotor angles going out of step, the type of voltage collapse related to voltage instability can occur where "angle stability" is not an issue. The gradual pulling out of step of machines, as rotor angles between two groups of machines approach or exceed 180°, results in very low voltages at intermediate points in the network (see Chapter 13, Section 13.5.3). However, in such cases the low voltage is a result of the rotors falling out of step rather than a cause of it.

Voltage stability, as described in Chapter 2, is concerned with the ability of a power system to maintain acceptable voltages at all buses in the system under normal conditions and after being subjected to a disturbance. A system enters a state of voltage instability when a disturbance, increase in load demand, or change in system condition causes a progressive and uncontrollable decline in voltage. The main factor causing instability is the inability of the power system to meet the demand for reactive power.

This chapter will review basic concepts related to voltage stability and characterize the "voltage avalanche" phenomenon. The dynamic and static approaches to voltage stability analysis will be described, and methods identified for preventing voltage instability.

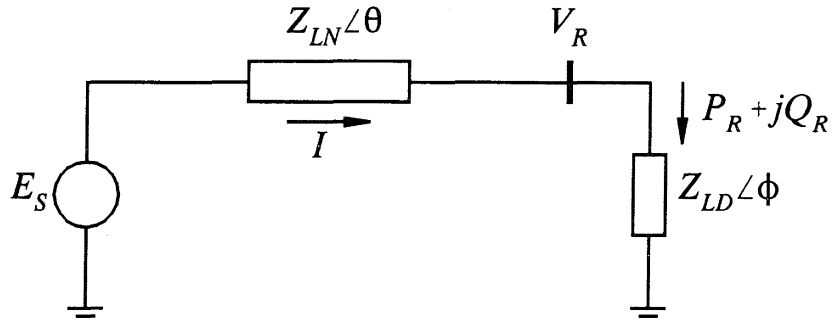
14.1 BASIC CONCEPTS RELATED TO VOLTAGE STABILITY

Voltage stability problems normally occur in heavily stressed systems. While the disturbance leading to voltage collapse may be initiated by a variety of causes, the underlying problem is an inherent weakness in the power system. In addition to the strength of transmission network and power transfer levels, the principal factors contributing to voltage collapse are the generator reactive power/voltage control limits, load characteristics, characteristics of reactive compensation devices, and the action of voltage control devices such as transformer under-load tap changers (ULTCs).

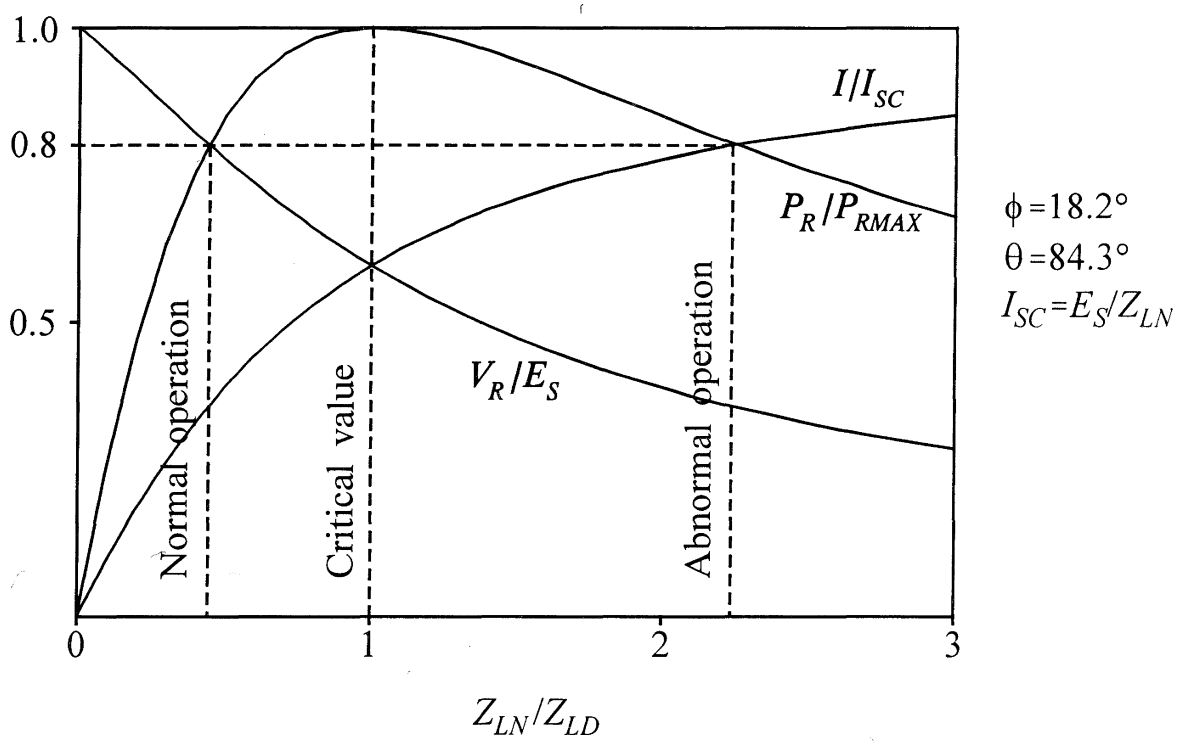
This section illustrates the basic concepts related to voltage instability by firstly considering the characteristics of transmission systems and then examining how the phenomenon is influenced by the characteristics of generators, loads, and reactive power compensation devices.

14.1.1 Transmission System Characteristics

The characteristics of interest are the relationships between the transmitted power (P_R), receiving end voltage (V_R), and the reactive power injection (Q_i). Such characteristics were discussed for a simple radial system in Chapter 2 (Section 2.1) and for transmission lines of varying lengths in Chapter 6 (Section 6.1). For complex systems with a large number of voltage sources and load buses, similar characteristics can be determined by using power-flow analysis (see Chapter 6).



(a) Schematic diagram



(b) Receiving end voltage, current and power as a function of load demand

Figure 14.1 Characteristics of a simple radial system

Let us briefly review the characteristics of the simple radial system considered in Chapter 2 (Figure 2.4). For reference the schematic diagram of the system is reproduced in Figure 14.1(a). As shown in Section 2.1.2, the current I and receiving end voltage V_R and power P_R are given by the following equations:

$$I = \frac{1}{\sqrt{F}} \frac{E_S}{Z_{LN}} \tag{14.1}$$

$$V_R = \frac{1}{\sqrt{F}} \frac{Z_{LD}}{Z_{LN}} E_S \tag{14.2}$$

$$P_R = \frac{Z_{LD}}{F}\left(\frac{E_S}{Z_{LN}}\right)^2 \cos\phi \tag{14.3}$$

where

$$F = 1+\left(\frac{Z_{LD}}{Z_{LN}}\right)^2 +2\left(\frac{Z_{LD}}{Z_{LN}}\right)\cos(\theta-\phi)$$

Plots of I, V_R, and P_R are shown in Figure 14.1(b) as a function of load demand (Z_{LN}/Z_{LD}), for the case with $\tan\theta=10.0$ and $\cos\phi=0.95$. To make the results applicable to any value of Z_{LN}, the values of I, V_R and P_R are appropriately normalized.

As load demand increases (Z_{LD} decreases), P_R increases rapidly at first and then slowly before reaching a maximum, and finally decreases. There is thus a maximum value of active power that can be transmitted through an impedance from a constant voltage source. The power transmitted is maximum when the voltage drop in the line is equal in magnitude to V_R, i.e., when $Z_{LD}/Z_{LN}=1$. The conditions corresponding to maximum power represent the limits of satisfactory operation. The values of V_R and I corresponding to maximum power are referred to as *critical values.*

For a given value of power P_R delivered ($P_R<P_{RMAX}$), two operating points may be found corresponding to two different values of Z_{LD}. This is shown in Figure 14.1(b) for $P_R=0.8$. The point to the left corresponds to normal operation. At the operating point to the right, I is much larger and V_R much lower than for the point to the left.

For a load demand higher than the maximum power, control of power by varying the load would be unstable, i.e., an increase in load admittance would reduce power. In this region, the load voltage may or may not progressively decrease depending on the load-voltage characteristic. With a constant-admittance load characteristic, the system condition stabilizes at a voltage level that is lower than normal. On the other hand, if the load is supplied by a transformer with ULTC, the tap-changer action will try to raise the load voltage, which has the effect of reducing effective Z_{LD}. This lowers V_R still further and leads to a progressive reduction of voltage. This is the phenomenon of *voltage instability.*

From Equation 14.3, we see that the maximum value of P_R can be increased by increasing the source voltage E_S and/or decreasing ϕ.

A more traditional method of illustrating the phenomenon is to plot the relationship between V_R and P_R, for different values of load power factor with E_S constant as shown in Figure 14.2. The locus of critical operating points is shown by dashed lines in the figure. Only the operating points above the critical points represent satisfactory operating conditions.

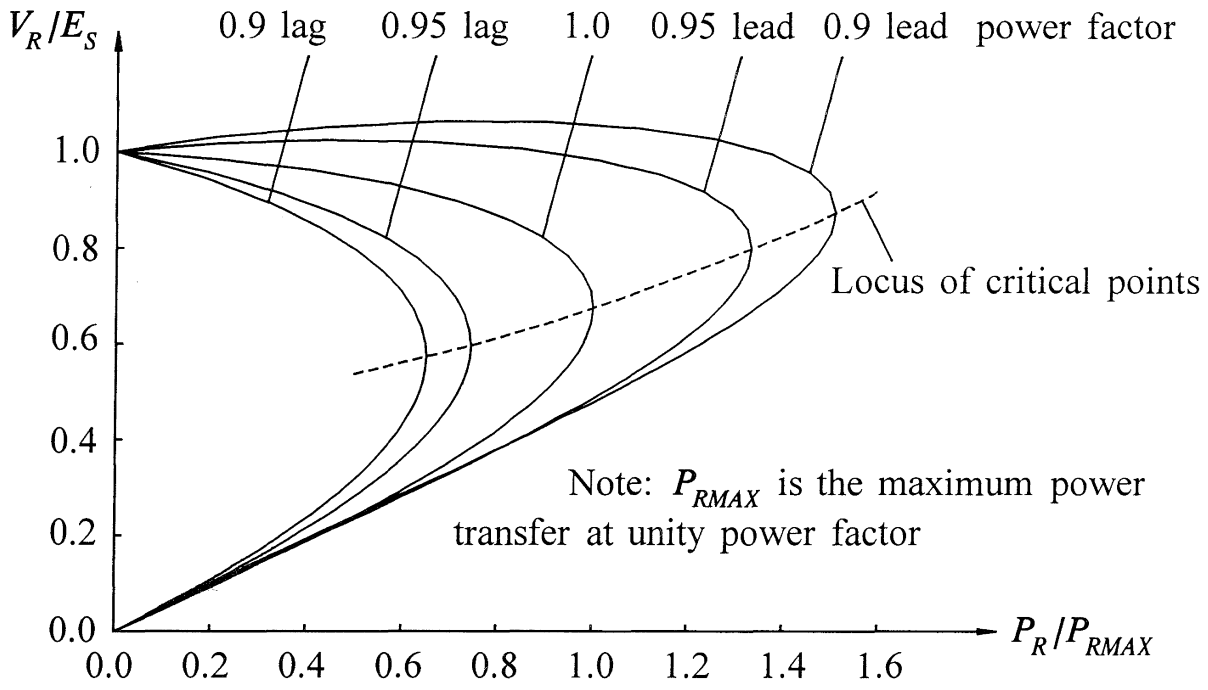


Figure 14.2 The V_R-P_R characteristics of the system of Figure 14.1

In Chapter 6 (Section 6.1), we developed similar *V-P* characteristics for transmission lines of different lengths. Practical power systems consisting of many voltage sources and load buses also exhibit similar relationships between active power transfer and load bus voltages. We will illustrate this for the system shown in Figure 14.3, consisting of 39 buses with nine generators and one synchronous condenser. Figure 14.4 shows the *V-P* curve for the system; it represents the variation in voltage at bus 530, a critical bus in the load area prone to voltage instability, as a function of total active power load in the shaded area. This curve has been produced by using a series of power-flow solutions for different load levels. The loads in area 1 (shaded) are uniformly scaled up while the power factor is kept constant. The active power outputs of generators are correspondingly increased in proportion to the size of generator. The *P* and *Q* components of each load are assumed to be independent of the bus voltage. At the "knee" of the *V-P* curve, the voltage drops rapidly with an increase in load demand (or nominal voltage load). Power-flow solution fails to converge beyond this limit, which is indicative of instability. Operation at or near the stability limit is impractical and a satisfactory operating condition is ensured by allowing sufficient "power margin."

We see that complex systems have *V-P* characteristics similar to those of the simple radial system of Figure 14.1. Such characteristics represent the basic property of networks with predominantly inductive elements.

We have so far considered the *V-P* characteristics with constant load power factor. Voltage stability, in fact, depends on how variations in *Q* as well as *P* in the load area affect the voltages at the load buses. Often, a more useful characteristic for certain aspects of voltage stability analysis is the *Q-V* relationship, which shows the

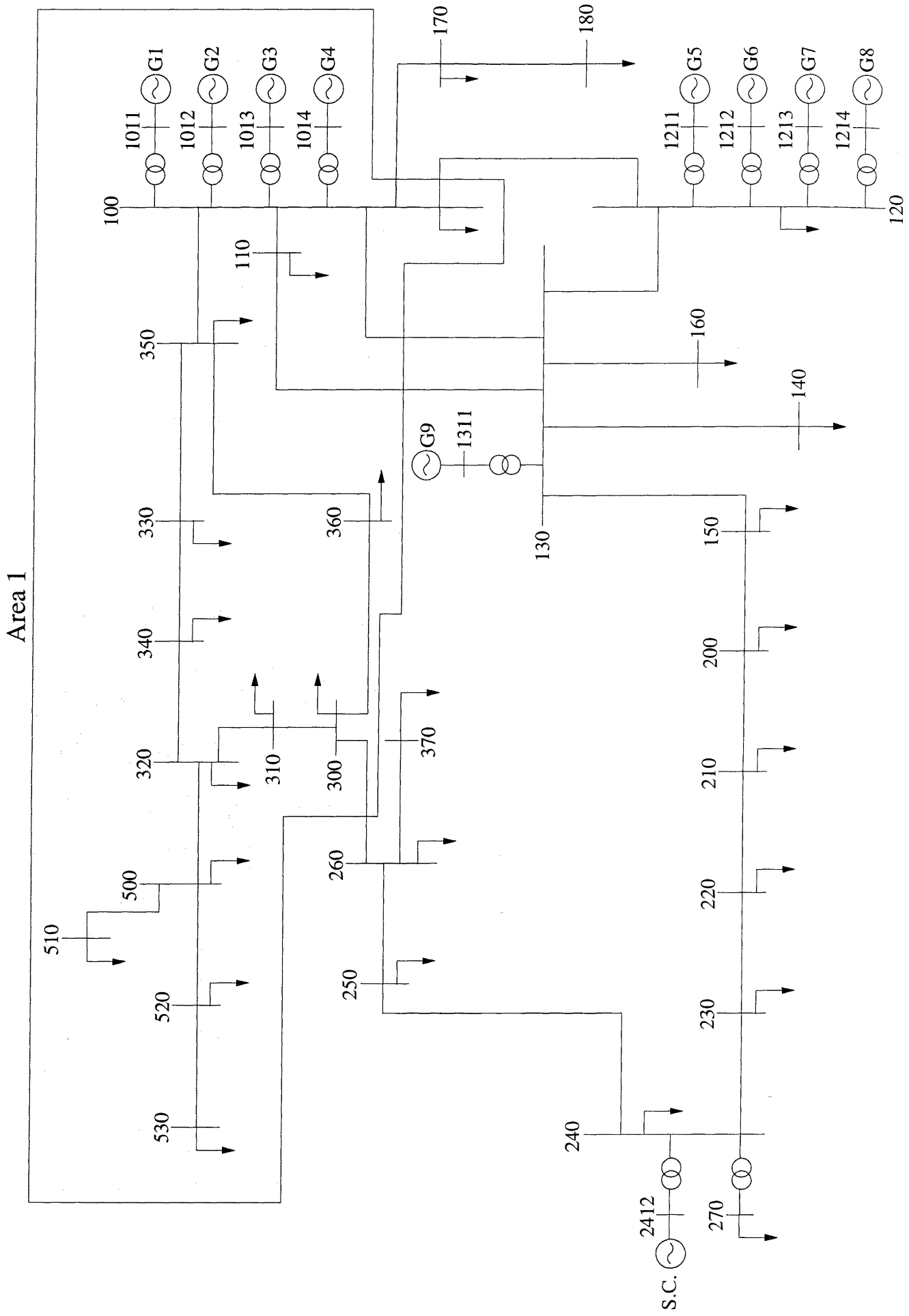


Figure 14.3 A 39-bus, 10-machine test system

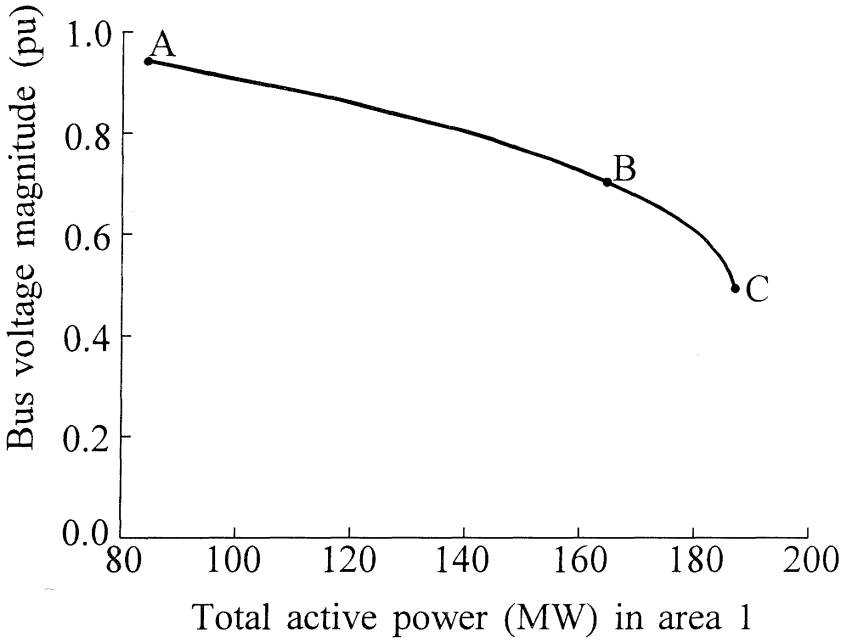
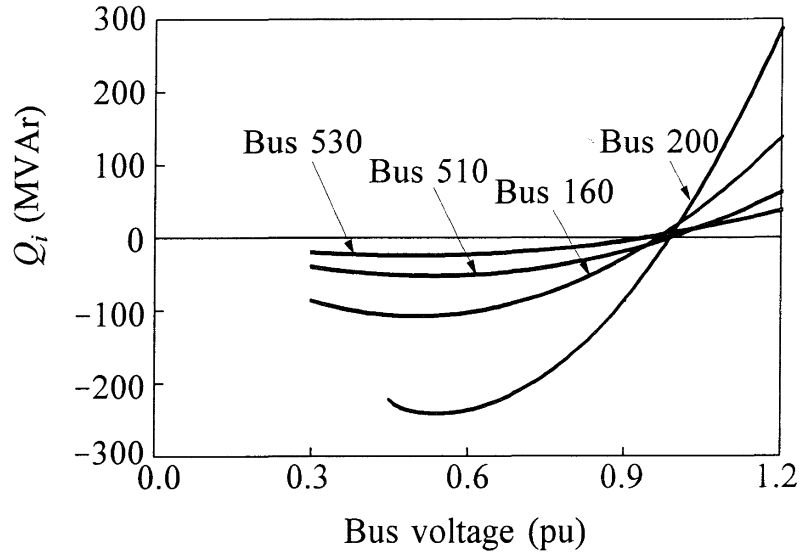


Figure 14.4 The *V-P* curve at bus 530 of the system shown in Figure 14.3

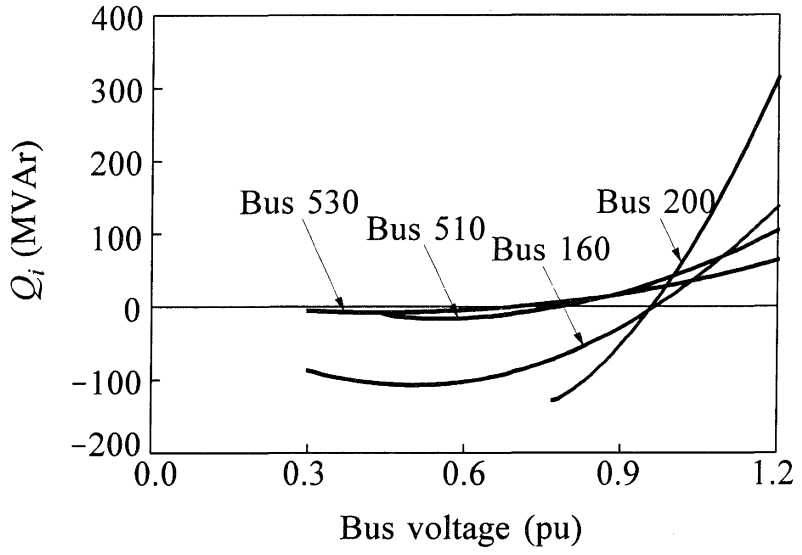
sensitivity and variation of bus voltages with respect to reactive power injections or absorptions. For the simple radial system of Figure 14.1, such characteristics for different values of load power are shown in Figure 2.8 of Chapter 2. These characteristics can be derived more readily than the *V-P* characteristics for systems with a non-radial type structure and are better suited for examining the requirements for reactive power compensation.

Figure 14.5 shows the *Q-V* curves computed at buses 160, 200, 510, and 530 for the three operating conditions represented by points A, B, and C on the *V-P* curve of Figure 14.4. Point A represents the base case, point B a condition near the critical operating point, and point C a condition at the critical operating point. Each of these *Q-V* curves has been produced by successive power-flow calculations with a variable reactive power source at the selected bus and recording its values required to hold different scheduled bus voltages. The bottom of the *Q-V* curve, where the derivative dQ/dV is equal to zero, represents the voltage stability limit. Since all reactive power control devices are designed to operate satisfactorily when an increase in Q is accompanied by an increase in V, operation on the right side of the *Q-V* curve is stable and on the left side is unstable. Also, voltage on the left side may be so low that protective devices may be activated. The bottom of the *Q-V* curve, in addition to identifying the stability limit, defines the minimum reactive power requirement for stable operation [3].

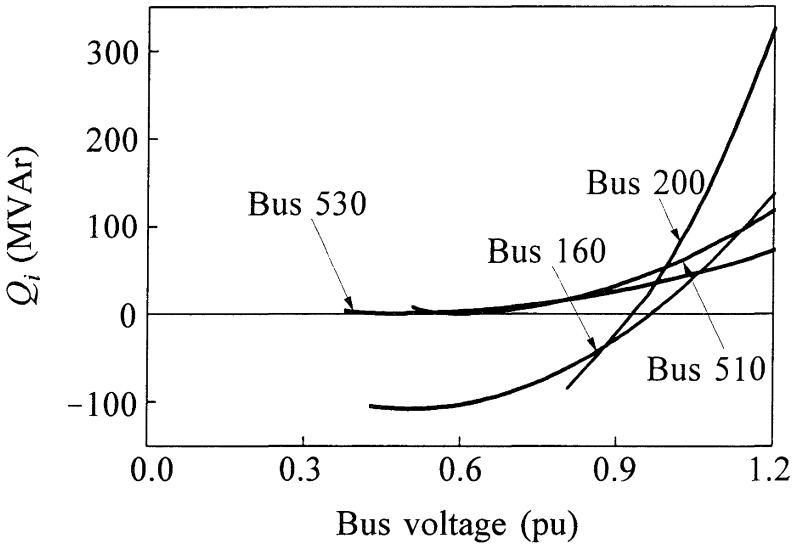
In this section we have examined the characteristics of transmission systems as impacted by the flow of active and reactive power through highly inductive elements. It is evident from the analysis presented here that the following are the principal causes of voltage instability:



(a) Base case, with a load of 84.5 MW, 53.3 MVAr in area



(b) Operating condition near the critical operating point, with a load of 164.4 MW, 103.7 MVAr in area 1



(c) Operating condition at the critical operating point, with a load of 186.9 MW, 117.9 MVAr in area 1

Figure 14.5 The Q-V curves for system shown in Figure 14.3

- The load on the transmission lines is too high.
- The voltage sources are too far from the load centres.
- The source voltages are too low.
- There is insufficient load reactive compensation.

The transmission system V-P and Q-V characteristics have been introduced here primarily to illustrate the basic phenomenon associated with voltage instability. The approach presented for deriving the characteristics by using conventional power-flow programs is, however, not necessarily the most efficient way of studying the voltage stability problem. Methods of analyzing voltage stability are discussed in Section 14.3.

14.1.2 Generator Characteristics

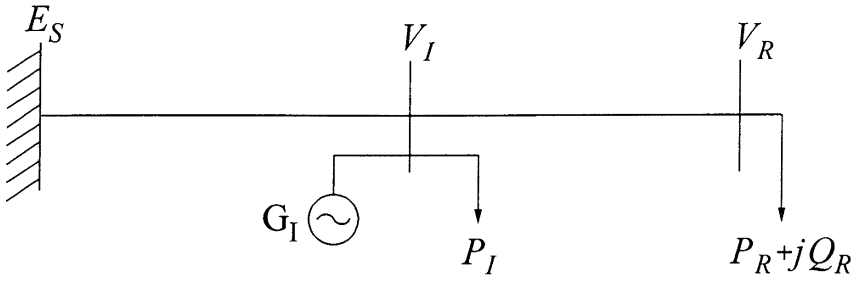
Generator AVRs are the most important means of voltage control in a power system. Under normal conditions the terminal voltages of generators are maintained constant. During conditions of low-system voltages, the reactive power demand on generators may exceed their field current and/or armature current limits (see Chapter 5, Section 5.4). When the reactive power output is limited, the terminal voltage is no longer maintained constant.

The generator field current is automatically limited by an *overexcitation limiter* (OXL). The function and modelling of such limiters are described in Chapter 8 (Sections 8.5 and 8.6). With constant field current, the point of constant voltage is behind the synchronous reactance (see Chapter 3, Figure 3.22). This effectively increases the network reactance significantly, further aggravating the voltage collapse condition.

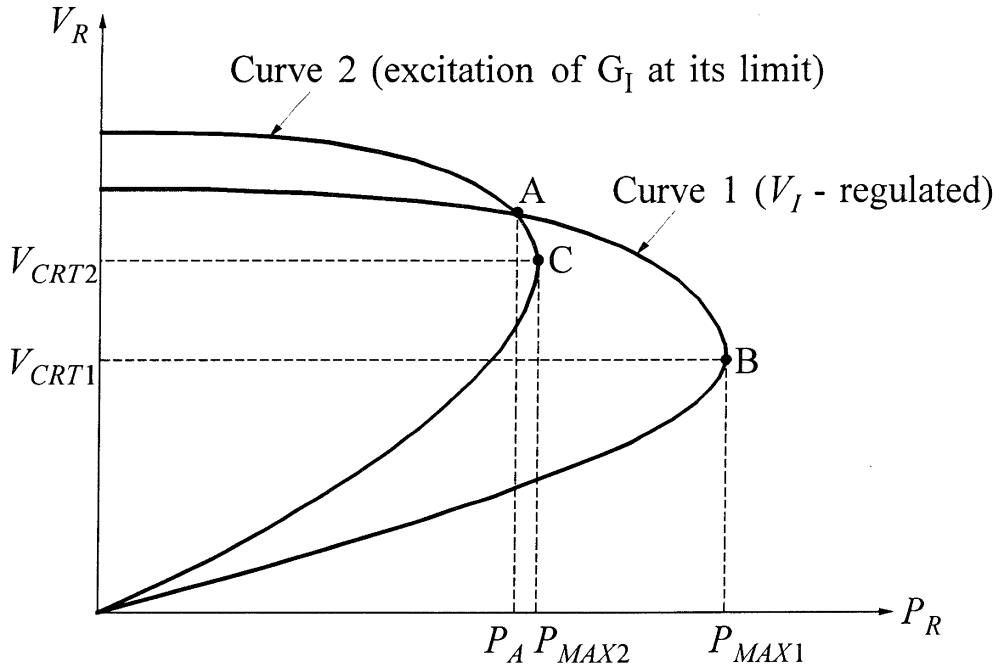
On most generators, the armature current limit is realized manually by operators responding to alarms. The operator reduces reactive and/or active power output to bring the armature current within safe limits. On some generators, automatic armature current limiters with time delay are used to limit reactive power output through the AVR [2].

To illustrate the impact of loss of generator voltage control capability, consider the system shown in Figure 14.6(a). It consists of a large load supplied radially from an infinite bus, with intermediate generation supplying part of the load and regulating voltage (V_I).

With voltage at the intermediate bus maintained, the V-P characteristic is shown by curve 1 in Figure 14.6(b). When the generating unit at the intermediate point hits its field current limit, the bus voltage (V_I) is no longer maintained and the V-P characteristic is shown by curve 2. An operating condition such as that represented by point A is considerably more stable when on curve 1 than when it is on curve 2. These results demonstrate the importance of maintaining the voltage control capability of generators. In addition, they show that the degree of voltage stability cannot be judged based only on how close the bus voltage is to the normal voltage level.



(a) Schematic diagram



(b) The V_R-P_R characteristics

Figure 14.6 Impact of loss of regulation of intermediate bus voltage

This situation is similar to that which led to voltage collapse in the Brittany region of the French system in December 1965 and in November 1975 [4].

14.1.3 Load Characteristics [1,5]

Load characteristics and distribution system voltage control devices are among the key factors influencing system voltage stability.

The characteristics and modelling of different types of loads are discussed in Chapter 7. Loads whose active and reactive components vary with voltage interact with the transmission characteristics by changing the power flow through the system. The system voltages settle at values determined by the composite characteristic of the transmission system and loads.

Distribution system voltage regulators and substation transformer ULTCs attempt to hold constant voltage at the point of consumption (see Chapter 11, Section 11.2). Within the normal control range, loads appear effectively as constant MVA loads. This may have a destabilizing effect during conditions of voltage collapse. The effect of ULTCs will be discussed further in Section 14.2.

When the ULTCs reach the end of their tap range, distribution system voltages begin to drop. The *residential* active and reactive loads will drop with voltage. This will in turn reduce line loading and, hence, the line reactive losses. The *industrial* loads, with large components of induction motors, will change little. However, the capacitors in the industrial area will supply less reactive power, thereby causing a net increase in the reactive load [1].

When the distribution voltages remain low for a few minutes, thermostats and other load regulation devices, as well as manual controls, tend to restore load. For example, heating-type loads will run longer to bring the temperature to the level called for by the thermostats. Consequently, more such devices will be operating at any given time. Many loads of this type will be restored to their normal full voltage value over a 10 to 15 minute period [5]. As voltage-sensitive controlled loads creep back, transmission and distribution voltages will drop further.

At voltages below 85 to 90% of the nominal value, some induction motors may stall and draw high reactive current. This brings the voltages down further. Industrial and commercial motors are usually controlled by magnetically held contactors; therefore, the voltage drop will cause many motors to drop out. The loss of load will result in the recovery of voltages. After some time, the motors are restored to service. This may cause voltages to drop again if the original cause of the voltage problem still persists.

It is evident from the above discussion that, for accurate analysis of voltage stability, the network representation must include the effects of distribution transformer tap-changer action and capacitors in the distribution systems. Depending on the scope of the study, the representation of load characteristics should take into consideration the effects of thermostats and other load regulation devices. In industrial areas, motors and capacitors may need to be represented explicitly.

14.1.4 Characteristics of Reactive Compensating Devices

In Chapter 11, we considered different types of reactive compensating devices. Here, we briefly describe how these devices influence voltage stability.

(a) Shunt capacitors

By far the most inexpensive means of providing reactive power and voltage support is the use of shunt capacitors. They can be effectively used up to a certain point to extend the voltage stability limits by correcting the receiving end power factor. They can also be used to free up "spinning reactive reserve" in generators and thereby help prevent voltage collapse in many situations.

Shunt capacitors, however, have a number of inherent limitations from the viewpoint of voltage stability and control:

- In heavily shunt capacitor compensated systems, the voltage regulation tends to be poor.
- Beyond a certain level of compensation, stable operation is unattainable with shunt capacitors (this is illustrated in Example 14.1).
- The reactive power generated by a shunt capacitor is proportional to the square of the voltage; during system conditions of low voltage the var support drops, thus compounding the problem.

(b) Regulated shunt compensation

A *static var system (SVS)* of finite size will regulate up to its maximum capacitive output. There are no voltage control or instability problems within the regulating range. When pushed to the limit, an SVS becomes a simple capacitor. The possibility of this leading to voltage instability must be recognized.

A *synchronous condenser*, unlike an SVS, has an internal voltage source. It continues to supply reactive power down to relatively low voltages and contributes to a more stable voltage performance.

(c) Series capacitors

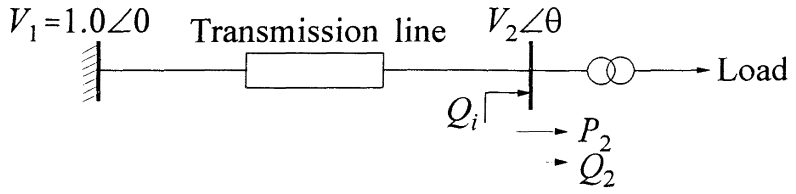
Series capacitors are self-regulating. The reactive power supplied by series capacitors is proportional to square of the line current and is independent of the bus voltages. This has a favourable effect on voltage stability.

Series capacitors are ideally suited for effectively shortening long lines. Unlike shunt capacitors, series capacitors reduce both the characteristic impedance (Z_C) and the electrical length (θ) of the line (see Chapter 11). As a result, both voltage regulation and stability are significantly improved.

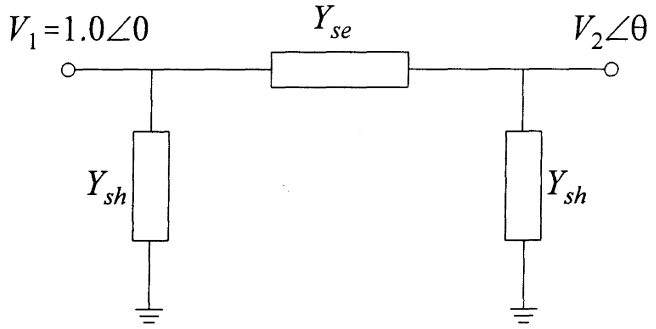
Example 14.1

Figure E14.1 shows the system representation applicable to a 322 km (200 mi), 500 kV transmission line supplying a radial load from a strong system. The line parameters are expressed in per unit on 100 MVA and 500 kV base.

(a) With the sending end voltage (V_1) maintained at 1.0 pu, generate Q-V curves at the receiving end for four different values of receiving end load power: 1300, 1500, 1700, and 1900 MW assumed at unity power factor. Together with the Q-V curves of the transmission system, plot the shunt capacitor Q-V characteristics with the reactive power injection at 1.0 pu voltage being 300, 450, 675, and 950 MVAr, respectively. Examine the effectiveness of shunt



(a) Schematic diagram



Y_{se} = 2.142 − *j*24.973 pu
Y_{sh} = 0 + *j*2.076 pu

(b) Equivalent π circuit representation of line

Figure E14.1 A 322 km, 500 kV line supplying a radial load

capacitor compensation as a means of providing reactive power compensation. Assume that the load at the receiving end exhibits a constant MVA steady-state characteristic due to the action of transformer tap changers.

(b) If the reactive compensation at the receiving end is in the form of an SVC with a capacitive limit of 950 MVAr, examine voltage stability of the system as P_2 is gradually increased from 1300 MW to 1900 MW.

Solution

(a) Figure E14.2 shows the steady-state Q_i-V_2 characteristics of the transmission line and the shunt capacitors.

The transmission line characteristics are shown in solid curves. These curves represent the relationship between voltage at the receiving end bus and injections of reactive power at that bus, each corresponding to a given level of receiving-end power, assumed at unity power factor.

The relationships between voltage and the reactive power produced by shunt capacitors are shown in dashed lines. The intersection between a solid curve and a dashed line establishes the steady-state operating point corresponding to the respective receiving-end power and shunt capacitor rating.

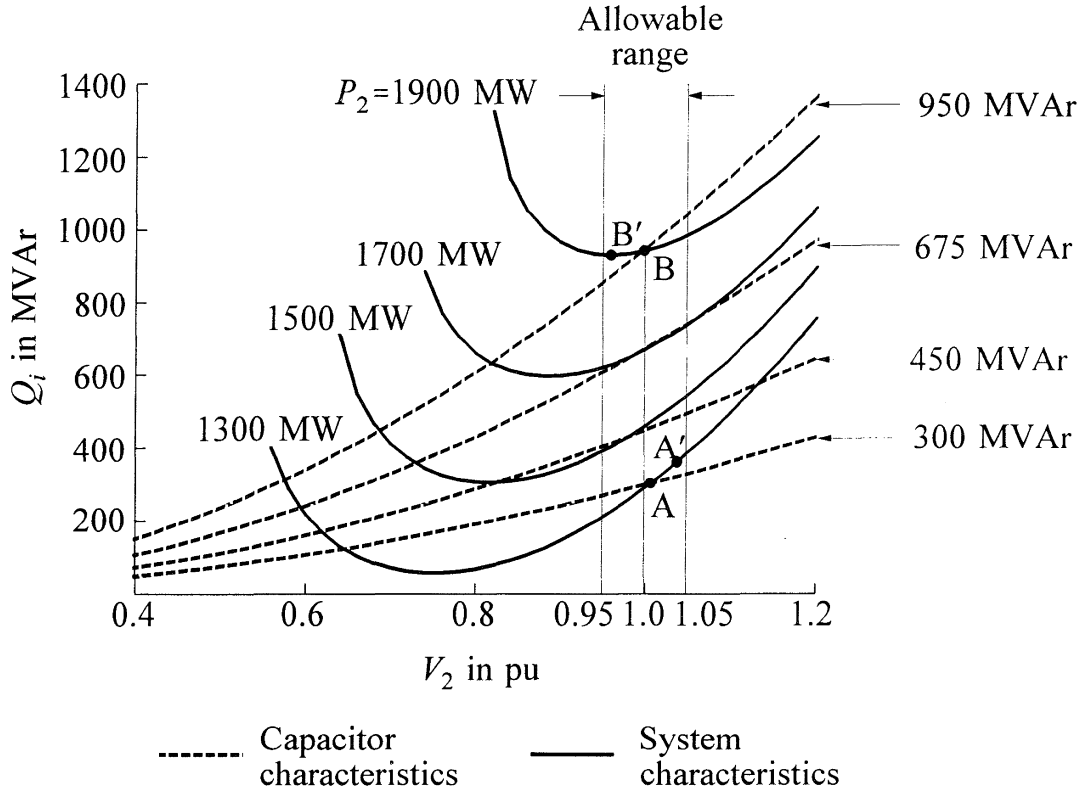


Figure E14.2 System and shunt capacitor steady-state Q-V characteristics; capacitor MVAr shown at rated voltage

Let us examine the steady-state system performance with a load level of 1300 MW and a capacitor bank of 300 MVAr, represented by the operating point A. At this point the slope $\Delta Q/\Delta V$ of the system is greater than that of the shunt capacitor; this represents stable operation. When perturbed by a small transient disturbance, the system returns to operating point A. The addition of a small amount of capacitance as represented by operating point A′ results in an increase in voltage, a characteristic normally expected.

The situation is quite different at operating point B, with a receiving power of 1900 MW and a capacitor bank of 950 MVAr. Now, the slope $\Delta Q/\Delta V$ of the system is less than that of the capacitor. A small perturbation leads to progressive deviation in V_2. An increase of shunt capacitor by a small amount, as represented by point B′, results in a decrease in bus voltage.

We thus see that at very high levels of shunt compensation, stable operation is not possible. The limiting load power level is about 1700 MW requiring a shunt capacitor of 675 MVAr. At this level, the slope $\Delta Q/\Delta V$ of the system is nearly equal to that of the shunt capacitor.

In the above analysis we have considered only the steady-state performance with the load at the receiving end maintaining constant MVA due to transformer ULTC action.

The transient response depends on the inherent load characteristics. For example, with a constant current load characteristic, switching additional load when operating at point B causes a transient reduction of V_2 and P_2. The system is voltage stable in the short term. However, the action of the transformer ULTC, as it attempts to raise the secondary voltage, causes an increase in primary (line) current. This results in a decrease in V_2 and P_2. The voltage V_2 decreases with each tap movement until the tap changer reaches its limit. The system settles at low values of V_2 and P_2.

(b) Figure E14.3 shows the steady-state Q_i-V_2 characteristics with a *static var compensator* (SVC). The SVC maintains constant voltage V_2 until its maximum capacitive output limit of 950 MVAr is reached. Consequently, for values of P_2 less than 1900 MW, the SVC maintains V_2 at 1.0 pu. When P_2 reaches 1900 MW, the SVC hits its capacitive limit and its characteristic is that of a simple capacitor. This leads to voltage instability.

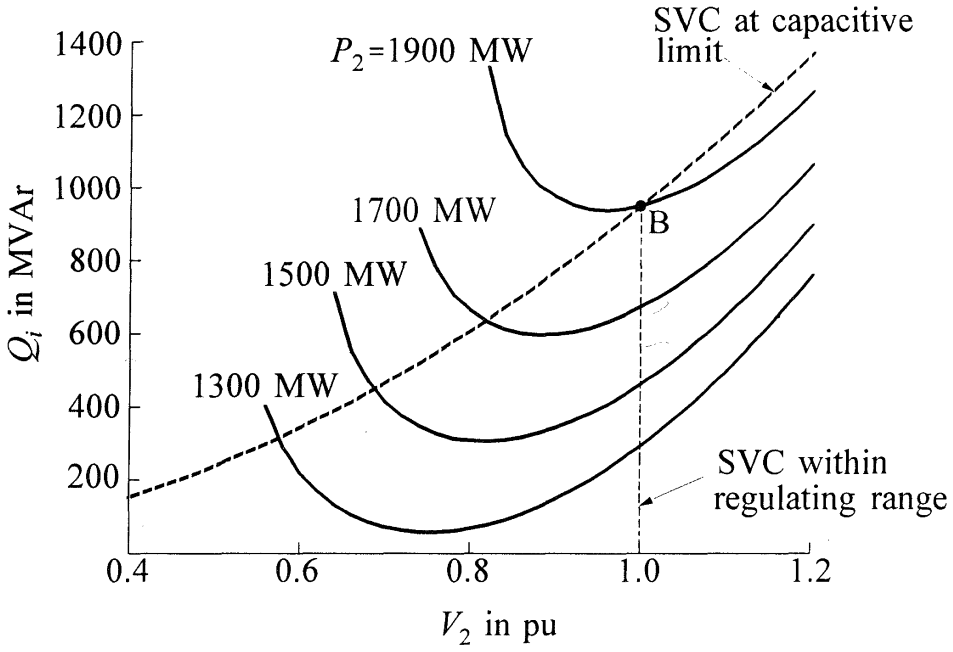


Figure E14.3 System and SVC Q-V characteristics; SVC capacitive limit 950 MVAr ■

14.2 VOLTAGE COLLAPSE

Voltage collapse is the process by which the sequence of events accompanying voltage instability leads to a low *unacceptable* voltage profile in a significant part of the power system.

Voltage collapse may be manifested in several different ways. We will describe a typical scenario of voltage collapse, and then provide a general characterization of the phenomenon based on actual incidents of collapse.

14.2.1 Typical Scenario of Voltage Collapse

When a power system is subjected to a sudden increase of reactive power demand following a system contingency, the additional demand is met by the reactive power reserves carried by the generators and compensators. Generally there are sufficient reserves and the system settles to a stable voltage level. However, it is possible, because of a combination of events and system conditions, that the additional reactive power demand may lead to voltage collapse, causing a major breakdown of part or all of the system.

A typical scenario of a voltage collapse would be as follows [6]:

- The power system is experiencing abnormal operating conditions with large generating units near the load centres being out of service. As a result, some EHV lines are heavily loaded and reactive power resources are at a minimum.

- The triggering event is the loss of a heavily loaded line which would cause additional loading on the remaining adjacent lines. This would increase the reactive power losses in the lines (Q absorbed by a line increases rapidly for loads above surge impedance loading), thereby causing a heavy reactive power demand on the system.

- Immediately following the loss of the EHV line, there would be a considerable reduction of voltage at adjacent load centres due to extra reactive power demand. This would cause a load reduction, and the resulting reduction in power flow through the EHV lines would have a stabilizing effect. The generator AVRs would, however, quickly restore terminal voltages by increasing excitation. The resulting additional reactive power flow through the inductances associated with generator transformers and lines would cause increased voltage drop across each of these elements.

  At this stage, generators would likely be within the P-Q output capabilities, i.e., within the armature and field current heating limits. The speed governors would regulate frequency by reducing MW output.

- The EHV level voltage reduction at load centres would be reflected into the distribution system. The ULTCs of substation transformers would restore distribution voltages and loads to prefault levels in about 2 to 4 minutes. With each tap change operation, the resulting increment in load on EHV lines would increase the line XI^2 and RI^2 losses, which in turn would cause a greater drop in EHV levels. If the EHV line is loaded considerably above the SIL, each MVA increase in line flow would cause several MVArs of line losses.

- As a result, with each tap-changing operation, the reactive output of generators throughout the system would increase. Gradually, the generators would hit

their reactive power capability limits (imposed by maximum allowable continuous field current) one by one. When the first generator reached its field current limit, its terminal voltage would drop. At the reduced terminal voltage for a fixed MW output, the armature current would increase. This may further limit reactive output to keep the armature current within allowable limits. Its share of reactive loading would be transferred to other generators, leading to overloading of more and more generators. With fewer generators on automatic excitation control, the system would be much more prone to voltage instability. This would likely be compounded by the reduced effectiveness of shunt compensators at low voltages.

The process will eventually lead to voltage collapse or avalanche, possibly leading to loss of synchronism of generating units and a major blackout.

14.2.2 General Characterization Based on Actual Incidents

There have been a number of voltage collapse incidents worldwide (see references 1, 2, 7 and 8 for descriptions). Based on these incidents, voltage collapse may be characterized as follows:

1. The initiating event may be due to a variety of causes: small gradual system changes such as natural increase in system load, or large sudden disturbances such as loss of a generating unit or a heavily loaded line. Sometimes, a seemingly uneventful initial disturbance may lead to successive events that eventually cause system collapse.

2. The heart of the problem is the inability of the system to meet its reactive demands. Usually, but not always, voltage collapse involves system conditions with heavily loaded lines. When transport of reactive power from neighbouring areas is difficult, any change that calls for additional reactive power support may lead to voltage collapse.

3. The voltage collapse generally manifests itself as a slow decay of voltage. It is the result of an accumulative process involving the actions and interactions of many devices, controls, and protective systems. The time frame of collapse in such cases could be on the order of several minutes.

   The duration of voltage collapse dynamics in some situations may be much shorter, being on the order of a few seconds. Such events are usually caused by unfavourable load components such as induction motors or dc converters [8]. The time frame of this class of voltage instability is the same as that of rotor angle instability. In many situations, the distinction between voltage and angle instability may not be clear, and some aspects of both phenomena may exist. This form of voltage instability may be analyzed by conventional transient stability simulations, provided appropriate models are used to represent the devices, particularly induction motor loads, and various controls

and protection associated with the generators and transmission equipment.

Based on the above considerations, the companion book by C.W. Taylor [8] classifies voltage stability into *transient* and *longer-term time frames*. Appendix F of the book groups known incidents of voltage instability by these time frames.

4. Voltage collapse is strongly influenced by system conditions and characteristics. The following are the significant factors contributing to voltage instability/collapse:

   - Large distances between generation and load
   - ULTC action during low voltage conditions
   - Unfavourable load characteristics
   - Poor coordination between various control and protective systems

5. The voltage collapse problem may be aggravated by excessive use of shunt capacitor compensation. Reactive compensation can be made most effective by the judicious choice of a mixture of shunt capacitors, static var systems, and possibly synchronous condensers.

14.2.3 Classification of Voltage Stability

It is helpful to classify voltage stability into two categories: *large-disturbance* voltage stability and *small-disturbance* voltage stability. These subdivisions essentially decouple phenomena that must be examined by using nonlinear dynamic analysis from those that can be examined by using steady-state analysis. This classification can simplify analytical tool development and application, and it can result in tools that produce *complementary* information.

Large-disturbance voltage stability is concerned with a system's ability to control voltages following large disturbances such as system faults, loss of load, or loss of generation. Determination of this form of stability requires the examination of the dynamic performance of the system over a period of time sufficient to capture the interactions of such devices as ULTCs and generator field current limiters. Large-disturbance voltage stability can be studied by using nonlinear time-domain simulations which include proper modelling.

Large-disturbance voltage stability, as discussed in Section 14.2.2, may be further subdivided into transient and long-term time frames.

Small-disturbance (or small-signal) voltage stability is concerned with a system's ability to control voltages following small perturbations, such as gradual changes in load. This form of stability can be effectively studied with steady-state approaches that use linearization of the system dynamic equations at a given operating point.

Following a disturbance, the system voltages often do not return to the original level. Therefore, it is necessary to define the region of voltage level considered acceptable. The system is then said to have *finite stability* within the specified region of voltage level.

14.3 VOLTAGE STABILITY ANALYSIS

The analysis of voltage stability for a given system state involves the examination of two aspects [9]:

(a) *Proximity to voltage instability*: How close is the system to voltage instability?

Distance to instability may be measured in terms of physical quantities, such as load level, active power flow through a critical interface, and reactive power reserve. The most appropriate measure for any given situation depends on the specific system and the intended use of the margin; for example, planning versus operating decisions. Consideration must be given to possible contingencies (line outages, loss of a generating unit or a reactive power source, etc.).

(b) *Mechanism of voltage instability*: How and why does instability occur? What are the key factors contributing to instability? What are the voltage-weak areas? What measures are most effective in improving voltage stability?

Time-domain simulations, in which appropriate modelling is included, capture the events and their chronology leading to instability. However, such simulations are time-consuming and do not readily provide sensitivity information and the degree of stability.

System dynamics influencing voltage stability are usually slow. Therefore, many aspects of the problem can be effectively analyzed by using static methods, which examine the viability of the equilibrium point represented by a specified operating condition of the power system. The static analysis techniques allow examination of a wide range of system conditions and, if appropriately used, can provide much insight into the nature of the problem and identify the key contributing factors. Dynamic analysis, on the other hand, is useful for detailed study of specific voltage collapse situations, coordination of protection and controls, and testing of remedial measures. Dynamic simulations also examine whether and how the steady-state equilibrium point will be reached.

In this section, we discuss static as well as dynamic analysis techniques and we illustrate how the two approaches can be used in a complementary manner.

14.3.1 Modelling Requirements

The following are descriptions of models of power system elements that have a significant impact on voltage stability:

Loads. Load characteristics could be critical in voltage stability analysis. Unlike in conventional transient stability and power-flow analyses, expanded subtransmission system representation in a voltage-weak area may be necessary. This should include transformer ULTC action, reactive power compensation, and voltage regulators in the subtransmission system.

It is important to account for voltage and frequency dependence of loads. It may also be necessary to model induction motors specifically. In some cases, appropriate representation of load characteristics at low voltages may be essential [11].

Generators and their excitation controls. For voltage stability analysis, it may be necessary to account for the droop characteristic of the AVR rather than to assume zero droop. If load (line drop) compensation (see Chapter 8, Section 8.5.4) is provided, its effect should be represented. Field current and armature current limits should be represented specifically rather than as a fixed value of the maximum reactive power limit.

Static var systems (SVSs). When an SVS is operating within the normal voltage control range, it maintains bus voltage with a slight droop characteristic. When operating at the reactive power limits, the SVS becomes a simple capacitor or reactor; this could have a very significant effect on voltage stability. These characteristics of SVS should be represented appropriately in voltage stability studies. Modelling of SVSs is described in Chapter 11 (Section 11.2.9).

Automatic generation control (AGC). For contingencies resulting in a significant mismatch between generation and load, the actions of primary speed control and supplementary tie line bias frequency control can change system generation significantly, sometimes to the detriment of voltage stability. Hence, these functions have to be represented appropriately.

Protection and controls. These include generating unit and transmission network protection and controls. Examples are generator excitation protection, armature overcurrent protection, transmission line overcurrent protection, capacitor bank controls, phase-shifting regulators, and undervoltage load shedding.

14.3.2 Dynamic Analysis

The general structure of the system model for voltage stability analysis is similar to that for transient stability analysis. As described in Chapter 13 (Section 13.3.5), the overall system equations, comprising a set of first-order differential

equations, may be expressed in the following general form:

$$\dot{\mathbf{x}} = \mathbf{f}(\mathbf{x}, \mathbf{V}) \tag{14.4}$$

and a set of algebraic equations

$$\mathbf{I}(\mathbf{x}, \mathbf{V}) = \mathbf{Y}_N \mathbf{V} \tag{14.5}$$

with a set of known initial conditions $(\mathbf{x}_0, \mathbf{V}_0)$, where

$\mathbf{x}$ = state vector of the system
$\mathbf{V}$ = bus voltage vector
$\mathbf{I}$ = current injection vector
$\mathbf{Y}_N$ = network node admittance matrix

Since we include the representation of transformer tap-changer and phase-shift angle controls, the elements of $\mathbf{Y}_N$ change as a function of bus voltages and time. The current injection vector $\mathbf{I}$ is a function of the system states $\mathbf{x}$ and bus voltage vector $\mathbf{V}$, representing the boundary conditions at the terminals of the various devices (generating units, nonlinear static loads, motors, SVSs, HVDC converters, etc.). Due to the time-dependent nature of devices such as field current limiters, the relationship between $\mathbf{I}$ and $\mathbf{x}$ can be a function of time.

Equations 14.4 and 14.5 can be solved in time-domain by using any of the numerical integration methods described in Chapter 13 (Section 13.2) and network power-flow analysis methods described in Chapter 6 (Section 6.4). The study period is typically on the order of several minutes. With the inclusion of special models representing the "slow system dynamics" leading to voltage collapse, the stiffness of the system differential equations is significantly higher than that of transient stability models. Implicit integration methods are ideally suited for such applications. Facilities to automatically change the integration time step, as the solution progresses and fast transients decay, greatly enhance the computational efficiency of such techniques [12].

Example 14.2

In this example we analyze the large-disturbance voltage stability of the system shown in Figure E14.4, using time-domain simulations. The test system considered here is based on the system originally described in reference 25, and used in references 2, 8, and 10 for analysis of the various aspects of voltage stability.

In addition to illustrating the time-domain approach to dynamic analysis of voltage stability, this example shows the effects of generator overexcitation limiter (OXL), transformer tap changer, and load characteristics on voltage stability.

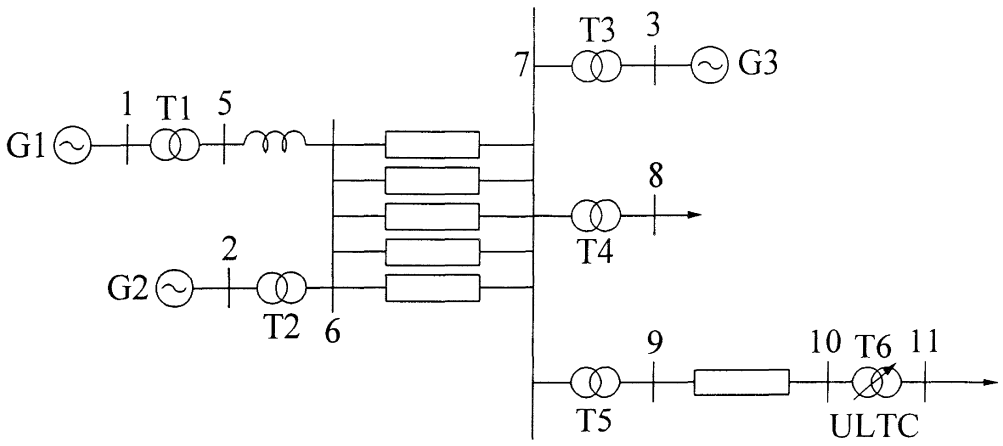


Figure E14.4 Test system

The test system data are as follows:

Transmission lines (R, X and B in pu on 100 MVA base):

Line	*R*	*X*	*B*
5-6	0.0000	0.0040	0.0000
6-7	0.0015	0.0288	1.1730
9-10	0.0010	0.0030	0.0000

Transformers (R and X in pu on 100 MVA base):

Transformer	*R*	*X*	Ratio	
T1	0.0000	0.0020	0.8857	
T2	0.0000	0.0045	0.8857	
T3	0.0000	0.0125	0.9024	
T4	0.0000	0.0030	1.0664	
T5	0.0000	0.0026	1.0800	
T6	0.0000	0.0010	0.9750	(load level 1)
			0.9938	(load level 2)
			1.0000	(load level 3)

ULTC for transformer T6 between buses 10 and 11:

Time delay for the first tap movement: 30 s
Time delay for subsequent tap movement: 5 s
Dead band: ±1% pu bus voltage
Tap range: ±16 steps
Step size: 5/8% (=0.00625 pu)

Shunt capacitors:

Bus	MVAr
7	763
8	600
9	1710

Loads:

Bus	P (MW)	Q (MVAr)	
8	3271	1015	(load level 1)
	3320	1030	(load level 2)
	3345	1038	(load level 3)
11	3384	971	(load level 1)
	3435	985	(load level 2)
	3460	993	(load level 3)

Generation:

Bus	P (MW)	V (pu)	
G1	3981	0.9800	(load level 1)
	4094	0.9800	(load level 2)
	4152	0.9800	(load level 3)
G2	1736	0.9646	(load level 1)
	1736	0.9646	(load level 2)
	1736	0.9646	(load level 3)
G3	1154	1.0400	(load level 1)
	1154	1.0400	(load level 2)
	1154	1.0400	(load level 3)

Machine parameters:

Machine 1: Infinite bus
Machine 2: H = 2.09, MVA rating = 2200 MVA
Machine 3: H = 2.33, MVA rating = 1400 MVA

The following are the parameters of machine 2 and machine 3 on their respective MVA ratings:

R_a = 0.0046 X_d = 2.07 X_q = 1.99
X_l = 0.155 X'_d = 0.28 X'_q = 0.49
X''_d = 0.215 X''_q = 0.215

$T'_{d0} = 4.10$ $T'_{q0} = 0.56$
$T''_{d0} = 0.033$ $T''_{q0} = 0.062$

Exciters:

Both machine 2 and machine 3 have thyristor exciters with a gain of 400 and the sensing circuit-time constant of 0.02 seconds.

Overexcitation limiter for machine 3:

$I_{fd\,max1} = 3.02$ pu $I_{fd\,max2} = 4.60$ pu
$I_{LIM} = 3.85$ pu $K_1 = 0.248$ $K_2 = 12.6$

The OXL is included for generator 3 only. The block diagram of the OXL is shown in Figure E14.5 and its functional characteristic is shown in Figure E14.6.

We will consider three system load levels:

Load level 1: 6655 MW, 1986 MVAr
Load level 2: 6755 MW, 2016 MVAr
Load level 3: 6805 MW, 2031 MVAr

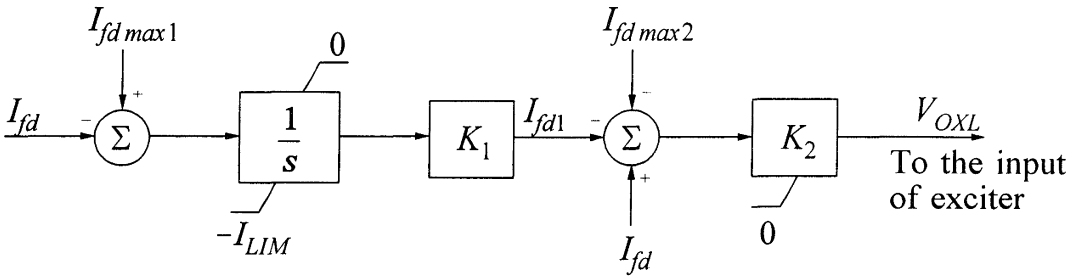


Figure E14.5 Block diagram of OXL

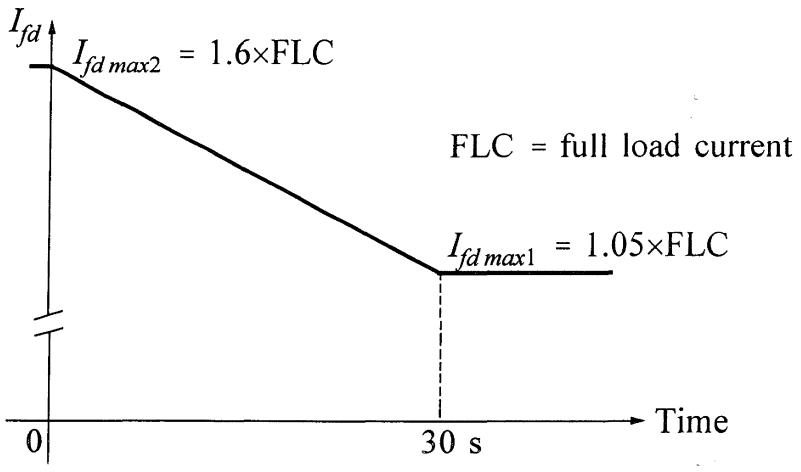


Figure E14.6 OXL characteristic

The disturbance considered is the loss of one of the lines between buses 6 and 7 (without a fault). Investigate the voltage stability of the system with the following representations of loads at buses 8 and 11:

(a) The load at bus 11 is modelled as 50% constant impedance and 50% constant current for both active and reactive components; the action of the ULTC transformer (T6) supplying this load is modelled in detail. The load at bus 8 is modelled as constant MVA for both active and reactive components. The transformer T4 supplying this load is assumed to have a fixed tap.

(b) The active power component of load at bus 8 is represented as an equivalent induction motor with the following parameters (see Chapter 7, Section 7.2.1 for description of model):

Motor rating = 3600 MVA, 60 Hz

X_m = 3.3 pu R_s = 0.01 pu X_s = 0.145 pu

R_r = 0.008 pu X_r = 0.145 pu H = 0.6 s

Load torque exponent m = 2.0 (that is, $T_L = T_0 \omega_r^2$)

All other components are modelled as in (a).

(c) The load at bus 11 is represented as in (a), with ULTC action of transformer T6. The load at bus 8 is represented as constant MVA for the reactive component and a thermostatically controlled load for the active component with the following parameters (see Chapter 7, Figure 7.4 for description of model):

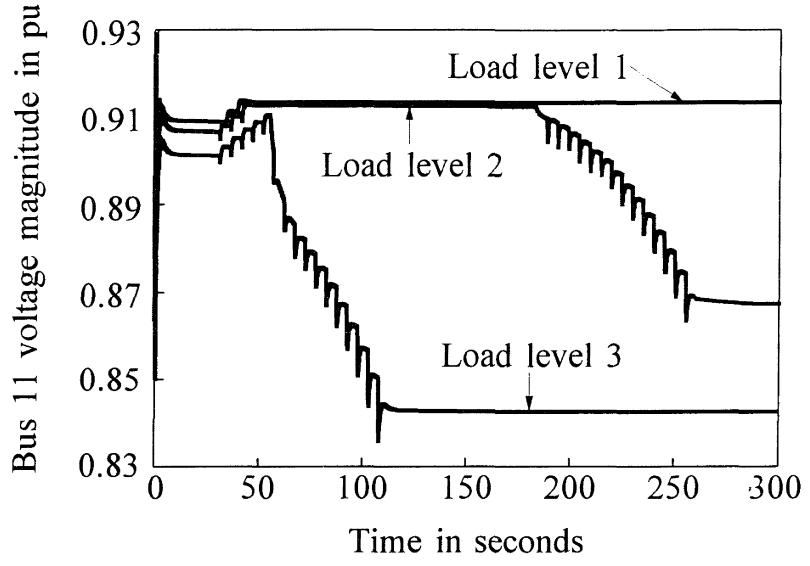
K_P = 0.1 K_I = 1.0 K_1 = 1.0

T_1 = 40 s T_A = 20 s $G_{max} = 1.5G_0$

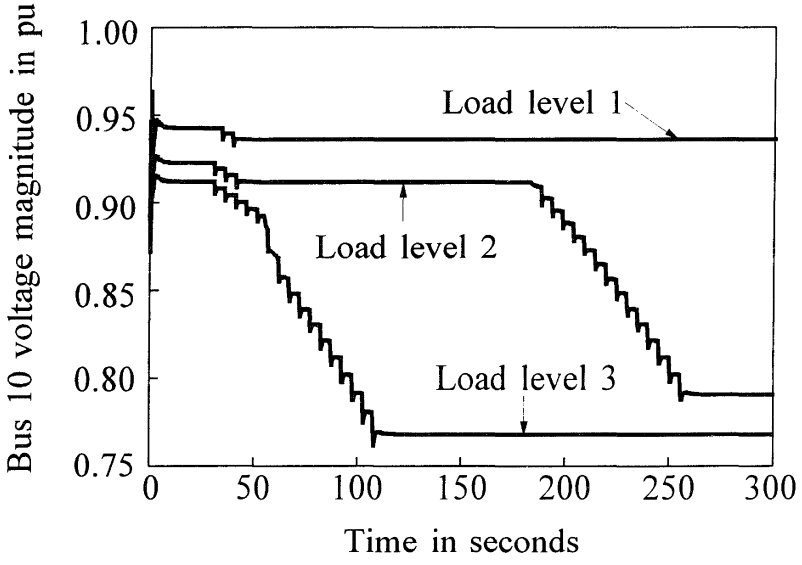
Solution

(a) Figures E14.7(a), (b), and (c) show the time responses of the voltages at buses 11, 10, and 7 following the loss of one of the lines between buses 6 and 7, for each of the three load levels. The corresponding plots of generator G3 field current, reactive power output, and terminal voltage are shown in Figures E14.8(a), (b), and (c).

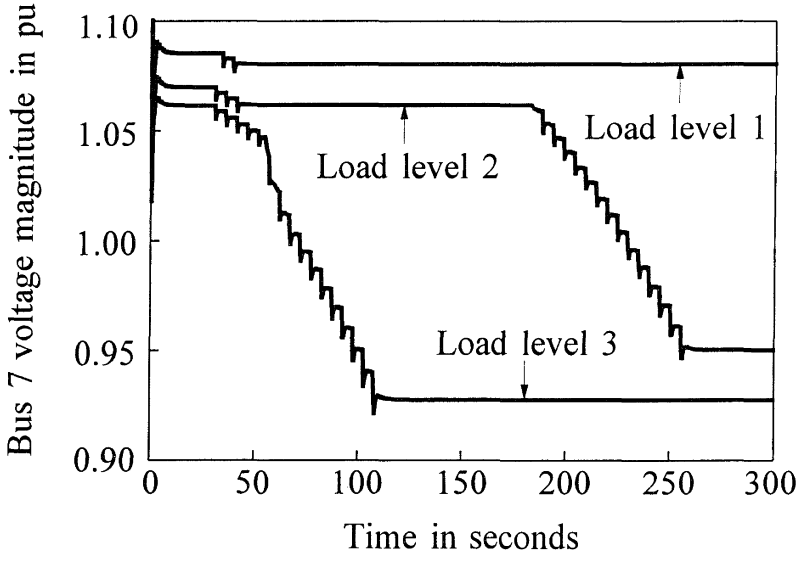
The effect of the loss of the line is to cause the system voltage to drop initially. For load level 1, the ULTC action of transformer T6 restores bus 11 voltage to nearly its reference value in about 40 seconds. Field current of G3 remains below its continuous limit and the terminal voltage is maintained at the initial value by the AVR. The voltages of buses 10 and 7 settle at values below the predisturbance values. The system is voltage stable.



(a) Bus 11 voltage

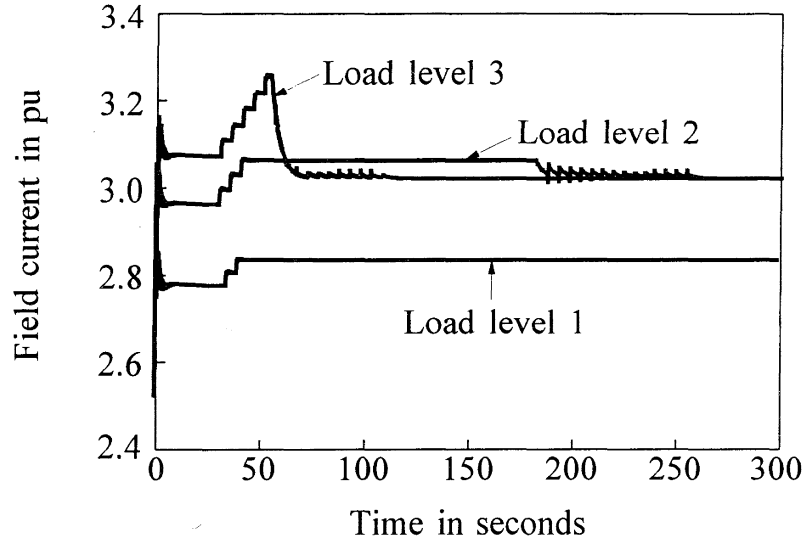


(b) Bus 10 voltage

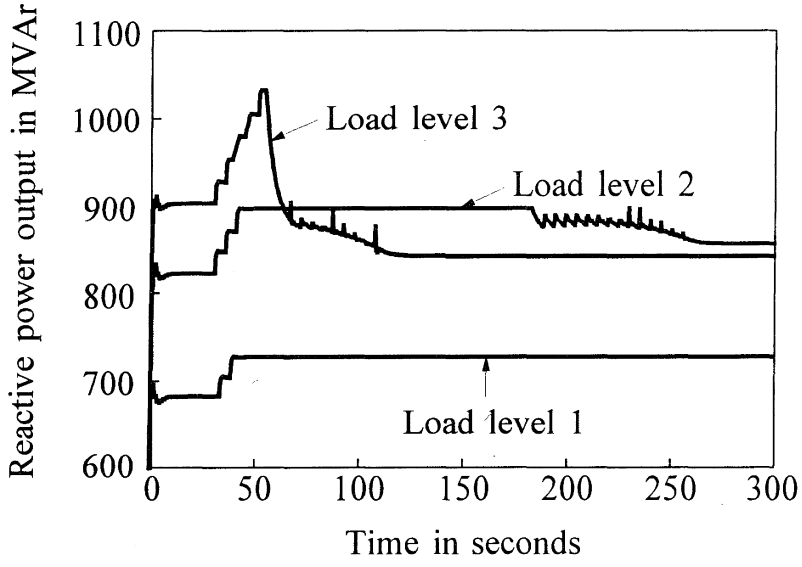


(c) Bus 7 voltage

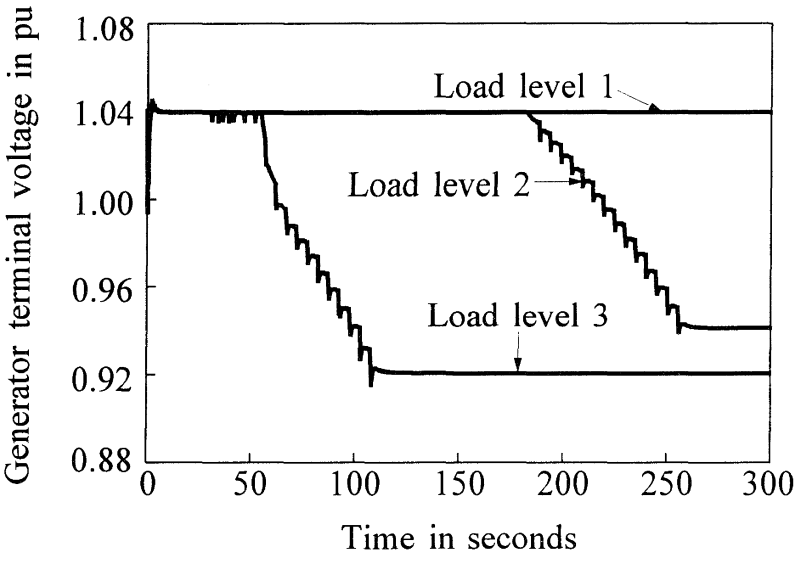
Figure E14.7 Voltages at buses 11, 10, and 7



(a) Field current



(b) Reactive power output



(c) Terminal voltage

Figure E14.8 Responses of generator G3 variables

With load level 2, the voltage of bus 11 is restored to nearly its reference value in about 40 seconds as in the case of load level 1. However, the reactive power demand on the generators is now higher and the field current of generator G3 exceeds its limit. The overexcitation limiter of G3 starts ramping the field current down at about 180 seconds. This in turn triggers the following chain of events:

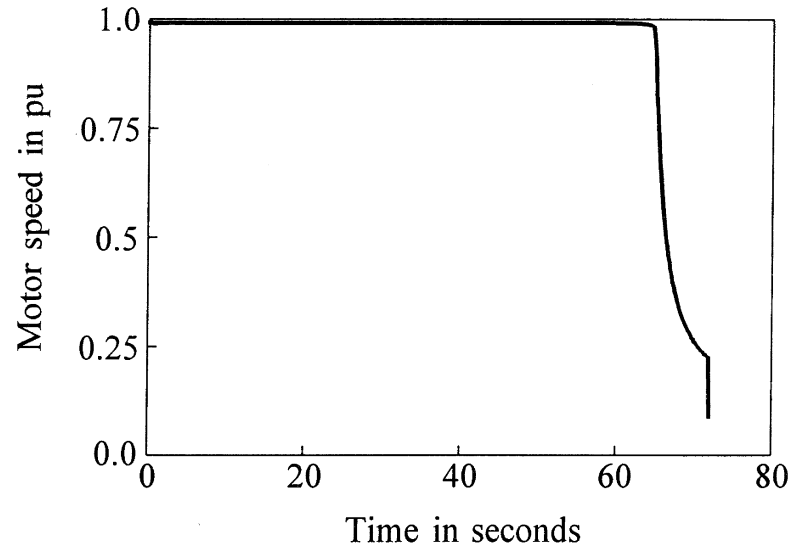
- The terminal voltage of G3, which is no longer being controlled by the AVR, drops.
- Voltages at buses 11, 10, and 7 drop.
- The ULTC on transformer T6 operates to restore the voltage and load at bus 11.
- The demand for reactive power on the generators increases. The OXL on G3 continues to hold the field current at its limit and the terminal voltage of G3 continues to drop.
- Voltage at the transmission level (bus 7) drops and this causes further reduction of bus 10 and bus 11 voltages.
- The ULTC on T6 operates again, repeating the above chain of events.

The net effect of each tap movement of transformer T6 is to reduce bus 11 voltage rather than increase it. The voltage at bus 11 falls progressively until the ULTC reaches its upper limit at about 260 seconds. The voltages stabilize at this point. The voltage at bus 11 settles at 0.865 pu.

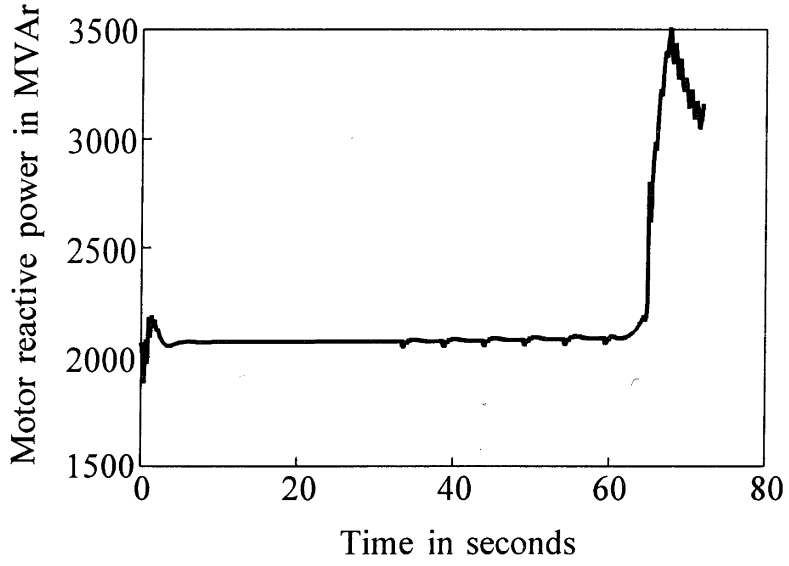
With load level 3, the demand for reactive power is higher. Consequently, the field current of G3 reaches its limit at about 50 seconds. With loss of voltage control by G3, the voltages at the transmission level and at bus 11 drop with each tap movement of the ULTC. The voltages stabilize when the ULTC reaches its limit at about 110 seconds. The voltage of bus 11 settles at nearly 0.84 pu.

(b) This case differs from the above in that the active power component of load at bus 8 is represented as an induction motor. Only load level 2 is considered. Figures E14.9(a), (b) and (c) show plots of the speed, reactive and active power of the induction motor. The motor stalls at about 65 seconds. This results in a decrease in active power absorbed by the motor. However, the reactive power drawn by the motor increases rapidly. This causes voltage collapse as depicted in Figures E14.10 and E14.11. For comparison, the voltage response with constant MVA load at bus 8, as computed in (a), is also shown in Figure E14.11.

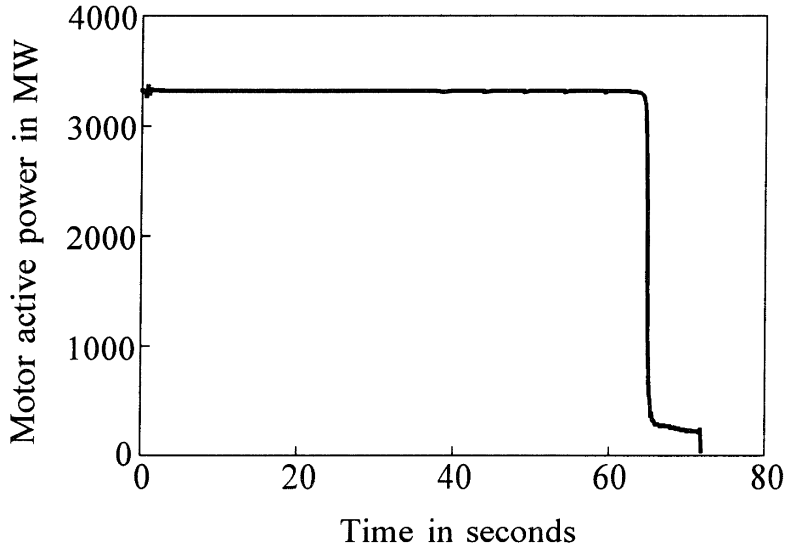
(c) This case considers a thermostatically controlled (TC) load at bus 8, with the system load at level 3. Figures E14.12(a), (b) and (c) show plots of the voltage at bus 8, the conductance of the TC load and active power drawn by the load. Figure E14.13 shows the corresponding plot of voltage at bus 11 (curve 1). For comparison, the response of bus 11 voltage with constant resistance load at bus 8 is also shown in Figure E14.13 (curve 2).



(a) Motor speed



(b) Reactive power absorbed by the motor



(c) Active power absorbed by the motor

Figure E14.9 Induction motor response, with load level 2

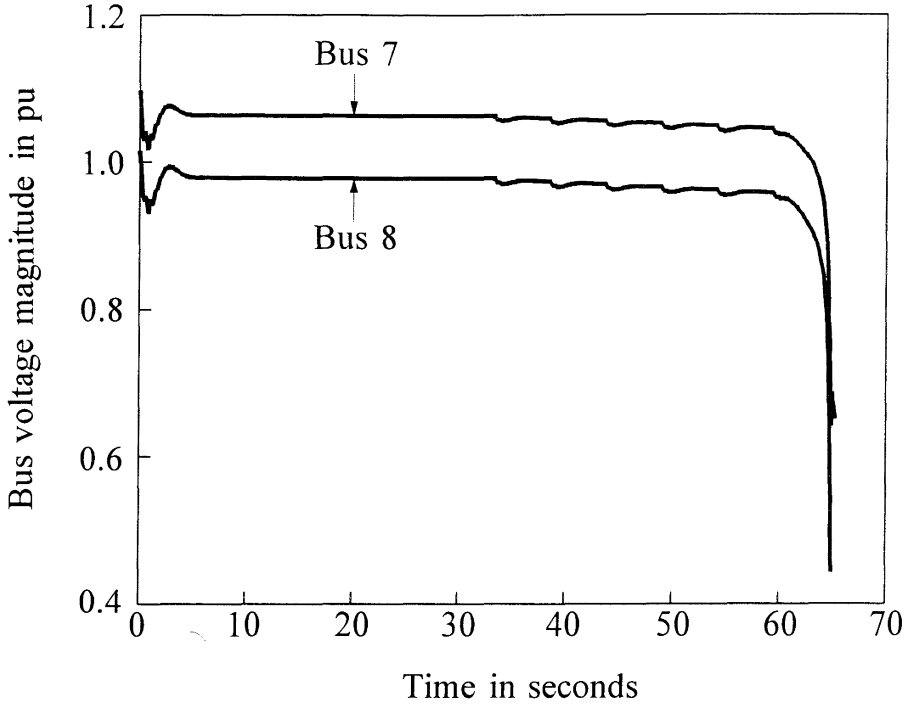


Figure E14.10 Voltage magnitude at bus 7 and bus 8 with induction motor load at bus 8; system at load level 2

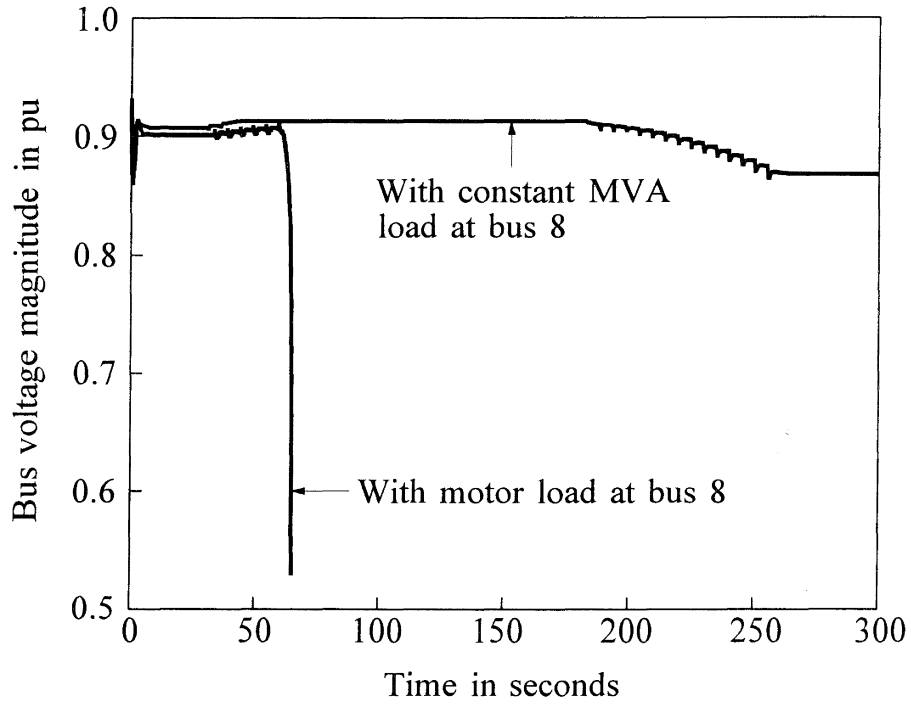
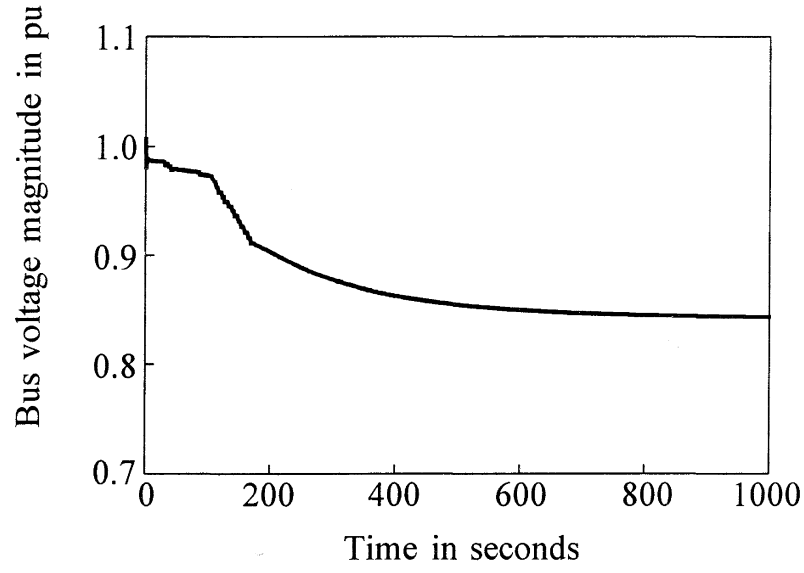
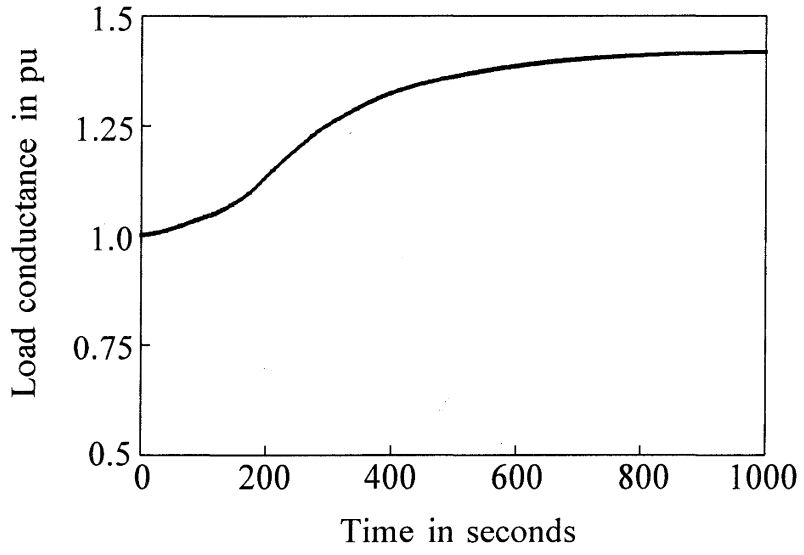


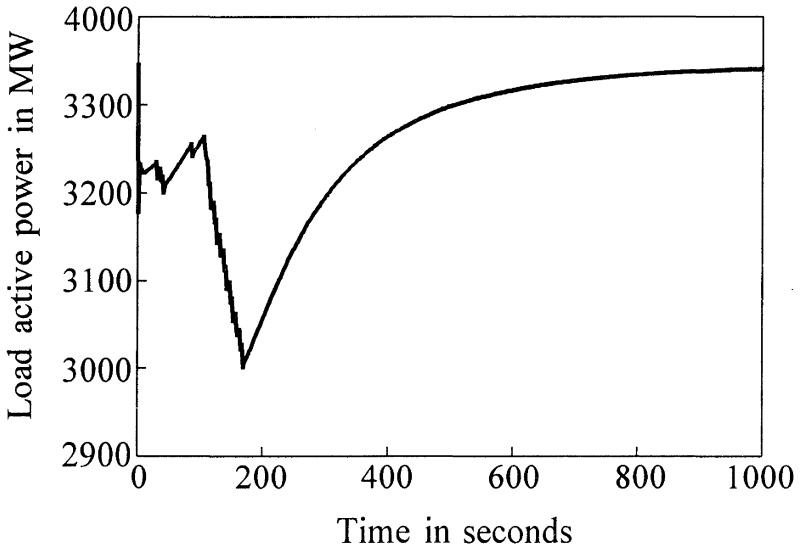
Figure E14.11 Response of voltage magnitude at bus 11 with (a) constant MVA load and (b) induction motor load at bus 8; system load at level 2



(a) Bus 8 voltage magnitude



(b) Conductance of TC load in per unit of the initial value G_0



(c) Active power supplied to TC load

Figure E14.12 Response of thermostatically controlled load at bus 8

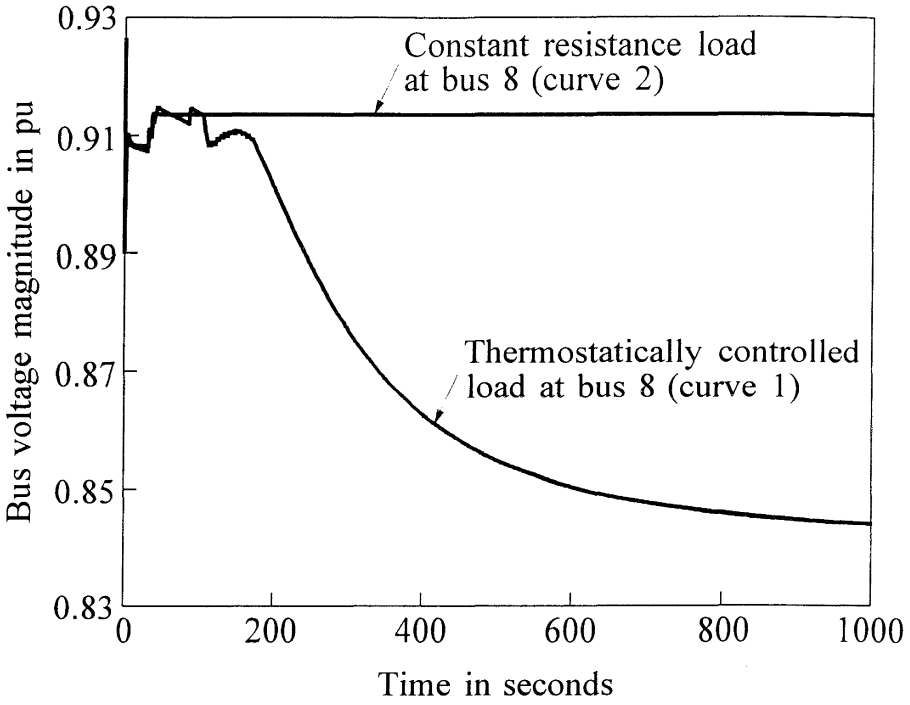


Figure E14.13 Response of voltage magnitude at bus 11 with TC load and constant resistance load at bus 8

Following the loss of a line between buses 6 and 7, the voltage of bus 11 drops. The ULTC of transformer T6 restores bus 11 voltage to its reference value at about 40 seconds. If the load at bus 8 were a constant resistance load, the voltage would stabilize as depicted by curve 2 of Figure E14.13. With a thermostatically controlled load, bus 11 voltage drops and the ULTC operates again at about 90 seconds. The action of the TC load causes the voltage to drop again. The interaction between the ULTC and the TC load continues until about 170 seconds, when the ULTC reaches its upper limit. The conductance of the TC load and the power continue to increase until the power reaches the predisturbance level of 3345 MW. The voltages at buses 8 and 11 stabilize at about 0.85 pu and 0.845 pu, respectively. ■

14.3.3 Static Analysis

The static approach captures *snapshots* of system conditions at various time frames along the time-domain trajectory. At each of these time frames, time derivatives of the state variables (i.e., $\dot{\mathbf{x}}$) in Equation 14.4 are assumed to be zero, and the state variables take on values appropriate to the specific time frame. Consequently, the overall system equations reduce to purely algebraic equations allowing the use of static analysis techniques.

In the past, the electric utility industry has largely depended on conventional power-flow programs for static analysis of voltage stability. Stability is determined by computing the *V-P* and *Q-V* curves at selected load buses. Generally, such curves are generated by executing a large number of power flows using conventional models. While such procedures can be automated, they are time-consuming and do not readily

provide information useful in gaining insight into causes of stability problems. In addition, these procedures focus on individual buses; that is, the stability characteristics are established by stressing each bus independently. This may unrealistically distort the stability condition of the system. Also, the buses selected for Q-V and V-P analysis must be chosen carefully, and a large number of such curves may be required to obtain complete information. In fact, it may not be possible to generate the Q-V curves completely due to power-flow divergence caused by problems elsewhere in the system.

A number of special techniques have been proposed in the literature for voltage stability analysis using the static approach. Some of these techniques are described in part 2 of the 1990 IEEE report [1]. In general, these have not found widespread practical application.

References 13 and 14 describe the practical applications of an approach based on V-Q sensitivity. The modal analysis approach described in references 9 and 10 has also been applied to voltage stability analysis of practical systems. In this section, we describe these two approaches. The advantages of these approaches are that they give voltage stability-related information from a *system-wide perspective* and clearly identify areas that have potential problems. The modal analysis approach has the added advantage that it provides information regarding the *mechanism* of instability. The principal reason for considering the V-Q sensitivity analysis here is that it serves as a good introduction to the modal analysis.

(a) V-Q sensitivity analysis

As shown in Chapter 6 (Section 6.4.3), the network constraints represented by Equation 14.5 may be expressed in the following linearized form:

$$\begin{bmatrix} \Delta \mathbf{P} \\ \Delta \mathbf{Q} \end{bmatrix} = \begin{bmatrix} \mathbf{J}_{P\theta} & \mathbf{J}_{PV} \\ \mathbf{J}_{Q\theta} & \mathbf{J}_{QV} \end{bmatrix} \begin{bmatrix} \Delta \boldsymbol{\theta} \\ \Delta \mathbf{V} \end{bmatrix} \tag{14.6}$$

where

$\Delta \mathbf{P}$ = incremental change in bus real power
$\Delta \mathbf{Q}$ = incremental change in bus reactive power injection
$\Delta \boldsymbol{\theta}$ = incremental change in bus voltage angle
$\Delta \mathbf{V}$ = incremental change in bus voltage magnitude

The elements of the Jacobian matrix give the sensitivity between power flow and bus voltage changes.

If the conventional power-flow model is used for voltage stability analysis, the Jacobian matrix in Equation 14.6 is the same as that derived in Chapter 6 for solving the power-flow equations by using the Newton-Raphson technique. With the enhanced device models represented by Equation 14.4, the linear relationship between power and voltage for each device when $\dot{\mathbf{x}} = 0$ may be expressed as follows:

$$\begin{bmatrix} \Delta \mathbf{P}_d \\ \Delta \mathbf{Q}_d \end{bmatrix} = \begin{bmatrix} \mathbf{A}_{11} & \mathbf{A}_{12} \\ \mathbf{A}_{21} & \mathbf{A}_{22} \end{bmatrix} \begin{bmatrix} \Delta \mathbf{V}_d \\ \Delta \boldsymbol{\theta}_d \end{bmatrix} \tag{14.7}$$

where

$\Delta \mathbf{P}_d$ = incremental change in device real power output
$\Delta \mathbf{Q}_d$ = incremental change in device reactive power output
$\Delta \mathbf{V}_d$ = incremental change in device voltage magnitude
$\Delta \boldsymbol{\theta}_d$ = incremental change in device voltage angle

The terms of the network Jacobian matrix in Equation 14.6 associated with each device are modified by $\mathbf{A}_{11}$, $\mathbf{A}_{12}$, $\mathbf{A}_{21}$ and $\mathbf{A}_{22}$ to form the system Jacobian matrix.

System voltage stability is affected by both P and Q. However, at each operating point we may keep P constant and evaluate voltage stability by considering the incremental relationship between Q and V. This is analogous to the Q-V curve approach. Although incremental changes in P are neglected in the formulation, the effects of changes in system load or power transfer level are taken into account by studying the incremental relationship between Q and V at different operating conditions.

Based on the above considerations, in Equation 14.6, let $\Delta \mathbf{P}=0$. Then

$$\Delta \mathbf{Q} = \mathbf{J}_R \Delta \mathbf{V} \tag{14.8}$$

where

$$\mathbf{J}_R = [\mathbf{J}_{QV} - \mathbf{J}_{Q\theta} \mathbf{J}_{P\theta}^{-1} \mathbf{J}_{PV}] \tag{14.9}$$

and $\mathbf{J}_R$ is the reduced Jacobian matrix of the system. From Equation 14.8, we may write

$$\Delta \mathbf{V} = \mathbf{J}_R^{-1} \Delta \mathbf{Q} \tag{14.10}$$

The matrix $\mathbf{J}_R^{-1}$ is the reduced V-Q Jacobian. Its i^{th} diagonal element is the V-Q sensitivity at bus i. For computational efficiency, this matrix is not explicitly formed. The V-Q sensitivities are calculated by solving Equation 14.8.

The V-Q sensitivity at a bus represents the slope of the Q-V curve at the given operating point. A positive V-Q sensitivity is indicative of stable operation; the smaller the sensitivity, the more stable the system. As stability decreases, the magnitude of the sensitivity increases, becoming infinite at the stability limit. Conversely, a negative V-Q sensitivity is indicative of unstable operation. A small negative sensitivity represents a very unstable operation. Because of the nonlinear nature of the V-Q relationships, the magnitudes of the sensitivities for different system conditions do not provide a direct measure of the relative degree of stability.

(b) Q-V modal analysis [9,15]

Voltage stability characteristics of the system can be identified by computing the eigenvalues and eigenvectors (see Chapter 12, Section 12.2) of the reduced Jacobian matrix $\mathbf{J}_R$ defined by Equation 14.9. Let

$$\mathbf{J}_R = \boldsymbol{\xi}\boldsymbol{\Lambda}\boldsymbol{\eta} \tag{14.11}$$

where

$\boldsymbol{\xi}$ = right eigenvector matrix of $\mathbf{J}_R$
$\boldsymbol{\eta}$ = left eigenvector matrix of $\mathbf{J}_R$
$\boldsymbol{\Lambda}$ = diagonal eigenvalue matrix of $\mathbf{J}_R$

From Equation 14.11

$$\mathbf{J}_R^{-1} = \boldsymbol{\xi}\boldsymbol{\Lambda}^{-1}\boldsymbol{\eta} \tag{14.12}$$

Substituting in Equation 14.10 gives

$$\Delta\mathbf{V} = \boldsymbol{\xi}\boldsymbol{\Lambda}^{-1}\boldsymbol{\eta}\Delta\mathbf{Q} \tag{14.13}$$

or

$$\Delta\mathbf{V} = \sum_i \frac{\boldsymbol{\xi}_i \boldsymbol{\eta}_i}{\lambda_i}\Delta\mathbf{Q} \tag{14.14}$$

where $\boldsymbol{\xi}_i$ is the i^{th} column right eigenvector and $\boldsymbol{\eta}_i$ the i^{th} row left eigenvector of $\mathbf{J}_R$.

Each eigenvalue λ_i and the corresponding right and left eigenvectors $\boldsymbol{\xi}_i$ and $\boldsymbol{\eta}_i$ define the i^{th} mode of *Q-V* response.

Since $\boldsymbol{\xi}^{-1} = \boldsymbol{\eta}$, Equation 14.13 may be written as

$$\boldsymbol{\eta}\Delta\mathbf{V} = \boldsymbol{\Lambda}^{-1}\boldsymbol{\eta}\,\Delta\mathbf{Q}$$

or

$$\mathbf{v} = \boldsymbol{\Lambda}^{-1}\mathbf{q} \tag{14.15}$$

where

$\mathbf{v} = \boldsymbol{\eta}\Delta\mathbf{V}$ is the vector of modal voltage variations

and

$\mathbf{q} = \boldsymbol{\eta}\Delta\mathbf{Q}$ is the vector of modal reactive power variations

The difference between Equations 14.10 and 14.15 is that $\boldsymbol{\Lambda}^{-1}$ is a diagonal matrix whereas $\mathbf{J}_R^{-1}$, in general, is nondiagonal. Equation 14.15 represents uncoupled first order equations. Thus, for the i^{th} mode we have

$$\mathbf{v}_i = \frac{1}{\lambda_i}\mathbf{q}_i \tag{14.16}$$

If $\lambda_i>0$, the i^{th} modal voltage and the i^{th} modal reactive power variations are along the same direction, indicating that the system is voltage *stable*. If $\lambda_i<0$, the i^{th} modal voltage and the i^{th} modal reactive power variation are along opposite directions, indicating that the system is voltage *unstable*. The magnitude of each modal voltage variation equals the inverse of λ_i times the magnitude of the modal reactive power variation. In this sense the magnitude of λ_i determines the *degree of stability* of the i^{th} modal voltage. The smaller the magnitude of positive λ_i, the closer the i^{th} modal voltage is to being unstable. When $\lambda_i=0$, the i^{th} modal voltage collapses because any change in that modal reactive power causes infinite change in the modal voltage.

Let us now examine the relationship between bus *V-Q* sensitivities and eigenvalues of $\mathbf{J}_R$. In Equation 14.14, let $\Delta\mathbf{Q}=\mathbf{e}_k$, where $\mathbf{e}_k$ has all zero elements except for the k^{th} element which is equal to 1. Then

$$\Delta\mathbf{V} = \sum_i \frac{\eta_{ik}\xi_i}{\lambda_i}$$

where η_{ik} is the k^{th} element of $\boldsymbol{\eta}_i$.

The *V-Q* sensitivity at bus k is given by

$$\frac{\partial V_k}{\partial Q_k} = \sum_i \frac{\xi_{ki}\eta_{ik}}{\lambda_i} \tag{14.17}$$

We see from the above equation that the *V-Q* sensitivities cannot identify individual voltage collapse modes; instead they provide information regarding the combined effects of all modes of voltage-reactive power variations.

If the transmission network resistances are neglected and the node admittance matrix $\mathbf{Y}_N$ is symmetrical, the reduced Jacobian matrix $\mathbf{J}_R$ is also symmetrical [15]. Then the eigenvalues and eigenvectors of $\mathbf{J}_R$ are real. In addition, the right eigenvector and the left eigenvector of an eigenvalue of $\mathbf{J}_R$ are equal.

With phase-shifting transformers (which make the matrix $\mathbf{Y}_N$ unsymmetrical) and line resistances, $\mathbf{J}_R$ is only nearly symmetrical; the eigenvalues of $\mathbf{J}_R$ for all practical purposes are real.

The magnitude of the eigenvalues can provide a relative measure of the *proximity* to instability. Eigenvalues do not, however, provide an absolute measure because of the nonlinearity of the problem. This is analogous to the damping factor in small-signal (angle) stability analysis, which is indicative of the degree of damping but is not an absolute measure of stability margin. If a megawatt distance to voltage instability is required, the system is stressed incrementally until it becomes unstable and modal analysis is applied at each operating point. The application of modal analysis helps in determining how stable the system is and how much extra load or power transfer level should be added. When the system reaches the voltage stability critical point, the modal analysis is helpful in identifying the voltage stability critical areas and elements which participate in each mode.

Example 14.3

For the 500 kV, 322 km line system considered in Example 14.1, write the equations of the power flow from the sending end to the receiving end in the following form:

$$P = f(\theta, V)$$
$$Q = g(\theta, V)$$

Find the expressions for $J_{P\theta}$, J_{PV}, $J_{Q\theta}$, and J_{QV} defined by the linearized load flow equations:

$$\begin{bmatrix} \Delta P \\ \Delta Q \end{bmatrix} = \begin{bmatrix} J_{P\theta} & J_{PV} \\ J_{Q\theta} & J_{QV} \end{bmatrix} \begin{bmatrix} \Delta\theta \\ \Delta V \end{bmatrix}$$

(a) When P_2=1,500 MW, calculate the eigenvalues of the reduced Q-V Jacobian matrix and V-Q sensitivities with the following different reactive power injections for each of the corresponding two voltages on the Q-V curve:

(i) Q_i = 500 MVAr
(ii) Q_i = 400 MVAr
(iii) Values of Q_i close to the bottom of the Q-V curve

Assume that, for the purpose of analysis, the load and reactive power source have constant P, Q characteristics.

(b) Determine the voltage stability by computing the eigenvalues of the reduced Q-V Jacobian matrix for the following cases:

(i) P = 1,500 MW, Q_i = 450 MVAr
(ii) P = 1,900 MW, Q_i = 950 MVAr

Assume that the reactive power Q_i is supplied by a shunt capacitor.

Solution

From Figure E14.1(b), the admittance matrix of the two-bus system is

$$Y = \begin{bmatrix} 2.142 - j22.897 & -2.142 + j24.973 \\ -2.142 + j24.973 & 2.142 - j22.897 \end{bmatrix} \tag{E14.1}$$

From Equation 6.101 of Chapter 6, the expressions for P and Q at any bus k are given by

$$\begin{aligned} P_k &= V_k \sum_{m=1}^{n} (G_{km} V_m \cos\theta_{km} + B_{km} V_m \sin\theta_{km}) \\ Q_k &= V_k \sum_{m=1}^{n} (G_{km} V_m \sin\theta_{km} - B_{km} V_m \cos\theta_{km}) \end{aligned} \tag{E14.2}$$

where $\theta_{km} = \theta_k - \theta_m$.

For the two-bus system, we have

$$\begin{aligned} P_1 &= V_1[(2.142V_1\cos\theta_{11} - 22.897V_1\sin\theta_{11}) + (-2.142V_2\cos\theta_{12} + 24.973V_2\sin\theta_{12})] \\ P_2 &= V_2[(-2.142V_1\cos\theta_{21} + 24.973V_1\sin\theta_{21}) + (2.142V_2\cos\theta_{22} - 22.897V_2\sin\theta_{22})] \\ Q_1 &= V_1[(2.142V_1\sin\theta_{11} + 22.897V_1\cos\theta_{11}) + (-2.142V_2\sin\theta_{12} - 24.973V_2\cos\theta_{12}] \\ Q_2 &= V_2[(-2.142V_1\sin\theta_{21} - 24.973V_1\cos\theta_{21}) + (2.142V_2\sin\theta_{22} + 22.897V_2\cos\theta_{22})] \end{aligned} \tag{E14.3}$$

where $\theta_{11} = \theta_{22} = 0$, and $\theta_{21} = -\theta_{12} = \theta$.

We are interested only in P_2 and Q_2. With $V_1 = 1.0$,

$$\begin{aligned} P_2 &= -2.142V_2\cos\theta + 24.973V_2\sin\theta + 2.142V_2^2 \\ Q_2 &= -2.142V_2\sin\theta - 24.973V_2\cos\theta + 22.897V_2^2 \end{aligned}$$

Hence the expressions for the Jacobian terms are given by

$$\begin{aligned} J_{P\theta} &= \frac{\partial P_2}{\partial \theta} = 2.142V_2\sin\theta + 24.973V_2\cos\theta \\ J_{PV} &= \frac{\partial P_2}{\partial V_2} = -2.142\cos\theta + 24.973\sin\theta + 4.284V_2 \\ J_{Q\theta} &= \frac{\partial Q_2}{\partial \theta} = -2.142V_2\cos\theta + 24.973V_2\sin\theta \\ J_{QV} &= \frac{\partial Q_2}{\partial V_2} = -2.142\sin\theta - 24.973\cos\theta + 45.794V_2 \end{aligned} \tag{E14.4}$$

(a) The linearized power-flow equations are

$$\begin{aligned} \Delta P_2 &= J_{P\theta}\Delta\theta + J_{PV}\Delta V_2 \\ \Delta Q_2 &= J_{Q\theta}\Delta\theta + J_{QV}\Delta V_2 \end{aligned} \tag{E14.5}$$

With $\Delta P_2 = 0$,

$$\Delta Q_2 = (J_{QV} - J_{Q\theta}J_{P\theta}^{-1}J_{PV})\Delta V_2$$

or

$$\Delta Q_2 = J_R \Delta V_2$$

where

$$J_R = J_{QV} - J_{Q\theta}J_{P\theta}^{-1}J_{PV}$$

The expressions for J_{QV}, $J_{Q\theta}$, $J_{P\theta}$, and J_{PV} are given by Equation E14.4. For this simple system, J_R is a 1×1 matrix. The eigenvalue (λ) of the matrix is same as the matrix itself. The *V-Q* sensitivity is equal to the inverse of the eigenvalue.

For each value of Q_i, there are two solutions for the receiving end voltage. Table E14.1 summarizes V, θ, λ, and dV/dQ with P=1,500 MW and Q=500, 400, 306, and 305.9 MVAr. For each case, the eigenvalue and *V-Q* sensitivity are both negative at the low voltage solution and are both positive at the high voltage solution. With Q=305.9 MVAr (close to bottom of the *Q-V* curve), dV/dQ is large and λ is very small.

Table E14.1

Q_i (MVAr)	High Voltage Solution				Low Voltage Solution			
	V_2	θ	λ	dV/dQ	V_2	θ	λ	dV/dQ
500.0	1.024	-37.3°	17.03	0.059	0.671	-66.7°	-39.87	-0.025
400.0	0.956	-40.1°	12.41	0.081	0.706	-60.3°	-20.96	-0.048
306.0	0.820	-48.2°	0.52	1.923	0.812	-48.8°	-0.95	-1.055
305.9	0.814	-48.7°	0.02	50.1	0.815	-48.6°	-0.70	-1.434

(b) With a shunt capacitor connected at the receiving end of the line, the self-admittance is

$$Y_{22} = 2.142 - j(22.897 - B_C)$$

(i) With P=1500 MW and a 450 MVAr shunt capacitor,

$$V_2 = 0.981 \qquad \theta = -39.1°$$

Since B_C=4.5 pu,

$$Y_{22} = 2.142 - j(22.897 - 4.5) = 2.142 - j18.397$$

With this new value of Y_{22}, the reduced Q-V Jacobian matrix, calculated by using Equation E14.4, is

$$J_R = 5.348$$

And J_R is positive, indicating that the system is voltage stable.

(ii) With P=1900 MW and a 950 MVAr shunt capacitor,

$$V_2 = 0.995 \qquad \theta_2 = -52.97°$$

Since B_C=9.5 pu,

$$Y_{22} = 2.142 - j(22.897 - 9.5) = 2.142 - j1.397$$

and the reduced Q-V Jacobian matrix, calculated by using Equation E14.4, is

$$J_R = -13.683$$

And J_R is negative, indicating that the system is voltage unstable. ■

Bus participation factors

The relative participation of bus k in mode i is given by the *bus participation factor*:

$$P_{ki} = \xi_{ki}\eta_{ik} \tag{14.18}$$

From Equation 14.17, we see that P_{ki} determines the contribution of λ_i to the V-Q sensitivity at bus k.

Bus participation factors determine the areas associated with each mode. The sum of all the bus participations for each mode is equal to unity because the right and left eigenvectors are normalized. The size of bus participation in a given mode indicates the effectiveness of remedial actions applied at that bus in stabilizing the mode.

There are generally two types of modes. The first type has very few buses with large participations and all the other buses with close to zero participations, indicating that the mode is very localized. The second type has many buses with small but

similar degrees of participations, and the rest of the buses with close to zero participations; this indicates that the mode is not localized. A typical localized mode occurs if a single load bus is connected to a very strong network through a long transmission line. A typical non-localized mode occurs when a region within a large system is loaded up and the main reactive support for this region is exhausted.

It is impractical and unnecessary to calculate all the eigenvalues of $\mathbf{J}_R$ for a practical system with several thousand buses. On the other hand, calculating only the minimum eigenvalue of $\mathbf{J}_R$ is not sufficient because there is usually more than one weak mode associated with different parts of the system, and the mode associated with the minimum eigenvalue may not be the most troublesome mode as the system is stressed. In practice, it is seldom necessary to compute more than 5 to 10 of the smallest eigenvalues to identify all critical modes.

Branch participation factors

Let us compute the branch participation factor associated with mode i by assuming that the vector of modal reactive power variations $\mathbf{q}$ has all elements equal to zero except for the i^{th}, which equals 1. Then from Equation 14.15, the corresponding vector of bus reactive power variations is

$$\Delta\mathbf{Q}^{(i)} = \boldsymbol{\eta}^{-1}\mathbf{q} = \boldsymbol{\xi}\mathbf{q} = \boldsymbol{\xi}_i \tag{14.19}$$

where $\boldsymbol{\xi}_i$ is the i^{th} right eigenvector of $\mathbf{J}_R$. We further assume that all the right eigenvectors are normalized so that

$$\sum_j \xi_{ji}^2 = 1 \tag{14.20}$$

With the vector of bus reactive power variations equal to $\Delta\mathbf{Q}^{(i)}$, the vector of bus voltage variations, $\Delta\mathbf{V}^{(i)}$, is

$$\Delta\mathbf{V}^{(i)} = \frac{1}{\lambda_i}\Delta\mathbf{Q}^{(i)} \tag{14.21}$$

and, the corresponding vector of bus angle variation is

$$\Delta\boldsymbol{\theta}^{(i)} = -\mathbf{J}_{P\theta}^{-1}\mathbf{J}_{PV}\Delta\mathbf{V}^{(i)} \tag{14.22}$$

With the angle and voltage variations for both the sending end and receiving end known, the linearized change in branch reactive loss can be calculated.

The relative participation of branch j in mode i is given by the participation factor:

$$P_{ji} = \frac{\Delta Q_{loss} \text{ for branch } j}{\text{maximum } \Delta Q_{loss} \text{ for all branches}} \tag{14.23}$$

Branch participation factors indicate, for each mode, which branches consume the most reactive power in response to an incremental change in reactive load. Branches with high participations are either weak links or are heavily loaded. Branch participations are useful for identifying remedial measures to alleviate voltage stability problems and for contingency selection.

Generator participation factors

As in the case of branch participation, for a given reactive power variation, voltage and angle variations are determined at each machine terminal. These in turn are used to compute the change in reactive power output for each machine.

The relative participation of machine m in mode i is given by the generator participation factor:

$$P_{mi} = \frac{\Delta Q_m \text{ for machine } m}{\text{maximum } \Delta Q \text{ for all machines}} \tag{14.24}$$

Generator participation factors indicate, for each mode, which generators supply the most reactive power in response to an incremental change in system reactive loading. Generator participations provide important information regarding proper distribution of reactive reserves among all the machines in order to maintain an adequate voltage stability margin.

Calculation of small eigenvalues [15,19]:

Several techniques are available for computing a selected subset of eigenvalues of a real matrix [16-18]. In the EPRI VSTAB program [19], an implicit inverse lopsided simultaneous iteration method is used. This is a combination of the *lopsided simultaneous iteration* (LOPSI) method and the *implicit inverse iteration* (IMPII) method.

LOPSI algorithm

Simultaneous iteration methods are suitable for obtaining dominant eigenvalues and corresponding eigenvectors of real unsymmetrical matrices. These methods involve an accurate eigensolution of a smaller iteration matrix at each iteration cycle, the dimension of which depends on the number of vectors processed simultaneously. A bi-iteration procedure is used to obtain left and right eigenvectors simultaneously. A lop-sided iteration procedure is used to obtain only one set of the eigenvectors, or

to obtain the right and left eigenvectors sequentially. A detailed description of the simultaneous iteration method can be found in reference 16. Here, we briefly describe the computational procedure for implementing the LOPSI algorithm for calculating a subset of dominant eigenvalues and corresponding right eigenvectors of a real matrix **A**. These dominant eigenvalues and corresponding left eigenvectors can be obtained by applying the same procedure to $\mathbf{A}^T$.

Each iteration cycle of the LOPSI algorithm involves a premultiplication and a reorientation, followed by a normalization and a convergence test. Let **A** be a real unsymmetrical matrix of order n for which the r dominant eigenvalues and corresponding right eigenvectors are required. Let $\mathbf{R}=[\mathbf{R}_1\ \mathbf{R}_2 \cdots \mathbf{R}_r]$ be a set of trial vectors normalized so that the maximum element for each column of **R** is 1. Premultiplying **R** by **A** and denoting the resulting set of vectors $\mathbf{S}=[\mathbf{S}_1\ \mathbf{S}_2 \cdots \mathbf{S}_r]$, we have

$$\mathbf{S} = \mathbf{AR} \tag{14.25}$$

Let $\mathbf{\Lambda}=[\mathbf{\Lambda}_a \mid \mathbf{\Lambda}_b]=\text{diag}[\lambda_1\ \lambda_2 \cdots \lambda_r \mid \lambda_{r+1} \cdots \lambda_n]$ be a diagonal matrix of the eigenvalues of **A** arranged in descending order of absolute magnitude, and let $\mathbf{\Phi}=[\mathbf{\Phi}_a \mid \mathbf{\Phi}_b]=[\boldsymbol{\phi}_1\ \boldsymbol{\phi}_2 \cdots \boldsymbol{\phi}_r \mid \boldsymbol{\phi}_{r+1} \cdots \boldsymbol{\phi}_n]$ be a matrix of the corresponding right eigenvectors of **A** so that

$$\mathbf{A\Phi}_a = \mathbf{\Phi}_a\mathbf{\Lambda}_a$$

and

$$\mathbf{A\Phi}_b = \mathbf{\Phi}_b\mathbf{\Lambda}_b \tag{14.26}$$

The trial vectors **R** may be represented as a linear combination of the full set of eigenvectors:

$$\mathbf{R} = \mathbf{\Phi}_a\mathbf{C}_a + \mathbf{\Phi}_b\mathbf{C}_b \tag{14.27}$$

where $\mathbf{C}_a$ and $\mathbf{C}_b$ are coefficient matrices of size $r\times r$ and $(n-r)\times r$, respectively. It follows from Equations 14.25 to 14.27 that

$$\mathbf{S} = \mathbf{\Phi}_a\mathbf{\Lambda}_a\mathbf{C}_a + \mathbf{\Phi}_b\mathbf{\Lambda}_b\mathbf{C}_b \tag{14.28}$$

The lower eigenvectors contribute relatively less to **S** than they do to **R**. After a number of iterations, due to the washing-out process of earlier iterations, the coefficients of $\mathbf{C}_b$ become much smaller than those of $\mathbf{C}_a$.

The reorientation process involves the complete eigensolution of the $r\times r$ iteration matrix **B** obtained from the solution of

$$\mathbf{GB} = \mathbf{H} \tag{14.29}$$

where $\mathbf{G}=\mathbf{R}^T\mathbf{R}$ and $\mathbf{H}=\mathbf{R}^T\mathbf{S}$.

By substituting the values of $\mathbf{R}$ and $\mathbf{S}$ given by Equations 14.27 and 14.28, and assuming the $\mathbf{C}_b$ coefficients to be negligible by comparison with the $\mathbf{C}_a$ coefficients, we can show that

$$\mathbf{R}^T\boldsymbol{\Phi}_a\mathbf{C}_a\mathbf{B} \approx \mathbf{R}^T\boldsymbol{\Phi}_a\boldsymbol{\Lambda}_a\mathbf{C}_a \tag{14.30}$$

If $\mathbf{R}^T\boldsymbol{\Phi}_a$ is nonsingular,

$$\mathbf{C}_a\mathbf{B} \approx \boldsymbol{\Lambda}_a\mathbf{C}_a \tag{14.31}$$

which shows that the matrix of left eigenvectors of $\mathbf{B}$ is an approximation to $\mathbf{C}_a$ and that the eigenvalues of $\mathbf{B}$ are approximations to $\boldsymbol{\Lambda}_a$. If $\mathbf{T}$ is the $r\times r$ matrix of right eigenvectors of $\mathbf{B}$, then

$$\mathbf{T} \approx \mathbf{C}_a^{-1} \tag{14.32}$$

Hence, the set of vectors obtained by the multiplication

$$\mathbf{W} = \mathbf{ST} = \boldsymbol{\Phi}_a\boldsymbol{\Lambda}_a + \boldsymbol{\Phi}_a\boldsymbol{\Lambda}_b\mathbf{C}_b\mathbf{C}_a^{-1} \tag{14.33}$$

gives an improved set of right eigenvectors.

The column vectors in the $\mathbf{W}$ matrix are normalized so that the maximum element for each vector is 1, and $\mathbf{W}$ with its column vectors normalized is denoted by $\mathbf{W}^*$.

Let $\Delta\mathbf{R}=|\mathbf{R}^i-\mathbf{R}^{i-1}|$, with $\mathbf{R}^i$ and $\mathbf{R}^{i-1}$ equal to the eigenvectors solved at iteration i and iteration $i-1$, respectively. The iterative process is continued until the maximum element of $\Delta\mathbf{R}$ is less than a prespecified tolerance.

In summary, the LOPSI procedure to calculate the r dominant eigenvalues and the corresponding right eigenvectors is

a. Select r initial trial vectors $\mathbf{R}=[\,\mathbf{R}_1\ \mathbf{R}_2\ \cdots\ \mathbf{R}_r\,]$.

b. Premultiply $\mathbf{R}$ by $\mathbf{A}$, $\mathbf{S}=\mathbf{AR}$.

c. Determine $\mathbf{G}=\mathbf{R}^T\mathbf{R}$, $\mathbf{H}=\mathbf{R}^T\mathbf{S}$.

d. Solve $\mathbf{GB}=\mathbf{H}$ for $\mathbf{B}$.

e. Do full eigensolution of $\mathbf{B}$.

f. Determine $\mathbf{W}=\mathbf{ST}$, with $\mathbf{T}$ the right eigenvector matrix of $\mathbf{B}$.

g. Set $\mathbf{R}=\mathbf{W}^*$, where $\mathbf{W}^*$ is $\mathbf{W}$ normalized such that all the vectors have their largest element equal to 1.

h. Check convergence; if converged, stop. Otherwise, go back to b.

Among all the r eigenvectors the ones corresponding to the eigenvalues with larger absolute magnitudes will converge first. Therefore, if $j-1$ vectors have already passed the convergence test, they are locked and iteration is carried only on the rest of the r vectors. Such a locking procedure results in savings in computation time, the majority of which is effected in the premultiplication stage.

The convergence of the LOPSI algorithm depends on $|\lambda_r/\lambda_{r+1}|$. If m dominant eigenvalues are required, it is advisable to make r greater than m by including a few extra guard vectors. This not only makes a fast convergence rate probable for the required eigenvalues and eigenvectors but also ensures that the occurrence of complex conjugate eigenvalues in positions λ_m and λ_{m+1} would be of no consequence.

IILSI algorithm

Let us return to the problem of eigensolution of $\mathbf{J}_R$. Since we are interested in the eigenvalues with the smallest absolute magnitudes, which correspond to the largest eigenvalues of $\mathbf{J}_R^{-1}$, the LOPSI algorithm has to be applied to $\mathbf{J}_R^{-1}$. At each iteration, the premultiplication is

$$\mathbf{S} = \mathbf{J}_R^{-1}\mathbf{R} \tag{14.34}$$

and the LOPSI algorithm becomes an inverse LOPSI algorithm.

Direct solution of Equation 14.34 involves matrix manipulation on $\mathbf{J}_R$. Recall that $\mathbf{J}_R = \mathbf{J}_{QV} - \mathbf{J}_{Q\theta}\mathbf{J}_{P\theta}^{-1}\mathbf{J}_{PV}$, which is not sparse due to reduction. To fully exploit the sparsity of the Jacobian matrix, $\mathbf{S}$ in Equation 14.34 is obtained by solving the following set of sparse linear equations:

$$\begin{bmatrix} \mathbf{J}_{P\theta} & \mathbf{J}_{PV} \\ \mathbf{J}_{Q\theta} & \mathbf{J}_{QV} \end{bmatrix} \begin{bmatrix} \mathbf{Z} \\ \mathbf{S} \end{bmatrix} = \begin{bmatrix} 0 \\ \mathbf{R} \end{bmatrix} \tag{14.35}$$

It can be readily shown that the $\mathbf{S}$ obtained by solving Equation 14.35 is same as the $\mathbf{S}$ given in Equation 14.34. Since Equation 14.34 is solved implicitly by solving Equation 14.35, the inverse LOPSI algorithm becomes an *implicit inverse lopsided simultaneous iteration* (IILSI) algorithm.

The IILSI algorithm is applied to $\mathbf{J}_R$ and $\mathbf{J}_R^T$ in turn to calculate the smallest eigenvalues and corresponding right and left eigenvectors.

Illustration of modal analysis

To illustrate the application of modal analysis, let us consider the 39-bus, 10-machine system of Figure 14.3. In Section 14.1.1, we computed the *V-P* and *Q-V* characteristics for this system (see Figures 14.4 and 14.5). We now perform modal

analysis at the three operating conditions represented by points A, B, and C on the V-P curve of Figure 14.4.

Table 14.1 gives the five smallest eigenvalues of $\mathbf{J}_R$ of each of the three operating points. We see that the magnitudes of the eigenvalues decrease as the system approaches instability. At the operating point C, the smallest eigenvalue is 0.0083, indicating that the system is on the verge of instability.

Table 14.2 gives the bus, branch, and generator participations for the least stable mode (λ=0.0083) for operating condition C. Figure 14.7 identifies the area prone to voltage instability (based on bus participations) and branches with higher participations in the least stable mode.

Table 14.1 Five smallest eigenvalues

Operating Point	A	B	C
λ_1	0.3867	0.1446	0.0083
λ_2	1.0271	0.5550	0.3209
λ_3	2.4049	1.5133	0.9334
λ_4	4.1031	2.6280	1.8757
λ_5	4.2699	3.0209	2.3373

Table 14.2 Bus, branch, and generator participations in the least stable mode for operating point C

Bus Participation		Branch Participation		Generator Participation	
Bus	Participation	Branch	Participation	Bus	Participation
530	0.2638	500-520	1.0000	1311	1.0000
520	0.2091	300-360	0.8414	2412	0.2786
510	0.1025	100-350	0.8175	1011	0.2103
500	0.0941	320-500	0.8093	1014	0.2036
320	0.0482	330-350	0.6534	1013	0.2036
310	0.0319			1012	0.2036
300	0.0296				
340	0.0279				

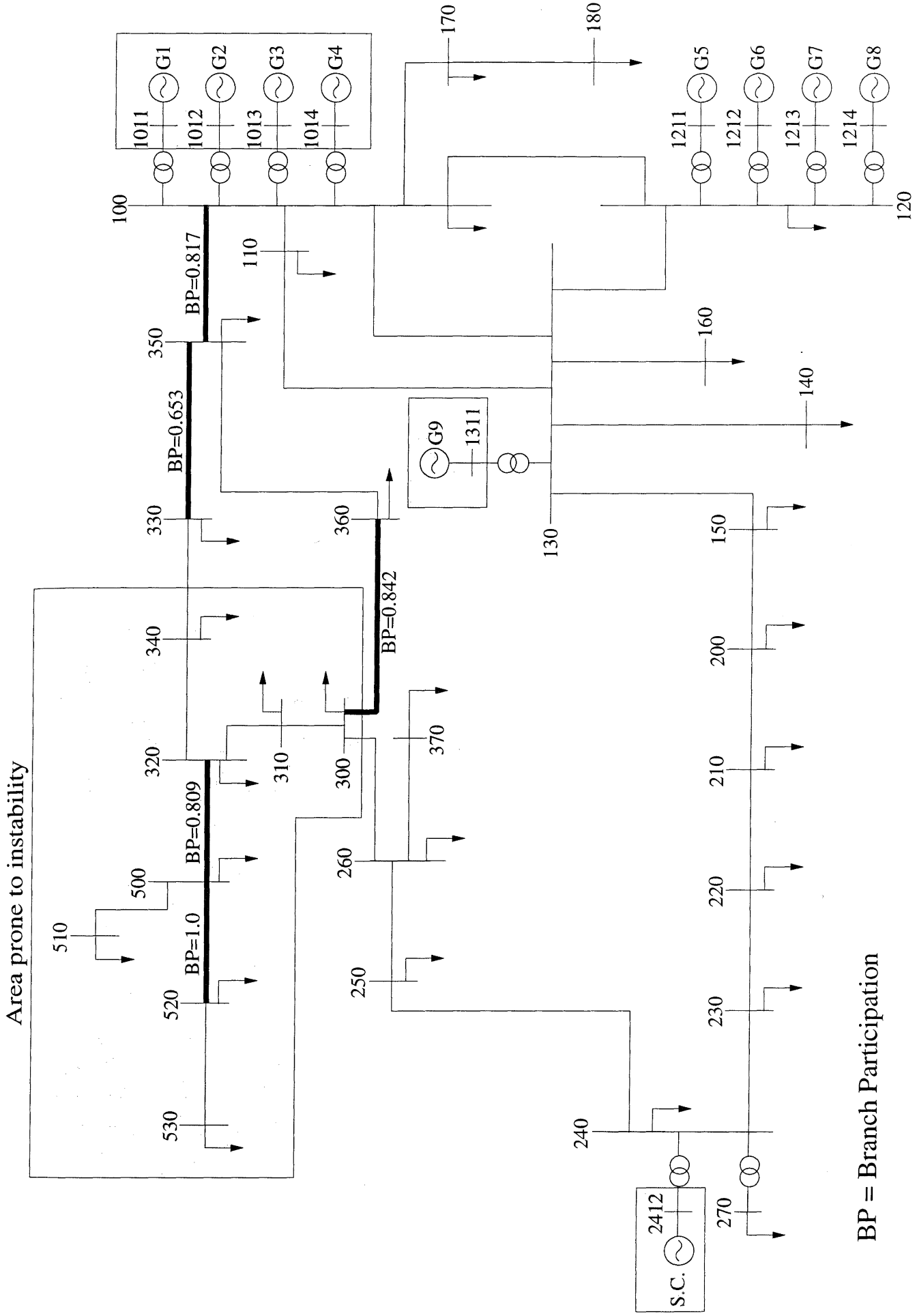


Figure 14.7 Buses and branches with high participation in the least stable mode

It is of interest to compare these results with the Q-V characteristics shown in Figure 14.5(c). The Q-V curves show that buses 530 and 510 have zero reactive margin. From Table 14.2, we see that these buses have high participation in the mode which is on the verge of becoming unstable. The advantage of modal analysis is that it clearly identifies groups of buses which participate in the instability. The Q-V analysis, being a single-bus approach, is unable to provide any connection between results obtained for individual buses. For large practical systems it may be necessary to compute a very large number of Q-V curves in order to find the problem area. Because of the way the Q-V curve stresses the system, it may not always be possible to complete the curve, in which case the search for a more critical bus must continue. The modal analysis approach eliminates this problem and easily identifies, on a system-wide basis, areas which are potentially troublesome.

Transient state approximations

In the analysis of voltage stability following a contingency, there are several distinct time frames in which different devices act to influence system performance. It is useful to be able to establish the condition of the system during each time frame, particularly if steady state cannot be achieved and we wish to determine what control actions cause instability. This leads to the concept of transient state approximations. Algebraic equations are used to represent system conditions which are approximations to various time frames along the transient trajectory of the system. These snapshots of system conditions represent transient state approximations.

Modal analysis can be applied to each snapshot to investigate the voltage stability of the system.

Proximity to instability

Proximity to small-disturbance voltage instability is determined by increasing load-generation in steps until the system becomes unstable or the power flow fails to converge. The increase in load may be by area, zone, or individual buses. The increase in generation follows a loading order that is usually system-specific. It is essential to capture nonlinearities encountered when moving from one system state to another.

Modal analysis performed at specified operating points provides information regarding areas prone to instability, and bus and generation participation factors. At the point of collapse, the left eigenvector identifies the most effective direction to steer the system to maximize voltage stability. Additionally, such measures as reactive reserves, losses, and bus voltages provide valuable information regarding the mechanism of instability.

References 20 to 25 describe special techniques for determining the point of voltage collapse and proximity to voltage instability. The following sections discuss two of these techniques.

14.3.4 Determination of Shortest Distance to Instability

The distance to voltage instability is normally determined by increasing the system load in a predefined manner, representing the most probable stressing scenario based on historical and forecast data. However, we are also interested in knowing the loading pattern that results in the smallest stability margin. The following is a description of a method of determining the minimum MVA stability margin, based on the technique described in reference 24.

Basic theory

What we want to find is the set of load MW and MVAr increments whose vector sum is a minimum and which, when imposed on the initial operating condition, cause the power-flow Jacobian to be singular. This may be achieved by organizing the power-flow equations in the form

$$\mathbf{f}(\mathbf{x}, \boldsymbol{\rho}) = g\begin{bmatrix}\mathbf{V}\\ \boldsymbol{\theta}\end{bmatrix} - \begin{bmatrix}\mathbf{P}\\ \mathbf{Q}\end{bmatrix} = 0 \tag{14.36}$$

where

$$\mathbf{x} = \begin{bmatrix}\mathbf{V}\\ \boldsymbol{\theta}\end{bmatrix} \qquad \boldsymbol{\rho} = \begin{bmatrix}\mathbf{P}\\ \mathbf{Q}\end{bmatrix}$$

Here $\mathbf{x}$ is the system state vector, and $\boldsymbol{\rho}$ is the parameter vector whose elements are active and reactive load power, and active generator power. Both $\mathbf{x}$ and $\boldsymbol{\rho}$ are $N=2N_{PQ}+N_{PV}$ dimensional vectors, with N_{PQ} the total number of PQ buses and N_{PV} the total number of PV buses. The dimension of the nonlinear vector function $\mathbf{f}$ is also N.

Let $\mathbf{J}_x$ and $\mathbf{J}_\rho$ be the Jacobian matrices of the vector function $\mathbf{f}$ with respect to $\mathbf{x}$ and $\boldsymbol{\rho}$, respectively. Matrix $\mathbf{J}_x$ is the same as the power-flow Jacobian matrix of Equation 14.6. For a given parameter vector $\boldsymbol{\rho}_i$, a system state vector $\mathbf{x}_i$ can be obtained by solving Equation 14.36 using any of the power-flow solution techniques described in Chapter 6. Each parameter vector $\boldsymbol{\rho}_i$ represents a specific system condition in terms of active and reactive loads, and active generation. The system reaches its voltage stability critical point if the parameter vector $\boldsymbol{\rho}_*$ and the corresponding system state vector $\mathbf{x}_*$ are such that the power-flow Jacobian matrix $\mathbf{J}_x$ is singular. Let S denote the hypersurface in the N-dimensional parameter space such that $\mathbf{J}_x(\mathbf{x}_*, \boldsymbol{\rho}_*)$ is singular if $\boldsymbol{\rho}_*$ is a point on S.

Given an initial system operating point $(\mathbf{x}_0, \boldsymbol{\rho}_0)$, we wish to find the parameter vector $\boldsymbol{\rho}_*$ on S such that the distance between $\boldsymbol{\rho}_0$ and $\boldsymbol{\rho}_*$, $k = |\boldsymbol{\rho}_* - \boldsymbol{\rho}_0|$, is a local minimum for the distance between $\boldsymbol{\rho}_0$ and S.

Assuming that S is a smooth hypersurface near $\boldsymbol{\rho}_*$, a normal vector to this hypersurface at $(\mathbf{x}_*, \boldsymbol{\rho}_*)$ is given by

$$\boldsymbol{\eta}_* = \mathbf{w}_* \mathbf{J}_\rho \tag{14.37}$$

where $\mathbf{w}_*$ is the left eigenvector of $\mathbf{J}_x(\mathbf{x}_*, \boldsymbol{\rho}_*)$ corresponding to the zero eigenvalue. And $\boldsymbol{\eta}_*$ is normalized such that $|\boldsymbol{\eta}_*| = 1$.

Starting from the initial system operating point $(\mathbf{x}_0, \boldsymbol{\rho}_0)$, the system is stressed by incrementally increasing $\boldsymbol{\rho}$ along a particular direction. Each time $\boldsymbol{\rho}$ increases, Equation 14.36 is solved to obtain the system state vector $\mathbf{x}$. And $\boldsymbol{\rho}$ is continuously increased along the same direction until, at the voltage stability critical point $(\mathbf{x}_*, \boldsymbol{\rho}_*)$, the power-flow Jacobian matrix $\mathbf{J}_x$ becomes singular; that is,

$$\boldsymbol{\rho}_* = \boldsymbol{\rho}_0 + k\boldsymbol{\eta} \tag{14.38}$$

where k is the distance between the initial system operating point $(\mathbf{x}_0, \boldsymbol{\rho}_0)$ and the voltage stability critical point $(\mathbf{x}_*, \boldsymbol{\rho}_*)$ as $k = |\boldsymbol{\rho}_* - \boldsymbol{\rho}_0|$.

For a given initial system operating point $(\mathbf{x}_0, \boldsymbol{\rho}_0)$, $\boldsymbol{\rho}$ can be increased along different directions. Obviously, the value of k depends on the direction along which $\boldsymbol{\rho}$ is increased. Our objective is to find the direction of the parameter vector $\boldsymbol{\rho}$ such that k is the local minimum.

The following procedure determines the vector $\boldsymbol{\eta}_*$ along which the distance between the initial equilibrium point $(\mathbf{x}_0, \boldsymbol{\rho}_0)$ and the singular point $(\mathbf{x}_*, \boldsymbol{\rho}_*)$ is the shortest:

(1) Let $\boldsymbol{\eta}_0$ be an initial guess for the direction $\boldsymbol{\eta}_*$, $|\boldsymbol{\eta}_0| = 1$.

(2) Stress the system by incrementally increasing $\boldsymbol{\rho}$ along the direction of $\boldsymbol{\eta}_i$ until $\mathbf{J}_x$ becomes singular; that is, determine k_i, $\boldsymbol{\rho}_i$ and $\mathbf{x}_i$ so that $\boldsymbol{\rho}_i = \boldsymbol{\rho}_0 + k_i\boldsymbol{\eta}_i$ is on the surface S.

(3) Set $\boldsymbol{\eta}_{i+1} = \mathbf{w}_i \mathbf{J}_\rho$, and $|\boldsymbol{\eta}_{i+1}| = 1$.

(4) Iterate steps 1, 2, 3 until $\boldsymbol{\eta}_i$ converges to a value $\boldsymbol{\eta}_*$. Then, $\boldsymbol{\rho}_* = \boldsymbol{\rho}_0 + k_*\boldsymbol{\eta}_*$ is the corresponding equilibrium condition.

A simple radial system example

For illustration, let us consider the radial system shown in Figure 14.8. Corresponding to Equation 14.36, we have

$$\mathbf{f}(\mathbf{x}, \boldsymbol{\rho}) = \begin{bmatrix} 4V\sin\alpha - P \\ 4V\cos\alpha - 4V^2 - Q \end{bmatrix} = \begin{bmatrix} 0 \\ 0 \end{bmatrix} \tag{14.39}$$

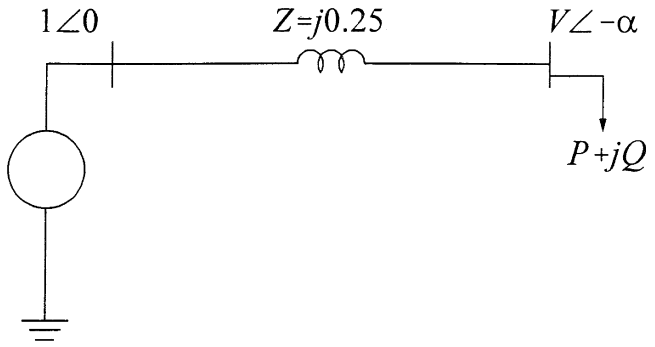


Figure 14.8 A simple radial system

with

$$\mathbf{x} = \begin{bmatrix} V \\ \alpha \end{bmatrix} \qquad \text{and} \qquad \boldsymbol{\rho} = \begin{bmatrix} P \\ Q \end{bmatrix}$$

The Jacobian matrices are

$$\mathbf{J}_x = \begin{bmatrix} 4V\cos\alpha & 4\sin\alpha \\ -4V\sin\alpha & 4\cos\alpha - 8V \end{bmatrix} \tag{14.40}$$

and

$$\mathbf{J}_\rho = \begin{bmatrix} -1 & 0 \\ 0 & -1 \end{bmatrix} \tag{14.41}$$

The determinant of $\mathbf{J}_x$ is

$$\det(\mathbf{J}_x) = 16V - 32V^2\cos\alpha \tag{14.42}$$

On the singular surface S, $\det(\mathbf{J}_x)=0$, that is,

$$16V - 32V^2\cos\alpha = 0$$

or

$$V = \frac{1}{2\cos\alpha} \tag{14.43}$$

Equation 14.43 describes the relationship between V and α, when $\mathbf{J}_x$ is singular. From Equations 14.39 and 14.43, we have the following expression describing the singular surface S in the parameter space:

$$P^2 + 4Q - 4 = 0 \tag{14.44}$$

Let us assume that the initial system operating condition is as follows:

$$P_0 = 0.8 \qquad Q_0 = 0.4 \qquad V_0 = 0.8554 \qquad \alpha_0 = 13.52°$$

Table 14.3 shows the iterative process of finding the point of voltage instability which is closest to the initial operating condition.

Table 14.3 Calculation of the shortest distance to voltage instability for the system of Figure 14.8

Iteration	Left Eigenvector $\boldsymbol{\eta}_i$	Distance to Instability (k_i)	P_i, Q_i
1	$[0.9725 \quad -0.2331]^T$	1.0725	1.8430, 0.1500
2	$[0.6776 \quad 0.7354]^T$	0.4173	1.0828, 0.7069
3	$[0.4869 \quad 0.8735]^T$	0.4061	0.9977, 0.7541
4	$[0.4443 \quad 0.8959]^T$	0.4024	0.9788, 0.7605
5	$[0.4405 \quad 0.8977]^T$	0.4016	0.9769, 0.7605
6	$[0.4378 \quad 0.8991]^T$	0.4015	0.9758, 0.7610

Figure 14.9 shows the singular surface S in a parameter space with active and reactive components of load as coordinates. On the figure, the point (P_0, Q_0) represents the initial operating condition. The surface S represents the locus of all combinations of P and Q which result in a zero eigenvalue of the Jacobian. All points below S represent voltage stable conditions, and all points above S represent unstable conditions.

General description of the procedure

For any system, the general procedure for finding the minimum distance from an initial load level $\mathbf{P}_0$, $\mathbf{Q}_0$ to S is as follows:

(1) Increase load from $\mathbf{P}_0$, $\mathbf{Q}_0$ in some direction (the choice of the initial direction will be discussed later) until an eigenvalue of the Jacobian is practically zero. The load level $\mathbf{P}_1$, $\mathbf{Q}_1$ corresponding to this point is the stability limit. This point $\mathbf{P}_1$, $\mathbf{Q}_1$ lies on, or is extremely near, S.

(2) For the conditions at $\mathbf{P}_1$, $\mathbf{Q}_1$, perform modal analysis and determine the left eigenvector of the *full Jacobian matrix*. The left eigenvector contains elements which provide the increments of MW and MVAr load for each bus. The eigenvector points in the shortest direction to singularity, which is therefore normal to S.

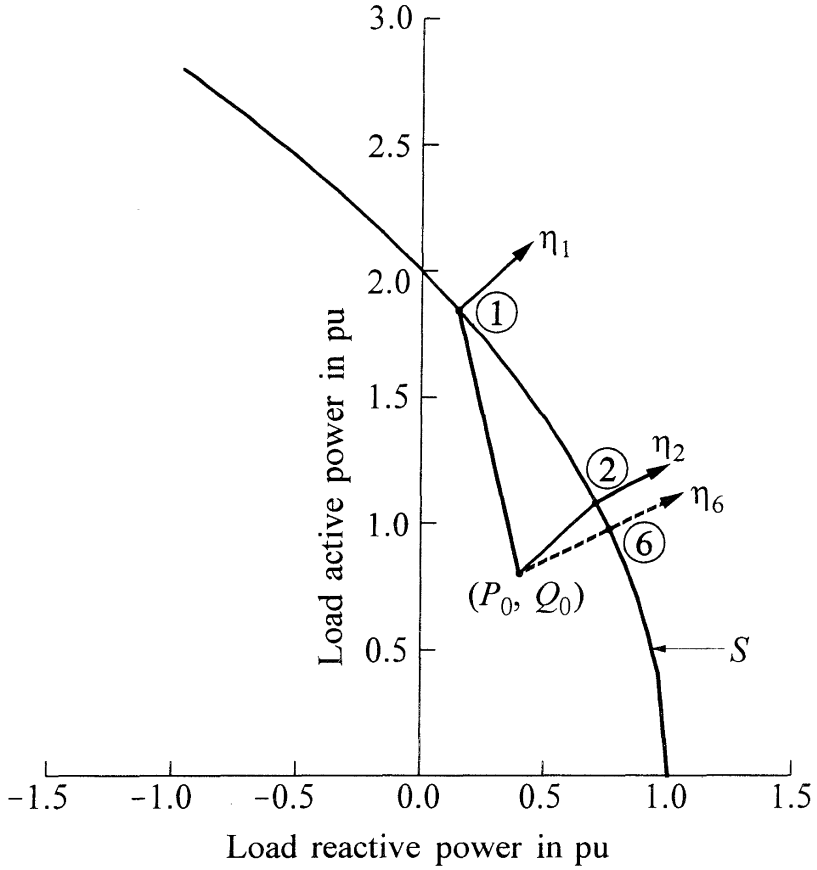


Figure 14.9 The singular surface S in the P-Q plane, and the convergence of the iterative process

(3) Go back to the base case load level $\mathbf{P}_0$, $\mathbf{Q}_0$ and load the system again, but this time in the direction given by the left eigenvector found in (2). When S is reached, a new left eigenvector is computed.

(4) Again we return to the base case $\mathbf{P}_0$, $\mathbf{Q}_0$ and load the system in the direction of the new eigenvector given in (3). This process is repeated until the computed eigenvector does not change with each new iteration. The process will then have converged.

When it has converged, the solution gives the minimum vector ($\mathbf{P}$ and $\mathbf{Q}$) distance to S from $\mathbf{P}_0$, $\mathbf{Q}_0$. This process can be applied to large practical systems; however, S is not a simple locus, but a hypersurface in a parameter space of dimension $2N$, where N is the total number of load buses (although we are free to choose the parameter space we use). The shape of this hypersurface is not known, and therefore we can expect that this process will find only a *local minimum*. Because of the nonlinearities encountered in loading the system from $\mathbf{P}_0$, $\mathbf{Q}_0$ to S, the local minimum we find is dependent on the initial direction we choose for loading. We could use the left eigenvector corresponding to the minimum eigenvalue of the Jacobian at $\mathbf{P}_0$, $\mathbf{Q}_0$ for this initial direction, but it may be more appropriate to use uniform loading based on an expected load pattern.

A large system example

This system has 600 buses. The total load power in the base case is 24,594 MW, 14,112 MVAr. The initial guess for the direction of stressing the system, i.e., $\boldsymbol{\eta}_0$ is such that the active and reactive load power in the base case is scaled up uniformly, and the increase in load active power is matched by uniformly scaling up active generation of all the generators. Table 14.4 summarizes the study results. Table 14.5 shows, at each iteration, the elements of the vector $\boldsymbol{\eta}_i$ associated with the top 20 buses with the largest increase in active power load.

Table 14.4 Summary of iterations to find the shortest distance to voltage instability of a 600-bus test system

Iteration	Distance to Instability (k_i)	Total Load P and Q at $(\mathbf{x}_*, \boldsymbol{\rho}_*)$	Smallest Eigenvalue of $\mathbf{J}_x$ at $(\mathbf{x}_*, \boldsymbol{\rho}_*)$
0		24,594 MW, 14,112 MVAr	0.034
1	116	25,729 MW, 14,763 MVAr	0.034
2	38	25,285 MW, 14,046 MVAr	-0.015
3	30	24,788 MW, 14,207 MVAr	-0.014
4	30	24,787 MW, 14,207 MVAr	0.013

From Table 14.4 we see that, with the initial uniform load increase, the stability limit is about 25,729 MW, an increase of about 1,135 MW. The corresponding vector sum of all active and reactive power load increases is 116. The smallest eigenvalue of $\mathbf{J}_x$ is 0.034, indicating that the system is on the verge of instability. The left eigenvector associated with the minimum eigenvalue gives the loading direction for the next iteration. Table 14.5 lists the top 20 entries of the left eigenvector; the load at each bus is increased in proportion to the corresponding eigenvector entries.

We see that the process converges quickly. At convergence, the load increase vector length k_i is only 30, significantly smaller than the initial direction of uniform load increase. The total megawatt load increase for the minimum loading direction is only 193 MW above the base case; this is 942 MW less than the margin found with uniform loading.

14.3.5 The Continuation Power-Flow Analysis

The Jacobian matrix of Equation 14.6 becomes singular at the voltage stability limit. Consequently, conventional power-flow algorithms are prone to convergence problems at operating conditions near the stability limit. The continuation power-flow analysis overcomes this problem by reformulating the power-flow equations so that they remain well-conditioned at all possible loading conditions. This allows the solution of the power-flow problem for stable as well as unstable equilibrium points (that is, for both upper and lower portions of the V-P curve).

Table 14.5 Top 20 elements of the vector $\boldsymbol{\eta}_i$ at each iteration

Iteration 1			Iteration 2			Iteration 4		
Bus	E_P	E_Q	Bus	E_P	E_Q	Bus	E_P	E_Q
279	0.146	-0.005	257	0.141	0.001	257	0.138	0.001
278	0.146	-0.005	260	0.140	0.000	260	0.138	0.000
281	0.146	-0.005	283	0.140	0.000	258	0.138	0.008
280	0.145	-0.005	282	0.140	0.000	283	0.137	0.000
293	0.142	-0.004	284	0.140	0.000	282	0.137	0.000
282	0.133	-0.002	258	0.138	0.008	284	0.137	0.000
283	0.133	0.000	256	0.137	0.005	256	0.137	0.005
284	0.132	0.000	246	0.137	0.005	247	0.137	0.008
260	0.131	-0.002	247	0.137	0.008	246	0.137	0.005
257	0.131	-0.002	293	0.136	0.001	248	0.136	0.004
256	0.120	0.000	248	0.136	0.004	294	0.135	0.011
246	0.118	0.000	279	0.135	0.001	265	0.134	0.004
265	0.117	0.000	278	0.135	0.002	293	0.134	0.001
248	0.117	0.000	280	0.135	0.001	261	0.133	0.007
258	0.117	0.002	281	0.135	0.001	267	0.133	0.010
247	0.116	0.002	265	0.134	0.004	250	0.133	0.006
270	0.112	0.000	294	0.134	0.011	269	0.133	0.010
292	0.112	0.000	261	0.133	0.007	281	0.132	0.001
261	0.111	0.001	250	0.132	0.006	268	0.132	0.009
277	0.111	0.000	267	0.132	0.010	279	0.132	0.002

Note: E_P and E_Q are the P and Q terms of the left eigenvector $\boldsymbol{\eta}_i$.

The continuation power-flow method described in this section is based on the approach described in reference 23. It uses a *locally-parameterized continuation method* and belongs to a general class of methods for solving nonlinear algebraic equations known as *path-following methods* [30, 31].

Basic principle

The continuation power-flow analysis uses an iterative process involving predictor and corrector steps as depicted in Figure 14.10. From a known initial solution (A), a tangent predictor is used to estimate the solution (B) for a specified pattern of load increase. The corrector step then determines the exact solution (C) using a conventional power-flow analysis with the system load assumed to be fixed.

The voltages for a further increase in load are then predicted based on a new tangent predictor. If the new estimated load (D) is now beyond the maximum load on the exact solution, a corrector step with loads fixed would not converge; therefore, a corrector step with a fixed voltage at the monitored bus is applied to find the exact solution (E). As the voltage stability limit is reached, to determine the exact maximum load the size of load increase has to be reduced gradually during the successive predictor steps.

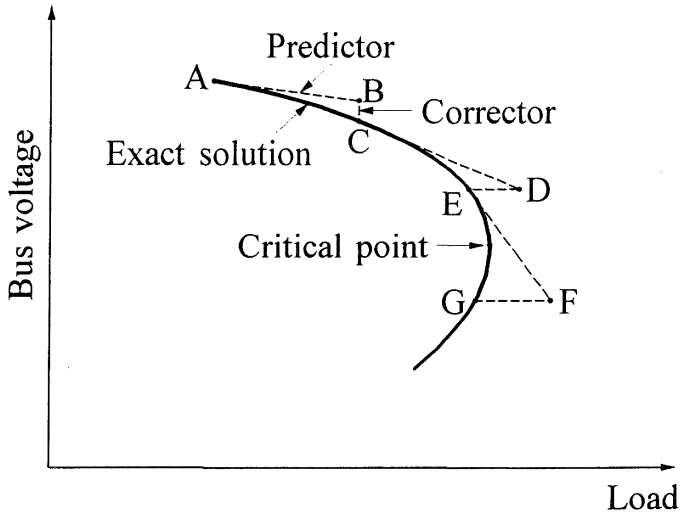


Figure 14.10 A typical sequence of calculations in a continuation power-flow analysis

Mathematical formulation

The basic equations are similar to those of a standard power-flow analysis except that the increase in load is added as a parameter. The reformulated power-flow equations, with provision for increasing generation as the load is increased, may be expressed as

$$\mathbf{F}(\boldsymbol{\theta},\mathbf{V}) = \lambda\mathbf{K} \tag{14.45}$$

where

λ is the load parameter
$\boldsymbol{\theta}$ is the vector of bus voltage angles
$\mathbf{V}$ is the vector of bus voltage magnitudes
$\mathbf{K}$ is the vector representing percent load change at each bus

The above set of nonlinear equations is solved by specifying a value for λ such that

$$0 \le \lambda \le \lambda_{critical}$$

where $\lambda=0$ represents the base load condition, and $\lambda=\lambda_{critical}$ represents the critical load.

Equation 14.45 may be rearranged as

$$\mathbf{F}(\boldsymbol{\theta},\mathbf{V},\lambda) = 0 \tag{14.46}$$

Predictor step:

In the predictor step, a linear approximation is used to estimate the next solution for a change in one of the state variables (i.e., θ, V, or λ).

Taking the derivatives of both sides of Equation 14.46, with the state variables corresponding to the initial solution, will result in the following set of linear equations:

$$\mathbf{F}_{\boldsymbol{\theta}} d\boldsymbol{\theta} + \mathbf{F}_{\mathbf{V}} d\mathbf{V} + \mathbf{F}_{\lambda} d\lambda = 0$$

or

$$[\ \mathbf{F}_{\boldsymbol{\theta}}\ \mathbf{F}_{\mathbf{V}}\ \mathbf{F}_{\lambda}\ ] \begin{bmatrix} d\boldsymbol{\theta} \\ d\mathbf{V} \\ d\lambda \end{bmatrix} = 0 \tag{14.47}$$

Since the insertion of λ in the power-flow equations added an unknown variable, one more equation is needed to solve the above equations. This is satisfied by setting one of the components of the tangent vector to +1 or −1. This component is referred to as the *continuation parameter*. Equation 14.47 now becomes

$$\begin{bmatrix} \mathbf{F}_{\boldsymbol{\theta}} & \mathbf{F}_{\mathbf{V}} & \mathbf{F}_{\lambda} \\ & \mathbf{e}_k & \end{bmatrix} \begin{bmatrix} d\boldsymbol{\theta} \\ d\mathbf{V} \\ d\lambda \end{bmatrix} = \begin{bmatrix} \mathbf{0} \\ \pm 1 \end{bmatrix} \tag{14.48}$$

where $\mathbf{e}_k$ is a row vector with all elements equal to zero except for the k^{th} element (corresponding to the continuation parameter) being equal to 1.

Initially, the load parameter λ is chosen as the continuation parameter and the corresponding component of the tangent vector is set to +1. During the subsequent predictor steps, for reasons given later, the continuation parameter is chosen to be the state variable that has the greatest rate of change near the given solution, and the sign of its slope determines the sign of the corresponding component of the tangent vector. As the maximum load is approached, a voltage will typically be the parameter with the largest change.

Once the tangent vector is found, the prediction for the next solution is given by

$$\begin{bmatrix} \boldsymbol{\theta} \\ \mathbf{V} \\ \lambda \end{bmatrix} = \begin{bmatrix} \boldsymbol{\theta}_0 \\ \mathbf{V}_0 \\ \lambda_0 \end{bmatrix} + \sigma \begin{bmatrix} d\boldsymbol{\theta} \\ d\mathbf{V} \\ d\lambda \end{bmatrix} \tag{14.49}$$

where the subscript "0" identifies the values of the state variables at the beginning of the predictor step. The step size σ is chosen so that a power-flow solution exists with the specified continuation parameter. If for a given step size a solution cannot be found in the corrector step, the step size is reduced and the corrector step is repeated until a successful solution is obtained.

Corrector step:

In the corrector step, the original set of equations $\mathbf{F}(\boldsymbol{\theta}, \mathbf{V}, \lambda) = 0$ is augmented by one equation that specifies the state variable selected as the continuation parameter. Thus the new set of equations is

$$\begin{bmatrix} \mathbf{F}(\boldsymbol{\theta}, \mathbf{V}, \lambda) \\ x_k - \eta \end{bmatrix} = [\mathbf{0}] \tag{14.50}$$

In the above, x_k is the state variable selected as the continuation parameter and η is equal to the predicted value of x_k. This set of equations can be solved using a slightly modified Newton-Raphson power-flow method. The introduction of the additional equation specifying x_k makes the Jacobian non-singular at the critical operating point. The continuation power-flow analysis can be continued beyond the critical point and thus obtain solutions corresponding to the lower portion of the *V-P* curve.

The tangent component of λ (i.e., $d\lambda$) is positive for the upper portion of *V-P* curve, is zero at the critical point, and is negative beyond the critical point. Thus the sign of $d\lambda$ will indicate whether or not the critical point has been reached.

If the continuation parameter is the load increase, the corrector will be a vertical line (for example, segment BC in Figure 14.10) on the *V-P* plane. If, on the other hand, a voltage magnitude is the continuation parameter, the corrector will be a horizontal line (for example, segment DE).

Selection of continuation parameter:

The selection of appropriate continuation parameters is particularly important for the corrector steps. A poor choice of the parameter can cause the solution to diverge. For example, the use of load parameter λ as the continuation parameter in the region of critical point can cause the solution to diverge if the estimate exceeds the maximum load. On the other hand, when the voltage magnitude is used as the continuation parameter the solution may diverge if large steps in voltage change are

used. A good practice is to choose the continuation parameter as the state variable that has the greatest rate of change near the given solution.

Sensitivity information

In the continuation power-flow analysis, the elements of the tangent vector represent differential changes in the state variables in response to a differential change in system load. Therefore, the dV elements in a given tangent vector are useful in identifying "weak buses", that is, buses which experience large voltage variations in response to a change in load.

Complementary use of conventional and continuation methods

The continuation method of power-flow analysis is robust and flexible. It is ideally suited for solving power-flow problems with convergence difficulties. However, the method is very slow and time-consuming.

The best overall approach for computing power-flow solutions up to and beyond the critical point is to use the conventional and continuation methods of power-flow analysis in a complementary manner. Starting from the base case, Equation 14.45 is solved using a conventional method (Newton-Raphson or Fast Decoupled) to compute power-flow solutions for successively increasing load levels until a solution cannot be obtained. From that point onward, the continuation method is used to obtain the power-flow solutions. Usually, the conventional methods can provide solutions right up to the critical point; the continuation method becomes necessary only if solutions exactly at and past the critical point are required.

Illustration of continuation power-flow application

To illustrate the application of continuation power-flow analysis, let us once again consider the system of Figure 14.3. The voltage stability properties of this system were analyzed in Section 14.1.1 by computing V-P and Q-V characteristics, and in Section 14.3.3 by applying modal analysis. As the power-flow solutions were obtained using conventional methods, the voltage stability analysis had to be limited to only stable equilibrium points, that is, to the upper portion of the V-P curve. At the limiting operating condition considered (point C on the V-P curve of Figure 14.4), as indicated by the eigenvalues of Table 14.1, the system is on the verge of instability but not actually unstable.

We now extend the analysis to operating conditions past the critical point by using continuation power-flow analysis. The load in area 1 of Figure 14.3 (shaded) is increased in the same way as described in Section 14.1.1 with loads assumed to have constant MVA characteristics. Figure 14.11 shows the *complete* V-P curve for the system. The upper portion of the curve (A to C) was computed using a conventional power-flow analysis (Fast Decoupled) and is identical to the characteristic shown in Figure 14.4. The lower portion of the curve (C to B) was, however, computed using the continuation power-flow analysis.

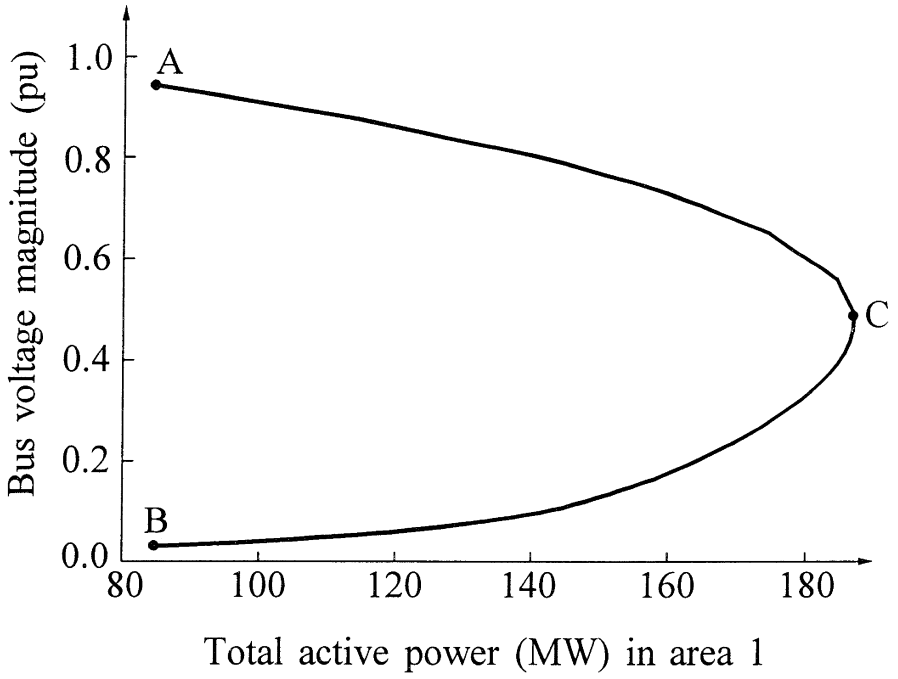


Figure 14.11 *V-P* curve at bus 530 of system shown in Figure 14.3

Table 14.6 Voltage sensitivity and participation factors for critical operating point

Continuation Power-Flow		Modal Analysis	
Bus	Voltage Sensitivity Factor	Bus	Bus Participation Factor
530	0.126	530	0.2654
520	0.112	520	0.2104
510	0.079	510	0.1025
500	0.075	500	0.0941
320	0.054	320	0.0481
310	0.044	310	0.0317
300	0.042	300	0.0294
370	0.041	340	0.0278
260	0.040	370	0.0267
340	0.040	260	0.0263

Note: Voltage sensitivity factor for bus k = $\dfrac{dV \text{ for bus } k}{\text{sum of } dV_s \text{ for all buses}}$

Point C represents the critical operating point, and the corresponding area 1 load is 186.98 MW. For this operating condition, the top 10 entries for the voltage sensitivity factors (dV elements of the tangent vector) are listed in Table 14.6. For comparison, the top 10 entries for the bus participation factors corresponding to the least stable mode (see Section 14.3.3) are also shown in the table. The areas prone to voltage instability identified by the two approaches are practically identical for this system. This is to be expected since, for the loading pattern considered, there is only one voltage weak area.

14.4 PREVENTION OF VOLTAGE COLLAPSE

This section identifies system design and operating measures that can be taken to prevent voltage collapse.

14.4.1 System Design Measures

(a) Application of reactive power-compensating devices

In Section 14.1.4, we discussed the effects of different types of reactive power-compensating devices on voltage stability. Adequate stability margins should be ensured by proper selection of compensation schemes. The selection of the sizes, ratings, and locations of the compensation devices should be based on a detailed study covering the most onerous system conditions for which the system is required to operate satisfactorily.

Design criteria based on maximum allowable voltage drop following a contingency are often not satisfactory from the voltage stability viewpoint. The stability margin should be based on MW and MVAr distances to instability. It is important to recognize voltage control areas and weak transmission boundaries in this regard.

(b) Control of network voltage and generator reactive output

Load (or line drop) compensation of a generator AVR regulates voltage on the high-tension side of, or partway through, the step-up transformer (see Chapter 8, Section 8.5.4). In many situations this has a beneficial effect on voltage stability by moving the point of constant voltage electrically closer to the loads.

Alternatively, secondary outer loop control of generator excitation may be used to regulate network side voltage. This should be much slower than the normal regulation of generator terminal voltage to minimize adverse interaction of the two controls. A response time of about 10 seconds is usually adequate for the outer loop control.

Several utilities are developing special schemes for control of network voltages and reactive power. For example, French and Italian utilities (EDF and ENEL) are

developing "secondary voltage control" schemes for centrally controlling network voltages and generator reactive outputs [26,27]. Tokyo Electric Power Company has an adaptive control of reactive power supply [28].

(c) Coordination of protections/controls

As identified in Section 14.2.2, one of the causes of voltage collapse is the lack of coordination between equipment protections/controls and power system requirements. Adequate coordination should be ensured based on dynamic simulation studies.

Tripping of equipment to prevent an overloaded condition should be the last resort. Wherever possible, adequate control measures (automatic or manual) should be provided for relieving the overload condition before isolating the equipment from the system.

(d) Control of transformer tap changers

Tap changers can be controlled, either locally or centrally, so as to reduce the risk of voltage collapse. Where tap changing is detrimental, a simple method is to block tap changing when the source side voltage sags, and unblock when the voltage recovers. Several utilities are using such schemes [1].

There is potential for application of improved ULTC control strategies. Such strategies must be developed based on a knowledge of the load and distribution system characteristics. For example, depressing the distribution voltages in substations which supply predominantly residential loads provides load relief at least temporarily. This will be partially offset eventually when the load is increased by the action of automatic or manually controlled devices. Increasing voltage on industrial loads does not materially affect the load supplied, but increases the reactive power supplied by the capacitors associated with such loads.

Microprocessor-based ULTC controls offer virtually unlimited flexibility for implementing ULTC control strategies so as to take advantage of the load characteristics. Where dropping the downstream voltage offers relief, the voltages may be reduced to a specific level when the primary voltage drops below a threshold. On the other hand, where maintaining secondary voltage is beneficial, normal ULTC controls should be applied. There is even a possibility of actually raising voltages slightly above normal [29]. The best strategy depends on the characteristics of the specific system.

(e) Undervoltage load shedding [1,32]

To cater to unplanned or extreme situations, it may be necessary to use undervoltage load-shedding schemes. This is analogous to underfrequency load shedding, which has become a common utility practice to cater to extreme situations resulting in generation deficiency and underfrequency. Load shedding provides a low-

cost means of preventing widespread system collapse. This is particularly true if system conditions and the contingencies leading to voltage instability are of low probability, but would result in serious consequences. The characteristics and locations of the loads to be shed are more important for voltage problems than they are for frequency problems.

Load-shedding schemes should be designed so as to distinguish between faults, transient voltage dips, and low voltage conditions leading to voltage collapse.

14.4.2 System-Operating Measures

(a) Stability margin

The system should be operated with an adequate voltage stability margin by the appropriate scheduling of reactive power resources and voltage profile. There are at present no widely accepted guidelines for selection of the degree of margin and the system parameters to be used as indices. These are likely to be system dependent and may have to be established based on the characteristics of the individual system.

If the required margin cannot be met by using available reactive power resources and voltage control facilities, it may be necessary to limit power transfers and to start up additional generating units to provide voltage support at critical areas.

(b) Spinning reserve

Adequate spinning reactive-power reserve must be ensured by operating generators, if necessary, at moderate or low excitation and switching in shunt capacitors to maintain the desired voltage profile. The required reserve must be identified and maintained within each voltage control area.

(c) Operators' action

Operators must be able to recognize voltage stability-related symptoms and take appropriate remedial actions such as voltage and power transfer controls and, possibly as a last resort, load curtailment. Operating strategies that prevent voltage collapse need to be established. On-line monitoring and analysis to identify potential voltage stability problems and possible remedial measures would be invaluable in this regard.

REFERENCES

[1] IEEE, Special Publication 90TH0358-2-PWR, *Voltage Stability of Power Systems: Concepts, Analytical Tools, and Industry Experience*, 1990.

[2] CIGRE Task Force 38-02-10, *Modelling of Voltage Collapse Including Dynamic Phenomena*, 1993.

[3] CIGRE Task Force 38-01-03, "Planning against Voltage Collapse," *Electra*, No. 111, pp. 55-75, March 1987.

[4] C. Barbier and J.P. Barret, "An Analysis of Phenomena of Voltage Collapse on Transmission System," *Revue Générale d' Electricité*, pp. 672-690, October 1980.

[5] H.K. Clark, "Voltage Control and Reactive Supply Problems," IEEE Tutorial Course Text on Reactive Power: Basics, Problems, and Solutions, 87EH0262-6-PWR, pp. 17-27, 1987.

[6] W.R. Lachs, "Voltage Collapse in EHV Power Systems," Paper No. A78057-2, presented at the 1978 IEEE PES Winter Meeting, New York, January 28-February 3, 1978.

[7] Y. Mansour and P. Kundur, "Voltage Collapse," *Control and Dynamic Systems*, Vol. 42: *Analysis and Control System Techniques for Electric Power Systems*, pp. 111-162, Academic Press, 1991.

[8] C.W. Taylor, *Power System Voltage Stability*, McGraw-Hill, 1993.

[9] B. Gao, G.K. Morison, and P. Kundur, "Voltage Stability Evaluation Using Modal Analysis," *IEEE Trans.*, Vol. PWRS-7, No. 4, pp. 1529-1542, November 1992.

[10] G.K. Morison, B. Gao, and P. Kundur, "Voltage Stability Analysis Using Static and Dynamic Approaches," Paper 92SM590-0 PWRS, Presented at the IEEE PES Summer Meeting, July 12-16, 1992, Seattle, Washington.

[11] K. Walve, "Modelling of Power System Components at Severe Disturbances," CIGRE Paper: 38-18, 1986.

[12] M. Stubbe, A. Bihain, J. Deuse, and J.C. Baader, "STAG - A New Unified Software Program for the Study of the Dynamic Behaviour of Electrical Power Systems," *IEEE Trans.*, Vol. PWRS-4, No. 1, pp. 129-138, 1989.

[13] N. Flatabø, R. Ognedal, and T. Carlsen, "Voltage Stability Condition in a Power Transmission System Calculated by Sensitivity Methods," *IEEE Trans.*, Vol. PWRS-5, No. 4, pp. 1286-1293, November 1990.

[14] C. Lemaitre, J.P. Paul, J.M. Tesseron, Y. Harmand, and Y.S. Zhao, "An Indicator of the Risk of Voltage Profile Instability for Real-Time Control Applications," IEEE Summer Meeting 1989, Paper 89SM713-9 PWRS.

[15] B. Gao, *Voltage Stability Analysis of Large Power Systems*, Ph.D. thesis, University of Toronto, 1992.

[16] W.J. Stewart and A. Jennings, "A Simultaneous Iteration Algorithm for Real Matrices," *ACM Trans. Mathematical Software*, Vol. 7, No. 2, pp. 184-198, June 1981.

[17] L. Wang and A. Semlyen, "Application of Sparse Eigenvalue Techniques to the Small Signal Stability Analysis of Large Power Systems," *IEEE Trans.*, Vol. PWRS-5, No. 2, pp. 635-642, May 1990.

[18] N. Martins, "Efficient Eigenvalue and Frequency Response Methods Applied to Power System Small-Signal Stability Studies," *IEEE Trans.*, Vol. PWRS-1, No. 2, pp. 217-225, February 1986.

[19] *Voltage Stability Analysis Program Application Guide*, EPRI Project RP3040-1, Prepared by Ontario Hydro, October 1992.

[20] F.L. Alvarado and T.H. Jung, "Direct Detection of Voltage Collapse Conditions," *Proceedings: Bulk Power System Voltage Phenomena - Voltage Stability and Security*, EPRI EL-6183, pp. 5.23-5.38, January 1989.

[21] H.D. Chiang, W. Ma, R.J. Thomas, and J.S. Thorp, "A Tool for Analyzing Voltage Collapse in Electric Power Systems," *Proceedings of the Tenth Power System Computation Conference*, Graz, Austria, pp. 1210-1217, August 1990.

[22] T. Van Cutsem, "A Method to Compute Reactive Power Margins with Respect to Voltage Collapse," *IEEE Trans.*, Vol. PWRS-6, No. 2, pp. 145-156, February 1991.

[23] V. Ajjarapu and C. Christy, "The Continuation Power Flow: A Tool for Steady State Voltage Stability Analysis," *IEEE PICA Conference Proceedings*, pp. 304-311, May 1991.

[24] I. Dobson and L. Lu, "Using an Iterative Method to Compute a Closest Saddle Node Bifurcation in the Load Power Parameter Space of an Electric Power

System," Bulk Power System Voltage Phenomena, Voltage Stability and Security NSF Workshop, Deep Creek Lake, Md., August 1991.

[25] A-P Löf, T. Smed, G. Andersson, and D.J. Hill, "Fast Calculation of a Voltage Stability Index," *IEEE Trans.*, Vol. PWRS-7, No. 1, pp. 54-64, February 1992.

[26] J.P. Paul, C. Corroyer, P. Jeanell, J.M. Tesseron, F. Maury, and A. Torra, "Improvements in the Organization of Secondary Voltage Control in France," CIGRE 38/39-03, 1990.

[27] V. Archidiacono, S. Corsi, A. Natale, C. Raffaelli, and V. Menditto, "New Developments in the Application of ENEL Transmission System Voltage and Reactive Power Automatic Control," CIGRE 38/39-06, 1990.

[28] S. Koishikawa, S. Ohsaka, M. Suzuki, T. Michigami, and M. Akimoto, "Adaptive Control of Reactive Power Supply Enhancing Voltage Stability of a Bulk Power Transmission System and a New Scheme of Monitor on Voltage Security," CIGRE 38/39-01, 1990.

[29] G. Brownell and H. Clark, "Analysis and Solutions for Bulk System Voltage Instability," *IEEE Computer Applications in Power*, pp. 31-35, July 1989.

[30] R. Seydel, *From Equilibrium to Chaos*, Elsevier, New York, 1988.

[31] W.C. Rheinboldt, *Numerical Analysis of Parameterized Nonlinear Equations*, John Wiley & Sons, New York, 1986.

[32] C.W. Taylor, "Concepts of Undervoltage Load Shedding for Voltage Stability," *IEEE Trans. on Power Delivery*, Vol. 7, No. 2, pp. 480-488, April 1992.

Subsynchronous Oscillations

In the analysis of power system dynamic performance so far, the rotor of a turbine generator was assumed to be made up of a single mass. Such a representation accounts for the oscillation of the entire turbine-generator rotor with respect to other generators. The frequency of this mode of oscillation is usually in the range of 0.2 to 2 Hz. In reality, a steam turbine-generator rotor has a very complex mechanical structure consisting of several predominant masses (such as rotors of turbine sections, generator rotor, couplings, and exciter rotor) connected by shafts of finite stiffness. Therefore, when the generator is perturbed, torsional oscillations result between different sections of the turbine-generator rotor.

The torsional oscillations in the *subsynchronous* range could, under certain conditions, interact with the electrical system in an adverse manner. Special problems related to torsional oscillations include the following:

(a) Torsional interaction with power system controls.

(b) Subsynchronous resonance with series capacitor-compensated transmission lines.

(c) Torsional fatigue duty due to network switching.

The torsional characteristics of hydro units are such that interaction with power system controls or transmission network has not been a source of concern.

This chapter describes the characteristics and modelling of a turbine-generator shaft system and discusses various problems related to subsynchronous torsional oscillations that require consideration in the design of power systems.

15.1 TURBINE-GENERATOR TORSIONAL CHARACTERISTICS

15.1.1 Shaft System Model [1-6]

The rotor of a thermal generating unit is a complex mechanical system. It may exceed 50 metres in total length and weigh several hundred tons. The rotor contains machined shaft sections of varying sizes and couplings that are either integral or shrunk on and keyed to the rotor. The turbine sections contain disks, blades, and other smaller components. The generator includes coil slots and retaining rings. Such a rotor system has a large number of torsional vibration modes both above and below the rated frequency. A *continuum model* of the rotor system would be required to account for the complete range of torsional oscillations [6]. However, the problem due to interaction between the electrical system and the rotor mechanical system is principally in the subsynchronous frequency range. This allows the representation of the rotor system by a simple *lumped-mass model* for electrical system interaction studies.

Figure 15.1 shows the structure of a typical lumped-mass model of a generating unit driven by a tandem compound reheat turbine. The five torsional masses represent the rotors of the generator, two low-pressure (LP) turbine sections, an intermediate-pressure (IP) turbine section, and a high-pressure (HP) turbine section. The generating unit is assumed to have a static exciter. For a unit with a rotating exciter driven by the same shaft system, there will be an additional mass representing the exciter rotor (see example shown in Figure 15.6).

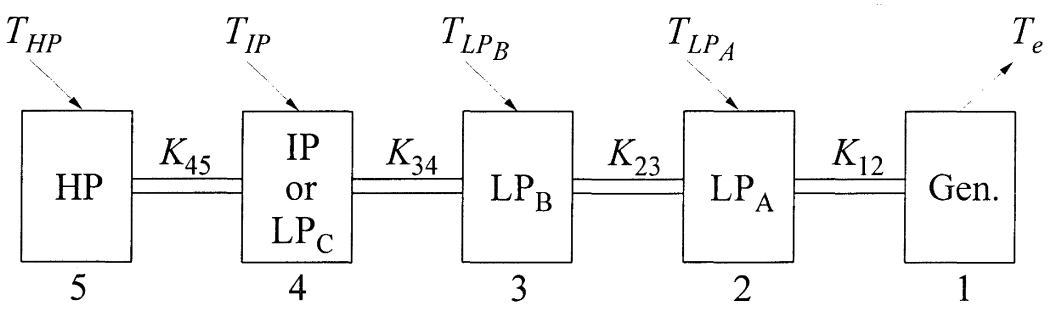


Figure 15.1 Structure of a typical lumped-mass shaft system model

In developing the mathematical equations of the shaft system, we use the following notation:

T_{HP}, T_{IP}, T_{LP_A}, T_{LP_B} = mechanical torques developed by the respective turbine sections in pu

T_e = generator air-gap torque in pu

ω_0 = rated speed in electrical rad/s = $2\pi f_0$ = 377 for 60 Hz
ω_{0m} = rated speed in mechanical rad/s = $(2/p_f)\omega_0$
p_f = number of field poles
ω_i = speed of mass i in electrical rad/s
δ_i = angular position of mass i in *electrical radians* with respect to a synchronously rotating reference = $\omega_i t - \omega_0 t + \delta_{i0}$
$\Delta\omega_i$ = speed deviation of mass i in pu = $(\omega_i - \omega_0)/\omega_0$
D = damping coefficient or factor in pu torque/pu speed deviation
H = inertia constant in MW·s/MVA
K = shaft stiffness in pu torque/electrical rad
t = time in seconds

The shaft system dynamic characteristics are defined by three sets of parameters: inertia constant H of the individual masses, torsional stiffness K of shaft sections connecting adjacent masses, and damping coefficient D associated with each mass. The following is a description of each of the parameters.

Inertia constant H

The inertia assigned to each rotor mass includes its share of shaft inertia. Turbine blades are assumed to be rigidly connected to the rotor. If the moment of inertia of a rotor mass is J kg·m^2, the per unit inertia constant H (see Chapter 3, Section 3.9) is given by

$$H = J\frac{1}{2}\frac{\omega_{0m}^2}{\text{VA}_{base}} = J\frac{1}{2}\frac{[2\pi\ (\text{r/min})/60]^2}{\text{VA}_{base}}$$

Torsional stiffness K

For a shaft of uniform cross-section undergoing elastic strain, the torsional stiffness or spring constant is given by [1]

$$K = \frac{GF}{l} \tag{15.1}$$

where

G = rigidity modulus of shaft material
F = form factor which defines the geometric property
l = length of shaft

For a solid shaft of circular cross-section with diameter d,

$$F = \frac{\pi d^4}{32} \tag{15.2}$$

The torsional stiffness defines the relationship between the torque transmitted and the angular twist between the two ends of the shaft:

$$T = K\theta \tag{15.3}$$

where

T = torque, N·m
θ = twist, rad
K = stiffness, N·m/rad

In a turbine-generator rotor, each shaft span consists of several sections of different diameters. The torsional stiffness of each section is determined and then a single equivalent stiffness is computed as follows:

$$\frac{1}{K_{total}} = \sum \frac{1}{K_{individual\,section}}$$

For the representation of turbine-generator shaft systems in power system studies, angles are expressed in electrical radians (or degrees). With the number of generator field poles equal to p_f,

$$\theta \text{ electrical rad} = (\theta \text{ mechanical rad})\frac{p_f}{2}$$

In system studies, torque is normally expressed in per unit with the base torque equal to

$$T_{base} = \frac{VA_{base}}{\omega_{0m}} = VA_{base}\frac{p_f}{2\omega_0}$$

The torsional stiffness is then given by

$$K \text{ pu torque/electrical rad} = \frac{K \text{ N·m/mechanical rad}}{(p_f/2)\, T_{base}}$$

$$= \frac{K \text{ N·m/mechanical rad}}{\text{VA}_{base}} \left(\frac{4\omega_0}{p_f^2} \right)$$

Damping coefficient or factor D [2-6]

There are a number of sources contributing to the damping of torsional oscillations:

(a) Steam forces on turbine blades. The oscillation of the turbine blades in the steady-state steam flow introduces damping. As an approximation, this may be represented as being proportional to the speed deviation of the respective turbine section.

(b) Shaft material hysteresis. When the interconnecting shaft sections twist, damping is introduced due to the mechanical hysteresis of the shaft material as it undergoes cyclic stress-strain variations.

(c) Electrical sources. Generator, exciter, and transmission networks contribute to damping of oscillations.

The damping levels associated with torsional oscillations are very small and are a function of the turbine-generator output. Time constants associated with the decay of torsional oscillations range from 4 to 30 seconds.

The various mechanisms contributing to torsional damping are complex and their contributions are difficult to predict. There is a high degree of variability in the torsional mode damping even among similar units. The best means of determining the actual damping levels is through station tests [3].

In our model of the shaft system, we will assume that all sources of damping may be represented in terms of damping torques proportional to speed deviations of individual masses; that is, damping torques between rotors are assumed to be negligible.

Shaft system equations

We will illustrate the development of equations of individual masses by considering the rotors of the generator and LP_A turbine shown in Figure 15.2.

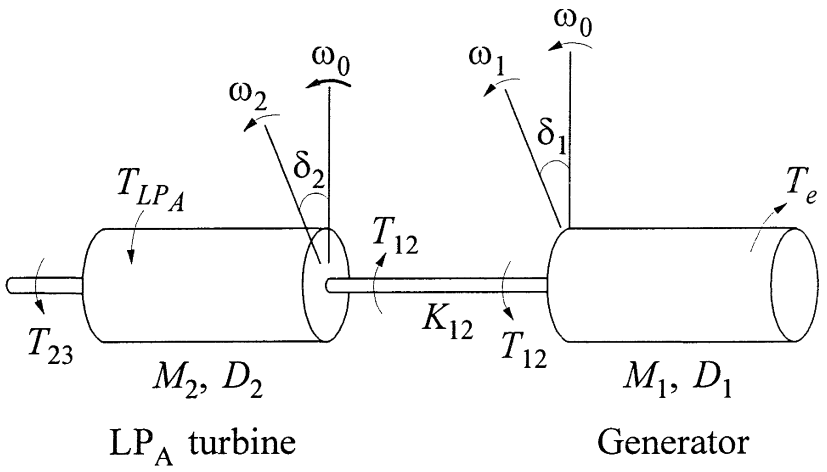


Figure 15.2

The various components of torque associated with the *generator rotor* are as follows:

Input torque $= T_{12} = K_{12}(\delta_2 - \delta_1)$
Output torque $= T_e$
Damping torque $= D_1(\Delta\omega_1)$
Accelerating torque $= T_a = T_{12} - T_e - D_1\Delta\omega_1$

The equations of motion of the generator rotor are

$$2H_1 \frac{d(\Delta\omega_1)}{dt} = T_a = K_{12}(\delta_2 - \delta_1) - T_e - D_1(\Delta\omega_1)$$

$$\frac{d(\delta_1)}{dt} = (\Delta\omega_1)\omega_0$$

Similarly, the following are the equations of the *LP_A turbine section*:

Input torque $= T_{LP_A} + T_{23} = T_{LP_A} + K_{23}(\delta_3 - \delta_2)$
Output torque $= T_{12} = K_{12}(\delta_2 - \delta_1)$
Damping torque $= D_2(\Delta\omega_2)$

Equations of motion:

$$2H_2 \frac{d(\Delta\omega_2)}{dt} = T_{LP_A} + K_{23}(\delta_3 - \delta_2) - K_{12}(\delta_2 - \delta_1) - D_2(\Delta\omega_2)$$

$$\frac{d\delta_2}{dt} = (\Delta\omega_2)\omega_0$$

The equations of the *complete rotor system* shown in Figure 15.1 may be summarized as follows :

GEN:

$$2H_1\frac{d(\Delta\omega_1)}{dt} = K_{12}(\delta_2-\delta_1) - T_e - D_1(\Delta\omega_1)$$

$$\frac{d(\delta_1)}{dt} = (\Delta\omega_1)\omega_0$$

LP_A:

$$2H_2\frac{d(\Delta\omega_2)}{dt} = T_{LP_A} + K_{23}(\delta_3-\delta_2) - K_{12}(\delta_2-\delta_1) - D_2(\Delta\omega_2)$$

$$\frac{d(\delta_2)}{dt} = (\Delta\omega_2)\omega_0$$

LP_B:

$$2H_3\frac{d(\Delta\omega_3)}{dt} = T_{LP_B} + K_{34}(\delta_4-\delta_3) - K_{23}(\delta_3-\delta_2) - D_3(\Delta\omega_3)$$

$$\frac{d(\delta_3)}{dt} = (\Delta\omega_3)\omega_0 \qquad (15.4)$$

IP:

$$2H_4\frac{d(\Delta\omega_4)}{dt} = T_{IP} + K_{45}(\delta_5-\delta_4) - K_{34}(\delta_4-\delta_3) - D_4(\Delta\omega_4)$$

$$\frac{d(\delta_4)}{dt} = (\Delta\omega_4)\omega_0$$

HP:

$$2H_5\frac{d(\Delta\omega_5)}{dt} = T_{HP} - K_{45}(\delta_5-\delta_4) - D_5(\Delta\omega_5)$$

$$\frac{d(\delta_5)}{dt} = (\Delta\omega_5)\omega_0$$

During a transient condition, the generator air-gap torque is determined by the dynamics of the generator and the power system to which it is connected. The torques generated by the individual turbine sections (i.e., T_{HP}, T_{IP}, T_{LP_A}, T_{LP_B}) depend on the dynamics of the steam turbine and its governing system (see Chapter 9).

Example 15.1

The data applicable to a five-mass torsional model (see Figure 15.1) of 960 MVA, 24 kV, 0.9 pf, 1,800 r/min (four poles) nuclear unit with a static exciter is as follows:

Mass No.	Rotor	Power* Fraction	WR^2 lb·ft^2	Shaft Section	Stiffness lb·ft/rad
1	GEN	–	1,114,382	GEN-LP_A	279,823,373
2	LP_A	0.24	1,831,389	LP_A-LP_B	235,204,647
3	LP_B	0.24	1,830,972	LP_B-LP_C	207,786,864
4	LP_C	0.24	1,830,417	LP_C-HP	133,530,219
5	HP	0.28	225,240		

* Fraction of total turbine power generated by the respective turbine sections under steady state

(a) Determine the inertia constant H in MW·s/MVA for each of the five masses and the stiffness K in pu torque/electrical rad for each of the four shaft sections.

(b) Compute the steady-state value of torque transmitted by each shaft section and the angular displacement between the generator and HP turbine section, when the generator is operating at rated output.

Solution

(a) The moment of inertia of the HP section rotor (mass 5) is

$$J_5 = (WR^2 \text{ lb·ft}^2)\frac{1.356}{32.2}$$

$$= 225{,}240 \times \frac{1.356}{32.2}$$

$$= 9485.3 \quad \text{kg·m}^2$$

The corresponding inertia constant is

$$H_5 = \frac{1}{2} J \left(\frac{2\pi \text{ r/min}}{60}\right)^2 \frac{1}{\text{VA rating}}$$

$$= \frac{1}{2} \times 9485.3 \times \left(\frac{2\pi \times 1800}{60}\right)^2 \frac{1}{960 \times 10^6}$$

$$= 0.1755 \quad \text{MW·s/MVA}$$

Similarly, the inertia constants of the other masses are

LP_C section : $H_4 = 1.4270$
LP_B section : $H_3 = 1.4275$
LP_A section : $H_2 = 1.4278$
Generator : $H_1 = 0.8688$

The torsional stiffness of the shaft between the HP and LP_C turbine sections is

$$K_{45} = 1.356K \text{ lb-ft/rad}$$
$$= 1.356 \times 133{,}530{,}219$$
$$= 181{,}066{,}980 \text{ N-m/mech. rad}$$

Expressing this in pu torque/electrical rad, we have

$$K_{45} = \frac{181{,}066{,}980}{\text{VA}_{base}} \left(\frac{4\omega_0}{p_f^2} \right)$$
$$= \frac{181{,}066{,}980}{960 \times 10^6} \times \frac{4 \times 377}{4^2}$$
$$= 17.78 \text{ pu torque/elec. rad}$$

The torsional stiffnesses of other shaft sections expressed in pu torque/electrical rad are

LP_C - LP_B : $K_{34} = 27.66$
LP_B - LP_A : $K_{23} = 31.31$
LP_A - GEN : $K_{12} = 37.25$

(b) The air-gap torque (T_e) in per unit on 960 MVA base is 0.9.

The torques developed by the different turbine sections are

$$T_{LP_A} = T_{LP_B} = T_{LP_C} = 0.24 \times 0.9 = 0.216 \text{ pu}$$
$$T_{HP} = 0.28 \times 0.9 = 0.252 \text{ pu}$$

The torque transmitted by the shaft section between the generator and LP_A is

$$T_{12} = T_e = 0.9 \text{ pu}$$

Therefore, the angle by which LP_A rotor leads the generator rotor is

$$\delta_{21} = \delta_2 - \delta_1 = T_{12}/K_{12}$$

$$= 0.9/37.25 = 0.02416 \quad \text{elec. rad}$$

The torque transmitted by shaft between LP_A and LP_B turbine sections is

$$T_{23} = T_{12} - T_{LP_A} = 0.9 - 0.216 = 0.684 \quad \text{pu}$$

Hence,

$$\delta_{32} = \delta_3 - \delta_2 = T_{23}/K_{23}$$

$$= 0.684/31.31 = 0.02185 \quad \text{elec. rad}$$

Similarly,

$$\delta_{43} = \delta_4 - \delta_3 = T_{34}/K_{34}$$

$$= (0.684 - 0.216)/27.66 = 0.01692 \quad \text{elec. rad}$$

and

$$\delta_{54} = \delta_5 - \delta_4 = T_{45}/K_{45}$$

$$= 0.252/17.78 = 0.01417 \quad \text{elec. rad}$$

Thus, the HP section rotor leads the generator rotor by

$$\delta_5 - \delta_1 = \delta_{54} + \delta_{43} + \delta_{32} + \delta_{21}$$

$$= 0.01417 + 0.01692 + 0.02185 + 0.02416$$

$$= 0.0771 \quad \text{elec. rad}$$

$$= 4.42 \quad \text{elec. degrees}$$

■

15.1.2 Torsional Natural Frequencies and Mode Shapes

The natural frequencies and mode shapes can be determined by using the modal analysis technique described in Chapter 12. This requires writing Equation 15.4 in the state-space form:

$$\dot{\mathbf{x}} = \mathbf{A}\mathbf{x} \tag{15.5}$$

For a small perturbation, the generator air-gap torque may be expressed as

$$T_e = K_S \Delta\delta_1 \tag{15.6}$$

where K_S is the synchronizing torque coefficient (see Chapter 12, Section 12.3).

The linearized equations of the rotor system may be readily written by inspection of Equations 15.4. For example, the generator rotor equations are

$$\frac{d(\Delta\omega_1)}{dt} = -\frac{D_1}{2H_1}(\Delta\omega_1) - \frac{K_{12}+K_S}{2H_1}(\Delta\delta_1) + \frac{K_{12}}{2H_1}(\Delta\delta_2)$$

$$\frac{d(\Delta\delta_1)}{dt} = \omega_0(\Delta\omega_1)$$

and the equations of the LP_A turbine section are

$$\frac{d(\Delta\omega_2)}{dt} = \frac{K_{12}}{2H_2}(\Delta\delta_1) - \frac{D_2}{2H_2}(\Delta\omega_2) - \frac{K_{12}+K_{23}}{2H_2}(\Delta\delta_2) + \frac{K_{23}}{2H_2}(\Delta\delta_3)$$

$$\frac{d(\Delta\delta_2)}{dt} = \omega_0(\Delta\omega_2)$$

Here, we have assumed that the mechanical torque T_{LP_A} developed by the turbine section is constant.

The state variables are thus the speed deviations $\Delta\omega_i$ and the rotor angle $\Delta\delta_i$, with i=1 to 5. The elements of the state matrix **A** of the rotor system depend on the torsional stiffness coefficients, the inertia constants of the individual masses, and the generator synchronizing torque coefficient K_S.

The eigenvalues of **A** give the natural frequencies of the shaft system. The corresponding eigenvectors give the "mode shape," i.e., the relative activity of a state variable in a given mode.

Examples of torsional characteristics

Figure 15.3 shows the natural frequencies and mode shapes of the rotor of a 555 MVA, 3,600 r/min fossil-fuel-fired generating unit with a static exciter. Also shown in the figure are the inertia constants of the masses and the stiffnesses of the shaft sections connecting them. The synchronizing torque coefficient (electrical stiffness) K_S is assumed to be 1.98 pu torque/rad. Damping coefficients are assumed to be negligible; this has no effect on the calculation of the natural frequencies or the mode shape.

Since we are considering a rotor with five masses, there are five modes of oscillation. The natural frequencies, as given by the imaginary components of the eigenvalues of the matrix **A**, are 1.67 Hz, 16.35 Hz, 24.1 Hz, 30.3 Hz, and 44.0 Hz.

H (MW·s/MVA)	0.124	0.232	1.155	1.192	0.855
K (pu torque/rad)	21.8	48.4	75.6	62.3	1.98

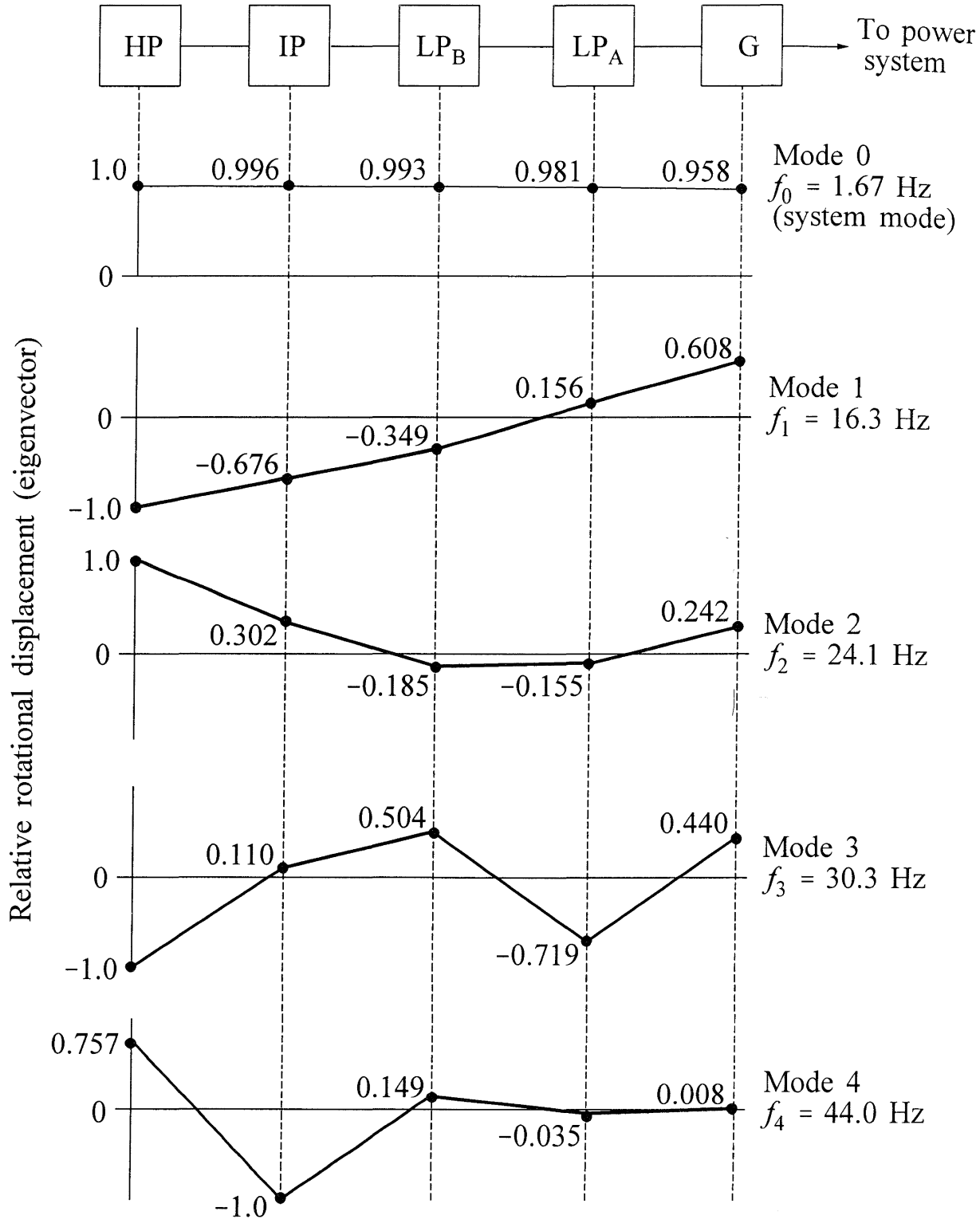


Figure 15.3 Rotor natural frequencies and mode shapes of a 555 MVA, 3,600 r/min steam turbine generator

The relative rotational displacements of the individual masses for each mode of oscillation are given by the right eigenvector of the corresponding eigenvalue. The elements of the eigenvector associated with either the speed deviations or the angle deviations may be used. In the plots shown in Figure 15.3, each eigenvector has been normalized so that its largest element is equal to 1.0.

The 1.67 Hz mode represents the oscillation of the entire rotor against the power system. This is the mode normally considered in system stability studies. It depends on the synchronizing torque coefficient K_S and the sum of the inertia constants of all the rotor masses. As seen by the mode shape, all five masses participate nearly equally in this mode.

The other four modes represent the torsional modes of oscillation. The first torsional mode has a natural frequency of 16.3 Hz. It has one polarity reversal in the mode shape. The polarities of eigenvector elements associated with the rotors of the generator and the LP_A section are opposite to those associated with the rotors of the LP_B, IP, and HP sections. This indicates that the generator and LP_A rotors oscillate against the other three rotors when this mode is excited.

The second torsional mode has a natural frequency of 24.1 Hz, and its mode shape has two polarity reversals. The third torsional mode, with a natural frequency of 30.3 Hz, has three polarity reversals in its mode shape. Finally, the fourth torsional mode, with a natural frequency of 44.0 Hz, has a mode shape with four polarity reversals.

In Figure 15.3, the rotors of the generator and the LP_A section have very low relative amplitudes of rotational displacement in the fourth torsional mode. This means that this mode cannot be easily excited by applying torques to the generator and LP_A turbine rotors.

In a general case, a rotor with n masses has $n-1$ torsional modes. The i^{th} torsional mode has the i^{th} highest torsional frequency, and its mode shape has i polarity reversals.

Figures 15.4 to 15.6 provide additional examples of torsional characteristics. Only the torsional modes are shown, and the system mode is omitted.

The torsional characteristic shown in Figure 15.4 is that of the 960 MVA, 1,800 r/min (four pole) nuclear unit considered in Example 15.1. This unit has one HP and three LP turbine sections. Its torsional frequencies are 8.4 Hz, 15.2 Hz, 20.3 Hz, and 23.6 Hz.

Figure 15.5 shows the torsional characteristics of a 191 MVA, 3,600 r/min (two pole) coal-fired unit with a static exciter. It has three turbine sections: HP, IP, and one LP. Hence, the rotor is represented by four lumped masses. The principal torsional frequencies are 22.4 Hz, 29.6 Hz, and 52.7 Hz.

H (MW·s/MVA)	0.176	1.427	1.428	1.428	0.869
K (pu torque/rad)		17.78	27.66	31.31	37.25

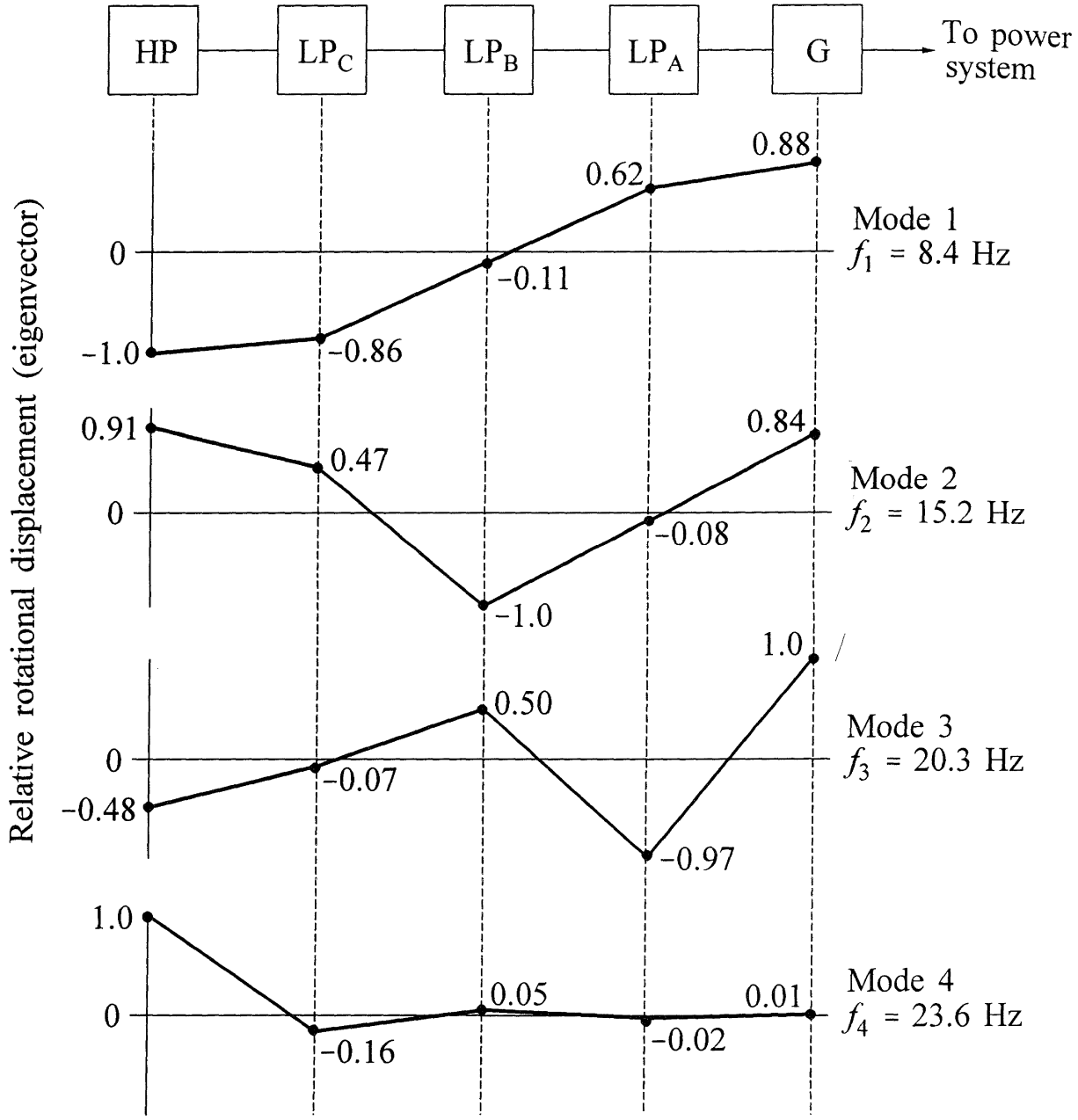


Figure 15.4 Torsional natural frequencies and mode shapes of a 960 MVA, 1,800 r/min turbine generator

H (MW·s/MVA)	0.099	0.337	3.68	0.946
K (pu torque/rad)	37.95	81.91	82.74	

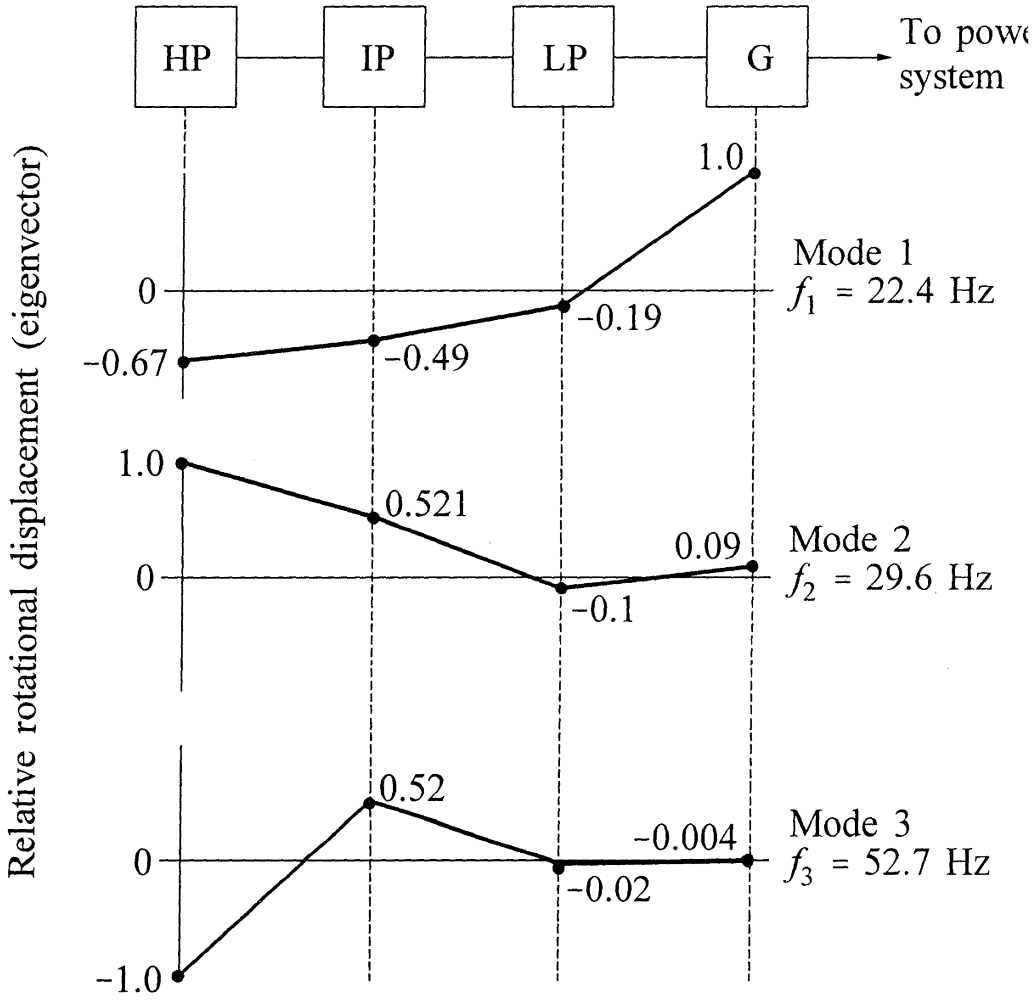


Figure 15.5 Torsional natural frequencies and mode shapes of a 191 MVA, 3,600 r/min turbine generator

Figure 15.6 shows the torsional characteristics of a 635 MVA, 1,800 r/min (four pole) unit with a rotating exciter (EX). The rotor is represented by six lumped masses.

H (MW·s/MVA)	0.254	0.983	1.001	1.009	1.035	0.013
K (pu torque/rad)		13.9	18.2	25.2	54.9	5.7

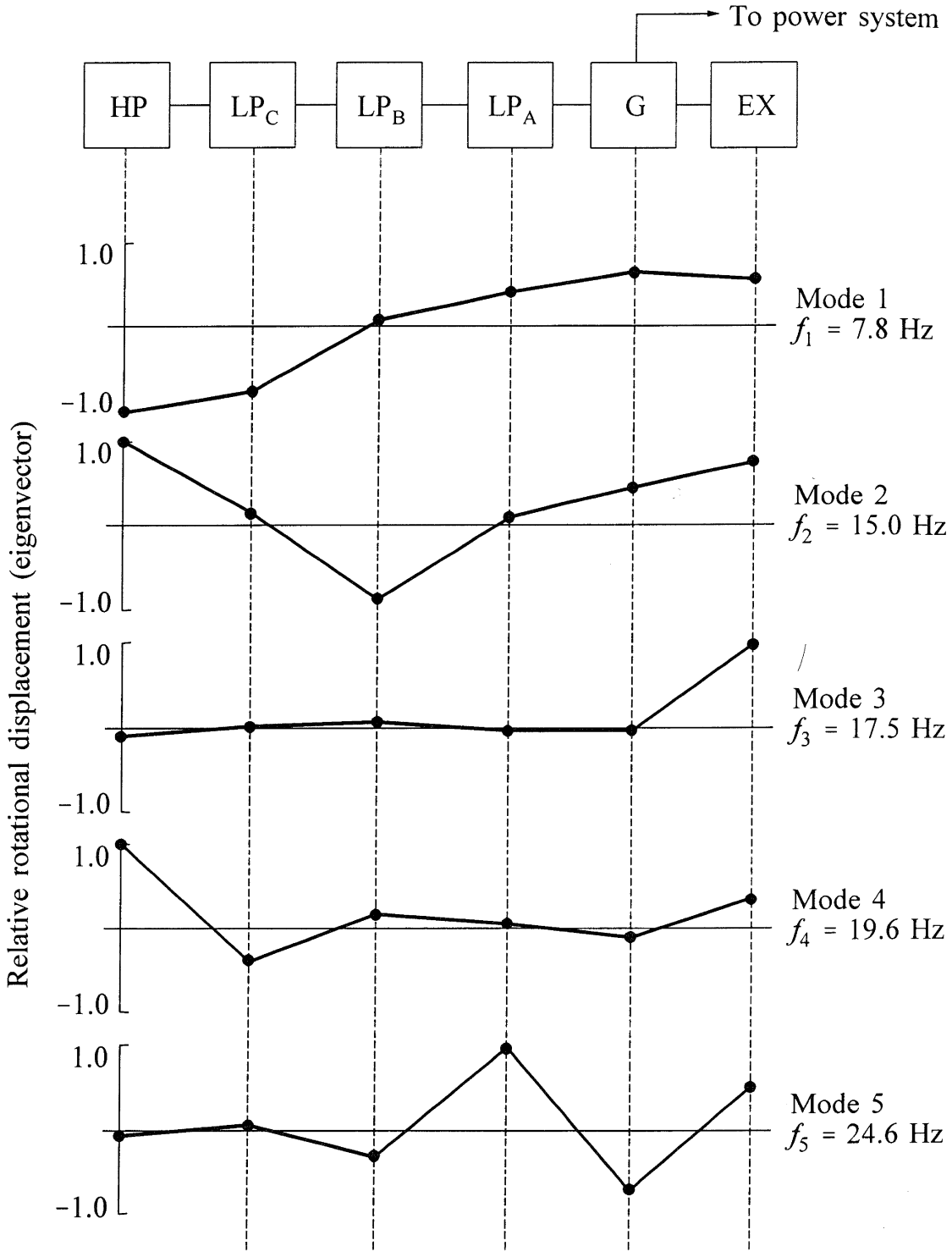


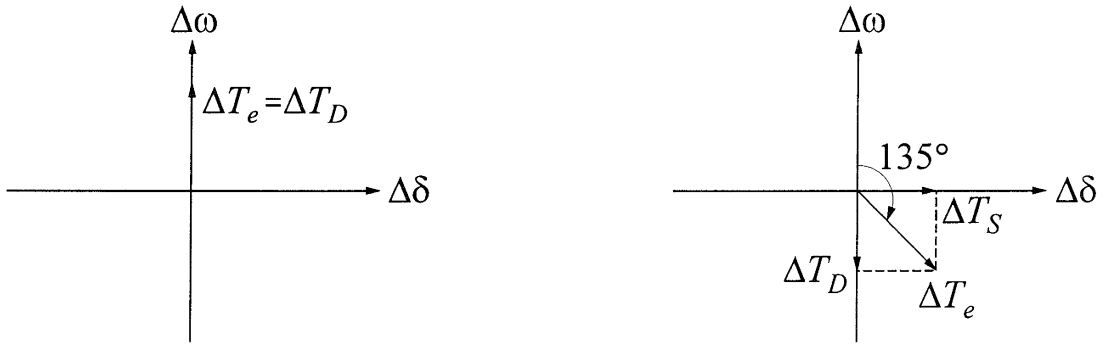
Figure 15.6 Torsional natural frequencies and mode shapes of a 635 MVA, 1,800 r/min turbine generator with a rotating exciter

15.2 TORSIONAL INTERACTION WITH POWER SYSTEM CONTROLS

As discussed in the previous section, torsional oscillations of turbine generators are inherently lightly damped. While the level of damping can vary to some extent with steam conditions and unit output, normally it is not affected by the generating unit or network controls. However, there have been several instances of torsional mode instability due to interactions with the generating unit excitation and prime mover controls, and with nearby HVDC converter controls. In this section, we describe the causes of such torsional instability problems and methods of analyzing and mitigating the problems.

15.2.1 Interaction with Generator Excitation Controls

Torsional mode destabilization by excitation control was first observed in 1969 during application of a power system stabilizer (PSS) on a 555 MVA, 3,600 r/min fossil-fuel-fired unit at the Lambton generation station in Ontario [7,8]. The PSS, which used a stabilizing signal based on speed measured at the generator end of the turbine-generator shaft, was found to excite the lowest torsional mode. The reason for this can be readily seen from the torsional characteristics shown in Figure 15.3, which are similar to those of the Lambton units. Shaft speed measured at the generator end has a high component of the 16 Hz torsional mode. The stabilizer transfer function is designed to provide zero phase shift between the input speed signal and air-gap torque at the system mode frequency of 1.67 Hz, so as to result in a purely damping torque component as shown in Figure 15.7(a) (see Chapter 12). However, the generator characteristics are such that this results in a phase lag of about 135° at 16 Hz [8]. As shown in Figure 15.7(b), the effect is to produce a negative damping torque component and hence instability of the 16 Hz torsional mode.



(a) Pure damping torque at 1.67 Hz

(b) Negative damping torque and positive synchronizing torque at 16 Hz

Figure 15.7 Torque components due to PSS

This problem was solved by sensing speed between the two LP turbine sections, close to the "node" of the 16 Hz torsional mode (see Figure 15.3). At this speed pickup location, other torsional modes also have very low amplitude. In addition, an electronic filter, with a notch at 16 Hz and substantial attenuation at other torsional frequencies, was used in the stabilizing path.

The modal analysis approach described in Chapter 12 is ideally suited for investigation of torsional stability problems. This is illustrated in Example 15.2.

Torsional mode instability through excitation control may also be caused by a terminal voltage limiter which uses feedback of terminal voltage to control excitation through a very high gain [8]. This can cause torsional instability, unless some kind of filtering is provided to attenuate high frequency components of the voltage signal.

Example 15.2

This example considers the effect of PSS on the torsional stability of an 889 MVA, 18.5 kV, 1,800 r/min generating unit with a tandem-compound turbine. The shaft system representation is shown in Figure E15.1. It is similar to that of Figure 15.4, except that each double flow LP turbine section is represented by two masses.

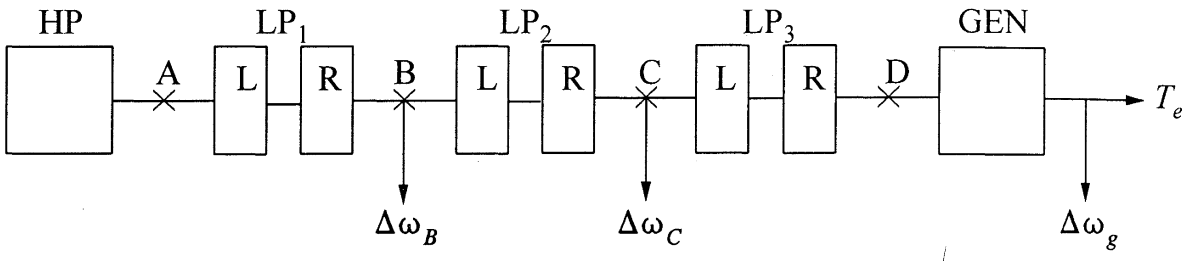


Figure E15.1 Shaft system representation

The shaft system data are as follows:

Mass	Inertia (WR^2 in lb·ft^2)	Damping Coefficient (pu torque/pu speed)
Generator	1,081,920	0
LP_{3R} or LP_{3L}	1,054,512	0.125
LP_{2R} or LP_{2L}	1,067,855	0.125
LP_{1R} or LP_{1L}	1,048,380	0.125
HP	258,000	0.125

Shaft Section	Stiffness (lb·ft/rad)	Shaft Section	Stiffness (lb·ft/rad)
Gen - Coupl D	844,391,342	LP_{2L} - Coupl B	625,948,703
Coupl D - LP_{3R}	859,316,929	Coupl B - LP_{1R}	626,684,214
LP_{3R} - LP_{3L}	2,545,306,455	LP_{1R} - LP_{1L}	2,548,322,567
LP_{3L} - Coupl C	627,555,327	LP_{1L} - Coupl A	566,819,519
Coupl C - LP_{2R}	628,294,620	Coupl A - HP	212,716,172
LP_{2R} - LP_{2L}	2,546,764,972		

The mechanical torque developed by each turbine section is assumed to be constant. The system is represented as shown in Figure E15.2 with parameters expressed in per unit on 889 MVA and 18.5 kV.

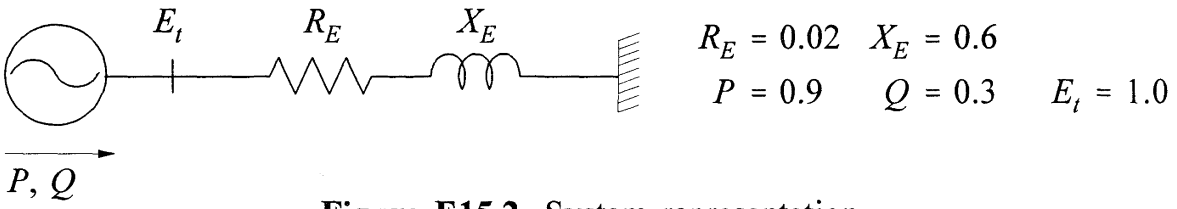


Figure E15.2 System representation

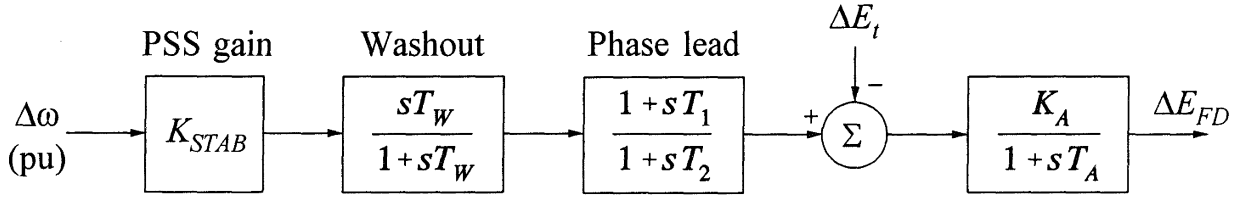
The generator parameters in per unit on 889 MVA and 18.5 kV are as follows:

$X_d = 1.72$ $X'_d = 0.36$ $X''_d = 0.24$ $T'_{d0} = 5.7$ s $T''_{d0} = 0.02$ s

$X_q = 1.69$ $X'_q = 0.40$ $X''_q = 0.23$ $T'_{q0} = 1.5$ s $T''_{q0} = 0.04$ s

The generator is equipped with a thyristor exciter. Our objective is to examine the system performance with the following alternative forms of PSS:

(a) A delta-omega stabilizer with shaft speed ($\Delta\omega$) as input signal and with speed measured at the generator end, at coupling B, at coupling C, or at both couplings B and C. The excitation system model is shown in Figure E15.3.



$K_A = 200$ $T_A = 0.005$ s $T_1 = 0.3$ s $T_2 = 0.06$ s $T_W = 1.5$ s

Figure E15.3 Thyristor exciter with delta-omega stabilizer

(b) A stabilizer as above, but with a torsional filter having a notch at 9 Hz and substantial attenuation at the higher torsional natural frequencies. The transfer function of the filter is

$$\frac{V_o}{V_i} = \frac{1 + s^2\, 0.00031258}{(1 + s\, 0.022 + s^2\, 0.000756)(1 + s\, 0.012 + s^2\, 0.009)}$$

(c) A stabilizer with electrical power deviation (delta-P) as stabilizing signal as shown in Figure E15.4. This system is similar to that of Figure E15.3, except that an equivalent speed ($\Delta\omega_{eq}$) derived from electrical power is used instead of actual shaft speed.

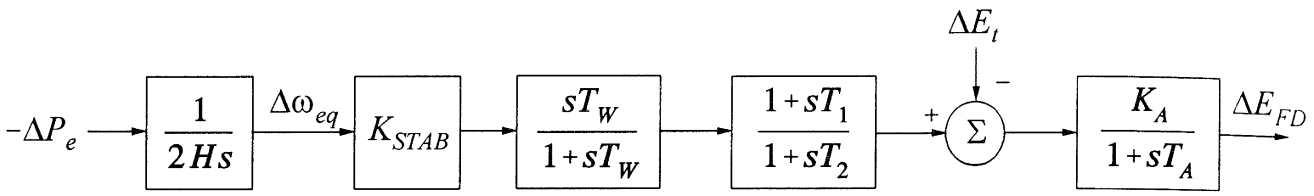


Figure E15.4 Thyristor exciter with delta-P stabilizer

Analysis

(a) *Delta-omega stabilizer.* The effects of PSS are examined by using the modal analysis approach described in Chapter 12. The analysis considers the effects of sensing speed ($\Delta\omega$) at different locations on the shaft. For each case, two or three values of the stabilizer gain K_{STAB} are considered to give an indication of the effect of varying the gain. The results are summarized in Table E15.1, where the six pairs of eigenvalues listed represent six modes which are important from the viewpoint of stabilizer application. The imaginary component of each complex pair of eigenvalues gives the frequency of oscillation in radians per second. The real component gives the rate of decay of the amplitude of oscillation (see Chapter 12).

The first four modes listed in Table E15.1 represent the dominant *torsional modes.* The fifth mode, identified as the *system mode*, is associated with the oscillation of the generator rotor with respect to the rest of the power system. Improving the damping of the system mode is the reason for using the speed signal feedback to the exciter. The sixth mode, identified as the *exciter mode*, is primarily associated with the field voltage and exists only in the presence of speed stabilization. This mode is usually heavily damped and becomes unstable only for high values of K_{STAB}. One of the considerations in choosing the parameters of the speed signal feedback circuit is to achieve maximum damping of the system mode without significantly sacrificing the damping of the exciter mode.

We see from the results that, without the speed signal stabilization (K_{STAB}=0), the system mode has a positive real part representing small-signal instability. The

eigenvalues associated with the torsional modes, without speed stabilization, give the original level of torsional damping and serve as a reference for purposes of comparison.

The results also show that the effect of sensing speed at the generator end is to cause either instability or decreased damping of all four torsional modes, while significantly damping the system mode.

Sensing speed only at coupling B has an adverse effect on the 23 Hz torsional mode, and sensing only at coupling C has an adverse effect on the 9 Hz torsional mode. Results obtained with the speed signal sensed at other possible locations along the shaft indicated that there is no single location that is acceptable for all torsional modes.

A combination of signals sensed at couplings B and C is seen to have favourable effects on all four torsional modes. The system mode itself is insensitive to speed sensing location and depends only on the stabilizer gain. The exciter mode is heavily damped for the entire range of the stabilizer gain considered, although a higher gain results in a slight reduction of its damping.

(b) *Delta-omega stabilizer with torsional filter.* The results of the analysis with the filter added in the speed signal loop are summarized in Table E15.2. The effect of the filter, as expected, is to make the torsional modes insensitive to the speed signal stabilization. The damping of the system mode with the filter is on the same order as that without the filter. However, the filter has an adverse effect on the exciter mode. This is because the characteristic of the filter circuit is such that it increases the gain in the frequency range associated with the exciter mode. As a consequence, the speed signal gain has to be limited to a value which gives sufficient stability margin for the exciter mode. The limiting value of the gain depends on the external system impedance, generator characteristics, and system-operating conditions [9]. With a lower value of X_E, the exciter mode is less stable.

(c) *Delta-P stabilizer.* The results are summarized in Table E15.3. They show that a delta-*P* stabilizer is effective without causing instability of the torsional modes. So far as the system and the exciter modes are concerned, there is very little difference between the delta-*P* stabilizer and the delta-omega stabilizer without a torsional filter.

Table E15.1 Effect of delta-omega stabilization without a torsional filter circuit

K_{STAB}	Speed Sensing Location	Torsional Modes				System Mode	Exciter Mode
		9 Hz	17 Hz	23 Hz	24 Hz		
0.0	-	-0.05±j56.2	-0.07±j105.7	-0.10±j146.1	-0.17±j151.2	+0.23±j5.7	-
9.5	Generator	+0.31±j57.6	+0.20±j106.0	+0.24±j146.4	-0.06±j151.3	-0.73±j5.0	-13.7±j13.1
9.5	Coupl - B	-0.25±j55.3	-0.17±j105.6	-0.01±j146.2	-0.19±j151.2	-0.75±j5.0	-16.7±j13.9
19.0	Coupl - B	-0.47±j54.3	-0.28±j105.5	+0.07±j146.3	-0.20±j151.2	-1.20±j4.2	-14.5±j19.7
9.5	Coupl - C	+0.06±j56.6	-0.26±j105.5	-0.21±j146.1	-0.18±j151.2	-0.74±j5.0	-15.5±j13.7
19.0	Coupl - C	+0.20±j57.0	-0.46±j105.3	-0.31±j146.1	-0.19±j151.2	-1.20±j4.2	-12.8±j18.5
9.5	Both B and C	-0.10±j56.0	-0.22±j105.5	-0.11±j146.1	-0.19±j151.2	-0.74±j5.0	-16.1±j13.8
19.0	Both B and C	-0.16±j55.7	-0.37±j105.4	-0.12±j146.1	-0.20±j151.2	-1.20±j4.2	-13.6±j19.1
28.5	Both B and C	-0.22±j55.5	-0.52±j105.2	-0.13±j146.1	-0.21±j151.2	-1.36±j3.6	-11.9±j22.9

Table E15.2 Effect of delta-omega stabilization with a torsional filter

K_{STAB}	Speed Sensing Location	Torsional Modes				System Mode	Exciter Mode
		9 Hz	17 Hz	23 Hz	24 Hz		
0.0	-	-0.05±j56.2	-0.07±j105.7	-0.10±j146.1	-0.17±j151.2	+0.23±j5.7	-
9.5	Generator	-0.06±j56.2	-0.07±j105.7	-0.11±j146.1	-0.17±j151.2	-0.91±j5.1	-10.4±j15.8
9.5	Coupl - B	-0.05±j56.2	-0.07±j105.7	-0.10±j146.1	-0.17±j151.2	-0.94±j5.0	-8.1±j14.1
19.0	Coupl - B	-0.05±j56.2	-0.06±j105.7	-0.10±j146.1	-0.17±j151.2	-1.42±j4.1	-1.9±j20.5
9.5	Coupl - C	-0.06±j56.2	-0.07±j105.7	-0.10±j146.1	-0.17±j151.2	-0.92±j5.0	-10.5±j20.0
19.0	Coupl - C	-0.06±j56.2	-0.06±j105.7	-0.10±j146.1	-0.17±j151.2	-1.41±j4.2	-3.2±j20.0
9.5	Both B and C	-0.05±j56.2	-0.07±j105.7	-0.10±j146.1	-0.17±j151.2	-0.93±j5.0	-9.4±j21.3
19.0	Both B and C	-0.05±j56.2	-0.06±j105.7	-0.10±j146.1	-0.17±j151.2	-1.42±j4.2	-2.5±j20.4
28.5	Both B and C	-0.05±j56.2	-0.06±j105.7	-0.10±j146.1	-0.17±j151.2	-1.54±j3.5	+0.5±j20.6

Table E15.3 Effect of delta-P stabilization

K_{STAB}	Torsional Modes				System Mode	Exciter Mode
	9 Hz	17 Hz	23 Hz	24 Hz		
0	-0.05±j56.2	-0.07±j105.7	-0.10±j146.1	-0.17±j151.2	+0.23±j5.7	-
9.5	-0.05±j56.2	-0.07±j105.7	-0.10±j146.1	-0.17±j151.2	-0.75±j5.0	-15.6±j13.7
19.0	-0.05±j56.2	-0.07±j105.7	-0.10±j146.1	-0.17±j151.2	-1.20±j4.2	-13.1±j18.6
28.5	-0.05±j56.2	-0.07±j105.7	-0.10±j146.1	-0.17±j151.2	-1.40±j3.6	-11.3±j22.0

■

15.2.2 Interaction with Speed Governors

The problem of speed-governing systems causing torsional mode instability surfaced in 1983 during the commissioning of a 635 MVA, 1,800 r/min nuclear unit at Ontario Hydro [9]. This unit is equipped with a fast-acting electrohydraulic governing system. The speed governor senses speed at the HP turbine end of the shaft. The torsional mode shape for this unit is similar to that shown in Figure 15.6, which indicates that the 7.8 Hz, 15 Hz, and 19.6 Hz torsional modes will appear in the end-of-shaft speed signal. The governing system uses an electronic linearizing circuit to compensate for the nonlinear flow versus valve position characteristics of the steam valves (see Chapter 9, Section 9.2).

During the commissioning tests, when the unit reached the 100 MW output level, abnormal vibrations were detected in the governor valves. Changes to the phase lead and the valve-linearizing circuits (see Chapter 9, Figure 9.34) partially eliminated the vibrations, and the loading could be increased to 475 MW (nearly 88% of rated output). Beyond this level, severe vibrations of the governor valves were experienced. Unit load was reduced to a safe level until the problem was investigated and satisfactorily solved.

Further field investigations and computer simulations using the modal analysis identified two factors which contributed to the problem:

(a) Inaccuracies in the valve-linearizing circuit, particularly in the 475 MW region. As a result, the effective governor droop suddenly increased by a factor of about 12, as loading increased.

(b) Large bandwidth of the electrohydraulic servo system. This allowed significant governor interaction at the higher frequencies associated with the torsional modes.

The problem was solved by providing accurate linearization of valve characteristics which maintained a constant droop of 4% over the entire loading range. As an additional precaution, filters were added to eliminate torsional components from the speed signal. In designing the filters, careful consideration was given to the performance during severe system disturbances and load rejections.

15.2.3 Interaction with Nearby DC Converters

The problem of subsynchronous torsional mode instability due to interaction with controls of nearby HVDC systems first came to light on the Square Butte dc system in North Dakota [10,11]. The Square Butte system consists of a ±250 kV, 500 MW dc link. The rectifier station is located adjacent to the Milton Young generating station consisting of two turbine generators, one rated at 234 MW and the other at 410 MW. The converters employ equidistant firing systems. The normal regulator control modes are constant current control at the rectifier and constant voltage control at the

inverter. In addition, a supplementary *frequency sensitive power controller* (FSPC) is provided between the sending end and receiving end systems. Field tests showed that the supplementary damping control destabilized the first torsional mode (11.5 Hz) of the 410 MW generating unit. The tests also showed that the normal constant current control acting without the supplementary damping control could cause instability of the 11.5 Hz torsional mode when some of the ac lines near the rectifier were switched out. Opening of the ac lines reduced the ac system strength which resulted in the instability of the torsional mode. The torsional oscillations stabilized when the dc power level was reduced.

At the time these instabilities were observed, the current control was modified, so as to allow safe operation, with some constraints on the dc power level and the ac system conditions. Subsequently, following a detailed analysis, the control systems were modified so as to allow safe operation under all but extreme system conditions.

This problem has been the subject of investigation of the EPRI research project RP1425-1. The work carried out under this project has led to a broader understanding of the phenomenon and the development of generic solutions [12].

Basic phenomenon

Torsional mode oscillations cause phase and amplitude modulation of the generated alternating voltage waveform. The modulated voltage has frequency components equal to the fundamental frequency minus the torsional frequency (see Figure 15.8). This modulated voltage is impressed on the dc system commutating bus.

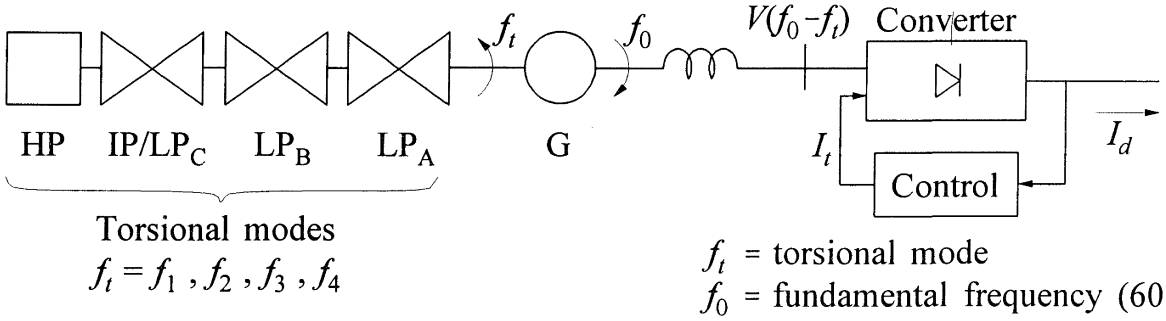


Figure 15.8 Torsional interaction with dc control

With the equidistant firing angle control used in modern HVDC converters, a shift in voltage phase due to a torsional mode causes a similar shift in the firing angle. This firing angle modulation, together with the alternating voltage magnitude modulation, will result in corresponding changes in direct voltage, current, and power. The closed-loop current control responds to correct for these changes. This in turn is reflected as a change in the generator power. If the net phase lag between the variation in shaft speed at the torsional frequency and the resulting change in

electrical torque of the generator exceeds 90°, the torsional oscillations become unstable. This situation is similar to that depicted in Figure 15.7(b).

Factors influencing torsional interaction [12,13]

The possibility of torsional instability due to interaction with nearby dc system controls depends on the rating of the dc system in relation to that of the generating unit and on the electrical distance between the two. Reference 12 recommends use of the *unit interaction factor* (UIF) defined below as a measure of the influence of dc system controls on torsional mode stability.

$$\text{UIF} = \frac{\text{MVA}_{dc}}{\text{MVA}_g}\left(1 - \frac{SC_g}{SC_t}\right)^2 \tag{15.7}$$

where

MVA_{dc} = MVA rating of the dc system
MVA_g = MVA rating of the generator
SC_t, SC_g = short-circuit capacity at the dc commutating bus (excluding ac filters) with and without the generator, respectively

If UIF is less than 0.1, there is little interaction between the torsional oscillation and the dc controls.

Parallel ac lines tend to minimize the possibility of torsional instability. Radial dc lines emanating from isolated thermal-generating stations are most prone to unfavourable torsional interaction.

The nominal firing angle of the rectifier has an impact on the degree of interaction. The tendency to cause torsional instability increases as the nominal firing angle is increased. Therefore, operating modes requiring the dc system voltages to be low may increase the possibility of torsional instability.

Effect of dc system controls [10,11]

In the case of the Square Butte project, the torsional instability was caused through two different control paths: the supplementary damping control and the rectifier current control.

The instability caused by the supplementary damping control was due to high gain and large phase lag in the frequency range at the lower end of the torsional natural frequencies. Only one of the two units near the rectifier had a torsional frequency (11.5 Hz) low enough to interact with the damping control. This problem could be readily solved by use of a notch filter at 11.5 Hz in the supplementary control. The other unit's first torsional frequency was so high as not to cause instability.

The influence of the current or power control depends on the regulator bandwidth. Typically, these controls have a bandwidth in the vicinity of 10 to 20 Hz. Only the torsional modes with frequencies below the upper range of the bandwidth have the potential for becoming unstable.

In the case of Square Butte, the problem due to the current control was solved by modifying the regulator frequency response characteristic. Some HVDC systems may require more than simple modifications of the current regulator to achieve stable operation. In such cases, an additional damping path may be required. In reference 12, a *subsynchronous damping control* (SSDC) has been developed to damp potentially troublesome torsional oscillations.

The problem of torsional interaction with the controls of HVDC systems may be investigated by using the modal analysis approach. Reference 13 describes other methods of studying the problem. Two effects must be accounted for in the simulations: (a) apparent shifts in the bridge firing angle due to shifts in phase of the bus voltage and (b) the speed variation (ω_r/ω_0) effects on the generator voltage [10].

15.3 SUBSYNCHRONOUS RESONANCE

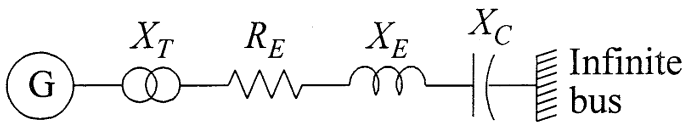
The phenomenon of *subsynchronous resonance* (SSR) occurs mainly in series capacitor-compensated transmission systems. The first SSR problem was experienced in 1970 resulting in the failure of a turbine-generator shaft at the Mohave plant in southern California. It was not until a second shaft failure occurred in 1971 that the real cause of the failure was recognized as subsynchronous resonance [14]. Since these failures, SSR has been a subject of considerable electric utility industry interest.

Before we discuss the SSR phenomenon, let us first examine the characteristics of a series capacitor-compensated system and the possibility of unstable subsynchronous oscillations.

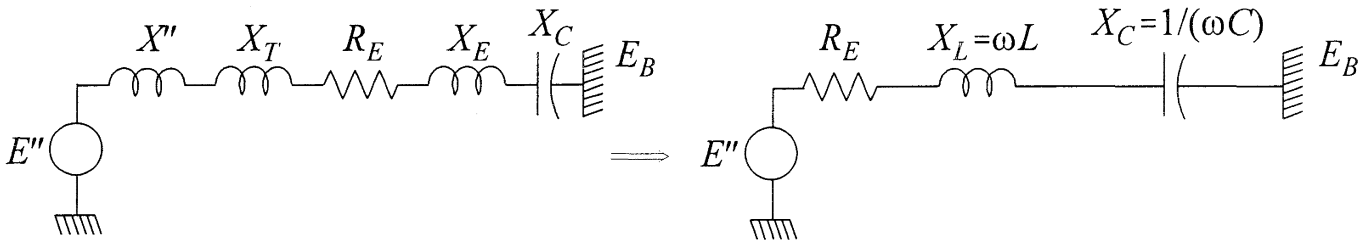
15.3.1 Characteristics of Series Capacitor-Compensated Transmission Systems [15,16]

In an *uncompensated* transmission system, faults and other disturbances result in dc offset components in the generator stator windings (see Chapter 3, Section 3.7.2). These currents, due to the space distribution of armature (stator) windings, result in a component of air-gap torque at the slip frequency of 60 Hz. In the case of unbalanced faults, the negative phase-sequence components of stator currents result in a 120 Hz (slip frequency) component of air-gap torque. Therefore, it is necessary to avoid having any of the torsional frequencies very near either 60 Hz or 120 Hz.

In *series capacitor-compensated* transmission systems, the situation can be very different. Consider, for example, the simple radial system shown in Figure 15.9. In this case, instead of the dc component of fault current, the offset transient current is also alternating current of frequency equal to the natural frequency (ω_n) of the circuit inductance and capacitance:



(a) Schematic diagram



(b) Equivalent circuit

Figure 15.9 Radial series compensated system

$$\omega_n = \frac{1}{\sqrt{LC}} = \frac{\omega_0}{\sqrt{(\omega_0 L)(\omega_0 C)}} = \omega_0 \sqrt{\frac{X_C}{X_L}} \text{ rad/s} \tag{15.8}$$

or

$$f_n = f_0 \sqrt{\frac{X_C}{X_L}} \text{ Hz} \tag{15.9}$$

where f_0 is the synchronous frequency in Hz, and $\omega_0 = 2\pi f_0$ rad/s.

Generator stator current components of frequency f_n induce rotor currents (and hence torque) of slip frequency $(60 - f_n)$ Hz. Table 15.1 shows the natural and slip frequencies as a function of the degree of compensation.

In practice, the frequency-dependent characteristic of the effective impedance of a network is complex and a more detailed system representation is required. A frequency scanning program such as that described in reference 18 can be used to determine this impedance.

The subsynchronous natural frequency (f_n) of the network and the frequency of the associated induced rotor currents (and torque) are said to be complementary, as their sum is equal to synchronous frequency. A series capacitor-compensated transmission network can cause sustained or negatively damped subsynchronous oscillations by two distinctive mechanisms: (a) self-excitation due to induction generator effect and (b) interactions with torsional oscillations.

Table 15.1

Percent Compensation $(X_C/X_L)\times 100$ (%)	Natural Frequency f_n (Hz)	Slip Frequency $60-f_n$ (Hz)
10	18	42
25	30	30
30	32.6	27.4
40	38	22
50	42.4	17.6

Shunt-compensated transmission systems normally have natural frequencies in the supersynchronous range; therefore, subsynchronous oscillations do not pose a problem. Exceptions are situations involving high degrees of shunt compensation and very long transmission.

15.3.2 Self-Excitation due to Induction Generator Effect

Figure 15.10 is a simplified equivalent circuit of a synchronous machine useful in explaining subsynchronous effects. The effect of saliency has been neglected and the machine has been represented by a circuit similar to that used for induction motors. The effects of the rotor circuits have been lumped and represented by a single circuit with a resistance R_r and a leakage reactance X_r. The power frequency quantities have been omitted and only subsynchronous frequency effects are considered.

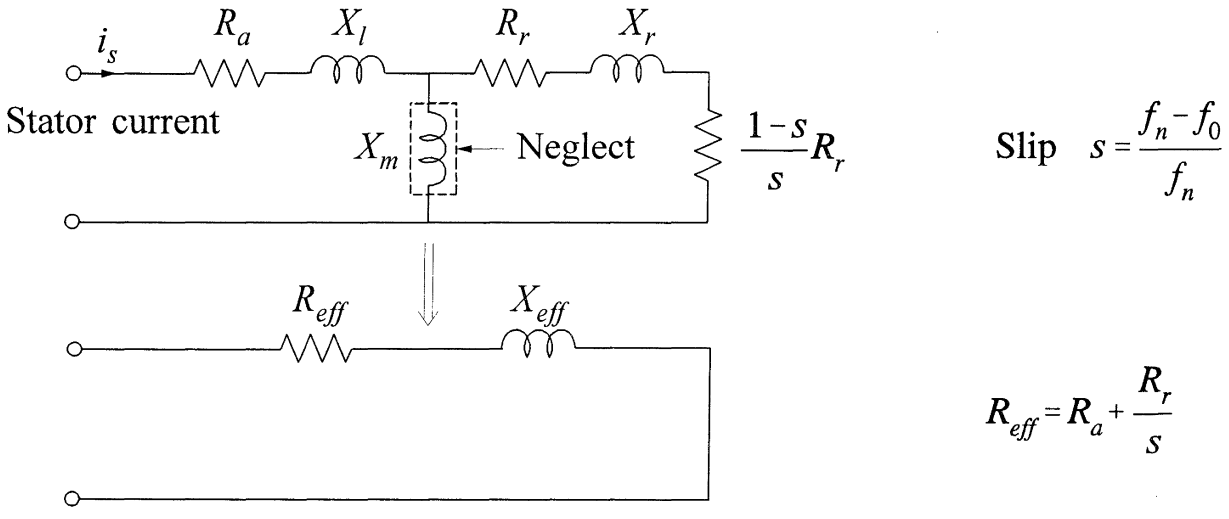


Figure 15.10 Simplified equivalent circuit of a synchronous machine applicable to subsynchronous frequency quantities

Since $f_n < f_0$, the slip s is negative, and the rotor behaves much like that of an induction machine running above synchronous speed. Depending on f_n, the effective resistance R_{eff} can be negative. At high degrees of compensation, this apparent negative resistance may exceed the network resistance, effectively resulting in an RLC circuit with negative resistance. Such a condition will result in self-excitation causing electrical oscillations of intolerable levels. The tendency toward this electrical subsynchronous instability is decreased by increasing the network resistance and by decreasing the resistance of generator rotor circuits (for example, by providing a good pole face damper winding).

This form of self-excitation is purely an electrical phenomenon and is *not* dependent on the shaft torsional characteristics.

15.3.3 Torsional Interaction Resulting in SSR

If the complement of the natural frequency (i.e., synchronous frequency minus the natural frequency) of the network is close to one of the torsional frequencies of the turbine-generator shaft system, torsional oscillations can be excited. This condition is referred to as *subsynchronous resonance* [16]. Under such conditions, a small voltage induced by rotor oscillations can result in large subsynchronous currents; this current will produce an oscillatory component of rotor torque whose phase is such that it enhances the rotor oscillation. When this torque is larger than that resulting from mechanical damping, the coupled electromechanical system will experience growing oscillations.

Subsynchronous resonance is thus a condition where the subsynchronous complement of the natural frequency of a series capacitor-compensated armature circuit of a turbine generator is close to its torsional natural frequencies, resulting in a strong coupling between the electrical and mechanical systems [17].

The consequences of subsynchronous resonance can be dangerous. If the torsional oscillations build up, the turbine-generator shaft will break with disastrous consequences. Even if the oscillations are not unstable, system disturbances can result in *shaft torques of high magnitude, causing loss of fatigue life* of the shaft.

15.3.4 Analytical Methods

Torsional interaction effects involve energy interchange between the generator shaft system and the inductances/capacitances of the network. Therefore, the analysis of SSR problems requires representation of both the electromechanical dynamics of the generating units and the electromagnetic dynamics of the transmission network. The generator stator circuits and the network cannot be represented by steady-state algebraic equations as in system stability studies. Consequently, the system model used for SSR studies is of a higher order and greater stiffness than the model used for stability studies.

Several methods have been used for the study of SSR. The following is a brief description of these methods.

(a) *Eigenvalue (modal) analysis.* The general approach is the same as that described in Chapter 12. The method is powerful and provides insight into the system characteristics. With the availability of special techniques for the analysis of very large systems (see Section 12.7.2), system size and computational burden are no longer considered as the limitations of this approach.

(b) *Frequency scanning* [18,19]. This technique computes the equivalent impedance as seen from the internal buses of generators looking into the network, for different values of frequency. It gives information about the natural frequencies of the system and the tendency toward self-excitation and SSR. This approach is particularly suited for preliminary analysis of SSR problems.

(c) *Frequency response analysis of full system* [20]. The stability of the subsynchronous oscillations is analyzed by using the multidimensional Nyquist criterion. This approach can handle detailed models and large systems.

(d) *Approximate frequency-domain analysis* [21,22]. This method analyzes the stability of individual torsional modes. It is limited to approximate detection of SSR.

(e) *Time-domain analysis.* The *electromagnetic transient program* (EMTP) may be used to compute the transient-time response [23]. A full three-phase representation of the system is used. It allows very detailed representation of equipment, including nonlinear effects. It is particularly suited for analyzing transient shaft torques due to SSR. However, this method is limited to the analysis of small systems.

Frequency dependent network equivalents may be used to facilitate the analysis of very large complex systems [24]. Such equivalents preserve the natural resonant characteristics of the network they represent.

Example 15.3

In this example, we illustrate the two forms of instability of subsynchronous oscillations associated with series capacitor-compensated systems: SSR and self-excitation. The test system considered is shown in Figure E15.5. It consists of a 555 MVA, 24 kV, 3,600 r/min turbine generator feeding power through a series capacitor-compensated transmission system to an infinite bus. The shaft system parameters and the torsional characteristics of the generating unit are as shown in Figure 15.3. The damping factors (D) of the individual masses are assumed to be negligible.

The generator and network parameters in per unit on 555 MVA, 24 kV base are as follows:

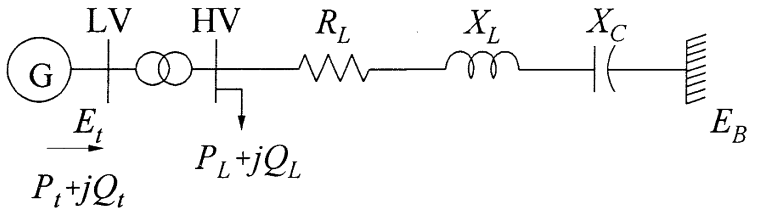


Figure E15.5 Series-compensated system

X_d = 1.81	X_q = 1.76	X_l = 0.16	X'_d = 0.3	X'_q = 0.61
X''_d = 0.217	X''_q = 0.254	R_a = 0.002	T'_{d0} = 7.8 s	T'_{q0} = 0.9 s
T''_{d0} = 0.022 s	T''_{q0} = 0.074 s	A_{sat} = 0.008	B_{sat} = 9.6	ψ_{T1} = 0.8
Z_T = 0.008+j0.13		R_L = 0.008	X_L = 0.75	

The power-flow condition is as follows:

P_t = 519.5 MW E_t = 1.08 E_B = 1.0

The degree of compensation (i.e., X_C/X_L) is varied and the reactive power output of the generator varies accordingly.

Our focus here is on the interaction between the lowest torsional (16 Hz) mode and the subsynchronous natural frequency oscillation of the network for the following values of load at the HV bus:

(a) P_L = 166.5 MW, Q_L = 0
(b) P_L = 0, Q_L = 0

Analysis

(a) With P_L=166.5 MW, Q_L=0:

We use the eigenvalue analysis approach described in Chapter 12 to analyze the modal interaction. However, the system model includes the dynamics of the transmission network and the generator stator circuits. The complete system equations are expressed in the *dq* reference frame.

Table E15.4 lists the eigenvalues, frequency and damping ratio (ζ) associated with the lowest torsional mode and the network mode as a function of the degree of series compensation (expressed in percent of line reactance X_L). In addition, participation factors associated with the generator speed deviation ($\Delta\omega_1$) and voltage across the series capacitor (Δv_c) are listed. These help identify the extent of interaction between the two modes. Since the network is modelled in the *dq* reference frame which rotates with the generator rotor, the frequency of the network mode computed is in fact the complement of the network natural frequency (i.e., synchronous frequency minus the natural frequency).

Table E15.4 Torsional and network modes as a function of the degree series compensation

With P_L = 166.5 MW, Q_L = 0

% Comp. of line 2-3	Torsional Mode					Network Mode (in *d-q* reference frame)				
	Eigenvalue	Freq. (Hz)	ζ	Participation Factors		Eigenvalue	Freq. (Hz)	ζ	Participation Factors	
				$\Delta\omega_1$	Δv_c				$\Delta\omega_1$	Δv_c
0.0	-0.04±j102.3	16.29	0.0004	0.90∠0.0°	–	–	–	–	–	–
25.0	-0.06±j102.6	16.32	0.0006	0.90∠0.0°	0.002∠153°	-2.9±j221.2	35.20	0.0130	0.03∠-177.0°	1.00∠1.0°
50.0	-0.10±j103.1	16.41	0.0010	0.90∠0.1°	0.01∠171.3°	-4.5±j155.5	24.75	0.0288	0.24∠89.3°	0.99∠-21.5°
60.0	-0.13±j103.7	16.50	0.0012	0.90∠0.0°	0.04∠172.7°	-3.2±j137.0	21.80	0.0231	0.01∠99.0°	1.00∠4.0°
65.0	-0.11±j104.4	16.61	0.0010	0.91∠-0.4°	0.09∠171.3°	-2.9±j126.2	20.09	0.0230	0.05∠164.0°	1.00∠1.7°
66.0	-0.10±j104.6	16.64	0.0010	0.91∠-0.4°	0.10∠170.0°	-2.9±j124.1	19.74	0.0230	0.07∠14.0°	1.00∠1.4°
68.0	-0.02±j105.2	16.74	0.0002	0.91∠-0.4°	0.17∠166.4°	-2.9±j119.6	19.04	0.0241	0.12∠164.0°	1.00∠0.4°
70.0	0.29±j106.3	16.90	-0.0027	0.91∠-7.8°	0.31∠152.5°	-3.1±j114.8	18.27	0.0273	0.26∠150.0°	1.00∠-6.3°
71.3	1.38±j107.3	17.08	-0.0128	0.91∠-30.0°	0.55∠109.0°	-4.2±j111.2	17.70	0.0376	0.47∠107.0°	0.98∠-28.0°
72.0	2.28±j107.5	17.10	-0.0212	0.91∠-37.7°	0.64∠84.5°	-5.0±j109.9	17.49	0.0460	0.55∠83.0°	0.98∠-36.0°
74.0	4.33±j106.6	16.96	-0.0406	0.92∠-31.4°	0.75∠48.0°	-7.0±j107.2	17.06	0.0658	0.64∠47.0°	0.96∠-29.4°
75.0	4.97±j105.9	16.85	-0.0468	0.93∠-25.5°	0.77∠37.3°	-7.6±j106.1	16.88	0.0721	0.65∠36.0°	0.95∠-23.2°
77.0	5.82±j104.4	16.60	-0.0557	0.93∠-13.0°	0.77∠18.0°	-8.5±j103.8	16.51	0.0814	0.66∠18.0°	0.95∠-9.0°
78.8	6.10±j103.1	16.41	-0.0590	0.93∠-3.8°	0.76∠5.1°	-8.7±j102.0	16.23	0.0850	0.64∠6.0°	0.95∠0.8°
80.0	6.12±j102.3	16.28	-0.0590	0.93∠1.9°	0.75∠-3.2°	-8.7±j100.9	16.05	0.0858	0.63∠-1.8°	0.95∠7.1°

With no compensation, the torsional mode has a frequency of 16.29 Hz and a small positive damping due to electrical sources. With 25% compensation, the torsional mode frequency and damping increase very slightly; the network mode has a frequency of 35.2 Hz and a damping ratio of 0.013. There is very little interaction between the two modes as indicated by the participation factors.

As the degree of compensation is increased, the frequency of the torsional mode varies slightly and its damping increases slightly at first and then decreases; the frequency of the network mode decreases and its damping increases. At 70% compensation, the torsional mode is just unstable and there is a noticeable amount of interaction between the two modes. Further increase in the degree of compensation strengthens the coupling between the two modes. This coupling effect tends to pull the two modes closer together in frequency but apart in damping. The torsional mode becomes unstable, while the network mode becomes more stable. With 75% to 80% compensation the two modes have nearly equal frequencies, and the coupling between the two modes is the greatest.

The effect of interaction between the network mode and the torsional mode on the characteristics of the network mode is more evident in Table E15.5. This table provides the frequency and damping ratio of only the network mode with and without the multimass representation of the turbine-generator rotor, that is, with and without the presence of the torsional mode. It is clear that, in this case, the interaction between the two modes increases the damping of the network mode.

(b) With $P_L=Q_L=0$

The results are summarized in Table E15.6. With the load removed, the effective resistance of the network is reduced significantly. Consequently, the network mode becomes unstable due to the induction motor effect. As the frequency of the network mode approaches the torsional mode frequency, the coupling between the two modes increases. In this case, the effect of the interaction is to increase the damping of the torsional mode and to decrease the damping of the network mode.

Table E15.7 compares the damping ratio and frequency of the network mode with and without multimass rotor representation. It is evident that the presence of the torsional mode makes the network mode more unstable. The stronger the interaction between the two modes, the less stable the network mode.

Table E15.5 Comparison of the network mode with and without multimass representation of the turbine-generator rotor

With P_L = 166.5 MW, Q_L = 0

% Comp. of line 2-3	Network mode with multimass representation of the turbine generator rotor		Network mode with single lumped-mass representation of the turbine-generator rotor	
	Freq. (Hz)	ζ	Freq. (Hz)	ζ
25.0	35.20	0.0130	35.32	0.0133
50.0	24.75	0.0288	25.13	0.0185
60.0	21.80	0.0231	21.82	0.0205
65.0	20.09	0.0230	20.27	0.0215
66.0	19.74	0.0230	19.96	0.0217
68.0	19.04	0.0241	19.37	0.0221
70.0	18.27	0.0273	18.78	0.0224
71.3	17.70	0.0376	18.39	0.0227
72.0	17.49	0.0460	18.20	0.0228
74.0	17.06	0.0658	17.63	0.0231
75.0	16.88	0.0721	17.35	0.0233
77.0	16.51	0.0814	16.74	0.0237
78.0	16.23	0.0850	16.27	0.0239
80.0	16.05	0.0858	15.96	0.0241

Note: Network mode shown above is in the *d-q* reference frame; the actual network frequency is equal to synchronous frequency (60 Hz) minus the above.

Table E15.6 Torsional and electrical network modes as a function of the degree of series compensation

With $P_L = Q_L = 0$

% Comp.	Torsional Mode					Network Mode				
	Eigenvalue	Freq. (Hz)	ζ	Participation Factors		Eigenvalue	Freq. (Hz)	ζ	Participation Factors	
				$\Delta\omega_1$	Δv_c				$\Delta\omega_1$	Δv_c
0.0	-0.03±j102.3	16.28	0.0003	0.896∠0.0°	–	–	–	–	–	–
25.0	-0.04±j102.5	16.32	0.0004	0.898∠0.0°	0.002∠153.0°	-1.94±j221.2	35.20	0.0088	0.03∠180.0°	1.00∠1.4°
70.0	-0.53±j106.4	16.94	0.0050	0.909∠5.0°	0.34∠-166.0°	0.67±j114.6	18.25	-0.0058	0.33∠-165.0°	1.00∠6.7°
75.0	-6.04±j105.5	16.79	0.0570	0.940∠28.0°	0.88∠-30.0°	6.51±j106.4	16.94	-0.0611	0.78∠-32.0°	1.00∠29.8°
78.8	-6.97±j102.3	16.28	0.0680	0.940∠3.9°	0.88∠1.7°	7.71±j102.8	16.36	-0.0750	0.79∠-4.1°	1.00∠4.6°
80.0	-6.92±j101.4	16.14	0.0681	0.930∠-2.7°	0.88∠10.0°	7.74±j101.8	16.20	-0.0758	0.78∠33.0°	1.00∠-2.0°
85.0	-5.03±j97.6	15.53	0.0500	0.871∠-34.°	0.83∠51.0°	6.22±97.1	15.46	-0.0639	0.71∠41.3°	1.00∠-32.0°
93.7	-0.13±j99.5	15.80	0.0013	0.870∠-1.0°	0.13∠-178.0°	1.96±j81.1	12.90	-0.0241	0.07∠167.1°	1.00∠3.8°

Note: Network mode shown above is in the *d-q* reference frame.

Table E15.7 Comparison of the network mode with and without multimass representation of the turbine-generator rotor

With $P_L = Q_L = 0$

% Comp. of line 2-3	Network mode with multimass representation of the turbine generator rotor shafts		Network mode with single lumped-mass representation of the turbine-generator rotor	
	Freq. (Hz)	ζ	Freq. (Hz)	ζ
25.0	35.20	0.0088	35.32	0.0088
70.0	18.25	-0.0058	18.78	-0.0018
75.0	16.94	-0.0611	17.35	-0.0050
78.8	16.36	-0.0750	16.26	-0.0080
80.0	16.20	-0.0758	15.96	-0.0090
85.0	15.46	-0.0639	14.62	-0.0138
93.7	12.90	-0.0241	12.38	-0.0246

Note: Network mode shown above is in the *d-q* reference frame ■

15.3.5 Countermeasures to SSR Problems [25,26]

A wide variety of methods have been proposed in the literature for counteracting SSR. These may be broadly classified as follows:

(a) *Static filter.* This can take the form of a blocking filter (parallel-resonance type) in series with the generator, or damping circuits in parallel with the series capacitors.

(b) *Dynamic filter.* This is an active device placed in series with the generator. It picks up a signal derived from rotor motion and produces a voltage in phase opposition so as to compensate for or even exceed the subsynchronous voltage generated in the armature.

(c) *Dynamic stabilizer.* This consists of thyristor modulated shunt reactors connected to the generator terminal. Control of subsynchronous oscillations is achieved by modulating the thyristor switch firing angles, using signals derived from the generator shaft speed.

(d) *Excitation system damper.* Generator excitation control is modulated by using a signal derived from the shaft speed so as to provide increased damping of

torsional oscillations.

(e) *Protective relays.* The SSR condition is detected by a relay and the affected units are tripped. The relay may take several forms: detection of excessive torsional motion by sensing rotor speed or detection of SSR condition by sensing the armature current.

(f) *NGH scheme [26].* This consists of a linear resistor in series with back-to-back thyristors connected across the series capacitor. The presence of SSR components in the capacitor voltage is detected and reduced by the action of the resistor discharge circuit.

An example of a comprehensive SSR protection scheme is the one at Salt River Project's Navajo Plant [27]. It consists of three forms of protection: (i) a tuned resonant blocking filter in series with the generator, (ii) an excitation system damper to damp subsynchronous oscillations, and (iii) a static relay which trips the units if the transient shaft response exceeds an acceptable level.

15.4 IMPACT OF NETWORK-SWITCHING DISTURBANCES

A generating unit encounters a multitude of switching duties during its lifetime. These include planned as well as unplanned events, such as simple line switching, system faults and fault clearing, reclosing of lines, and faulty synchronizing. Such disturbances can produce high levels of oscillatory shaft torques. The resulting cyclic stress variations undergone by the shaft material may cause loss of fatigue life. This is a cumulative process, with each incident using up a portion of the total fatigue life.

Traditionally, turbine generators have been designed to withstand terminal short circuits in accordance with industry standards [28]. Terminal short circuits are rare events; consequently, a generating unit would not be expected to experience more than a few such events over its entire life. In the early 1970s, it was realized that network-switching operations could contribute to shaft fatigue damage. This recognition came about as a result of studies prompted by the shaft failure of Mohave units due to SSR. Although the SSR phenomenon is of a different nature, it drew attention to other possible transmission network conditions that may lead to shaft damage. The effects of network disturbances and switching events on turbine-generator shafts, independent of SSR conditions, have been examined by a number of investigators [2-6,29,30]. A procedure for estimating torsional fatigue life expenditure has also been developed under an EPRI research project, based on extensive testing of shaft specimens [31].

This problem has been examined by an IEEE working group, and general recommendations have been made to the industry concerning (a) steady-state switching [32] and (b) successive network switching [33].

Steady-state switching

Switching operations involving opening or closing of circuit breakers can result in transient torques which impose severe stress on nearby generators. Usually, the most severe switching operation with the network initially under steady state is the reclosing of transmission lines across a large breaker angle. Depending on the network impedances, the resulting sudden increase in the air-gap torque of a nearby generator could be very large. This causes the mechanical system to respond to the principal torsional natural frequencies. If the resulting torques are high, this may result in loss of shaft fatigue life. For the purpose of explaining the basis used for determining the acceptability of the shaft duty imposed by a switching operation, it is helpful to briefly review the fatigue characteristics of shaft materials.

Torsional fatigue characteristics [2,3,16,33]:

Fatigue is defined as the process of progressive localized permanent structural change occurring in a material subjected to conditions which produce fluctuating stresses and strains at some point or points and which may culminate in cracks or complete fracture after a sufficient number of fluctuations [16].

Fatigue is a cumulative process in which additional events add to previous life expenditure. Observable defects such as cracks will not be formed until all the fatigue life is consumed.

A typical fatigue characteristic of a shaft specimen subjected to a fully reversed cyclic stress is shown in Figure 15.11. The figure shows how the number of cycles to failure is related to the magnitude of the cyclic stress. The figure also defines the

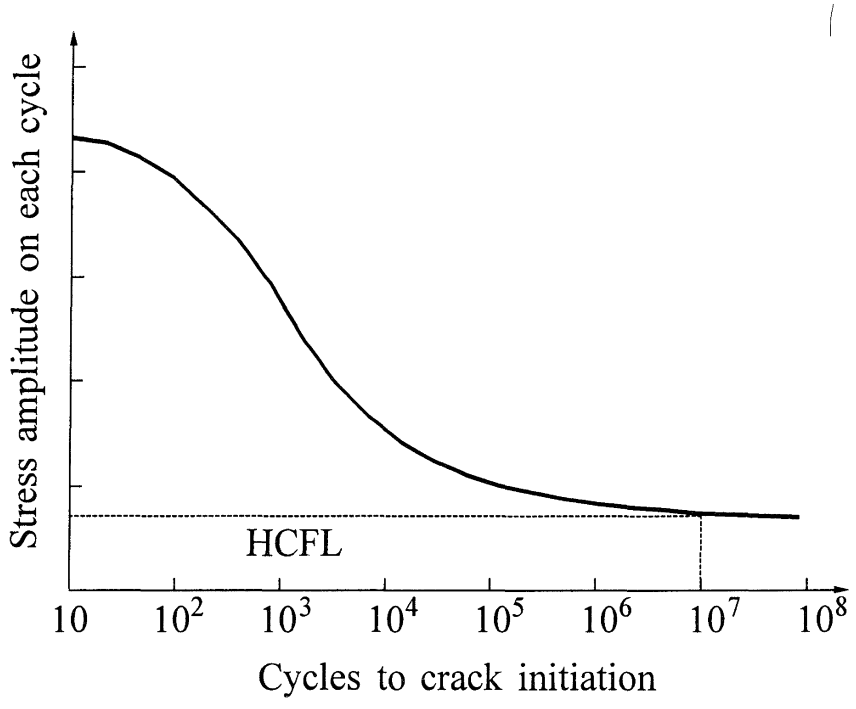


Figure 15.11 A typical fatigue characteristic showing cycle life curve for fully reversed stress

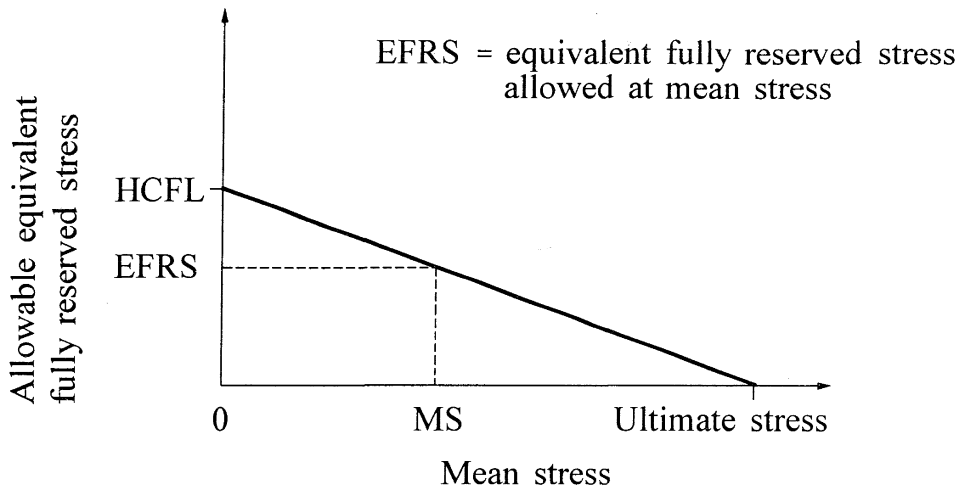


Figure 15.12 Mean stress effect

high-cycle fatigue limit (HCFL) which is the limiting value of the cyclic stress to which the shaft can be subjected such that practically no cumulative fatigue damage occurs. In addition to the alternating stress, the effect of the mean stress should be considered. Figure 15.12 illustrates how the mean stress or the steady-state torque lowers the allowable cyclic torque. The allowable cyclic torque is equal to HCFL when the mean stress is equal to zero, and it is equal to zero when the mean stress is equal to the ultimate stress of the material. For any other value of mean stress between these two extremes, the allowable cyclic torque is determined as shown in Figure 15.12.

Figure 15.13 shows a typical stress-strain curve for a material. The linear region of the curve is known as the region of *elastic strain.* A material which is elastically deformed will return to its original shape and strength after deformation. Values of strain in the nonlinear region are known as *plastic strain.* Plastic strain results in permanent deformation of the material.

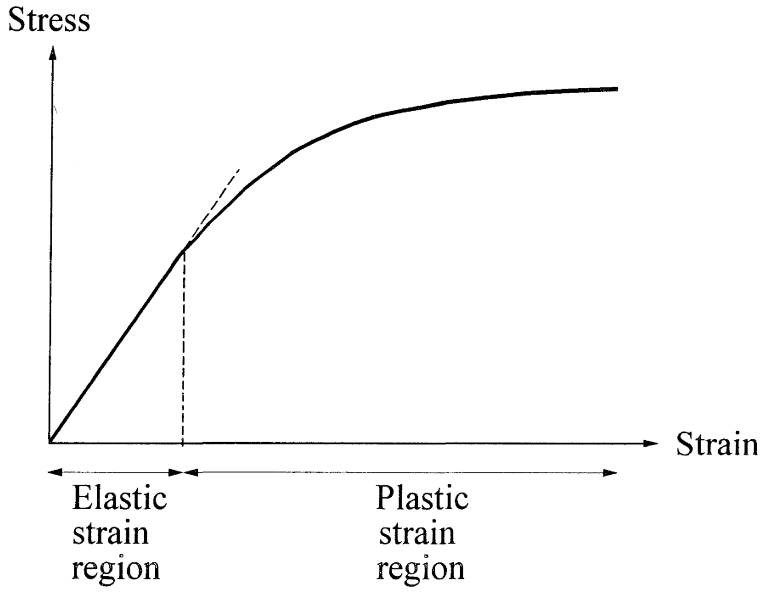


Figure 15.13 Stress-strain curve

High-cycle fatigue is caused by a large number of low amplitude fluctuations; it results in elastic deformation. Conversely, *low-cycle fatigue* is caused by a small number of large amplitude fluctuations; it involves local plastic deformation in regions such as keyways and fillets.

Recommendations:

For planned switching operations, such as a simple line restoration, IEEE guidelines [32] recommend that the switching be conducted so that it does not contribute significantly to cumulative shaft fatigue. This means that the magnitude of the cyclic shaft stress, with mean stress effects included, should be kept mostly below the high cycle fatigue limit (see Figures 15.11 and 15.12). In this way, nearly all of the fatigue capability of the shafts will be preserved to withstand the impact of unplanned and unavoidable disturbances such as faults, fault clearing, reclosing into system faults, and emergency line switching.

Guidelines for screening acceptable line-switching duties:

A detailed investigation of all possible line-switching cases would be impractical. Therefore, the IEEE [32] has suggested general guidelines to permit the utilities to screen switching operations and to determine if any of the cases requires a detailed study. These guidelines assume a *simple line restoration from steady state*; hence, they are applicable only for delayed reclosing, with a reclosing time of about 10 seconds or more. The guidelines are based on detailed studies performed on a number of cases where a large angle across the open breaker indicated that there could be excessive shaft torques.

The breaker angle is not by itself very useful in judging the severity of a switching operation. The circuit impedances play a significant role. Therefore, the severity is measured in terms of the sudden change in the generator power (ΔP), as computed by a conventional transient stability program. A rule-of-thumb limit proposed by the IEEE for ΔP is 0.5 per unit of generator MVA rating. A line-switching case resulting in ΔP of less than 0.5 per unit may be considered safe. Switching operations resulting in ΔP greater than the 0.5 per unit limit have to be studied in detail to assess the shaft duty.

Successive network-switching disturbances

Successive network disturbances, such as automatic high-speed line reclosing following a fault, can result in dangerously high torques. The concern here is for the *compounding effects* of the different switching operations. For example, in the case of high-speed reclosing, the following successive switching disturbances are involved:

- Transmission line fault
- Clearing of fault
- Reclosing of the line, either successful or unsuccessful

The torsional oscillations due to successive impacts may reinforce the initial oscillations. The risk of amplifying vibrations to damaging levels is a function of the type of disturbance and the timing of subsequent switching operations.

In the analysis of the effects of network-switching operations on shaft torques, the 60 Hz component of air-gap torque associated with the dc offset in the stator current is generally found to have a significant effect. Therefore, it is necessary to model the generator stator and network transients. To simulate the circuit-breaker operation adequately, as affected by the current zero crossing in each phase, it is necessary to use a three-phase cycle-by-cycle representation.

The electromagnetic transient program [23] provides a means of representing these effects. It also has facilities for computing shaft torques and determining torsional fatigue life expenditure.

Reference 33 prepared by the IEEE working group gives a summary of the predicted range of fatigue life expenditure for various network disturbances: different types of faults, fault clearing, successful reclosing, and unsuccessful reclosing. Automatic high-speed reclosing of multiple faulted lines near generating plants is identified as posing a significant risk in shaft fatigue life expenditure. Where high-speed reclosing strategies are contemplated, a study to assess the shaft fatigue duty is recommended. The following are possible alternative reclosing strategies with reduced risk of shaft damage:

(a) Delayed reclosing, with a delay of 10 s or more.

(b) Sequential reclosing; i.e., automatic reclosing from the end remote from the plant, followed by synchro-check reclosing of the plant end.

(c) Selective reclosing; i.e., limiting automatic high-speed reclosing to single line-to-ground faults and line-to-line faults.

Reference 30 provides a comparative assessment of the fatigue life expenditure with unrestricted high-speed reclosing and the above alternative reclosing strategies.

15.5 TORSIONAL INTERACTION BETWEEN CLOSELY COUPLED UNITS

A single generator of M masses connected to a power system has M modes of oscillation (for example, see Figure 15.3). One of these modes is the system mode or the rigid-body mode in which all rotor masses move in phase with nearly equal magnitude. The other $M-1$ modes are torsional modes whose frequencies differ from one another and in which the M rotor masses have differing degrees of participation.

If there are N machines operating in parallel, their shaft systems are coupled through the electrical system. The electrical stiffness of such coupling is an order of magnitude smaller than the mechanical stiffness of shafts interconnecting adjacent

rotor masses. Therefore, the rigid-body modes of oscillation have frequencies in the range of 0.2 to 3.0 Hz.

The interaction between the shaft systems of parallel units has an effect on the torsional modes. The need to consider this interaction was first recognized during field tests conducted at the Mohave generating station [4]; a double resonant peak was observed near one of the torsional frequencies with two generating units operating in parallel.

The effect of interaction between torsional dynamics of two closely coupled units is depicted in Figure 15.14. Each unit is assumed to have the torsional characteristics shown in Figure 15.3.

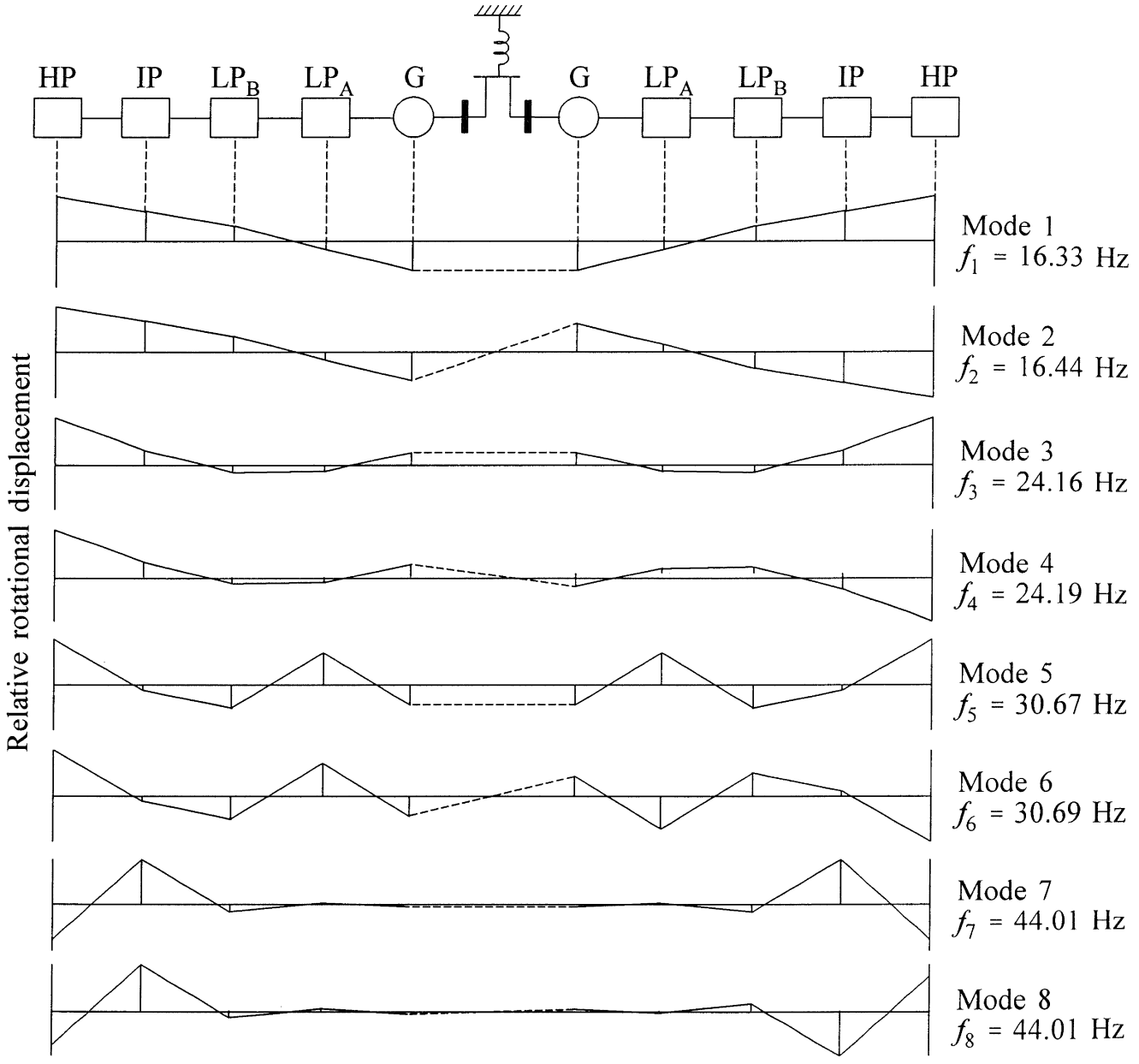


Figure 15.14 Torsional frequencies and mode shapes of two coupled turbine generators

Modes 1 and 2 represent the lowest torsional modes. In mode 1 (f_1=16.33 Hz) the corresponding masses in the two units oscillate in phase, whereas in mode 2 (f_2=16.44 Hz) the corresponding masses oscillate in antiphase. The difference in frequencies of the two modes is 0.11 Hz. This difference is a function of the stiffness coefficient of the electrical coupling between the two units. With a low coupling, the two frequencies would be equal. As the coupling is increased, the frequency difference increases.

Similarly, there are in-phase and antiphase modes corresponding to each of the other three torsional modes of the individual units.

In a general case of N identical machines (each having M masses) operating in parallel, the following torsional modes exist [34]:

- One group of M modes in which the corresponding rotors in each unit oscillate in unison. These modes are stimulated by symmetrical disturbances on all N units, and are designated *in-phase modes.*

- The M groups of $N-1$ identical modes representing intermachine dynamics. These modes have linearly independent mode shapes and are designated *antiphase modes.*

The above analysis assumes that the N units are truly identical. If the units are only nominally identical, there will be families of N modes slightly separated in frequency. Each torsional mode family will consist of one in-phase mode, in which the generators participate at slightly different magnitudes, and $N-1$ antiphase modes with slight differences in frequency. The torsional interaction in this case will be less because of the differences in the individual torsional frequencies of the units.

The possible spread of antiphase torsional modes as additional units are brought on-line is significant in situations where notch filters are used to solve torsional-related problems.

15.6 HYDRO GENERATOR TORSIONAL CHARACTERISTICS

The rotor of a hydraulic generating unit consists of a turbine runner and a generator rotor. If the unit has a shaft-driven exciter, there is an additional rotor mass. Consequently, there are at most two torsional modes of oscillation.

The inertia of the generator rotor is about 10 to 40 times higher than that of the turbine runner (waterwheel). The torsional natural frequencies lie in the range of 6 Hz to 26 Hz [35].

There are no reported cases of adverse dynamic interaction between the hydro generator rotor and the electrical network. The following are the principal reasons for the absence of adverse interaction [35,36]:

1. The high value of the generator rotor inertia in relation to the inertias of the turbine runner and exciter rotor. This effectively shields the rotor mechanical system. As a result, it is difficult to excite torsional oscillations through disturbances on the generator.

2. Viscous waterwheel damping. This makes the inherent damping of torsional oscillations for hydro units significantly higher than for steam-turbine generators.

REFERENCES

[1] J.P. Den Hartog, *Strength of Materials*, Dover, 1961.

[2] M.C. Jackson, S.D. Umans, R.D. Dunlop, S.H. Horowitz, and A.C. Parikh, "Turbine-Generator Shaft Torques and Fatigue: Part I - Simulation Methods and Fatigue Analysis; Part II - Impact of System Disturbance and High Speed Reclosure," *IEEE Trans.*, Vol. PAS-98, No. 6, pp. 2299-2328, November/ December 1979.

[3] D.N. Walker, S.L. Adams, and R.J. Placek, "Torsional Vibration and Fatigue of Turbine-Generator Shafts," *IEEE Trans.*, Vol. PAS-100, No. 11, pp. 4373-4380, November 1981.

[4] D.N. Walker, C.E.J. Bowler, R.L. Jackson, and D.A. Hodges, "Results of Subsynchronous Resonance Test at Mohave," *IEEE Trans.*, Vol. PAS-94, No. 5, pp. 1878-1889, September/October 1975.

[5] R. Quay and A.C. Schwalb, discussion of reference 4, *IEEE Trans.*, Vol. PAS-94, No. 5, pp. 1887-1888, September/October 1975.

[6] R.G. Ramey, A.C. Sismour, and G.C. Kung, "Important Parameters in Considering Transient Torques on Turbine-Generator Shaft Systems," *IEEE Trans.*, Vol. PAS-99, No. 1, pp. 311-317, January/February 1980.

[7] W. Watson and M.E. Coultes, "Static Exciter Stability Signal on Large Generators - Mechanical Problems," *IEEE Trans.*, Vol. PAS-92, pp. 205-212, January/February 1973.

[8] D.C. Lee and P. Kundur, "Advanced Excitation Controls for Power System Stability Enhancement," CIGRE paper 38-01, 1986.

[9] D.C. Lee, R.E. Beaulieu, and G.J. Rogers, "Effects of Governor Characteristics on Turbo-Generator Shaft Torsionals," *IEEE Trans.*, Vol. PAS-104, No. 6, pp.

1255-1261, June 1985.

[10] M. Bahrman, E.V. Larsen, R.J. Piwko, and H.S. Patel, "Experience with HVDC - Turbine Generator Torsional Interaction at Square Butte," *IEEE Trans.*, Vol. PAS-99, pp. 966-975, May/June 1980.

[11] N. Hingorani, S. Nilsson, M. Bahrman, J. Reeve, E.V. Larsen, and R.J. Piwko, "Subsynchronous Frequency Stability Studies of Energy Systems Which Include HVDC Transmission," Paper presented at the Symposium on Incorporating HVDC Power Transmission into System Planning, Phoenix, Ariz., March 24-27, 1980.

[12] EPRI Report EL-2708, "HVDC System Control for Damping Subsynchronous Oscillations," Final Report of Project RP1425-1, Prepared by General Electric Company, October 1982.

[13] CIGRE/IEEE guide for "Planning DC Links Terminating at AC Locations Having Low Short-Circuit Capabilities, Part I: AC/DC Interaction Phenomenon," 1992.

[14] E. Katz, "Subsynchronous Resonance," Paper presented at the panel discussion on Dynamic Stability in the Western Interconnected Power Systems, IEEE PES Summer Meeting, July 18, 1974.

[15] C. Concordia, J.B. Tice, and C.E.J. Bowler, "Sub-synchronous Torques on Generating Units Feeding Series-Capacitor Compensated Lines," Paper presented at the American Power Conference, Chicago, May 8-10, 1973.

[16] IEEE Committee Report, "Proposed Terms and Definitions for Subsynchronous Oscillations," *IEEE Trans.*, Vol. PAS-99, No. 2, pp. 506-511, March/April 1980.

[17] C. Concordia, discussion of reference 16.

[18] B.L. Agrawal and R.G. Farmer, "Use of Frequency Scanning Techniques for Subsynchronous Resonance Analysis," *IEEE Trans.*, Vol. PAS-98, pp. 341-349, March/April 1979.

[19] P.M. Anderson, B.L. Agrawal, and J.E. Van Ness, *Subsynchronous Resonance in Power Systems*, IEEE Press, 1990.

[20] J.M. Undrill and T.E. Kostyniak, "Subsynchronous Oscillations Part I - Comprehensive System Stability Analysis," *IEEE Trans.*, Vol. PAS-95, pp. 1446-1455, July 1976.

[21] L.A. Kilgore and D.G. Ramey, "Transmission and Generator System Analysis Procedures for Subsynchronous Resonance Problems," tutorial session, IEEE PES Summer Meeting, July 1975.

[22] EPRI Report EL-2614, "Study of Turbine Generator Shaft Parameters from the Viewpoint of Subsynchronous Resonance," Final Report of Contract TPS81-794, Prepared by Power Technologies Inc., September 1982.

[23] EPRI/DCG Report EL-7321, "Electromagnetic Transients Program - Version 2: Revised Application Guide," November 1991.

[24] A.S. Morched, J.H. Ottevangers, and L. Marti, "Multi-port Frequency Dependent Network Equivalents for the EMTP," Paper 92 SM 461-4 PWRD, Presented at the IEEE PES Summer Meeting, Seattle, July 1992.

[25] IEEE Committee Report, "Countermeasures to Subsynchronous Resonance Problems," *IEEE Trans.*, Vol. PAS-99, No. 5, pp. 1810-1817, September/October 1980.

[26] N.G. Hingorani, "A New Scheme for Subsynchronous Resonance Damping of Torsional Oscillations and Transient Torque - Part I," *IEEE Trans.*, Vol. PAS-100, pp. 1852-1855, April 1981.

[27] R.F Wolff, "Stop Subsynchronous T/G - Shaft Damage," *Electrical World*, pp. 129-133, April 1981.

[28] ANSI Standard C50.13-1977, *Requirements for Cylindrical Rotor Synchronous Generators.*

[29] J.S. Joyce, T. Kulig, and D. Lambrecht, "The Impact of High-Speed Reclosure of Single and Multi-Phase System Faults on Turbine-Generator Shaft Torsional Fatigue," *IEEE Trans.*, Vol. PAS-99, No. 1, pp. 279-291, January/February 1980.

[30] C.E.J. Bowler, P.G. Brown, and D.N. Walker, "Evaluation of the Effect of Power Breaker Reclosing Practices on Turbine-Generator Shafts," *IEEE Trans.*, Vol. PAS-99, No. 5, pp. 1764-1779, September/October 1980.

[31] EPRI Report EL-3083, "Determination of Torsional Fatigue Life of Large Turbine Generator Shafts," Final Report of Project 1531-1, Prepared by General Electric Company, April 1984.

[32] IEEE Working Group Report, "IEEE Screening Guide for Planned Steady-State Switching Operations to Minimize Harmful Effects on Steam Turbine-

Generators," *IEEE Trans.*, Vol. PAS-99, No. 4, pp. 1519-1521, July/August 1980.

[33] IEEE Working Group Interim Report, "Effects of Switching Network Disturbances on Turbine-Generator Shaft Systems," *IEEE Trans.*, Vol. PAS-101, No. 9, pp. 3151-3157, September 1982.

[34] R.T.H. Alden, P.J. Nolan, and J.P. Bayne, "Shaft Dynamics in Closely Coupled Identical Generators," *IEEE Trans.* Vol. PAS-96, pp. 721-728, May/June 1977.

[35] G. Andersson, R. Almuri, R. Rosenquist, and S. Torseny, "Influence of Hydro Units' Generator-to-Turbine Inertia Ratio on Damping of Subsynchronous Oscillations," *IEEE Trans.*, Vol. PAS-103, pp. 2352-2361, August 1984.

[36] L.E. Eilts and E. Campbell, "Shaft Torsional Oscillations of Hydrogenerators," U.S. Bureau of Reclamation Report REC-ERC-79-6, Denver, Colo., August 1979.

Chapter 16

Mid-Term and Long-Term Stability

Mid-term stability and long-term stability are associated with the response of power systems to severe upsets. Severe upsets are those disturbances that result in excursions of frequency, voltage, and power flows either so great or so long-lasting that they invoke the actions of slow processes, protective systems, and controls not modelled in conventional transient stability studies.

This chapter illustrates the nature of system response when subjected to severe upsets and examines the need for distinction between mid-term and long-term stability. It describes modelling considerations and analytical techniques for simulation of long-term dynamic response. In addition, it gives illustrative examples and provides guidelines for enhancing the ability of power systems to cope with severe upsets.

16.1 NATURE OF SYSTEM RESPONSE TO SEVERE UPSETS

In considering the nature of system response to major disturbances, it is helpful to visualize the power system operating conditions in terms of the five states depicted in Figure 16.1. A description of these states and the ways in which the transition takes place from one state to another is provided in Chapter 1 (Section 1.3). This chapter focuses on events and system conditions associated with the *in extremis* state.

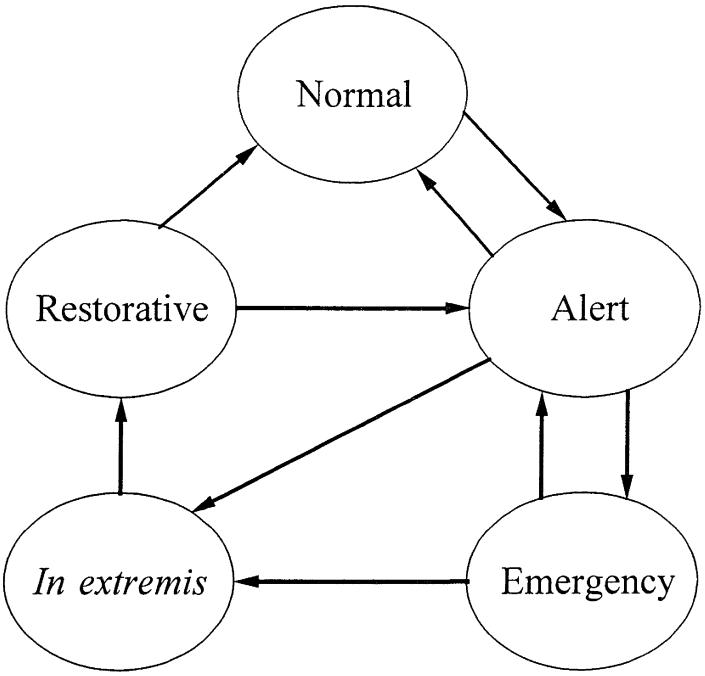


Figure 16.1 Power system operating states

An examination of actual system disturbances [1-6] shows that an underlying pattern exists with regard to the events leading to system failures. This is depicted in Figure 16.2 which shows the events that could cause transition from the alert state to the *in extremis* state. The initiating event could be a disturbance of natural origin, a malfunction of equipment, or a consequence of human factors. Modern power systems are designed and operated to ensure secure operation for the more probable contingencies (see Chapter 1 for a description of the design contingencies). In the vast majority of cases, power systems are able to withstand any single contingency and many multiple contingencies. The protective and control systems act to prevent the propagation of the disturbance to other parts of the network.

Occasionally, however, an unusual combination of circumstances and events causes a portion of the interconnected system to separate completely and form one or more *electrical islands*. The initiating event is usually a contingency more severe than those covered by the normal design criteria: for example, tripping of several transmission lines as the result of a tornado, an ice storm, or a malfunction of communication equipment. The events triggered as a consequence of the initiating event, by stressing the system further, cause uncontrolled cascading outages. Wide variations of frequency (from 58 to 63 Hz) and voltage (from 50% to 120% of pre-disturbance value) may exist during the ensuing system conditions [1]. The system can thus deteriorate to the *in extremis* state, the result being the loss of significant portions of system load. Generally, the actions of control and protective systems dominate the system response during these conditions. The situation is often aggravated by poorly coordinated protection and control systems. Emergency control action should be directed toward saving as much of the system as possible from total collapse.

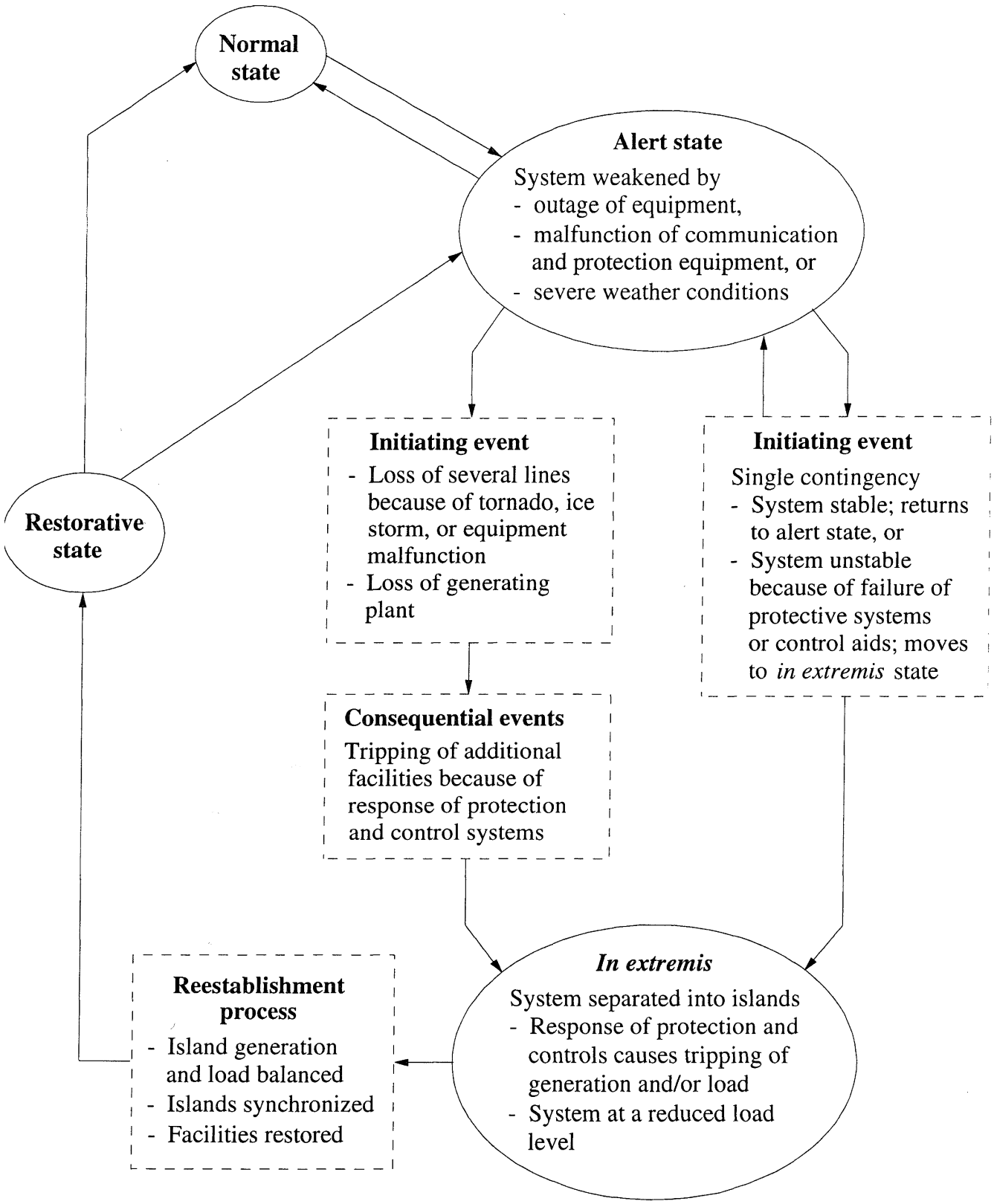


Figure 16.2 Transition of system states during severe upsets

System response to islanding conditions

The system response to an islanding condition is basically a sustained-frequency transient. Therefore, the speed control and the subsequent responses of prime mover and energy supply systems play a major role in determining the nature of the system dynamic performance. Often, the situation is compounded by high- or low-voltage conditions.

Undergenerated islands:

In an island with total initial generation less than the total load, the frequency will decline. If there is sufficient spinning reserve within the island, the system frequency returns, in a few seconds, to a near normal value. If sufficient generation with the ability to rapidly increase output is not available, the frequency may reach levels that could lead to tripping of thermal generating units by underfrequency protective relays, thus aggravating the situation further. Therefore, underfrequency load-shedding schemes are usually employed to reduce the connected load to a level that can be satisfactorily supplied by the available generation (see Chapter 11, Section 11.1.7).

Consequently, in an undergenerated island, the initial transient is dependent on the responses of spinning generation reserve and load-shedding relaying. The minimum value of frequency is reached in a few seconds. The system frequency response beyond this point depends on the prime mover characteristics.

Overgenerated islands:

In an island with an initial excess generation, the frequency will rise, and the speed-governing system will respond by reducing the mechanical power generated by the turbines. The power plants, in effect, experience a "partial load rejection." The performance of the island and its ability to stabilize without loss of load depend on the ability of the power plants to sustain a partial load rejection. This is discussed further in Section 16.3.

Reactive power balance:

The system performance is also influenced by the reactive power balance within the island. A significant mismatch in the total reactive power generated and absorbed could lead to high- or low-voltage conditions. Generator over/underexcitation limiters and controls may be activated. In extreme situations, the response of protective relays could lead to the tripping of generating units. For example, an island with lightly loaded EHV lines and/or cables may cause the generators to absorb high amounts of reactive power; this situation, if not corrected quickly, could lead to tripping of the units by loss-of-excitation protection.

Power plant auxiliaries:

Variations, especially a decrease, in power supply voltage and frequency can degrade the performance of power plant auxiliaries driven by induction motors. For example, pumps associated with circulating water, condensate, heater drain, and feedwater are driven by induction motors. Degraded performance of these pumps may lead to loss of condenser vacuum, high turbine-exhaust temperature, and insufficient condensate/feedwater flow. Many nuclear plants are, therefore, equipped with undervoltage and underfrequency relays set to trip the plant at low voltages (typically, 70% of rated value) and at low frequencies (typically, 59.2 Hz) [8].

Power plant motors commonly use electromagnetic contactors and relays in the starting and protection circuits. The response of these contactors and relays to severe or long voltage dips could disconnect the motors.

System restoration

When the islands reach steady-state conditions, operators take steps to restore the interconnected system. These involve adjusting of generation and load in each island, resynchronizing of islands, and restoration of generating units, loads, and other facilities tripped during the system disturbance. Start-up and reloading of thermal units are constrained by a number of factors, and full power may not be available for several hours. The restoration of power can be speeded up considerably if the thermal units are available quickly for reloading. Many utilities have, therefore, adopted the "tripping to house load" technique. The following are the different methods used to achieve this [9,10]:

(a) Trip the fire at the moment of disconnection and rely on the thermal storage of the boiler for about 20 minutes.

(b) As (a), but re-ignite the fire and leave the boiler running on the ignition burners.

(c) Apply a special firing technique at very low load.

(d) Leave the boiler at full power or reduce power to minimum load. Dump excess steam into the atmosphere, and draw upon feed-water storage, usually for several hours.

(e) Leave the boiler at minimum load and bypass excess steam into the condenser.

16.2 DISTINCTION BETWEEN MID-TERM AND LONG-TERM STABILITY

As noted in Chapter 2, the terms *long-term stability* and *mid-term stability* are new in the literature on power system stability. They were introduced as a result of the need to deal with problems associated with the dynamic response of power systems to severe upsets.

Long-term stability analysis as defined in references 11 to 15 assumes that inter-machine synchronizing power oscillations have damped out, the result being uniform system frequency. The focus is on slower and longer duration phenomena that accompany large-scale system upsets and on the resulting sustained mismatches between generation and consumption of active and reactive power. Boiler dynamics of thermal units, penstock and conduit dynamics of hydro units, automatic generation control, power plant and transmission system protections/controls, transformer saturation, and off-nominal effects on loads and the network are likely to be significant.

The term *mid-term stability* was introduced in references 14 and 15. It represents the transition between the transient responses and the long-term responses. In mid-term stability, the focus is on synchronizing power oscillations between machines, as well as on the effects of some of the slower phenomena, and possibly large-voltage and/or frequency excursions.

It is clear, by these definitions, that the distinction between mid-term and long-term stability is weak. What makes long-term stability different is that it assumes that the system frequency is uniform and that fast dynamics are not significant. This is helpful if analytical tools require these assumptions to facilitate simulation. But with today's software that utilizes advanced sparsity and efficient implicit integration techniques, simulating long time frames with fast-dynamic modelling is becoming less of a concern.

There is no well-defined distinction between the mid-term time frame and the long-term time frame so far as modelling requirements are concerned. For time periods beyond the transient period, the choice of models to be included in a simulation should be based on the phenomena being analyzed and the system representation used, rather than on the actual duration of the simulation. For example, neglecting boiler dynamics or steam process control in a "mid-term" simulation may be acceptable for simulation of disturbances in which the driving functions to these dynamics are small. However, neglecting these slower dynamics for more severe disturbances that may invoke protections associated with variables such as steam pressures could have a tremendous impact on the simulation results. The experiences of a number of utilities have identified the need to represent intermachine oscillations and fast transients associated with excitation systems in long-term stability studies [16]. Thus, the distinction between mid-term and long-term stability cannot be satisfactorily based on a fixed time-frame basis, nor on modelling requirements. In light of this, the best approach to classifying stability problems associated with severe

system upsets is to eliminate the concept of mid-term as a separate category and to use long-term to encompass all studies beyond the transient time frame.

Long-term stability would then be described as the ability of a power system to reach an acceptable state of operating equilibrium following a severe system disturbance that may or may not have resulted in the system being divided into subsystems. The time frame of interest extends beyond the transient period sufficiently to include, in addition to fast dynamics, the effects of slow dynamics of automatic system controls and protections. Long-term simulations may include severe disturbances, beyond the normal design contingencies, that have resulted in cascading and splitting of the power system into a number of separate islands with the generators in each island remaining in synchronism. *Stability in this case is a question of whether each island will reach an acceptable state of operating equilibrium with minimal disruption to services.* In an extreme case, the system and unit protections may compound the adverse situation and lead to a collapse of the island in whole or in part.

Generally, the long-term stability problems are associated with inadequacies in equipment responses, poor coordination of control and protection equipment, or insufficient active/reactive power reserve.

The characteristic times of the processes and devices activated by the large voltage and frequency shifts will range from a matter of seconds, corresponding to the responses of devices such as generator controls and protections, to several minutes, corresponding to the responses of devices such as prime mover energy supply systems and load-voltage regulators.

From an analytical standpoint, long-term stability programs become extensions of transient stability programs with the desired capability of adjusting the integration time-step according to the dominant transients [17].

One application of long-term stability simulation gaining interest is the dynamic analysis of voltage stability (discussed in Chapter 14) requiring simulation of the effects of transformer tap-changing, generator overexcitation protection and reactive power limits, and thermostatic loads. In this case, intermachine oscillations are not likely to be important and energy supply system transients may not be critical. However, care should be exercised before neglecting some of the fast dynamics.

16.3 POWER PLANT RESPONSE DURING SEVERE UPSETS

16.3.1 Thermal Power Plants

The ability of power plants to survive partial load rejections is of crucial importance in minimizing the impact of a severe upset and quickly restoring normal operation of the power system. References 18 to 21 describe the responses of power plants to partial load rejections and problems experienced in successfully withstanding such disturbances.

Reference 22, prepared by an IEEE Working Group, provides guidelines for enhancing power plant response to partial load rejections. The following is a summary of these guidelines:

(a) *Overall plant control.* To withstand a partial load rejection, the overall plant control must promptly decrease the input power (fuel flow) to correspond to the output electrical power. As there are time lags in this decrease, the power input must temporarily undershoot the power output. The ideal source of intelligence to determine the input power reduction is the actual power output.

(b) *Boiler control.* Without a turbine bypass system, a partial load rejection appears to the boiler as a step decrease in steam flow. Prompt reduction of fuel flow is essential, as noted above.

For a *once-through boiler*, prompt reduction of the feedwater flow, tightly coupled to the fuel flow, is also required. However, once-through boilers normally have superheater/turbine bypass systems of limited capacity to protect the furnace tubes and to assist in pressure control. This bypass capability can be used to ease the rate of reduction of fuel and feed-water flow.

For a *drum type boiler*, the reduction of feed-water flow should be delayed because the immediate response of the drum water level is to decrease with steam flow and the resulting rise in drum pressure. In addition, overfeeding is required to obtain the higher-level water inventory required at the lower power level. Adequate water-level control is particularly important for large changes in steam flow. To enhance the ability of water-level control during a partial load rejection, consideration should be given to temporarily increasing the range between high and low water-level trip limits, or delaying the trip for high feedwater flow.

For either type of boiler, a delay in the reduction of air flow is generally desirable since the cooling effect of the excess air flow will tend to compensate for the lags in fuel flow response. However, the air flow to the operating burners must be controlled relative to the fuel flow to maintain stable combustion.

For feed pumps driven by auxiliary steam turbines, the closure of intercept valves will interrupt the steam flow; therefore, it is necessary either to provide an alternate steam source to the auxiliary turbine or to switch to motor-driven pumps.

(c) *Turbine-generator control.* The turbine overspeed controls are designed to limit overspeed following full-load rejection to about 1% below the overspeed trip settings. This will obviously prevent overspeed trips during partial load rejection.

While the control valves and the intercept valves are closed, there is no steam flow through the turbine. To prevent overheating of the reheater tubes, boiler firing must be tripped off if the interruption of steam flow through the reheater is sustained. However, since the closure of the steam valves is temporary, tripping of the boiler firing can be avoided by proper coordination of boiler protection and fuel control with the turbine controls.

In addition, as recommended in reference 4, the overspeed controls must

(i) Not interfere with normal speed governing in such a way that the performance of the islanded system is adversely affected

(ii) Be capable of discriminating between unit rejections and transient system disturbances, e.g., transmission system faults that temporarily reduce unit power

(d) *Power plant auxiliaries.* The effect of voltage and frequency variations experienced during partial load-rejection conditions should be checked to ensure vital auxiliaries will not trip out.

(e) *Steam turbine bypasses.* The use of a steam bypass system permits the reduction of boiler power in a controlled manner. A well-designed turbine bypass system significantly enhances the capability of the power plant to withstand a partial load rejection.

Nuclear plants normally have steam turbine bypass systems. In North America, fossil-fuelled power plants with drum type boilers are not usually equipped with turbine bypass systems. Power plants with once-through boilers have turbine and superheater bypass systems; these are installed primarily for start-up and shutdown duty.

16.3.2 Hydro Power Plants

Experience with the operation of hydraulic units under system islanding conditions has demonstrated that governor tuning is critical [23]. The requirement for good stability of speed control under islanding conditions or other isolated modes of operation is in conflict with the governor settings required for fast loading and unloading under normal synchronous operation. For rapid load changes, it is desirable to have a fast governor response. However, the governor settings that result in a fast response usually cause frequency instability under system-islanding conditions. References 23 to 25 provide general guidelines for selection of the governor settings.

As described in Chapter 9 (Section 9.1.3), the governor settings that can be varied to control the dynamic performance of the generating unit are the dashpot reset time T_R, the temporary droop R_T, and the gate servo system gain K_S. A convenient method of analyzing the effects of variations in these parameters on the stability of

frequency oscillations is the eigenvalue analysis described in Chapter 12. For a determination of the optimum governor parameters, the stability of the generating unit when supplying an isolated non-synchronous load must be considered. This represents the most severe condition from the viewpoint of frequency control.

Table 16.1 shows the effects of varying the governor parameters on the stability of a hydraulic unit with a mechanical starting time T_M of 6.2 seconds and a water starting time T_W of 1.0 second. The unit is assumed to be supplying rated power to an isolated load having a constant power characteristic (equivalent to having a damping coefficient of -1).

Table 16.1 Effects of governor parameters under isolated operation

Governor Parameters			Eigenvalues		
K_S	R_T	T_R	Mode 1	Mode 2	Mode 3
5.0	0.38	1.5	+0.048±j0.60	-1.058	-5.96
5.0	0.38	2.0	-0.006±j0.59	-0.799	-3.87
5.0	0.38	5.0	-0.173±j0.65	-0.255	-3.77
5.0	0.38	10.0	-0.212±j0.72	-0.104	-3.75
5.0	0.24	5.0	-0.003±j0.75	-0.277	-3.44
5.0	0.30	5.0	-0.081±j0.71	-0.237	-3.58
5.0	0.35	5.0	-0.141±j0.68	-0.248	-3.70
5.0	0.40	5.0	-0.193±j0.64	-0.262	-3.82
2.5	0.38	5.0	-0.107±j0.54	-0.252	-2.86
10.0	0.38	5.0	-0.251±j0.73	-0.256	-5.72
5.0	0.30	1.5	+0.095±j0.65	-0.920	-3.68
5.0	0.50	1.5	-0.010±j0.54	-1.140	-4.32
2.5	0.38	1.5	+0.044±j0.51	-0.954	-2.93
10.0	0.38	1.5	+0.039±j0.68	-1.058	-5.96

Table 16.1 lists eigenvalues associated with three modes that are sensitive to variations in governor parameters. The first mode is an oscillatory mode represented by a pair of complex conjugate eigenvalues having a frequency (given by the imaginary component) on the order of 0.6 rad/s or 0.1 Hz. The stability of this mode is of primary concern for isolated operation and during system-islanding conditions. The other two modes listed are non-oscillatory modes represented by real eigenvalues. The reciprocals of the real eigenvalues represent time constants and are a measure of the responsiveness of the governor under isolated operating conditions.

For isolated operation, selection of governor parameters to ensure that the oscillations are very well damped is of primary concern. It is desirable to achieve this without unduly slowing down the speed of response since speed of response affects

the maximum frequency deviation when an island is formed. The results of Table 16.1 show that the variations in the governor parameters have the following effects on the dynamics of the unit under *isolated* operating conditions:

- An increase in dashpot reset time T_R results in an increase in damping, accompanied by a reduction in rate of response.
- An increase in temporary droop R_T results in an increase in damping and a slight decrease in the time to reach steady state.
- An increase in servo system gain K_S results in an improvement in damping as well as in the rate of response. The improvement in the rate of response is primarily through reduction in the time constant associated with mode 3.

The results in Table 16.1 are for a select combination of governor parameters chosen to illustrate the overall nature of the problem. Because a large number of combinations of parameters is possible and because damping of mode 1 is of primary concern, the selection of optimum governor parameters can be better achieved by presenting the results as shown in Figure 16.3. The results are shown in the form of loci of constant damping ratio ζ in an R_T-T_R parameter plane when K_S is held constant. The variations in the natural frequency of oscillation are also shown in the figure.

The results suggest that, for a unit with T_M=6.2 s and T_W=1.0 s, values of R_T less than 0.225, and T_R less than 1.5 s result in unstable frequency oscillations. As T_R is increased from 1.5 s to about 5.0 s, the damping increases significantly. Increasing T_R beyond 5.0 s results in a small improvement in damping at the expense of slowing down the speed of response. This suggests that an appropriate value for T_R is about 5.0 s. The value of R_T can be chosen to give any desired damping ratio. A good value for the damping ratio is 0.25. This can be achieved by setting R_T=0.3 s with T_R=5.0 s. A higher value of R_T would result in higher damping and a slight reduction in time to reach steady state. However, the peak overshoot or maximum frequency deviation would be higher with higher values of R_T.

The effect of the servo system gain K_S is shown in Figure 16.4. These results are an extension of those of Figure 16.3 and show loci of ζ=0 (absolute stability limit) and of ζ=0.25 for three values of K_S. We see that higher values of K_S increase the regions of stability throughout the ranges of R_T and T_R considered.

Similar analyses performed on units having different combinations of water and machine starting times indicate that the optimum choices of the temporary droop R_T and the reset time T_R are represented by the following expressions [23]:

$$R_T = [2.3-(T_W-1.0)0.15]\frac{T_W}{T_M} \tag{16.1}$$

$$T_R = [5.0-(T_W-1.0)0.5]T_W \tag{16.2}$$

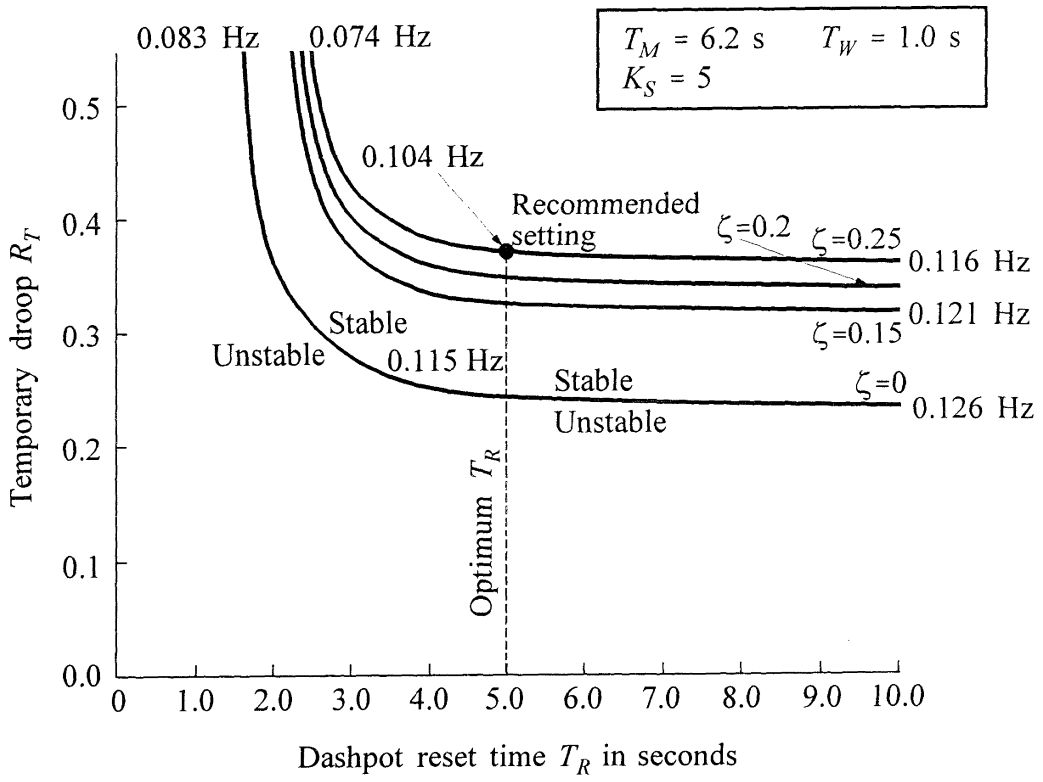


Figure 16.3 Loci of constant damping ratio (ζ) for isolated operation

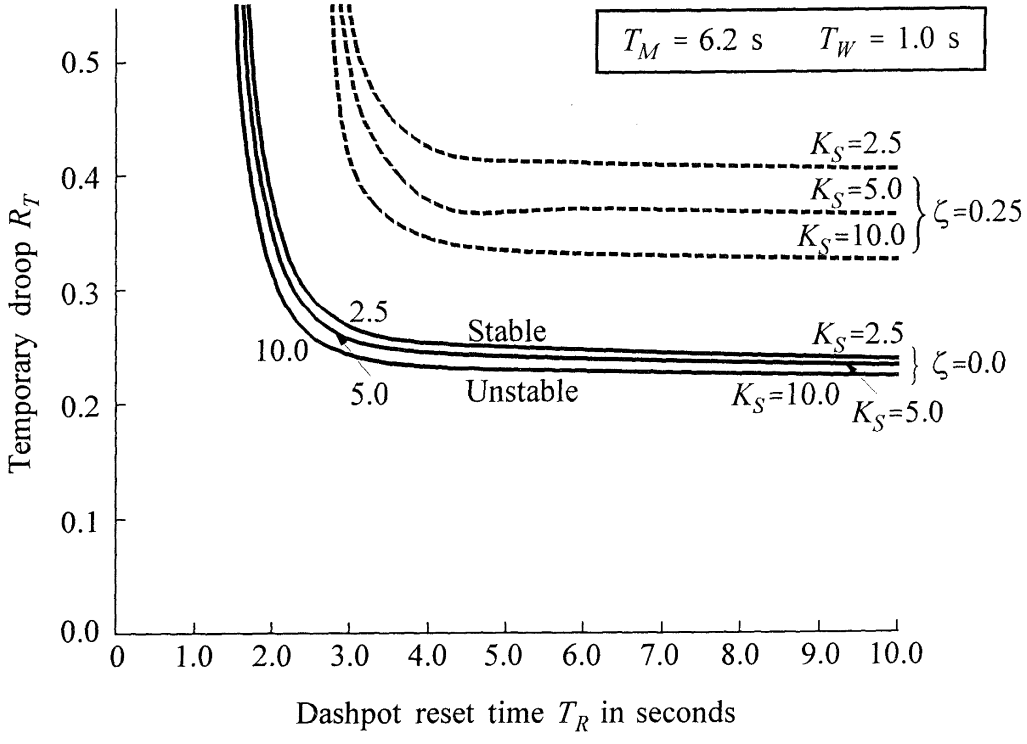


Figure 16.4 Effect of servomotor gain

In addition, the servosystem gain K_S should be set as high as is practically possible. *The above settings ensure good stable performance when the unit is at full load supplying an isolated load; this represents the most severe requirement and ensures stable operation for all situations involving system islanding.*

For loading during normal operation, the above settings result in too slow a response [23]. For satisfactory loading rates, the reset time T_R should be less than 1.0 s, preferably close to 0.5 s.

As discussed in Chapter 9, these conflicting requirements can be met by a dashpot bypass arrangement in which, with the dashpot not bypassed, the settings satisfy the requirements for system islanding conditions or isolated operation; and with the dashpot bypassed, the reset time T_R has a reduced value that results in acceptable loading rates. The dashpot is normally not bypassed so that, in the event of a disturbance leading to an islanding operation, the speed control would be stable. The dashpot is bypassed for brief periods during loading and unloading.

16.4 SIMULATION OF LONG-TERM DYNAMIC RESPONSE

16.4.1 Purpose of Long-Term Dynamic Simulations

The objectives of analysis of long-term dynamics include the following:

(a) Post-mortem analysis of severe upsets [32]. This will help identify the underlying causes of such incidents and develop corrective measures.

(b) Evaluation of the ability of power plants to ride through disturbances. This will help identify deficiencies in equipment responses and in the coordination of control and protective systems.

(c) Examination, at the system planning and design stage, of the system response to extreme contingencies, that is, contingencies that exceed the severity of normal design contingencies. As discussed in Chapter 1 (Section 1.4), the purpose of extreme contingency assessment is to develop measures for reducing the frequency of occurrence of such contingencies and to mitigate the consequences.

(d) Examination of emergency procedures and provision of operator training.

(e) Evaluation of load-shedding practices and policies.

16.4.2 Modelling Requirements

The long-term stability simulation program should include, in addition to the models used in conventional transient stability simulations, adequate representation

of the prime mover and energy supply systems. It should also include appropriate models for the wide range of protection and control systems that are invoked when the system is in the emergency and *in extremis* states.

An examination of major power system disturbances [1-4,26,27] shows that the following protection and control devices have a significant influence on the system dynamic performance during severe system upsets:

(a) Generator and excitation system protection and controls:

- Loss-of-excitation relays
- Underexcitation limiters (UEL)
- Overexcitation limiters (OXL)
- V/Hz limiter and protection

Chapter 8 provides descriptions of these devices.

(b) Electrical network protection and controls:

- Transmission system relays
- Distribution system relays
- Transformer underload tap-changer (ULTC) controls
- Distribution system voltage regulators
- Underfrequency and undervoltage load-shedding relays

Chapters 6 and 11 include descriptions of these devices.

(c) Prime mover/energy supply system protection and controls:

- Turbine overspeed controls and protections
- Turbine underfrequency protection
- Boiler/reactor controls and protections
- Automatic generation control (AGC)

Chapters 9 and 11 provide descriptions of the above. The representation of prime mover and energy supply systems should include appropriate representation of the power plant auxiliaries. Induction motors driving some of these auxiliaries are

affected by off-nominal voltage and/or frequency of the power supply.

For situations involving high network voltage conditions, representation of transformer saturation is important. Where appropriate, the characteristics of motor loads as influenced by off-nominal frequency and voltage variations should be represented.

Off-nominal frequency effects on the representation of the transmission network, synchronous machine stator circuits, and reactive power compensation devices should be accounted for.

The EPRI *long-term stability program* (LTSP) developed under project RP 3144-1 includes most of the above modelling capabilities.

16.4.3 Numerical Integration Techniques

The early long-term dynamic simulation programs, such as LOTDYS [28], assumed uniform frequency and modelled only slow phenomena to achieve computational efficiency. This allowed the use of low order explicit integration techniques, but required special means of initialization. A disadvantage of this approach is that it neglects many important fast transients that influence long-term dynamic response; consequently, many potential system problems are masked.

The present trend is to model fast as well as slow phenomena in long-term dynamic simulations. This is facilitated by the use of implicit integration methods. As discussed in Chapter 13, the implicit integration methods are numerically very stable; stiffness of the differential equations affects accuracy but not numerical stability. With large time-steps, high-frequency modes are filtered out and solutions of slower modes are accurate.

In reference 29, a unified approach to short- and long-term dynamic simulation is implemented by using the trapezoidal integration method. The simulation mode (short- or long-term) is determined by integration step-size. An artificial damping is added to suppress synchronizing power oscillations and to allow larger integration time-steps when simulating the long-term mode. Facilities are provided for switching from one mode to the other by adding or removing the artificial damping and changing the time-step.

Another attractive integration technique for long-term dynamic simulation is the Gear-type backward differentiation formula [30,31]. The second-order Gear method is an implicit self-starting integration algorithm of the predictor-corrector type. The EUROSTAG program described in reference 17 applies this method. The key feature of this application is the automatic adjustment of the integration time-step based on the truncation error. When fast modes are excited, the time-step is reduced to a value below that corresponding to the smallest eigenvalue. As the fast modes decay during the solution process, the time-step is gradually increased. If the fast modes are excited due to a subsequent switching operation, the time-step is automatically reduced. During a long-term dynamic simulation, the time-step may vary between 1 ms and 100 s.

16.5 CASE STUDIES OF SEVERE SYSTEM UPSETS

In this section we consider two case studies: one involving an overgenerated island and the other an undergenerated island.

16.5.1 Case Study Involving an Overgenerated Island

This case study is intended to demonstrate the impact of turbine-generator overspeed controls on the performance of a generation-rich island. It is based on experiences with auxiliary governors (described in Chapter 9, Section 9.2.2) used on some of the generating units in Ontario [4].

An island formed as a result of separation from the rest of the interconnected system of an area consisting of 9,650 MW of generation and 4,750 MW of consumption (load plus losses) is considered (see Figure 16.5). Prior to separation, the area is exporting 4,900 MW; MVAr generation and consumption within the area are nearly equal.

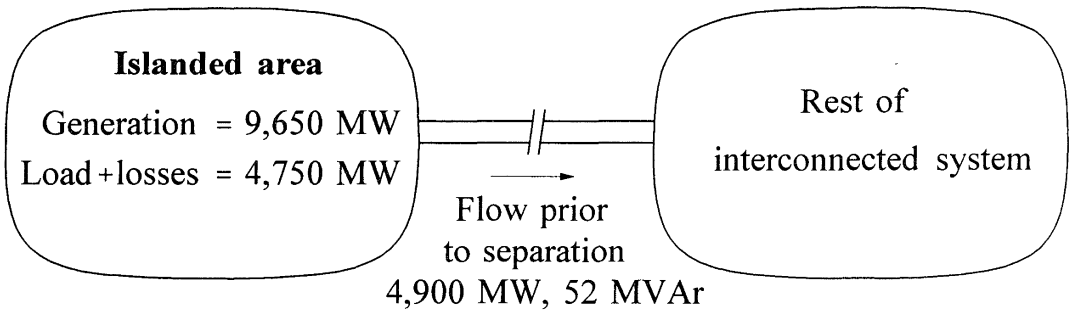


Figure 16.5

The area generation

The generation within the area consists of the following:

- 4,000 MW of nuclear generation at a plant with eight 500 MW units
- 3,850 MW of fossil-fuelled generation at two plants, each with four 500 MW units
- 1,800 MW of hydraulic generation at six plants

Turbine-governing systems

The nuclear units are equipped with *mechanical-hydraulic control* (MHC) governors whose block diagram is shown in Figure 9.31 of Chapter 9. A singular feature of this governing system is the use of an *auxiliary governor*, which becomes operative when the speed exceeds its setting V_1=1%. The auxiliary governor acts in parallel with the main governor to effectively increase the gain of the speed control loop by a factor of about 8. This limits overspeed by rapidly closing the control valves (CVs) as well as the intercept valves (IVs).

The fossil-fuelled units have MHC governors whose block diagram is shown in Figure 9.32.

The model for the governing systems of the hydraulic units is shown in Figure 9.10, with settings given by Equations 16.1 and 16.2 so as to result in heavily damped control under islanding conditions.

Figures 9.7 and 9.24 show the representation of hydraulic turbines and steam turbines, respectively.

Simulation

The disturbance simulated is the simultaneous opening of all ties connecting the area to the rest of the system, the result being an island with generation nearly twice the load. The generators and excitation system are represented in detail. Loads are represented as nonlinear functions of voltage and frequency.

The performance of the islanded system is examined with the auxiliary governors of the nuclear units in service and out of service.

(a) With auxiliary governor in service:

Figure 16.6 shows plots of speed deviation, CV and IV positions, and mechanical power of one of the nuclear units. All units in the area swing together; therefore, the speed plot shown is representative of the area frequency.

As a consequence of islanding, the speed increases rapidly to a maximum of about 6.4% above the normal speed of 1,800 r/min and then oscillates with little damping between 3.5% above and 0.7% below the normal speed. The sustained oscillation is due to the action of the auxiliary governors. When the overspeed exceeds the setting V_1 of 1%, the auxiliary governors close the steam valves and reduce the mechanical power of the nuclear units to zero. The deficit in the generated power reduces the speed rapidly, and the valves open again. The resultant increase in mechanical power is such that the speed exceeds the auxiliary governor setting of 1%, and the valves close again. The cycle repeats with a period of about 7 seconds.

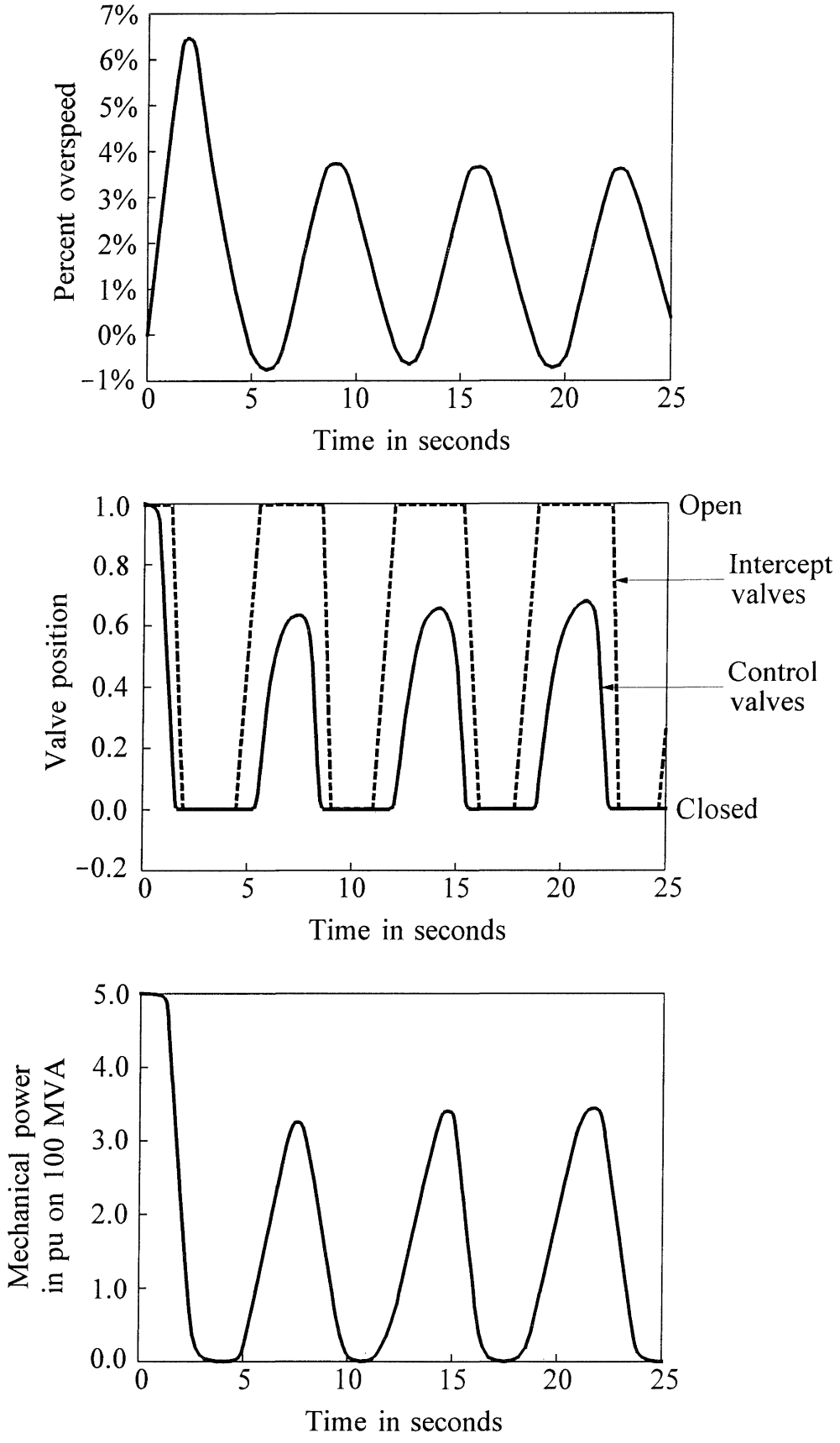


Figure 16.6 Transient response of nuclear units with auxiliary governor

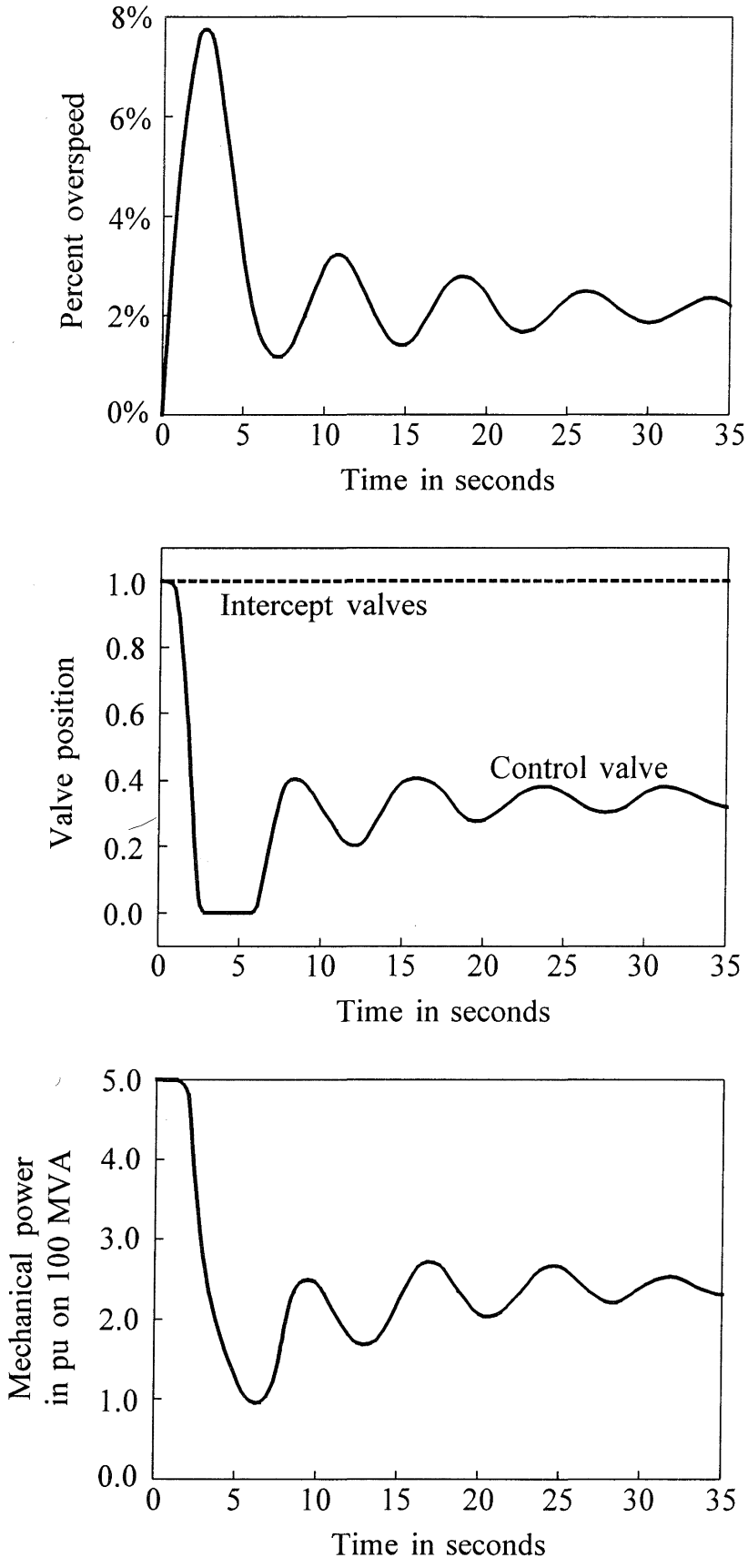


Figure 16.7 Transient response of nuclear units with auxiliary governor out of service

(b) With auxiliary governor out of service:

Figure 16.7 shows the results with the auxiliary governors of nuclear units out of service. The speed deviation reaches a maximum of about 7.7% and damps to a steady state value of nearly 2% above the nominal. The removal of the auxiliary governor results in stable frequency control. Only the CVs respond to speed changes and the IVs remain fully open because the main governor alone is not enough to overcome the intercept valve-opening bias.

From the above results, it is clear that the auxiliary governors cause instability of the speed control during system-islanding conditions. The other units in the island respond to oscillations of the units with auxiliary governors; the overall effect is to cause oscillations of all units. The resulting movements of steam valves or wicket gates continue until the hydraulic systems of the governors run out of oil and cause unit tripping and possibly a blackout of the island. The power oscillations may also give rise to "priming" of the boilers of the fossil-fuel-fired units that causes water from the boilers to come in contact with the high temperature superheat and HP stages.

A possible solution to this problem is to replace the auxiliary governor with an electronic acceleration detector [4].

This case study has assumed that the steam generation systems perform satisfactorily by following the demands of the turbine. Reference 33 illustrates the types of problems that may be caused by unsatisfactory response of steam generation system protections and controls of a nuclear unit.

16.5.2 Case Study Involving an Undergenerated Island

This case study is intended to illustrate the performance of an undergenerated island as influenced by underfrequency load shedding and power plant control. In addition, it demonstrates the requirement for adequate voltage and reactive control.

Power generation and conditions

An island formed as a result of separation of an area consisting of 2,218 MW generation and 3,283 MW load is considered. Prior to islanding, the area is importing 1,103 MW and exporting 1,590 MVAr, as shown in Figure 16.8.

The generation mix within the area is as follows:

- 1,200 MW nuclear generation supplied by two units in one plant
- 1,018 MW of hydraulic generation supplied by six plants

The two nuclear units are operating at their load limits. The hydraulic generation has a spinning reserve of about 170 MW.

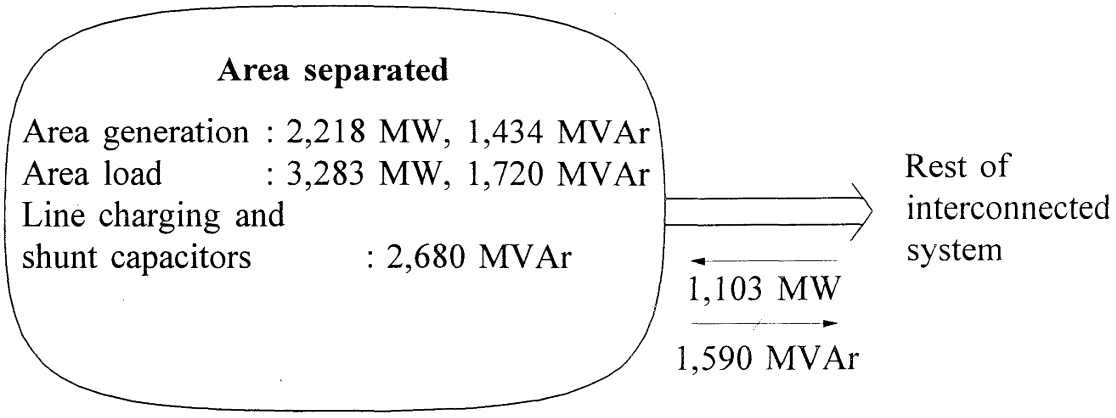


Figure 16.8 Active and reactive power conditions prior to separation

Underfrequency load shedding

Frequency trend relays (see Chapter 11, Section 11.1.7) are used to shed up to 50% load in four blocks depending on the frequency drop and the rate of frequency decline as depicted by Figure 11.31. The load shedding is delayed by about 0.5 second after the relay has operated.

Simulation of islanding condition

The islanding condition is simulated by opening the ties between the area under consideration and the rest of the interconnected system. The detail of representation of the power plants and other elements of the system is similar to that of the case study described in Section 16.5.1. The nuclear units are equipped with thyristor exciters with power system stabilizers and electrohydraulic governing systems. The hydraulic units are equipped with rotating dc exciters and mechanical hydraulic governors. Two cases are considered: one with no capacitor switching and the other with capacitors having a nominal rating of 700 MVAr switched out following islanding. Loads are represented as nonlinear functions of voltage and frequency.

(a) With no capacitor switching:

The switching sequence, including that resulting from load-shedding relays, is as follows:

Time (seconds)	Event
0.5	Island is formed by simultaneous tripping of ties.
0.9	System frequency drops to 59.5 Hz and rate of frequency decline is 1.25 Hz/s; the conditions for tripping the first two blocks of load are satisfied.

1.4	25% of area load is rejected.
1.6	System frequency drops to 58.8 Hz; the condition for tripping the fourth block of load is satisfied.
2.2	Additional 15% of load is rejected.
50.0	Simulation is terminated.

(Note: The rate of frequency does not exceed 2 Hz/s; hence, the third block of load is not shed.)

Figures 16.9 to 16.11 show plots of frequency, terminal voltage and reactive power output of one of the nuclear units, voltage of a load bus, total mechanical power and electrical power of all the generators, and the total active power supplied to the area loads. From Figure 16.9, we see that the system frequency drops below 58.5 Hz in about 2 seconds and remains below this level in spite of shedding about 40% of the area load. The reason for this is evident from Figures 16.10 and 16.11. Because of surplus reactive power in the area, the system voltages increase significantly after islanding, and this keeps the load power high even after shedding load.

The total reactive power absorbed by the nuclear units exceeds the continuous end-region heating limit of the generators (see Chapter 5, Section 5.4.1).

Figure 16.12 shows the apparent impedance seen by a loss-of-excitation (LOE) relay located at the terminals of one of the nuclear units. We see that the impedance locus does not enter the trip characteristic of the relay.

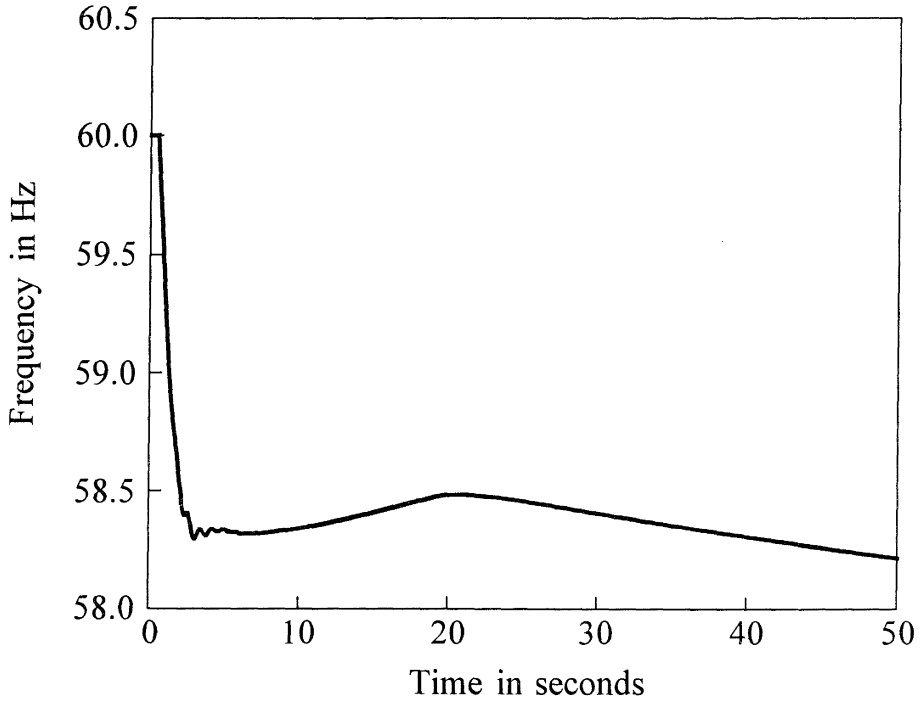


Figure 16.9 System frequency with underfrequency load shedding and no capacitor switching

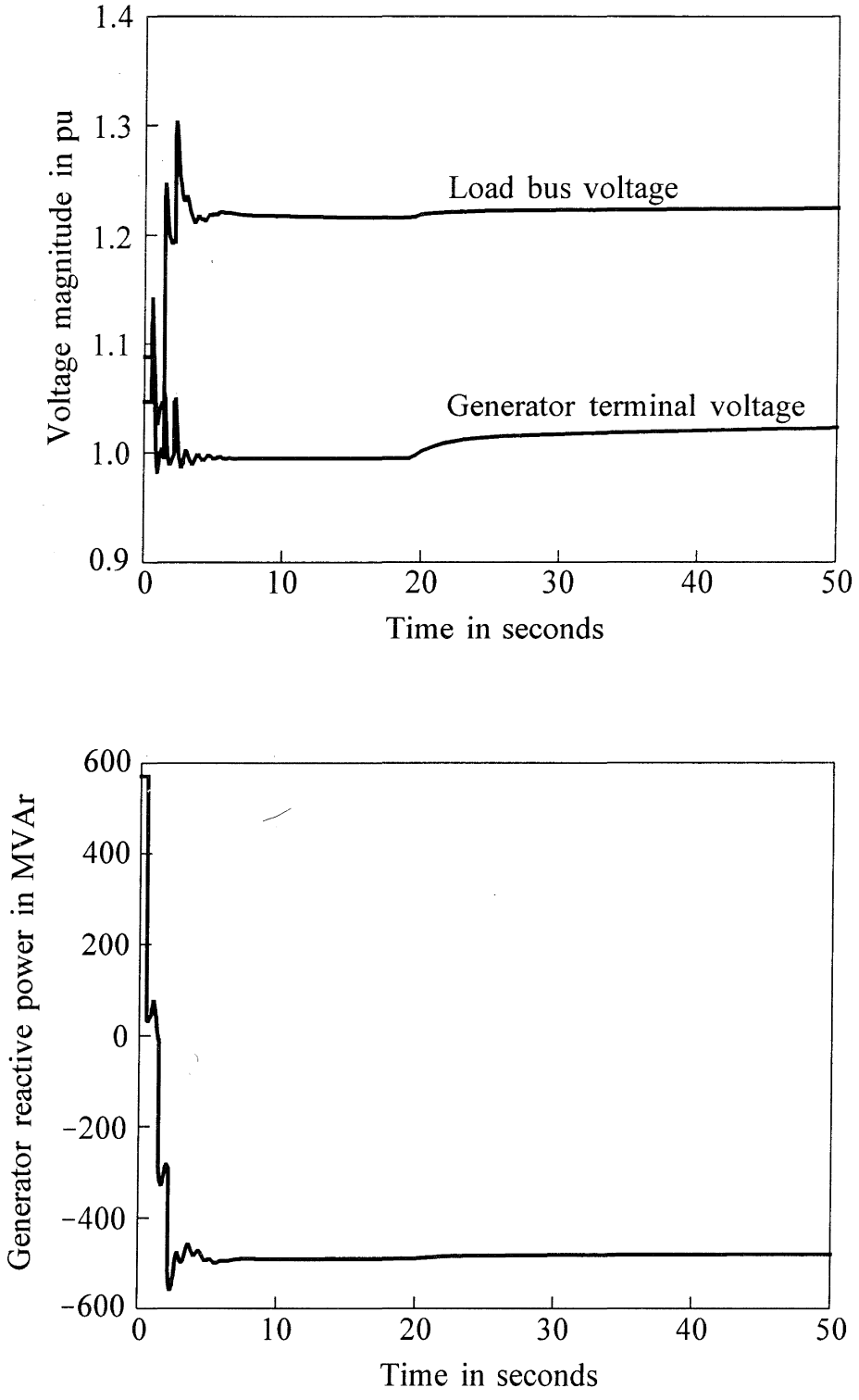


Figure 16.10 Nuclear unit terminal voltage and reactive power and load bus voltage with load shedding and no capacitor switching

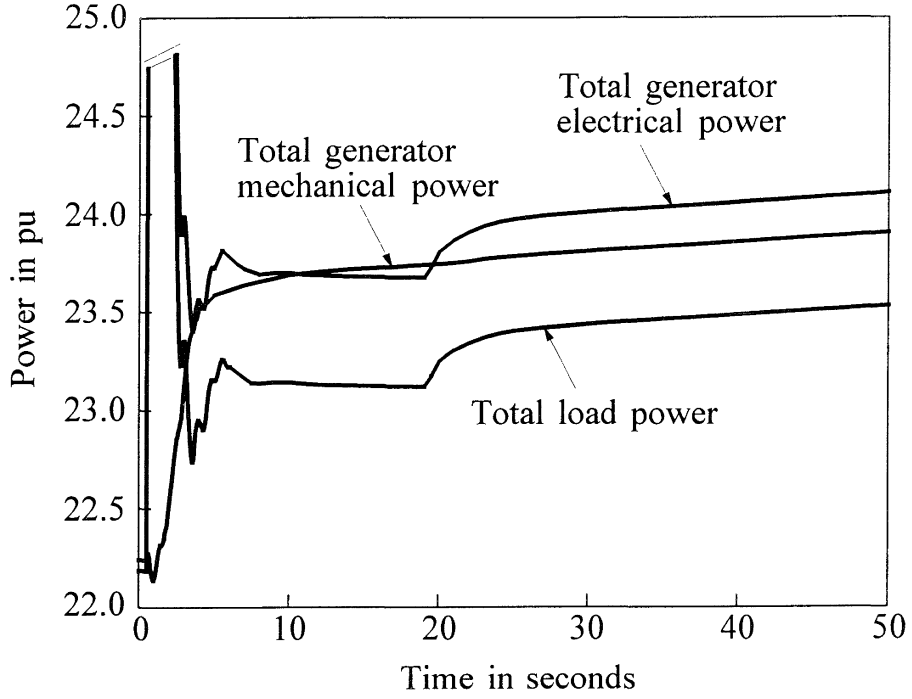


Figure 16.11 Total generated mechanical and electrical power and load power with load shedding and no capacitor switching

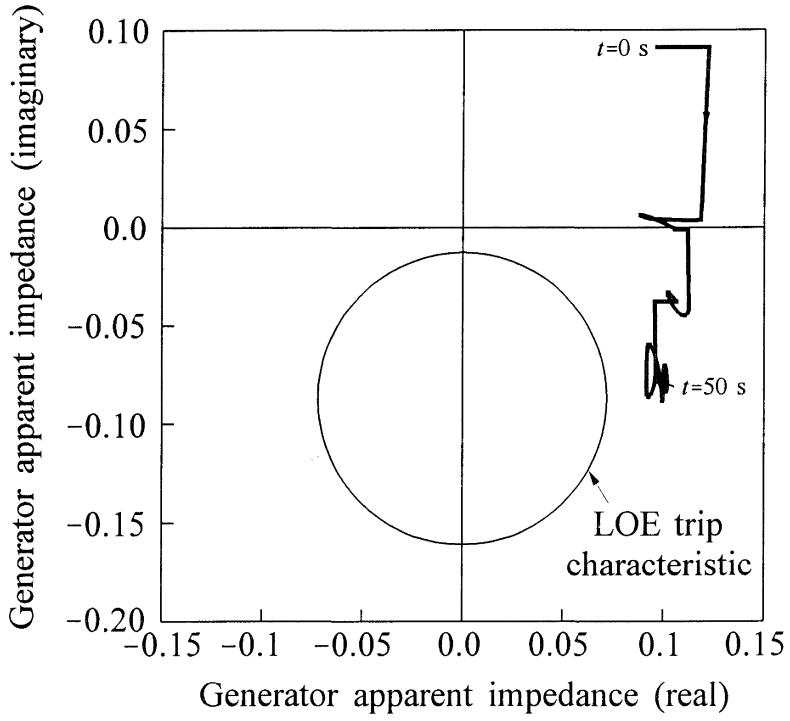


Figure 16.12 Locus of apparent impedance seen by LOE relay; impedance expressed in per unit on 100 MVA base

(b) With 720 MVAr of shunt capacitors switched out:

The switching sequence in this case is as follows:

Time (seconds)	Event
0.5	Island is formed.
0.9	The conditions for tripping first two blocks of load are satisfied.
1.4	25% of load is shed; 485 MVAr capacitors are switched out.
1.8	Frequency drops below 58.8 Hz; the condition for tripping the fourth block of load is satisfied.
2.3	Additional 15% of load is shed; 235 MVAr capacitors are switched out.
50.0	Simulation is terminated.

Figures 16.13 to 16.15 show the corresponding results. In this case, the system voltages do not rise as high as in the previous case. Following load shedding, the total active power supplied to the loads falls below the available generation. The system frequency recovers to the nominal value (60 Hz) in about 20 seconds and reaches a maximum value of about 60.1 Hz. The steady-state frequency settles at a value slightly above the nominal value as determined by the droop characteristics of the speed governors of all the generating units in the area.

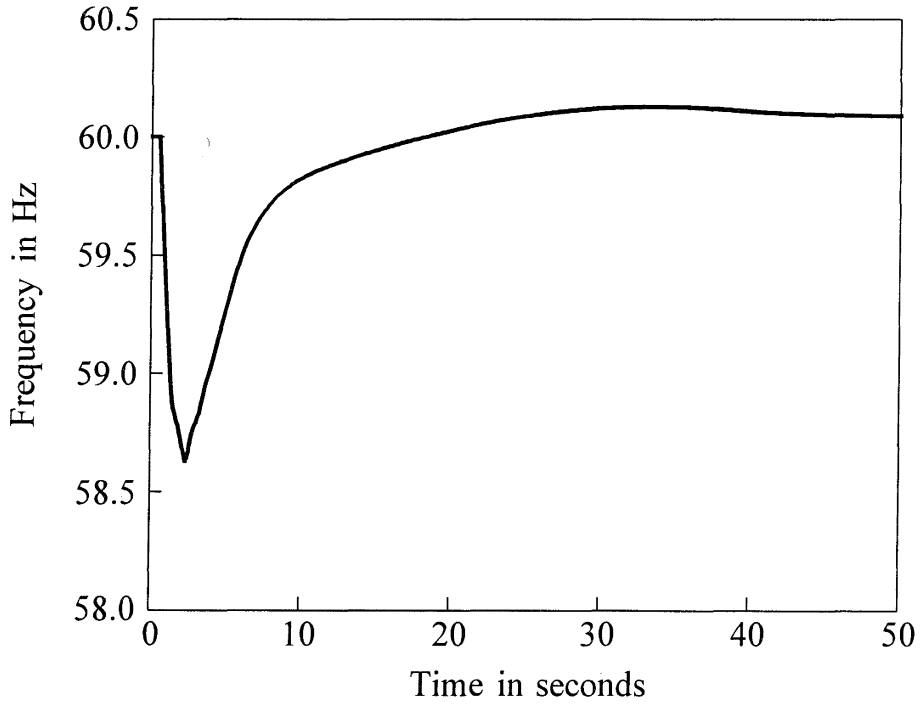


Figure 16.13 System frequency with underfrequency load shedding and capacitor switching

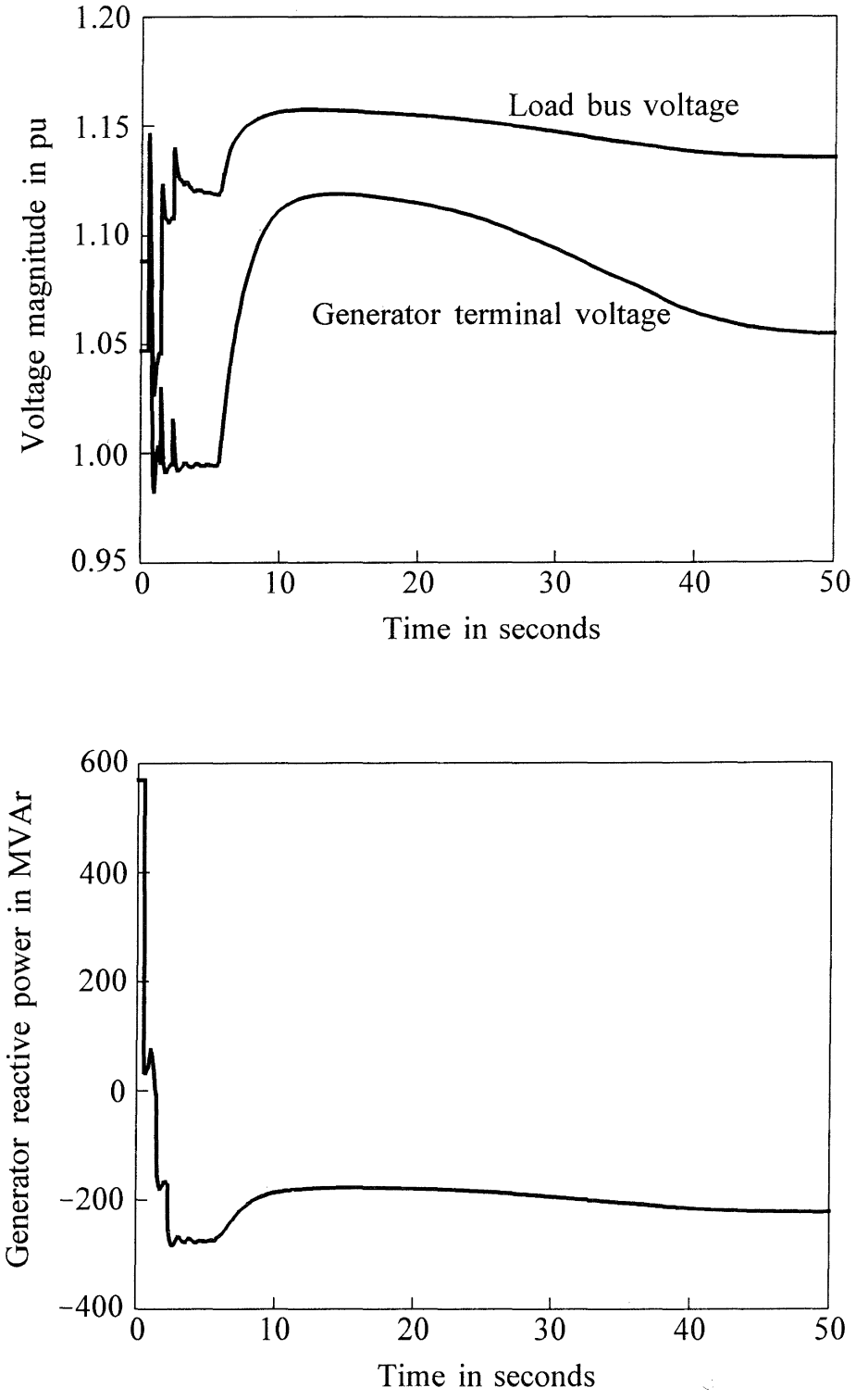


Figure 16.14 Nuclear unit terminal voltage and reactive power and load bus voltage with load shedding and capacitor switching

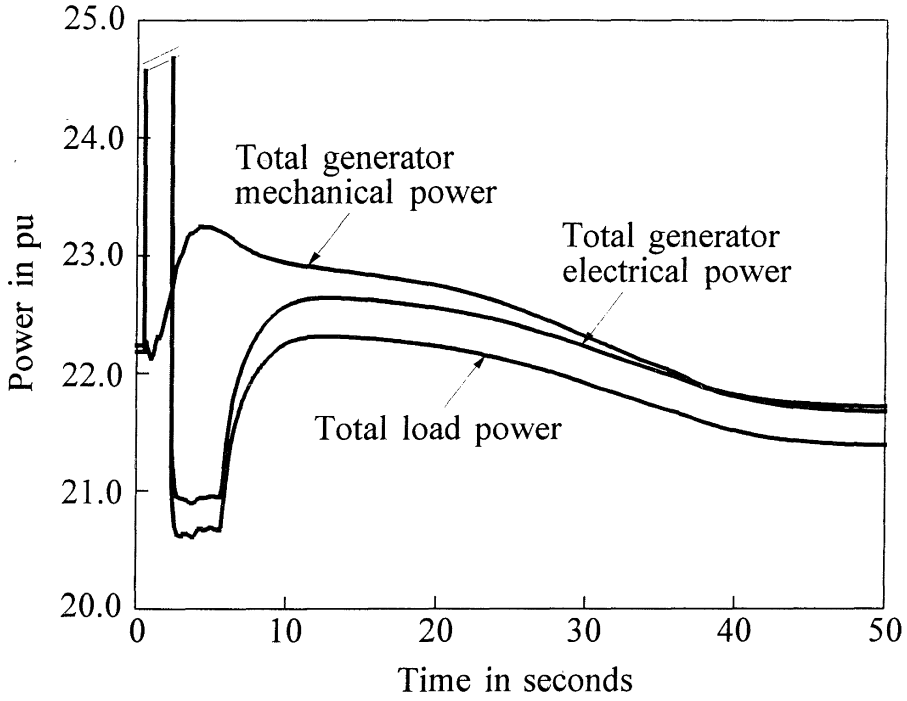


Figure 16.15 Total generated mechanical and electrical power and load power with load shedding and capacitor switching

Figure 16.14 shows that the terminal voltage of the nuclear unit increases rapidly during the period between 5 and 10 seconds and then gradually drops to about 1.05 pu. This response of the generator voltage is due to the action of the power system stabilizer and can be modified to some extent by changing the parameters of the PSS (see Chapter 17, Section 17.2.1).

With capacitor switching, the reactive power absorbed by the nuclear unit is within the continuous capability of the generator.

REFERENCES

[1] D.R. Davidson, D.N. Ewart, and L.K. Kirchmayer, "Long-Term Dynamic Response of Power System Disturbance: An Analysis of Major Disturbances," *IEEE Trans.*, Vol. PAS-94, No. 3, pp. 819-826, May/June 1975.

[2] C. Concordia, D.R. Davidson, D.N. Ewart, L.K. Kirchmayer, and R.P. Schulz, "Long-Term Power System Dynamics - A New Planning Dimension," CIGRE Paper 32-13, 1976.

[3] U.G. Knight, "International Survey of Major Disturbances," CIGRE SC32/WG01 Report, 1978.

[4] P. Kundur, D.C. Lee, J.P. Bayne, and P.L. Dandeno, "Impact of Turbine Generator Overspeed Controls on Unit Performance under System Disturbance Conditions," *IEEE Trans.*, Vol. PAS-104, No. 6, pp. 1262-1267, June 1985.

[5] D.N. Ewart, "Whys and Wherefores of Power System Blackouts," *IEEE Spectrum*, pp. 36-41, April 1978.

[6] L.H. Fink and K. Carlsen, "Operating under Stress and Strain," *IEEE Spectrum*, pp. 48-53, March 1978.

[7] R.M. Maleszwski, R.D. Dunlop, and G.L. Wilson, "Frequency Actuated Load Shedding and Restoration," *IEEE Trans.*, Vol. PAS-90, No. 4, pp. 1452-1459, 1971.

[8] G.A. Weber, M.C. Winter, and S.M. Follen, "Nuclear Plant Response to Grid Electrical Disturbances," EPRI Report NP-2849, February 1983.

[9] V.F. Carvalho, "Power Plant Control," CIGRE SC39/WG04 Survey Paper D, CIGRE SC39/IFAC Meeting, Florence, September 1983.

[10] D. Rumpel et al., "Tripping to Houseload - Methods, Application, Experience," CIGRE SC39/IFAC Meeting, Florence, September 1983.

[11] CIGRE Working Group 32-03, "Tentative Classification and Terminologies Relating to Stability Problems of Power Systems," *Electra*, No. 56, 1978.

[12] EPRI Report EL-596, "Midterm Simulation of Electric Power Systems," Project RP745, June 1975.

[13] K. Hemmaplardh, J.W. Manke, W.R. Pauly, and J.W. Lamont, "Considerations for Long Term Dynamic Simulation Program," *IEEE Trans.*, Vol. PWRS-1, pp. 129-135, February 1986.

[14] V. Converti, D.P. Gelopulos, M. Housley, and G. Steinbrenner, "Long-Term Stability Solution of Interconnected Power Systems," *IEEE Trans.*, Vol. PAS-95, No. 1, pp. 96-104, January/February 1976.

[15] Discussion of reference 14 by R.P. Schulz and H.H. Happ.

[16] CIGRE Task Force 38-02-08, "An International Survey of the Present Status and the Perspective of Long Term Dynamics in Power Systems," Final Report, January 1992.

[17] M. Stubbe, A. Bihain, J. Deuse, and J.C. Badder, "STAG - A New Unified

Software Program for the Study of the Dynamic Behaviour of Electrical Power Systems," *IEEE Trans.*, Vol. PWRS-4, No. 1, pp. 129-138, February 1989.

[18] P. Kundur, "A Survey of Utility Experiences with Power Plant Response during Partial Load Rejections and System Disturbances," *IEEE Trans.*, Vol. PAS-100, No. 5, pp. 2471-2475, May 1981.

[19] T.D. Younkins and L.H. Johnson, "Steam Turbine Overspeed Control and Behaviour during System Disturbances," *IEEE Trans.*, Vol. PAS-100, No. 5, pp. 2504-2511, May 1981.

[20] O.W. Durrant, "Boiler Response to Partial Load Rejections Resulting from System Upsets," IEEE Paper 81-JPGC-922-4, presented at 1981 Joint Power Generation Conference, St. Louis, MO. October 4-8, 1981.

[21] A.H. Rawdon and F.A. Palacios, "Effects of Partial Load Rejection on Fossil Utility Steam Generators," IEEE Paper 81-JPGC-907-5, presented at 1981 Joint Power Generation Conference, St. Louis, MO, October 4-8, 1981.

[22] IEEE Working Group Report, "Guidelines for Enhancing Power Plant Response to Partial Load Rejections," *IEEE Trans.*, Vol. PAS-102, No. 6, pp. 1501-1504, June 1983.

[23] P.L. Dandeno, P. Kundur, and J.P. Bayne, "Hydraulic Unit Dynamic Performance under Normal and Islanding Conditions - Analysis and Validation," *IEEE Trans.*, Vol. PAS-97, No. 6, pp. 2134-2143, November/ December 1978.

[24] L.M. Hovey, "Optimum Adjustment of Hydro Governors on Manitoba Hydro System," *AIEE Trans.*, Vol. 81, Part III, pp. 581-587, December 1962.

[25] F.R. Schleif and A.B. Wilbor, "The Coordination of Hydraulic Turbine Governors for Power System Operation," *IEEE Trans.*, Vol. PAS-85, pp. 750-758, July 1966.

[26] R.P. Schulz, "Capabilities of System Simulation Tools for Analyzing Severe Upsets," *Proceedings of International Symposium on Power System Stability*, Ames, Iowa, pp. 209-215, May 13-15, 1985.

[27] EPRI Report EL-6627, "Long-Term Dynamic Simulation: Modelling Requirements," Final Report of Project 2473-22, Prepared by Ontario Hydro, December 1989.

[28] EPRI Report, "Long-Term Power System Dynamics," Final Report of Project

RP 90-7, Prepared by General Electric Company, April 1974.

[29] R.J. Frowd, J.C. Giri, and R. Podmore, "Transient Stability and Long-Term Dynamics Unified," *IEEE Trans.*, Vol. PAS-101, pp. 3841-3850, October 1982.

[30] C.W. Gear, "Simultaneous Numerical Solution of Differential-Algebraic Equations," *IEEE Trans.*, Vol. CT-18, No. 1, pp. 89-95, January 1971.

[31] C.W. Gear, "The Automatic Integration of Ordinary Differential Equations," *Communications of the ACM*, Vol. 14, No. 3, March 1981.

[32] N.J. Balu, H.W. Mosteller, and R.P. Schulz, "LOTDYS Analysis of August 1973 Gulf Coast Area Power System Disturbance," *IEEE Trans.*, Vol. PAS-100, pp. 2471-2475, May 1981.

[33] Q.B. Chou, P. Kundur, P.N. Acchione, and B. Lautsch, "Improving Nuclear Generating Station Response for Electrical Grid Islanding," *IEEE Trans.*, Vol. EC-4, No. 3, pp. 406-413, September 1989.

Chapter 17

Methods of Improving Stability

The preceding five chapters have described the physical aspects of the various categories of power system stability, and methods of their analysis. As well, key factors influencing stability problems and methods of mitigation have been covered. This chapter discusses special methods used for enhancing transient and small-signal stability. These two categories of system stability have received considerable attention since the 1960s, and methods for their improvement are further evolved than those for other categories.

For a given system, any one method of improving stability may not be adequate. The best approach is likely to be a combination of several methods judiciously chosen so as to most effectively assist in maintaining stability for different contingencies and system conditions. In applying these methods to the solution of specific stability problems, it is important to keep in mind the overall performance of the power system. Solutions to the stability problem of one category should not be effected at the expense of another category.

Many of the methods for stability enhancement described in this chapter are options normally available for economic design of the system. With proper design and application they should greatly contribute to the flexibility of system operation without compromising other aspects of system performance.

Some of the methods described are, however, somewhat "heroic" in nature and can be justified only in special situations. While improving system stability, they impose duty on some of the equipment. Their application, therefore, has to be based on a careful assessment of the benefits and costs.

17.1 TRANSIENT STABILITY ENHANCEMENT

Methods of improving transient stability try to achieve one or more of the following effects:

(a) Reduction in the disturbing influence by minimizing the fault severity and duration.

(b) Increase of the restoring synchronizing forces.

(c) Reduction of the accelerating torque through control of prime-mover mechanical power.

(d) Reduction of the accelerating torque by applying artificial load.

The following are various methods of achieving these objectives.

17.1.1 High-Speed Fault Clearing

The amount of kinetic energy gained by the generators during a fault is directly proportional to the fault duration; the quicker the fault is cleared, the less disturbance it causes.

Two-cycle breakers, together with high-speed relays and communication, are now widely used in locations where rapid fault clearing is important.

In special circumstances, even faster clearing may be desirable. Reference 1 describes the development and application of a one-cycle circuit breaker by Bonneville Power Administration (BPA). Combined with a rapid response overcurrent type sensor, which anticipates fault magnitude, nearly one-cycle total fault duration is attained. One-cycle breakers are not yet in widespread use. Reference 2 describes an ultra-high-speed relaying system for EHV lines based on travelling wave detection.

17.1.2 Reduction of Transmission System Reactance

The series inductive reactances of transmission networks are primary determinants of stability limits. The reduction of reactances of various elements of the transmission network improves transient stability by increasing postfault synchronizing power transfers. Obviously, the most direct way of achieving this is by reducing the reactances of transmission circuits, which are determined by the voltage rating, line and conductor configurations, and number of parallel circuits. The following are additional methods of reducing the network reactances:

(a) Use of transformers with lower leakage reactances.

(b) Series capacitor compensation of transmission lines.

Typically, the per unit transformer leakage reactance ranges between 0.1 and 0.15. For newer transformers, the minimum acceptable leakage reactance that can be achieved within the normal transformer design practices has to be established in consultation with the manufacturer [3]. In many situations, there may be a significant economic advantage in opting for a transformer with the lowest possible reactance.

Series capacitors directly offset the line series reactance. We discussed the application of series capacitors for reactive power and voltage control in Chapter 11. As shown in Section 11.2.8, the maximum power transfer capability of a transmission line may be significantly increased by the use of series capacitor banks. This directly translates into enhancement of transient stability, depending on the facilities provided for bypassing the capacitor during faults and for reinsertion after fault clearing (see Section 11.2.5). Speed of reinsertion is an important factor in maintaining transient stability [4]. Early designs of protective gaps and bypass switches limited the benefits achievable by series capacitor compensation. However, with the present trend of using nonlinear resistors of zinc oxide, the reinsertion is practically instantaneous.

As discussed in Chapter 15 (Section 15.3), one problem with series capacitor compensation is the possibility of subsynchronous resonance with the nearby turbo alternators. This aspect must be analyzed carefully and appropriate preventative measures must be taken.

Traditionally, series capacitors have been used to compensate for very long overhead lines. Recently, there has been an increasing recognition of the advantages of compensating shorter, but heavily loaded, lines by using series capacitors.

For transient stability applications, the use of *switched series capacitors* offers some advantages. Upon detection of a fault or power swing, a series capacitor bank can be switched in and then removed about 0.5 second later. Such a switched bank can be located in a substation where it can serve several lines.

In reference 5 it is shown that, for a given transient stability limit, the aggregate rating of series capacitors required is less if some are switched than if all are unswitched. The scheme with a portion of the capacitors switched reduces the angular swings of the machines, and this in turn reduces fluctuation of loads, particularly those near the electrical centre.

Protective relaying is made more complex when series compensation is used, particularly if the series capacitors are switched.

17.1.3 Regulated Shunt Compensation

Shunt compensation capable of maintaining voltages at selected points of the transmission system can improve system stability by increasing the flow of synchronizing power among interconnected generators. Synchronous condensers or static var compensators described in Chapter 11 (Sections 11.2.6 to 11.2.8) can be used for this purpose.

As illustrated in Section 11.2.8, regulated shunt compensation increases the maximum power transfer capability of a long transmission line. This clearly enhances transient stability.

17.1.4 Dynamic Braking [6-10]

Dynamic braking uses the concept of applying an artificial electrical load during a transient disturbance to increase the electrical power output of generators and thereby reduce rotor acceleration.

One form of dynamic braking involves the switching in of *shunt resistors* for about 0.5 second following a fault to reduce the accelerating power of nearby generators and remove the kinetic energy gained during the fault. BPA has used such a scheme for enhancing transient stability for faults in the Pacific northwest [8]; the brake consists of a 1400 MW, 240 kV resistor made up of 45,000 ft of 1/2 inch stainless steel wire strung on three towers. Reference 9 provides brief reports of braking resistor applications in Japan, China, Russia, and Australia.

To date, braking resistors have been applied only to hydraulic generating stations remote from load centres. Hydraulic units, in comparison to thermal units, are quite rugged; therefore, they can withstand the sudden shock from the switching in of resistors without any adverse effect on the units.

If braking resistors are applied to thermal units, the effect on shaft fatigue life must be carefully examined (see Chapter 15, Section 15.4). If the switching duty is found unacceptable, the switching in of the resistors may have to be performed in three or four steps spread over one full cycle of the lowest torsional mode [10].

The braking resistors used to date are all shunt devices. Alternatively, *series resistors* may be used to provide the braking effect. In this case, the energy dissipated is proportional to the generator current rather than to the voltage. One way of inserting the resistors in series is to install a star-connected three-phase resistor arrangement with a bypass switch in the neutral of the generator step-up transformer to reduce resistor insulation and switch requirements [10]. The resistor is inserted during a transient disturbance by opening the bypass switch.

Another form of braking resistor application that enhances system stability for unbalanced ground faults only, consists of a resistor connected permanently between the ground and the neutral of the Y-connected high-voltage winding of the generator step-up transformer [30]. Under balanced conditions no current flows through the neutral resistor. When line-to-ground or double line-to-ground faults occur, current flows through the neutral connection and the resistive losses act as a dynamic brake.

With the switched form of braking resistors, the switching times should be based on detailed simulations. If the resistors remain connected too long, there is a possibility of instability on the "backswing."

17.1.5 Reactor Switching

Shunt reactors near generators provide a simple and convenient means of improving transient stability. The reactor normally remains connected to the network. The resulting reactive load increases the generator internal voltage, and this is beneficial to stability. Following a fault, switching out the reactor further improves stability.

17.1.6 Independent-Pole Operation of Circuit Breakers

Independent-pole operation refers to the use of separate mechanisms for each phase of the circuit-beaker so that the three phases are closed and opened independently of each other. As a result, the failure of one pole will not restrict the operation of the other two poles. Although the breaker poles operate independently of each other, the relaying system is normally arranged to trip all three poles for any type of fault.

Independent-pole operation can be used advantageously at locations where the system design criteria include a three-phase fault compounded by breaker failure. Maintaining system stability for the contingency of a three-phase fault with all three poles of a primary circuit-breaker failing to open is extremely difficult. With breakers designed for independent-pole operation, a failure of all three poles is highly improbable. The use of duplicate relay systems, circuit-breaker trip coils, and operating mechanisms practically guarantees that at least two poles will open. Therefore, the independent operation of the failed breaker will reduce a three-phase fault to a single line-to-ground fault when two of the poles open. Thus, the severity of a three-phase fault with a stuck breaker is significantly reduced.

17.1.7 Single-Pole Switching

Single-pole switching uses separate operating mechanisms on each phase; for single line-to-ground faults, the relaying is designed to trip only the faulted phase, followed by fast reclosure within 0.5 to 1.5 seconds. For multiphase faults, all three phases are tripped.

During the period when one phase is open, power is transferred over the remaining two phases.

As most faults on transmission lines are of the single line-to-ground type, opening and reclosing of only the faulted phase results in an improvement in transient stability over three-phase tripping and reclosing.

Single-pole switching is particularly attractive for situations where a single major line connects two systems or where a single major line connects a generating station to the rest of the system. It may also be used on systems with multiple lines to improve system security against multiple contingency disturbances [11].

There are three potential problems that need to be considered in applying single-pole switching:

- Secondary-arc extinction.
- Fatigue duty on turbine-generator shafts and turbine blades.
- Thermal duty on nearby generators due to negative-sequence currents.

Secondary-arc extinction

When one phase of a three-phase line is open at both ends, the faulted phase is capacitively and inductively coupled to the two unfaulted phases, which are still energized (see Figure 17.1). A voltage will be induced in the isolated phase because of the capacitive coupling, and to a lesser extent because of the inductive coupling. The magnitude of the induced voltage is a direct function of the phase-to-phase and phase-to-ground capacitances. The induced voltage may sustain the fault arc for an extended period following the opening of the phase. The arc on the faulted phase conductor after it has been switched off is called the *secondary arc*. The secondary-arc current is primarily determined by the circuit voltage and the length of the line section that is switched out. It is also influenced by the fault location, any shunt reactors connected directly to the open phase, and line transposition.

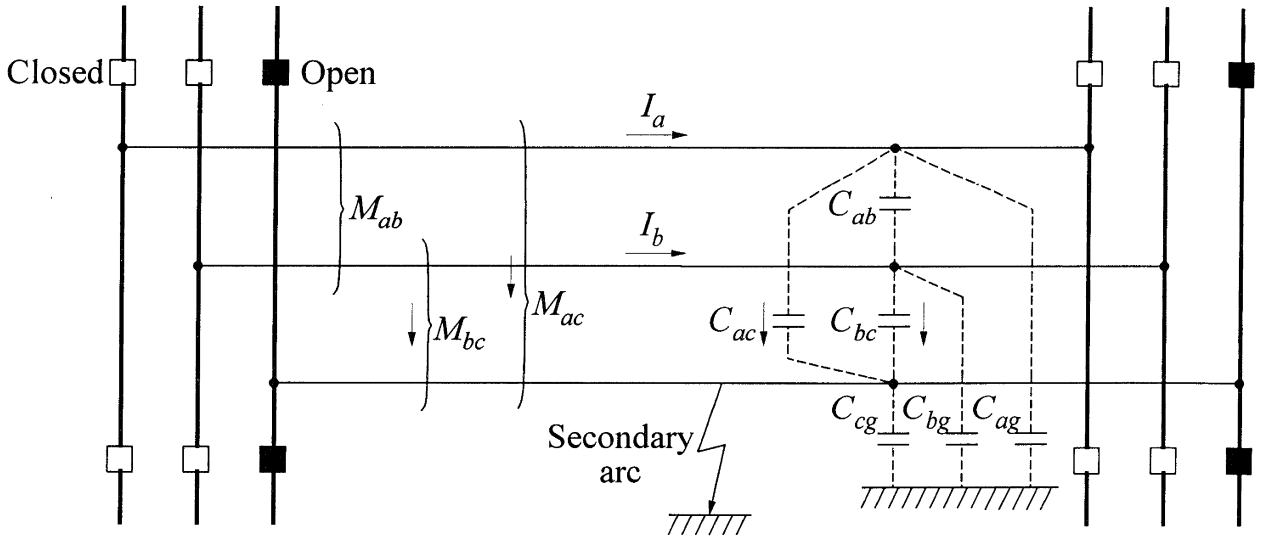


Figure 17.1 Secondary-arc current

The capacitive component of the secondary-arc current is essentially independent of the fault location and the load current. The inductive component of the current is very dependent on the load currents on the two energized phases and on the location of the fault; it is nearly zero for a fault at the middle of the line and is maximum for a fault at either end. Reference 12 gives typical values of the secondary-arc current for 765 kV and 345 kV lines: the capacitive component of the current per 100 mi (160 km) of line length is on the order of 50 A for 765 kV lines and 30 A for 345 kV lines; the maximum inductive component of the current is in the range of 10 to 15 A for 765 kV lines when the power transfer on the two energized phases corresponds to the surge impedance loading.

In reference 13, the results of arc extinction tests carried out on the American Electric Power system are compared with the published results of tests on other

systems and laboratory tests. The general conclusion is that the secondary arc should self-extinguish within 500 ms if the arc current is on the order of 40 A or less on lines with shunt reactor compensation and 20 A or less on uncompensated lines.

For applications where the secondary-arc current is higher than the above values, it is necessary to neutralize the capacitive reactance. One method is to use shunt inductive reactors. The four-legged reactor scheme described in references 14 and 15 has been used in a number of single-pole switching applications for reduction of secondary-arc current [11]. In this scheme, a phase reactor is connected between each phase and a neutral point, and a neutral reactor is connected between ground and the neutral point. This method is particularly attractive if shunt reactors are required to compensate the normal line-charging current for voltage control (see Chapter 11, Section 11.2.3). By appropriate connection, these reactors can be made to serve the additional purpose of reducing secondary-arc current.

Another method of secondary-arc suppression is to use high-speed grounding switches as described in reference 16. This method is attractive for lines without shunt reactors.

Fatigue duty on turbine-generator turbine blades and shafts

As discussed in Chapter 9 (Section 9.2.3), one of the design considerations of long low-pressure turbine blades is that the frequencies of the fundamental vibratory modes must not coincide with multiples of running speed. Single-pole switching during the reclosing dead time when one phase is open can excite 120 Hz torque oscillations. These oscillations may resonate with the blade natural-vibration modes and thus damage the blades.

A single-pole switching sequence imposes successive disturbances on the turbine-generator shaft system. The initial disturbance is due to the fault itself, which for a line-to-ground fault is not very severe. When the fault is cleared by opening the faulted phase, a second disturbance is imposed. Reclosing of the opened phase, either successful or unsuccessful, imposes an additional disturbance. As discussed in Chapter 15 (Section 15.4), the shaft torsional oscillations resulting from successive impacts may amplify the transient shaft torques. Each such incident of single-pole switching operation may contribute to a small loss of shaft system fatigue life. If the turbine-generator is subjected to a large number of such incidents, their cumulative effect may cause shaft failure.

The effects of single-pole switching on the fatigue life of shafts and blades have been investigated for specific units in reference 17. The results showed no significant loss of life to either the blades or the shaft sections. In addition, experience to date has not indicated any turbine-generator blade or shaft problems resulting from single-pole switching [11]. However, it would be prudent to study each application individually before implementation.

Thermal duty on nearby generators

System unbalance during the period when one phase is open results in negative-sequence currents in the stators of nearby generators and synchronous condensers. The negative-sequence stator currents induce 120 Hz rotor currents that cause heating. Standards have been established defining generator continuous and short-time unbalanced current capability [18]. The short-time capability is expressed in terms of I_2^2t, the integrated product of machine negative-sequence phase current (I_2) and time (t). The permissible I_2^2t depends on the type of machine as shown in Table 17.1.

Table 17.1 Short-time unbalanced current capability

Type of Machine	Permissible I_2^2t
Salient pole generator	40
Synchronous condenser	30
Round rotor generators	
- Indirectly cooled	30
- Directly cooled: up to 800 MVA	10
- Directly cooled: 800-1600 MVA	10-[(MVA-800)×0.00625]

I_2 expressed in per unit of rated armature current;
t expressed in seconds.

Studies of specific applications of single-pole switching applied to lines near thermal units have shown the thermal duty to be not limiting (for example, see reference 12). However, each application should be examined individually to be sure that the negative-sequence heating duty is not excessive.

17.1.8 Steam Turbine Fast-Valving

Fast-valving (or early valving, as it is sometimes referred to) is a technique applicable to thermal units to assist in maintaining power system transient stability. It involves rapid closing and opening of steam valves in a prescribed manner to reduce the generator accelerating power following the recognition of a severe transmission system fault.

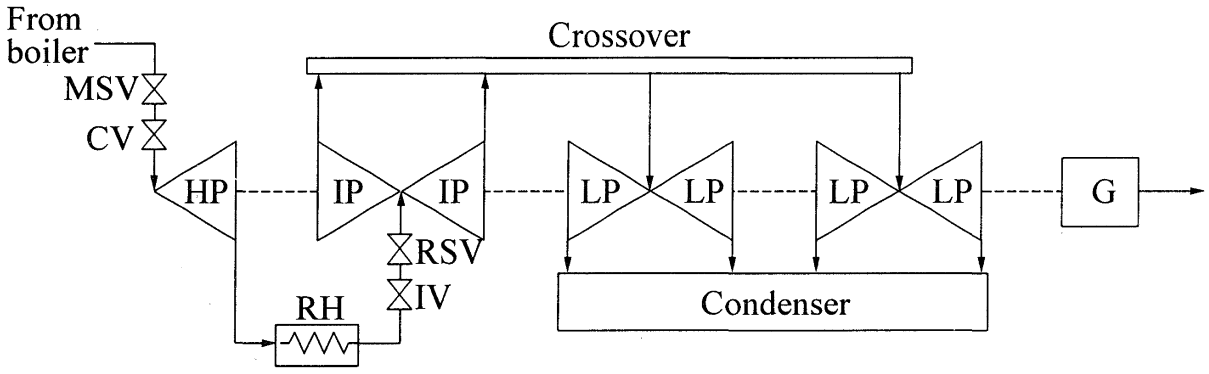
Although the principle of fast-valving as a stability aid was recognized in the early 1930s [19], the procedure has not been very widely applied for several reasons. Among them are the concerns for any possible adverse effects on the turbine and energy supply system.

Since the mid-1960s, utilities have realized that fast-valving could be an effective method of improving system stability in some situations. A number of technical papers have been published describing the basic concepts and effects of fast-

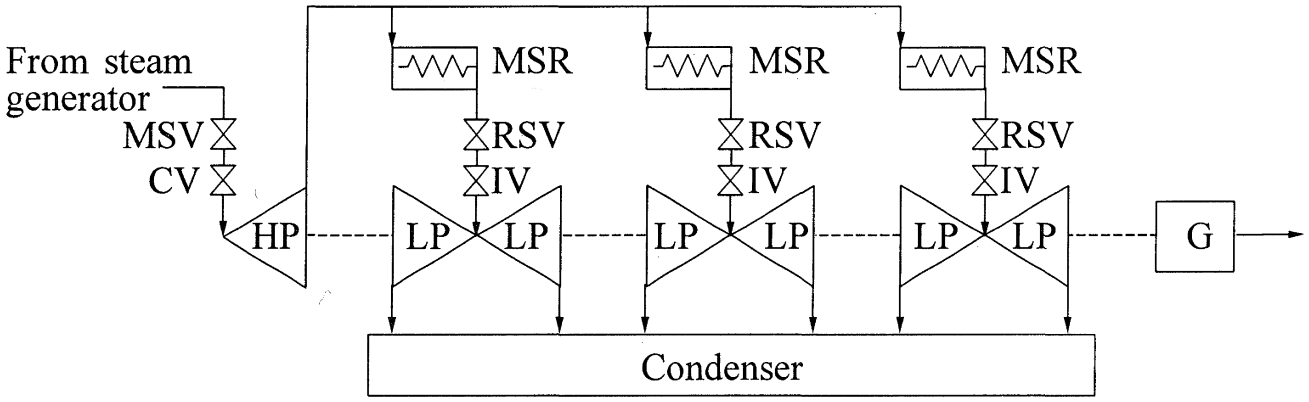
valving [20-23]. Several utilities have tested and implemented fast-valving on some of their units [24-27].

Fast-valving procedures

Chapter 9 discussed steam turbine configurations for fossil-fuel and nuclear-generating units. For illustration of fast-valving applications, let us consider a fossil-fuel generating unit with a tandem-compound single reheat turbine and a nuclear unit. The turbine configurations are shown in Figure 17.2. For these units, the main inlet control valves (CVs) and the reheat intercept valves (IVs) provide a convenient means of controlling the turbine mechanical power. Depending on how these valves are used to control the steam flow, a variety of possibilities exists for the implementation of fast-valving schemes.



(a) Tandem-compound single reheat steam turbine of a fossil-fuel unit



(b) Turbine of a nuclear unit

HP = high-pressure (turbine)
IP = intermediate-pressure (turbine)
LP = low-pressure (turbine)
MSV = main (inlet) safety valve
RSV = reheat safety valve
IV = intercept valve
MSR = moisture separator reheater
CV = control valve
RH = reheater

Figure 17.2 Typical steam turbine configurations

In one commonly used scheme, only the intercept valves are rapidly closed and then fully reopened after a short time delay. Since the intercept valves control nearly 70% of the total unit power, this method results in a fairly significant reduction in turbine power. A more pronounced temporary reduction in turbine power can be achieved through actuation of both control and intercept valves. The procedure of rapid closing and subsequent full opening of the valves is called *momentary fast-valving.*

In some situations where the postfault transmission system is much weaker than the prefault one, it is desirable to have the prime mover power, after being reduced rapidly, return to a level lower than the initial power. One approach is to provide for rapid closure of control and intercept valves, followed by partial opening of control valves and full opening of intercept valves. An alternative approach is to provide for rapid closure and full opening of intercept valves, coupled with partial closure of control valves. This procedure whereby, in addition to a rapid temporary reduction, a sustained reduction in turbine power is achieved is referred to as *sustained fast-valving.*

Improvement of system stability

Fast-valving assists in maintaining system stability following a severe fault by reducing the turbine mechanical power. Results of studies on the effectiveness of fast-valving in enhancing the stability of individual systems have been reported in references 27 to 32. Many of these studies also consider other means of enhancing system stability such as high-response exciters, series capacitor compensation, independent-pole switching, braking resistors, and generator tripping.

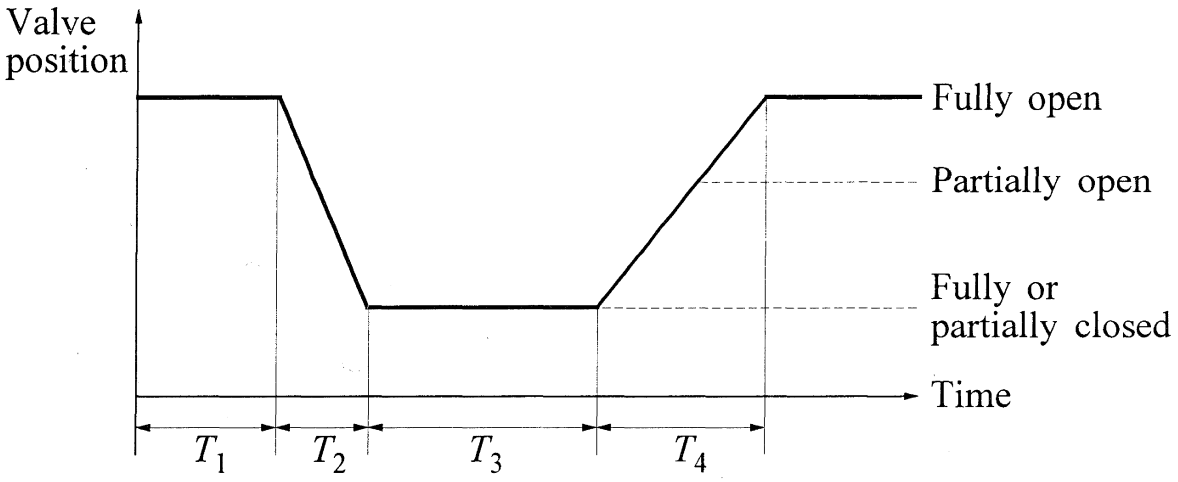
Generally, fast-valving has been found to be an effective and economical method of meeting the performance requirements of power systems whose design and operating criteria require stability to be maintained for a three-phase fault with delayed clearing because of a stuck breaker. The transient stability problem in such cases is generally associated with a swing mode local to a generating station and having a period of about 0.5 to 1.2 seconds.

Although not very widely recognized, fast-valving could be very effective in situations where instability occurs through a slow interarea swing having a period of about 2.0 to 4.0 seconds. The problem is usually caused by generators in one area, because of a fault in the area, advancing with respect to the generators in other interconnected areas. This causes heavy power flows through weak ties connecting the areas, which in turn leads to separation of the areas. Fast-valving of one or more units within the area where the fault occurs minimizes the accelerating power and hence reduces the transient power swings through the weak ties. Fast-valving is particularly effective in such situations, since the periods of the power swings are long; this, therefore, allows more time for the reduction in power to be achieved.

The cost of implementing fast-valving is usually small. However, in view of the concerns about possible adverse effects on the turbine and boiler/steam generator, fast-valving should be used only in situations where other less "heroic" measures are

not able to maintain system stability. In such situations, often the only other effective means of maintaining system stability is to use generator tripping. Compared to generator tripping, fast-valving has the advantage that the unit remains connected to the system. As a result, the total system inertia is not reduced and full or partial power output is restored within a few seconds. In addition, the resulting stress on the prime mover is believed to be significantly less severe. However, fast-valving is not as effective in aiding stability as generator tripping.

The fast-valving logic can take several forms, depending on the supplier and the intended use of fast-valving. Generally, such logic will contain two main circuits: one for generating the valve control sequence and the other for generating an unloading signal if fast-valving is to be followed by a reduced generator output. The valve control sequence will generate a signal to close the valves at a preset rate, hold them closed for an adjustable period of time and reopen them at a preset rate. Figure 17.3 shows a typical valve closing- and opening-sequence. The allowable valve actuation times are influenced by equipment as well as system considerations.



T_1 = delay between the time of initiation and the time when the valve begins to close
T_2 = valve-closing time
T_3 = time during which the valve remains closed
T_4 = valve-opening time

Figure 17.3 Typical valve closing- and opening- sequence

The ability of steam valves to rapidly close and reopen depends on the type of governor system used. The electrohydraulic turbine governor system that uses solid-state electronics and a high-pressure hydraulic actuator system is capable of rapid control. A common practice, particularly of North American manufacturers, is to use fast-acting hydraulic valves arranged to dump oil from the spring-loaded actuating cylinders of the intercept and control valves to facilitate rapid valve closure.

This permits complete valve closure in 0.08 to 0.4 second. Reopening after a fast closure is inherently delayed for approximately 0.3 to 1.0 second to allow for restoration of oil to the hydraulic cylinder. The valve-opening time depends on the size of the hydraulic operating cylinder but is usually in the range of 3 to 10 seconds. For some applications, faster valve-reopening may be needed for fast-valving than is used in normal electrohydraulic governing operations. This can be achieved with the aid of accumulators on the hydraulic system [22,33].

In contrast, some European manufacturers tend to use large servo valves with facilities for fast operation; this achieves reopening times of less than 1 second.

Fast-valving can also be applied to units with mechanical-hydraulic turbine governors, but it is less flexible and somewhat more difficult to implement.

For fossil-fuel-fired units, reheater metal protection considerations dictate the intercept valve-opening time. The problem is one of reheater tube heating when the steam flow is shut off and subsequently restored. The time within which reheater steam flow should be reestablished is typically on the order of 10 to 12 seconds.

From a system stability viewpoint, the valves should be closed as rapidly as possible. With momentary fast-valving, it may also be desirable to initiate valve reopening slightly before the first peak of rotor angle is reached. Slow reopening increases the backswing, and this could lead to second-swing instability [22,29]. If the delay in valve opening is significant, it could also accentuate the swinging of generators in one area against the rest of the system, and this could lead to instability [22]. For any specific system, acceptable valve actuation times should therefore be based on detailed stability studies.

Fast-valving action can be initiated by power load unbalance relays, acceleration detectors, or relays that recognize severe transmission faults [6]. References 23 and 33 describe typical fast-valving initiating logics used in the standard circuitry provided by North American turbine-generator manufacturers. The logic is usually a simple extension of the scheme used to limit overspeed and depends on the comparison of mechanical input power and electrical output power. The former is measured by monitoring the reheat steam bowl pressure. In order to avoid unnecessary initiation of fast-valving action, it is usually necessary to introduce additional logic to discriminate against faults that do not require fast-valving. In most cases, since rapid closing of the valves is critical, it is important to ensure that the delay introduced by the selectivity of the logic is minimal.

The time delay introduced by the feedback control logic, such as detection based on power-load imbalances, is on the order of 0.1 second and this may be unacceptable in some cases. A feedforward control logic derived directly from protective relay systems could reduce the initiating time to one or two cycles [22].

The effectiveness of fast-valving in improving transient stability is demonstrated in Figure 17.4. The figure shows the responses with and without fast-valving of a fossil-fuel-fired power plant consisting of two 500 MW units. The fast-valving sequence assumed closing and full reopening of intercept valves only, with T_1=0.1 s, T_2=0.25 s, T_3=0.1 s, and T_4=0.85 s. The units have a thyristor excitation system with power system stabilizers. The disturbance considered is a three-phase

fault on a major transmission line close to the station, cleared by primary relaying in 60 ms. Without fast-valving, the generating units exhibit a dominant interarea swing having a period of about 4.5 seconds. Consequently, the fast-valving sequence is very effective in limiting the peak of the first swing in rotor angle. Here, very fast valve closing and opening times have been assumed. With slower valve-opening times, the fast-valving sequence, as shown in reference 29, results in second-swing instability.

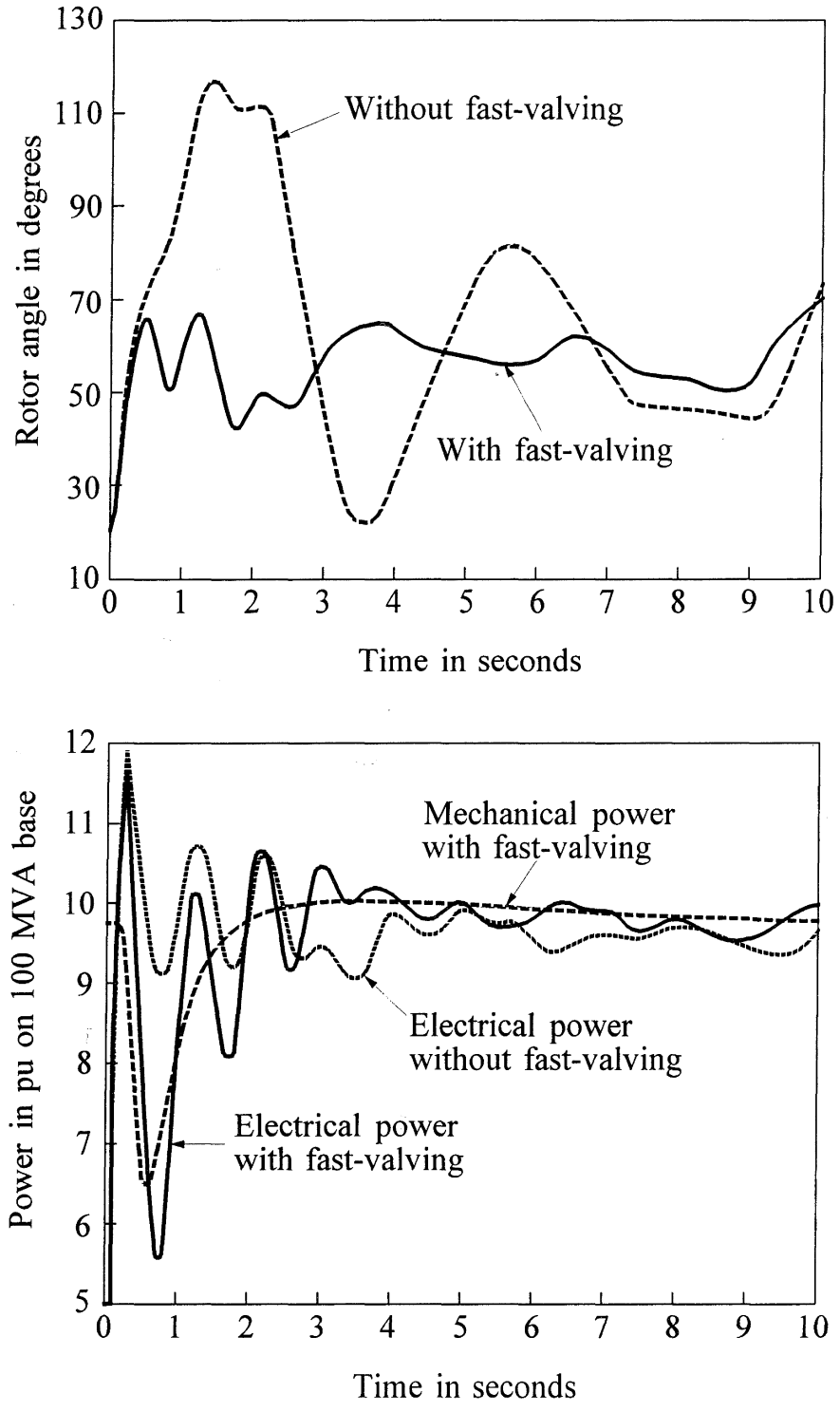


Figure 17.4 Effect of fast-valving on the stability of a fossil-fuel-fired station exhibiting a slow interarea swing

Plant considerations

Fast-valving imposes a relatively severe transient on the turbine and steam generator system. There are several potential problem areas that must be considered in the application of fast-valving. The following is a brief discussion of the equipment considerations that must be addressed.

Fossil-fuel-fired unit steam generator considerations:

Closing the intercept valves results in a temporary increase in reheater pressure that could cause the reheat safety relief valves to lift. The safety valves may not reseat properly following this operation. Also, any noise impact on the environment resulting from the escaping steam must be addressed. Closing both the control and intercept valves reduces the possibility of a lifting of the reheat relief valves but this merely transfers the problem to the main relief valves.

As noted earlier, reheater tube protection is a limiting factor that determines how soon the steam flow should be restored to the reheater. For a typical reheater design, the limiting time is on the order of 11 seconds. If power-operated relief valves are utilized on the reheater outlet and automatically reopened, the problem is minimized in any occurance where only the intercept valves are closed.

Sustained fast-valving appears to the boiler as a partial load rejection. Without a turbine or superheater bypass system, the sudden closure of turbine inlet valves requires venting of the throttled steam to the atmosphere. If this is done by means of spring-loaded safety valves, it may be followed by an outage required to repair these valves. Therefore, power-assisted pressure relief valves and/or a turbine bypass should be used. Under optimum conditions, however, a once-through boiler can be run back quickly enough to withstand sustained fast-valving without lifting the safety valves; this was demonstrated by TVA tests on the Cumberland units [26].

With a drum-type boiler, if a bypass system is not used, sustained fast-valving causes a reduction of drum level. This could result in tripping of the unit by low drum-level protection that is provided to prevent overheating of the furnace firewalls. Improvements in control of feedwater, drum level and rate of reduction of fuel input to the furnace and the use of power-operated relief valves should enhance the ability of drum-type boilers to cope with sustained fast-valving.

Nuclear unit steam generator considerations:

Compared to fossil-fuel-fired units, nuclear units have smaller reheater time constants, and hence closing of only the intercept valves results in a faster rise in reheater pressure. Reheat safety valve lifting is therefore more likely in a nuclear unit. In addition, the probability of a damaged safety valve seat is higher because less superheat in the steam can lead to water-cutting during lifting of the safety valves. The reheater pressure rise can be of greater concern if large bursting disks, rather than safety relief valves, have been used in the reheat system. The bursting of a disk

essentially takes the unit out of service and adds to the system upset.

The closing of both the control and intercept valves has the same effect as for the fossil-fuel units; that is, it passes the problem on to the main safety-relief valves. The closing of the control valves results in a rise in steam generator pressure, and steam must be bypassed either to the condenser or to the atmosphere. The boiler pressure-control system uses the turbine or the bypass system to control the boiler pressure.

Turbine considerations:

The integrity of control-valve (CV) seat and stem is of some concern. The dumping of the actuator fluid results in an accelerated closing of the valve that may lead to valve-bouncing or stem-bending. On existing units, it may be necessary to add more solenoid dump valves to achieve the fast-closing time for the CVs.

The combined action of the control and intercept valves necessitates a review of the extraction steam system to determine if there is a likelihood of actuating any start-up bypass valve from the HP turbine to the condenser. The sustained fast-valving cycle may therefore require the addition of a time delay in the control logic for this bypass valve.

The decay of pressure downstream of the intercept valves means that the valve actuators must be capable of reopening the valves against a high-differential pressure. As in the case of the control valves, the control system must have fast-acting dump solenoids and an adequate-control fluid supply for resetting the valves without initiating a low-control oil pressure trip.

The intercept valves are larger than the control valves; thus the effect of higher impact loading on the devices used for stopping the valves at the end of their stroke must be evaluated. Avoiding a full closure would be preferable.

In the case of a nuclear unit with a moisture separator reheater, higher-than-normal steam velocities are created in part of the tubing; the result is higher stress on the tubes. The tubing response to this excitation must be evaluated.

The rapid decay of the pressure in the LP turbine raises the possibility of steam flashing in the feed-water heaters and hence a water induction incident that would result in the feed train being closed by the protection system.

The turbine-generator rotors must not suffer a significant loss of life from the torsional stresses imposed on them by a fast-valving event. Results of simulations of specific applications have shown that the resulting shaft stresses are acceptable [24].

Reference 34 describes fast-valving tests on two units at the Pickering-B nuclear station in Ontario. The tests revealed no obvious adverse effects on equipment. From the plant viewpoint, fast-valving appeared to be a nonevent. From the system viewpoint, the fast-valving sequence was found to be effective in causing a rapid and substantial reduction of turbine power.

17.1.9 Generator Tripping

The selective tripping of generating units for severe transmission system contingencies has been used as a method of improving system stability for many years. The rejection of generation at an appropriate location in the system reduces power to be transferred over the critical transmission interfaces. Since generating units can be tripped rapidly, this is a very effective means of improving transient stability. (See Chapter 13, Section 13.6 for illustration.)

Historically, the practice of generator tripping as a stability aid was confined to hydro plants. Such plants are usually remote from load centres and there is little risk of damage to the unit from a sudden trip. Since the 1970s, this practice has been gradually extended to fossil-fuel-fired and nuclear units as a means of solving severe stability problems.

The scheme used for detection of system conditions requiring unit tripping is often an extension of trip circuits from various remote and local line protections. If the faulted line is restored within minutes, the rejected units are brought back on-line quickly.

Unless special facilities are provided, the rejected unit goes through a standard shut-down and start-up cycle; consequently, full power may not be available for several hours. A practice used by many utilities is to design thermal units so that, after tripping, they continue to run, supplying unit auxiliaries. This permits the units to be resynchronized to the system and restored to full load in about 15 to 30 minutes [35].

The sequence of events that follow generator tripping is as follows: the boiler is tripped; turbine controls limit overspeed (the turbine is not tripped) and the speed is returned to near-rated speed; the unit then operates either at no load or supplies the unit auxiliary load; the boiler is purged and refired in preparation for reloading; the unit is resynchronized to the power system and reloaded at a predetermined rate.

Evidently, the tripping of a unit subjects it to sudden changes in mechanical and electrical loading, with the associated impact on the generator, prime mover, and energy supply system. While thermal units and their controls are designed to withstand such shocks, there is some possibility that controls will not function correctly. Also, thermal units are not designed for frequent full-load rejection; significantly increasing the number of full-load rejections may increase unit maintenance requirements and reduce unit availability. Therefore, this type of control measure for improving system stability should not be used indiscriminately.

The following are the major turbine-generator concerns:

(a) The overspeed resulting from tripping the generator

(b) Thermal stresses caused by the rapid load changes

(c) High levels of shaft torques as the result of successive disturbances

Overspeed considerations

The turbine controls should be capable of full-load rejection without a turbine trip. As discussed in Chapter 9 (Section 9.2.2), the controls of steam turbines are generally designed to limit the overspeed following a full-load rejection to about 1% below the overspeed trip level of 110 to 115% of rated speed. Prevention of turbine trip is essential if the unit has to carry its auxiliary load until it is resynchronized to the power system.

Following the initial overspeed, the unit will reach a steady-state speed determined by the governor droop characteristic. The standard 5% regulation will result in a steady-state speed slightly below 105% of rated speed (corresponding to a frequency of 63 Hz). Continuous operation at this frequency is forbidden as it may cause damage to the low-pressure turbine blades (see Section 9.2.3). On older units with mechanical-hydraulic control (MHC), the operator has to adjust the speed-load changer to return the unit to rated speed. On modern units with electrohydraulic control (EHC), this speed reduction to rated speed is automatic.

If frequent generator tripping is required to maintain system stability, there is a greater risk of turbine-generator runaway because of equipment malfunction. To ensure safe and reliable operation of speed controls, greater emphasis should be placed on preventive maintenance and on periodic testing of the turbine valves and protective system.

Thermal stress considerations

Generator tripping imposes a high thermal stress on the turbine because of the variation of unit output over a wide range. Prior to the disturbance, the unit output is relatively high and the turbine metal temperatures in the critical parts would be near rated conditions. When the unit is tripped, the unit operates for about 20 minutes at very light load or no load; this results in rapid cooling of the turbine metals, followed by resynchronization and reloading of the unit. The turbine metals continue to cool during the initial reloading until the steam temperatures match turbine metal temperatures in the critical areas. An increase in load beyond this point begins to heat the metals, the rate of heating being a function of the loading rate and the degree of cooling that occurred during light-load operation. The parts of the turbine that are critical from thermal stress considerations are high-temperature regions of the HP turbine section.

The thermal stresses resulting from generator tripping can be limited to acceptable levels by appropriate operating procedures developed in consultation with the turbine-generator manufacturer.

Shaft fatigue-life considerations

When a generating unit in a multiunit power plant is tripped, all units in the plant experience successive disturbances that can result in high levels of shaft torques.

As discussed in Chapter 15 (Section 15.4), the torsional oscillations caused by successive impacts may reinforce the initial oscillations. Detailed simulations should be carried out to ensure that there are no adverse effects on the shaft fatigue-life from the compounding effects of a network fault, clearing of the fault, and unit tripping. For the unit that is tripped, the electric torque is suddenly reduced to a very low value. The remaining units initially experience a sudden proportionate increase in the electric torque. If two or more units are tripped, it is very unlikely that they will be tripped at precisely the same instant. Therefore, a multiunit tripping scheme may impose a more severe duty.

References 36 and 37 describe a generation and load rejection scheme implemented by Ontario Hydro at the Bruce Nuclear Power Development Complex having a total generation capacity of about 6000 MW. The scheme, implemented as a stopgap measure because of delays in acquiring transmission right-of-way provided for rejection of up to four 750 MW units and 1500 MW of customer load, depending on total generation at the complex, the number of transmission circuits in service, and the type of fault. The decision to implement the rejection scheme was based on a detailed evaluation of the benefits and impacts. The following factors were given consideration in the selection of the scheme:

(a) The cost of displacing locked-in nuclear energy with fossil-fuelled generation

(b) The expected frequency of transmission system faults and the estimated number of units trips

(c) The impact on generating units with regard to risk of turbine-generator runaway, increased forced and maintenance outage rates, increased cost because of additional wear and tear, and cumulative loss of component life, including shaft fatigue-life

17.1.10 Controlled System Separation and Load Shedding

Controlled separation may be used to prevent a major disturbance in one part of an interconnected system from propagating into the rest of the system and causing a severe system breakup. The initiating disturbance may be the loss of a major transmission line (ac or dc) carrying a large amount of power or loss of a significant amount of generation. The incipient instability in such cases is usually characterized by sudden changes in tie line power. If this is detected in time and the information is used to initiate corrective actions, severe system upsets can be averted.

The impending system instability is detected by monitoring one or more of the following system quantities: sudden change in power flow through specific transmission circuits, change of bus voltage angle, rate of power change, and circuit-breaker auxiliary contacts.

Upon detection of the impeding instability, controlled system separation is initiated by opening the appropriate tie lines before cascading outages can occur. In

some instances it may be necessary to shed selected loads to balance generation and load in the separated systems.

In other instances, only load shedding can be initiated so that transient stability is maintained without resorting to system separation.

An example of relaying used for controlled separation is the $\Delta P/\Delta\theta$ relay on the tie lines between Ontario Hydro and Manitoba Hydro. The relay monitors sudden changes in power flow (ΔP) over the tie lines and changes in phase angle ($\Delta\theta$) of the bus voltage at the Ontario end of the tie lines. The $\Delta\theta$ element supervises the ΔP element. The settings of the relay are chosen so that the ties are tripped for disturbances in Manitoba that cause instability in Ontario. For some system conditions, tie line tripping is accompanied by load shedding to ensure satisfactory post-separation system conditions.

Reference 38 describes a local independent detection scheme developed to isolate the U.S. southwest power system from the U.S. northwest system for outages of the Pacific ac intertie. The scheme uses the power rate of change at two locations for detection of conditions requiring northwest/southwest separation. This involves separation of the Utah and Colorado power systems from the Arizona system by opening five ties, and separation of the Nevada system from the California system north of San Francisco by opening three ties.

Reference 39 describes a load-shedding scheme used by the U.S. Northwest Power Pool to maintain transient stability of the Western System Coordinating Council (WSCC) systems.

17.1.11 High-Speed Excitation Systems

Significant improvements in transient stability can be achieved through rapid temporary increase of generator excitation. The increase of generator field voltage during a transient disturbance has the effect of increasing the internal voltage of the machine; this in turn increases the synchronizing power.

During a transient disturbance following a transmission system fault and clearing of the fault by isolating the faulted element, the generator terminal voltage is low. The automatic voltage regulator responds to this condition by increasing the generator field voltage, and this has a beneficial effect on the transient stability. The effectiveness of this type of control depends on the ability of the excitation system to quickly increase the field voltage to the highest possible value. High-initial-response excitation systems with high-ceiling voltages are most effective in this regard. Ceiling voltages are, however, limited by generator rotor insulation considerations. For thermal units, the ceiling voltages are limited to about 2.5 to 3.0 times the rated-load field voltage.

Fast excitation response to terminal voltage variations required for improvement of transient stability often leads to degrading the damping of local plant mode oscillations (see Chapter 12, Sections 12.4 and 12.5). Supplementary excitation control, commonly referred to as *power system stabilizer* (PSS), provides a convenient means of damping system oscillations that enables the high-response excitation system

to be used. The use of high-initial-response excitation systems supplemented with PSS is by far the most effective and economical method of enhancing the overall system stability [40]. As an example of such a system, Figure 17.5 shows a general block diagram representation of a thyristor exciter with an automatic voltage regulator (AVR), a PSS, and a terminal voltage limiter. The function of the limiter is to prevent the terminal voltage from exceeding a set level of typically 1.15 pu. The effectiveness of the excitation system in improving the overall system stability depends on proper control design and tuning procedures. This is covered in Section 17.2.

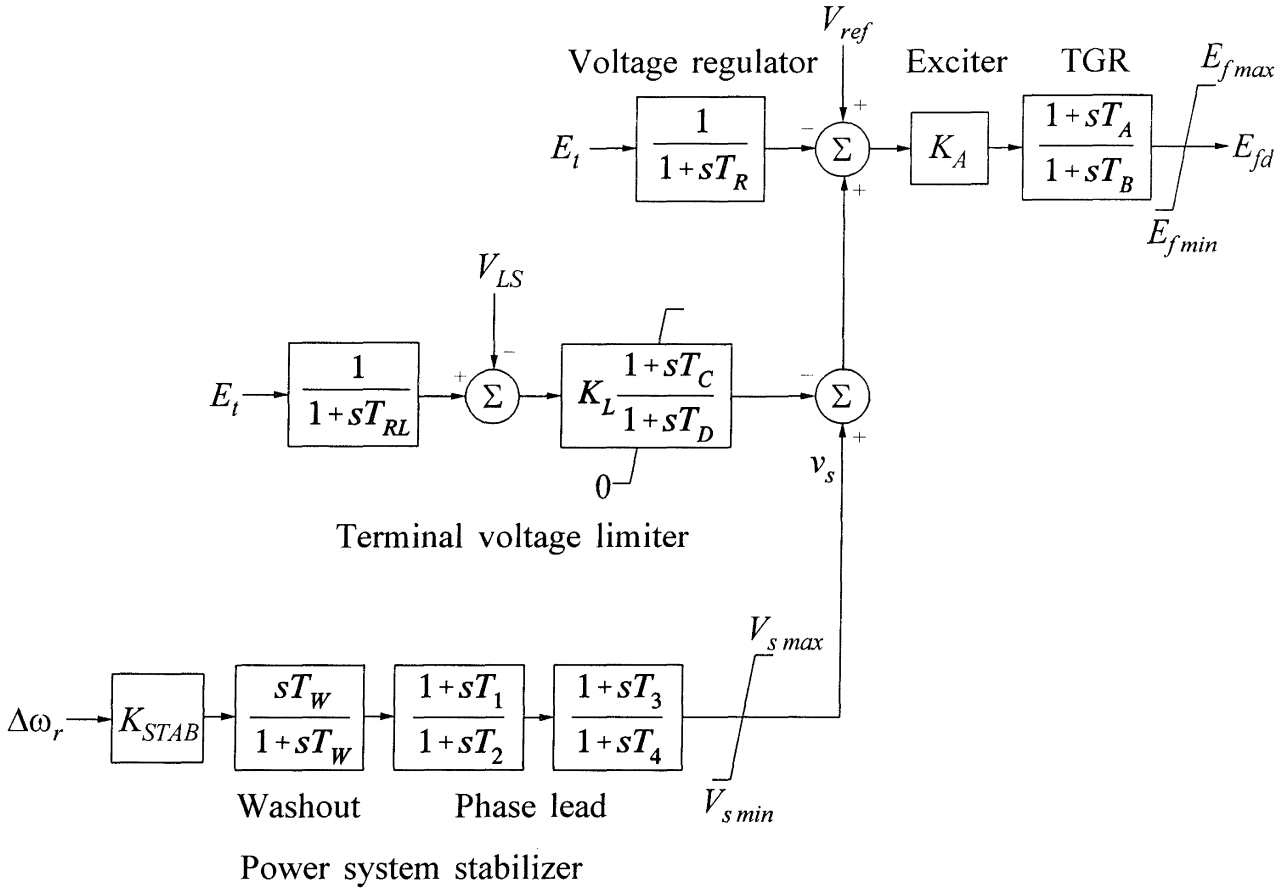


Figure 17.5 Block diagram of thyristor excitation system with PSS

The influence of excitation system response on transient stability is illustrated in Figure 17.6. The figure compares the responses of the fossil-fuel-fired plant considered in Section 17.1.8 with two alternative forms of excitation system: (a) an ac exciter with diode rectifiers, having a response ratio of 2.0, and (b) a bus-fed thyristor exciter with a PSS. The disturbance considered is a three-phase fault on a major transmission line near the power plant, cleared in 60 ms. The system is unstable with the rotating exciter and is stable with the high-initial-response thyristor exciter. The critical fault-clearing time with the ac exciter is 47.5 ms, and 62.5 ms with the thyristor exciter.

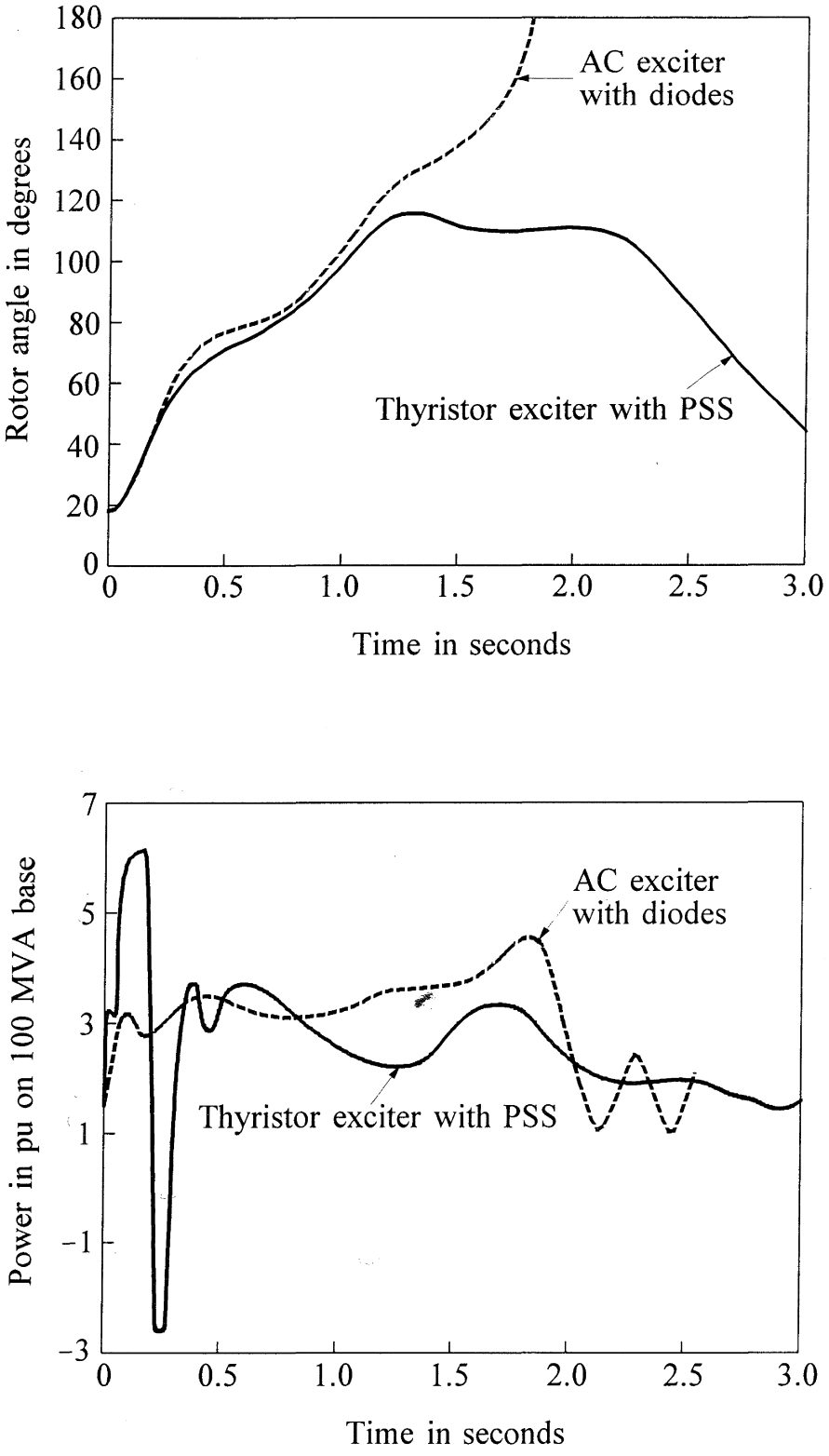


Figure 17.6 Comparison of transient stability with an ac exciter and a bus-fed thyristor exciter

17.1.12 Discontinuous Excitation Control [40]

A properly applied power system stabilizer provides damping to both local and interarea modes of oscillations. Under large-signal or transient conditions, the stabilizer generally contributes positively to first-swing stability. In the presence of both local and interarea swing modes, however, the normal stabilizer response can allow the excitation to be reduced after the peak of the first local-mode swing and before the highest composite peak of the swing is reached. Additional improvements in transient stability can be realized by keeping the excitation at ceiling, within terminal voltage constraints, until the highest point of the swing is reached.

A discontinuous excitation control scheme referred to as *transient stability excitation control* (TSEC) has been developed by Ontario Hydro to achieve the above [40]. This control improves transient stability by controlling the generator excitation so that the terminal voltage is maintained near the maximum permissible value of about 1.12 to 1.15 pu over the entire positive swing of the rotor angle. The scheme uses a signal proportional to the change in angle of the generator rotor, in addition to the terminal voltage and rotor speed signals. However, the angle signal is used only during the transient period of about 2 seconds following a severe disturbance, since it results in oscillatory instability if used continuously. The angle signal prevents premature reversal of field voltage and hence maintains the terminal voltage at a high level during the positive swing of the rotor angle. Excessive terminal voltage is prevented by the terminal voltage limiter.

Figure 17.7 shows a block diagram of the discontinuous excitation control scheme. The TSEC circuitry is integrated with the PSS circuitry. The speed signal ($\Delta\omega_r$) provides continuous control to maintain small-signal stability under normal operation. The angle signal is derived by integrating the speed signal. The TSEC block shown in the figure is an integrator with a washout. The value of T_{ANG} is such

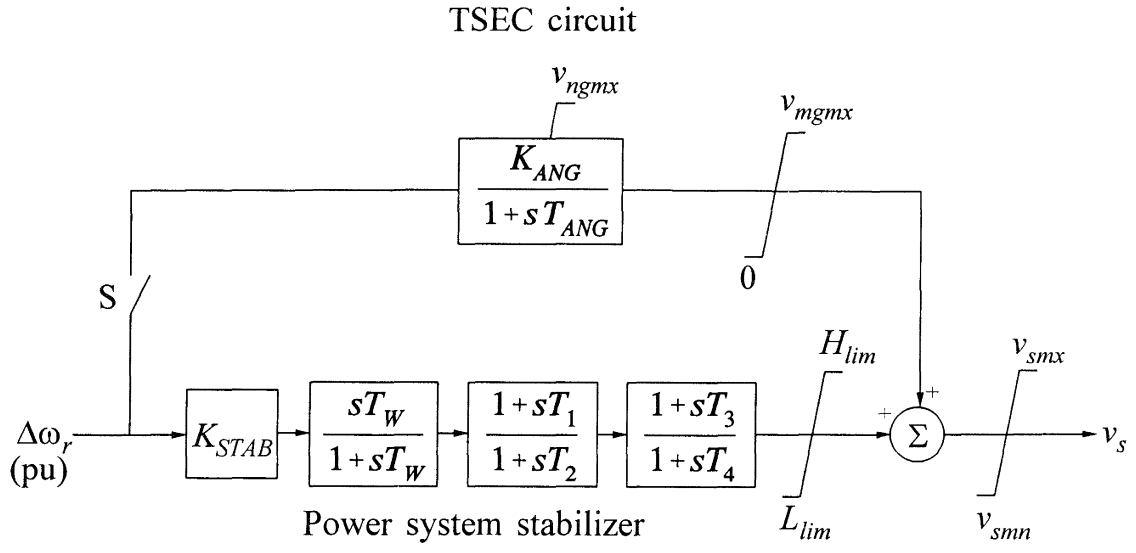


Figure 17.7 Block diagram of TSEC scheme

that, at the frequency range of interest, the output is proportional to the angular deviation. The TSEC is in effect a closed-loop control based on local measurements. The relay contact (S) is closed if the terminal voltage drop exceeds a preset value, field voltage is at positive ceiling, and the speed increase is above a preset value. The relay contact is opened when either the speed drops below a threshold value or the exciter comes out of saturation; the output of the TSEC block then decays exponentially with a time constant T_{ANG}.

The discontinuous excitation control is most effective in improving the transient stability of generating units exhibiting low-frequency interarea swings.

When TSEC is applied to several generating stations in an area, the system voltage level in the entire area is raised. This increases the power consumed by the voltage-dependent loads in the area, thereby contributing to further improvement in transient stability.

To illustrate the performance of TSEC, we once again consider the fossil-fuel-fired power plant used in Sections 17.1.8 and 17.1.11 to demonstrate the effectiveness of fast-valving and high-initial-response excitation system. As seen from the rotor angle plots of Figure 17.6, the generators at this plant exhibit a dominant low-frequency interarea swing. Figure 17.8 shows the responses of the generators with and without TSEC. Clearly, the system transient stability is very significantly improved by TSEC. The critical clearing time, which is 62.5 ms with a thyristor exciter and PSS, is increased to 117.5 ms by the discontinuous excitation control.

Figure 17.9 shows an extended simulation of the system with and without TSEC. For purposes of comparison, the response obtained with fast-valving of intercept valves as described in Section 11.1.8 is also shown in Figure 17.9. The discontinuous excitation control is seen to be as effective as fast-valving for this particular application.

Compared to other methods of improving system stability, such as fast-valving and generator-tripping, TSEC imposes very little duty on the turbine-generator shaft and steam supply system. However, parts of the power system will experience a rise in voltage of up to 15% (depending on the setting of the terminal voltage limiter) for 1 to 2 seconds. This excitation control scheme must be coordinated with other overvoltage protection and control functions. It must also be coordinated with transformer differential protection to ensure that the increased magnetizing current resulting from the elevated voltage level does not cause this protection to operate.

The discontinuous control described above for transient boosting of excitation uses local intelligence to detect a severe system disturbance condition. In some applications, it may be necessary to initiate the transient excitation boosting by using remote telemetered signals. Reference 41 describes such an application.

17.1.13 Control of HVDC Transmission Links

As discussed in Chapter 10 (Section 10.4), an HVDC transmission link is highly controllable. It is possible to take advantage of this unique characteristic of the HVDC link to augment the transient stability of the ac system.

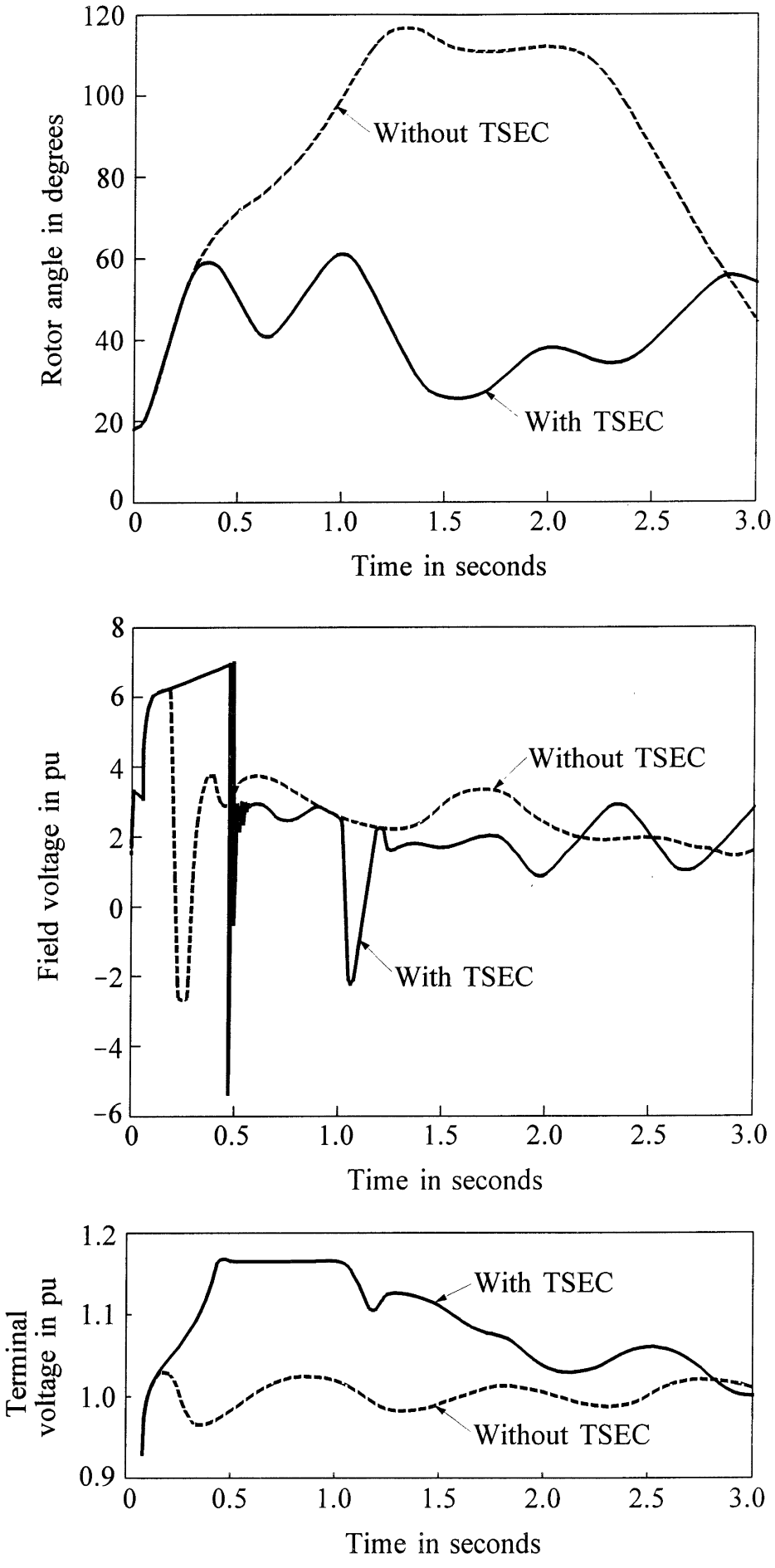


Figure 17.8 Effect of TSEC on transient stability

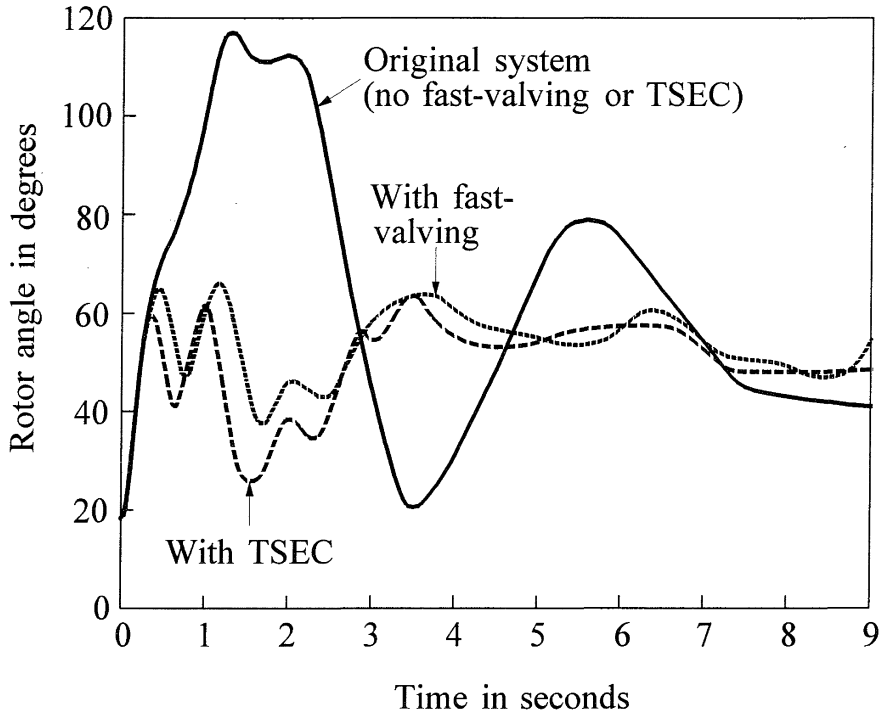


Figure 17.9 Effects of TSEC and fast-valving on extended system response

During a transient disturbance, the dc power can be ramped down rapidly to reduce generation/load unbalance of the ac system on both sides. In some situations, it may be necessary to ramp up the dc power to assist system stability by taking advantage of the short-term overload capability of the HVDC system. From the viewpoint of the ac system performance, the rapid control of dc power has the same beneficial effect as generator/load tripping. References 42 and 43 provide descriptions of special controls used in a number of HVDC installations for transient stability augmentation.

Transient stability augmentation can also be achieved by controlling the HVDC converters so as to provide reactive power and voltage support [44].

17.2 SMALL-SIGNAL STABILITY ENHANCEMENT

The problem of small-signal stability, as described in Chapter 12, is usually one of insufficient damping of system oscillations. The use of power system stabilizers to control generator excitation systems is the most cost-effective method of enhancing the small-signal stability of power systems. Additionally, supplemental stabilizing signals may be used to modulate HVDC converter controls and static var compensator controls to enhance damping of system oscillations.

The controls used for small-signal stability enhancement should perform satisfactorily under severe transient disturbances. Therefore, while the controls are designed using linear techniques, their overall performance is assessed by considering small- as well as large-signal responses.

17.2.1 Power System Stabilizers

Section 12.5 of Chapter 12 developed the theoretical basis for a PSS. The function of a PSS is to add damping to the generator rotor oscillations. This is achieved by modulating the generator excitation so as to develop a component of electrical torque in phase with rotor speed deviations. Shaft speed, integral of power and terminal frequency are among the commonly used input signals to the PSS.

Alternative types of PSS

(a) Stabilizer based on shaft speed signal (delta-omega):

PSS based on shaft speed signal has been used successfully on hydraulic units since the mid-1960s. Reference 45 describes a technique developed to derive a stabilizing signal from measurement of shaft speed of a hydraulic unit. Among the important considerations in the design of equipment for the measurement of speed deviation is the minimization of noise caused by shaft run-out and other causes [45,46]. The allowable level of noise is dependent on its frequency. For noise frequencies below 5 Hz, the level must be less than 0.02%, since significant changes in terminal voltage can be produced by low-frequency changes in the field voltage. A frequency corresponding to shaft rotational speed and resulting from shaft run-out is generally the most important noise component in this range. Lateral movements of the shaft of 0.075 cm are typical at points close to the generator guide bearing. Such low-frequency noise cannot be removed by conventional electric filters; its elimination must be inherent to the method of measuring the speed signal. This is achieved by summing the outputs from several pick-ups around the shaft. At gate positions below 70%, the stabilizing signal is disconnected automatically by an auxiliary (pallet) switch to prevent excessive modulation of the field voltage by vibrations generated in the turbine at partial gate openings.

The application of shaft speed-based stabilizers to thermal units requires a careful consideration of the effects on torsional oscillations. The stabilizer, while damping the rotor oscillations, can cause instability of the torsional modes. This problem is discussed in Chapter 15 (Section 15.2.1). One approach successfully used to circumvent the problem is to sense the speed at a location on the shaft near the nodes of the critical torsional modes [47,48]. In addition, an electronic filter is used in the stabilizing path to attenuate the torsional components.

While stabilizers based on direct measurement of shaft speed have been used on many thermal units, this type of stabilizer has several limitations. The primary disadvantage is the need to use a torsional filter. In attenuating the torsional components of the stabilizing signal, the filter also introduces a phase lag at lower frequencies. As demonstrated in Example 15.2 of Chapter 15, this has a destabilizing effect on the "exciter mode", thus imposing a maximum limit on the allowable stabilizer gain. In many cases, this is too restrictive and limits the overall effectiveness of the stabilizer in damping system oscillations. In addition, the stabilizer has to be

custom-designed for each type of generating unit depending on its torsional characteristics. The delta-*P*-omega stabilizer described next was developed to overcome these limitations.

(b) Delta-P-omega stabilizer [40,49,50]:

The principle of this stabilizer is illustrated by the following equation that shows how a signal proportional to rotor speed deviation can be derived from the accelerating power:

$$\Delta\omega_{eq} = \frac{1}{M}\int(\Delta P_m - \Delta P_e)\,dt \tag{17.1}$$

where

M = inertia constant, $2H$
ΔP_m = change in mechanical power input
ΔP_e = change in electric power output
$\Delta\omega_{eq}$ = derived or equivalent speed deviation

The objective is to derive the equivalent speed signal $\Delta\omega_{eq}$ so that it does not contain torsional modes. As shown in Chapter 15 (Example 15.2), torsional components are inherently attenuated in the integral of ΔP_e signal. The problem is to measure the integral of ΔP_m free of torsional modes.

In many applications, the ΔP_m component is neglected. This is satisfactory, except when changing load on the unit and other system conditions when the mechanical power changes. Under such conditions, a spurious stabilizer output is produced if ΔP_e alone is used as the stabilizing signal. This in turn results in transient oscillations in voltage and reactive power.

The integral of mechanical power is related to shaft speed and electrical power as follows:

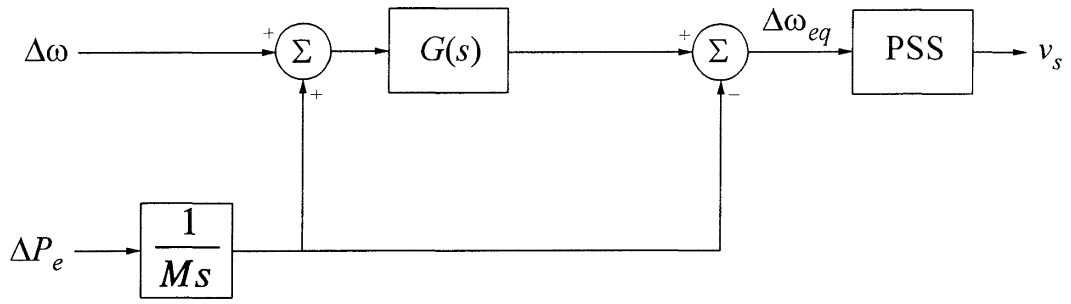
$$\int \Delta P_m\,dt = M\Delta\omega + \int \Delta P_e\,dt \tag{17.2}$$

The delta-*P*-omega stabilizer makes use of the above relationship to simulate a signal proportional to the integral of mechanical power change by adding signals proportional to shaft-speed change and integral of electrical power change. This signal will contain torsional oscillations unless a filter is used. Because mechanical power changes are relatively slow even for fast-valve movements, the derived integral of the mechanical power signal can be conditioned with a simple low-pass filter to remove torsional frequencies.

The overall transfer function for deriving the equivalent rotor speed deviation signal from shaft speed and electrical power measurements is given by

$$\Delta\omega_{eq}(s) = -\frac{\Delta P_e(s)}{Ms} + G(s)\left[\frac{\Delta P_e(s)}{Ms} + \Delta\omega(s)\right] \tag{17.3}$$

where $G(s)$ is the transfer function of the torsional filter. A realization of this is shown in the block diagram of Figure 17.10.



ω_0 = base frequency, rad/s
M = inertia coefficient = $2H$
s = d/dt

Figure 17.10 Block diagram realization of delta-*P*-omega stabilizer

The delta-*P*-omega stabilizer has two major advantages over the delta-omega stabilizer:

1. The ΔP_e signal has a high degree of torsional attenuation, and hence there is generally no need for a torsional filter in the main stabilizing path. This eliminates the exciter mode stability problem, thereby permitting a higher stabilizer gain that results in better damping of system oscillations.

2. An end-of-shaft speed-sensing arrangement with a simple torsional filter can be used with electrical power to derive the mechanical power signal. This allows the use of a standard design for all units irrespective of their torsional characteristics.

(c) Frequency-based stabilizers:

Terminal frequency has been used as the stabilizing signal for several PSS applications. Normally, the terminal frequency signal is used directly as the stabilizer input signal. In some cases, terminal voltage and current are used to derive the frequency of a voltage behind a simulated machine reactance so as to approximate the machine rotor speed.

In these systems, as in the case of speed-based stabilizers, care must be taken to filter torsional modes when they are used on steam turbine units.

The sensitivity of the frequency signal to rotor oscillations increases as the external transmission system becomes weaker, tending to offset the reduction in gain from stabilizer output to electrical torque that results from a weaker transmission system [51]. Hence, the gain of a frequency-based stabilizer may be adjusted to obtain the best possible performance under weak ac transmission system conditions where the contribution of the stabilizer is required most.

The frequency signal is more sensitive to modes of oscillation between large areas than to modes involving only individual units, including those between units within a power plant. Thus it seems possible to obtain greater damping contributions to interarea modes of oscillation than would be obtainable with the speed input signal.

The frequency-based stabilizer, however, suffers from several shortcomings:

1. During a rapid transient, the terminal frequency signal will undergo a sudden phase shift. This results in a spike in the field voltage that is reflected in the generator output quantities.

2. The frequency signal often contains power system noise caused by large industrial loads such as arc furnaces. In many cases this has prevented the use of frequency as an input signal.

3. Torsional filtering is required. Hence, a frequency-based stabilizer has the same basic limitation as the delta-omega stabilizer.

(d) Digital stabilizer:

Digital versions of some of the above stabilizers have been developed and are now commercially available [52].

Manufacturers are producing excitation systems with complete digital circuitry. In this environment, if the appropriate inputs are provided, the stabilizer becomes just another program in the excitation control processor.

Excitation control design [40,53]

The parameters of the PSS and other elements of the excitation system are chosen to enhance the overall system stability. Specifically, the following are the objectives of excitation control design:

- Maximization of the damping of the local plant mode as well as interarea mode oscillations without compromising the stability of other modes.

- Enhancement of system transient stability.

- Prevention of adverse affects on system performance during major system upsets that cause large frequency excursions.

- Minimization of the consequences of excitation system malfunction because of component failures.

The procedure used for meeting the above objectives is illustrated by considering a thyristor excitation system whose block diagram is shown in Figure 17.5. The input to the PSS may be either the shaft speed deviation ($\Delta\omega_r$) or the equivalent rotor speed deviation ($\Delta\omega_{eq}$) . The terminal voltage transducer circuitry is represented by time constants necessary for filtering the rectified terminal voltage waveform. These can usually be reduced to a single time constant (T_R) in the range of 0.01 to 0.02 seconds. Other time constants through to the exciter output, including any associated with the exciter itself, are negligible, and the main path can be represented simply by the gain K_A.

The following is a description of the considerations and procedures used for selection of the various parameters.

Exciter gain:

A high value of K_A is desirable from the viewpoint of transient stability. A suitable value of K_A is about 200 with no *transient gain reduction* (TGR) [40,53].

A common industry practice is to reduce the gain of the exciter at high frequencies by use of TGR [51,52]. Typical values of T_A and T_B used for this purpose are one and ten seconds, respectively. On excitation systems with large values of T_R, TGR is required for satisfactory operation of the generating unit on open-circuit. With T_R on the order of 0.02 seconds, TGR is unnecessary for stable open-circuit operation (see closure of reference 53).

The need to use TGR should be based on a careful assessment of the overall system dynamic performance and on how TGR affects selection of other parameters of the excitation system. References 40 and 53 discuss in detail the impact of using TGR for specific applications.

Phase-lead compensation:

To damp rotor oscillations, the PSS must produce a component of electrical torque in phase with rotor speed deviation. This requires phase-lead circuits to be used to compensate for the lag between the exciter input (i.e., PSS output) and the resulting electrical torque (see Section 12.5). Two first-order phase-compensation blocks are shown in Figure 17.5. If the degree of phase compensation required is small, a single first-order block may be used. For hydraulic generators with low values of *d*-axis open-circuit time constant (T'_{d0}), the phase compensation required is small and phase-lead circuitry may in fact not be utilized.

The PSS is often required to enhance damping of either a local plant mode or

an interarea mode of oscillation. While this mode receives special attention, the phase compensation should be designed so that the PSS contributes to damping over a wide range of frequency covering both interarea and local modes of oscillation.

The first step in determining the phase compensation is to compute the frequency response between the exciter input and the generator electrical torque, using a tool such as the MASS program which was described in Chapter 12. In computing this response, however, the generator speed and rotor angle should remain constant. This is because when the excitation of a generator is modulated, the resulting change in electrical torque causes variations in rotor speed and angle that in turn affect the electrical torque. As we are interested only in the phase characteristic between exciter input and electrical torque, the feedback effect through rotor angle variation should be eliminated by holding the speed constant. (See the block diagram of Figure 12.13 in Chapter 12.) Therefore, the phase characteristic as a function of frequency is obtained with a large inertia assumed for the machine under consideration (say 100 times the actual inertia). This ensures that the speed and angle do not change over the frequency range of importance for stabilizer design (0.1 to 3 Hz).

The required frequency response of any machine is sensitive to the Thevenin equivalent system impedance at its terminals but relatively independent of the dynamics of other machines. It is, therefore, appropriate to assume that all other machines act as infinite buses. This has the effect of eliminating their dynamics from the response calculation while retaining the correct Thevenin impedance at the terminals of the machine under study. The resulting phase characteristic has a relatively simple form free from the effects of natural frequencies of the external machines.

The phase characteristic to be compensated varies to some extent with system conditions. Therefore, a characteristic acceptable for different system conditions is selected. Generally, slight undercompensation is preferable to overcompensation so that the PSS does not contribute to the negative synchronizing torque component (see Section 12.5). An undercompensation by about 10° over the entire frequency range of interest provides the required degree of tolerance to allow for uncertainties in machine and system modelling.

Stabilizing signal washout:

The signal washout is a high-pass filter that prevents steady changes in speed from modifying the field voltage. The value of the washout time constant T_W should be high enough to allow signals associated with oscillations in rotor speed to pass unchanged.

From the viewpoint of the "washout function," the value of T_W is not critical and may be anywhere in the range of 1 to 20 seconds. The main considerations are that it should be long enough to pass stabilizing signals at the frequencies of interest relatively unchanged, but not so long that it leads to undesirable generator voltage excursions as a result of stabilizer action during system-islanding conditions. Ideally, the stabilizer should not respond to system-wide frequency variations.

For local mode oscillations in the range of 0.8 to 2.0 Hz, a washout of 1.5 seconds is satisfactory. From the viewpoint of low-frequency interarea oscillations, a washout time constant of 10 seconds or higher is desirable, since lower-time constants result in significant phase lead at low frequencies. Unless this is compensated for elsewhere, it will reduce the synchronizing torque component at interarea frequencies. This desynchronizing effect is detrimental to interarea transient stability as it will cause the areas to swing farther apart following a disturbance.

Stabilizer gain:

The stabilizer gain, K_{STAB}, has an important effect on damping of rotor oscillations. The value of the gain is chosen by examining the effect for a wide range of values. The damping increases with an increase in stabilizer gain up to a certain point beyond which further increase in gain results in a decrease in damping. Ideally, the stabilizer gain should be set at a value corresponding to maximum damping. However, the gain is often limited by other considerations. With a delta-omega stabilizer, as a result of the effect of the torsional filter, the stability of the "exciter mode" becomes an overriding consideration. With a delta-P-omega stabilizer, exciter mode stability is not a problem, and a considerably higher value of gain is acceptable provided that the phase-lead compensation has been chosen to provide satisfactory phase characteristics over a range of frequencies that includes all dominant modes. In such cases, the maximum value of the stabilizer gain is likely to be limited by practical considerations such as the effect on signal noise.

Stabilizer gain is normally set to a value that results in as high a damping of the critical system mode(s) as practical without compromising the stability of other system modes or causing excessive amplification of signal noise.

Stabilizer limits:

The positive output limit of the stabilizer is set at a relatively large value in the range of 0.1 to 0.2 pu. This allows a high level of contribution from the PSS during large swings. With such a high value of stabilizer output limit, it is essential to have a means of limiting the generator terminal voltage to its maximum allowable value, typically in the 1.12 to 1.15 pu range. Therefore, a terminal voltage limiter is used as shown in Figure 17.5. To be effective, the limiter gain K_L must be very high. The terminal voltage signal, however, contains small components of torsional components. Hence, feedback of this signal to the excitation system through a high gain may cause torsional mode instability. Therefore, T_C and T_D are chosen so as to provide high attenuation at torsional frequencies, in addition to ensuring an adequate degree of limiter loop stability.

On the negative side, a limit of −0.05 to −0.1 pu is appropriate. This allows sufficient control range while providing satisfactory transient response. In the unlikely event of the PSS output being held at the negative limit because of a failure of the stabilizer, this will not result in a unit trip.

Check on selected settings:

The final stage in stabilizer design involves the evaluation of its effect on the overall system performance. First, the effect of the stabilizer on various modes of system oscillations is determined over a wide range of system conditions by using a small-signal stability program. This includes analysis of the effects of the PSS on local plant modes, interarea modes, and control modes. In particular, it is important to ensure that there are no adverse interactions with the controls of other nearby generating units and devices such as HVDC converters and SVCs.

After checking the PSS performance under small perturbations, it is important to examine its effect on transient stability and long-term stability.

For systems with voltage problems, the acceptability of the chosen PSS output limits should be carefully assessed. In some situations, it is possible for the machine terminal voltage to fall below the exciter reference level while the speed is also falling. This can lead to the stabilizer overriding the voltage signal to the exciter, causing reduced transient recovery. It is important to limit the stabilizer output to prevent this.

It is also important to coordinate the performance of the PSS with other protections and controls such as V/Hz limiters and overexcitation/underexcitation protection.

Reference 53 provides a detailed account of the application of the above procedure for the design of the PSS of a large nuclear power plant.

General comments on excitation control design:

The excitation control systems, designed as described above, provide effective decentralized controllers for the damping of electromechanical oscillations in power systems. Generally, the resulting design is much more robust than can be achieved through use of other methods such as pole placement techniques and multivariable state space techniques. The overall approach is based on a knowledge of the physical aspects of the power system stabilization problem. The method used for establishing the phase characteristics of the PSS is simple and requires only the dynamic characteristics of the concerned machines to be modelled in detail. Detailed analysis of the performance of the power system is used to establish other parameters and to ensure adequacy of the overall performance of the excitation control. The result is a control that enhances the overall stability of the system under different operating conditions. Since the PSS is tuned to increase the damping torque component for a wide range of frequencies, it contributes to the damping of all system modes in which the respective generator has a high participation. This includes any new mode that may emerge as a result of changing system conditions. It is possible to satisfy the requirements for a wide range of system conditions with fixed parameters; hence, there has been little incentive to date to consider an adaptive control system.

Example of excitation control design

This example illustrates the application of power system stabilizers to a two-unit thermal generating station. Each unit has a rating of 488 MVA and is equipped with a thyristor excitation system. The power system characteristics are such that these units exhibit two dominant rotor oscillation modes: an interarea mode of about 0.5 Hz and a local intermachine mode of about 2.0 Hz. The objective of excitation control design is to enhance the transient as well as small-signal stability of the power system.

For the purpose of comparison, we will also examine the performance of the two thermal units when equipped with slow-rotating exciters.

The power system:

The power system consists of two areas, as shown in Figure 17.11. Area 1 has a peak load of 805 MW and is supplied by the two-unit thermal plant (G1 and G2) for which we are designing the excitation control. Area 2 has a peak load of 360 MW and is supplied by seven smaller power plants.

The parameters of each of the two 488 MVA units of area 1 in per unit on its rating are as follows:

X_d	= 1.81	X_q	= 1.76	X_l	= 0.16	X'_d	= 0.3	X'_q	= 0.61
X''_d	= 0.217	X''_q	= 0.217	R_a	= 0.002	T'_{d0}	= 7.80 s	T'_{q0}	= 0.90 s
T''_{d0}	= 0.022 s	T''_{q0}	= 0.074 s	H	= 3.53	K_D	= 0		

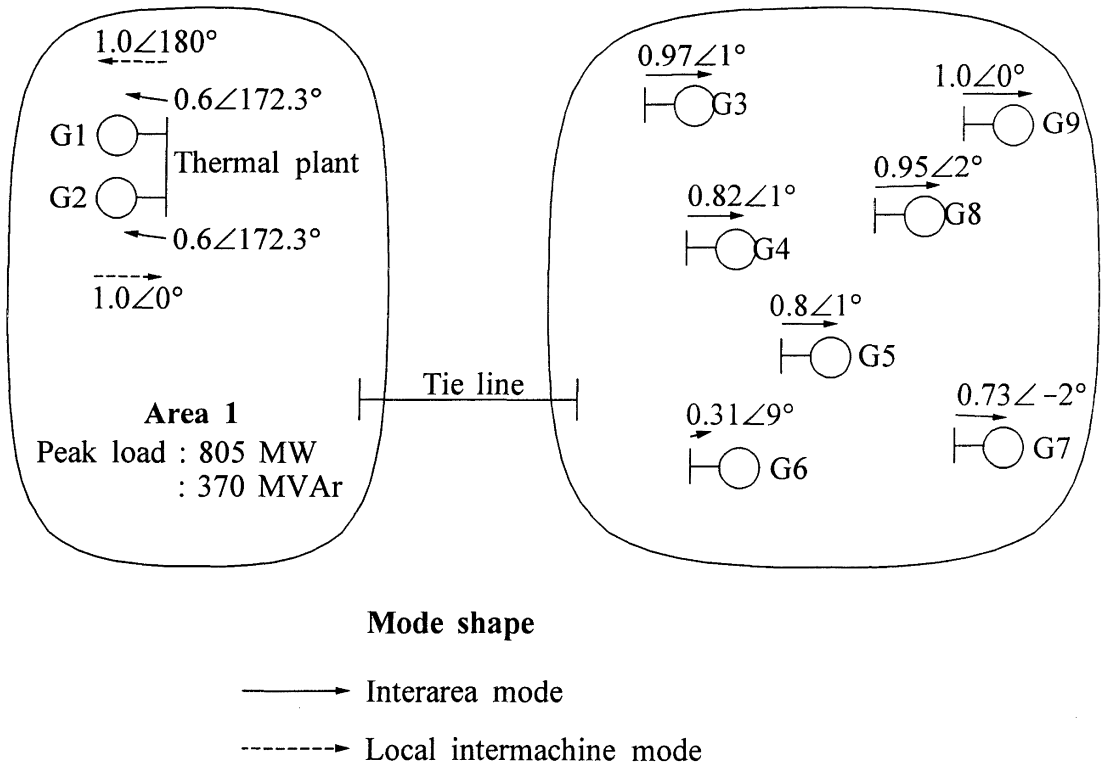


Figure 17.11 Two-area system

Thyristor excitation system:

The block diagram of the thyristor excitation system is shown in Figure 17.5. The parameters of the exciter and AVR are as follows:

$K_A = 212$ $T_R = 0.01$ $E_{fmax} = 7.77$ $E_{fmin} = -6.86$

A high exciter gain of 212 (with no transient gain reduction) is used to ensure good transient stability performance.

Slow rotating excitation system:

The alternative excitation system considered is a self-excited dc exciter with the following parameters (see block diagram of Figure 8.40, Chapter 8):

$K_A = 19.2$ $T_A = 0.1$ $T_E = 0.65$ $T_C = 0$ $T_B = 0$
$A_{ex} = 0.46$ $B_{ex} = 0.19$ $K_F = 0.05$ $T_F = 0.7$ $T_R = 0.02$
$V_{RMAX} = 1.15$ $V_{RMIN} = -1.15$ $R_C = 0$ $X_C = 0$

Small-signal stability performance:

The frequencies and damping ratios (ζ) of the rotor angle modes associated with units G1 and G2 are summarized in Table 17.2. These results were computed by using the MASS program with a detailed representation of all generating units. Peak system load conditions were considered and a major transmission circuit in area 1 near the generating station was assumed to be out of service. The network was represented by 83 buses, with the active component of loads modelled as 50% constant current and 50% constant impedance, and the reactive component of loads modelled as constant impedance.

With thyristor exciters (no PSS), the interarea mode has a frequency of 0.55 Hz and is just stable with a damping ratio of 0.006; the local intermachine mode has a frequency of 1.823 Hz and a damping ratio of 0.049. The mode shapes are shown in Figure 17.11.

With the rotating exciters, the frequencies of the two modes decrease slightly and the damping ratios increase slightly. The mode shapes are essentially similar to those with thyristor exciters.

Table 17.2 Rotor angle modes of units G1 and G2

Type of Exciter	Local Intermachine Mode		Interarea Mode	
	Frequency	ζ	Frequency	ζ
(a) Thyristor (no PSS)	1.823 Hz	0.049	0.550 Hz	0.006
(b) Rotating exciter	1.793 Hz	0.075	0.498 Hz	0.046

Selection of PSS parameters for the thyristor exciter:

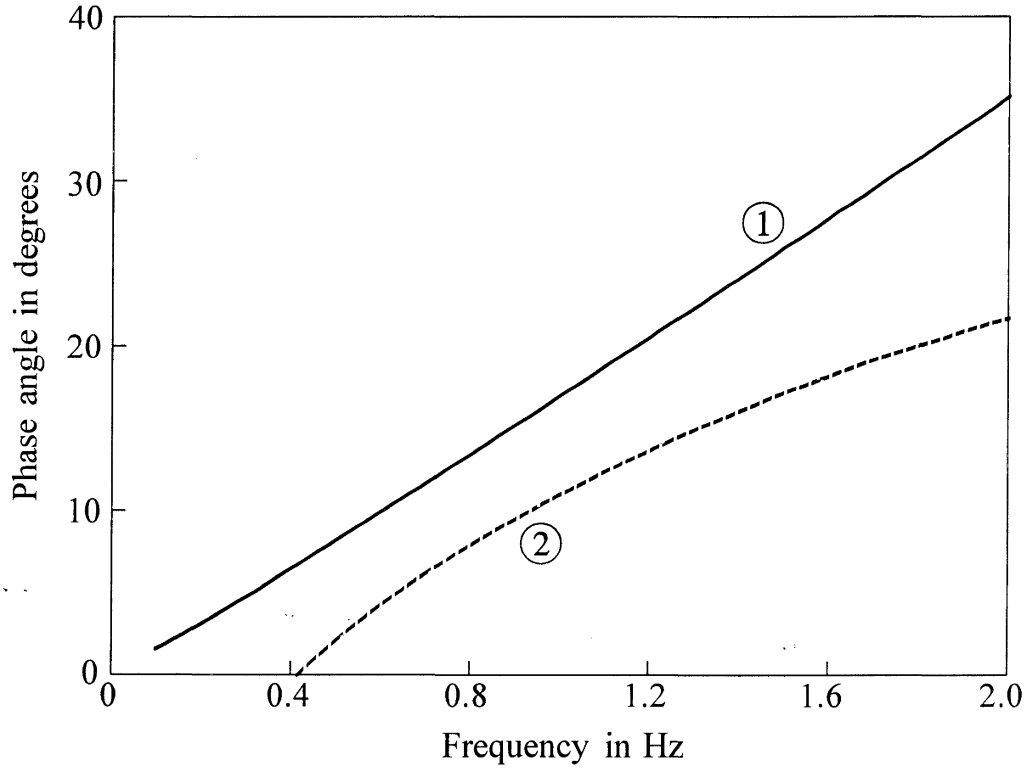
The basis for the selection of the phase-lead compensation is illustrated in Figure 17.12. Curve 1 of the figure shows the phase lag between the exciter input and the generator electrical torque as a function of frequency. This characteristic was computed using the MASS program with G1 and G2 represented in detail as a single equivalent generator having a large inertia, and the generators at all other generating stations as infinite buses. Curve 2 of the figure shows the phase-lead compensation provided by choosing the following PSS parameters (see Figure 17.5):

$T_1 = 0.06$ $T_2 = 0.02$ $T_3 = 1.5$ $T_4 = 4.0$ $T_w = 7.5$

The effect of supplementing the thyristor excitation system of units G1 and G2 with the PSS on the small-signal stability is shown in Table 17.3 for different values of stabilizer gain K_{STAB}. The damping of both modes of rotor oscillation increases as K_{STAB} is increased. A gain of about 30 is considered satisfactory.

Other parameters of the PSS (including the terminal voltage limiter) that affect the large-signal performance are chosen as follows:

$V_{s\,max} = 0.2$ $V_{s\,min} = -0.05$ $V_{LS} = 1.15$ $K_L = 17$
$T_C = 0.025$ $T_D = 1.212$ $T_{RL} = 0.01$



① Phase lag to be compensated
② Phase compensation provided

Figure 17.12 Determination of phase-lead compensation

Table 17.3 Effect of PSS gain on rotor angle modes

K_{STAB}	Local Intermachine Mode		Interarea Mode	
	Frequency	ζ	Frequency	ζ
0	1.823 Hz	0.049	0.550 Hz	0.006
20	2.079 Hz	0.156	0.547 Hz	0.087
30	2.218 Hz	0.197	0.548 Hz	0.124
40	2.366 Hz	0.227	0.533 Hz	0.156

Transient stability performance:

The results of transient stability simulations for a contingency involving a three-phase fault on a circuit close to the thermal station in area 1 are shown in Figures 17.13 and 17.14. The fault is applied when time is equal to 50 cycles and cleared 5 cycles later by opening both ends of the faulted circuit simultaneously. Three types of excitation control are considered for units G1 and G2: the thyristor exciter without and with PSS (K_{STAB}=30), and the slow dc exciter.

The results shown in Figure 17.13 are for the peak system load conditions. The system is transiently unstable with the rotating exciter. It is stable with the thyristor exciter (no PSS), but poorly damped. The PSS, in addition to significantly increasing the damping of system oscillations, improves transient stability performance by reducing the first rotor swing.

The results shown in Figure 17.14 are for system conditions with 94.5% of peak load and the output of the thermal station in area 1 proportionately reduced. With the rotating exciters, units G1 and G2 are in this case first-swing stable but become unstable in the second swing. With thyristor exciters, the stability performance is similar to that for the peak load case. Clearly, thyristor exciters with the PSS result in very good overall stability performance.

Selection of PSS location

In large systems, the selection of units on which to install the PSS to damp interarea oscillations may not be readily apparent. Although the principles of PSS design for damping of local and interarea modes are similar, the mechanisms by which a PSS contributes to the damping of the two types of oscillation are different. A PSS adds damping to an interarea mode largely by modulating system loads, whereas the performance of the PSS with regard to a local mode is only slightly affected by the load characteristics [54,55]. Understanding these mechanisms is essential to the effective application of the PSS.

Participation factors corresponding to speed deviations of generating units are very useful for initial screening of generating units on which to add stabilizers. However, a high participation factor is a necessary, but not a sufficient, condition for a PSS at the unit to effectively damp interarea oscillations. Following the initial screening based on participation factors, a more rigorous evaluation using residues and frequency responses should be carried out to determine appropriate locations for the stabilizers [54].

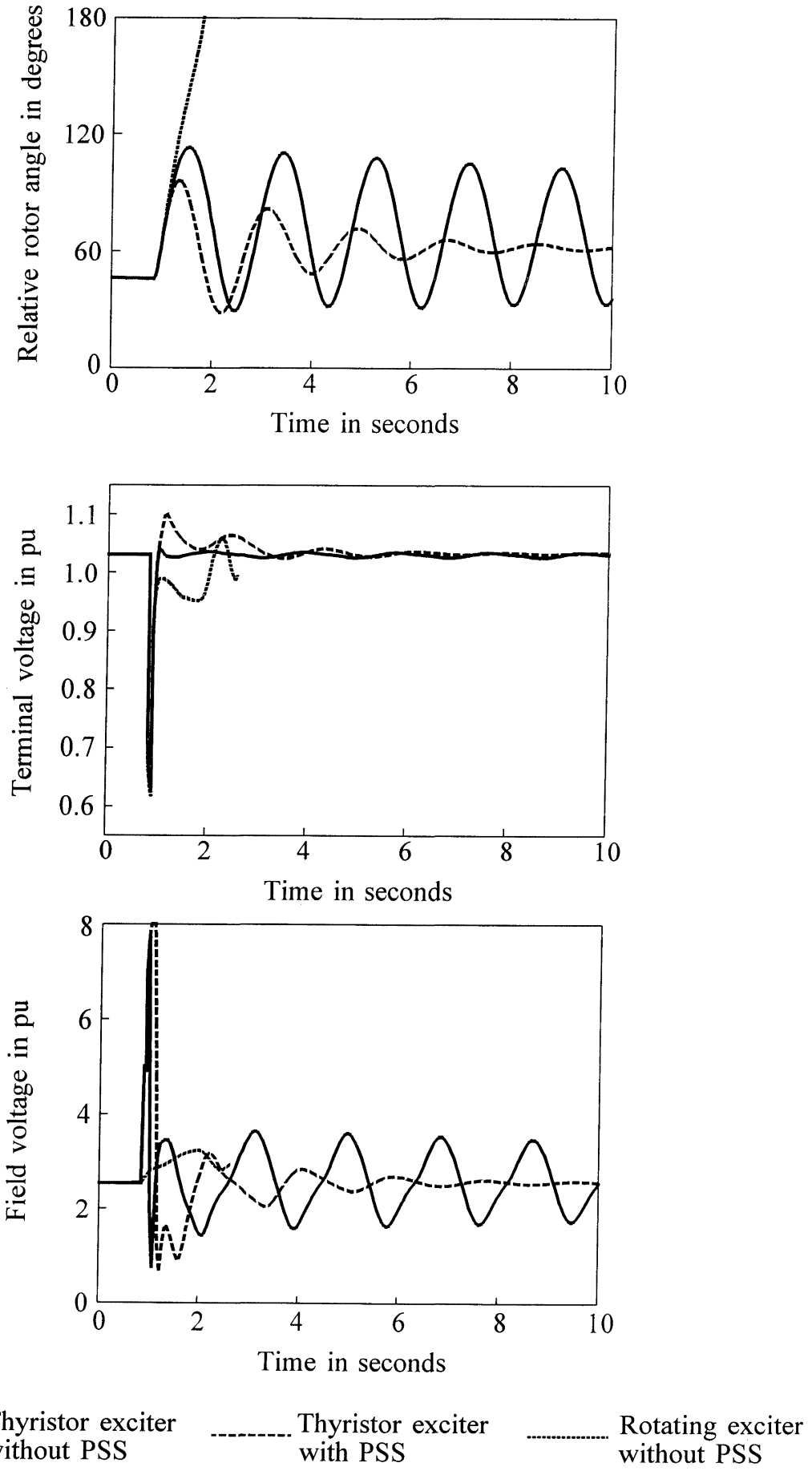


Figure 17.13 Response of unit G1 to a five-cycle three-phase fault; peak load conditions

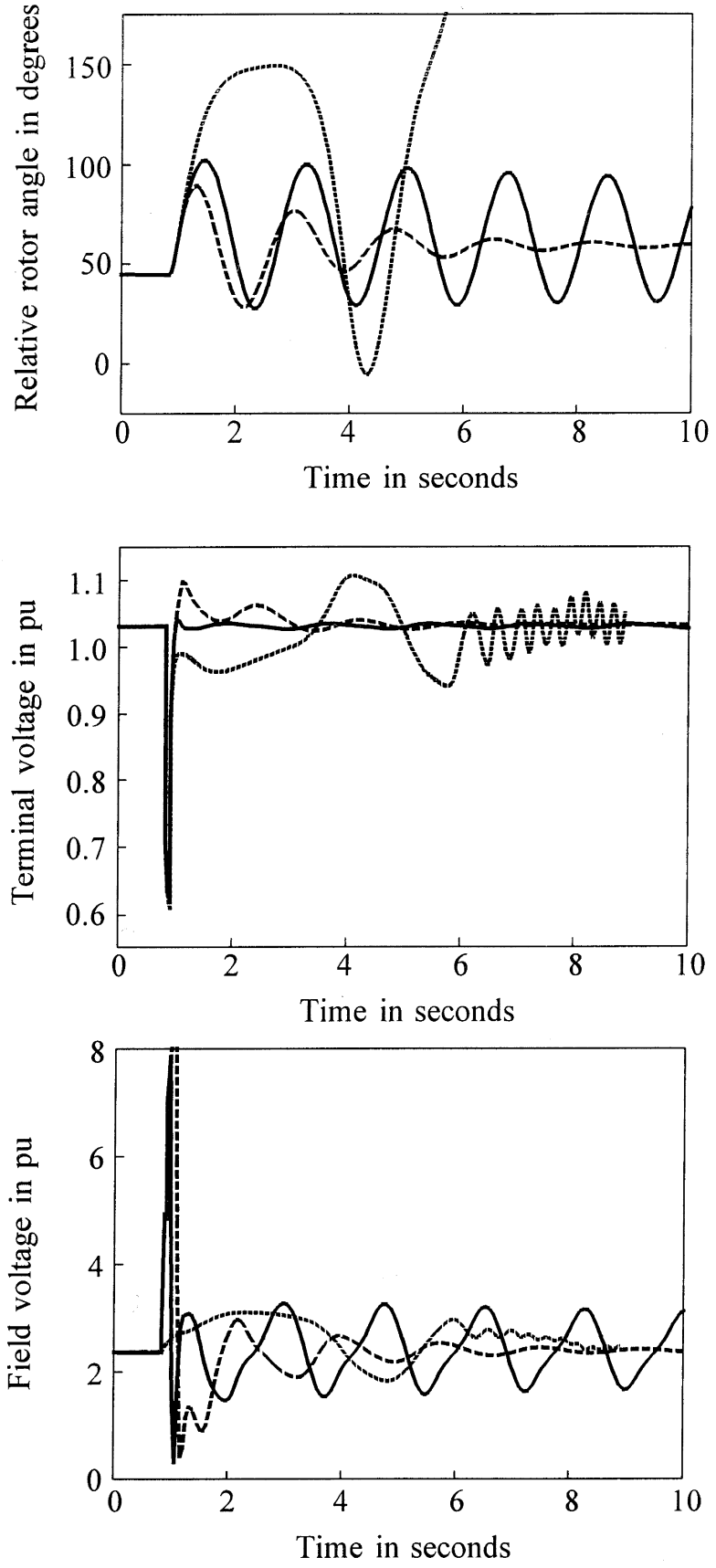


Figure 17.14 Response of unit G1 for a five-cycle three-phase fault; 94.5% peak load conditions

17.2.2 Supplementary Control of Static Var Compensators

In Chapter 11, the characteristics and modelling of static var compensators (SVCs) were described, along with the basic principles of their application. By rapidly controlling the voltage and reactive power, an SVC can contribute to the enhancement of the power system dynamic performance. Normally, voltage regulation is the primary mode of control, and this improves voltage stability and transient stability. However, the contribution of an SVC to the damping of system oscillations resulting from voltage regulation alone is usually small; supplementary control is necessary to achieve significant damping. The effectiveness of an SVC in enhancing small-signal stability depends on the location of the SVC, input signals used, and controller design.

Example of SVC application

The simple two-area system shown in Figure 17.15 is used to illustrate the application of an SVC for the enhancement of system stability. This system is identical to the one used in Example 12.6 of Chapter 12 except for slight differences in power-flow conditions because of additional shunt capacitor compensation at bus 8. All four generators are assumed to have self-excited dc exciters.

System performance without an SVC:

Figure 17.16 shows the system response to a three-phase fault near bus 9 on one of the lines between buses 8 and 9. The fault is assumed to be cleared in 74 ms by isolating the faulted line. We see from the results that the system becomes unstable through growing oscillations of about 0.4 Hz.

Stability enhancement with an SVC:

The first step is to determine a suitable location for the SVC. For this simple system, an obvious choice would be the middle of the interconnection between the two areas, where voltage swings are the greatest without the SVC [56,57].

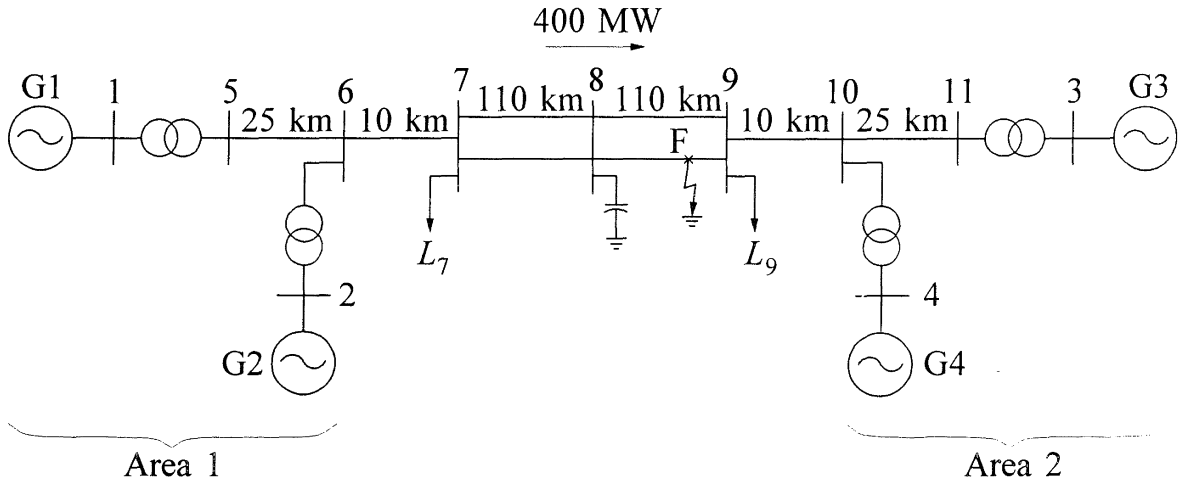


Figure 17.15 A simple two-area system

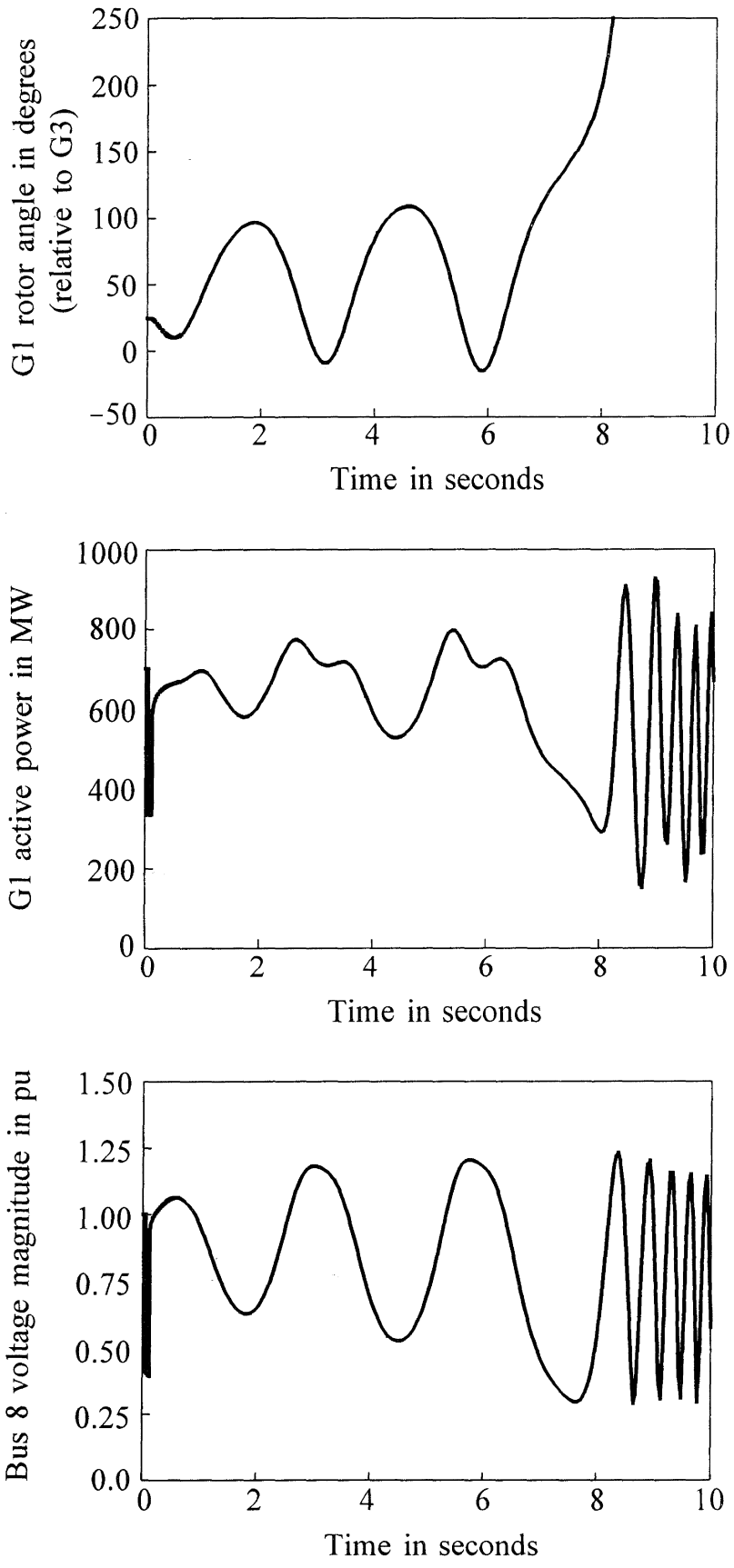


Figure 17.16 System response to a severe disturbance with no SVC

For large complex systems, the best SVC location is not obvious. In such situations, the PEALS (described in Chapter 12) or the VSTAB program (described in Chapter 14) may be used to identify the SVC locations. The bus participations computed by the VSTAB program and the voltage participation factors computed by PEALS serve as useful sensitivity indices for identifying SVC locations. Tables 17.4 and 17.5 give these indices for the prefault system conditions. The VSTAB results show bus 8 to be the best location. PEALS results indicate that bus 9 has the highest voltage participation factor (sensitivity to susceptance change), while buses 10, 4, 8, and 11 also have large factors. Considering that the power transfer might be in either direction between the two areas, bus 8 would obviously be the best choice.

An SVC comprising a fixed capacitor and a thyristor-controlled reactor (TCR) is considered for enhancement of system stability. The rating of the SVC is assumed to be 0 to 200 MVAr (capacitive). Figure 17.17 shows the block diagram of the SVC, including the

Table 17.4 Bus participation computed by VSTAB

Bus	Participation
8	0.5100
9	0.1711
7	0.1613
10	0.0668
6	0.0617
11	0.0153
5	0.0138

Table 17.5 Bus voltage eigenvector magnitude for interarea mode computed by PEALS

Bus	Voltage Vector Magnitude Factor
9	1.0000
10	0.8852
4	0.7294
8	0.6547
11	0.6147
3	0.3645

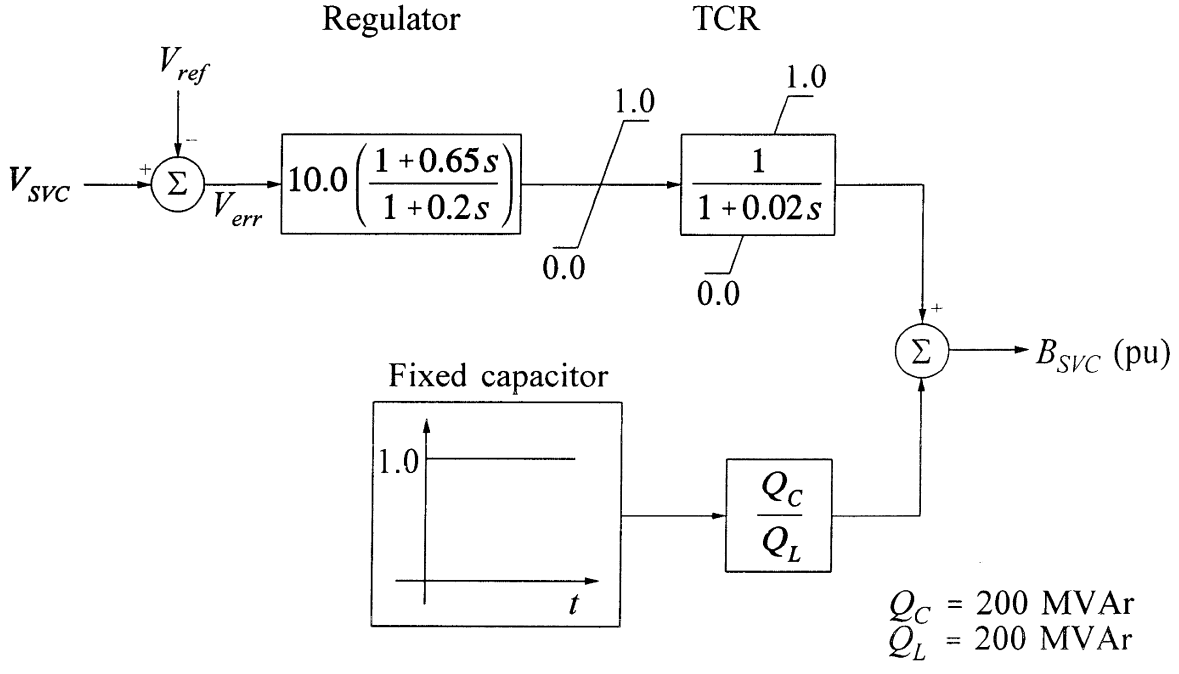


Figure 17.17 Block diagram of SVC and voltage regulator

voltage regulator. The voltage regulator gain is set at 10 to provide a 10% slope in the control range. The parameters of the lead-lag block have been selected so that the voltage regulator enhances system transient stability (i.e., high initial response).

Small-signal stability performance:

Table 17.6 summarizes the frequencies and damping ratios of the interarea mode with and without the SVC, for prefault and postfault system conditions. While the SVC has stabilized the interarea mode, the damping is still very low.

Table 17.6 Effect of SVC on interarea mode (frequency and damping ratio)

System Condition	No SVC		With SVC	
	Frequency	ζ	Frequency	ζ
Prefault	0.540 Hz	0.0064	0.547 Hz	0.0096
Postfault	0.417 Hz	-0.0228	0.476 Hz	0.0154

Supplementary control to improve damping:

The input signal used for supplementary control of the SVC should be responsive to the modes of oscillation to be damped. This can be determined by residues and observability using the MASS program described in Chapter 12. Table 17.7 gives the residues and observability factors for various input signals for both prefault and postfault conditions. Clearly, a good choice for the input signal is the magnitude of current in the line between buses 9 and 10. Figure 17.18 shows the frequency response characteristics of the transfer function between the SVC input and this current. It has a high gain at the frequency of interarea mode – an indication of good selectivity of this signal.

Table 17.7 Residues and observability factors

Signal	Prefault		Postfault	
	Residue	Observability	Residue	Observability
$\Delta\omega$ of G1	$-0.2680-j0.1156$	0.8738	$-0.9522-j0.3651$	0.5471
$\Delta\omega$ of G2	$-0.2121-j0.1004$	0.7025	$-0.7733-j0.3347$	0.4510
$\Delta\omega$ of G3	$0.4588+j0.1121$	1.4140	$2.6200+j0.2945$	1.4140
$\Delta\omega$ of G4	$0.4064+j0.0947$	1.2510	$2.4380+j0.2469$	1.3140
ΔP, line 6-7	$-0.2286+j0.4914$	1.6230	$-0.6551+j1.5160$	0.8861
ΔP, line 10-9	$0.2122-j0.8560$	2.6400	$0.5305-j4.3570$	2.3550
ΔQ, line 6-7	$-0.0310+j0.2107$	0.6375	$0.1289+j1.2020$	0.6847
ΔQ, line 10-9	$-0.0400+j0.2346$	0.7126	$-0.0924+j1.6290$	0.8752
ΔI, line 6-7	$-0.3157+j0.8618$	2.7980	$-0.8919+j3.4640$	1.9120
ΔI, line 10-9	$0.2615-j0.8732$	2.7290	$0.6484-j3.8810$	2.1110

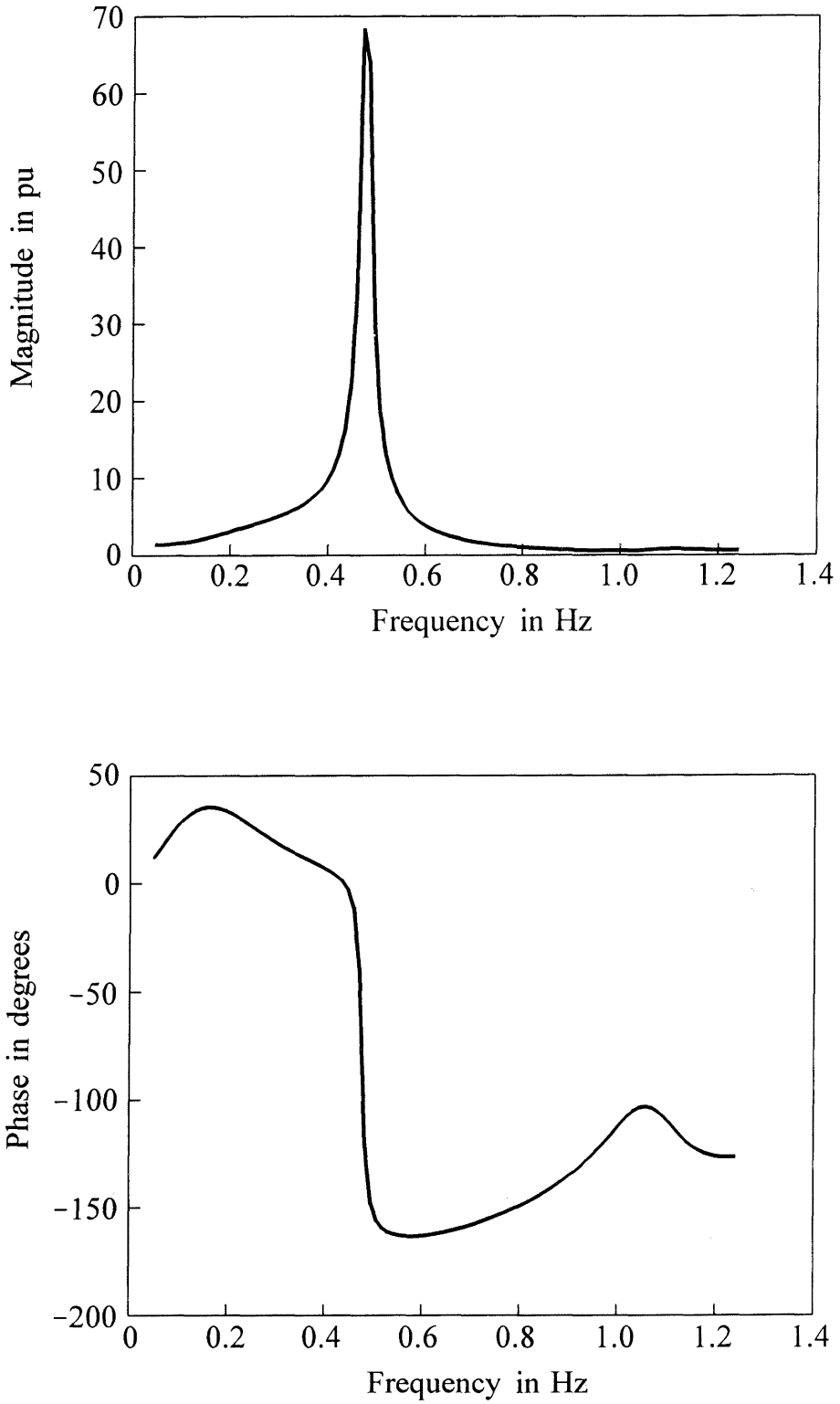


Figure 17.18 Frequency response of the transfer function between the SVC input and the current in line between buses 9 and 10

Control design:

Several alternative control design techniques may be used for determining the control parameters for SVCs [55]:

- Pole placement technique
- Phase and gain margin technique
- H-infinity technique

Here, we will illustrate the use of the pole placement technique. First, we will provide a brief description of the method.

The pole placement technique uses root locus rules to shift a pair of dominant poles to a newly assigned location in the s-plane. After the initial design the controller is tested for robustness and, if necessary, appropriate modifications are made. At this stage, the nonlinearities may be included and the compensator limits may be set.

Let the transfer function of the open-loop plant and the controller (compensator) be $G(s)$ and $H(s)$, respectively, as shown in Figure 17.19.

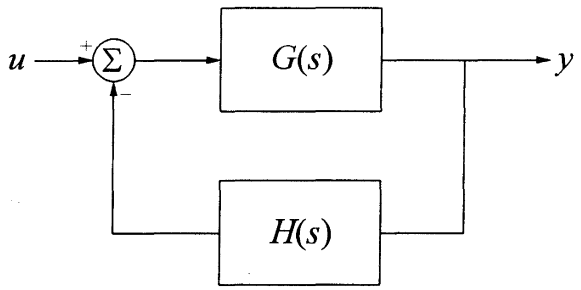


Figure 17.19 Transfer function of a plant with feedback

The closed-loop transfer function of the compensated plant is

$$G_c(s) = \frac{G(s)}{1+G(s)H(s)}$$

The zeros of $1+G(s)H(s)$ are the poles of the closed-loop system.

Assume that the system eigenvalue λ is to be shifted to a new location in the s-plane denoted by λ_0. Since λ_0 must satisfy the characteristic equation of the closed-loop system,

$$H(\lambda_0) = -\frac{1}{G(\lambda_0)}$$

This can be expressed in terms of magnitude and phase, as follows:

$$|H(\lambda_0)| = \frac{1}{|G(\lambda_0)|}$$

$$arg(H(\lambda_0)) = 180° - arg(G(\lambda_0))$$

Thus, the magnitude and phase of the compensator at λ_0 can be calculated from the magnitude and phase of the plant at λ_0; that is, from the complex frequency response of the plant at the new pole location. The new pole location is chosen to satisfy the specified damping ratio. Its imaginary part is usually chosen slightly larger than that of λ.

The compensator generally consists of a washout and a series of lead and/or lag functions to satisfy the argument equation, as shown below.

$$K\frac{sT_W}{1+sT_W}\frac{1+sT_1}{1+sT_2}\cdots\frac{1+sT_{2n-1}}{1+sT_{2n}}$$

The washout is intended to eliminate the dc component or reduce the close-to-dc component of the measured signal and has a large time constant. Each lead or lag block compensation is limited to a maximum of 60° for practical reasons. The maximum angle, θ_m, that the i^{th} block can provide, is given by

$$\sin\theta_m = \frac{1-a_i}{1+a_i}$$

where $a_i = T_{2i}/T_{2i-1}$.

The frequency at which this maximum occurs is

$$\omega_m = \frac{1}{\sqrt{a_i}T_{2i-1}}$$

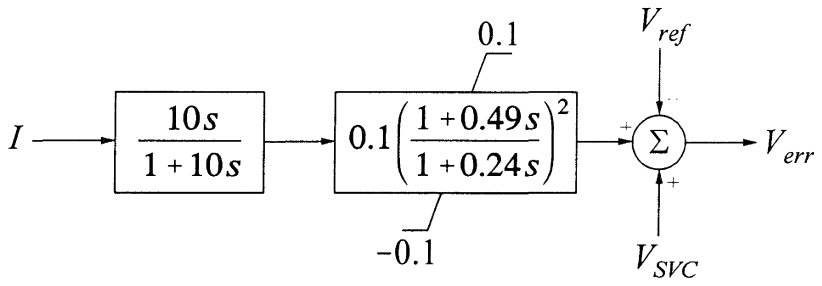
which is usually chosen to be near the frequency of λ_0. Finally, the gain K is chosen to satisfy the magnitude equation.

For the system of Figure 17.15, the magnitude and phase of the transfer function between the SVC input and the current in the line from bus 10 to bus 9 are computed for a number of values of λ_0. This is done for the prefault as well as the postfault system conditions. The objective is to find satisfactory values of λ_0 that result in approximately the same magnitude and phase for both operating conditions. These values of λ_0 are given in Table 17.8.

Table 17.8 The desired location of the eigenvalues and the value of the system transfer function

Prefault System		Postfault System	
New Eigenvalue Location	Value of Transfer Function	New Eigenvalue Location	Value of Transfer Function
$-0.127\pm j3.544$	$4.262\angle 137.8°$	$-0.576\pm j3.498$	$4.177\angle 132.3°$

Figure 17.20 shows the block diagram of the supplementary control. The output limits of the controller are set to provide the desired large-signal response.



I = magnitude of current in line between buses 9 and 10

Figure 17.20 Supplementary control block diagram

The frequency and damping ratios of the interarea mode with supplementary control of the SVC are as follows:

Prefault: f=0.564 Hz ζ=0.036
Postfault: f=0.557 Hz ζ=0.163

The transient stability performance of the system with and without supplementary control of the SVC is depicted in Figure 17.21. The disturbance considered is, as before, a 74 ms three-phase fault on one of the lines between buses 8 and 9. The SVC with voltage regulation stabilizes the system, but the damping is poor. The oscillations are well damped with the supplementary control of the SVC.

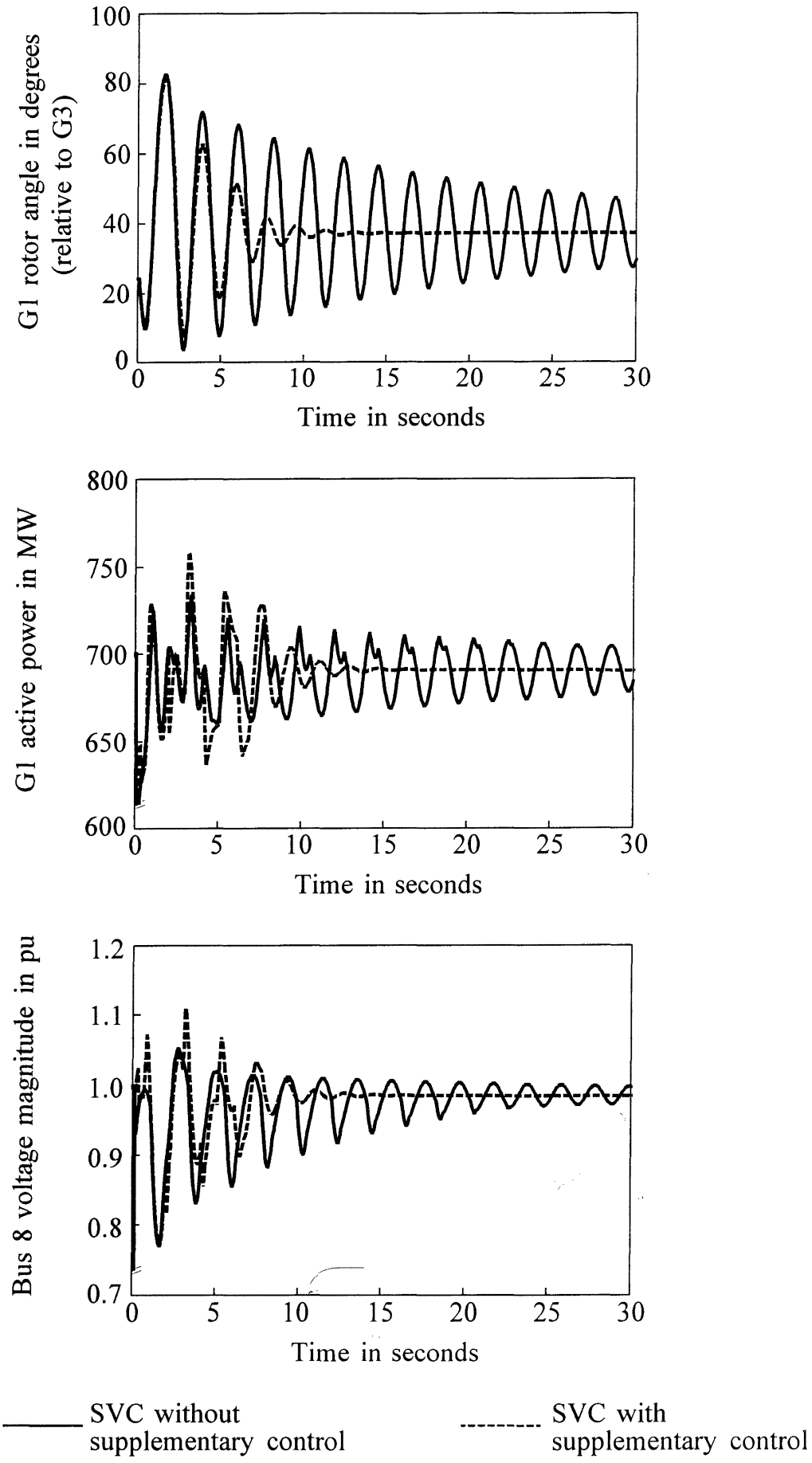


Figure 17.21 System response to a severe disturbance with and without supplementary control of an SVC at bus 8

17.2.3 Supplementary Control of HVDC Transmission Links

As described in Chapter 10, the basic controlled quantity in an HVDC transmission link is the direct current. Normally, the direct current is controlled by the rectifier, and the dc line voltage is maintained near the rated value by inverter control. Damping of the ac system electromechanical oscillations can be increased by modulating the current order at the rectifier. Alternatively, both the current order at the rectifier and the voltage order at the inverter can be modulated.

The HVDC link may either be embedded in an ac system or form an asynchronous link between two ac systems. Supplementary control with either of these types of HVDC links is effective in damping ac system oscillations. References 42 and 43 describe dc modulation schemes used in several HVDC transmission links.

The following example illustrates the use of supplementary control of HVDC links for the enhancement of system stability.

Example of HVDC link supplementary control

The system used to illustrate the application of HVDC supplementary control is shown in Figure 17.22. It is based on the simple two-area system considered in the previous section (Figure 17.15) and in Example 12.6. A 200 MW bipolar dc link has been added between buses 7 and 9 in parallel with two ac ties. The dc link is represented as a monopolar link with a voltage rating of 56 kV and a current rating of 3,600 A. The dc line resistance is 1.5 Ω, and inductance is 100 mH. The commutating reactance (X_c) associated with each converter is 0.57 Ω. A smoothing reactor of 50 mH is used at each end of the line.

The ac portion of the system is very similar to that of Example 12.6. The principal difference is the reactive support of 125 MVAr provided at the rectifier and inverter buses.

Modelling of converter controls:

Figures 17.23 to 17.28 show models used to represent the dc link controls. The master control, shown in Figure 17.23, determines the current order for the rectifier and inverter. If

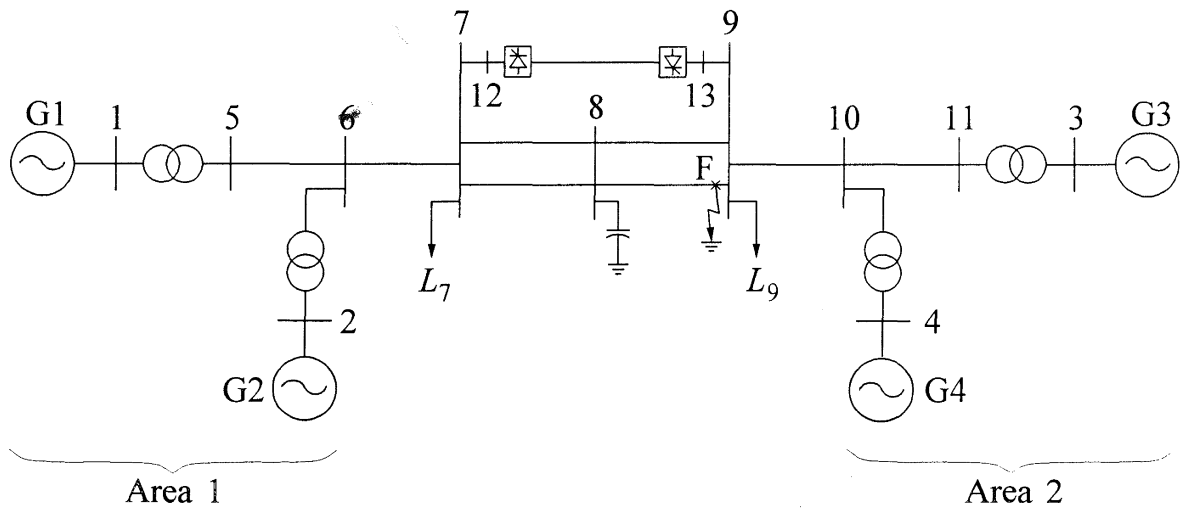


Figure 17.22 A two-area system with parallel dc and ac ties

the rectifier end dc voltage falls below 90% of rated value, the control switches to constant current mode. The hysteresis characteristic represented by block MC1 prevents hunting between constant power and constant current control modes. The current order is limited by the voltage-dependent current order limit (VDCOL) shown in Figure 17.24.

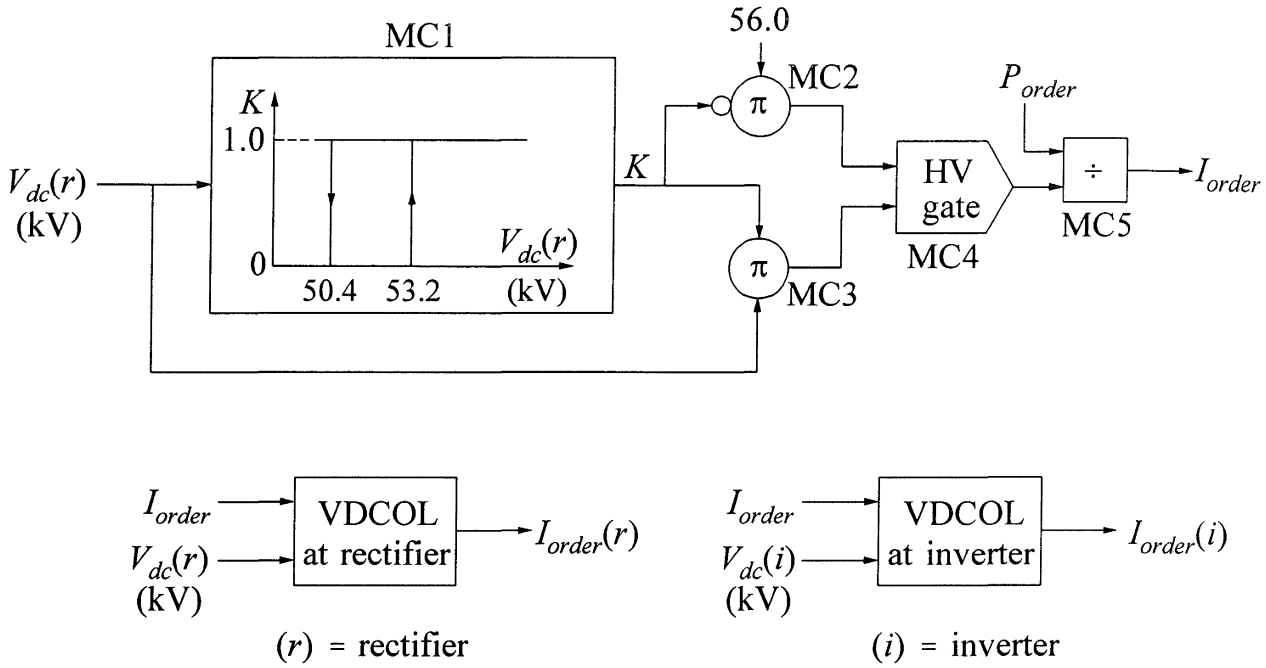
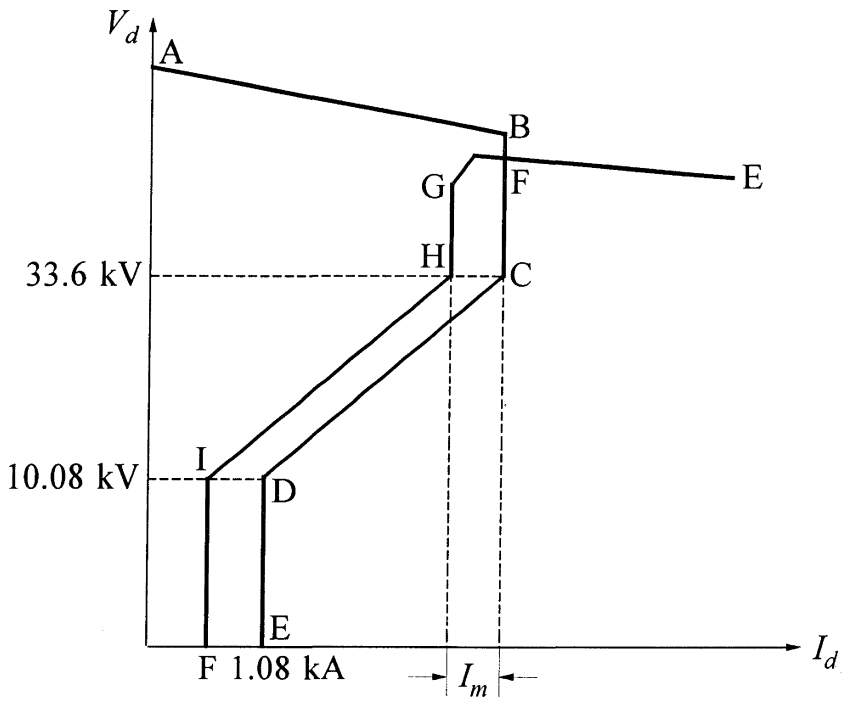


Figure 17.23 Master control



I_m = 0.36 kA

The downtime constant is 5 ms.
The uptime constant is 100 ms.

Figure 17.24 Voltage-dependent current order limits

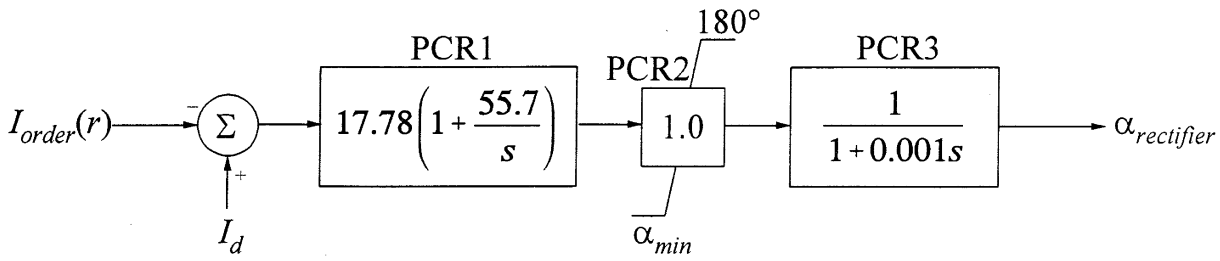


Figure 17.25 Rectifier pole control

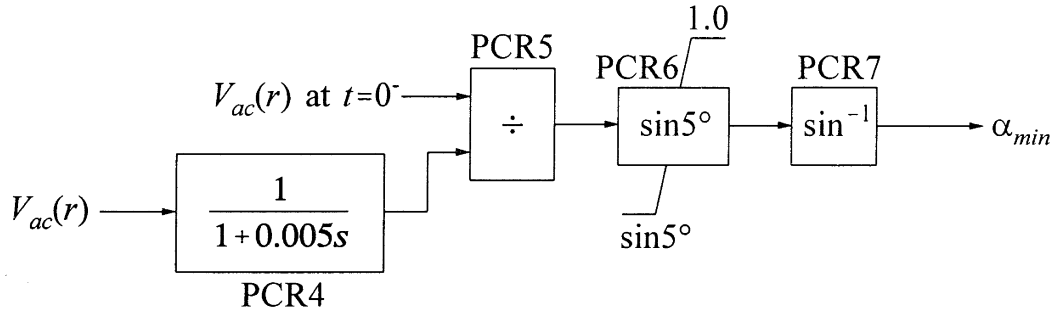


Figure 17.26 α_{min} calculation

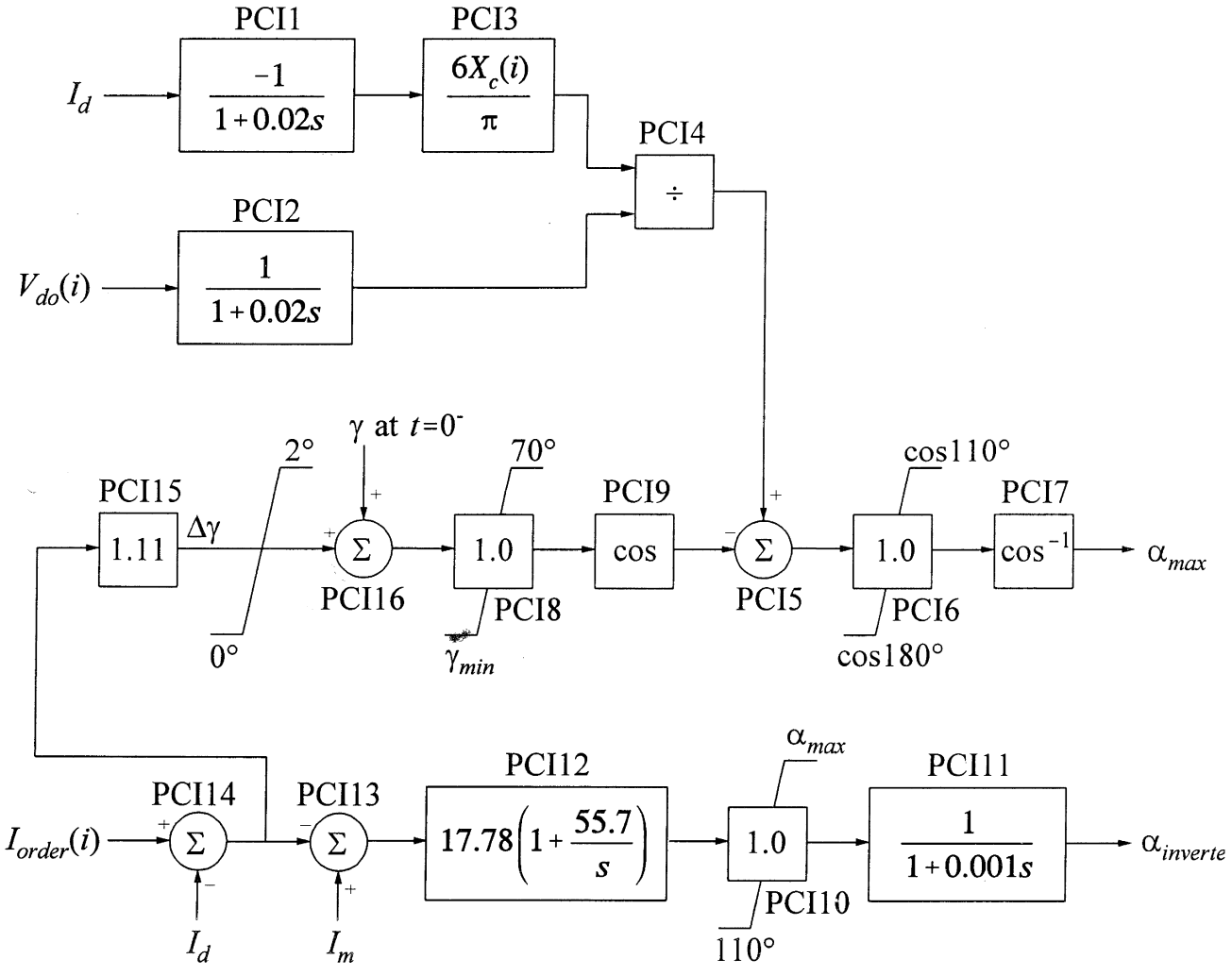


Figure 17.27 Inverter pole control

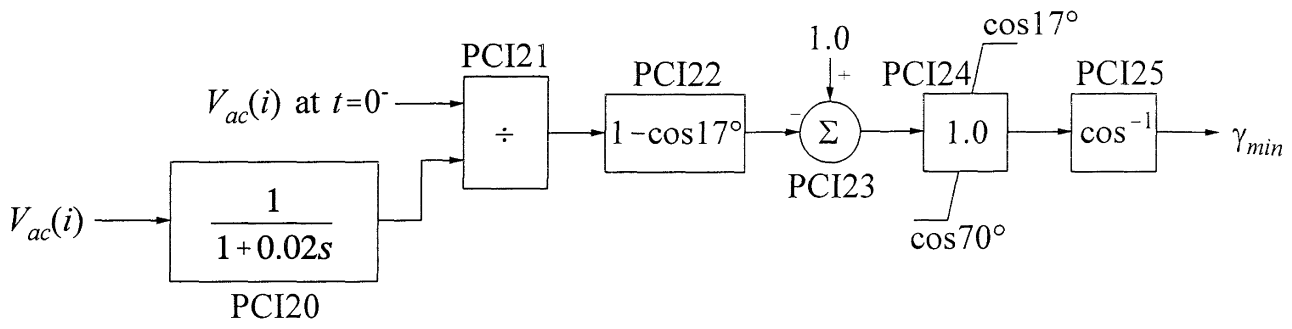


Figure 17.28 γ_{min} calculation

The rectifier pole control representation is shown in Figure 17.25. The normal mode of rectifier operation is current control. A proportional plus integral controller (block PCR1) is used to control the direct line current. The ignition delay angle α is limited between α_{min} and 180°. The lower limit α_{min} ensures that there is sufficient forward voltage across the thyristor for a successful turn-on. This limit, as shown in Figure 17.26, varies with the ac line voltage at the rectifier (blocks PCR4 to PCR7) so that there is always a minimum amount of forward voltage across the thyristor.

Figure 17.27 shows the inverter pole control representation. Under normal conditions, the inverter is on constant extinction angle (CEA) control represented by

$$\cos\alpha = \frac{6X_c I_d}{\pi V_{d0}} - \cos\gamma$$

The control ensures that cosα corresponds to a condition with γ constant (see Chapter 10, Section 10.9.3).

The inverter is also equipped with a current controller that is active only when the firing angle derived from current control is smaller than the firing angle derived from the CEA controller. The inverter switches to the current control mode when the rectifier hits α_{min} and is unable to maintain the desired direct current.

The lower limit of the extinction angle (γ_{min}) is varied with the inverter ac bus voltage so that a minimum commutation margin area is maintained. Figure 17.28 shows the logic for the calculation of γ_{min}.

If the inverter ac bus voltage drops below 0.5 pu, it is assumed that commutation failure occurs. The rectifier and inverter are blocked if the inverter experiences more than two commutation failures. The inverter recovers following a commutation failure when the ac bus voltage subsequently goes above 0.7 pu.

System performance without supplementary control:

Figures 17.29 and 17.30 show the system response to a three-phase fault near bus 9 on one of the circuits between buses 8 and 9. The fault is cleared by isolating the faulted circuit in 83 ms. We see from the results that the system is transiently stable. However, oscillations between area 1 and area 2 generators have zero or slightly negative damping.

Table 17.9 summarizes the results of small-signal stability analysis. The frequency and damping ratio of the interarea mode are listed for different system conditions. The interarea mode is poorly or negatively damped in all the cases considered.

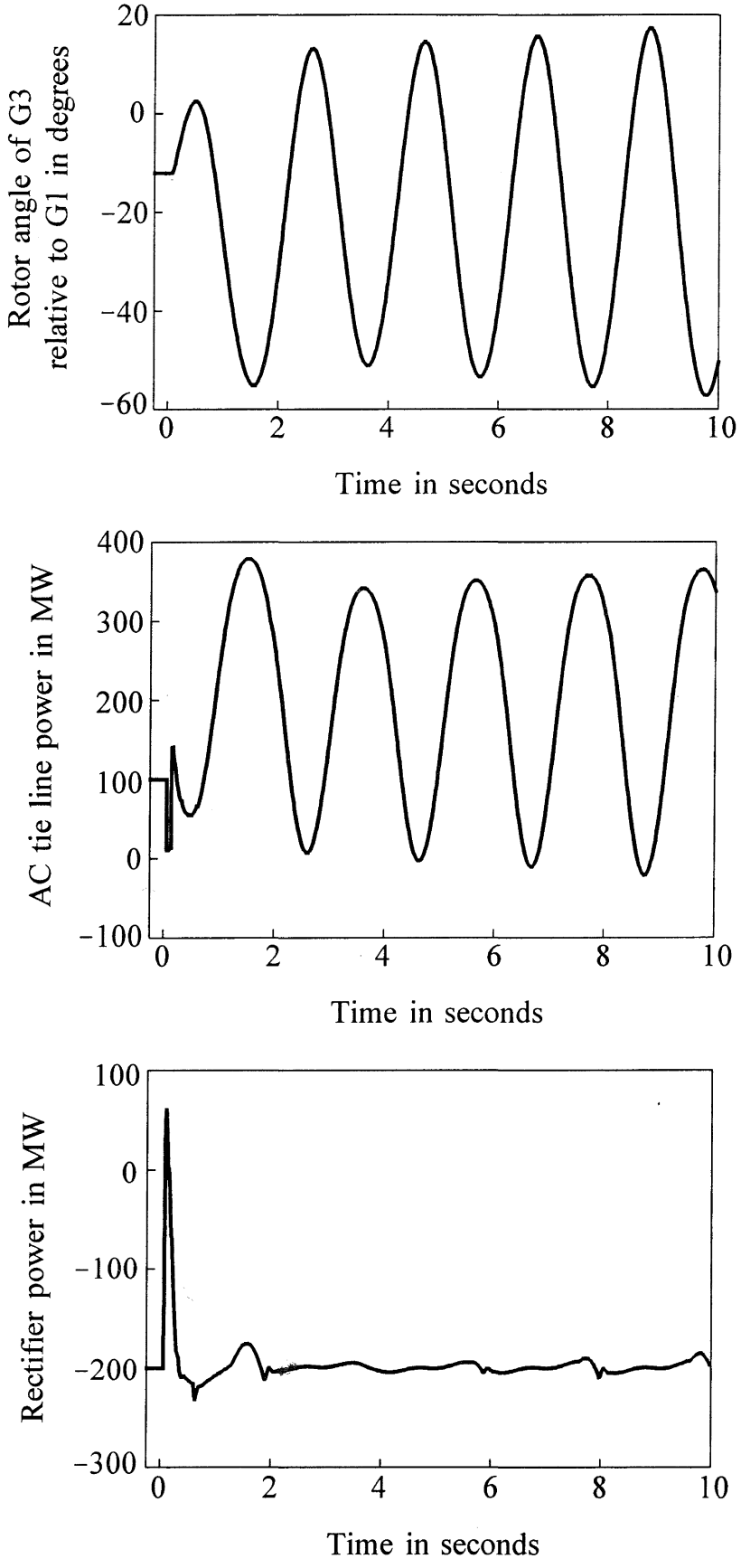


Figure 17.29 System response to an ac system fault near the inverter, with no supplementary control

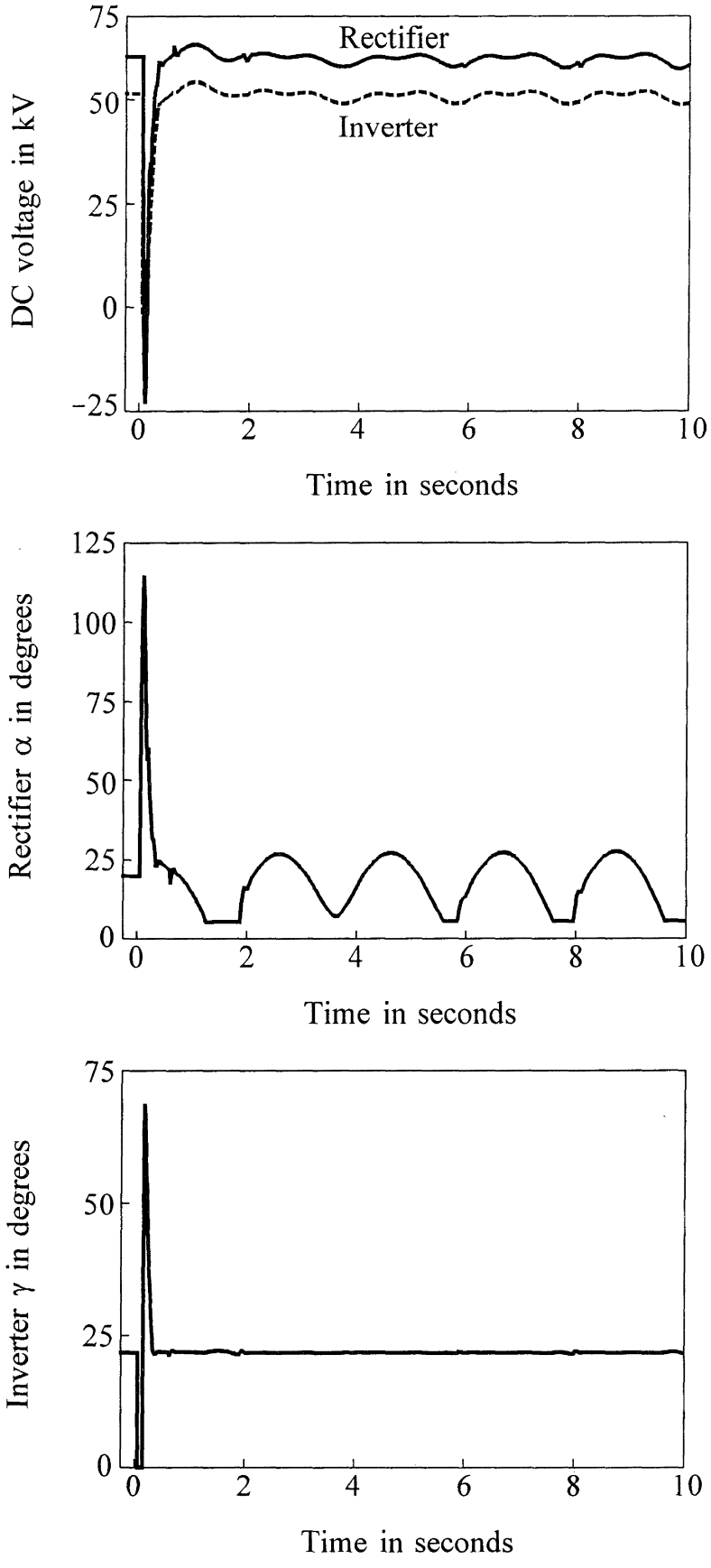


Figure 17.30 HVDC link response to an ac system fault near the inverter, with no supplementary control

Table 17.9 Frequency and damping ratio of interarea mode without supplementary control

Case No.	MW Flow from Area 1 to Area 2		Circuits out of Service	Interarea Mode	
	DC Tie	AC Tie		Freq. (Hz)	ζ
1(a)	200	200	None	0.575	0.0076
1(b)	200	200	8 to 9 (1 cct)	0.495	-0.0054
1(c)	200	200	7 to 8 (1 cct) 8 to 9 (1 cct)	0.440	-0.0167
2(a)	50	352	None	0.560	0.0052
2(b)	50	352	8 to 9 (1 cct)	0.466	-0.0110
2(c)	50	352	7 to 8 (1 cct) 8 to 9 (1 cct)	0.397	-0.0254

Supplementary control to improve damping:

The general procedure for designing the supplementary control is the same as that for an SVC using the pole placement technique as described in Section 17.2.2.

Based on observability considerations, active power through the line between buses 7 and 8 is selected as the feedback signal. The initial target for the placement of the eigenvalue associated with the interarea mode is chosen to be $-0.64\pm j3.1$. This corresponds to a frequency of 0.5 Hz and a damping ratio of 0.2. The magnitude and phase of the open-loop transfer function between the power order signal of HVDC master control and the active power flow in the line between buses 7 and 8 at a complex frequency $s=-0.64\pm j3.1$ for different operating conditions are listed in Table 17.10. The results show that the phase compensation required is between 85° and 150°. As a compromise, the phase compensation is chosen to be 100°. Figure 17.31 shows the block diagram of the supplementary control.

Table 17.10 Magnitude and phase of the open-loop transfer function at $s=-0.64\pm j3.1$

Case No.	Open-Loop Transfer Function
1(a)	$0.815\angle -146.92°$
1(c)	$0.773\angle -86.84°$
2(a)	$0.716\angle -142.20°$
2(c)	$0.237\angle -112.90°$

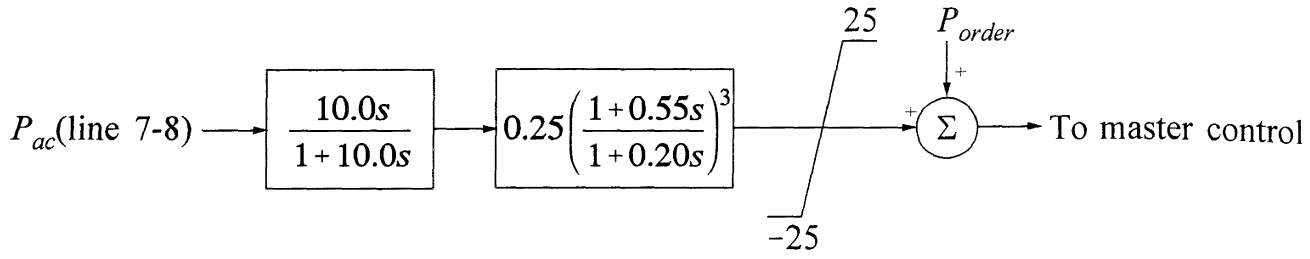


Figure 17.31 Supplementary control block diagram

The washout time constant is 10 s. The parameters of the phase-lead block are chosen to provide 100° at the complex frequency $-0.64\pm j3.1$. The gain is limited to 0.25 so as to ensure adequate damping of all system modes. Relatively large output limits (±25 MW) are used to allow a high level of contribution from the supplementary controller during large swings.

The frequency and damping ratio of the interarea mode with the supplementary control are summarized in Table 17.11 for the different operating conditions considered in Table 17.9. The interarea mode is well damped in all cases with the supplementary control.

Table 17.11 Frequency and damping ratio of interarea mode with supplementary control

Case No.	Interarea Mode	
	Freq. (Hz)	ζ
1(a)	0.607	0.1730
1(b)	0.506	0.1572
1(c)	0.467	0.2512
2(a)	0.588	0.1474
2(b)	0.475	0.1007
2(c)	0.422	0.1031

Figures 17.32 and 17.33 show the transient response of the system with supplementary control for a three-phase fault near bus 9 on a circuit between buses 8 and 9. The oscillations are now well damped.

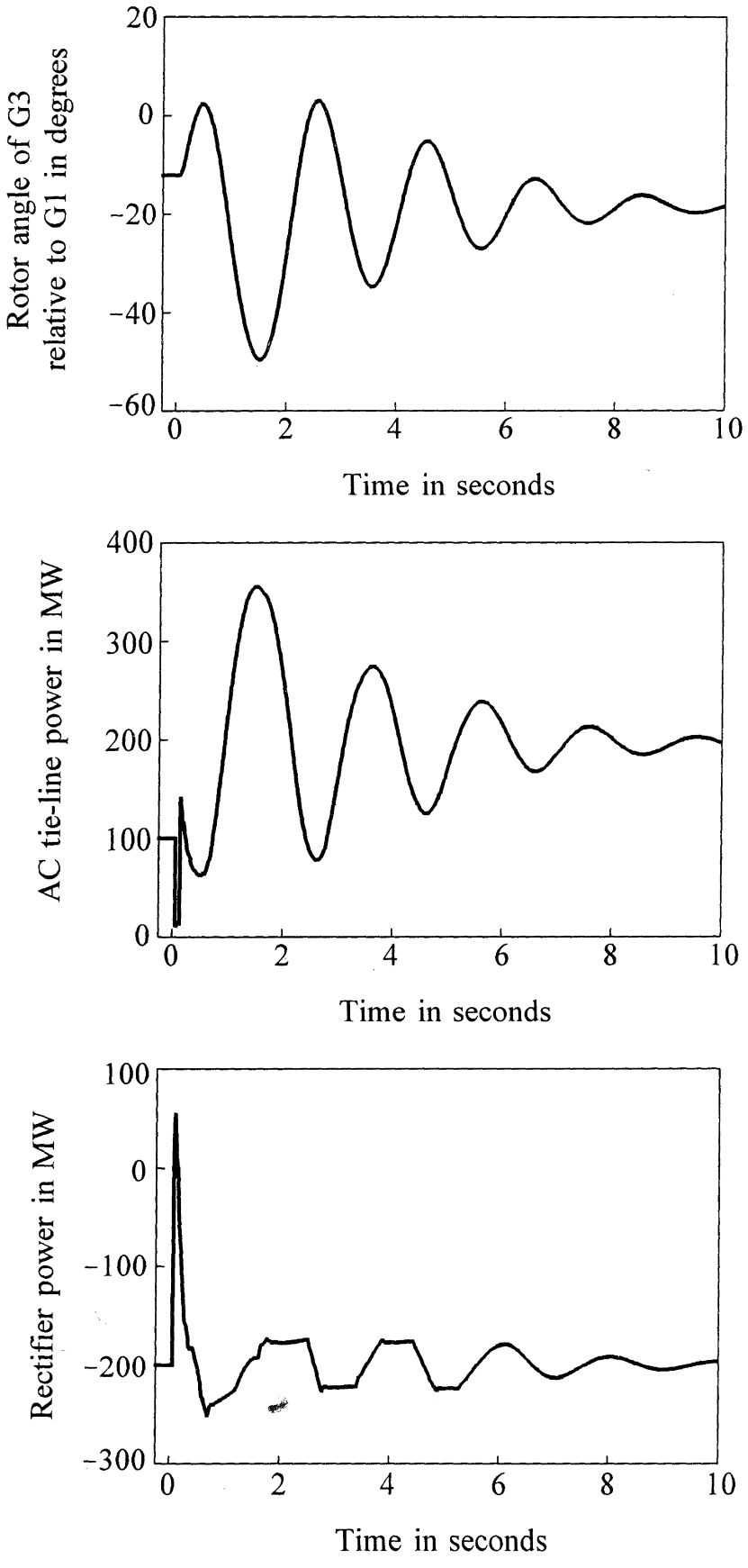


Figure 17.32 System response to an ac system fault nea the inverter, with supplementary control

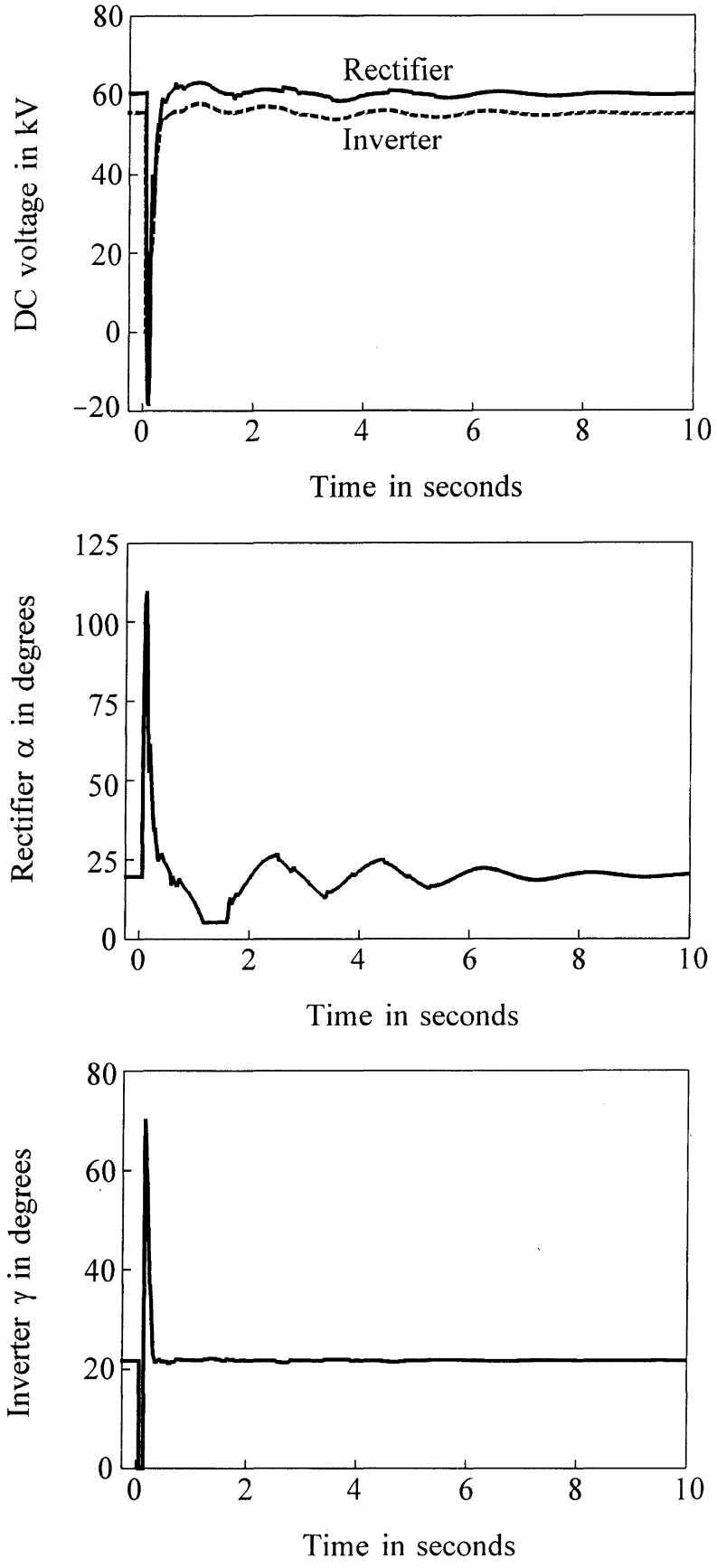


Figure 17.33 HVDC link response to an ac system fault near the inverter, with supplementary control

REFERENCES

[1] R.O. Berglund, W.A. Mittelstadt, M.L. Shelton, P. Barkan, C.G. Dewey, and K.M. Skreiner, "One-Cycle Fault Interruption at 500 kV: System Benefits and Breaker Design," *IEEE Trans.* Vol. PAS-93, pp. 1240-1251, September/ October, 1974.

[2] J. Esztergalyos, M.T. Yee, M. Chamia, and S. Liberman, "The Development and Operation of an Ultra High Speed Relaying System for EHV Lines," CIGRE 34-04, 1978.

[3] C. Lindsay and V. Shenoy, "Reliability and Selection of Characteristics for EHV Transformers," CIGRE 12-08, 1978.

[4] G.D. Breuer, H.M. Rustebakke, R.A. Gibley, and H.O. Simmons, "The Use of Series Capacitors to Obtain Maximum EHV Transmission Capability," *IEEE Trans.,* Vol. PAS-83, pp. 1090-1101, November 1964.

[5] E.W. Kimbark, "Improvement of System Stability by Switched Series Capacitors," *IEEE Trans.,* Vol. PAS-85, pp. 180-188, February 1966.

[6] IEEE Task Force Report, "A Description of Discrete Supplementary Controls for Stability," *IEEE Trans.,* Vol. PAS-97, pp. 149-165, January/February 1978.

[7] H.M. Ellis, J.E. Hardy, A.L. Blythe, and J.W. Skooglund, "Dynamic Stability of the Peace River Transmission System," *IEEE Trans.*, Vol. PAS-85, pp. 586-600, June 1966.

[8] M.L. Shelton, R.F. Winkleman, W.A. Mittelstadt, and W.L. Bellerby, "Bonneville Power Administration 1400 MW Braking Resistor," *IEEE Trans.,* Vol. PAS-94, pp. 602-611, March/April 1975.

[9] CIGRE SC38-WG02 Report, "State of the Art in Non-Classical Means to Improve Power System Stability," *Electra*, No. 118, pp. 88-113, May 1988.

[10] EPRI Report EL-5859, "Technical Limits to Transmission System Operation," Final Report of Project 5005-2, prepared by Power Technologies Inc., June 1988.

[11] IEEE Working Group, "Single Pole Switching for Stability and Reliability," Report of a panel discussion held at the 1984 PES Summer Meeting, *IEEE Trans.,* Vol. PWRS-1, No. 2, pp. 25-36, May 1986.

[12] R.D. Dunlop, R.M. Maliszewski, and B.M. Pasternack, "Application of Single Phase Switching on the AEP 765-kV System," *Proceedings of the American Power Conference*, Vol. 42, pp. 461-462, 1980.

[13] A.J. Fakheri et al., "The Use of Reactor Switches in Single Phase Switching," CIGRE 13-06, 1980.

[14] N. Knudsen, "Single-Phase Switching of Transmission Lines Using Reactors for Extinction of the Secondary Arc," CIGRE 310, 1962.

[15] E.W. Kimbark, "Suppression of Ground-Fault Arcs on Single-Pole Switched Lines by Shunt Reactors," *IEEE Trans.*, Vol. PAS-83, pp. 285-290, March 1964.

[16] R.M. Hasibar, A.C. Legate, J.H. Brunke, and W.G. Peterson, "The Application of High-Speed Grounding Switches for Single-Pole Reclosing on 500-kV Power Systems," *IEEE Trans.*, Vol. PAS-100, pp. 1512-1515, April 1981.

[17] A.J. Gonzales, G.C. Kung, C. Raczkowski, C.W. Taylor, and D. Thonn, "Effects of Single-and-Three Pole Switching and High-Speed Reclosing on Turbine-Generator Shafts and Blades," *IEEE Trans.*, Vol. PAS-103, pp. 3218-3228, November 1984.

[18] ANSI Standard C50.13-1989.

[19] R.C. Buell, R.J. Caughey, E.M. Hunter, and V.M. Marquis, "Governor Performance during System Disturbances," *AIEE Trans.*, Vol. 50, pp. 354-369, March 1931.

[20] F.P. deMello, D.N. Ewart, M. Temoshok, and M.A. Eggenberger, "Turbine Energy Controls Aid in Power System Performance," *Proceedings of the American Power Conference*, Vol. 28, pp. 438-445, 1966.

[21] R.H. Park, "Improved Reliability of Bulk Power Supply by Fast Load Control," *Proceedings of the American Power Conference*, Vol. 30, pp. 1128-1141, 1968.

[22] R.H. Park, "Fast Turbine Valving," *IEEE Trans.*, Vol. PAS-92, pp. 1065-1073, May/June 1973.

[23] E.W. Cushing, G.E. Drechsler, W.P. Killgoar, H.G. Marshall and H.R. Stewart, "Fast Valving as an Aid to Power System Transient Stability and Prompt Resynchronization and Rapid Reload after Full Load Rejection," *IEEE Trans.*, Vol. PAS-91, pp. 1624-1636, July/August 1972.

[24] H.F. Martin, D.N. Tapper and T.M. Alston, "Sustained Fast Valving Applied to TVA's Watts Bar Nuclear Units," Paper 76-JPGC-PWR-5, presented at the 1976 Joint Power Generation Conference, Buffalo, N.Y., September 1976, *ASME Trans.,* Series A, Vol. 99, No. 1, 1977.

[25] P.L. McGaha and T.L. Dresner, "A Nuclear Steam Turbine Intercept Valve and Control System for Fast Valving," Paper presented at the 1977 Joint Power Generation Conference, Long Beach, Calif., September 1977.

[26] L. Edwards, R.J. Thomas, D.C. Hogue, P. Hughes, W. Novak, G. Weiss and J.E. Welsh, "Sustained Fast Valving at TVA's Cumberland Steam Plant: Background and Test Results," *Proceeding of the American Power Conference*, Vol. 43, pp. 142-152, April 1981.

[27] IEEE Working Group Report of panel discussion, "Turbine Fast Valving to Aid System Stability: Benefits and Other Considerations," *IEEE Trans.*, Vol. PWRS-1, pp. 143-153, February 1986.

[28] W.A. Morgan, H.B. Peck, D.R. Holland, F.A. Cullen, and J.B. Ruzek, "Modern Stability Aids for Calvert Cliffs Units," *IEEE Trans.*, Vol. PAS-90, pp. 1-10, January/February 1971.

[29] P. Kundur and J.P. Bayne, "A Study of Early Valve Actuation Using Detailed Prime Mover and Power System Simulation," *IEEE Trans.*, Vol. PAS-94, pp. 1275-1287, July/August 1975.

[30] D.L. Osborn, "Fast Valving and Neutral Resistor Application on a 600 MW Fossil Unit," Paper A76608-0, presented at the 1976 Joint Power Generation Conference, Buffalo, N.Y., September 1976.

[31] N.J. Balu, "Fast Turbine Valving and Independent Pole Tripping Breaker Applications for Plant Stability," *IEEE Trans.*, Vol. PAS-99, pp. 1330-1342, July/August 1980.

[32] R.M. Maliszewski, B.M. Pasternack, and R.D. Rana, "Temporary Fast Turbine Valving on the AEP System," *Proceedings of the American Power Conference*, Vol. 44, pp. 118-125, 1982.

[33] T.D. Younkins, J.H. Chow, A.S. Brower, J. Kure-Jensen, and J.B. Wagner, "Fast Valving with Reheat and Straight Condensing Steam Turbines," *IEEE Trans.*, Vol. PWRS-2, pp. 397-405, May 1987.

[34] P. Kundur, R.E. Beaulieu, C. Munro, and P.A. Starbuck, "Steam Turbine Fast Valving: Benefits and Technical Considerations," ST267 position paper,

presented at the Canadian Electrical Association, spring meeting, March 1986.

[35] R.H. Hillery and E.D. Holdup, "Load Rejection Testing of Large Thermal Electric Generating Units," *IEEE Trans.*, Vol. PAS-87, pp. 1440-1453, June 1968.

[36] V.F. Carvalho, "Use of Generator and Customer Load Rejection to Increase Power Transfer Limits," CIGRE Paper 32-79-00-56, presented at the Study Committee 32 Meeting, Minneapolis, Minn., 1979.

[37] P. Kundur and W.G.T. Hogg, "Use of Generation Rejection in Ontario Hydro to Increase Power Transfer Capability," Paper presented at panel session on generator tripping, IEEE PES winter meeting, New York, January/February 1982.

[38] R.G. Farmer, "Independent Detection Scheme to Initiate Western System Islanding for Pacific AC Intertie Outages," Paper presented at the panel session on controlled separation and load shedding, IEEE PES summer meeting, July 1985.

[39] C.W. Taylor, F.R. Nassief, and R.L. Cresap, "Northwest Power Pool Transient Stability and Load Shedding Controls for Generation-Load Imbalances," *IEEE Trans.*, Vol. PAS-100, pp. 3486-3495, July 1981.

[40] D.C. Lee and P. Kundur, "Advanced Excitation Control for Power System Stability Enhancement," CIGRE 38-01, 1986.

[41] C.W. Taylor, J.R. Mechenbier, and C.E. Matthews, "Transient Excitation Boosting at Grand Coulee Third Power Plant: Power System Application and Field Test," Paper 92 SM 533-0 PWRS, presented at the IEEE PES summer meeting, Seattle, July 12-16, 1992.

[42] IEEE Committee Report, "Dynamic Performance Characteristics of North American HVDC Systems for Transient and Dynamic Stability Evaluations," *IEEE Trans.*, Vol. PAS-100, pp. 3356-3364, July 1981.

[43] IEEE Committee Report, "HVDC Controls for System Dynamic Performance," *IEEE Trans.*, Vol. PWRS-6, No. 2, pp. 743-752, May 1991.

[44] C.E. Grund, G.D. Breuer, and R.P. Peterson, "AC/DC System Dynamic Performance - Transient Stability Augmentation with Dynamic Reactive Power Compensation," *IEEE Trans.*, Vol. PAS-99, pp. 1493-1502, July/August 1980.

[45] P.L. Dandeno, A.N. Karas, K.R. McClymont, and W. Watson, "Effect of High-

Speed Rectifier Excitation Systems on Generator Stability Limits," *IEEE Trans.*, Vol. PAS-87, pp. 190-201, January 1968.

[46] W. Watson and G. Manchur, "Experience with Supplementary Damping Signals for Generator Static Excitation Systems," *IEEE Trans.*, Vol. PAS-92, pp. 199-203, January/February 1973.

[47] W. Watson and M.E. Coultes, "Static Exciter Stabilizing Signals on Large Generators - Mechanical Problems," *IEEE Trans.*, Vol. PAS-92, pp. 204-211, January/February 1973.

[48] P. Kundur, D.C. Lee, and H.M. Zein El-Din, "Power System Stabilizers for Thermal Units: Analytical Techniques and On-Site Validation," *IEEE Trans.*, Vol. PAS-100, pp. 81-95, January 1981.

[49] F.P. deMello, L.N. Hannett, and J.M. Undrill, "Practical Approaches to Supplementary Stabilizing from Accelerating Power," *IEEE Trans.*, Vol. PAS-97, pp.1515-1522, September/October 1978.

[50] D.C. Lee, R.E. Beaulieu, and J.R.R. Service, "A Power System Stabilizer Using Speed and Electrical Power Inputs - Design and Field Experience," *IEEE Trans.*, Vol. PAS-100, pp. 4151-4167, September 1981.

[51] E.V. Larsen and D.A. Swan, "Applying Power System Stabilizers, Parts I, II, and III," *IEEE Trans.*, Vol. PAS-100, pp. 3017-3046, June 1981.

[52] F.P. deMello, J.S. Czuba, P.A. Ruche, and J. Willis, "Developments in Application of Stabilizing Measures through Excitation Control," CIGRE Paper 38-05, 1986.

[53] P. Kundur, M. Klein, G.J. Rogers, and M.S. Zywno, "Application of Power System Stabilizers for Enhancement of Overall System Stability," *IEEE Trans.*, Vol. PWRS-4, pp. 614-626, May 1989.

[54] M. Klein, G.J. Rogers, S. Moorty, and P. Kundur, "Analytical Investigation of Factors Influencing Power System Stabilizer Performance," *IEEE Trans.*, Vol. EC-7, pp. 382-388, September 1992.

[55] Canadian Electrical Association Report, "Investigation of Low Frequency Inter-Area Oscillation Problems in Large Interconnected Power Systems," Report of Project 294 T 622, prepared by Ontario Hydro, 1993.

[56] E.V. Larsen and J.H. Chow, "SVC Control Design for System Dynamic Performance," IEEE Special Symposium on Application of SVS for System

Dynamic Performance, Publication 87TH0187-5-PWR, 1987.

[57] N. Martins and L.T.G. Lima, "Determination of Suitable Locations of PSS and SVC for Damping Electromechanical Oscillations in Large Power System," *Proceedings of the 1989 Power Industry Computer Application Conference*, pp. 74-82, May 1989.

Index

AC/DC system interaction, 528
  influence of ac system strength, 528
AC excitation system, 318, 320
  rotating rectifier system, 322
  stationary rectifier system, 320
AC exciter, 353
AESOPS, 800
Alternative transformations, 83
Amortisseurs, 47, 782
Amplidyne voltage regulator, 319
Amplidyne, 320
Arc-back, 498
Area control error, 606
Area frequency-response characteristic, 607
Armature current limit, 191
Armature time constant, 161
Asymptotic stability, 702
Asynchronous link, 464
Attenuation constant, 203
Automatic generation control, 377, 601
  control performance criteria, 618
  effect of speed-governor dead band, 622
  emergency mode operation, 621
  frequency of AGC execution, 619
  implementation of, 617
  in interconnected power systems, 601
  in isolated power systems, 601
  performance of, 610, 621
  tuning, 621
Automatic line reclosing, 922
Autotransformer, 231
Average direct voltage of dc converters,
  with ignition delay, 475
  with no ignition delay, 473

Backswing, 1106
Baum, F.G., 665
Bias factor, 606, 607
Bipolar HVDC link, 465
Blinders, 920
Boiler, 451
  drum type, 451
  once-through, 451
Boiler-following mode of control, 453
BPA, 1104, 1106
Braking resistor, 1106
Brushless excitation system, 322
Bulk power system, 6
Bundled conductor, 230
Bus classification, 255
Bypass valve, 498

CANDU reactor, 457
control modes, 457
Centre of inertia, 946
Characteristic harmonics, 525
Characteristic impedance of a line, 203
Commutating voltage, 481
Commutation angle, 479
Commutation failure, 499, 537
double, 500
Commutation in dc converters, 473
Commutation overlap, 479, 482
Complex frequency, 717
Complex turns ratio of transformers, 245
Composite regulating characteristic, 595
Composition of load, 271
Compounding curve of synchronous machine, 126, 197
Concordia, C., 728
Contingency,
extreme, 14
normal design, 13
Continuation parameter 1015
Continuation power-flow analysis, 1012
Control mode, 25
Control of HVDC system, 500
augmenting transient stability, 1125
Controllability, 716
Controlled system separation, 1120
Converter, 467
Converter circuit, 470
Converter faults, 535
Converter firing control system, 516
Converter theory, 468
Converter transformer, 470
Critical operating condition, 965
Crowbar, 340

d-q transformation of induction machine equations, 283
Damper winding, 47
Damping coefficient, 1029
Damping torque, 23
Dashpot bypass, 400, 1085
DC braking torque, 173
DC excitation system, 318, 319
DC line faults, 533
deMello, F.P., 728
Design criteria for stability, 13
Direct (*d*) axis, 53
Direct method, 706, 941
Direct offset current, 108
Discharge lamp, 275
Discharge lighting load, 278
Discontinuous excitation control, 1124
Displacement factor, 479
Distance relay characteristics, 905
Distribution system, 6
feeder regulation, 680
substation bus regulation, 680
voltage regulation, 679
Disturbance, 18
dq0 transformation of synchronous machine equations, 67, 73
Dynamic braking, 1106
Dynamic overvoltage, 530

Edison, T., 3
Effective short-circuit ratio, 529
Eigenvalue, 707
computation of, 726
eigenvalue and stability, 711
sensitivity, 714
Eigenvector, 707, 714
calculation of, 806
left eigenvector, 708
right eigenvector, 707
Elastic strain, 1063
Electrical centre, 916
Electrical island, 1074
Electromagnetic transient program, 1065
End region heating limit, 194
Equal-area criterion, 831
Equations of motion of synchronous machines, 128

Equidistant pulse control system, 519
Equilibrium point, 701
Equivalent commutating resistance, 485
ETMSP, 274
Euler method of integration, 836
EUROSTAG, 1087
Excitation control design, 1131
Excitation system, 315, 1121
  ac regulator, 333
  basic function, 315
  ceiling current, 328
  ceiling voltage, 328
  control and protective functions, 333
  dc regulator, 333
  discontinuous control, 1124
  effect on small-signal stability, 758
  elements of, 317
  high initial response, 328, 1121
  line-drop compensator, 318, 336
  load compensator, 318, 335, 361
  modelling of, 341
  nominal response, 328
  performance measures, 327, 330
  per unit system, 342
  reactive-current compensator, 336
  requirements, 315, 317
  stabilizing circuits, 334, 357
  types of, 318
  voltage response time, 328
  voltage time response, 328
Exciter, 318
Exciter mode, 1044
Explicit integration method, 841, 861
Extinction advance angle, 487
Extinction angle, 480
Extinction delay angle, 487

Fast decoupled load flow, 264
Fast-valving, 1110
Fault,
  simulation of, 885
Fault-clearing time, 911
Ferranti effect, 215, 629
Field current limit, 192
Field current limiter, 318, 339, 370
Field shorting circuit, 340
  representation of, 857
Finite stability, 702
Flue gas system, 451
Forced commutation, 532
Fossil-fuelled power plant, 449
Francis turbine, 378
Free motion of a dynamic system, 709
Frequency bias setting, 619
Frequency bias tie line control, 606
Frequency control, 581
Frequency dependency of load, 273
Frequency response,
  calculation of, 807
  characteristics of synchronous machine, 159
Fuel system, 450
Full-wave bridge circuit, 470
Furnace, 449

Gauss-Seidel method, 259, 267
Gear method, 1087
Generator out-of-step protection, 925, 926
Generator tripping, 1118
Global stability, 702
Graetz bridge, 470

Harmonic resonance, 531
Harmonics in HVDC systems,
  ac side, 524
  dc side, 526
Hazards of underfrequency operation, 624
High-cycle fatigue limit, 1063
High-speed fault clearing, 1104
High-speed line reclosure, 922, 1065
High value gate, 361
Homopolar HVDC link, 466

HVDC system,
abnormal operation, 498
ac system faults, 535
classification, 464
components, 464, 467
configurations, 464
detailed flexible model, 569
functional block diagram, 567
guidelines for selection of modelling detail, 575
per unit system, 564
representation for power flow solution, 544
representation for stability studies, 566
response model, 566
reversal of power flow, 522
simple model, 566
supplementary control of, 1151
HVDC system control, 500
actual characteristics, 505
auxiliary controls for ac system, 512
basic means of, 502
basic principles, 500
basis for selection of, 502
blocking, 522
constant current, 504
constant extinction angle, 504
constant margin angle, 504
control characteristics, 503
control implementation, 514
current limits, 509
deblocking, 522
enhancement of ac system performance, 523
hierarchy, 515
power control, 512
tap changer control, 509
Hydraulic turbine, 377
classical transfer function, 383
governors for, 394
nonlinear model, 387
special characteristics, 384
Hydraulic turbine governors, 394
electrohydraulic governor, 399
mechanical-hydraulic governor, 396
PID governor, 404
tuning of, 399, 1081

Ideal no-load direct voltage, 475
Ignition advance angle, 487
Ignition delay angle, 487
Implicit integration method, 842, 862, 979
Impulse turbine, 377
Independent-pole operation, 1107
Individual phase control, 516
Induction generator, 280
Induction motor, 279
basic equations, 280
deep-bar rotor, 294
double squirrel-cage rotor, 293, 294
equivalent circuit, 289, 295
modelling of, 279
parameters, 304
per unit representation, 297
representation of saturation, 296
rotor constructions, 293
squirrel-cage rotor, 280
torque-slip characteristic, 290
wound rotor, 280, 293
Induction voltage regulator, 680
Inertia constant, 129, 132, 1027
Infinite bus, 728, 827
Initial pressure regulator, 443
Integrated boiler-turbine control, 454
Interarea mode, 25, 39, 817
Inverter control modes, 507
mode stabilization, 508
Inverter equivalent circuit, 490
Inverter operation, 486
Isochronous governor, 587
IV trigger, 442

Jacobian, 262, 264

Kalman, R.E., 717
Kaplan wheel, 378
K constants, 747, 748, 762

Linearization, 703
Line drop compensator, 682, 684
Line loadability, 228
Loadability curve, 228, 229
Load angle, 221
Load characteristics, 310
Load classes, 309
Load compensator, 361
Load components, 309
Load-frequency control, 377, 582, 601
Load modelling, 271
  acquisition of parameters, 306
  composite load model, 275
  dynamic model, 272, 274
  exponential model, 272
  motor loads, 279
  polynomial model, 273
  static model, 272, 274
Load reference setpoint, 592
Load sharing by parallel units, 591
Load shedding, 623, 1020, 1120
LOADSYN, 309
Local mode, 25, 39, 817
Local stability, 702
Long-term dynamic response, 1085
  simulation of, 1085
Long-term stability, 33, 1073, 1078
Loss-of-excitation protection, 337, 927, 1076
LOTDYS, 1087
Low value gate, 361
LTSP, 1087
Lyapunov's first method, 706
Lyapunov's second method, 706

Mason, C.R., 928
MASS, 795
Maximum excitation limiter, 318, 337
Mechanically switched capacitor, 652
Mercury-arc valve, 469
Metadyne, 320
Mho relay, 920
Mid-term stability, 33, 34, 1073, 1078
Miller, T.J.E., 655
Minimum excitation limiter, 337
Modal matrix, 708
Mode controllability matrix, 717
Mode observability matrix, 717
Mode shape, 714
Modified Arnoldi method, 807
Modified Euler method, 838
Mohave generation station, 1066
Monopolar HVDC link, 464, 465
Multiple bridge converters, 493
Multiterminal HVDC system, 466, 538
  control of, 540
  parallel connected system, 541
  series connected system, 542

Natural load, 205
Navajo plant, 1061
Negative-sequence braking torque, 891
Nepier, J., 717
NERC, 13, 618
Network equations, 257
Network reduction, 268
Network-switching disturbance, effects on turbine-generator shafts, 1061
Newton-Raphson method, 260, 267
NGH scheme, 1061
Node admittance matrix, 257
Non-characteristic harmonics, 525
Non-windup limits, 359
Northeast blackout of Nov. 1965, 38
NPCC, 13
Numerical integration, 836
Numerical stability, 837

Observability, 716
Off-nominal turns ratio, 235
Ontario Hydro, 930, 1120, 1124
Open-conductor condition, 898
Operating criteria for stability, 13
Oscillatory instability, 23
Out-of-step blocking, 921
Out-of-step condition, 923
  effect of, 923
Out-of-step relaying, 921
  principle of, 921
Out-of-step tripping, 921
  for generators, 924
Overexcitation limiter, 337, 370, 967
Overhead line, 200, 209
Overlap angle, 487

Partial load rejection, 1076
Participation factor, 715
PEALS, 799
Pearl Street Station, 3
Per unit system, 75, 342, 564
Phase constant, 203
Phase variable, 775
Phase-shifting transformer, 245
  representation of, 246
Plastic strain, 1063
Pole placement technique, 1147
Pole slipping, 916
Poles of a transfer function, 718
Potential energy boundary surface, 942, 943
Potier reactance, 119
Power load unbalance relay, 442
Power plant auxiliaries,
  effect of system islanding on, 1077
Power system control, 8
  hierarchy, 12
Power system operating states, 10, 1073
  alert, 10, 1074, 1075
  emergency, 11, 1074
  in extremis, 11, 1074, 1075
  normal, 10, 1074, 1075
  restorative, 11, 1074, 1075
Power system stability, 17
  basic concepts, 17
  classification, 17, 34, 36
  definition, 17
  historical review, 37
Power system stabilizer, 318, 335, 766, 1121, 1128
  alternative types of, 1128
  delta-omega, 1128
  delta-P-omega, 1129
  digital, 1131
  frequency-based, 1130
Power transfer between two sources,
  factors influencing, 250
Power versus angle relationship, 20
Power-factor correction, 631, 632
Power-flow analysis, 255, 687
  AGC response power flow, 690
  governor response power flow, 690
  inertial power flow, 690
  postfault power flow, 688
  prefault power flow, 687
PQ bus, 255, 264
Pressurized water reactor, 455
Propagation constant, 203
Propeller turbine, 378
PV bus, 255, 264

QR transformation method, 726
Quadrature (q) axis, 53
Quality of power supply, 8
Q-V characteristics, 967

Reaction turbine, 377
Reactive-ampere limiter, 337
Reactive capability curves, 196
Reactive capability limits, 191
Reactive compensating devices,
  modelling of, 672

Reactive power,
production and absorption, 627
Reactive power loss, 254
Rectifier equivalent circuit, 486
Reference frame transformation, 793
Regulated shunt compensation,
970, 1105
Relaying quantities during swings, 914
Reliability criteria, 13
Residue of a transfer function, 720
Richardson's formula, 841
Rigid-body mode, 1065
Rotor angle, 98
Rotor angle stability, 18
Runge-Kutta methods, 838

Saturation characteristics of synchronous
machines,
air-gap line, 110
improved modelling of, 117
incremental saturation, 745
open-circuit characteristic, 110
representation of, 112
saturation factor, 113, 114
short-circuit characteristic, 111
short-circuit ratio, 112
total saturation, 744
SCADA, 12
Secondary-arc extinction, 1107
Selective modal analysis, 799
Self-excitation, 1052
Self-excited dc exciter, 352
Separately excited dc exciter, 347
Series capacitor, 633, 970, 1105
bypassing and reinsertion, 635
bypass protective schemes, 636
Severe system upset, 1073,
case studies, 1087
hydro power plant response, 1081
nature of system response, 1073
thermal power plant response, 1079
Shaft system model, 1026
continuum model, 1026
lumped-mass model, 1026
Short-circuit ratio of ac system, 528
Shunt capacitor, 631, 969
Shunt reactor, 629
Signal washout, 770
Single-pole switching, 1107
Singular point, 701
type of, 712
Slack bus, 255
Sliding pressure mode, 454
Small-signal stability, 23, 228, 699
enhancement, 1127
Smoothed ACE, 618
Smoothing reactor, 467, 527
Sparse matrix methods, 268
Speed-changer motor, 592
Speed droop, 589, 590
Speed droop characteristic, 594
Speed regulation, 590
Speed voltage, 71
SSR protection scheme, 1061
Stability of dynamic systems, 700, 702
Stable equilibrium point, 942
State matrix, 707
State space, 701
State-space representation, 700
State variable, 701
redundant, 798
Static excitation system, 318, 323
bus-fed, 323
compound controlled rectifier
excitation system, 325
compound-source rectifier system,
324
field flashing, 326
potential-source controlled-rectifier
system, 323
transformer-fed, 323
Static var compensator, 639
application of, 654
supplementary control of, 1142
types of, 639

Static var system, 639
modelling of, 672
Stator decrement test, 162
St. Clair curves, 228
Steam turbine, 418
cross-compound, 418
detailed generic model, 430
enhanced model, 430
modelling of, 422
non-reheat, 421
off-frequency capability, 444
reheat, 421
simplified transfer function, 427
tandem-compound, 418
Steam turbine bypass, 1081
Steam turbine controls, 432
digital electrohydraulic control, 442
electrohydraulic control, 439
emergency trip, 433
generic model, 444
mechanical-hydraulic control, 434
overspeed control, 433
overspeed trip, 433
Step voltage regulator, 681
Stiffness of differential equations, 841, 1087
Stiffness of power systems, 596
electrical, 1065
mechanical, 1065
torsional, 1027
Subsynchronous resonance, 638, 1025, 1050
countermeasures to, 1060
Subtransmission system, 6
Surge impedance, 205
Surge impedance load, 205
Swing equation, 128, 131
Symmetrical components, 872
Synchronizing torque, 23, 751
Synchronous condenser, 638
Synchronous machine, 45
basic equations, 59
characteristics, 19
equivalent circuits, 88, 90
fault current, 107
magnetic saturation, 110
mechanical starting time, 132
modelling, 45
per unit equations, 84
per unit reactances, 87
phasor diagram, 181
phasor representation, 95
physical description, 46
rotor structure, 47
salient pole rotor, 47
solid round rotor, 48
Synchronous machine model,
classical model, 184
representation in stability studies, 169
simplified models, 190
Synchronous machine parameters, 139
basic parameters, 139
determination of, 161
negative-sequence reactance, 878
operational parameters, 139
sequence impedances, 877
standard parameters, 147, 150
subtransient parameters, 144
synchronous parameters, 144
transient parameters, 144
Synchronous motor, 306
Synchronous speed, 47
System generation control, 10
System islanding, 1074
overgenerated island, 1076
undergenerated island, 1076
System restoration, 1077

Tap-changing transformer, 231, 678
application to transmission systems, 678
Taylor, C.W., 976
Terminal voltage limiter, 318, 1122
Thermostatically controlled load, 275, 277
Three-winding transformer, 240

equivalent circuit, 240
Thyristor-controlled reactor, 645
Thyristor-switched capacitor, 649
Thyristor valve, 469
Time deviation correction, 619
Torsional characteristics, 1026
examples of, 1035
hydro generator, 1067
turbine generator, 1026
Torsional fatigue, 1025, 1062
Torsional interaction, 1041
between closely coupled units, 1065
with generator excitation controls, 1041
with nearby dc converters, 1047
with power system controls, 1041
with speed governors, 1047
Torsional mode, 25
Torsional mode shape, 1034
Torsional natural frequency, 1034
Torsional oscillations, 1025
special problems, 1025
Torsional stiffness, 1027
Transformer, 231
π circuit representation, 236
equivalent circuit, 232, 234
representation of ONR, 235
sequence impedances, 884
zero-sequence equivalent, 886
Transformer voltage, 71, 109
Transient droop, 396
Transient energy function, 941
Transient energy margin, 943
Transient energy of a power system, 948
critical energy, 948
kinetic energy, 942, 948
potential energy, 942, 948
Transient saliency, 184
Transient stability, 25, 38, 827
elementary view of, 827
enhancement, 1104
factors influencing, 835
Transmission control, 10
Transmission line, 200
classification of line length, 208
electrical characteristics, 200
equivalent circuit, 206
loadability, 228
performance requirements, 211
power transfer, 221
reactive power requirements, 224
sequence impedances, 884
stability considerations, 221
stability limits, 228
thermal limits, 226, 228
typical parameters, 208
voltage and current profile, 211
voltage drop limits, 228
voltage-power characteristics, 216
Transmission line protection, 903
directional comparison scheme, 909
distance relaying, 904
overcurrent relaying, 904
permissive overreaching scheme, 907
pilot-relaying schemes, 906
Transmission network classification, 6
distribution system, 6
subtransmission system, 6
transmission system, 6
Transmission system compensation, 654
degree of series compensation, 656
degree of shunt compensation, 656
effect on line voltage, 657
effect on maximum power, 657
regulated shunt compensation, 663
series compensation, 655
shunt compensation, 655
Trapezoidal integration method, 842
Triangular factorization, 268
Tripping to house load, 1077
TSEC, 1124
Turbine,
hydraulic, 377
steam, 418
Turbine-following mode of control, 453
Two-winding transformer, 232

ULTC, 231, 275, 960
control system model, 684, 685
Unbalanced faults, 872
Underexcitation limiter, 318, 337
Underfrequency load shedding, 623, 1093
Underground cable, 201, 210
Undervoltage load shedding, 1020
Underwater cable, 463
Unstable equilibrium point, 949

V curve of a synchronous machine, 126, 197
Valve blocking, 520
Valve bypassing, 520
Valve characteristics, 469
Varistor, 340
VDCOL, 510, 568
Vector power factor, 479
V/Hz limiter, 339, 340, 370
V/Hz protection, 340
Voltage avalanche, 960
Voltage collapse, 27, 959, 973
general characterization, 975
prevention of, 1019
typical scenario of, 973
Voltage control, 627
methods of, 628
objectives, 627
Voltage flicker, 531, 654
Voltage instability, 959
causes of, 965, 967
mechanism of, 977
proximity to, 977, 1006
Voltage stability, 27, 530, 959
basic concepts, 960
branch participation factor, 999
bus participation factor, 998
classification of, 976
effect of load characteristics, 979
effect of overexcitation limiter, 979
effect of transformer tap changer, 979
generator participation factor, 1000
large disturbance, 976
small disturbance, 976
Voltage stability analysis, 977
dynamic analysis, 978
IILSI algorithm, 1003
LOPSI algorithm, 1000
modelling requirements, 978
Q-V modal analysis, 993
static analysis, 990
transient state approximations, 1006
V-Q sensitivity analysis, 991
V-P characteristics, 963

Water hammer, 378
Water starting time, 382, 389
Wavelength 204
Windup limits, 358

Zeros of a transfer function, 718